DISPERSION OF HEAVY PETROLEUM GASES IN THE ATMOSPHERE

Abdullah Alakalabi

Doctor of Philosophy

Submitted in partial fulfilment of the requirements for the degree of
Doctor of Philosophy

School of Engineering
University of Central Lancashire
March 2020

Statement of Original Authorship

The work contained in this thesis has not been previously submitted to meet requirements for an award at this or any other higher education institution. To the best of my knowledge and belief, the thesis contains no material previously published or written by another person except where due reference is made.

Signature: 

Date: 05 May 2021

Acknowledgements

This thesis is based on the research conducted to study **Dispersion of Heavy Petroleum Gases in the Atmosphere**. This study became a reality because due to the unlimited support and efforts given by many people whom guided me at different phases of this journey. For this, I would like to extend my gratitude to each and every one of them.

First and foremost, my praises and gratitude to the **Allah Almighty** for His showers of blessings throughout my research to complete the research positively, and successfully. Whenever I felt hopeless during this research, it was His divine guidance that guided me and showed me the correct path every time I needed.

I am extremely grateful to the government of **Saudi Arabia** for providing me the opportunity to study at this prestigious institution. I am glad that I was able to complete my research and can give to the country, but this cannot be equal to what the government has provided me at the time of my need. I cannot express my gratitude in words for the help they provided me awarding me a scholarship.

I would like to express my profound and genuine appreciation to my Director of Research Studies **Dr. Weiming Liu** for giving me the opportunity and providing me the guidance throughout this research. His valuable feedback, dynamism vision, truthfulness and inspiration have profoundly motivated me throughout this journey. During the lows of my research Dr. Weiming Liu's guidance and encouragement as a supervisor pushed me to motivation and thus completion of my PhD. It has been an exceptional experience and beneficial to work and study under his direction. I am very thankful for what Dr. Weiming Liu has offered me during these years. The bond of mentorship along with friendship made between us will remain an important part of my life. Not only have I learnt blossomed academically, but also in my life. Dr. Weiming Liu has taught me valuable lessons and will serve as a torch in my darkness. I am also thankful to the 2nd supervisor Dr. Tony Graham, and 3rd supervisor Dr. Xiaojun Gu for their continuous support, and valuable feedback.

I would also like to express my sincere heartfelt gratitude and appreciation to the Research Student Registry staff especially Mrs. Clare E Altham, and Mr. Khalil Patel for providing me the correct guidance and support to complete my research. This would not have been possible without their assistance. With the heartfelt gratitude and appreciation.

Furthermore, with endless love and gratefulness, I would like to thank my mother, my beloved wife and my siblings for their continuous support and moral encouragement. Completing this research study would not have been possible without their prayer, cheer and reassurances.

Finally, I would also like to express my gratitude to all my close friends whom I call 'the real brotherhoods' Prof. Abdulrhman Dhabbah, Dr. Saeed Alzahrani, Dr. Bander Aldossari and Mr. Mohammad Alghamdi. Without their support and advise this would not have been possible. It is rightly said that friends are needed at all stages of life and a friend in need is a friend indeed. The support of my brothers provided during the times when I was in difficulty and the smiles, they brought in me whenever I was feeling homesick is invaluable. Besides my University colleagues, one of my friends in the UK also helped me a lot was Dr. Naif Alwahebi. Without his help, I would have quit a long time ago and it was because of this invaluable support that I am able to complete my research today. These moments will remain in my heart for all of my life and will cheer me at the time of need.

Thank you all for your untiring support.

Keywords

Dispersion of petroleum heavy gases, formation of heavy gas cloud, mixing of heavy gases at the atmosphere, heavy gas cloud, dense gas, chemical gas leakage, complex structure, computational fluid dynamics.

Abstract

This research addresses hazards of liquefied petroleum gases in its applications. The hazards are caused by the leakage of gases and valued by risk analysis and assessment in safety management. However, to accurately calculate the risks, detailed knowledge on processes and development of leaked gases are critical. Hence, the aim of this PhD is to investigate the processes and development of the gas leakage dispersion.

The leakage of a liquefied natural gas or liquefied petroleum gas experiences evaporating and mixing with ambient air to form a vapour cloud, heavier than air. When concentration of the vapour cloud lies within the limit of flammability and if the cloud make contact with the source of ignition and then the cloud could ignite that in case, a large and strong explosion will firstly occur and then fire follows, which could cause damage to the people and properties. This research study is therefore developing a novel approach for analysing vapour cloud dispersion at petroleum gas processing facilities. This is achieved based on existing computational fluid dynamics technology and tools such as ANSYS-CFX, FDS, and in-house solvers. Using these tools, the process for liquefied gas leakages and dispersions are simulated and the characteristics of petroleum gas vapour clouds are analysed. Three main case studies and flashing jets of liquefied petroleum gases are simulated and explored. Effects of the obstacles which are placed behind the leakage source with different height on heavy gas dispersion in the atmosphere are investigated under various conditions of the stratified flows. Sub-scale structures, which are of the order of obstacle lengths, heights and dominated by obstacle configurations were created in the gas clouds. Such sub-scale structures significantly impact the formation of gas clouds. Finally, recommendations for computational modelling of petroleum gas clouds are developed. The achieved results from this research evidently show consistency when compared intensively with published data by other researchers.

The study discusses thermodynamic properties of atmosphere along with the properties of petroleum gas. Properties of heavy gas clouds and the process of their formation has been discussed. Also, combustion reactions are reviewed alongside the happened accidents and the simulation of fire explosions is discussed.

In this work, the formation of flashing jet has been analysed with an example of liquefied petroleum gas. Two-phase flow has been brought into consideration through the Eulerian Lagrangian model and gas phase calculations are done through Navier-Stokes's equation.

Thermodynamic properties of the liquefied gas along with their storage conditions inside the liquefied tanks are discussed. Furthermore, Liquefied mist has been tracked through Lagrangian particles. Procedure for the mathematical modelling of liquefied mist along with the dynamics of the particle has been discussed. Distribution of the mist droplets size have been discussed. Change in the droplet's temperature has been linked with heat and mass transfer through different equations.

The findings from this work will provide a framework to analyse the behaviour of liquefied natural gas or liquefied petroleum gas leakages that will be benefitted to investigate accidental fires and explosions. The findings also provide a basis for risk assessment and management.

Table of Contents

List of Tables

Nomenclature

Acronyms & Abbreviations

ANSYS - Analysis System……/

BLEVE - Boiling Liquid Expanding Vapor Explosion……/

CAD - Computer-Aided Design ……/

CFD - Computational Fluid Dynamics……/

CFL - Courant-Friedrichs-Lewy number……/

CNF - Cumulative Number Fraction……/

DSEAR - Dangerous Substances and Explosive Atmospheres Regulations……/

DNS - Direct Numerical Simulation……/

FDM - Finite Difference Methods……/

FEM - Finite Element Methods……/

FVM - Finite Volume Methods……/

FDS - Fire Dynamics Simulator……/

ESD - Emergency Stop Buttons……/

ICE - Internal Combustion Engine……/

LES - Large Eddy Simulations……/

LNG - Liquefied Natural Gas ……/

LPG - Liquefied Petroleum Gas……/

LFL - Lower Flammable Limit……/

PDA - Phase Doppler Anemometry……/

PRV - Pressure Release valve……/

PDF - probability density function……/

PHAST - Process Hazard Analysis Software……/

QRA - Quantitative Risk Assessment……..…….…../

ROM - Reduced Order Method……..…../

RNG - Renormalization Group……..…../

SST - Shear Stress Transport……..…../

SGS - Sub-Grid Scale……..…../

TDMA - Tri Diagonal Matrix Algorithm……..…../

UFL - Upper Flammability Limit……..…../

VDI - Verein Deutscher Ingenieure……..…../

Latin Symbols

A *- Convection diffusion coefficient*……..…../

C_D *- Discharge coefficient*……..…../

d *- Coefficient relating to pressure difference*……..…../

d_m *- mean diameter*……..…../

G *- Mass flux (kg/m^2.s)*……..…../

h *- Pool liquid depth (m)*……..…../

k *- Turbulent kinetic energy (m^2/s^2)*……..…../

r *- Radial Coordinate*……..…../

Yi *- Mass fraction of specie i*……..…../

Re *- Reynolds number*……..…../

u *- Velocity field in x direction*……..…../

v *- Velocity field in y direction*……..…../

Vz - Volume or volume/kg……..…../

l_t *- turbulent length scale*……..…../

U_t *- turbulent velocity scale*……..…../

S_φ *- φ source per unit volume*……..…../

w - Velocity field in z direction……..…../

∇ *- Global position vector*……..…../

∇_{φ} - *φ gradient……/*

Greek Symbols

α - *Gas volume fraction……/*

∂ - *Partial derivative sign……/*

ε - *Turbulent dissipation rate (m 2/s3)……/*

η - *Ratio of orifice pressure and storage pressure……/*

γ - *Thermal diffusivity (m^2/s)……/*

λ - *Thermal conductivity ($^W/m.K$)……/*

μ - *Dynamic viscosity (kg/m.s)……/*

ν - *Specific volume (m^3/kg)……/*

ρ - *Density (kg/m^3)……/*

σ - *Surface tension for a liquid (N/m)……/*

$\sigma 0$ - *Standard deviation of the log-normal distribution……/*

τ_p - *Particle relaxation time (s)……/*

Γ_{φ} - *coefficient of diffusion for φ……/*

Subscripts	
e	*Control volume face in-between E and P*
w	*Control volume face in-between W and P*
i	*Iteration number*
T	*positive Z direction neighbour*
N	*Positive y direction neighbour*
P, E	*Mid grid points*
t	*Control volume face in-between T and P*
n	*Control volume face in-between N and P*
nb	*Neighbouring grid node*
Superscripts	
$*$	*Previous iteration/guessed value*
$'$	*Correction value (e.g., pressure Correction)*

Chapter 1 Introduction

Heavy gases in the environment consists of molecules with high molecular mass or density. Mostly, these gases are made up of hydrocarbons like propane, butane and methane etc. all of which come from petroleum products. Traces of these gases are already present in nature. However, due to accidents caused within industries whilst handling release the gasses into the environment in large amounts. The sources of release of heavy gasses can be categorised into two types:

- Releases of heavy gases directly from the gaseous source
- Release of heavy gases from liquified petroleum source

Petroleum and gas industries handle these products in large amounts both in gaseous and liquid form, for example, methane gas is stored and used as a fuel source in many process and chemical plants. For domestic use and liquified natural gas (LNG) it is used as fuel and as raw material for the production of other chemical products. Strict safety protocols are being followed in industries for the handling these heavy chemical gases. However, on some occasions large quantities of these gasses are released into the environment resulting either from instrumental or human error. In this study, investigations some of the major incidents, which have occurred at various sites around the world and the possibilities that resulted in the release of heavy gases leading to explosion are studied. Most of these accidents are due to instrument failure.

Many precious lives and industrial equipment have been lost resulting from each occurrence of such incidents. As a consequence of this industrial safety standards have become stricter and been divided into the areas where heavy gases are handled into three zones, defined as zone 0, zone 1, and zone 2.

These zones incredibly strict safety protocols starting from the most stringent policies at zone 0 right through to zone 2. This research study explains these safety protocols in detail with reference to the examples and safety of risk management, which includes the equipment used for the safety of the containers. As they contain heavy gases like smoke detectors, industrial safety shower and fire extinguishers. Furthermore, these types of equipment are categorised and standardised by the safety standards management for use in different zones.

Thermodynamic properties of the heavy gases such as density and, vapour pressure based on their temperature have also been explained. The saturation curve of propane and butane show many similarities exist between their properties. Although butane is heavier than propane, the physical properties shown by it, is less when compared to the boiling point of propane.

As the hazards related to the release of heavy gases are so extreme accidents cannot be fully avoided. Advanced engineering simulation tools help researchers to study the behaviour of heavy gas cloud to predict its flow, velocity, temperature and other important parameters. It is useful to be aware of these parameters in order to know and understand the amount of area the heavy gases will cover in case of any accidental release and hence applying safety protocols in those areas including the zones concept.

In this research, a series of experimental studies were performed for the heavy gases cloud dispersion and flashing jets. In these simulation experiments' effect of obstacles considered are in the form of buildings for the dispersion of heavy gaseous cloud. The obtained results are of the following properties: temperature, velocity, density, flow rate, source point position, turbulence for the heavy gases cloud and the studied of the effect of atmospheric parameters like ambient pressure, wind velocity and ambient temperature on the behaviour of heavy gas cloud dispersion.

Using the advanced computational fluid dynamics (CFD) approaches like ANYSYS-CFX and fire dynamic simulator (FDS), various cases were simulated, and results were obtained different parameters. The results of numerical simulations are compared with the experimental observations. It is found that wind velocity, temperature, and ambient pressure are the major factors affecting the behaviour of heavy gas dispersion.

The numerical simulations are carried out for the heavy gases released in the environment, directly in gaseous form or from a flashing jet. For the flashing jet, a comparison of our CFD simulations results with the experiments conducted by Witlox et. al. [55,56], which employed the testing equipment manufactured for a cylinder containing the liquified heavy gas and a nozzle are done.

In this study the investigation of the effects for obstacles on heavy and neutral gas dispersion is assessed. Previous studies have found out that obstacles play an important role in the cloud shape formation of heavy gas dispersion. Therefore, in this research study, CFD simulations were performed based on a similar setup to experiments conducted by Ayrault et. al. [57,58]. Their studies were conducted in EDF-ECL atmospheric wind tunnels.

This study of heavy gas dispersion in three groups of buildings and/or structures is studied using CFD approach. The buildings and/or structures have varying shape, cuboidal-shaped, cylindrical-shaped, and spherical-shaped. In each group, these buildings are of collocated and staggered layouts. The perimeters are varied along with the release source location and the effect of the difference in the values of these perimeters is analysed. The results obtained from these studies are compared with the experimental results of Heidorn et. al. [59].

This research explains the dispersion of heavy gasses that are not influenced by any atmospheric parameters for example: wind, temperature of pressure to understand the overall dependencies of the parameters on various factors. Consequently, a comparative study is performed to have an in-depth understanding of the factors that affect the heavy gas cloud for its dispersion.

1.1 Background

The petroleum gas supply chain involves production and examination, re-gasification, storage, liquefaction, and distribution. From a safety perspective, each of these processes have ability to give rise to leaks, cause fires and alternative safety hazards. Leakage of (LPG) or (LNG) generates a heavier-than-air vapour, which is therefore known as heavy or dense gas. The heavier gas mixes with the air in the surrounding and disperses in the atmosphere. If the cloud is ignited, fast flame or explosion occurs because the fuel is pre-mixed with air. After explosion, the unburned mixture could be re-ignited by the high temperature gas and result in secondary fires. Fire and explosion could cause severe damage to life and property, such as the Qingdao pipeline explosion incident Ruwitch et. al.[1]. For this reason, a critical understanding of LPG/LNG vapour cloud dispersion phenomenon is of importance.

Several experimental investigations into heavy gas dispersions have been performed, which have been reviewed by Cleaver and Hob et. al. [2]. Based on the experimental results, Empirical Correlations, Integral Model, Shallow-Layer Model have been developed Ichard et. al. [3]. These models help predict and analyse LPG/LNG vapour dispersions and helps in the assessment of risk and management. Dispersion, however, is a complex multi-phase problem, where flows occur in complex geometric configurations, including phase-changing and heat and mass transfer conditions. Therefore, these models are unable to characterise the phenomenon accurately.

Liquefied gas leakage into the atmosphere give rise to different terms involving jetting and flashing. Thus, the complete study of the thermodynamic properties of the liquefied mist enables to analyse the factors effecting the mass transfer, heat transfer and the size of mist droplets.

Atmosphere and petroleum gas have different properties and it is necessary to know the comparison between them. Since the petroleum gas release may prove hazardous thus all the characteristics and the conditions inside the tank must be known to prevent any hazard. Previous works involved 1D simulation of the heavy gas dispersions, but 3D modelling gives a better concept about the heavy gas dispersion, thus 3D modelling of the heavy gas dispersion should be known, and the results are of great importance. Without knowing the properties, it is not possible to model any dispersion thus the properties of heavy gas cloud must be known. With the help of computational fluid dynamics (CFD), large scale numerical simulations of heavy gas dispersions could largely enhance the prediction processes accuracy and enhance

our understanding of hazards. CFD models can solve equations that are time-dependent using conservation of mass, species, and energy and momentum phenomena. In principle, CFD models can produce detailed and accurate processes. Due to the limitations of existing numerical methods and computational resources, it is challenging to obtain accurate numerical solutions for the petroleum gas dispersion problem. Based on this understanding, this study will develop CFD techniques to investigate dispersion of heavy gas and the results.

1.2 Aim and objectives

Based on the reasons explained in in the above, the aim and objectives of this research are detailed as follows.

1.2.1 Aim – the aim of this research is at enhancing knowledge on formation and dispersion of heavy petroleum gas cloud from a leakage within complex geometries, using computational fluid dynamics (CFD) approach.

1.2.2 Objectives – the objectives are defined below:

1. Develop and test accurate turbulence models for dispersion of vapour clouds of petroleum gases.
2. Simulate and explore the heavy gas dispersion over four types of obstacles of different heights, and study the influences of these obstacles to the heavy gas dispersion with various leakage sources in the atmosphere.
3. Explore the heavy gas cloud formations and the gas mixing processes in the situations of stratified flows and characterise the dispersive behaviours of petroleum gas clouds within the following complex geometries:
    a. Vapour cloud dispersion in a group of buildings.
    b. Vapour cloud dispersion in an oil storage tanks area.
    c. Vapour cloud dispersion in a gas storage tanks area.
4. Develop novel approach for risk assessment and safety management for petroleum gas leakages based on the works above.

1.3 Originality of this research

To obtain accurate knowledge about the formation and behaviour of heavy gas clouds when a leakage occurs is a vital component of risk assessment and management processes. Traditional models often predict the dispersion of heavy gas clouds inaccurately and poorly. This research study, therefore, incorporates turbulence modelling, phase changing and mass transfer calculations to improve predictions.

Using the CFD approach, this investigation simulates the movement and development of LNG/LPG vapour clouds in areas, that have irregular terrains and unstructured building layouts. This will facilitate the prediction and influence of building layout, wind speed, leakage rate, and ambient temperature variation. Furthermore, these approaches will enhance the results of this investigation with higher levels of precision. This is an important contribution to the existing body of knowledge and is additional novel feature within this research.

Finally, characteristics of hazardous clouds will be quantified. Since the outcomes of this investigation enhance risk assessment and safety management, the results are useful for the industry and yet again is a novel feature of the investigation.

Chapter 2 Accidents and Risk Management

2.1 Previous accidents of gas leakage

Heavy gases including natural gas, hydrogen gas, and other associated fuels are widely used as a type of energy. Thus, heavy gas clouds in the atmosphere occasionally are a contribution form industrial accident. It is important to analyse previous accidents such as the discussed following accidents, to learn the risks and hazards from the real scenarios. In this chapter, three typical methods of dispersions of harmful heavy gases in the environment are explored Woodward et. al. [4]. Based on the investigation of these accidents, risk assessment approach on hazardous zone concept is reviewed.

Previously, there have been many catastrophic gas leakage accidents all over the world resulting in a huge loss of human lives as well as losses of business . Most prominent of these include the Buncefield Petroleum gas leakage occurred in the UK located at Hemel Hempstead in Hertfordshire near to the M1 motorway, that resulted in more than 40 injuries including 2 very serious. Furthermore, millions of dollars of businesses were impacted, and the explosion resulted in the contamination of the underground water seriously affecting the Eco life. Further details of this are in (section 2.1.1).

Similarly, another accident took place in the facility of Bayamon located in Puerto Rico, a Caribbean island. The Caribbean Petroleum Corporation (CAPECO) was one of the largest petroleum suppliers to the Puerto Rico. The explosion resulted in the release of more than 30 million gallons of crude petroleum oil into the water bodies resulting in the death of hundreds of fish and wildlife causing a major deadly health impact on the population, and is discussed in details in (section 2.1.2).

In the U.S.A a devastating explosion occurred at the PEAK Shaving Plant located in Washington due to the Liquified Natural Gas leakage. The explosion resulted in many injuries and a huge loss to the company in terms of loss in production and damage to the equipment, and in more details will discussed in following (section 2.1.3).

2.1.1 Buncefield explosion and fire

On 10th December 2005, Buncefield fire explosion took place at the terminal when a fuel storage tank was being filled with gasoline at Buncefield tank farm. The terminal was owned by Total UK limited and is reported to be the fifth largest storage depot in the UK with a

capacity of 273 million litres of fuel. Figure 2.1 shows the smoke containing heavy particles rising above the sky from the fire.

Figure 2.1: *Buncefield fire explosion (Courtesy Wikipedia)*

The blast was initiated from tank no. 912 and led to successive blasts of 20 tanks nearby. From analysis, the cause of the blast was identified to be initiated by the level indicator of the gasoline tank which was stuck at 2/3. As a result of continuous overfilling of the tank, the temperature increased, causing a huge explosion of the unleaded gasoline, releasing large amounts of lead and other heavy gases into the atmosphere. Figure 2.2 shows a heavy gas cloud rising in the atmosphere Witlox and Cleary et. al. [5]. These major accidents are a consequent of continuous negligence and do not happen instantaneously. Below are two main highlighted reasons and solutions that could have prevented the incident from occurring:

1) Faulty indicator level in the tank. This accident could have been prevented if a regular maintenance regime were adhered to for all equipment installed at the site was set-up Kay et. al. [6].
2) Increase in temperature of the tank causing ignition of the fuel. A temperature sensor on site could also have prevented this accident.

A heavy gas is defined as a gas containing heavy elements like chlorine, LNG, LPG, and other petroleum gases. Heavy gases are said to be incredibly harmful for human health. Fortunately, the concentration of heavy gases is reduced with distance. However, the dispersion of these cause a gas cloud, which is very different from a normal vapour cloud. Normal vapour clouds rise above and form clouds due to the pressure difference. Whereby, heavy gases move both

above the ground and towards the low slope, and the concentration of these gases change as they move with the air.

Figure 2.2: *Buncefield fire cloud (Courtesy Wikipedia)*

The Buncefield fire accident resulted in the vapour cloud covering an area of more than 200,000 m^2. The smoke resulted from the burning of structures made of different chemical compositions, which consequently resulted in high concentrations of harmful materials within the neighbourhood. Ultimately all residential and commercial areas surrounding the terminal were immediately evacuated. Figure 2.3 shows the aftermath of Buncefield fire explosion.

Buncefield fire occurred close to a busy motorway resulting in the disruption of traffic within the vicinity. All motorway activity was shut down and almost 30 km of the road remained closed. Thus, disrupting the transport business and causing a huge economical loss to the nearby industries.

In the latter part of July 2010, the investigations concluded, and report published, announced that it had detected abnormal amounts of biochemicals and heavy waste products in underground drinking water. Underground water was polluted to an extent that a criterion of more than one hectare limit was used to provide information about the environmental impacts on the atmosphere. Later that year, water was purified to remove PFOS and fuel content from the drinkable water costing an almost one million pounds expenditure Nicholas et. al.[7].

Table 2.1: *Consequences of accident of Buncefield explosion*

Consequences and facts	
Area affected	200,000 m2
Injuries	43
Smoke cloud altitude	9000 ft (2700 m)

Figure 2.3: *Aftermath of Buncefield fire (Courtesy Wikipedia)*

2.1.2 Caribbean petroleum explosion and fire - Bayamon

On 23rd October 2009, a huge explosion hit the CAPECO facility in Bayamon, Puerto Rico. This incident occurred when gasoline was being offloaded from the ship tanker, the Cape Bruny, to the CAPECO tank farm onshore. Figure 2.4 shows the Caribbean petroleum explosion fire Atkinson et. al. [8].

Heavy gas dispersion is dependent on numerous environmental conditions, for example: ambient air temperature, air density and air temperature. Nonetheless, the behaviour of heavy gas dispersion in the unfortunate accident is also observed to be identical as other such accidents which can also be verified from the general characteristics of heavy gases (or their behaviour) when a leak occurs. As shown in (Figure 2.4), a cloud of heavy gases resulting from explosion is rising above the ground and expanding with the air. The concentration of the cloud is at its maximum at the base where it is produced from the fire. This concentration decreases with the distance.

Figure 2.4: *Caribbean fire explosion (Courtesy Wikipedia)*

It was investigated that the aerosolization of the gasoline spray resulted in the formation of a huge vapour cloud. This vapour cloud ignited in the wastewater treatment facility area after reaching an ignition source. The blast also caused the explosion of 17 other storage tanks.

The key reasons of the accident noted by the investigation team are as follow:

1) The investigation report claimed that aerosolization of the gasoline spray resulted in the explosion. Aerosolization is the phenomenon in which the molecules of the liquid are carried away with the wind.
2) The explosion could have been prevented if there was no contact of the air with the fuel. There were no safety checks at the site available to ensure this.
3) The ignition source was the a nearby waste-water management. This incident could also have been prevented if the temperature of the wastewater were checked and controlled frequently.

The fire from the explosion lasted approximately 60 hours with continuous smoke cloud rising above and mixing in the atmosphere. It affected approximately 45000 residents living nearby and around 300 houses were damaged from this explosion. Contamination of the atmosphere from the fire with the heavy metals resulted in many health complications of the people in that area.

Table 2.2: *Consequences of accident of Carribean petroleum explosion and fire*

Consequences and facts	
Homes affected	300
Petroleum released	30 million gallons

Fatal injuries	3
People affected	45000

According to below figures, nearly 30 million gallons of petroleum was released on site and off site through the storm water channels. 100,000 and seventy-one thousand million gallons of oil, fire suspension foam and twenty-two million gallons of contact water contaminated the environment as a result of the accident. Figure 2.5 shows the aerial view of the Caribbean Fire explosion and Figure 2.6 shows the minute stamps view of the explosion, finally Figure 2.7 shows the Aftermath of Caribbean explosion.

Figure 2.5: *Aerial view of Caribbean fire explosion (Courtesy Wikipedia)*

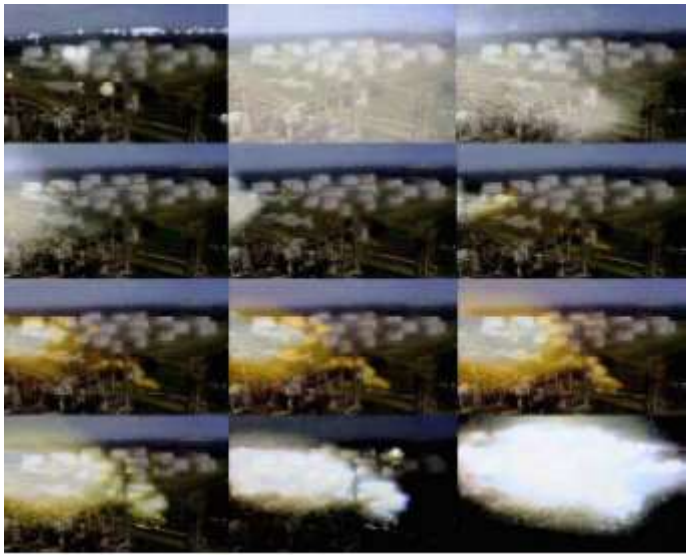

Figure 2.6: *Minute timestamps view of the explosion (Courtesy Wikipedia)*

Figure 2.7: *Aftermath of Caribbean explosion (Courtesy Wikipedia)*

2.1.3 LNG peak shaving plant - Plymouth

On 31st March 2014 at 8:19 am, (LNG) peak shaving plant operated by Williams company at Plymouth, Washington faced a disastrous failure and explosion in LNG-1 regeneration system and purification facility area. This occurred during the annual liquefaction start-up operation. Figure 2.8 shows the aerial view of LNG peak shaving plant Atkinson et. al. [9].

Key reasons of explosion noted by investigation team are:

1) The explosion was caused by operator error. The temperature of the air-gas mixture increased in the pipe and resulted in the ignition of the mixture. There should have been some temperature sensor present on the line to protect the equipment.
2) Purging the pipes containing combustible vapours must be carried out at regular intervals to prevent the accumulation of these gases.

Figure 2.8: *Aerial view of LNG Peak shaving plant (Courtesy google earth)*

The reason of this explosion was that the salt bath heater was located at the piping of the tank, as shown in Figure 2.9. A gas-air mixture that was flammable remained for a long period in the system and entered the salt bath heater. This mixture auto ignited after the start up. Figure 2.10 shows the aftermath of the explosion.

Table 2.3: *Consequences and facts of LNG Peak shaving plant explosion*

Consequences and facts	
Cost occurred	$ 50,000,000
Fatal injuries	5
People affected	30,000

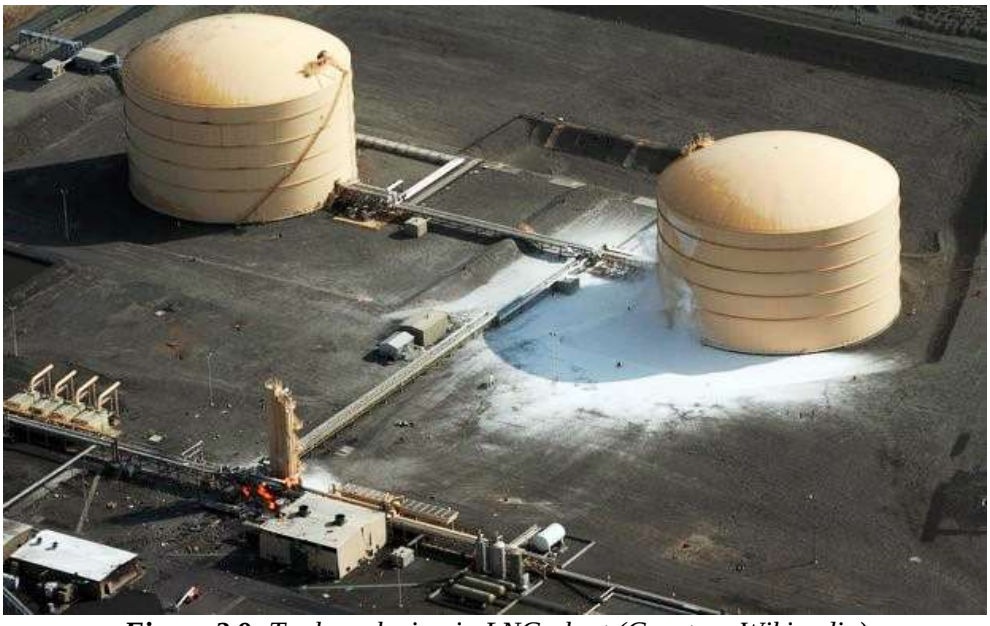

Figure 2.9: *Tank explosion in LNG plant (Courtesy Wikipedia)*

Figure 2.10: *Aftermath of explosion fire (Courtesy Wikipedia)*

2.2 Hazardous zones concept

According to DSEAR (dangerous substances and explosive atmospheres regulations. 2013) Zohdirad et. al.[10], any environment that contains hazardous or explosive material must be accompanied with safety protocols to protect the employees and the surroundings. Heavy gas leakage from various equipment's, processes and its contact with inflammable fluids may cause explosion in the adjacent environment leading to severe dames. Therefore, a new concept was introduced, whereby identification of potential ignition sources coupled with reducing possibilities for the various heavy gas clouds to combine. This concept is known as hazardous area/zone classification. The DSEAR classified the hazardous areas into three zones as zone 0, zone 1 and zone 2 based on the period in hours for which the area remains explosive per year. This duration is explained in detail below.

Research shows there are several methodologies presented to identity and design hazardous zones with the aim to reduce accidents. However, these techniques are limited by inaccurate identification of such areas due to the fact that combined effects of multiple leak sources and weather conditions are not included in the process. Thus, a new approach was presented by Zohdirad et. al. [10] where an optimisation methodology is adopted to define better hazardous zone while considering varying weather conditions and number of leak sources. The results show that better hazardous are definition and classification is possible since this method incorporated the wind direction, leak sources and their combined influence on the process.

An additional study was carried out focused on estimate the potential area where the heavy gas leakage may occur based on concepts of VDI (Verein Deutscher Ingenieure – German developed Models) dispersion model to predict the dispersion of gas. However, this model VDI Guideline 3783 provides no technique for estimating dimensions of potentially leaked heavy

gas cloud. Hence, this study provides a comprehensives strategy in finding these dimensions and were validated against experimental data. The study divides the hazardous areas where heavy materials are stored such as petroleum products into three zones. This concept of zones is explained in detail below. To fully understand the classification, some of the terms related to the hazardous area and fire triangle are explained below:

2.2.1 Definition

Any place or area where a potential of explosion is possible resulting from accumulation of heavy gases is termed as 'hazardous area'.

For any explosion to take place, the three conditions that must be satisfied are:

(1) Fuel, (2) Ignition sources, and (3) Oxygen

For each of these conditions, explained below is a short description of the conditions that must be fulfilled for an explosion to occur:

Fuel must be present in large concentration for an explosion to occur. For example, if a gas burner is left on for a period of time and then ignited with a lighter nearby, a small explosion will occur.

The ignition source is required to burn the fuel in the air.

Oxygen is required to carry out the chemical reaction. This chemical reaction will consequently produce heat and light.

2.2.2 Hazardous area classification - Zones

Hazardous areas are divided into three categories based on the percentage of risk: zone 0, zone 1, and zone 2. These zones refer to continuous, secondary, and primary grades of release, respectively. Furthermore, this is also defined as term Vz, a volume within, which flammable gas based on the mean concentration increases because of the release.

2.2.2.1 Zone 0

Zone 0 is the place where the explosive fuel is present frequently for a longer period. Zone 0 is the area where precautionary measures taken by the plant team are most strict and has no chance of leverage is provided to any member of the workers regardless of the position or state of the employee. The risk management protocols remain the same for persons. According to DSEAR, if an environment contains explosive substance for more than 1000 h/year, it is

classified as zone 0 Zohdirad et. al. [10]. This zoning concept must be kept in mind by the risk management team in order to account for safety measures.

2.2.2.2 Zone 1

Zone 1 is still considered as a high probability of explosion but is less than zone 0. According to DSEAR, if an environment contains explosive substance for more than 10 h/year but less than 1000 h/year, it is classified as zone 1 Zohdirad et. al. [10]. In this zone, the explosive materials are present while working on the equipment, which contain those materials. Zone 1 is an area where some leverage can be provided in some cases, but the risk is nonetheless considered to be high. In this zone all precautionary measures must be adopted to avoid any accident at zone 1.

2.2.2.3 Zone 2

Zone 2 has the lowest probability of explosion even if the explosion occurs, it is short and small scaled. According to DSEAR, if an environment contains explosive substance for less than 10 h/year, it is classified as zone 2 Zohdirad et. al.[10]. Zone 2 has the lowest probability of any accident hence the safety is also not so strict but still some measures are taken to ensure the safety of the workers.

2.2.3 Example applying hazardous zone approach

A hazardous area is defined as the place where there is a presence of any flammable substance that has ability to cause an explosion. However, these hazardous places contain different concentrations of flammable substances and based on such factors, these areas are divided into different zones i.e. zone 0, zone 1 and zone 2 Witlox et. al. [11]. Thus, for any explosion to occur, three components should be present: Any flammable substance, ignition source or heat, and air or oxygen.

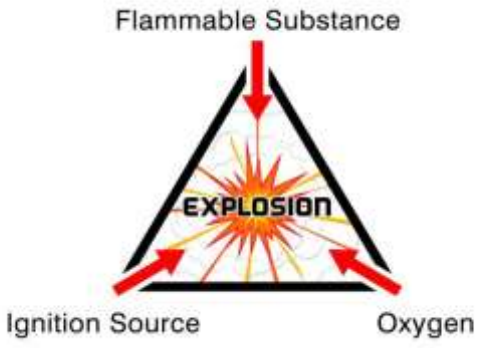

Figure 2.11: *Fire triangle (Courtesy: raytecled.com)*

2.2.4 Importance of zones

2.2.4.1 Locating the dangerous areas

These zones are important in understanding the severity of the danger. Many safety standards are existent which help to identify such zones. Colour coding is used to help locate these areas. For example, in some industries, red coloured fittings and piping are used to identify zone 0, yellow-coloured fittings and piping are used to identify zone 1, and grey colour are used to identify zone 2.

2.2.4.2 Providing safety measures

If in any area, there is a chance that these three components can be present, fire safety measures must be provided. Zone 0 is the most hazardous area that is directly exposed to the flammable gases if there is any leakage. Hence, zone 0 will contain maximum safety measures to prevent any loss. Moreover, further safety measures will also be provided that includes restrictions for specified personnel only and not allowing ignition sources inside the zone 0. Similarly, zone 2 is least dangerous so there will be less safety measures.

2.2.4.3 Conserving the resources

The concept of zones helps save resources that are spent on safety measures and help to identify the most affected areas in case of any leakage Witlox et. al. [11]. For example, zone 0 is the most dangerous area and must contain maximum safety measures.

To understand the concept of zones, consider a gasoline filling station, Figure 2.12. A petrol yard (where the petrol is directly filled into the vehicles) is declared as zone 0, as this place is exposed to hazardous and explosive material directly and frequently. The maintenance workshop located behind petrol station is declared as zone 1, as this involves maintenance activities sometimes which involve release of hazardous gases. The area surrounding the filling station can be declared as zone 2 as it has less probability of explosion.

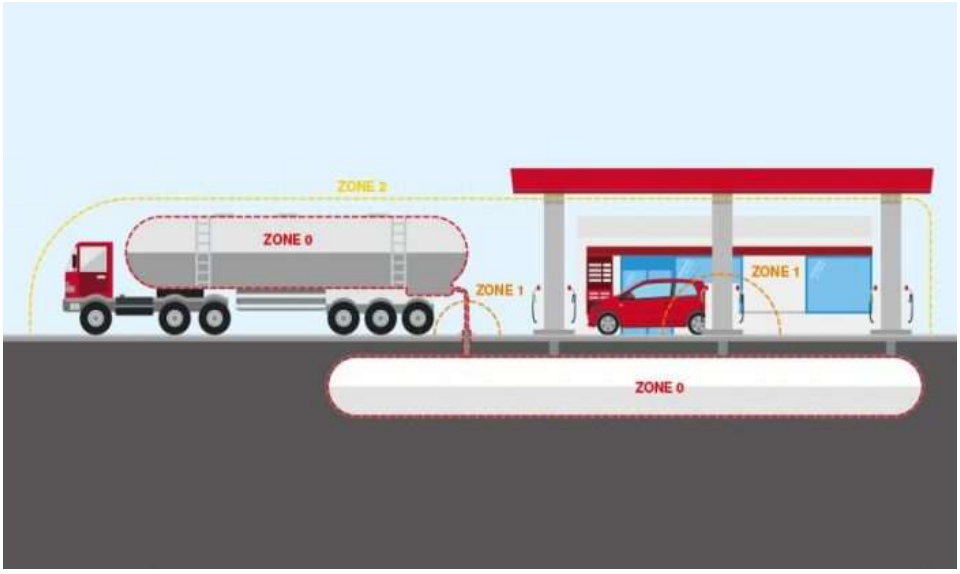

Figure 2.12: *Petrol station example (Courtesy leansixsigma.com)*

2.3 Other consequences and hazards

Besides the harmful effects caused by the direct release of the heavy gas into the environment, there are many other consequences and hazards which are caused by the heavy gas release into the environment. To understand the effects of industrial release of harmful gases into the atmosphere, the hazards of these gases should be known in case they are released in the environment beyond safe limits. For instance, consider CO_2 emissions during its transport can cause health problems such as respiratory problems and other related medical issues. Moreover, it was also found that the higher the concentration of CO_2 released into the atmosphere and the soil, causes reduction of pH level of soil, thus soil slowly loses its fertilising ability. Additional environmental implications include degradation in groundwater quality also causing some irreversible effects on microbial species Tian et. al.[12], Jossi et. al. [13]. Similarly, for the heavy gas release into the environment, there are many other implications besides the explosion which can affect the life on Earth.

2.3.1 Consequences of Pre-mixed combustible mixture

The energy from liquids and gaseous fuels is produced by mixing together with a combustible oxidiser, which in this case is air containing oxygen. Pre-mixed combustible mixtures result due to the prior mixing of fuel and the oxidiser to the passage of the burning zone. A good example of pre-mixed flame is the flame burning on the common household burner. Any atmosphere with the deficiency of oxygen is due to the accumulation of the LPG vapours. This type of atmosphere causes the formation of a cloud that sometimes seems to be either bigger

or smaller than the actual cloud, which mainly depends on air humidity. To enter such a zone with clouds, an explosimeter should be utilised, otherwise entering for anyone could be an introduction of an ignition source in such a fatal and hazardous zone.

2.3.2 Consequences of fast flame

Upon the complete LPG combustion mainly water and the carbon dioxide are released, both of which are not extremely hazardous when burned completely and taken care of the residue. However, with LPG leakages the flame takes ignition from the lowest possible area because of the gases are heavier. The flame can ignite from the source and move up to the leakage rapidly causing an overpressure zone and a very fatly burning flame. In lieu of safety, correct and adequate ventilation system and a proper vent for the combustion as well as the formation of products from the combustion to eradicate the chances of fire catching by the LPG must be present.

2.3.3 Consequences of explosion

Principally, the potential hazard of LPG is fire and explosion. It can be concluded that this is due to the inherited quality of the discussed product including high flammability and combination of gases in extreme conditions. Such gases can lead to a phenomenon called BLEVE (Boiling Liquid Expanding Vapour Explosion). BLEVE occurs only when the vessel containing the pressurised gas is ruptured due to the high temperatures and pressure. All explosions as mentioned above proved to be extremely dangerous.

The pressure is the main aspect and circle of discussion when discussing explosions or combustions. Being inherited with a very high volumetric expansion LPG tanks must never be filled. The explosion causes a release of a large amounts of flammable gas and vapours which cause an area of lesser vacancy to the production of larger cloud causing the pressure to be over-excited during the explosion. In these cases, the significant flame has a fast-moving flame front from about one hundred to several hundreds.

2.3.4 Consequences of ignition of other materials

Any sort of uncontrolled release or usage of LNG/LPG would always result in a hazardous outcome. Whenever LPG is released in the air by any means, a 200 times expansion in the original liquid is seen. The vapours being heavier than the LPG always move closer to the ground and any ignition source would therefore be risk takingly ready to ignite a fire, which would rapidly cross the safe limits by combusting the nearby ignitable material and leading to

an explosion. As the heavy gas cloud spreads overall a large surface area, the explosion that takes place cannot be controlled easily.

The LPG pipeline failures often lead to a scenario that is different for fire which may include pool fires and explosions and may vary by the mode of ignition to the LPG.

2.4 Pollution to the environment

LPG industry plays an important role in the economic and social development of society. LPG is extracted from crude oil by the distillation process. The burning of the LPG generates an extensive amount of CO_2 as a by-product. CO_2 is a major pollutant to the atmospheric environment and no doubt has a less contribution to environmental degradation but still plays a part in damaging the environment. This means that not only the direct release of LPG is harmful, but the burning of the petroleum gas also releases harmful pollutants into the environment.

2.5 Impact on human health

LPG has direct effects on human health despite making a difference indirectly through environmental pollution. It vaporises rapidly and causes cold burns to the skin. Furthermore, eyes must be protected at all times with safety goggles as LPG at a very high concentration is mixed with air and hence diluting the available oxygen.

Statistics data from a questionnaire interview along with the haematological and biochemical analysis on venous blood samples were collected from approximately 30 workers from filling and distribution stations. All LPG workers were diagnosed with high red blood cell count, corpuscular haemoglobin, and platelets count. Furthermore, it was also determined that these workers had significantly high risks of kidney and liver function failure. It is clearly evident that LPG has a direct effect not only on the workers but also on people present within LPG surrounded areas resulting from leakages or from the presence of such chemicals/gases.

2.6 Risk assessment and management

Today, comprehensive statistical analysis of protection against explosions is usually based on analysing the influence of all related factors for example: materials, possible ignition sources, related process of the system and interrelated interaction of different factors. All risk assessment studies are carried out based on various factors: such probable undesirable event, the frequency of their occurrence and potential results of damage that may occur. In this regard, a basic formation of risk was given based on triplet concept by Kaplan et. al. [14]. Where, risk

R is defined as a function of all possible scenarios for an undesirable accident. After that, the next step would be correct identification of hazards considering as to why, how, and what may cause an unforeseen accident followed by a risk intensity estimation (frequency of potential occurrence of event). Consequently, the next step is important as it requires the comparison between estimated risk potential with some standards in the field. Finally, the risk management policies as defined by world standards are adopted and implemented in the hope to prevent possible catastrophe Gavranic et. al. [15]. Moreover, the risk management step involves management of consequences and the probability of any sort of potential accident. Additionally, all of the described process primarily depends upon the accurate and reliable risk assessment and it is evident from the literature that a perfect risk assessment should properly identify the potential accidents, causes of the incident as well as they prescribe ways to reduce the risk as shown in Figure 2.13.

Figure 2.13: *Risk management (Courtesy riskmanagement.org)*

Based on the classification, hazardous zones must be supplied with the necessary protective and safety equipment. Zone 0 must have anti-ignition provisions and fire protection equipment available. This risk assessment can be classified into qualitative and quantitative methods. Consequently, proper prevention, protection, and the emergency responses would be brought into light as a result of conducting a risk assessment study Witlox and Clear et. al. [5].

2.6.1 Prevention

Prevention, is taking any measures to avoid any accident. This is a leading indicator to identify the causes of any accident before its occurrence. The above-mentioned accidents of the heavy gas leakage and explosion (Buncefield, Shaving plant accident etc.) could have been prevented if the necessary precautionary measures were taken by the plant teams.

The risk management department take care of such activities at the plants and provide recommendations of the measures to reduce the hazards.

The risk assessment must be in lieu to keep working of their own must also have an eye on the hidden causes of the occurrence of the incidence. So, they can be prevented by precautionary measures including the identification of LPG cylinders, their storages, and their pipelines. Employees should be educated upon starting employment to prevent accidents. Hence, such measures can be taken by ensuring the display markings, warning signs, and precautionary instructions are clearly vigilant and adhered to. All import and export products could be separate avoiding any sort of mixing and thus improve the degree of purity.

2.6.2 Protection

Protection, is a lagging indicator because it is useful in the case of an occurrence of an accident which has already occurred. In the absence of the national regulation tags, the minimum safety information, the name of the supplier, the quantity filled, and all necessary symbols must be present on the cylinder. Furthermore, the tanks and storage compartments should be explosion-proof.

Additionally, it is noticed that a language barrier is present occasionally in industry due to the varying range of backgrounds of workers. Hence, these measures should be taken not only in the local language but also in an international language. Upon compliance font size should be easily readable, and in a noticeable colour contrasting with the rest of the cylinder.

2.6.3 Emergency response

Although it is ideal to have an existing safety systematic approach in case of any sort of emergencies, a backup option is necessary to control and limit the rate of danger or accidents caused. Hence, an option is to have an increase number of LPG detectors in working areas along with controlled valves present in the vaporizing section which can be operated should an emergency arise. Heat intensities from storages often reach approximately 4KW/ m^2 at roughly 550 meters due to the catastrophic failures. For this, a solution could be to separate rooms which have ability to remain insulated from explosions to keep situations under control in times of emergency.

The shock waves can also reach at about 0.2 bars for the facilities nearby. Major accidents are also caused resulting from employees smoking, and this should be limited to restricted smoking zones only, which help prevention of further accidents.

Research shows numerous software are devised to model certain wind stability and contour of different concentration levels. The point of release has about 38 m and the falling flame can go as far as to approximately 143 m in the downwind direction which needs to be coped in emergency situations. According to the lower explosive limits (LEL) and lower flammability limits (LFL), the electrical appliances and other ignition sources must be kept at the safe distances.

2.7 Protection requirements

2.7.1 Detection system installed

Identification of any type of hazard is one of the crucial steps to consider when carrying out a risk assessment. To identify the hazards in an LPG system, the temperature detection of operations, pressure range of working modules, conditions of storage, and the composition of inventories should be identified. Site visits should be carried on daily basis in order to have a verification and overview with flow diagrams, discussions with the plant manager and/operator to ensure suitable changes for the detection of any sort of hazardous after affecting activity can be made. Working in such environments always demand a highly qualified system. Hence, knowing the behaviour of LPG, it is possible to predict the behaviour in advance using a technological approach. For accurate and reliable detection systems, an intelligent safety system should be adopted. These systems, use previous data, and help to take intelligent decisions. Based on the nature of the hazards and all consequences the quantitative risk analysis (QRA) should be identified and studied to learn the significant factors that may potentially cause an accident. Thus, the selected hazards are consequently taken out on a new platform for modelling and future restrictions that may occur.

2.7.2 Protection set-up

The primary policy in any operation must be to minimise the risks involved. Management of LPG operators must be given guidelines to operate, work and manipulate the operational equipment, which should all be included within the protection of the individual in such a modernised industrialised society Hebrard et. al. [16].

The protection setups include all the equipment, plant storages, LPG storages, and effective implementation of the precautionary measures. Illegal working should be prevented which may include transferring products by the incompetent person or by unapproved connections such as under the table transactions and other such ways. For such types of setups, the software can be

aided with PHAST 6.5, which is a prime example of obtaining results in a graphical form, making it easier for detection and elimination of potential gas leak sources. The main hazards, which can be associated are: The production of toxic gases with a fair chance of thermal radiation emissions. Thus, for such cases, the sudden release of the LPG in substantial amounts into the atmosphere may result in explosions similar to the BLEVE incident as discussed earlier in previous accidents of gas leakage (section 2.1), and the BLEVE termed reviewed in (section 2.3.3).

2.7.3 Emergency rescue planned

Emergency rescue planning is an incredibly important task to deal with as shown in Figure 2.14. Key responsibilities may include the determination of the exact scenarios, resulting in calculating the exact amount of damaged caused to a property and the exact number of accidental leakages in the tanks and all the leading failures in a system due to the malfunction of any sort of component within the system.

There is a vital need to have a fire protection system in place in order to avoid any sort of emergency. Generally, the typical fire prevention system requires a 200mm water supply hose along with sets of fire extinguishers. The system consists of:

1) Deluge sprays cover the heat sensor or fragile bulbs in the area.
2) Activation of emergency stop buttons (ESD) placed around the terminal.

Figure 2.14: *Emergency rescue planning (Courtesy industrial safety planning)*

During normal working hours, trained personnel with brief knowledge regarding first aid must be present on site. These personnel can be traced by notice board signs placed in common

communal areas, for example in the front or nearby to a first aid kits, canteens, or even at entrances /reception. Inclusive on such boards should be all techniques that would be able to help device ways to find the probability of failures. Several examples of powerful tools that help in the prediction of the failure rates have been seen.

2.8 Summary

Overall, it is concluded that majority of such actions generally resulted from human error and adoption of indifferent attitude. The gas leak accident in Buncefield resulted in the explosions of the storage tanks. Hundreds of lives were lost due to the accident. To avoid such accident, it is suggested to a comprehensive system with many protection layers or stages. These layers could be developed at the design stage followed by fabrication stage and including operation and related risk prevention system and potential damage mitigation systems. The explosion at CAPECO, which was caused by number of factors including overflow of gas, inefficient tank level control, out of order gauge systems and absence of alarm and overfilling prevention system. The consequences were severe in financial and environmental context, which could have been avoided by proper implementation of industry standard rules backed by the state-of-the-art safety equipment's. Lastly, the main causes behind shaving plant fire were identified to be the entrapped air fuel mixture in the pipe, which was left during the last maintenance and could have been avoided if such negligence on human resource part do not occurred. All accidents caused a lot of havoc and devastating damage to the environment and inhabitants of adjacent areas. Focussing on the prevention of such future accidents, concepts of hazardous zones were presented and widely implemented all across the globe. zone 0, zone 1, and zone 2 are continuous, secondary, and primary grades of release respectively. While the term of Vz is the volume within which flammable gas mean concentration arising from the release will be 25% (primary release) and 50% (secondary release) of the lowest explosive limit. If $Vz < 0.3\ m^3$, the ventilation should be high. The implementation of proper and reliable safety management protocols must be implemented at the sites dealing with the petroleum products. These systems are in the form of the fire protection equipment or intelligent safety analytics that help the user to take decisions based on the previous data. There must be a standard emergency response system in place and proper trainings of the employees and safety personnel must be carried out so that loss of precious lives can be prevented in case of any future accidents.

Chapter 3 Source of Heavy Gas Leakages

3.1 Attributes of gas leakage sources

Prior to estimating the extent and the hazards of a vapour cloud, it is first required to evaluate its release source. The source of vapour clouds can be sorted in four categories depending on the properties of the involved substance. The source is a gas source when the substance is in vapour form both at ambient conditions and inside the leaking system (e.g. natural gas leak). When the substance is in liquid form, both at ambient conditions and inside the leaking system (e.g., leak of gasoline) the source is considered to be a liquid source. A liquefied gas source is when the substance is in vapour form at ambient conditions but is in liquid form inside the leaking system (e.g., leak of liquefied natural gas or of pressure liquefied propane). A condensing vapour source: is when the substance is in liquid form at ambient conditions (boiling point is above ambient temperate) but is in vapour form inside the leaking system (e.g., in some industrial processes). A summary of the different types of vapour sources is given by Ponchaut et. al. [17].

3.1.1 Low-temperature liquefied gas leakage

When the source is in a liquid state and remains liquid when spilt on the ground, a three-step procedure is required to estimate the vapour cloud source. The first step is to determine the spill rate of the substance on the ground or in the containment structure. Consequently, the second step determines how fast the liquid pool is growing, and finally the third step is to calculate how quickly the pool vaporises. Although the evaporation of the pool can influence its growth, for most practical applications the effect of the vaporisation rate on pool growth is small. Considering the pool grows as if it were not evaporating, leads to a slight overestimate of its size, and therefore produces somewhat of an overestimated evaporation rates.

3.1.2 High-pressure liquefied gas leakage

A liquefied gas source refers to substances stored in a liquid form which vaporise at ambient conditions. The gas can be liquefied in two different ways, these being:

1. Pressure liquefied gas
2. Sub-cooled gas

In the pressure liquefied gas case:, the substance is pressurised in the system to remain a liquid at a temperature above its boiling point in ambient conditions (e.g., propane or butane bottles).

In the sub-cooled gas case (refrigerated liquid), the gases are kept sufficiently cold in order to remain liquid (e.g., cryogenic liquids, liquefied natural gas). When contained under pressures above ambient, the liquefied gas source leak creates a two-phase jet that is commonly referred to as "jetting and flashing."

A portion of the liquid ejected through the breach flashes immediately and becomes vapour, while the remainder remains liquid and forms small droplets that can either remain suspended and evaporate before reaching the ground or rain-out and pool on the ground. The speed of the jet and the amount of flashing depends on the pressure at which the liquid is stored and on the size of the breach.

3.2 Thermodynamics involved in the suspension of heavy particles

Heavy particles in the air can be suspended in the form of solid, liquid and gas. These particles are injurious to health and enter the human body once inhaled. Hence, it is important to study the suspension dynamics and thermodynamic properties involved in the presence of these particles in the air.

These particles in the form of liquid are present in petroleum products like gasoline, natural gas, and industrial lube oils. When they are exposed to the atmosphere, the products evaporate and result in the heavy particles dispersing into the air Webber et. al. [18].

Petroleum products like diesel, gasoline, LPG, or LNG, etc. are obtained by the distillation of crude oil in a large vessel containing bubble traps. The crude oil consists of different components having different boiling points. The oil is heated, and vapour rise and get trapped within the bubble traps as shown in the Figure 3.1:

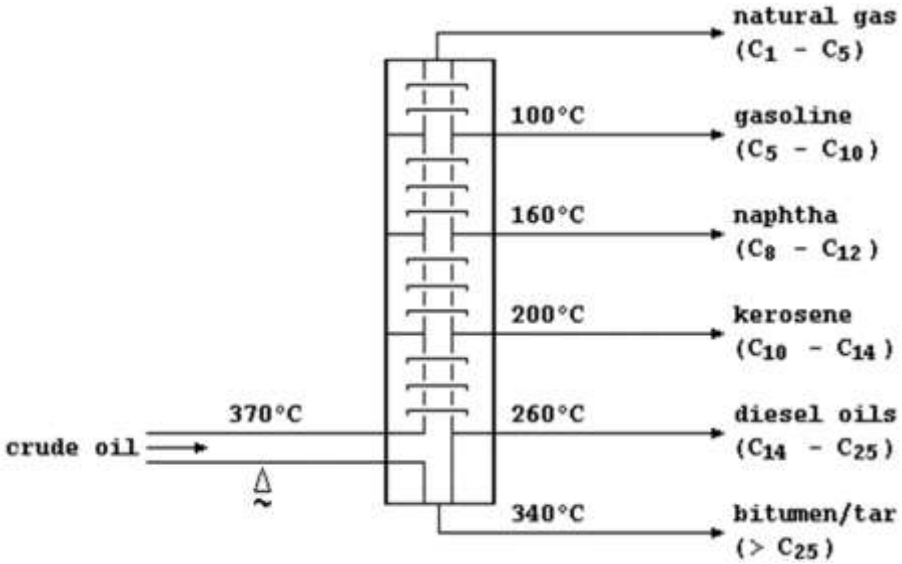

Figure 3.1: *Distillation of petroleum (Courtesy Wikipedia)*

Liquefied petroleum gas (LPG) is composed of hydrocarbon gases that are kept under pressure for liquefication and are used as a source of fuel. This comes from processing of natural gases and refining of petroleum. These gases change to liquid by compression at incredibly low pressures. The storage of LPG is done in steel vessels as liquid. These vessels vary from small bottles to large cylinders and tanks. Refrigeration is used for LPG separation from natural gas which is unprocessed. Distillation tower extracts LPG from heated crude oil. LPG can be divided into three part: butane, isobutene and propane. Its process of refining is shown in the Figure 3.2 below Witlox and Cleary et. al. [5].

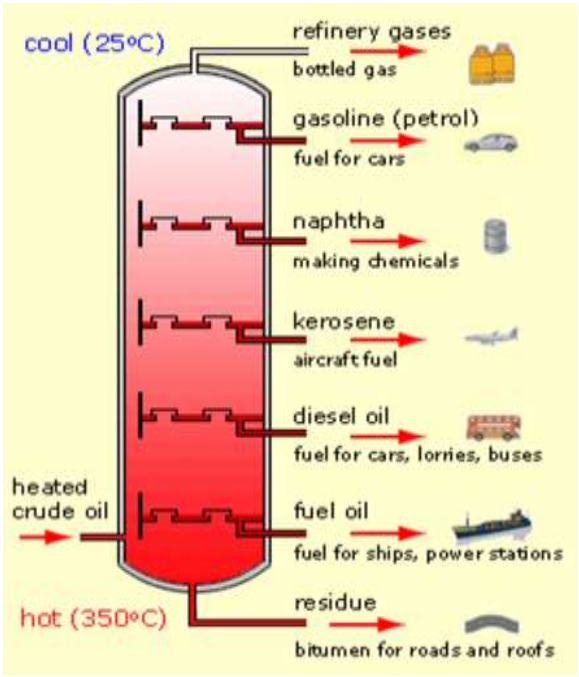

Figure 3.2: *Boiling temperatures of petroleum products [5]*

3.2.1 Release of LNG into the atmosphere

Liquified natural gas', LNG consists of methane in liquid form. Methane exists naturally in gaseous state, at high pressure and low temperature, which is converted into the liquid state and is stored within cylinders. LPG, 'Liquified Petroleum Gas' consists of propane and butane. The major differences between the two materials are shown in the following Table:

Table 3.1: *Difference between LPG and LPG (Courtesy: pioneerlng.com)*

	LNG	Propane
BTU Gallon	82,644	91,000
Gallons per MMBTU	12.10	10.99
Energy Density (Btu/gal)	1.00	1.10
Ignition Temperature (DegF)	1004	842
Leaks and Spills	Vaporizes to Atmosphere	Gathers in low lying areas
Boiling Pointy (DegF)	-260	-44

The storing of LNG requires very low pressure i.e., 10 kPa. The LNG cylinders are specially designed for this purpose to withstand very low storage pressures. Moreover, the cylinders are also insulated to prevent any major heat loss. Upon leakage, LNG vaporises into the atmosphere. The vapours of Methane are colourless.

In contrary, the storage pressure of the LPG varies with the temperature. The variation of the pressure with temperature is shown in the Table 3.2. It is clear from the chart that at 27 degrees Celsius, the storage pressure of the LPG cylinder must be 883 kPa. Upon leakage if the LPG consists mostly of propane and forms a mist cloud. If it mostly consists of butane, and is spilled on the ground, small droplets are carried away with the wind.

Table 3.2: *LPG Cylinder Pressure Chart (Courtesy: Elgas Limited)*

LPG (Propane) Cylinder Pressure Chart			
Temperature		Vapour Pressure	
C	F	kPa	PSIG
54	130	1794	257
43	110	1358	197
38	100	1186	172
32	90	1027	149
27	80	883	128
16	60	637	92
-1	30	356	51
-18	0	152	24
-29	-20	74	11
-43	-45	0	0
Copyright © 2015 Elgas Ltd.			

Handling of LNG is more difficult than LPG because of the following reasons:

1) The LNG cylinders require very low pressures to be maintained inside them to keep the methane gas in liquid form. The cylinders used for this purpose are called ‘Cryogenic Cylinders’. These cylinders are designed to maintain very low pressures inside them. The tanks must be equipped with many safety fittings to prevent the leakage of the gas into the atmosphere.
2) The spill of LNG in the atmosphere is more dangerous and difficult to control as compared to LPG. The LNG if released vaporises instantly and forms flammable clouds of methane gas which are carried by the wind. LPG on the other hand is heavier than air and forms mist of liquid which is easier to control.

Under the influence of heat and in the absence of pressure relief, LNG could generate a significant amount of vapour in the container. This could result in pressure build-up in the

container. When the container is opened, LNG vapour mixes with the surrounding air. This vapour cloud could move downwind, resulting in a heavier-than-air vapour cloud. If this LNG source is at an elevation, a dense gas plume could result when the fractional density is greater than zero Witlox and Cleary et. al. [5]. Fractional density is defined as the relative density of a substance in a mixture relative to the overall density of the mixture.

$$\Delta \cong 1.0 - \frac{28.9}{m_0}\left(\frac{T_0}{T} - 8\frac{\dot{M}_w}{\dot{M}_0}\right) \quad (3.1)$$

In the above equation, T_0 is the reference temperature of the mixture and T is temperature of the mixture. $\dot{M}_w$ is the total mass of the mixture and $\dot{M}_0$ is the mass of the substance.

Cleaver et. al. [2] found that LNG clouds could spread in horizontal, downwind, or crosswind directions depending on wind characteristics. LNG vapour clouds are analysed by solving equations for momentum, mass, and transport. Qi et. al. [19] concluded LNG vapour clouds are well represented by CFD methods.

3.3 Thermodynamic properties of Atmosphere and petroleum gas

To understand the behaviour of petroleum particles in the air, we must understand the thermodynamic properties of both air and petroleum. Earth atmosphere is composed of nitrogen and oxygen and their mixture forms atmospheric air. Nitrogen being 78.08% and oxygen 20.95% along with 0.94% of inert gases and 0.03% CO_2. The air with such composition is called dry with molecular weight of 28.96 g/mole. Water vapours are also present in air at the lower atmosphere strata. Its concentration is variable, which depends on the vapour pressure of water at a relative humidity and temperature. For example, 0.02% water vapours are present in air at 20^o Cand 80% relative humidity. Other components may also be present at layers of air adjacent to the surface of earth. At ambient temperature and pressure, air can be referred to as perfect gas and described using the equation 3.2:

$$v = RT \quad \text{and} \left(\frac{\partial u}{\partial p}\right)_y = 0 \quad (3.2)$$

where v = specific volume, u = specific internal energy, R = air gas constant

Air is liquefied at low temperatures. Oxygen typically boils (condensate) at -183°C and nitrogen at -195.8°C at approximately 0.1013 MPa pressure . At nearly atmospheric pressure, liquid air behaves as ideal solution and follows Raoult's Law. Condensation temperature of air normally is -191.4°C and the boiling temperature is -194°C.

As the temperature of the air, various changes occur. Physicochemical transformations are undergoing at elevated temperatures by air. Various oxides are produced by nitrogen when it reacts with oxygen: N_2O, NO, NO_2, NO_3. Moderate pressure and temperature greater than 2000K, oxygen and nitrogen start to dissociate and at atmospheric pressure and temperature greater than 4000K, ionisation of nitrogen, oxygen become evident. The thermodynamic properties of air are shown in Table 3.3 given by Qi et. al. [19].

Table 3.3: *Properties of air [19]*

T,K	p_b	p_c	v'	v''	h'	h''	s'	s''
1	2	3	4	5	6	7	8	9
65	0.1468	0.08613	1.065	2154	−149.6	+64.6	.669	6.040
70	0.3234	0.2052	1.090	968.4	−140.6	+69.2	.797	5.867
80	1.146	0.8245	1.148	269.6	−122.6	+77.8	3.034	5.585
90	3.036	2.397	1.216	100.2	−103.5	+84.8	3.251	5.376
100	6.621	5.599	1.302	44.67	−83.3	+89.3	3.456	5.204
110	12.59	11.22	1.418	22.15	−61.9	+90.1	3.649	.045
120	21.61	20.14	1.569	11.45	−37.5	+84.8	3.850	4.877
130	34.16	33.20	2.075	5.425	+0.4	+66.1	4.136	4.644
132	—	37.69	—	3.196	—	+37.4	—	4.410

p_b, p_c, bar,—pressure respectively at the boiling and condensing curves;
v', v'', 10^{-3} m^3/kg—specific volumes respectively of the liquid and vapor;
h', h'', kJ/kg—specific enthalpies of the liquid and vapor;
s', s'', kJ/kg · K—specific entropies of the liquid and vapor.

Flammable gaseous mixture mainly composed of methane is called natural gas. The composition follows; 13% C_2H_6, 70.99% CH_4, 0.2% C_3H_8, and small concentrations of N_2, CO, H_2O, CO_2, and He, etc. Underground cavities contain natural gas, either with access to petroleum fields (e.g., Saudi Arabia, Nigeria) or free deposits (e.g., Algeria, Indonesia, New Zealand). Non-hydrocarbons components of natural gases are removed during the liquefication of gas i.e., carbon dioxide, water, and hydrogen sulphide. This prevents corrosion and solid plugs. Before the market, it is sweetened (CO_2 and H_2S are removed by amine absorption), some liquefying fractions are extracted (isentropic expansion produces LPG), dehydrated (to avoid hydrate formation and water freezing by the absorption of glycol).

LPG are mixtures of the derivative of petroleum, are gaseous at ambient temperature but at 200-900 kPa. It is composed of n-butane, propylene, iso-butane, propane, and butylene with a composition that varies from approximately 100% propane in colder countries and approximately 20-30% propane in the warmer climatised.

Physical properties of LPG include boiling point, specific gravity, vapour expansion, combustion facts, flashpoint, pressure, and temperature and are partially shown in the Table 3.4:

Table 3.4: *Properties of LPG [19]*

Properties		Diesel fuel	LPG	
			Propane	Butane
Density	[kg/m³]	800-840	503	-
Vaporization heat	[kJ/kg]	465	420	-
Self ignition temperature	[°C]	355	481	544
Inflammability limits	[%]	0.6-5.5	2.1-9.5	-
A/F ratio	[kg/kg]	15	15.71	15.49
Flame temperature	[°C]	2054	1990	-
Lower heating value	[MJ/m³]	36000	23000	-
Lower heating value	[MJ/kg]	42.5	46.34	45.55
Cetane number CC	[-]	40-55	-2	-

3.4 Heavy particles due to evaporation

Evaporation is the natural phenomena, and it occurs at all temperatures. During evaporation, liquid molecules absorb the heat from the environment and leave the liquid surface and are released into the atmosphere. The introduction of the liquid to the open air above its threshold pressure gives rise to the heated liquid. Under these conditions, the dynamic expansion of the vapours shatters the steam of liquid and thus, resulting in atomised spray which is called flashing. For example, when LPG is introduced into the air at atmospheric pressure, the liquid flashes to produce gas. Two-phase flow of the liquid gas involving the change of phase (liquid-to-gas) is a flashing jet. Eulerian-Lagrangian multiphase model is used to bring this two-phase flow under consideration. Gas phase calculations are done through Navier-Stokes's equation and the representation and tracking of the liquefied mist are done through Lagrangian particles. The flow of incompressible liquids in Fluid Mechanics is described through the Navier-Stokes's equation. It can be regarded as the generalised form of the equation given by Euler at the start of the eighteenth century. Turbulence and the complex vortices occurring in the 3-D fluid flow results in the increase of velocity Giannissi et. al. [20].

A mixture of hydrocarbons liquefies to form a clear odourless and colourless liquid called LNG. This is normally transported and is stored at a temperature near to its boiling point at atmospheric pressure (nearly -160 degree C). Natural gas is cold liquid form is normally called LNG. Natural gas is the fuel that is burned in stoves, heaters, and electricity power plants. When it heats up, LNG become natural gas once again. Natural gas cannot be liquefied without cooling. LNG is exported and imported through ships. LNG cannot be burnt itself. First, it needs to be in vapour form and needs to be mixed with air to burn. It is combustible about five % to fifteen % volume concentration in the air. It is a cryogenic substance, and any physical

contacts results in danger. The major component is methane. It violently gasifier after the direct introduction of natural gas into a cargo tank at ambient temperature. Pressure rapidly increases inside the cargo tank and makes the atmosphere flammable. After the rapid cooling of the tank, large thermal stresses occur on the cargo skin and on the piping system. As a result, preparatory work must be followed the dry docking. Liquefied gas compresses to a little fraction of its original volume when subjected to liquefaction. Liquefaction reduces the cost of the transport by the reduction of volume. It can be very dangerous if not handled. The properties of LNG are shown in Table 3.5 Woodward et. al. [4].

Table 3.5: *Properties of LNG [4]*

Property	Value	Remarks
Boiling Point	-161.5^0C	@ 1 atm
Freezing Point	-182.6^0C	@ 1 atm
LNG Specific Gravity	$0.43 \sim 0.47$	rel to water = 1
Gas density	$0.7 \sim 0.9$	kg/m^3 @ STP
Flammability limits	$4 \sim 15$	by volume in air
Ignition Temperature	538^0C	@ 1 atm
Carbon content	73	by weight
Hydrogen content	24	by weight
Oxygen content	0.4	by weight
Hydrogen/Carbon atomic ratio	$3.0 \sim 4.0$	
Relative Density	$0.72 \sim 0.8$	at 15^0C
Octane Number	$120 \sim 130$	
Methane Number	$69 \sim 99$	

LNG's source and the process of liquefaction will decide its real composition. In the majority of the cases, the major percentage is methane along with ethane, propane, pentane, and butane. A small amount of nitrogen might also be present.

3.5 Heavy particles due to mists

Sometimes petroleum products are released into the atmosphere in the form of minute liquid particles. These particles can come from the unburnt gasoline with exhaust gases of the vehicles. Mists have got a large number of applications including IC engines, turbines, combustion engines, pesticides, and fertilisers. A large amount of research has been done to figure out the physical processes involved in the production of sprays and mists. Three basic ways in which mists are formed are explained below:

1) Discharge of spray from Liquid Reservoir under pressure

   Both accidental and intentional releases are the part of this. The breakup of the spray in the jet results in mist formation and as a result solid surfaces nearby will be hit by the liquid droplets.

Condensation of saturated vapour: The contact of liquid with hot surface results in the formation of hot vapour which cools and as a result, aerosol-cloud is produced. This is like the droplets being formed from the boiling kettle.

2) Splashing and Agitation

   In this case, the external force moves the liquid and induces breakup.

3) Stripping of air

   The flow of the fast-moving current of air over the pool of liquid and as a result stripping droplet from the liquid surface.

3.6 Tests for heavy gases detection

Testing of heavy gas for its concentration and composition is very important as it will help to identify the type of gas present in the cloud and the ways to deal with it. INERIS is a French organisation which stands for National Institute for Environmental Technology and Hazards. The organisation funded a European project named "Flashing Liquids in Industrial Environment". As part of this project, different experiments were performed for ammonia and LPG to improve the already present knowledge of the interactions between two-phase jets and obstacles. A schematic of the device that was used to carry out the discharge for LPG is shown in Figure 3.3 below:

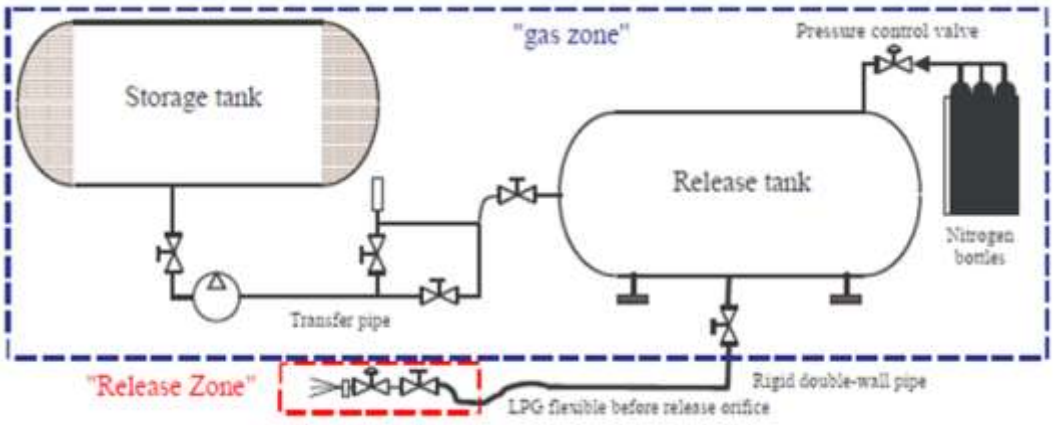

Figure 3.3: *Heavy gas detection method Woodward et. al.[4]*

The discharge device had of components including a buffer tank, a $5m^3$ discharge tank, nitrogen frames, an LPG buffer tank, a point of discharge, and a $5m^3$ feeding tank for point of discharge. The ratio of calculated mass flow rate and the experimental mass flow rate was used to validate the prediction of different models. Five different models namely the Bernoulli model for estimation of two-phase flow rate, Lackme model for calculating the two-phase discharge, Fauske model based on the Equilibrium Rate Model, Wheatley model for choked flows, and

omega model for mass flow rate estimation, were used for different conditions of the experimentation.

The results of the experiments predicted that two-phase models are suitable for full section ruptures while the Bernoulli model is suitable for small leaks. Similarly, for bigger leaks, none of the models could give suitable results. The ratio between the calculated and experimental mass flow rate against the overpressure for butane and propane is shown in figures below for diameters ranging between 5 to 25mm.

3.7 Liquefied gas flashing jets

Liquified gas flashing jets occur when the fuel come out of the nozzle and expand. This sudden expansion causes the sudden decrease in pressure which results in the vaporisation of the liquid particles into the gaseous form. These heavy particles in liquid form have very low boiling points and sudden expansion causes these low boiling points liquids to evaporate.

Three zones/areas are produced during this expansion and evaporation process which are named as shown in Figure 3.4.

1) Expansion area

   In this area, the liquid fuel or heavy molecular fluid from a compressed low area comes into a very large area. This sudden change in the area results in a sudden change of pressure according to the Continuity Equation and Bernoulli's theorem. At this point, the heavy fluid in liquid form is at its boiling because as the liquid expands, the molecules move quickly apart which results in evaporation as in gaseous form the molecules are far apart as shown in (Figure 3.4).

2) Entrainment area

   In this zone, two processes have occurred. One is the breakage of the turbulent zone and the other is the evaporation of liquid droplets. The velocity of the jet makes the liquid particles to move (hap) hazard. The energy required to evaporate the liquid comes from the surrounding air.

3) Final dispersion area

   The final dispersion zone is the area in which the vapours of the liquid droplets are finally spread into the air. At this point, the velocity of the fluid is reduced so much that it is now equal to velocity of the air.

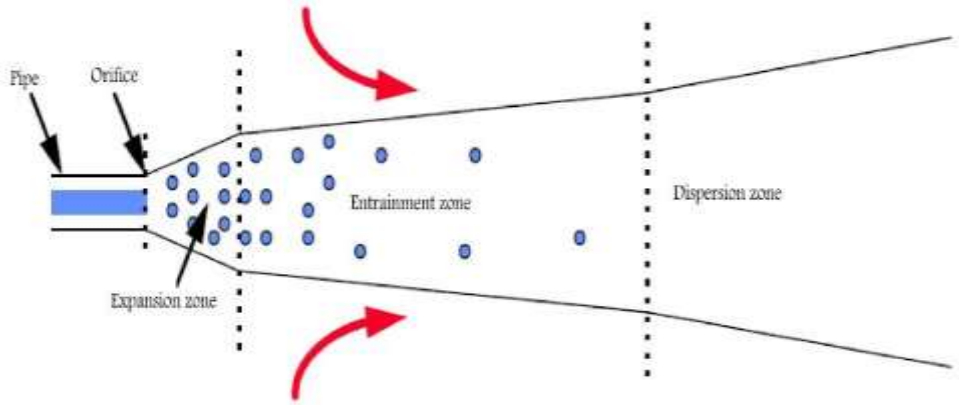

Figure 3.4: *Liquified gas jet zones Cleaver et.al. [2]*

3.7.1 Modelling of liquified gas flashing jet

Modelling of liquified gas dispersion is required to measure the vapour mass of the liquid fuel at the end. This vapour mass is required to measure the amount of vapours an amount of liquid will produce which can help to determine the limits of the vapours in the atmosphere.

There are two approaches to model the liquified gas dispersion. These two models are based on two different thermodynamic approaches. These approaches will directly influence the boundary conditions required to model the cases. The description of these two models is as follow:

1) Isenthalpic approach

   In this method, the enthalpy of the liquid during its transformation is considered to be constant but the entropy of the process changes i.e., increases.

2) Isentropic approach

   In this method, the entropy of the liquid during its transformation is considered to be constant but the enthalpy of the process changes i.e., decreases.

There are still some assumptions made to simply the complex equations which are as follow:

1. The fluid is homogenous i.e., the properties and composition of the fluid are assumed to be constant throughout the liquid and gas mixture.
2. The flow will always follow the mass and energy balance principle, no matter what happens.
3. The enthalpy or entropy of the fluid is considered to be constant. Both cannot be constant at the same time.

3.7.2 Two-phase flashing jets

Two-phase flashing jets are produced during the high-pressure escape of the sub-cooled liquid into some low-pressure atmosphere. This results in two-phase flashing jets. Modelling of these jets is required to determine the amount of vapours and fluid droplets. Sub-cooled fluid falls in the region below the saturated liquid vapour mixture. This region has such a low temperature and pressure that all the fluid in this region is in the liquid form.

Two types of two-phase flashing jets are discussed here:

1) Free Jet
2) Impingement jet

3.7.2.1 Free Jet

A free jet forms when a rupture or hole occurs in a large reservoir of any fluid. As a result, the fluid flows freely due to the pressure difference through the hole. It is a very commonly observed phenomenon in fluid mechanics and is very often explained in terms of water flow from a ruptured pipe [6].

Free jet which is shown in Figure 3.5 showing the release of sub-cooled liquid into the lower pressure region freely without any restriction at the end of the fluid.

The pressure distribution curve of the free jet is shown in the figure. It is clear that the pressure is maximum at the centreline of the jet and minimum near the jet boundaries. To understand the pressure distribution, consider that the free jet of the liquid released consists of different layers. When the jet is released, the pressure is same throughout the layers and with time, the layers at the extreme end's loss the pressure due to interaction with the atmosphere. In contrary, the layers at the centre do not come in contact with the atmosphere and hence retain their pressure.

Same is the case with the jet velocities which is maximum at the centre and minimum near the boundaries [6]. In figure 3.5, it is clear shows that the pressure profile and, the velocity profile is similar.

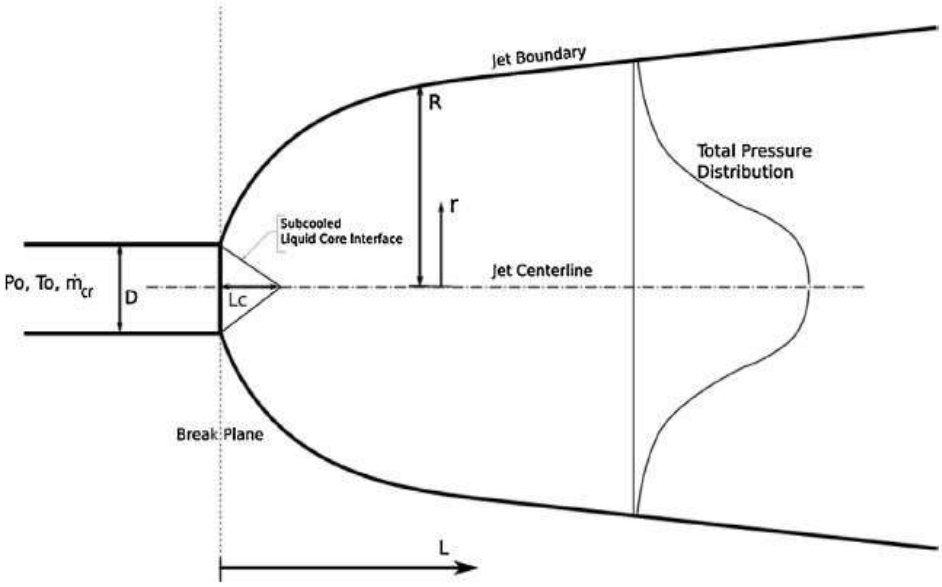

Figure 3.5: *Free jet of Sub-cooled liquid having no restriction at the end Kay et. al. [6]*

3.7.2.2 Impingement jet

In fluid mechanics, the impingement jet is similar to the free jet but has a flow restriction at the end. This flow restriction plate breaks the fluid velocity. This phenomenon can be observed in the T-joints in which the flow from the pipe is divided into two parts through a flow restriction at the end [8].

Impingement jet which is shown in the Figure 3.6 showing the release of high pressure sub-cooled liquid into the atmosphere but have a restriction at the end.

From the Figure 3.6, it is clear that the flow restriction results in a huge pressure drop at the centreline of the jet. The pressure distribution curve shows that at the centreline, the pressure is minimum as compared to the pressure at the jet boundaries. It is very important to monitor the pressure of the impingement jets to prevent the cavitation of the restriction plate at the centreline. This is because at the centreline the pressure may drop to such a value that evaporation may occur which can damage the equipment [8].

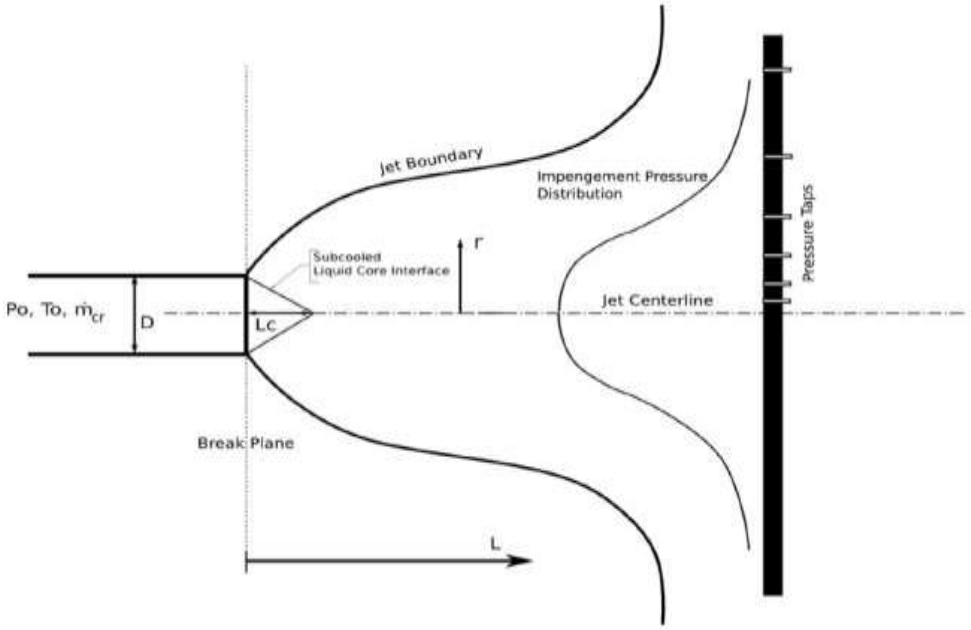

Figure 3.6: *Impingement jet of Sub-cooled liquid having restriction at the end Atkinson et. al. [8]*

3.7.3 Importance of pressure distribution curve

3.7.3.1 Preventing the cavitation

It is very important to monitor the pressure of the impingement jets to prevent the cavitation of the restriction plate at the centreline. Cavitation occurs when the pressure of the fluid becomes lower than the vapour pressure of the liquid. The bubbles of the evaporation formed hit the impingement plate and collapse. This action damages the plate. In case of impingement jet, at the centreline the pressure may drop to such a value that evaporation may occur which can damage the equipment [8].

3.7.3.2 Understanding the wake region at the centre

At the centre line of the flow, the flow restriction causes the formation of the vacuum. This results in the creation of the wake region at the centre that makes the fluid to move in circles. The pressure distribution curve helps to understand the flow mechanics for the jet which in turn helps to understand the dispersion.

3.7.3.3 Modelling the flow using CFD

The pressure distribution curve also helps to model the flow using the Computational Fluid Dynamics (CFD) approach. The pressure co-efficient value obtained from the analysis of the pressure distribution curve help to understand the flow properties.

3.7.4 Two-phase dispersion

Most of the accidents involving the release of heavy gases cloud in the atmosphere involve two-phase dispersion of liquid molecules in the atmosphere. This two-phase dispersion means that the molecules of heavy gas released into the atmosphere are in both liquid and gaseous forms. This two-phase dispersion remains longer into the atmosphere than single-phase dispersions as when released the vapours rise above the ground and liquid flow in the streams. This liquid, also turns into vapours when heated by the sunlight.

3.7.4.1 Droplet evaporation

Droplet evaporation involves similar phenomena. The liquid droplets of the heavy gases are carried away with the rainwater which later evaporates and forms more heavy gases vapours as shown in Figure 3.7.

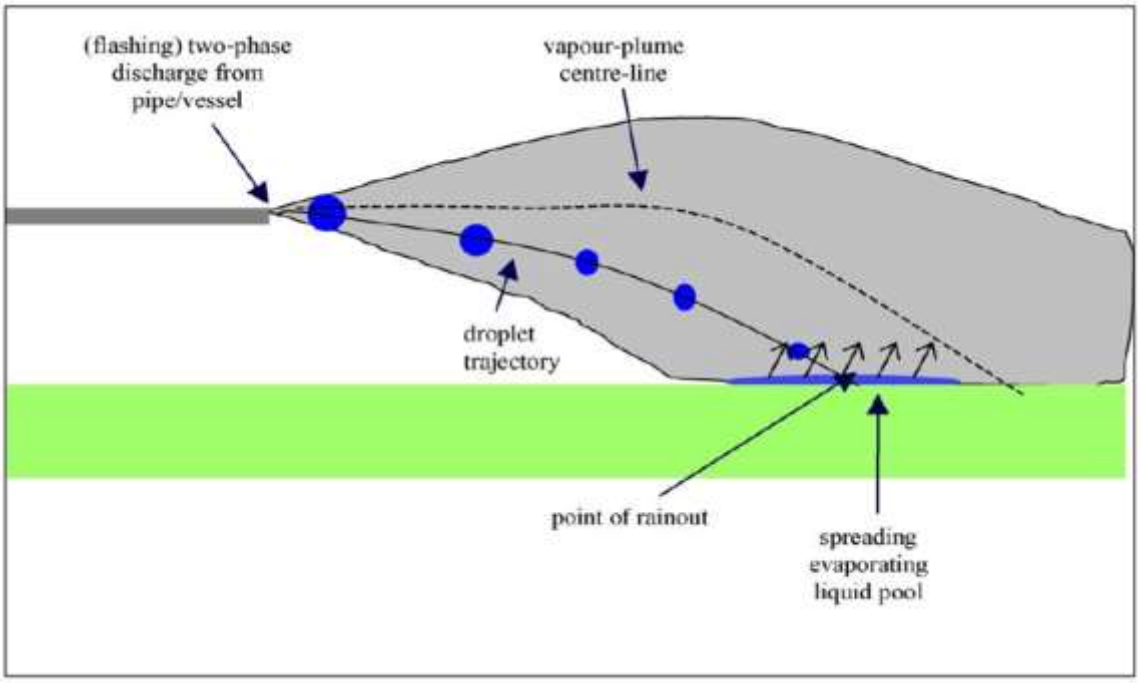

Figure 3.7: *Droplet evaporation Kay et. al. [6]*

Kay et. al. [6] explained the process in detail and provided recommendations based on his findings which are as follow:

1. First step for the modelling of droplet evaporation involves modelling of a jet to produce a stream of flashing liquid. This requires some boundary conditions i.e., pressure, velocity, and temperature of the jet.
2. Second step is to provide the model the ambient conditions i.e., atmospheric pressure and atmospheric temperature.

3. Sometimes the air also gets entrapped in the stream of the jet which effects the flashing of the jet.
4. The evaporation of the particles also depends on the size of the droplets and other droplets characteristics like droplet velocity etc.

3.7.4.2 Rainout formulations

Rainout of the liquid particles also occurs on similar principles as the droplet formation. Figure 3.8 shows the release of heavy liquid jet into the atmosphere. This liquid when released into the atmosphere evaporates and forms vapours of heavy gases. During the flashing of the liquid into vapours, the small liquid droplets move with velocity and fall with a trajectory and make a small pool of the heavy liquid at the ground.

This liquid is carried away with the rain and evaporates to produce more heavy gas cloud.

Witlox et. al. [5] performed certain tests at the Cardiff University to understand the behaviour of the rainout formations which is explained as follow:

1. First of all, tests were performed using water to understand the behaviour of the flashing liquid. The conditions were created for the water to evaporate as it flashes out of the nozzle.
2. The tests were expanded on other liquids to test the procedure on other liquids. The same results were obtained.
3. The other liquids on which the experiments were carried out are cyclohexane, propane and butane.

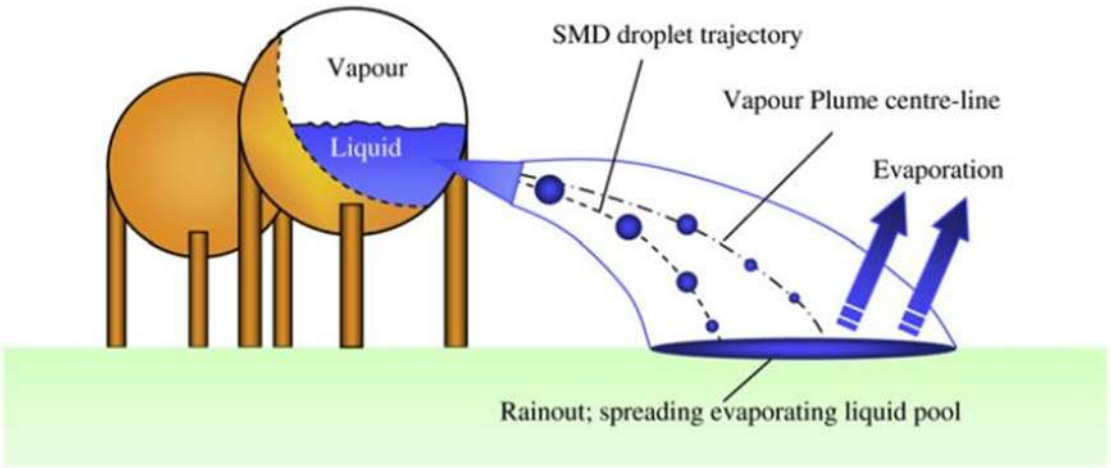

Figure 3.8: *Rainout formations Witlox et. al. [5]*

The experimental setup adopted to carry out the experiment consist of a large cylinder having a filling port and a pressure release (PRV) port. The filling port is used to fill the cylinder with the liquid and the PRV is used to protect the cylinder from over-pressure.

A heating element is also placed in the cylinder to control the temperature of the flashing liquid according to the experiment requirements. A nozzle is present at the bottom of the cylinder with an opening and closing valve to control the flow of the flashing liquid outside the cylinder.

Figure 3.9 shows the cylinder and its auxiliaries:

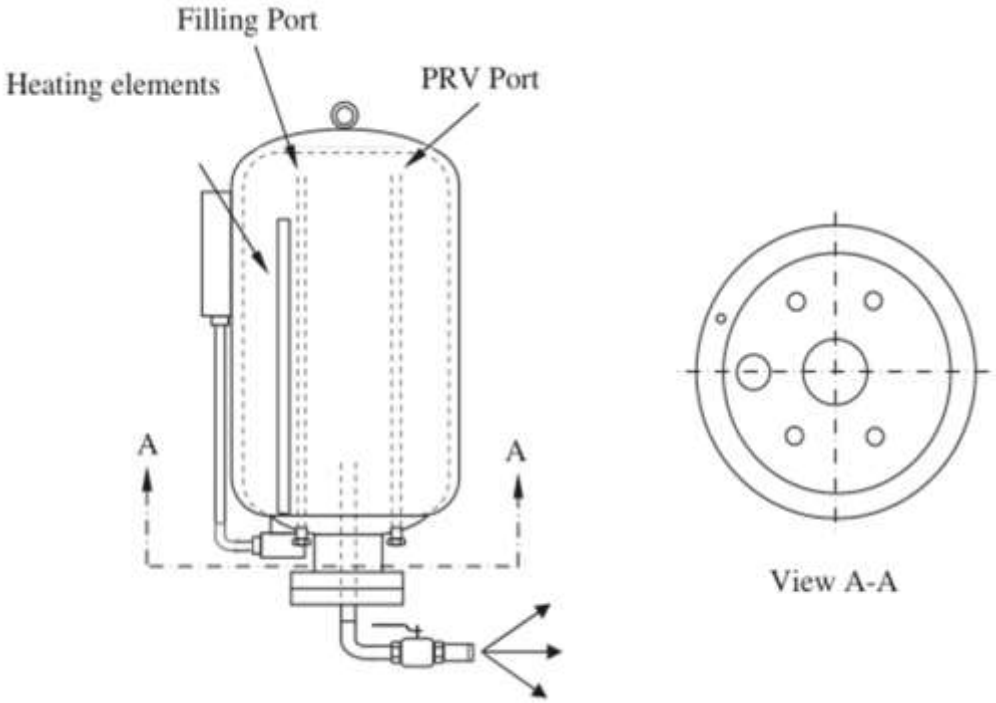

Figure 3.9: *Experimental setup Witlox et. al.[5]*

3.8 Mathematical models involved in heavy particles suspension

Owing to the importance to eliminate the heavy particles from the atmosphere or to prevent its release into it, it is important to analyse the dynamics of them. To help understand the behaviour of these particles in the atmosphere. For this purpose, many scientists and mathematicians developed mathematical models. Some of these models will be discussed here in detail.

For a practical perspective, these models are split into sub-models which are referred to as "reduced models". Mathematical interpretations of any model are not independent, but the

physical conditions are part of the results of the equation. Small changes in the physical methods, allow one to easily see a large change in the mathematical models.

Firstly, the procedure is to determine calculations of different phases of mist. After this model is proposed, which not only throws light on movements and motion but also enlightens the theoretical method behind the procedure. Here we need to discuss the motion of liquefied gas mist.

Some of the mathematical models which explain the behaviour of the heavy particles are:

1) Navier-Stokes Equation
2) Lagrangian Approach

3.8.1 Droplet size calculations

The size of the droplets produced during the two-phase flashing jet is important because of the following reasons:

1. The flashing jet calculations depend on the droplet size. The greater the size of the droplet, the more the liquid droplets are produced instead of vapours and are gathered in the puddle form on the ground.
2. The more the velocity of the jet is required if the size of the droplet is large to move it the same distance as that of a small droplet.
3. Droplet size matters a lot in vapour calculations i.e., the amount of vapour cloud produced during flashing of the liquid.

One of the problems of the theoretical model is to determine the dimensions and the number of Lagrangian particles. For this, the assumption is to consider the particles of spherical shape. Therefore, we must deal with the radiuses of the particles for their geometric dimensions. It is convenient to work with an average or mean diameter rather than the complete droplet size distribution. Hence, for the radius estimation, droplet size distribution is required. The number of stochastic differential equations control the droplet size distribution. These reflect the stochastic processes of the particles. In order to avoid these equations, a pre-defined droplet size distribution is preferred, employing combinations and distributions of Rosin-Rammler and log-normal for the combined volume of particles.

$$F = \begin{cases} \frac{1}{\sqrt{2\pi}} \int_0^D \frac{1}{\sigma x} exp\left(-\frac{[\ln x - \ln d_m]^2}{2\sigma^2}\right) dx & D \leq d_m \\ 1 - exp\left[-0.693\left(\frac{D}{d_m}\right)^{\gamma}\right] & D > d_m \end{cases} \quad (3.3)$$

where d_m = mean diameter and D = particle diameter.

The size of the droplet is very critical and important in specific applications and needs to be measured accurately. In mass transfer and other flow processes, it is convenient to deal with mean or average diameter.

3.8.2 Heat and Mass transfer

Heat and mass transfer are important aspects to study related to the dispersion of heavy particles into the atmosphere. At high temperatures, the particle's s rate of evaporation increases, and these particles are released into the atmosphere.

During the flashing of a liquid jet, heat is transferred into the liquid molecules of the jet and the molecules gain energy and evaporate. The energy required for this transformation comes from the atmosphere or air itself.

Four physical processes govern the rate of change of the dropping temperature namely, conduction, convection, radiation, and phase change. Phase changes involve evaporation or condensation. For most of the cases, the radiation is ignored.

As the vast greater part of the information is for the instance of water, the absence of information for various materials is considered the most critical lack at this phase of comprehension. Consequently, albeit an enhancement for past models for superheated discharges, there is yet impressive innovative work required to evaluate, combine and build up a portion of the suspicions, and demonstrating approaches received in this work. Besides, the simultaneous estimation of source splash conditions with estimated rainout has not been embraced in this arrangement.

3.9 High momentum release

Richardson's number determines the amount of turbulence of any gas flow. Such releases gradually transition to low momentum releases as the distance from the source begins to increase.

The releases which do not fall in Richardson's number range 0.8-30 are regarded as high momentum releases.

In negative buoyancy dominated flows, vapour clouds feature gravity-induced slumping and lateral spreading. This is typical for Richardson numbers between 10 and 30. Stably stratified regimes have vapour clouds embedded in the mean wind flow. Turbulence in damped and

vertical mixing is reduced by the stratification of density. The typical Richardson number is between 1 and 30. For passive dispersion, the typical Richardson number regime is between 0.8 and 1. Releases that do not fall in any of these three mentioned categories are regarded as high momentum releases. For this scenario, jet-induced turbulence strongly influences the dispersion process. High-momentum jets entrain more air and lead to a rapid reduction of vapour concentration, especially close to the leak. Such releases gradually transition to low momentum releases as they move away from the source. Other approaches for classifying releases include the duration of continuous and instantaneous releases. An instantaneous release occurs when the time of release is lesser than the time which the vapour cloud requires to reach the location. Based on the same logic, a release is continuous when the time of release is greater than the time which the vapour cloud requires to reach the location. Thus, a release could be classified as instantaneous or continuous depending on its relative position.

Vapour clouds could be dense gas clouds, jets, and neutral clouds. When the density is sufficiently greater than the ambient density, dense gas clouds are formed. The associated phenomena are different from those observed for momentum-driven or positively buoyant clouds. Negatively buoyant clouds have a larger width and lower average cloud height in comparison to neutral clouds. This low-degree dispersion seems sensitive to the obstacles.

The properties of jet releases depend on the characteristics of the jet. The transfer of momentum between ambient and high-speed release results in the entrainment of air into the jet, which reduces concentration and velocity. Sources with low or negligible initial momentum generate buoyant jets. Characteristics of negatively buoyant jets include higher than ambient densities.

When the molecular weight of chemical compounds is like the molecular weight of air, passive clouds are formed. Passive clouds could also be formed when dense vapour clouds dilute sufficiently for ambient air entrainment. Low concentrations could also result in passive clouds. Atmospheric turbulence controls the dispersion of neutral clouds Qi et. al. [19].

3.10 Summary

In this work, the analysis and brief explanation for the formation of flashing jet with an example of liquefied petroleum gas. Two-phase flow was brought into consideration through the Eulerian-Lagrangian model and gas-phase calculations were done through the Navier-Stokes's equation. Thermodynamic properties of the liquefied gas along with their storage conditions inside the liquefied tanks were discussed. Furthermore, Liquefied mist was tracked through Lagrangian particles. Procedures for the mathematical modelling of liquefied mist

along with the dynamics of the particle has been discussed. Distribution of the mist droplets' size has been discussed. Change in the droplet's temperature was linked with heat and mass transfer through different equations. An additional non-depersonalised connection for the forecast of mean bead size in isothermal water planes discharged in the mechanical separation system is created dependent on Stage Doppler Anemometry information. New relationships for the expectation of bead size circulation in sub-cooled and completely blazing planes have further been created utilising the information. A quantitative exploratory strategy for recognising change from mechanical separation to full glimmering has been planned and actualised, permitting examination of the progress information for cases progressively normal for environmental scattering discharges (higher Weber number) with a relationship which previously exhibited in research conducted by Kitamura. Using a comparable progress rule to that embraced by Kitamura, the current dataset is reliable with the relationship pushed by Kitamura dependent on Jakob and Weber number. It is recommended that the altered relationship proposed by Kitamura, considering air pocket development rates, is utilised until a more extensive dataset for a scope of material discharges gets accessible.

This study depicts the thermodynamics properties of atmospheric and petroleum gases which explain the behaviour of the phase changing of LPG/LNG products when released from a container. The physiochemical transformation of air at elevated temperatures has also been discussed in this section. The study also contributes to the explanation of vapour clouds formed due to the leakages of the LNG/LPG from containers and incorporates Froude number, wind speed, roughness conditions, and stratification conditions to predict the propagation of vapour clouds formed after the leakage. Finally, the experiments performed for propane and butane for small, medium, and large diameters showed that the Bernoulli, and the two-phase models are suitable for small leaks and full-section ruptures, respectively.

Chapter 4 Heavy Gas Dispersion

4.1 Dispersion of heavy gases to form a cloud

After a liquefied gas, either through refrigeration or undergoing liquefaction under high pressure, leaks to the atmosphere, it will disperse, and a gas cloud will be formed eventually see Figure 4.1. Process concentration equals the concentration at the release point (gas cloud). Movement of the gas cloud will be in a pre-determined manner based on the prevailing wind and gas density. Hot also called light gases with lower density than air will float. On the other hand, the cold gases will sink since they are denser than air. The cloud uniformity changes with respect to time and distance irrespective of its density or buoyancy. It does not remain constant.

The heavy gases dispersion can be both in the form of gaseous cloud and liquid puddles over the liquid ponds. The gaseous dispersion spreads easily with the air to the surrounding regions but the liquified heavy particles remain over the water and are moved away to other areas with the flow and evaporate according to the temperature.

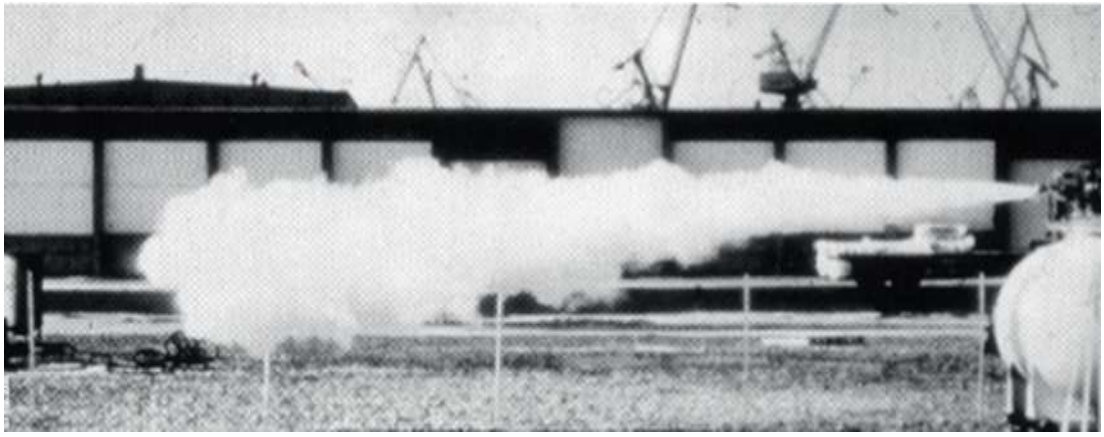

Figure 4.1: *Heavy gases cloud Giannissi et. al. [20]*

A plume of gas is formed due to the gas dispersion from its release point. The movement of this plume changes the concentration within it and it either falls or rises. Random gas measurements will be generated by the gas plumes being moved across the detector. Sometimes, the detector measures low concentration and sometimes larger. This type of dispersion is known as Gaussian Dispersion.

The medium pressure release of gas is different from that of overpressure release. Adiabatic expansion occurs here as a proper thermodynamic effect. After the escape of high-pressure gas, it cools down after expansion and the forming cold cloud of a gas behaves as a dense gas. In the case of a high-pressure release, there is a variation in the distance and shape of the jet of

the released gas however, the format is highly stable, and its shape is tapered with the distance on the outer side Giannissi et. al. [20].

Upon the leakage of the heavy gas into the atmosphere, there are many factors that come into play that results in the dispersion of the gas Gaber et. al. [21]. The dispersion is mainly influenced by the thermodynamic properties of the gas that include temperature, pressure etc. These properties not only directly affect the buoyancy of the gas. but the dispersion is also affected by the atmospheric conditions such as ambient temperature, pressure, and wind velocity. Hence, it is very difficult to design an accurate dispersion of the heavy gas as it is dependent on many variable factors. In the paragraphs below, we shall discuss the dispersion of the three types of gases that are buoyant gas, neutral gas, and heavy gas Gaber et. al. [21]

4.1.1 Dispersion of buoyant gas

Buoyant gas is defined as the gas which has the density less than the atmospheric air. Upon release, the buoyant gas is immediately converted into the vapor state, Since the density of the buoyant gas is less than the atmosphere, it always rises. The rising motion of the gas into the atmosphere creates turbulence around the boundaries that results in the swift mixing of the gas with air. This results in the dilution and hence reduction in the overall buoyancy. After that, the gas becomes so diluted that its density becomes equal to the air and is carried away in the direction of the wind Gaber et. al. [21]. Such a release of the buoyant gas can be detected by placing a gas detector directly near the potential leak source. The examples of the buoyant gas include the release of hydrogen gas, methane gas etc.

4.1.2 Dispersion of neutral gas

Neutral gas is defined as the gas whose density is equal to that of the air. The dispersion of the neutral gas is not driven by the buoyancy but is carried away with the wind. Upon leakage, the gas is immediately mixed with the atmospheric air due to the vortices, diffusion and the turbulence resulting from wind and gas release velocity Gaber et. al. [21]. Modelling the dispersion of these gases requires very much attention towards the wind velocity. Examples of these gases include ethane, ethylene etc.

4.1.3 Dispersion of heavy gas

Heavy gas is defined as the gas whose density is greater than that of surrounding air. Heavy gas dispersion forms the largest cluster of dispersion gases. The main driving force in the dispersion of heavy gas is the gravity which causes the heavy gas to flow like water. As a result

of which, the heavy gas is carried away to long distances. Moreover, heavy gases are not easily altered by the wind, but the dispersion is greatly influenced by the surrounding obstacles and buildings present in the path of the gas Gaber et. al. [21].

The dispersion of the heavy gas is unique in another way that at the beginning, the temperature of the gas is very low and as such the density is high making the gas flows like water but as the temperature of the heavy gas increases, the gas becomes less dense. The heavy gas cloud is formed by the process which is explained in the next paragraphs.

4.2 Heavy gas clouds formation

Experiments carried out regarding the heavy gas leakage suggests that the formation of the heavy gas cloud takes place in three steps Eidsvik et. al. [22]:

1) Initial speedy tumbling of the heavy gas
2) Intermediate process of less rapid dispersion
3) Final phase of cloud formation and diffusion

4.2.1 Initial speedy tumbling of the heavy gas

Upon leakage, the liquified petroleum gas (LPG) is discharged rapidly into the low-pressure surroundings. The liquified gas instantly vaporises. The rapid release of the vapours forms results in the vortex generation at the cloud boundaries. The vortex ring contains major portion of the leaked gas due to the suction created by the vortex. Along with the heavy gas, some amount of air is also entrapped [22].

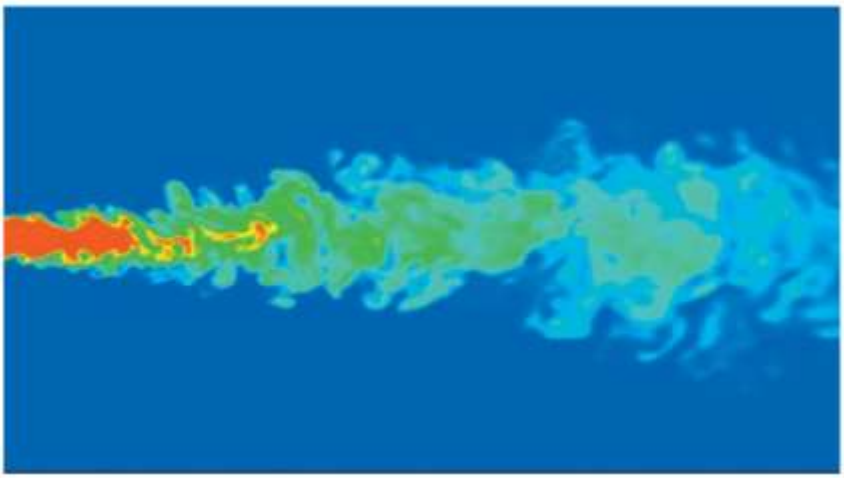

Figure 4.2: *Heavy gas cloud formation Eidsvik et. al. [22]*

In the above Figure 4.2, the high-pressure release of LPG gas is shown. It is clear from the clouds of the heavy petroleum gas that three regions are produced. The first region shown in

the red colour has the highest concentration of the heavy gas and contains high velocity vortices of air and the heavy gas. The second region shown in green colour is the intermediate region in which the temperature of the gas is increased, and concentration is decreased due to diffusion into the air and the last region shown in green/blue colour is the final phase in which the properties of the air are more dominant [22].

4.2.2 Intermediate process of less rapid dispersion

In the intermediate stage, the vortex of the heavy gas cloud formed disperses. The temperature and density come into play and the vortex is created due to the discharge velocity is reduced. The low temperature and high density cause the heavy gas to settle down and flow like water which is inclined more towards to the lower areas. The surface stress and the heat transfer with the environment results in turbulent behaviour of the heavy gas. This turbulence aids the diffusion process. In case of the heavy gas, the horizontal dispersion distance is many times larger than the vertical dispersion owing to the large density [22].

4.2.3. Final phase of cloud formation and diffusion

At the last stage, the heavy gas cloud becomes mature. At this stage, the areas where is high turbulence has the large concentrations of heavy gas. Moving further, as more air is diffused into the heavy gas cloud, the density of both the atmosphere and the heavy gas equalises [22]

4.3 Properties of heavy gas clouds and its effect on the environment

Physical properties and processes help characterise the dispersion of LNG in the atmosphere shows in Table 4.1. The environment includes confined or semi-confined areas, urban canopies, and buildings. The strategy for analysis is the comparison of pre-release and after-release dispersion models Safitri et. al. [23] argue that the amount of gas released depends on pressure. The dispersion is affected by the amount of gas released and the ambient conditions Scargiali et al. [24] found that the presence of structures does not have much influence on dispersion for clouds with regular shapes. Such clouds are free to move in the direction of the wind. The clouds move faster in the direction of the wind in flat terrains. Cloud dispersion is slowed by the presence of vortices, though, because the presence of structures causes larger dispersions, which slow down the plume. According to Liu et. al. [25], concentrations are sensitive to source location and wind direction. Concentration is influenced by wind speed and an increase in wind speed increases the velocity of the cloud. These findings show that dispersion is mainly influenced by convection. Havens et. al. [26] also argue that the

flow of the cloud is influenced by its properties. The density of the cloud influences dispersion. The density of a cloud decreases when gas is mixed with air. The effects of buoyancy are negatively influenced until the cloud density equals ambient density. For this reason, a larger quantity of mass experiences slower dilution and maintains the buoyant behaviour for a longer duration.

Table 4.1: *Influencing Factors*

Factor	Characteristics	Study
Properties	Concentration, shape, and size	Scargiali *et al*. [24]; Safitri, Gao, and Mannan [23]; Havens, Walker, and Spicer [26].
Processes	Wind motion, influence of gravity, cloud behaviour in relation to time, and transient zones	Kothari and Meroney [27]; Meroney [28]; Heidorn *et al*. [29]; Ohba *et al*. [30]; Cleaver, Johnson, and Hob [2]; Liu, Niu, and Kwok [25]; Safitri, Gao, and Mannan [23]

In the absence of turbulence models for simulating the effects of ambient air, Pontiggia et. al. [31] argue that the approach should focus on considering atmospheric properties in models that have been validated with experimental data Cleaver et. al. [2] argue that one of the challenges for modelling LNG clouds is the lack of large-scale data. This gives rise to a high degree of uncertainty while simulating LNG dispersion behaviour. The main uncertainly in the application of a model is the approximation required to represent the distribution of obstacles, which raises issues for grid resolution. For such scenarios, a risk-based approach is useful for the prediction of a numerical measure of risk. While modelling hazardous scenarios, the Health and Safety Executive recommends simplifying the model by limiting the simulation to a dense cloud instead of simulating the ambient air Hall et. al. [32].

A dense gas could be formed by gases with large molecular masses such as ethane or propane, or those with small molecular masses such as liquefied natural gas. Hence, any leakage or release in the petroleum industry results in a heavy gas cloud. According to Hurley et. al. [33], gas source leaks create two-phase jets, which are jetting and flashing in Figure 4.3.

The introduction of the liquid to the open air above its threshold pressure gives rise to the heated liquid. Under these conditions, the dynamic expansion of the vapours shatters the steam of liquid and thus, resulting in an atomised spray which is called flashing. For example, when

LPG is introduced into the air at atmospheric pressure, the liquid flashes to produce gas. Two phase flow of the liquid gas involving the change of phase (liquid-to-gas) is a flashing jet as shown in Figure 4.3.

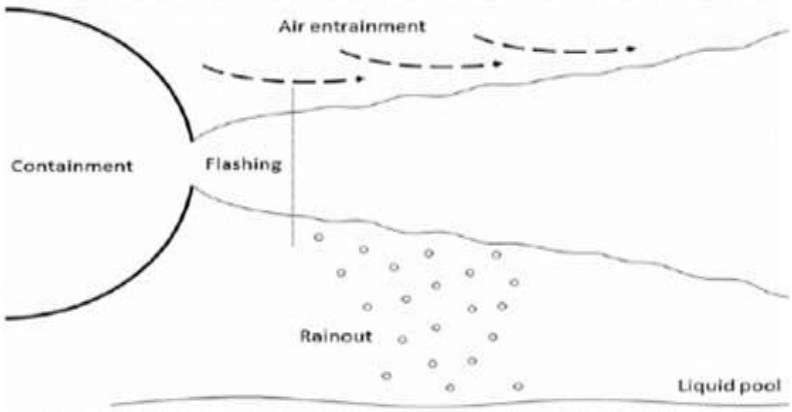

Figure 4.3: *Flashing jet dispersion of heavy gases Hurley et. al. [33]*

A portion of pressurised liquefied gas source vaporises when the pressure drops across the leakage. If ambient pressure is less than the critical pressure then the flow is said to be choked, but the gas continues to flash until the ambient pressure is achieved. This phase change causes the jet to cool down. The gas turns into vapour if the jet has not cooled to the required mark. On the other hand, vaporisation stops, and a small portion of the gas remains in liquid droplet form in the cold pool. The jet entrains the surrounding air, providing more heat to the jet, which results in more vapour formation.

The release of heavy cloud begins with a flashing jet and it expands to atmospheric pressure forming an aerosol-gas mixture which is followed by liquid droplets evaporation. Thus, the resulting cloud has different characteristics from the normal or traditional vapour cloud. Physical phenomena that occur during the cloud dispersion are:

1) Flashing, when the liquid which is pressurised reaches temperature beyond the boiling point of the atmosphere.
2) During expansion to atmospheric pressure, liquid stream atomises.
3) Air entrainment by the jet of liquid particle.
4) Evaporation of droplet.
5) Rainout: Liquid droplets deposition which hits the ground or objects before evaporation.

Cloud dispersion behaviour is dependent on the leaked nature. These include released material, release nature, and atmospheric conditions Hurley et. al. [33] argue vapour clouds could be classified using Richardson number, release, and wind velocity as Dong et. al. [34]: Negative

buoyancy dominated flows: In positive buoyant surface discharge, buoyancy, free surface, and seabed (shallow water receiving's) restrict the entrainment and thus limits the initial mixing. However, in this case, namely plunging of negative buoyant surface discharge has the potential to enhance near field mixing.

Stably stratified shear flows: Mixing is a very normal feature with both density variation and vertical velocity. Vapour clouds are embedded in the mean wind flow in case of stably stratified regimes. These flows have a characteristic lifecycle where velocity shear is intensified by some external force. The bulk Richardson number is given as:

$$J = \frac{g p_o d_o}{\rho a {U_o}^2} \tag{4.1}$$

In the above equation, g is the value of gravitational acceleration that the earth exerts on the heavy gas cloud, $U_o$is the component of the velocity in the direction of the flow, d_o is the reference boundary layer thickness, ρ_o is the reference density at release temperature and ρ is the density at atmospheric temperature.

The value of the bulk Richardson number represents the turbulence that is caused by the turbulence kinetic energy due to the wind shear and is given as Eidsvik et. al. [22]:

$$R_B = \frac{g_c \Delta\theta_v \Delta z}{T_v((\Delta U)^2+(\Delta V)^2)} \tag{4.2}$$

In the above equation, g is the gravitational acceleration, T_v is the virtual temperature of the gas, θ_z is the temperature difference between the boundary layers, Δz is the thickness of the boundary, ΔU and ΔV is the components of the wind velocity.

Another phenomenon that explains the dispersion of the heavy gas with wind currents is called as the 'Passive Dispersion Regime' and is explained below.

4.4 Passive dispersion regime

Passive dispersion is defined as the dispersion of the gases with the atmospheric currents. The condition for the passive dispersion regime is that the typical Richardson number must lie between 0.8 and 1. The diffusion of passive which is released at the ground into stratified turbulent shear flow is given by Wheatley's model. The solution is provided if the diffusion equation for law profiles of wind speed and diffusivity of the atmosphere. The vertical concentration profile of its solution is given as:

$$Fv\,(z) = \exp\left[-\left(\frac{z}{a}\right)s\right] \tag{4.3}$$

In the above equation, ‘a’ is the vertical extent measure and ‘s’ is the diffusivity power law index. For the Gaussian vertical profile (s = 2) and exponential (s = 1) in case of neutral atmospheric stability, exp = expansion, (z) component, Fv = vertical distribution function, dimensionless.

An example of the passive dispersion is shown in below Figure 4.4

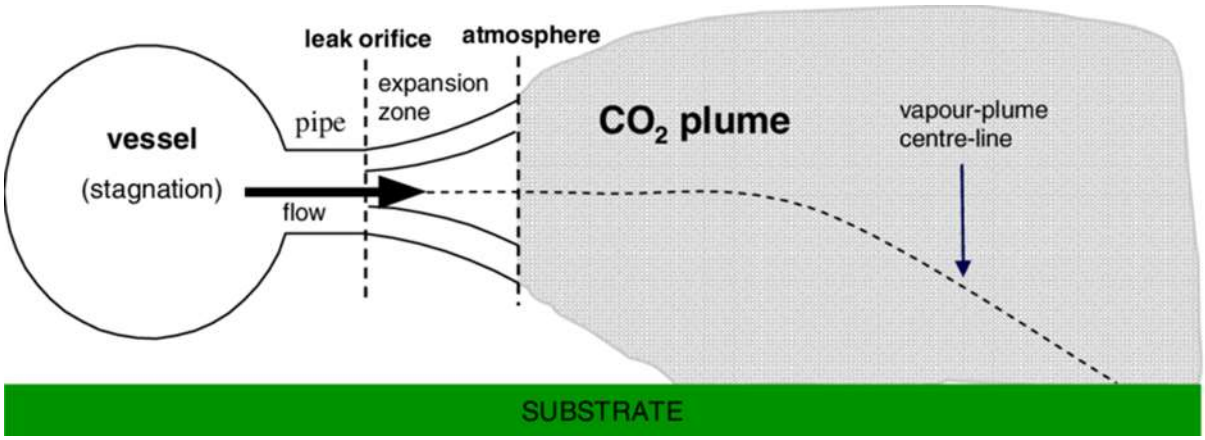

Figure 4.4: *Passive dispersion Dong et. al. [34]*

In the above Figure 4.4, a vessel is shown containing liquid carbon dioxide at high pressure. When the CO_2 is released into the atmosphere through its nozzle, the vapours of the CO_2 gas are produced and are then carried with the atmosphere through the air velocity.

This dispersion of the vapours through the atmosphere is called ‘Passive Dispersion’.

Richardson's number is used to determine the validity of passive dispersion. If the Richardson number is within 0.8 to 1, the passive dispersion of the vapours will take place. Apart from the Richardson Number, there are many properties that are specific to the heavy gas cloud. Properties such as flammability and explosivity are important to study, owing to their large influence on the environment.

4.5 Flammability of the heavy gas clouds

Flammability is characterised by the concentration of heavy gas and the thermodynamic state of the pre-mixed combustible cloud. Baukal et. al. [35] explains the role of the two limits of flammability, which are the lower flammability (LFL) and upper flammability limits (UFL) respectively. The resulting types of blast waves are known as detonations and deflagrations. Fires could also occur after the ignition of heavy gas clouds. According to DeMarco et al. [36] fires could be categorised as; (1) pool fire and trench fire, (2) jet fire, (3) flash fire, and (4) fireball. Detonations are characterised by an immediate pressure increase, while the increase

in pressure is less rapid in deflagrations. The detonations and deflagrations curves are shown in Figure 4.5

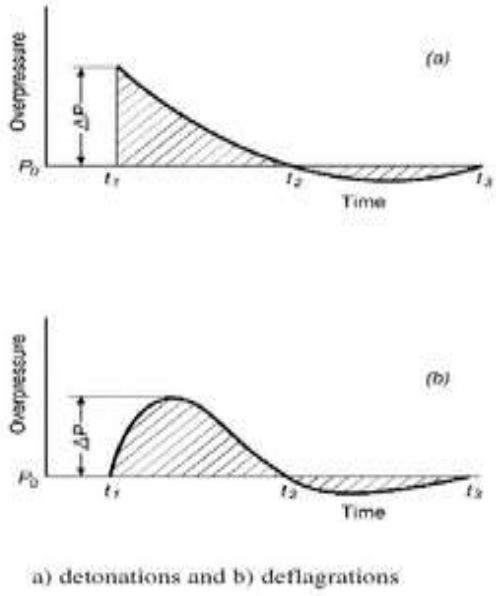

a) detonations and b) deflagrations

Figure 4.5: *Gas Cloud Explosions Casal et. al. [37]*

In the case of the large vapour-air mixture volume, and slow rate of the release of energy, vapour cloud explosions are deflagrations. Blast wave is relatively smoother and propagates at subsonic velocity. In the beginning stage of a gas cloud explosion, laminar flame propagation occurs, and overpressures are small. The rate of combustion increases, and turbulence is generated with the further proceeding of the explosion.

4.6 Explosivity of the heavy gas clouds

A vapour cloud's explosive potential is proportional to the amount of fuel in the cloud or depends on the amount of the material that is flammable. The value of the proportionality factor, also known as efficiency or yield factor, deduced from damage patterns is observed in vapour cloud explosions. Explosive combustion could result from turbulence, which is caused by the high-velocity flow of fuel such as LNG from a pressurised vessel or leaking pipe. A partially confined environment could also cause turbulence. In this case, turbulence is caused by the expansion of flow due to combustion. According to the Centre for Chemical Process Safety [38], speed and pressure could contribute to an exponential increase in combustion, which could result in several blasts. This multi-energy model is useful for modelling an intense turbulent mixture or partially confined areas. In this model, vapour cloud explosions are modelled as sub-explosions corresponding to the number of areas in the cloud that burn under intense turbulent conditions. The TNT equivalent weight method is also useful for evaluating

gas leakage explosive shock. The technique is an empirical model to compare the explosion of TNT with a gas vapour cloud and is relevant for this study, as it seeks to simulate the explosion of a vapour cloud. Guo et. al.[39] found that the technique is reliable for analysing explosion scenarios. The simulation of fire and explosion are shown in the Figure 4.6 and Figure 4.7. (Typically, used to describe the energy released in an explosion. The ton of TNT is a unit of energy defined by that convention to be 4.184)

Figure 4.6: *Fire explosion modelling and dispersion of heavy gases [39]*

Figure 4.7: *Simulation of heavy gases due to explosion [39]*

Combustion of the air gas mixture, which is flammable may result in an explosion. An acceleration of reaction because of temperature rises or by the increase in of chain reactions results in the transition from combustion to the explosion. Consequently, this gives rise to two explosions namely, chain explosion and thermal explosion. In the thermal explosion, progressive heat increases the rate at which the reaction releases heat, and this continues until it exceeds the heat loss rate from the area. It accounts for fuel consumption and rise of temperature during the induction period. The explosion will not occur at high rates of consumption. In branched chain reactions, ignition and explosion have certain limitations.

When the probabilities of branching chains are equal, chain explosion occurs. The stages of combustion that leads to fire and explosion are shown in Figure 4.8

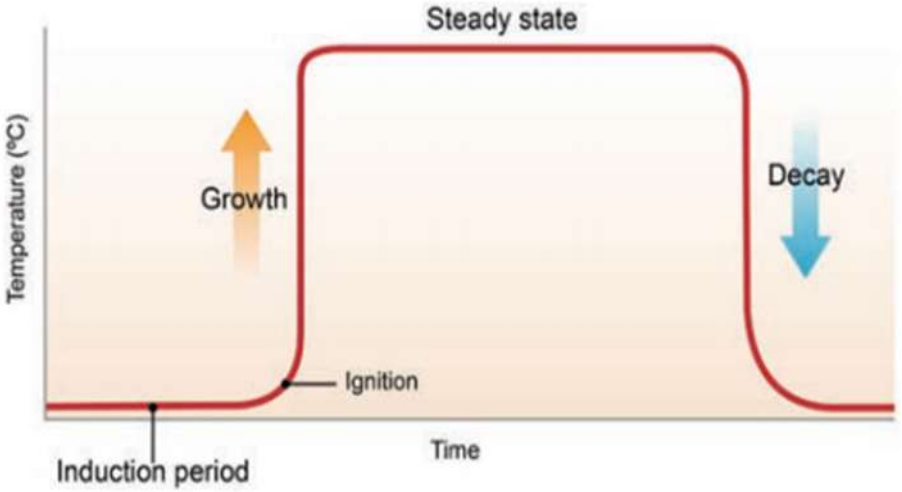

Figure 4.8: *Stages that may lead to explosion [37]*

During the induction period of explosion, vapours are produced by the heat that mixes with the air above the fuel and flammable mixture generates. The reaction is initiated by ignition and hence requires no further external heat source. The fire starts to grow either due to direct burning or by any mechanism of the transmission of heat.

Owing to the dangers of the heavy petroleum gas dispersion in the environment, various models are developed to predict the behaviour of the heavy gas cloud upon accidental leakage. These models use advance turbulence and density equations, in order to predict the concentration and dispersion area depending upon the mass flow and velocity.

4.7 CFD modelling for dispersion of heavy gas clouds

CFD modelling, based on numerical solutions for the Navier-Stokes's problems, is a more accurate approach for calculating the dispersion of heavy gas clouds, compared with plume modelling. It can well predict the spreading of the cloud, entrainment processes of the air, and effects of thermodynamic properties of the mixture. This approach also well deals with the structures such as buildings, roads, and trees, all of which could affect the dispersion of the heavy gas clouds significantly, and the characteristics of heat and mass transport phenomena.

4.7.1 Reynold's Averaged Navier Stokes (RANS) turbulence model

Since turbulence is always involved in dispersion of heavy gas clouds, Reynold's Averaged Navier Stokes (RANS) equations are solved of the most reliable models of the heavy gas

dispersion along with the various obstacles. The RANS model utilises the continuity and momentum equations for the prediction of the dispersion behaviour Dong et. al. [34].

$$\frac{\partial \rho}{\partial t} + \frac{\partial}{\partial x_i}(\rho u_i) = 0 \tag{4.4}$$

$$\frac{\partial}{\partial t}(\rho u_i) + \frac{\partial}{\partial x_j}\left(\rho u_i u_j\right) = -\frac{\partial \rho}{\partial x_i} + \frac{\partial}{\partial x_j}(\mu \frac{\partial u_i}{\partial x_j} - \rho(u_i u_j)') \tag{4.5}$$

In the above equations, ρ is the density of the heavy gas, u_i is the horizontal or vertical components of the mean velocity respectively and t is the time. The Reynolds stresses of (4.6) in the equations (4.5) are calculated through various the turbulence models, e.g., k-epsilon model. The turbulence models will be discussed in detailed in coming sections.

$$-\rho(u_i u_j)' = \mu_t \left(\frac{\partial u_i}{\partial x_j} + \frac{\partial u_j}{\partial x_i}\right) - \frac{2}{3}(\rho k + \mu_t \frac{\partial u_i}{\partial x_i})\delta_{ij} \tag{4.6}$$

Dong et. al. [34] found that the RANS model performed better and produced reliable results for the dispersion of the lower layers of the heavy gas dispersion.

4.7.2 Renormalisation group and shear stress transport (SST) model

Renormalisation group (RNG) theory and shear stress transport (SST) models are often employed to calculate Reynolds stresses in equations (4.7). Xing et. al. [42] argued that the standard renormalisation group (RNG) and shear stress transport (SST) models are reliable methods for the modelling of the heavy gas dispersion. Complex terrains such as hills, valleys, and sloping grounds cannot be modelled using conventional heavy gas models. Conventional models do not account for wind shifts, which move the dispersion in unpredictable ways. The presence of obstacles within the initial plume and subsequent cloud path can be modelled using CFD techniques. CFD heavy gas models benefit from the customisation of codes, which have been validated.

4.7.3 Stochastic model

Akaike (1974) used the stochastic model for the heavy gas dispersion. In this model, the mass 'M' of the gas dispersed at any time 't' can be modelled by using the equation Eidsvik et. al. [22]:

$$M(t) = \pi \rho(t) r^2(t) h(t) = M_g + M_a(t) \tag{4.7}$$

In the above equation, ρ is the density of the heavy gas at any time 't', h is the height of the gas cloud, r is the cloud radius. The density, height and radius combined determine the

characteristics of the gas cloud in the model. To model the speed of the heavy gas cloud, Akaike used the terminal velocity equation [22] which is given as follow:

$$\frac{dr}{dt} = U_g = \alpha_1 (gh\frac{\Delta\rho}{\rho})^{1/2} \quad (4.8)$$

In the above equation, α_1 accounts for the turbulent behaviour of the cloud which is given as $\sqrt{2}$ in case of heavy LPG gas.

4.7.4 Limitations of the RANS model

Heavy cloud CFD models, however, have limitations Cameron and Raman et. al. [40] argue that hazard ranges could be overestimated by a factor of 5 and wind directions could vary by 90 degrees for flat terrains.

One of the major limitations of the RANS model is that it is not able to generate reliable results for the higher layers for the dispersion of the heavy gas. Furthermore, the model is also not able to predict the variation of the tracer clouds in the spatial-temporal layer of the heavy gas dispersion.

4.8 Validated heavy gas dispersion models

Validation of the CFD models is to check whether the model represents the real-world phenomenon. The validation of the models is dependent on several factors such as the complexity of the problem, usage of the results obtained from the model etc. The validation is carried out by comparing the results obtained from the actual experiments with those from simulation. Qi et. al. [19] used a similar technique for the validation, by first carrying out the experiments and then CFD modelling the dispersion of the LNG. Heidorn et. al. [29] argue that the approach for modelling is to simulate physical processes that influence gas dispersion phenomena. Components of a vapour dispersion CFD model include geometry creation, meshing, domain, atmosphere boundary, pool boundary, and ground boundary. Each of these components have input parameters for the specific scenarios under investigation. Figure 4.9 shows the comparison between simulation results and test data performed by Qi et. al. [19], who found that the height and width of the plume is similar to the real plume at the source as well as in the downwind area, and the effects of geometry features on the cloud are well represented. The experiment shows that wind velocity and turbulence have strong influence on the thermodynamics of the cloud, which affects the downwind distance.

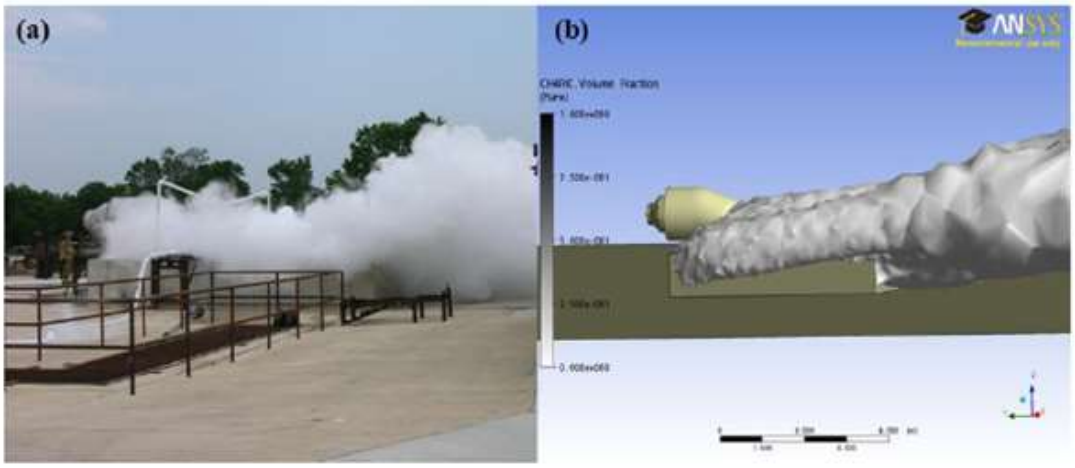

Comparison of the plume shape of on-site photo and the simulation results. (a) On-site photo and (b) ANSYS CFX simulation

Figure 4.9: *LNG Dispersion Model Qi et. al. [19]*

Scargiali et. al. [24] investigated heavy clouds with properties including concentration, shape, and size. They found that concentration changes under the influence of convection during dispersion. They also found that field results and experimental results are in good agreement, within a standard deviation of 6%. Another technique is the construction of 3D urban models using spatial geodatabases, which could be imported into CFD models. This domain design technique is integrated with codes for concentration and exposure time Pontiggia et. al. [41] found that such models could overestimate and underestimate the magnitude of consequences related to gas releases in urban areas.

This method of the CFD validation requires a lot of resources and expenditure because it is the real time, full scale experiment of the heavy gas dispersion. It may also happen that the many attempts may be required to get the accurate results from the experiment. Moreover, there are many safety concerns that are involved in carrying the full-scale experiments.

In another approach to validate CFD models, a small-scale model of the real world is developed, so that the experiments are carried out in wind tunnels. The results obtained from the experiments are compared with the simulation results. Langlo et. al. [43], used the wind tunnel model for the validation of their dispersion CFD models. It is argued that the use of small-scale models can help the industries and the petroleum companies to determine the safe flammability distance for their storage locations.

4.8.1 Validation process

The concentration of the heavy gas along the axis x is plotted from the results obtained from the model, and on the same graph data from the actual experiment carried out is also plotted. If any scaling is done on the real models, the concentration values are multiplied with the calculated numbers to obtain the off-scale values of the concentration. Rauchegger et. al. [44] used a similar technique to validate the accidental release of the heavy gas model with the actual tests carried out in the lab. The graph obtained is as follow:

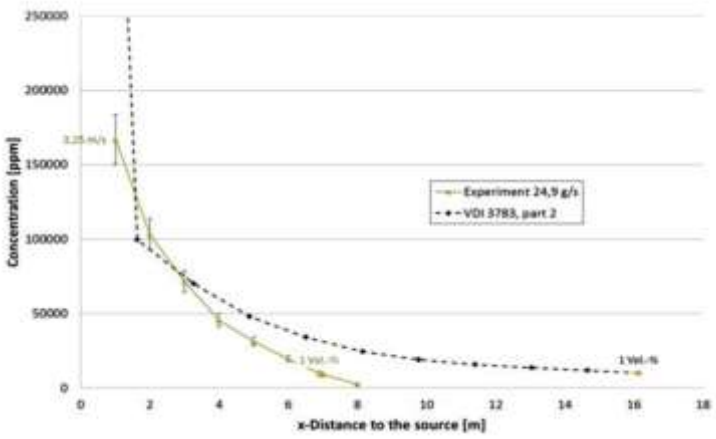

Figure 4.10: *x-axis showing the distance from the source in meters and y-axis showing the concentration in ppm Rauchegger et. al. [44]*

In above Figure 4.10, x-axis represents the horizontal distance in meters from the source location and y-axis represents the concentration of the heavy gas in ppm. The graph is plotted for the experiment of the heavy gas at the release rate of 24.9 g/s which is represented by the green solid line. Similarly, a graph is plotted for the results obtained from the model. Although it is evident that there is some difference in the concentration values of the heavy gas from the two results, nonetheless the trend is still the same. In both cases, the concentration of the heavy gas decreases while moving away from the release source. This suggests that the model is accurate is determining the results.

4.9 Summary

In the oil and gas industry, different heavy substances such as methane, propane, butane etc. are stored in large storage tanks. There is a risk of potential leakage of the heavy petroleum substances from these tanks. In case of leakage, a jet is released into the environment that is vaporised to form a cloud of heavy gas. The gas cloud is dispersed by the wind and the difference in the density. The formation of the heavy gas takes place in three steps that is vortex formation due to the high release velocity, flow of the heavy gas cloud resulting from gravity and wind, and finally the diffusion of the heavy gas with the atmospheric air. It is imperative

to study the dispersion of the heavy gas cloud to predict its behaviour under the presence of various obstacles. The accumulation of heavy gas molecules around the obstacles and tanks poses a serious threat of explosion and fire hazard. Various models have been developed to visualise the dispersion of the heavy gas into the environment. Shear stress transport model utilises the conventional shear stress equations to model the dispersion. A major shortcoming of the model is that it is not able model the wind directions properly. Another reliable model is the Reynold's Averaged Navier Stokes (RANS) model that makes use of the momentum and turbulence equations to model the dispersion of the heavy gas and the wind. Similarly, stochastic model utilises the mass and terminal velocity equations to model the heavy gas dispersion. These models are validated with the help of real time experimentation with full scale and small-scale models. By using the graphs containing concentrations on the y-axis and distance from the release source on the x-axis and plotting the curves for the model and experiment, which consequently allows the model to be validated.

Chapter 5 Methodology

One of the major global issues since the beginning of twenty first century has been ensuring a green and sustainable environment for mankind due to it being under constant threat from the continuous release of toxic substances into the atmosphere, adversely impacting the quality of life. Dispersion of hazardous and toxic gaseous matter into the atmosphere often renders the adjacent lands inhabitable for human population. Therefore, it is essential to understand, investigate and estimate the harmful effects of such materials.

Various methodologies for conducting such investigations feature in the literature. These include experimental studies, quantitative analyses for predicting the risks associated with potential accidents and use of empirical models for predicting loss and risk. While all of these techniques have their own merits and demerits, one widely used methodology is computational fluid dynamics (CFD). This is used for conducting more accurate and detailed virtual simulations of the phenomena concerned under varying governing conditions. This chapter aims to discuss in detail the proposed methodology for conducting simulation studies of heavy gas dispersion phenomena Sklavounos et. al. [45].

First, it is essential to understand why CFD based analysis tools are becoming popular in this domain. The main reason is that the specially developed analytical and mathematical models such as DEGADIS and others, which are still in use, primarily because they are easy and quick to use, do not produce an accurate prediction of dispersion phenomena Rigas et. al. [46,47]. Although the characteristic of providing quick solutions appears an attractive advantage when seen in terms of computation and time saved, these models are not capable of accurately modelling the physical phenomena behind the interaction of scattered gas particles and the various obstacles. Moreover, the results obtained are restricted to single dimension dispersion behaviour of gas, which is evident from the fact that 1D models are easily solvable using analytical methods because they provide information about behaviour of dispersed gaseous particles under many assumptions. Moreover, as the actual flow is so complex and occurs in a 3D space, the related mathematical models become so complex that they cannot be solved analytically [48]. Therefore, CFD is widely used in the industry; it facilitates more accurate flow visualisation of complicated physical phenomena by employing appropriate mathematical models to describe the transport of mass and heat phenomena associated with the heavy dispersion of toxic gases in the environment. These numerical models provide better and more

physically accurate results as they fully incorporate the effects of phenomena such as mixing of air and gas particles (turbulent mixing) and influence of building wakes on flow fields.

This chapter will cover theoretical and mathematical explanations of the turbulence model utilised in the study, followed by the various discretisation schemes, the technique used in this study and information about the choice of solution methods. Moreover, all the information is presented in an orderly fashion, beginning with a detailed discussion about the turbulence model used and ending with the settings adopted for meshing and turbulence, as well as solution methods.

5.1 Mathematical models

There are two approaches for an investigation into heavy gas dispersion. One is the experimental approach, for example, experimental investigations into heavy gas dispersions performed by Cleaver et. al. [2]. Through a combination of the experimental results and simplified theoretical models, Empirical Correlations, Integral Model, Shallow-Layer Model, etc. can be developed Ichard et. al. [3]. These models help predict and analyse heavy gas vapour dispersions and play a major role in risk assessment and management. However, the dispersion is a complex multi-phase problem, where flows occur in complex geometric configurations, including phase-changing and heat and mass transfer conditions. Moreover, these experiments are costly to conduct and cannot be carried out for all probable geometric configurations. Therefore, the second approach, which is based on the Navier-Stokes equations, has been developed. Theoretically, the second approach can predict the heavy gas dispersion with complex conditions, environments, and configurations and therefore of complex mathematical models. In order to solve such mathematical models, computational fluid dynamics (CFD) techniques are employed. The mathematical models and their numerical solutions are addressed in this chapter and coming chapter, respectively.

5.1.1 Basic equations for flow field

The basic equation used in this work will be the equation of mass, moment and energy conservations. The flow processes will be described by the basic equations which satisfy the law of conservation of mass (5.1), the law of conservation of momentum (5.2) and the law of conservation of energy (5.3).

$$\frac{\partial \rho}{\partial t} + (u \cdot \nabla)\rho + \rho \nabla \cdot u = 0 \tag{5.1}$$

$$\rho \frac{\partial u}{\partial t} + \rho(u \cdot \nabla)u + \nabla p = \rho g + \mu \nabla \cdot \{\nabla u + (\nabla u)^T\} \tag{5.2}$$

$$\rho \frac{\partial e}{\partial t} + \rho(u \cdot \nabla)e + p(\nabla \cdot u) = \nabla \cdot (\lambda \nabla T) + \Phi \quad (5.3)$$

In the above equations, the term "t" denotes time, "u" denotes velocity vector, "ρ" denotes density, "T" denotes temperature, "p" denotes pressure, "e" denotes internal energy, "Φ" denotes dissipation function and "g" denotes gravity vectors. The conduction co-efficient is denoted by "λ" and viscosity of the gas mixture is denoted by "μ". The term$(\nabla u)^T$represents the transpose of (∇u). The relationship between temperature and internal energy can be obtained by the following relation according to laws of thermodynamics:

$$e = c_v T \quad (5.4)$$

Here, c_v is the specific heat capacity at constant volume.

5.1.2 Mass transfer equations

The present work does not study the chemical reactions, only the mixing of inert heavy gas with the surrounding air and dispersion. For the individual species, a set of mass transfer equations can be used to describe the mixing and dispersion. Another assumption involved in this work is that the flows and mass transfer advance in a single-phase only, which is the gaseous phase. Since gaseous leakage is assumed in this work, the following basic equation can be used to write the mass transfer of the individual gaseous species:

$$\rho \frac{\partial Y_i}{\partial t} + \rho(u \cdot \nabla)Y_i = \nabla \cdot (\rho D_i \nabla Y_i) \quad (5.5)$$

Here, the fraction of concentration for the species i is Y_i and its diffusion coefficient is D_i.

The continuity equation (5.1), $\sum[\nabla \cdot (\rho D_i \nabla Y_i)] = 0$ is required because of $\sum Y_i = 1$.

5.1.3 State equations

The following equation represents the equation of state:

$$p = \frac{\rho R T}{W} \quad (5.6)$$

Here, R represents the universal gas constant and, Wrepresents the local mean molecular mass of the gas mixture can be calculated using the following equation:

$$W = \sum_i \left(\frac{Y_i}{W_i}\right)^{-1} \quad (5.7)$$

where W_i is the molecular mass of the species i. It can be seen that the molecular mass of the mixture is not a constant but varies due to the leaked gas mixing with the surrounding air.

In the present work, the processes studied are described by these basic equation (5.1) – (5.7). They are complete and enclosed theoretically. The processes to be studied can be uniquely defined by these equations with proper initial and boundary conditions. In the following section, the numerical solutions for these equations can be found.

5.1.4 Flashing jet

The leaked materials, stored with either high pressure or low temperature, have a state of liquid before leaking out. When they leak out, jets are formed from the leaking cracks and two-phase dispersions take place. The overheated liquid evaporates directly with its own heat after leakage. This is called a flashing jet.

The flashing jets are governed by the Navier-Stokes equations with the gas dispersion that can be written as follows:

$$\frac{\partial \rho}{\partial t} + \nabla \cdot (\rho \vec{v}) = 0 \tag{5.8}$$

$$\rho \frac{\partial \vec{v}}{\partial t} + \rho(\vec{v} \cdot \nabla)\vec{v} + \nabla p - \rho g - \nabla \cdot \tau = f_p \tag{5.9}$$

$$\rho \frac{\partial h}{\partial t} + \rho \nabla \cdot (h\vec{v}) - \frac{dp}{dt} - \nabla \cdot (k \nabla T) = 0 \tag{5.10}$$

$$\rho \frac{\partial Y}{\partial t} + \rho \nabla \cdot (Y\vec{v}) - \nabla \cdot (\rho D \nabla Y) = s_p \tag{5.11}$$

where $\vec{v}$ is the velocity vector, ρ is the density, p is the pressure, T is the temperature, g is actually gravitational acceleration , τ is the viscous stress , k and h are the conductivity of mixture and enthalpy of mixture respectively. The equations (5.8) – (5.11) are used for the control lance of processes of flow with the gas mixture and the air in the surroundings. The equation (5.11) is used for the governance of the mass transfer of the gas, where Y is used for the denotation of the mass fraction, D is used for the denotation of mass diffusivity of the gas and the air fraction is denoted by $1-Y$. Furthermore, the viscous stress tensor can be given as

$$\tau = \mu(\nabla \vec{v} + \nabla \vec{v}^T) - \frac{2}{3}\mu(\nabla \cdot \vec{v})I \tag{5.12}$$

where viscosity of the mixture is represented by μ and I is used for the denotation of tensor. Thermodynamically we can determine the equation represented as

$$p = \frac{R}{W}\rho T \tag{5.13}$$

where R is the universal gas constant, and W is used for the denotation of the averaged molecular weight. The mass fraction relation of the gas acts as a variable to the molecular weight of the gas. When the air holds the mixture, the air weighs approximately 29 g/mol at the standard state. The averaged molecular weight will rise and cause a change in the density of the mixture.

The flow of the test material in this work is actually turbulent and a large eddy simulation of turbulence is experienced being employed in the process. The large eddy simulation requires a set of grid Reynolds stresses. Coupled with the filtered Naiver-Stokes equations, the integral equations can be solved theoretically. However, many individuals have solved them. Here, we take the model of Smagorinsky et. al. [49] to keep up the work. The turbulent viscosity is calculated by

$$\mu_t = \rho(c_s\Delta)^2\left[2\nabla u : \nabla u - \frac{2}{3}\nabla \cdot u\right] \tag{5.14}$$

Where, turbulent viscosity μ_t, $c_s = 0.2$ is an empirical constant and Δ denotes the length of a grid cell. The scale product of two tensors is denoted by the symbol "$:$" .

The equations from (5.8) - (5.13) are for the fully compressible and workable flows. To integration of these equations, the time step width is restricted by the Courant-Friedrichs-Lewy (CFL) number. In the CFL number, the velocity for compressible flows is the sum of flow velocity and local sonic speed. Therefore, when the sonic speed is much larger than the flow velocity then the case is directly solving (5.8) - (5.13), this is very time-consuming for the concerned time interval. We can see a minute influence by the acoustic mode on the result of the work in the discussion in Chapter 6. So, in order to filter them, the acoustics mode is removed, which causes a reduction in the computational time Safitri et. al. [23]. Thus, two kinds of problems need to be solved numerically. Poisson equations along with the transport equation are the two sets of equations used in this case. The discretisation of the Poisson equation results in a system of linear equations that is solved using an elliptic solver.

5.1.4.1 A mathematical model for the motions of liquid particles

The transition of the liquid gas flow and the liquid to gas flow is call the flashing jet. Due to the surface tension force of the liquid, the stability of the liquid jet starts to be gradually lost,

after disintegrating, atomization occurs. The characteristic ratio of the inertia and the surface tension, which is used to measure the condition of the spray, is known as the Weber number. This is a dimensionless number. This section will address the two-phase atomization flow and the transition of phases will be discussed later.

5.1.4.2 Dynamics of the particles

The previous section discussed equations (5.9) and (5.11) in which there are two additional terms, f_p and s_p. The preceding expression is an additional force that can be said to be produced by the movement of the liquefied gas mist in comparison to the local gas and air mixture. The latter term is the source, which is generated during the liquid-to-gas phase change. The mathematical model for the liquefied gas mist deals with the determination of the force and source accurately. The liquid particles vaporise into the gas phase which then mixes with the air. This is all because of the heat exchange with the air and we can also say that the phase changes. The equation (5.15) is used for these additional terms.

A model called the Lagrangian and Eulerian will be used in Chapter 6, as well as for further calculations. Therefore, an additional force of the liquid and gaseous and liquified mixtures is also given as follows:

$$f_p = \sum \left\{ 0.5 \cdot \rho c_d a_p (u_p - u) |u_p - u| - \frac{dm_p}{dt} (u_p - u) \right\} \tag{5.15}$$

The particle velocity is denoted by u_p and the particle mass is denoted by m_p. The forces represented in equation (5.14) make movements and act upon these particles. By applying Newton's second law, the movement of each particle can be found, including the velocity acceleration and the location of particle. Meanwhile the other two coefficients in equation (5.14), c_d and a_p, are the coefficient of drag and the area of the particles, respectively.

$$s_p = \sum \left\{ \frac{dm_p}{dt} \right\} \tag{5.16}$$

Evaporating the droplets and diffusing them forms an ignitable mixture with high temperature. The dilution of spray shows that the distance between them is large in comparison to the droplet's diameter. Thus, the process involving the ignition and combustion can be called the droplet examination. Denser spray shows that the droplets are too close to have an interaction which can be neglected. So, in order to model the spray combustion, the spray should be taken as a collection of non-interacting single droplets which are burning, meaning of a droplets cloud.

In terms of mass of the Lagrangian particles, because of the phase change, it will vary with the movement, i.e., equation (5.15). The phase change depends on the heat transfer between the particle and gas mixture which have been discussed in chapter 3. These additional terms and relevant coefficients are related to the geometric dimensions and relative movements of the Lagrangian particles with respect to the local gas flow and will be modelled in Chapter 6.

5.1.4.3 The size distribution of the particles

When talking about the remaining problem in the theoretic models, one needs to know how to determine the number of the Lagrangian particles and their geometric dimensions. To that end, it has been assumed that the particles are of a spherical shape. Therefore, the geometry of spherical shapes is characterised by their radiuses. Calculations of the mass transfer show convenience to work instead of complete drop size distribution with mean or average diameter. In order to estimate the radius, the droplet size distribution is required. Theoretically, the droplet size distribution is controlled by a number of stochastic differential equations that reflect the stochastic processes of the particles. To avoid solving the stochastic differential equations, however, a pre-defined droplet size distribution is employed, namely, employing the combination and distributions of Rosin-Rammler and log-normal for the cumulative volume of the particles.

$$F = \begin{cases} \frac{1}{\sqrt{2\pi}} \int_0^D \frac{1}{\sigma x} exp\left(-\frac{[\ln x - \ln d_m]^2}{2\sigma^2}\right) dx & D \le d_m \\ 1 - exp\left[-0.693\left(\frac{D}{d_m}\right)^{\gamma}\right] & D > d_m \end{cases} \tag{5.17}$$

Here, F is flow vector field, mean diameter is d_m and D is the particle diameter, the mean diameter, d_m, is related to the local flow and leakage orifice geometry. What is determined by the Weber number, $\frac{\rho_p u_p^2 R_o}{\sigma_p}$, here ρ_p, R_o and d_m is known to be the particles density, orifice radius and the surface tension of the liquefied particles. σ and γ are constants, which are dependent on the requirements of the distribution, and are approximately 2.4 and 0.48 respectively.

5.1.4.4 Number and geometry of the particles

The previous equation numbered (20) is derived by considering the diameter of the particle, we use the probability density function (PDF) is used for the particle diameters. After the integration of the PDF the cumulative number fraction CNF can be derived for all the particles.

Having the cumulative volume distribution in equation (5.18), for the particles a number associated with a formula can be designated, which can be easily obtained. We are talking about the cumulative number fraction of the particles under the following equation:

$$U(D) = \frac{\int_0^D \frac{dF}{dx} dx}{\int_0^\infty \frac{dF}{dx} dx} \tag{5.18}$$

For application purposes, it is critical to decide the size of droplets for a specific application that is most for useful, for the usual calculations in many of the flow processes and mass transfer, it is thought to be particularly convenient to work with instead of complete droplet size mean or taking the average diameter.

The distribution of the Lagrangian particles along their radiuses is expressed by equation (5.17) discussed above. This distribution theoretically determines the number of Lagrangian particles and their geometric dimensions.

It can be stated that, theoretically, the number of particles is infinitesimally large. The following mass balance equation is also encountered:

$$m_p = C \sum_{i=1}^{N} \frac{4}{3} \pi \rho_p \left(\frac{d_i}{2}\right)^3 \tag{5.19}$$

5.1.4.5 Phase transformation of liquid particles

The ambient temperature is always higher than the saturation temperature of the liquid at the correlating temperatures. Furthermore, in the case of the flashing jet, it is known that heat exchange between the liquid and ambient air is always considerable. This presence of heat exchange results in the change of phases from liquid and gas. These exchanges by the heat and mass transfer equations can be addressed as follows:

$$\frac{dm_p}{dt} = -A_p h_m \left(Y_p - Y_g\right) \tag{5.20}$$

$$m_p c_p \frac{dT_p}{dt} = A_p h \left(T_g - T_p\right) + q_r + h_v \frac{dm_p}{dt} \tag{5.21}$$

Here, the two variables are the mass fractions of the liquid and the other is the mass fraction of the gas. Thus, is a surface area, temperature and the specific heat of the particles. The properties of the gas and the liquid can also be ascertained from the relevant handbook with the emission of the radiation. The surface area of the particles can be obtained from the Chapter 3. The temperature and the mass equation are from one and six respectively and the equation number thirteen has a temperature variant, which also becomes the solid wall temperature.

The Clausius equation is shown below used for the calculations of the liquid equilibrium vapour mass fraction:

$$X_p = exp\left\{\frac{h_v W_p}{R}\left(\frac{1}{T_b} - \frac{1}{T_p}\right)\right\} \tag{5.22}$$

$$Y_p = \frac{X_p}{X_p + \frac{W_a}{W_g}(1 - X_p)} \tag{5.23}$$

In this section we know that the equations from (5.19) and (5.22) are then coupled together for the phase transition which also provides the source term.

5.1.4.6 Heat and mass transfers

The problem of thermal explosion and expansion in the mixture of the gas and liquid phases in most cases have been studied. These studies have shown that this process in the mixture takes place in a consistent way. During the process, there is a collision between the droplets, droplets dispersion, the change of temperature along with mass and heat transfer, and the break-up of droplets and all the possible procedures to be involved between the phases of gas with liquid for the mass and heat transfers. At this point of discussion, the following equations are used:

$$\frac{dm_p}{dt} = -A_p h_m (Y_p - Y_g) \tag{5.24}$$

where Y_p and Y_g are the mass fractions of the liquid and gas phases respectively. The physical assumptions can be described as follows: The constant is the density of the liquid fuel; the evaporating droplet temperature and the saturation temperature are taken to be equal. So, in the relation of mass and heat transfer during the process, elaboration on the combustion process is required first.

The combustion is actually atomised into a combustion gas environment. The liquid used in the process is then broken up into larger droplets, which eventually causes an increase in the surface area of the oxide. This more increased exposure causes an enhancement in the rates of the mass and heat transfer. In terms of the range of the droplet's distribution, it can be placed in the bracket of a few microns to about 500 micrometres. It is known that the nozzles must produce droplets of approximately the same size. In terms of the practicality of the nozzles they cannot typically produce spray droplets of the same or uniform size at the operating conditions. Furthermore, the production of many of the large droplets is catered by their break down into smaller droplets in the initial liquid disintegration.

$$m_p c_p \frac{dT_p}{dt} = A_p h\left(T_g - T_p\right) + h_v \frac{dm_p}{dt} \tag{5.25}$$

where T_p , A_p and c_p are the temperature, specific heat and surface area of the particles respectively, while h_m, h and h_v are the mass, heat transfer coefficients, and latent heat of vaporisation of the liquid respectively. Equations (5.16) and (5.17) are applied to calculate the phase change in each computational cell. The detailed numerical schemes as well as the working principles are addressed in the contexts below.

5.1.5 Leakage flow rates

Leakages can occur either as a continuous steady process or transient leakage can occur. The leakage rate can be calculated by the following equation Danie et. al. [50]:

$$Q_m = \rho A\, C_0 \left[2\left(\frac{P_0}{\rho} + g h_r\right)\right]^{1/2} \tag{5.26}$$

where Q_m is mass leaking rate, P_0 Tank internal pressure, ρ density of LNG, A the leaking area, h_L the distance between the leakage point and liquid level, and the leaking coefficient is C_0. Percentage F of the liquid directly evaporated at the time of leakage is given by the formula:

$$F = C_p \left(\frac{T - T_0}{H}\right) \tag{5.27}$$

where C_p is the constant pressure specific heat and T is the temperature of liquid before leakage. The boiling temperature of liquid at atmospheric pressure is T_0. The liquid vaporised at the time of leakage will form a cloud of fine smog which will mix with the air and vaporise by absorbing heat. In order to calculate the rate of release through a hole in a storage tank of LNG [38], a mechanical energy balance associated with a fluid flow is used and clearly shown in flowing equation (5.28):

$$\int \frac{dP}{\rho} + \Delta\left(\frac{\bar{u}^2}{2\alpha g_c}\right) + \frac{g}{g_c}\Delta z + F = -\frac{W_s}{\dot{m}} \tag{5.28}$$

where the normal momentary speed of liquid is ū, thickness of fluid is p, the unit less speed profile redress factors and is with qualities a =1.0 for attachment stream, a = 0.5 for laminar stream and a - > 1.0 for violent stream, g is the gravitational steady to get increasing speed because of gravity and z is the tallness above datum, F is the net grating deficit term, W, is the pole work and TM is the mass stream rate. For incompressible fluid, the density is constant;

therefore, equation (5.29) shows that $\frac{dP}{\rho}$ is equal to the $\frac{\Delta P}{\rho}$. Assuming a constant gauge pressure P_{Tank} in the storage tank, ΔP will become equal to that of P_{Tank} as shown in equation (5.30):

$$\frac{dP}{\rho} = \frac{\Delta P}{\rho} \tag{5.29}$$

$$\Delta P = P_{Tank} \tag{5.30}$$

The shaft work is zero, and velocity of the fluid in the tank is assumed negligible. The frictional losses in the leak can be approximated by a constant discharge coefficient C_1, which is defined in the form of equation (5.31). A hole develops at a height h_L below the liquid level, namely $\Delta z = h_L$. The average discharge velocity is described in the form of equation (5.32):

$$-\frac{\Delta P}{\rho} - F = {C_1}^2\left(-\frac{\Delta P}{\rho}\right) = {C_1}^2\frac{P_{Tank}}{\rho} \tag{5.31}$$

$$\underline{u} = C_1\sqrt{\alpha}\sqrt{2\frac{g_c P_{Tank}}{\rho} + g h_L} \tag{5.32}$$

Defining a new discharge coefficient c_d as $c_d = C_1\sqrt{\alpha}$, the mass flow rate Q_m from a hole of area A in the LNG tank is given in form of equation (5.33)

$$Q_m = \rho \underline{u} A = \rho A c_d\sqrt{2\frac{g_c P_{Tank}}{\rho} + g h_L} \tag{5.33}$$

where the mass flow rate is Q_m, the mean liquid velocity is $\underline{u}$, the density of liquid is ρ, the orifice area is A, the discharge coefficient is c_d, the gauge pressure is P_{Tank} of the tank, the level of liquid in the tank is h_L, the gravitational constant is g_c and the acceleration due to gravity is g.

5.1.6 Initial and boundary conditions

In the simplest possible terms, the boundary and initial conditions are constraints that help formulate an accurate mathematical model that best represents the associated physical phenomena. In nature, all the natural phenomena and systems can be assumed to have infinite degrees of freedom. However, in order to formulate their respective mathematical models, infinite degrees of freedom have to be converted into finite degrees of freedom. In other words, a finite number of equations will be required, with some values known and others unknown, to solve any problem. This is achieved by defining a variety of initial and boundary conditions depending on the problem because, by doing so, all the required input data for solution of mathematical model is provided. Consequently, any physical phenomenon can be explained

mathematically by a number of equations proportional to their degree of freedom. Moreover, many real-world systems show transient behaviour in that their properties vary with time. So, such systems are usually mathematically expressed by set of differential equations (to represent change of properties with time).

The solution of these differential equations is achieved by transforming the problem into a boundary value problem (differential equations with boundary conditions) Zwillinger et. al. [51]. On one hand, boundary conditions restrict the practical system while initial conditions provide an initial state of that system and, on basis of this initial state, the various numerical methods solve complex behaviour of such systems. These conditions must be specified even before solving the governing equations of the flow. They are setup by providing a set of thermodynamic variables, including fluid saturation temperature and saturation pressure Wu et. al. [52]. These initial conditions directly influence the way in which state of practical systems is accurately represented by mathematics Jouaneh et. al. [53]. The well-defined initial and boundary conditions generally lead to accurate numerical modelling and resulting behaviour of systems such as leakage of heavy gas.

In context to CFD modelling of heavy gas dispersion, it is evident from the literature surveyed that various kinds of boundary conditions have been used. Dong et. al. [34], for example conducted a numerical investigation of heavy gas leakage in an indoor space with turbulence $K-\omega$ turbulence model and compared results with experimentally measured concentration. The author utilised velocity as an inlet boundary condition as dictated by direction of flow of air and outflow condition was specified for windows and ventilation ducts. Moreover, the actual source was given a mass flow boundary condition and other surfaces pertaining to walls, floor and obstructions were all specified to have no slip wall conditions.

A similar study conducted by J Fiates et. al. [54] specified leakage source as under condition of outgoing mass flow rate while the uniform velocity was chosen for air flow. Moreover, the inlet and outlet of computation domain which was made at least twice the actual model dimensions was prescribed at pressure boundary conditions. Scargial et. al. [55] also conducted a study and employed vertical velocity and temperature distribution fields as an inlet condition for a 3D simulation study. Moreover, the effects of turbulence in the flow were also catered for by specifying a turbulence field initial condition at inlet. Their study assumed that overall behaviour of dispersion of the gaseous fluids in the study is not highly influenced by the initial leakage and dispersion of heavy gas. In a very recent study, Jiang et. al. [56] developed a real time prediction model based on CFD for lethal gas dispersion and set up following types of

boundary conditions: velocity inlet condition at multiple inlets of computational domain and respectively outflow condition for outlets of the domain. In accordance with the previous literature, the leakage source itself is specified a mass-flow inlet condition Jiang et. al. [56]. From the literature, it can be seen that there exists a pattern in boundary and initial conditions settings for heavy gas dispersion numerical modelling and the specific conditions at different locations are summarised in Figure 5.1 shown below:

Therefore, in the present study, as per the norm in the literature, all the boundary conditions and initial conditions are specified in a similar manner as shown above. Moreover, as far as initial conditions are concerned, they are usually utilised only in the beginning of any analysis and are meant for conducting non-steady analysis Zhang et. al. [57]. In the present study, the initial condition reflects the initial thermodynamics state of the considered domain before the leakage takes place that is the initial state of the system characterised by the absence of any eternal influencing parameters. Here, in this work, the initial conditions are assumed to be at the standard atmospheric conditions without the airflow, i.e., a pressure of 101.3 kPa and a temperature of 20°C. All initial conditions, including standard atmospheric conditions, are generally setup in accordance with the experimental setup specifications. Meanwhile, boundary conditions refer to those conditions which are noted after the leakage takes place.

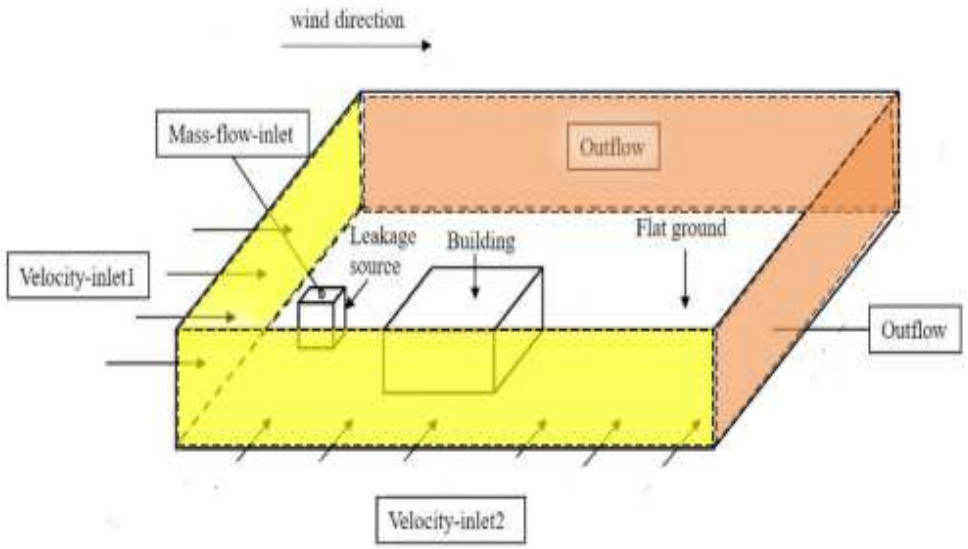

Figure 5.1: *General Initial & Boundary Condition setup for Heavy Gas Dispersion Modelling[55]*

These are usually limiting conditions that bound the system; that is the numerical model do not go beyond these restrictions. However, it should also be noted, in case of bad boundary conditions, that the model may provide certain discrepancies, such as reverse flow and stability

issues, and may not converge to any solution at all. In such scenarios, if the boundary conditions are not flexible, either the meshing should be fine-tuned, or the model geometry should be modified within the allowable limit. One solution for eliminating reverse flow that is common in the literature is to increase the length of computational domain - not the model - so that the flow under given conditions will become stable until it reaches the actual inlets of the concerned geometry. These conditions are usually derived after performing number of experiments or sometimes even from predictions based on previous studies conducted in the domain.

In the present work, boundary conditions refer to mainly for the liquefied mist inlet that occurs over the outlet of the leakage orifice. As is well known, the orifice that the dimension of the orifice, compared with the size of the computational domain, is significantly smaller; so, the orifice outlet cannot be meshed. This therefore cause the mist inlet to be tested as a point source with mass flow boundary conditions. The temperature at the outer ending of the exit orifice during the earlier stages is transient when the valves are opened until the achievement of equilibrium and stabilisation of exit temperature bellow the vessel temperature. Here, the question arises as to what causes this change in temperature. So, of this difference in temperature, the potential causes are the transfer of heat and the change of the phase before the orifice exit due to the fact that flow rushes out of orifice by facing certain geometrical hindrances; thus, its temperature along with flow velocity changes very quickly. Although it is common to make an assumption of steady state flow owing to a less computationally intensive solution with limiting accuracy, in doing so, the actual physics behind the phenomenon is eliminated. This affects the results which are usually far from the actual behaviour of the system. As the jet temperature increases, the breakup form of fluid flow passes through different transition regimes throughout the cross-section in the validation rates become very high at the edge of the spray where we know that the spray density is at its minimum and vice versa.

One additional problem faced was gas behaviour when sprayed under the influence of the sub-cooled conditions, which led to issues in terms of data truncations. In the present study, these issues were minimised by adopting configuration optically. However, ideally, it is never possible to be sure that the truncation has been eliminated. As the mist inlet is tested as a point source, this automatically makes a predefinition of the fact that the mist flow rate, velocity and thermodynamic state are given at a spatial point. The CFD simulations can be calculated using the flux over the boundary cell faces.

5.1.7 Simplified Solution

In the present study, the main focus is on modelling atmospheric dispersion of hazardous fluids such CO2 using mathematical expressions. The transportation and turbulent dispersion of such gases must be estimated to prevent a potential accident. A study of the literature leads to the conclusion that two main modelling strategies have been adopted for modelling of heavy gas dispersion in the atmosphere: Air Quality Models and CFD Based Models. The former category involves such methods which estimate the potential dispersion of these fluids into the environment utilising Dense Gas Models mostly referred to as Gaussian Gas Models, as done in studies conducted by Kruse et. al. [58], Vending et. al. [59] and Turner et. al. [60].

From the literature studied, it was observed that, until the past few decades, the Gaussian models dominated the field of estimating gas dispersions mainly due to their relatively reliable and quick estimates. However, this quick convergence to solution is highly dependent on the conditions in which the fluid flows as the quickness of the model is only evident in the models where the flow remains uninterrupted on flat surfaces, as is evident in the previous studies Reynolds et. al. [61], Smith et. al. [62]. These models, based on analytical solving methodologies, on the other hand, provide inaccurate and unreliable results where the surfaces or terrains become complex. This is because, in such a scenario, the mathematical models become so complex that can be no longer solved by analytical procedures Mazzoldi et. al. [63]. This is what led to the development of CFD tools to better predict and visualise these flow dispersions. At present, because of high computational power available at economic conditions, these CFD models are becoming increasingly popular. Furthermore, these models are proven to provide better results when modelling dispersion of gas plume for complex terrains and large buildings in built up areas Scargiali et. al. [55], Tang et. al. [64]. The Gaussian or heavy gas dispersion model was firstly presented by Mohan et. al. [65] where all the related physical phenomena were considered by formulating specific governing equations. Some of these physical processes included air suction, heating of gas clouds, slumping behaviour, and others such phenomena that typically occur in heavy gas leakage. This model is further classified into two sub-categories: Heavy Gas Dispersion Model-1 and Heavy Gas Dispersion Model-2. Both of these models numerically solve the governing flow equations with leaking rate and related meteorological properties as inputs by utilising discretisation schemes such as Runge Kutta model and Finite Difference Scheme respectively. The typical outputs obtained from the model include air flow entrained and associated temperature, as well as dimensions of cloud formation.

5.1.8 Mathematical formulation of Gaussian method

All the gas dispersion models usually involve mathematical expressions representing diffusion phenomenon occurred due to turbulent flow motion. Average dispersion flow gives rise to advection process and leakage/dispersion sources. These terms makeup a mathematical model representing transportation phenomenon of hazardous gases that are released near to Earth's surface in the environment Stockie et. al. [66].

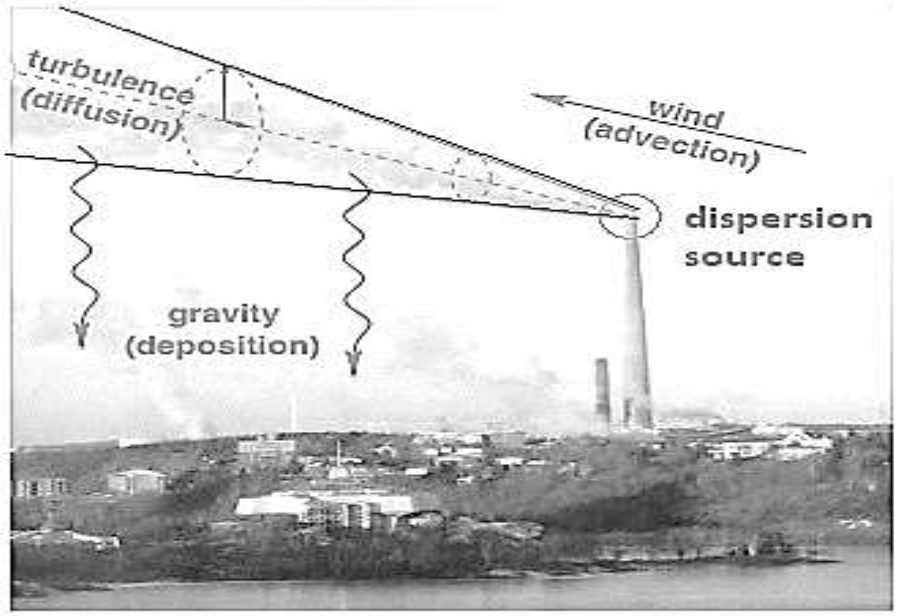

***Figure 5.2*:** *Atmospheric Hazardous Gases Transport Phenomenon Stockie et. al. [66]*

Considering a plume of containment gases that could be represented by a function (mathematically representing the plume geometry) termed 'G' with known density at point 'x' in space at time 't', the basic mass conservation law can be described as follows:

$$\frac{\partial G}{\partial t} + \nabla . \vec{M} = \tag{5.34}$$

The spatial vector $\vec{M}$ refers to transport of containment associated with convection and diffusion phenomenon, whereas 'S' refers to source of dispersion and Greek letter noble represent a 3D position vector. The diffusion phenomenon is characterized by considering that mass flux obtained due to diffusion is directly proportional to concentration of gases and more specifically, the gradient representing concentration variation, which is represented by the equation

$$\overrightarrow{M_d} = -K\nabla G \tag{5.35}$$

The notion of flow of contamination from high density area to low density area (high concentration to low concentration) is signified by the negative sign. The term 'K' refers to the coefficient of diffusion. Another component of flux is represented by the diffusion of containment occurring due to external factors in the form of wind with '$\vec{u}$' as its velocity:

$$M_w = D\vec{u} \tag{5.36}$$

$$\vec{M} = \overrightarrow{M_d} + \overrightarrow{M_w} \tag{5.37}$$

Putting all these equations in above equation (5.34), a diffusion-advection equation for 3D space is obtained:

$$\frac{\partial G}{\partial t} + \nabla.(D\vec{u}) = \nabla.(K\nabla G) + S \tag{5.38}$$

After applying certain assumptions including SteadyState dispersion from source, fixed velocity of wind, isotropic diffusion, x-axis win velocity is neglected and considering the flat terrain, the above equation becomes:

$$\mathrm{u}\frac{\partial G}{\partial x} = K\frac{\partial^2 G}{\partial y^2} + K\frac{\partial^2 G}{\partial z^2} + \mathrm{Q}\delta(\mathrm{x})(\delta(\mathrm{x})\delta(\mathrm{y})\delta(\mathrm{z}-\mathrm{H})) \tag{5.39}$$

Here, $\frac{\partial G}{\partial(x,y,z)}$ represents distribution of mass flux in three spatial coordinates, Q refers to fixed flow rate of containment from the source and δ represents Dirac delta function. For the development of accurate model, the partial differential equations of the models must be restricted by some boundary conditions as follows:

$$D(x,y,z) = D(0,y,z) = 0, D(\infty,y,z) = 0, D(x,\pm\infty,z) = 0, D(x,y,\infty) = 0, \frac{K\partial C}{\partial z}(x,y,0) = 0 \tag{5.40}$$

The very first boundary condition is representation of wind flow in a single direction and no gas flow in the x-axis. The last condition represents zero flux in vertical direction on the ground surface and the remaining ones refers to the overall restriction posed on the model that sum of mass of hazardous fluids must have a finite value.

Now that the problem has been well-defined, the solution begins with eliminating the terms referring to source of containment in equation 6 and replacing term 'x' with another independent variable 'r' such that

$$\mathrm{u}\frac{\partial G}{\partial r} = K\frac{\partial^2 G}{\partial y^2} + K\frac{\partial^2 G}{\partial z^2} \tag{5.41}$$

The initial form of the solution is thereby obtained by applying a variable separation method:

$$d(r, y, z) = \frac{Q}{u} a(r, y).\,\mathrm{b(r, z)} \tag{5.42}$$

'a' and 'b' are new variables after the separation as function of coordinates for a 2nd problem. After partial differentiation of the above equation, two reduced forms of 2nd equations for diffusion are obtained:

$$\frac{\partial a}{\partial r} = \frac{\partial^2 a}{\partial y^2} \text{ for } 0 \leq \mathrm{r} < \infty \text{ and } -\infty < \mathrm{y} < \infty$$

$$\frac{\partial b}{\partial r} = \frac{\partial^2 b}{\partial z^2} \text{ for } 0 \leq \mathrm{r} < \infty \text{ and } 0 < \mathrm{z} < \infty$$

After applying the Laplace transform to the above equations, the following simplified solution to convection advection equation is obtained:

$$c(r, y, z) = \frac{Q_L}{2\pi\mu r} \exp\left(-\frac{z^2}{4r}\right) \exp \int_{-\infty}^{\infty} \left(-\frac{y^2}{4r}\right) dy \tag{5.43}$$

$$c(r, y, z) = \frac{Q_L}{\sqrt{\pi\mu}} \exp\left(-\frac{z^2}{4r}\right) \tag{5.44}$$

The two models for the Gaussian plumes are described in the form of equations. Equation (5.45) shows the simple model equation for the shape of disk depends on the stability category.

$$concentration\ of\ air\ at\ 2 = \frac{mass\ emission\ rate}{(wind\ speed)(area\ of disk\ 2)} \tag{5.45}$$

$$\frac{\partial C}{\partial t} = 0 \tag{5.46}$$

$$o'^2_z = \frac{2K_z x}{u} \tag{5.47}$$

$$o'^2_y = \frac{2K_y x}{u} \tag{5.48}$$

$$\int_{-\infty}^{\infty} \int_{-\infty}^{\infty} C dy dz = Q \qquad [for\ x > 0] \qquad \{\mu g/sec\} \tag{5.49}$$

The Gaussian plume equation is a particular solution that follows certain assumptions. The first assumption is a steady-state condition, which is shown above as equation (5.46). The second assumption is constant wind speed with height. The third is constant eddy diffusivity, which is shown above as equation (5.47) and equation (5.48). The fourth assumption is the conservation of mass, which is described as equation (5.49)

5.2 Turbulence models

The flow for leaked heavy gas is essentially a turbulent one. Such turbulent flow is characterised by the instantaneous velocity field $U(x,t)$, which is three-dimensional, time dependent and random.

A broad range of scales distinguishes the turbulent flows. The substantial scales of the flow are as huge as the geometrical obstructions present in the flow field (L), and the smallest scales of the flow, η vary as [67] and shown as equation (5.50).

$$\eta \sim (Re_L)^{-\frac{3}{4}} \tag{5.50}$$

Here, Re_L is dependent on the huge size of the stream L and is known as the Reynolds number. Hence, the Reynolds number increments (in agreement to either diminishing inconsistency or an expansion in the speed) as, though the stream around a hindrance of size L is considered, the smallest size of the stream diminishes, and along these lines, the scope of scales one needs to determine becomes more extensive. The vitality range demonstrates the appropriation of vitality in wavenumber space among the different sizes of a fierce stream. Huge scale whirlpools contain the underlying vitality, which is then exchanged to the small-scale vortexes by means of a course like procedure through the inertial sub-run. The vitality is at last disseminated by the small-scale vortexes. Hence, in the event that one needs to unravel precisely a tempestuous stream field, one must determine the entire scope of scales.

Turbulence modelling remains one of the most challenging fields in the computational fluid dynamics field to this day. The difficulty lies in determining Reynolds' stresses. The unsolved scale flow's effects on the solved quantities are reflected by Reynolds' stresses. Based on the methods for Reynolds' stresses, turbulence modelling can be classified into three approaches: Large Eddy Simulation (LES), Direct Numerical Simulation (DNS) and Reynolds-Averaged Navier-Stokes Simulation (RANS), which are detailed in the following sections.

5.2.1 Direct numerical simulation (DNS)

Direct numerical simulation (DNS) is a method in computational fluid dynamics which is used to solve the Navier-Stroke's equations numerically without the use of a turbulence model. This means that the whole range of all the scales of turbulence needs to be resolved. Special care in numerical solutions is to be taken as a requirement for the wide range of scales in turbulent flows. DNS has helped offer a significant insight into turbulence physics of certain idealised flows that were very difficult to obtain from the laboratory.

DNS it is the accurate approach that is used for the turbulence simulation for solving the Navier-Stokes equations without involving any approximations except the numerical discretisation. In numerical discretisation, the errors are estimated. The realisation of flow is equal to that of computed flow field. This is known as DNS that is direct numerical simulation approach.

DNS results in detailed information about the flow. This is not used as a design tool as it is too costly. It is applicable for many examples, such as for understanding the turbulence production mechanism, aerodynamics nose production and its simulation, to see the effect of compressibility on turbulence, combustion, and turbulence interactions, as well as to reduce the drag on a solid surface.

In DNS, fine grids are used for solving Navier-Stokes's equations. All the eddy's whether small or large turbulent scales, are captured. The result is 3D, transient behaviour and are accurate. The overall cost of the computational effort is directly proportional to Re_L^3.

The grid points/dimensions to resolve the small scales are:

$$N_{1D} \sim Re_L^{3/4} \quad , \qquad Re_L = \frac{\rho\sqrt{k}\, l}{\mu}$$

The grid points need for three dimensional DNS are:

$$N_{3D} \sim Re_L^{9/4}$$

In direct numerical simulations (DNS), a small-time step is used to solve the Navier-Stokes equations on a fine grid. Small turbulence scales when neglected can affect the outcome of the results. So, in direct numerical simulations, the aim is that all eddy sizes are captured, including the smallest turbulent scales. The result of DNS is an accurate model of transient 3D behaviour. It can be said that the DNS are good for simple flows, but computationally they are very intensive. In DNS, the computational effort is proportional to Re_l^3 where Re_l^3 is the Reynold's number. In view of the CPU resources currently available, DNS are not recommended for industrial applications.

5.2.2 Large eddy simulation (LES)

Large eddy simulation (LES) is a technique in computational fluid dynamics in which the small eddies are removed and modelled using a subgrid-scale model. The large eddies are retained and solved using a transient calculation directly. The requirements for LES include the spatial and temporal resolution of scales in the inertial subrange and transient modelling. Large scales

of motion (large eddies) are usually much more energetic than the small-scale ones. In contrast to the small eddies, which are usually much weaker and have therefore very limited role in mass momentum and energy exchange, these large eddies are the most effective transporters of conserved quantities mass, momentum, and energy. Therefore, it is more important to solve these large eddies more accurately keeping in view their significant effect on the transport of the conserved quantities mass, momentum and energy.

The basic idea behind large eddy simulations (LES) is to model the small-scale eddies more universal using a subgrid-scale (SGS) model and to treat the large eddies with precision. LES are inherently time dependent and are three-dimensional simulations. Large eddy simulations (LES) are less costly than direct numerical simulations (DNS).

For flows with complex geometry and a high Reynolds number, large eddy simulations (LES) are the preferred method for obtaining the time history. In LES, a spatial filtering method is employed to separate the large eddies from the small eddies, keeping in view the basic idea of the method that small-scale eddies are to be treated differently (universally) to the large eddies (accurately). The large eddy simulation (LES) equations are derived by the application of a low-pass filter, parameterised with width *D*, to the transport equations for mass, momentum and energy. The filtered fields in the LES equations can be thought of as cell means. By applying a low-pass filter of width *D* to the DNS equations, the LES equations can be derived:

As an example, for a cell of width *D* in 1D the filtered density is:

$$\rho(x,t) = \frac{1}{\Delta}\int_{x-\frac{\Delta}{2}}^{x+\frac{\Delta}{2}} \rho(r,t)dr \tag{5.51}$$

where ρ is density and the filter width Δ in FDS is in equivalence to the local cell size *dx*.

In the sub-models, it is a key parameter for the turbulent viscosity and the reaction time scale later discussed. Implicit filtering is a term used for the practice of taking *D=dx*. However, it is important to appreciate that implicit filtering does not mean dissipative numeric. Kinetic energy conserving central difference schemes are applied in FDS for momentum with physically based closures for the turbulent stress.

The LES approach models the outcomes of small-scale swirls and decides the large-scale eddies. Spatial filtering is utilised to separate the resolved from the unresolved scales. The LES approach is well suited to handle bluff-body flows such as the flow around buildings or in urban areas. Some engineering or large-scale scenarios can be treated with the LES approach Harms et. al. [68], Salim et. al. [69].

Large Eddy Simulation (LES) is a preferred method for the floes where the Reynolds number is much greater or where the geometry is too much complicated to permit the application of Direct Numerical Simulation (DNS). This explicitly solves for large-eddies in the calculation and accounts implicitly for small eddies using SGS (subgrid-scale model). Mathematically, it separates the velocity field into a sub-grid and a resolved part. The resolved part specifies large eddies, while the sub-grid part specifies small eddies whose effect can be understood with the SGS model.

$$u_i\,(x) = \int G\,(x-\xi)u(\xi)d\xi \tag{5.52}$$

Resulting in $u_i = \overline{u_\iota} + u_i'$, where $\overline{u_\iota}$ is the resolved scale part and u_i' is the sub grid scale ξ part. Incompressible Navier-Stokes's equations develop filtered equations:

$$\frac{\partial ui}{\partial x} + \mathrm{u_j}\frac{\partial ui}{\partial xj} = -\frac{1}{\rho}\frac{\partial p}{\partial xi} + \frac{\partial}{\partial xj}\left(v\frac{\partial ui}{\partial xj}\right) \tag{5.53}$$

Substituting in the final equation above, the following is obtained:

$$\frac{\partial ui}{\partial x} + \mathrm{u_j}\frac{\partial ui}{\partial xj} = -\frac{1}{\rho}\frac{\partial p}{\partial xi} + \frac{\partial}{\partial xj}\left(v\frac{\partial ui}{\partial xj}\right) + \frac{1}{\rho}\frac{\partial \tau \mathrm{ij}}{\partial xj} \tag{5.54}$$

SGS stresses can also be found using Boussinsq hypothesis:

$$\tau_{ij} - \frac{1}{3}\tau_{kk}\delta_{ij} = -2\mu_t S_{ij} \tag{5.55}$$

This work takes the suggestion of Smagorinsky [49]: The Reynolds stresses have the same formulae as the viscous ones, but the turbulent viscosity is calculated by the following equation:

$$\mu_t = \rho(c_s\Delta)^2\left[2\nabla u : \nabla u - \frac{2}{3}\nabla\cdot u\right] \tag{5.56}$$

where μ_t= turbulent viscosity, $c_s = 0.2$, an empirical constant, and Δ = length of a grid cell.

The symbol ":" is used to denote the scale product of two tensors.

5.2.3 Reynolds Averaged Navier Stokes (RANS) methods

This approach gives rise to the turbulent closure problem by producing six new unknowns, the turbulent Reynolds stresses. The instantaneous flow field can be decomposed into an altering and a mean flow field. Hence, it is called the Reynolds decomposition which for the velocity field is given on the form of equation (5.57)

$$U_i^{inst} = u_i + \underline{U_i} \quad i = 1,2,3 \tag{5.57}$$

where u_i is the altering velocity and the mean velocity is u_i. As complete instantaneous flow vector field is decomposed in a 3D space, it will be equivalent to mean and altering velocity in x direction, velocity components in y direction and velocity decomposition in z direction. These are all different notations that represent components of flow field in a space. In this case, $U_1^{inst} = u_1 + U_1$ represents x-component of instantaneous flow field of velocity divided into associated mean and altering components u_1 and U_1 respectively. In a similar manner, $U_2^{inst} = u_2 + U_2$ and $U_3^{inst} = u_3 + U_3$ represent decomposition of instantaneous velocity filed in y and z directions into their respective components as described above. The compressible Reynolds Averaged Navier-Stokes's equations are written as follows:

$$\overline{U_i} = \frac{1}{\Delta t}\int_t^{t+\Delta t} U_i dt \tag{5.58}$$

$$\frac{\partial \rho}{\partial t} + \frac{\partial}{\partial x_j}\left(\rho U_j\right) = 0 \tag{5.59}$$

$$\frac{\partial \rho U_i}{\partial t} + \frac{\partial}{\partial x_j}\left(\rho U_i U_j\right) = -\frac{\partial p}{\partial x_i} + \frac{\partial}{\partial x_j}\left(\tau_{ij} - \rho\overline{u_i u_j}\right) + S_M \tag{5.60}$$

$$\frac{\partial}{\partial t}(\beta_v \rho) + \frac{\partial}{\partial x_j}\left(\beta_j \rho \underline{U_j}\right) = S_{m_{p\to f}} \tag{5.61}$$

$$\frac{\partial}{\partial t}\left(\beta_v \rho \underline{U_i}\right) + \frac{\partial}{\partial x_j}\left(\beta_j \rho \underline{U_i}\underline{U_j}\right) = -\beta_v \frac{\partial P}{\partial x_i} + \frac{\partial}{\partial x_j}\left(\beta_j \tau_{ij}\right) - \frac{\partial}{\partial x_j}\left(\beta_j \rho \underline{u_i u_j}\right) + S_0 + \beta_v(\rho - \rho_0)g_i + \rho S_{U_{p\to f,i}} \tag{5.62}$$

$$\frac{\partial}{\partial t}(\beta_v \rho H) + \frac{\partial}{\partial x_j}\left(\beta_j \rho \underline{U_j} H\right) = \frac{\partial}{\partial x_j}\left(\beta_j \rho \underline{h u_j}\right) + \beta_v \frac{DP}{Dt} + \dot{q} + S_{h_{p\to f}} \tag{5.63}$$

where the mean particular enthalpy of fluid is *H*. The source term accounting for the flow resistance due to the presence of sub-grid objects is S_0, β_v and β_j are the volume and area porosities of the cell respectively. For a compressible Newtonian fluid, the stress tensor τ_{ij} can be written as equation (5.64)

$$\tau_{ij} = \mu\left(\frac{\partial U_i}{\partial x_j} + \frac{\partial U_j}{\partial x_i} - \frac{2}{3}\frac{\partial U_k}{\partial x_k}\delta_{ij}\right) \tag{5.64}$$

The source terms $S_{m_{p\to f}}$, $S_{U_{p\to f,i}}$ and $S_{h_{p\to f}}$ model the effects of the dispersed phase on the continuous phase in the Euler-Lagrange approach. The exact expression of these equations contains 42 single phase turbulent jet flows terms. In the RANS approach, models need to be developed to estimate the Reynolds-stresses $\underline{u_i u_j}$ and enthalpy transport by turbulent

fluctuations $\underline{u_i h}$. Several models exist with different degrees of complexity; the $k-\omega$, the $k-\epsilon$ and the Reynolds-stress model, are among the most commonly models David et. al. [70] carried out an extensive description of these models. The Reynolds averaged energy equation is given below as equation (5.65)

$$\frac{\partial \rho h_{tot}}{\partial t} - \frac{\partial \rho}{\partial t} + \frac{\partial}{\partial x_j}(\rho(U_j h_{tot}) = \frac{\partial}{\partial x_j}\left(\lambda \frac{\partial T}{\partial x_j} - \rho\overline{u_j h}\right) + \frac{\partial}{\partial x_j}\left[U_i\left(\tau_{ij} - \rho\overline{u_i u_j}\right)\right] + S_E \tag{5.65}$$

The mean total enthalpy is given by following equation (5.66)

$$h_{tot} = h + \frac{1}{2}U_i U_i + k \tag{5.66}$$

Note that the total enthalpy contains the contribution from k, which is turbulent kinetic energy and given in following equation that is equation (5.67)

$$k = \frac{1}{2}\overline{u_i^2} \tag{5.67}$$

The additional variable equation becomes like equation (5.68). Where, $\rho\overline{u_j \varphi}$ is the Reynolds flux.

$$\frac{\partial \rho \varphi}{\partial t} + \frac{\partial}{\partial x_j}\left(\rho U_j \varphi\right) = \frac{\partial \varphi}{\partial x_j} - \left(T \frac{\partial \varphi}{\partial x_j} - \rho\overline{u_j \varphi}\right) + S_\varphi \tag{5.68}$$

5.2.3.1 Eddy viscosity turbulence models

Equation (5.69) shown below represents the relationship between stress and strain tensors in laminar Newtonian flow.

$$-\rho\overline{u_i u_j} = \mu_t\left(\frac{\partial U_i}{\partial x_j} + \frac{\partial U_j}{\partial x_i}\right) - \frac{2}{3}\delta_{ij}\left(\rho k + \mu_t \frac{\partial U_k}{\partial x_k}\right) \tag{5.69}$$

Similar to the eddy viscosity hypothesis, the eddy diffusivity hypothesis also states that the Reynolds fluxes of a scalar are linearly connected to the average scalar gradient. Here, Γ_t is the eddy diffusivity, and it prescribed in the equation along with other factors as shown in form of equation (5.70).

$$-\rho\overline{u_i \varphi} = \Gamma_t \frac{\partial \Phi}{\partial x_i} \tag{5.70}$$

The eddy diffusivity can be written in the form of following equation.

$$\Gamma_t = \frac{\mu_t}{Pr_t} \tag{5.71}$$

In light of the above hypothesis, the Reynolds averaged momentum and the scalar transport equation is converted in the following form of equation (5.72). Pr_t is the turbulent Prandtl number.

$$\frac{\partial \rho U_i}{\partial t} + \frac{\partial}{\partial x_j}\rho\left(U_i U_j\right) = -\frac{\partial P'}{\partial x_i} + \frac{\partial}{\partial x_j}\left[\mu_{eff}\left(\frac{\partial U_i}{\partial x_j} + \frac{\partial U_j}{\partial x_i}\right)\right] + S_M \tag{5.72}$$

Here, S_M is the sum of the body forces and μ_{eff} is known as effective viscosity, which is defined in form of following equation:

$$\mu_{eff} = \mu + \mu_t \tag{5.73}$$

where p' is a pressure that is actually a modified pressure and defined as equation (5.74) below:

$$p' = p + \frac{2}{3}\rho k + \frac{2}{3}\mu_{eff}\frac{\partial U_k}{\partial x_k} \tag{5.74}$$

The Reynolds averaged energy equation is given below in equation (5.75) below:

$$\frac{\partial \rho h_{tot}}{\partial t} - \frac{\partial p}{\partial t} + \frac{\partial}{\partial x_j}\left(\rho U_j h_{tot}\right) = \frac{\partial}{\partial x_j}\left(\lambda\frac{\partial T}{\partial x_j} + \frac{\mu_t}{Pr_t}\frac{\partial h}{\partial x_j}\right) + \frac{\partial}{\partial x_j}\left[U_i\left(\tau_{ij} - \rho\overline{u_i u_j}\right)\right] + S_E \tag{5.75}$$

Similarly, the Reynolds mean transport equation is shown below along with additional variables as equation (5.76)

$$\frac{\partial \rho\varphi}{\partial t} + \frac{\partial}{\partial x_j}\left(\rho U_j \varphi\right) = \frac{\partial}{\partial x_j}\left[\left(T_\varphi + \frac{\mu_t}{\sigma_\varphi}\right)\frac{\partial \varphi}{\partial x_j}\right] + S_\varphi \tag{5.76}$$

5.2.3.2 k-epsilon turbulence models

Accurate Turbulence modelling of fluid flow is of critical importance to the numerical model development of physical systems. Over the last two centuries, the introduction and rapid development of technology in domain of achieving higher and higher computational power has facilitated scientists and researchers to build large, complicated mathematical models representing the complex nature of flow of practical systems. Owing to the availability of such a computational resource, models based on equations representing kinetic energy of flow with turbulence effects have become the foundation for modern numerical method approaches for solving real world flows. This section will focus on two equation models, which are different from conventional one-dimensional models in that the former models incorporate the influence of scale length of turbulence phenomenon by providing an additional equation for eddy viscosity.

The significance of these models lies in the fact that they not only cover the aspects of turbulence in flow but also related phenomena. Moreover, an important fact to note is that these models are fully capable of estimating turbulent flow characteristics without having any base knowledge of potential structures of turbulence. There exist only two kinds of such models: one is $K-\omega$ (K-omega model) while other is $K-\epsilon$ (K-epsilon Model).

The basic foundation of these models initiates with a widely known approximation for Boussinesq represented in form of tensors for Reynolds Stresses given in equation (5.77)

$$\tau_{ij} = 2v_T S_{ij} - \frac{2}{3} k\delta_{ij} \tag{5.77}$$

where τ represents dissipation rate, k is equivalent to specific turbulent kinetic energy and S represents mean stress tensor in x and y direction. Lastly, v_T represents kinematic eddy viscosity of flow. The other foundation equation is of kinetic energy equation for turbulent flows.

$$\frac{\partial k}{\partial t} + U_j \frac{\partial k}{\partial x_j} = \tau_{ij} \frac{\partial U_i}{\partial x_j} - \epsilon + \frac{\partial[(v+\frac{v_T}{\sigma_k})\frac{\partial k}{\partial x_j}]}{\partial x_j} \tag{5.78}$$

where U is a representation of flow velocity and ϵ represents rate of dissipation per unit mass in K- ϵ model while, for the $K-\omega$ model, the term w represents specific rate f dissipation as first introduce by Kolmogorov et. al. [71].

Historically speaking, the similarities between the two models is evident from the terms in the equations representing eddy viscosity, rate of dissipation and turbulence length scale, all of which are represented by the empirical dimensional parameters which, on the down side, do not reveal any flow features that occur in physical flow. In terms of limitations of these models, which in the present age became evident in form of two-phase models for equilibrium and non-equilibrium flows, these two equation models are restricted to certain conditions and cannot be applied universally to any fluid flow having turbulence and are proven to produce inaccuracies for various turbulent flows which develop non-equilibrium state. Moreover, since an additional equation catering for ϵ and ω is infused in the model, the model becomes complex and presents many difficulties while solving the flow Wilcox et. al. [72].

From the practical aspect of implementing these models, it should be noted that the $K-\epsilon$ model is proven to provide inaccurate and less reliable results near the walls of the computational flow domain. This is because the most appropriate scale for flow velocity in the context of transportation of turbulence near the walls should be v^2, not the term k in the existing

model, as indicated by Durbin et. al. [73]. Moreover, this model when implemented for flows where near wall flows are of critical significance, employs a specific wall function. One of the most important aspects of the two equation models pertains to widely known Law of the wall, which is essentially empirical equation for flow with turbulence flowing adjacent to the solid boundaries. This law is generally related shear stress with distance from the boundary surface 'y'. The modified term 'y+' provides the critical value of near wall distance (usually approximately 30), at which the velocity profile obtained from the model matches with the physically accurate behaviour observed experimentally. Another important point to understand is that this value of 30 is not fixed and is directly influenced by flow regimes represented by the Reynolds number Re [72]. One pioneering study conducted on development of a modified $K-\epsilon$ model for near wall treatment of flow specified that, when y+ lies in range of 60-150, the value of turbulence becomes constant and thus shear stresses in the flow also attains a constant value and flow quality improves Patel et. al. [74]. Therefore, the previous discussion led to the observation that, as the Reynolds number increases and flow regimes change, the associated y+ must also increase so as to match the law of wall with actual flow velocity characteristics near the solid boundaries.

This model adds two new variables into the system of equations. The continuity equation then becomes as equation (5.79). The equation of momentum is shown as equation (5.80).

$$\frac{\partial \rho}{\partial t}+\frac{\partial}{\partial x_j}\left(\rho U_j\right)=0 \tag{5.79}$$

$$\frac{\partial \rho U_i}{\partial t}+\frac{\partial}{\partial x_j}\left(\rho U_i U_j\right)=-\frac{\partial p'}{\partial x_i}+\frac{\partial}{\partial x_j}\left[\mu_{eff}\left(\frac{\partial U_i}{\partial x_j}+\frac{\partial U_j}{\partial x_i}\right)\right]+S_M \tag{5.80}$$

where

$$\mu_{eff}=\mu+\mu_t$$

Here, μ_t is turbulence viscosity and this model assumes that μ_t is linked to the turbulence kinetic energy and dissipation. μ_{eff} is the effective viscosity accounting for turbulence. This linkage is shown in the form of equations (5.81), (5.82), and (5.83) below. In these equations, C_μ is constant.

$$\mu_t=C_\mu \rho\ \frac{k^2}{\varepsilon} \tag{5.81}$$

$$\frac{\partial(\rho k)}{\partial t}+\frac{\partial}{\partial x_j}\left(\rho U_j k\right)=\frac{\partial}{\partial x_j}\left[\left(\mu+\frac{\mu_t}{\sigma_k}\right)\frac{\partial k}{\partial x_j}\right]+P_k-\rho\varepsilon+P_{kb} \tag{5.82}$$

$$\frac{\partial(\rho\varepsilon)}{\partial t}+\frac{\partial}{\partial x_j}\left(\rho U_j\varepsilon\right)=\frac{\partial}{\partial x_j}\left[\left(\mu+\frac{\mu_t}{\sigma_\varepsilon}\right)\frac{\partial\varepsilon}{\partial x_j}\right]+\frac{\varepsilon}{k}\left(C_{\varepsilon1}P_k-C_{\varepsilon2}\rho_\varepsilon+C_{\varepsilon1}P_{\varepsilon b}\right) \quad (5.83)$$

Here, $C_{\varepsilon1}, C_{\varepsilon2}$ and σ_ε are constants. where, P_{kb} and $P_{\varepsilon b}$ represent the influence of buoyancy forces.

$$P_k=\mu_t\left(\frac{\partial U_i}{\partial x_j}+\frac{\partial U_j}{\partial x_i}\right)\frac{\partial U_i}{\partial x_j}-\frac{2}{3}\frac{\partial U_k}{\partial x_k}\left(3\mu_t\frac{\partial U_k}{\partial x_k}+\rho k\right) \quad (5.84)$$

In equation (5.84) above, P_k is turbulence production because of the viscous forces. It is modelled with help of this equation. In the case of incompressible flow, $\frac{\partial U_k}{\partial x_k}$ is small. For the compressible flow, this term will only be large in areas where high velocity divergence exists.

Buoyancy turbulence, when the buoyancy is being modelled, the buoyancy turbulence option is used. The buoyancy production term P_{kb} is modelled as

$$P_{kb}=-\frac{\mu_t}{\rho\sigma\rho}g_i\frac{\partial\rho}{\partial xi} \quad (5.85)$$

If the Boussinesq model is being used,

$$P_{kb}=-\frac{\mu_t}{\rho\sigma\rho}\rho\beta g_i\frac{\partial\rho}{\partial xi} \quad (5.86)$$

when the buoyancy turbulence option is set to production or dissipation, the production term is included in the k equation. $P_{\varepsilon b}$ is proportional to P_{kb} and should be positive.

$$P_{\varepsilon b}=C_3.\max[0,P_{kb}] \quad (5.87)$$

Modification can be done for any angle ɵ between the velocity and gravity vectors.

$$P_{\varepsilon b}=C_3.max[0,P_{kb}].sin\emptyset \quad (5.88)$$

where Turbulence Schmidt Number σρ, and Boussinesq buoyancy (σρ= 0.9)

Full buoyancy model(σρ=1), Dissipation co-efficient (C_3 = 1) $\sigma_{\varepsilon RNG.}$ $\emptyset$ the angle between velocity and gravity vectors.

5.2.3.3 RNG k-epsilon model

When the renormalisation group analysis of the Navier-Stokes Equations is done, this gives basis to the k-epsilon model. The transport equations are similar to that of the standards model, but the only change is to replace $C_{\varepsilon1}$. by $C_{\varepsilon1RNG}$

$$\frac{\partial\rho\varepsilon}{\partial t}+\frac{\partial}{\partial xj}(\rho U_j\varepsilon)=\frac{\partial}{\partial xj}\left[\left(\mu+\frac{\mu t}{\sigma_\varepsilon RNG}\right)\frac{\partial\varepsilon}{\partial xj}\right]+\frac{\varepsilon}{k}(C_{\varepsilon1RNG}P_k-C_{\varepsilon2RNG}\rho\varepsilon+C_{\varepsilon1RNG}P_{\varepsilon b}) \quad (5.89)$$

where, $C_{\varepsilon 1\text{RNG}} = 1.42 - f_{\eta}$

The other factors are given as $C_{\mu\text{RNG}}$

$$f_{\eta} = \frac{\eta\left(1-\frac{\eta}{4.38}\right)}{1+\beta\text{RNG}\eta 3} \quad , \quad \eta = \sqrt{\frac{Pk}{\rho C\mu\text{RNG}\varepsilon}}$$

5.2.4 Boundary conditions

Sometimes, two CFD calculations have the same grid or even the same computational domain. Thus, the imposed boundary conditions determine the type of flow to be modelled. Accurate CFD solution is obtained by appropriate boundary conditions. CFD uses different terminologies. In 2D flow, face or plane are used instead of edge or line. Several options are present at the boundaries through which the fluid enters or leaves the computational domain. They may be either pressure specified, or velocity specified conditions.

5.2.4.1 Inlet

Here, the velocity of the incoming fluid along the inlet face at the velocity inlet is specified. Sometimes, the temperature of the incoming flow also needs to be specified. Similarly, at the pressure inlet, total pressure along the inlet face is specified. The Cartesian velocity component may be written as:

$$U_{inlet} = U_{spec(i)} + V_{spce(j)} + W_{spec(k)} \tag{5.90}$$

Similarly, the cylindrical velocity components are given as

$$U_{inlet} = U_{r,spec(r)} + V_{\theta,\text{spec}(\theta)} + W_{z,spec(z)} \tag{5.91}$$

The boundary mass flow rate can also be specified with a directional component:

$$\text{P U} = \frac{\dot{m}}{\int dA} \tag{5.92}$$

Here the integral shows none other than the integrated surface boundary area.

The inlet temperature is specified as

$$T_{ststic,inlet} = T_{spec}$$

$$Q_{inlet} = Q_{advect} + Q_{diffusion}(inlet\ energy\ flow) \tag{5.93}$$

5.2.4.2 Outlet

Fluid essentially flows out of the computational domain here. At the pressure outlet, the static pressure along the outlet face is specified. This is mostly set as zero-gauge pressure. Turbulence

and temperature properties are also specified at the outlet. If there is reverse flow at the pressure outlet, this means that that the working domain is not large enough:

$$U_{outlet} = U_{spec(i)} + V_{spce(j)} + W_{spec(k)} \tag{5.94}$$

Similarly, for the static pressure, equation is given as

$$P_{spec} = \frac{1}{A} \int p_{ip} \, D_a \tag{5.95}$$

where p_{ip} = imposed pressure at every integration point.

$$P_{ip} = P_{spec} + (P_n - \acute{p}_n) \tag{5.96}$$

5.2.4.3 Opening

These are also known as outflow boundary conditions. No flow properties are specified at the outflow boundary i.e. velocity or temperature properties. In fact, all the flow properties are forced to have zero gradients which are normal to the face of outflow. For example, outflow boundary conditions would be most appropriate if the flow of the duct is fully developed at the outlet. Fluid can cross the boundary surface in either direction.

$$U_{openimg} = U_{spec(i)} + V_{spce(j)} + W_{spec(k)} \tag{5.97}$$

The relative pressure value for the opening condition can be specified in the same way,

$$P_{opening} = P_{spec} \tag{5.98}$$

Similarly, we can also specify the lost coefficient $f = f_{spec}$

$$P_{loss} = \frac{1}{2} \rho f U_{n^2} \tag{5.99}$$

$$P_{spec} + \frac{1}{2} \rho f U_{n^2} = P_{stat} \tag{5.100}$$

The temperature condition can also be specified in same way as shown above.

5.2.4.4 Walls

As the fluid cannot pass through a wall, thus the velocity's normal component is set at zero relative to the wall along the boundary condition prescribed face. Similarly, the velocity's tangential component is also set to zero because of the no-slip condition at the wall.

$$U_{WALL} = 0$$

Similarly, the normal component of the velocity and the shear stresses at the wall are:

$$U_{n,WALL} = 0, \quad \tau_n = 0$$

The velocity components in Cartesian and cylindrical are given as

$$U_{WALL} = U_{spec(i)} + V_{spce(j)} + W_{spec(k)} \tag{5.101}$$

$$U_{WALL} = U_{r,spec(r)} + V_{\theta,spce(\theta)} + W_{z,spec(z)} \quad (5.102)$$

5.3 Numerical methods

There are three methods for numerically solving the equations in the above chapters: Finite element methods (FEM), finite difference methods (FDM) and finite volume methods (FVM). Finite difference methods (FDM) are the oldest method, introduced in the18th century. FDM require structured or block-structured grids and are therefore limited in the applications with simple and regular geometrical domains. On the grids, FDM approximates differential equations into a set of algebraic equations for each node of the grids and then calculates the algebraic equations numerically. The major advantage of the finite difference method is that it is straightforward as a concept and easy to apply. For irregularly shaped geometries, however, the differential equations must be transformed into a regular shaped domain before finite difference schemes are applied. This transformation introduces various sorts of problems, e.g., additional cross-coupling equations and convergent issues.

The second numerical method is the finite element method (FEM). This method requires transforming the differential equations in the mathematic models into Galerkin formulation. The equivalent Galerkin formulation is projected into finite element space so as to make a set of discrete algebraic equations which are computable. The finite element method is employed mostly for the structural analysis and flow with a low Reynolds number. The major advantages of finite element methods are mastering element formation and that the same effort is required for any shaped geometry that can be modelled using this method. This method is much an appropriate to use, but it requires a great deal of computational effort, particularly in the case of density stratifies flows. Its disadvantage is heavy use of mathematics while being of less physical significance.

The third method is finite volume methods (FVM) for numerical solutions. This method is based on the control volume integration form of the basic equations that are often partial differential equations. The control volume can be built up by meshing a computational domain, and FVM discretises the integrations of the basic equations into algebraic form of the equations. Compared with FDM, the finite volume method can be applied to very complex geometric domains. Because of these properties, FVM will be used in the present research.

The small volume around each node point in the mesh is actually termed as the finite volume. The 1D problem is defined as partial differential equation shown below as equation (5.103)

$$\frac{\partial \rho}{\partial t} + \frac{\partial f}{\partial x} = 0\ ,\ t \geq 0 \tag{5.103}$$

The implementation of this method in the case of one dimensional (1D) steady-state heat transfer includes the generation of the grid as its initial step in which the control volume surrounds each node and the physical boundaries match with the control volume boundaries. The next step is discretisation, which involves the basic concept of this method i.e., to integrate these equations (governing equations) for a control volume. And at the nodal point, it provides the discretised equation. This discretised equation will need the gradient at the west and east and interface diffusion coefficient. After having useful discretised equations, the next step is to find a solution for them. Finite volume methods are not only for 1D diffusion problems, but they are also for 2D and 3D diffusion problems as well. Equation (5.104) is the general form of discretised equations for 1D, 2D, and 3D diffusion problems. In this equation, a_{nb} represents the neighbouring coefficients that will be two (a_W, a_E) for one-dimensional problem. Whereas, a_{nb} will be a_W, a_E, a_S and a_N. However, for a diffusion problem with three dimensions, a_{nb} will be a_W, a_E, a_S, a_N, a_B and a_T, the equation (5.105) will be satisfied by all coefficients around P. This equation will be applicable for all cases in finite volume methods.

$$a_p \varphi_p = \sum a_{nb}\, \varphi_{nb} + S_u \tag{5.104}$$

$$a_p = \sum a_{nb} + S_p \tag{5.105}$$

According to Versteeg & Malalasekera [75], the finite volume methods are also implemented for the problems of the discretising and diffusion equation by assuming that there is a known flow field. The problems that have both convection and diffusion at the same time are solved through finite volume methods by using the coefficients that came from a weighted combination of convex mass flux and diffusion conductance and are used in discretised equations. In these equations, through the source terms, boundary conditions are encountered. For two main reasons, method of central differencing failed for general purpose convection diffusion problems. They are the lack of transporters and providing solutions that are unrealistic at higher values of the Cell Peclet Number.

Finite volume methods are not limited to this, but they are also implemented for unsteady flows. The techniques developed to solve such problems are also based on the convection-diffusion discretised equations discussed above. An explicit technique is used when variable ϕ from the previous time level, but for the values at the new time level, the/an implicit technique is used.

However, when there is a hybrid of both, the crank time stepping algorithm is preferably used for finding the variable ϕ at a new time level.

Rahitby et. al. [76]; Chui et. al. [77,78]; Chui et. al. [50] provide a CV (control volume) integration method for the calculation of radiative transfer of heat, which has some similarities with the discrete ordinate method. Along with this method Chai et. al.[80,81] they describe the finite volume (FV) method by using the control angle integration.

In the finite volume method, one is constantly dealing with fluxes, but not so with finite elements. The advantages of using this method include its applicability for the unstructured grid, integral formation of conservation laws, and being based on cell averaged values. The disadvantage of this method is in case of an irregular mesh that needs calculation, and will lead to an unbearable number of fluxes and a major bookkeeping effort to ensure all the fluxes have been calculated properly.

5.3.1 Discretization of the mathematical equations

To solve the equations in section 5.1 and 5.2, they are firstly discretized in space and time coordinates. For the computations of the discrete Navier-Stokes's equations, there are two numerical techniques: Pressure-based and density-based approaches. For the flows with a low Mach number, the pressure-based method presents more advantages over the density-based method and therefore is used in the present work. In the pressure-based technique, the manipulation of momentum and the continuity equation provides a pressure equation. The solution of this equation provides a pressure field. A general solution is stepped by:

- Utilisation of the computational grid to divide the domain into discrete control volume.
- Constructing algebraic equations for dependent discrete variables i.e. pressure, velocity, scalars, and temperature by integrating the set of governing equations on every control volume (individual).
- Solving the linear equations obtained by linearising the set of discretised equations and yielding new values of dependent variables.

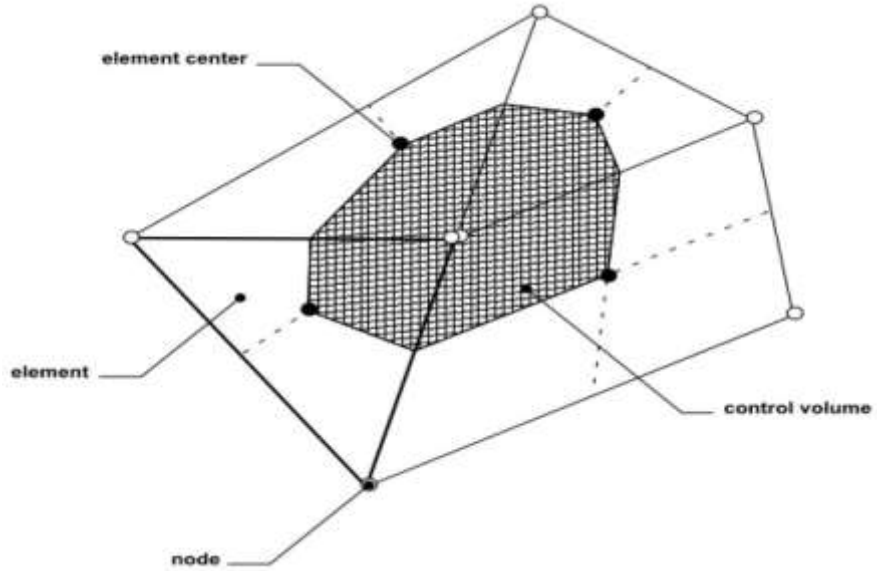

Figure 5.3: *Control Volume Definition [83]*

The discretisation process is completed using the finite volume method. Consider the following equations:

$$\frac{\partial \rho}{\partial t} + \frac{\partial}{\partial x_j}\left(\rho U_j\right) = 0 \tag{5.106}$$

$$\frac{\partial (\rho U_i)}{\partial t} + \frac{\partial}{\partial x_j}\left(\rho U_j U_i\right) = \frac{\partial P}{\partial x_i} + \frac{\partial}{\partial x_j}\left(\mu_{eff}\left(\frac{\partial U_i}{\partial x_j} + \frac{\partial U_j}{\partial x_j}\right)\right. \tag{5.107}$$

$$\frac{\partial (\rho \varphi)}{\partial t} + \frac{\partial \left(\rho \varphi U_j\right)}{\partial x_j} = \frac{\partial}{\partial x_j}\left(\mu_{eff}\left(\frac{\partial \varphi}{\partial x_j}\right)\right) + S_\varphi \tag{5.108}$$

By the integration of these equations over each of the control volumes, Gauss's theorem of divergence can be applied to convert these volume integrals also involving divergence operators to the surface integrals. The derivatives can be also moved outside the volume integrals in case the control volume deformation is not in time. Thus,

$$\frac{d}{dt}\int_v \rho dV + \int_S \rho U_j dn_j = 0 \tag{5.109}$$

$$\frac{d}{dt}\int_v \rho U_i dV + \int_S \rho U_j U_i dn_j = \int_S P dn_j + \int_S \mu_{eff}\left(\frac{\partial U_i}{\partial x_j} + \frac{\partial U_j}{\partial x_j}\right) dn_j + \int_V S\, U_i dV \tag{5.110}$$

$$\frac{d}{dt}\int_v \rho \varphi dV + \int_S \rho U_j \varphi dn_j = \int_S \mu_{eff}\left(\frac{\partial \varphi}{\partial x_j}\right) dn_j + \int_V S\, \varphi dV \tag{5.111}$$

where S and V correspond to surface and volume regions of integration and Cartesian differential component is represented by dn_j.

The next step is the discretisation of the surface and volume integrals. For this consider a single mesh element shown below:

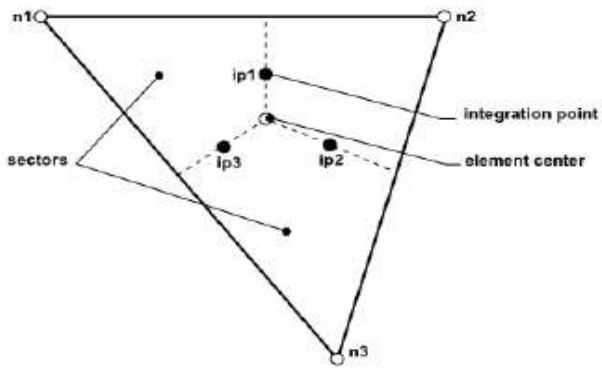

Figure 5.4: *Mesh Element [83]*

Discretisation of volume integral is done within each sector element, whereas discretisation of the surface integral is done at the integration points which are located at every surface segment's centre and then its distribution is done adjacent to every control volume. Surface integrals are considered to be locally conservative. Thus, the equations become:

$$V\left(\frac{\rho-\rho^0}{\Delta t}\right) + \sum_{ip} \dot{m}_{ip} = 0 \quad (5.112)$$

$$V\left(\frac{\rho U_i-\rho^0 U_i{}^0}{\Delta t}\right) + \sum_{ip} \dot{m}_{ip} (U_i)_{ip} = \sum_{ip}(P\Delta n_i)_{ip} + \sum_{ip} \mu_{eff}\left(\frac{\partial U_i}{\partial x_j} + \frac{\partial U_j}{\partial x_j} \Delta n_j\right)_{ip} + S_{Ui} V \quad (5.113)$$

$$V\left(\frac{\rho\varphi-\rho^0\varphi^0}{\Delta t}\right) + \sum_{ip} \dot{m}_{ip} (\varphi)_{ip} = \sum_{ip} \mu_{eff}\left(\frac{\partial U_i}{\partial x_j} + \frac{\partial U_j}{\partial x_j} \Delta n_j\right)_{ip} + S_{\varphi} V \quad (5.114)$$

Where, ip represents the integration point and Δt is the time step. Meanwhile, Δn_j represents the outward discrete surface vector.

5.3.2 Segregated and coupled algorithms

The projection method is employed to calculate the discrete Navier-Stokes's equations. Because of the pressure-velocity coupling, in practical calculations, two algorithms are commonly used, that is, segregated and coupled algorithms.

5.3.2.1 Segregated algorithm

The segregated algorithms are to solve the equations of flow velocities and pressure separately. The major advantage of this algorithms requires least amount of memory when compared to coupled algorithms, however, this algorithm suffers from slow convergence Kelecy et. al. [85].

The modern segregated solution algorithms were developed to satisfy the following requirements:

- Capability to solve both steady and transient flow equations.
- The results obtained must be equivalent to results obtained from coupled algorithms for same flow problem.

In order to explain the steps in details, a specific pressure based segregated algorithm should be considered as shown in Figure 5.5. This is called a SIMPLE algorithm Patankar et. al. [86]. Each time the solver runs, the following steps are repeated:

1. Properties of the fluid are usually updated by considering the values obtained in the last iteration. These properties usually include pressure, velocity, temperature, concentration and turbulence entities, but may also include viscosity, specific heat or even density depending upon the nature of flow problem being solved. The first step is making a prediction for the entire pressure field P*.
2. Utilising the updated values of the face and pressure mass fluxes for solving the momentum equations to obtain first obtain starred velocity (Velocity field not satisfying continuity equation) components u, v and w are given below:

$$a_e u_e^* = \sum a_{nb} u_{nb}^* + b + \left(P_p^* - P_E^*\right) A_e \tag{5.115}$$

$$a_n v_n^* = \sum a_{nb} u_{nb}^* + b + \left(P_p^* - P_N^*\right) A_n \tag{5.116}$$

$$a_t w_t^* = \sum a_{nb} u_{nb}^* + b + \left(P_p^* - P_E^*\right) A_t \tag{5.117}$$

3. The imperfect velocity field obtained is utilised for solving the pressure equation. In order to obtain specific values of velocity in the above set of equations that will satisfy the continuity equation, the value of pressure P is calculated by summing up the pressure guessed above P* and pressure correction P' by following equation:

$$p = p^* + p' \tag{5.118}$$

The pressure correction found from the step above can be utilised to correct the pressure and mass-fluxes, and calculate velocity field in terms of u , v and w. The following correction formulae are employed to obtain perfect velocity field. The unknowns can be established using a simultaneous solution of the following expressions:

$$u_e = u_e^* + d_e(P_P' - P_E') \tag{5.119}$$

$$v_n = v_n^* + d_n(P_P' - P_N') \tag{5.120}$$

$$w_t = w_t^* + d_t(P_P' - P_T') \tag{5.121}$$

The unknowns can be found using a simultaneous solution of following expressions:

$$a_e u_e' = (P_P' - P_E')A_e \tag{5.122}$$

$$u_e' = (P_P' - P_E')d_e \tag{5.123}$$

$$d_e = \frac{A_e}{a_e} \tag{5.124}$$

4. Using these values obtained, discretisation equations are solved for only those flow quantities that actually influence flow behaviour such as temperature, turbulent viscosities, etc. It should be noted that those flow characteristics that do not influence the flow field are usually after obtaining the solution for a flow problem.
5. The equation set's convergence is checked.
6. Continue these steps by now considering the correct version of pressure P as a new guess value P* and then repeat the procedure unless the convergence is achieved [82,83,84]

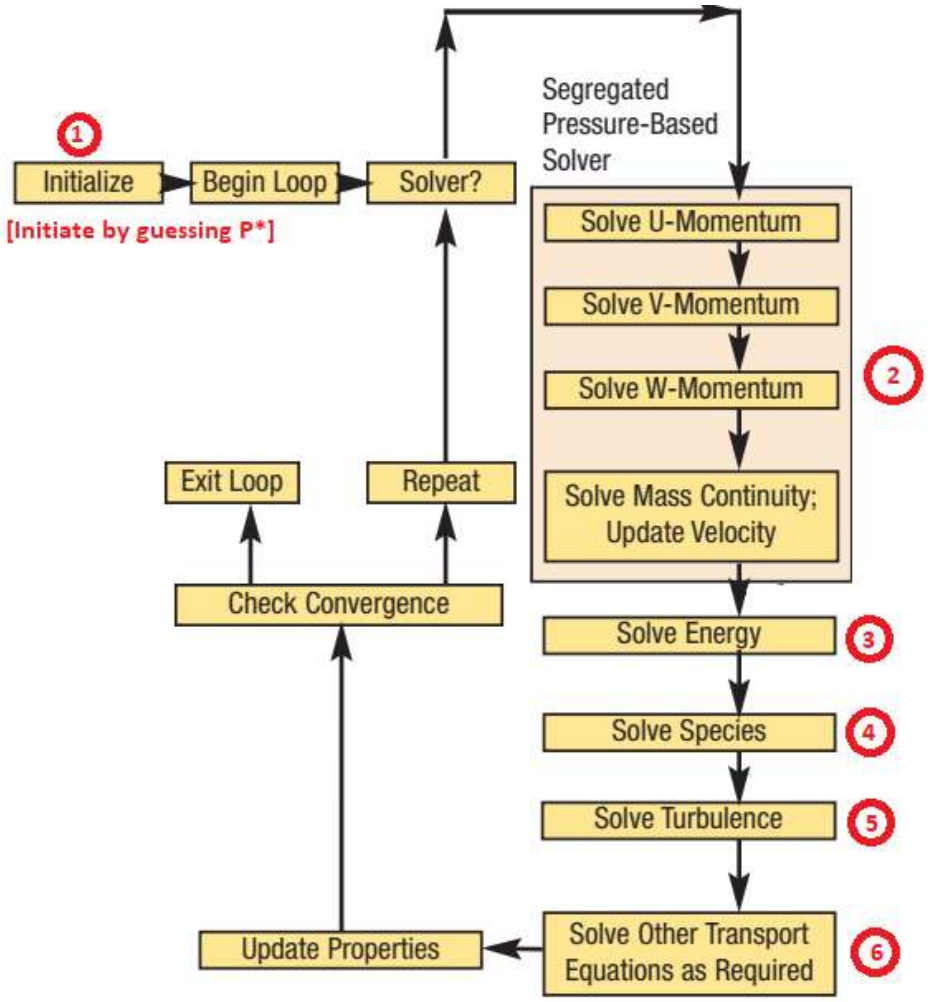

Figure 5.5: *Segregated Algorithm Flowchart Kelecy et. al. [85]*

5.3.2.2 Coupled algorithm

In this algorithm also termed the semi-direct method, solutions for the discretized version of continuity and momentum conservation equations are coupled with each other and the consequent set of equations are solved simultaneously. This method was introduced by

Caretto et. al. [86]. This type of algorithms has been proven to provide a close linkage between pressure and velocity components, thus improving rate of convergence and efficiency. However, the limitation is its requirement of large computational memory which it has attempted to solve by solving the set of governing equations on a number of sub-domains. This approach suffers from the issue of connectivity between various subdomains. This results in a very heavy convergence rate penalty Vanka et. al. [87,88], Braaten et. al.[89].

A coupled algorithm is generally of the following procedure Hanby et. al. [90]:

1) Predict and obtain initial values of pressure and velocity fields in terms of Po and U_0 , V_0, W_0 respectively.
2) Obtain the solution of a coupled system of flow governing equations given below:

$$\frac{1}{r}\frac{\partial}{\partial r}(\rho r v_i u^*) + \frac{\partial}{\partial z}(\rho u_i u^*) - \mu\nabla^2 u^* + \frac{\partial_p^*}{\partial z} = f_u \quad (5.125)$$

$$\frac{1}{r}\frac{\partial}{\partial r}(\rho r v_i v^*) + \frac{\partial}{\partial z}(\rho u_i v^*) - \mu\left(\nabla^2 v^* - \frac{v^*}{r^2}\right) - \frac{2\rho}{r} w_i w^* + \frac{\partial_p^*}{\partial r} = f_v \quad (5.126)$$

$$\frac{1}{r}\frac{\partial}{\partial r}(\rho r v_i w^*) + \frac{\partial}{\partial z}(\rho u_i w^*) - \mu\left(\nabla^2 w^* - \frac{w^*}{r^2}\right) - \frac{\rho}{r} w_i v^* + \frac{\rho}{r} v_i w^* = f_w \quad (5.127)$$

$$\frac{\partial u^*}{\partial z} + \frac{1}{r}\frac{\partial}{\partial r}(rv)^* = g \quad (5.128)$$

3) In order to facilitate the faster convergence, the following under-relaxation factor is applied to all flow variables:

$$x_{i+1} = \varepsilon x^* + (1-\varepsilon)x_i \quad (5.129)$$

4) Check the specified convergence criterion.
5) Continue the above procedure unless the converged solution is not obtained. Note that, in this case, both pressure and velocity equations are solved simultaneously in step 2, in contrast to segregated algorithms, which complete the same procedure in 2-3 steps.

Thus, this approach solves a coupled equation system that comprises both the pressure-based and momentum continuity equations. For further clarifications are shown in Figure 5.6 below:

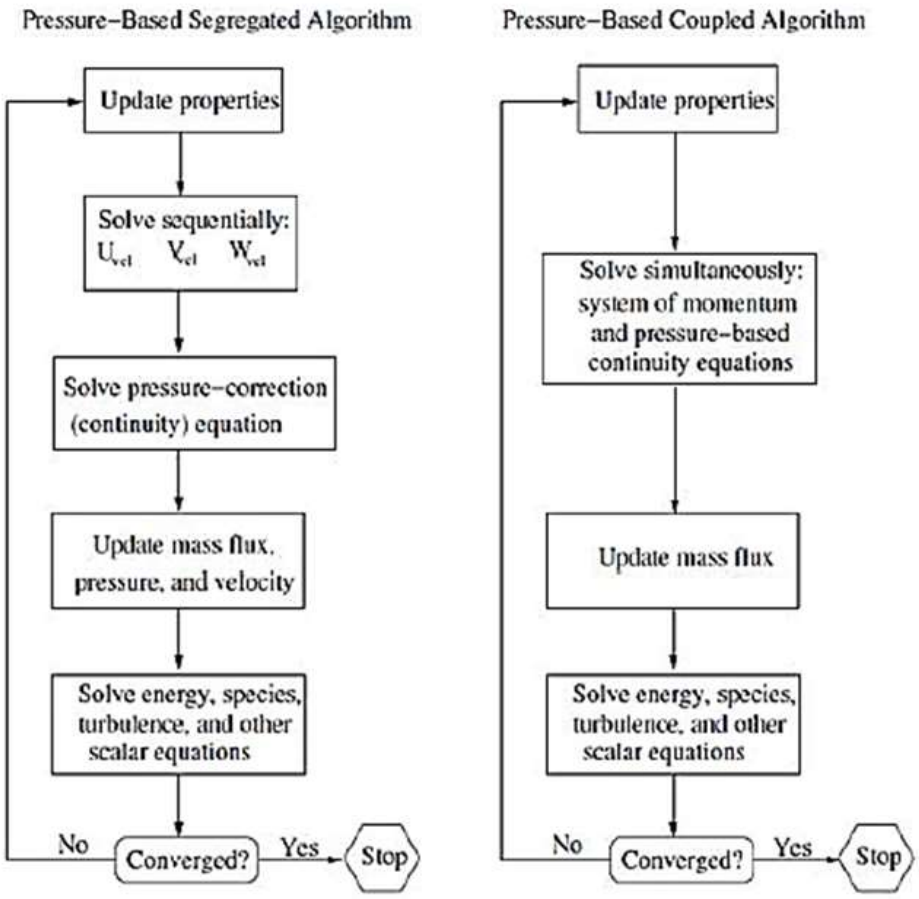

Figure 5.6: *Comparison of segregated and coupled algorithm [82,83]*

5.3.3 Numerical schemes for turbulence

Numerical methods for the computation of turbulent flows are classified on the basis of several features. They are classified into three main categories. The first is the discretisation method, which the approximation of the differential and integral conservation equations by a system of the algebraic equations that can be solved using a computer. The second category belongs to various classes of turbulence models.

The third main category is the pressure velocity density coupling method. In discretisation methods, finite difference, finite element, spectral and finite volume methods are mostly used. This has been discussed in previous sections 5.3 (Numerical Methods).

The methods for integration in time are called the Explicit and Implicit methods. In the explicit method, the solution is calculated at a new time interval using only the variable values from the previous step. However, in the implicit method (used in evaluation of integrals) the new values are unknown and hence need a solution of an equation system. This can be explained

using conservation equation, which is rewritten in form of equation (5.130) where F and φ are the functions of time.

$$\frac{\partial \varphi}{\partial t} = F \tag{5.130}$$

In case of the two-level methods, the explicit Euler method is represented as equation (5.131) in which all the quantities on the right-hand side of the equation are known. Therefore, a new value is directly obtained:

$$\varphi^{n+1} = \varphi^{n} + F^{n}\Delta t \tag{5.131}$$

On the other hand, the implicit Euler method is presented as equation (5.132) in which the new value is used. Therefore, the method is called the implicit Euler method.

$$\varphi^{n+1} = \varphi^{n} + F^{n+1}\Delta \tag{5.132}$$

The iterative solver is mostly preferred for linear equations systems as well. Lilly's analysis for the turbulent flows is shown below in the form of equations. Equation (5.133) is for the incompressible flows. Equation (5.134 is for the case when the Reynolds number μ_t is too much larger than of μ. By assuming that the width is Δ for the flow of the high Reynolds number, the Kologorov kinetic energy spectrum can be represented in the form of equation (5.135). However, by considering a spectral cut off filter, the equation can be written as equation (5.136) McGranttan et. al.[91].

$$\nabla . u = 0 \tag{5.133}$$

$$2v_t\overline{S_{ij}S_{ij}} = 2vS_{ij}S_{ij} \tag{5.134}$$

$$E(k) = C_K \varepsilon^{\frac{2}{3}} k^{-\frac{5}{3}} \tag{5.135}$$

$$2v\overline{S_{ij}S_{ij}} = 2v\int_0^{\frac{\pi}{\Delta}} k^2 E(k)dk \tag{5.136}$$

5.3.4 Two phase flows

In the past, for the sake of quick and acceptably good results, the one phase models were widely used owing to their ease of solution. However, these models are based on assumptions, and the models are simplified to such an extent that physical behaviour of flow is not captured. These two-phase flow types are evident in a large number of applications, including ejectors, slurry fluid flow, flow of fluid droplets and others. These models are mainly classified into the subcategories Equilibrium Model and Non-Equilibrium Model [92,93]. Although these models

are still in the research and development stage, they still provide a better approximation of the physical flow compared to single phase models.

Usually, these models as the name suggests, involve flow in two different physical states, such liquid-liquid flow and liquid vapour fluid flow, or solid-gaseous particles flow and liquid solid flow. On a practical level, there exist large number of processes in which two or more immiscible fluids in multiphase are utilised in industrial devices. Their interaction (of two different phases of non-moving fluids) led to the development of the process known as interface tracking. Many different methods are available and categorised on the basis of grid methods or techniques employed for the solution. These include Fixed Grid methods, Moving Grid Methods and Grid-less or Grid-Free methods. In the present study, the focus will be restricted to first category i.e., the volume of fluid (VOF) method, level set methods and front tracking methods will be briefly discussed. VOF was first introduced by Borrell et. al. [94]. It involves introducing a function having values in the range of 0 to 1, which consequently represents the portion of volume that is actually filled with the fluid. At every cell of the computational domain, the VOF function F is reconstructed by implementing various methods, including piecewise reconstruction and other methods. On the basis of the interface, the reconstructed complete velocity vector field is calculated at all faces of every cell. Then the fluid transfers itself to an adjacent cell (from donor to acceptor cell) and the process continues for the whole domain. Similarly, the level set method employs a distance function F as function of time t and distance x, which provides information about the location of initial interface from specific distance x. The advantage of this method lies in its capability to tackle distortion in fluid interfaces and related topology variations, but it is usually limited by its lack of capability to incorporate conservation of mass phenomenon Kleefsman et. al. [95]. The last front tracking method is generally aimed at solving flow problems where flow discontinuities are essential characteristic to investigate. This method models the discontinuities by specifying the explicit degree of freedom (DOF) supported by DOF referring to values of continuous solution of flow. The method was first introduced by Morton et. al. [96] and was widely implemented in CFD studies of aerodynamics Glimm et. al. [97]. These two-phase flows and their modelling are still under development. Different methods have not been proposed yet. These main methods, including the volume of fluid method, the level set method, and the front tracking method are briefly discussed above. These methods are mostly concerned with a trade-off between the maintenance of a sharp interface or conversion mass. It is crucial as the evaluation of the viscosity, density and surface tension is based on the values averaged over the

interface. Lagrangian multiphase models that are used for dispersed media are based on solving the Lagrangian equation of motion for the dispersed phase.

5.3.5 Meshes used in this project

Mesh generation is required both to match complex computational domain configuration and to have sufficiently high resolution. Quality-high meshes are essential to accurately produce CFD simulations. Two types of elements during meshing are employed: hexahedral and tetrahedral. For a mesh of the same number of nodes, the tetrahedral element mesh has a number of elements approximately five times greater than that of the hexahedral element mesh, which means that the tetrahedral element mesh entails more computational cost over the hexahedral element mesh in the computations. Hexahedral element mesh, however, cannot be generated in a complex geometric domain.

Therefore, when the computational domain can be topologically mapped to multiple cuboid blocks, the hexahedral element mesh of multiple blocks is generated, i.e., structured mesh (for example, sees Figure 5.6). Otherwise, the tetrahedral element is applied in mesh generation, i.e., unstructured mesh (see Figure 5.7).

A computer-aided design (CAD) programme, Salome, is used to generate the geometries for computational domains. Salome is an open-source CAD programme. It is produced and maintained by Open CASCADE Technology, France. The generated geometries are input into ANSYS mesh generation tools for mesh generation.

It should be pointed out that there are also mesh generation tools in ANSYS for mixed element meshes. The researcher's experience testing these tools, however, found that they are not capable of generating elements with the desired sizes. Accordingly, the hexahedral and tetrahedral elements are applied in the present study. The following figures show some examples of the meshes generated.

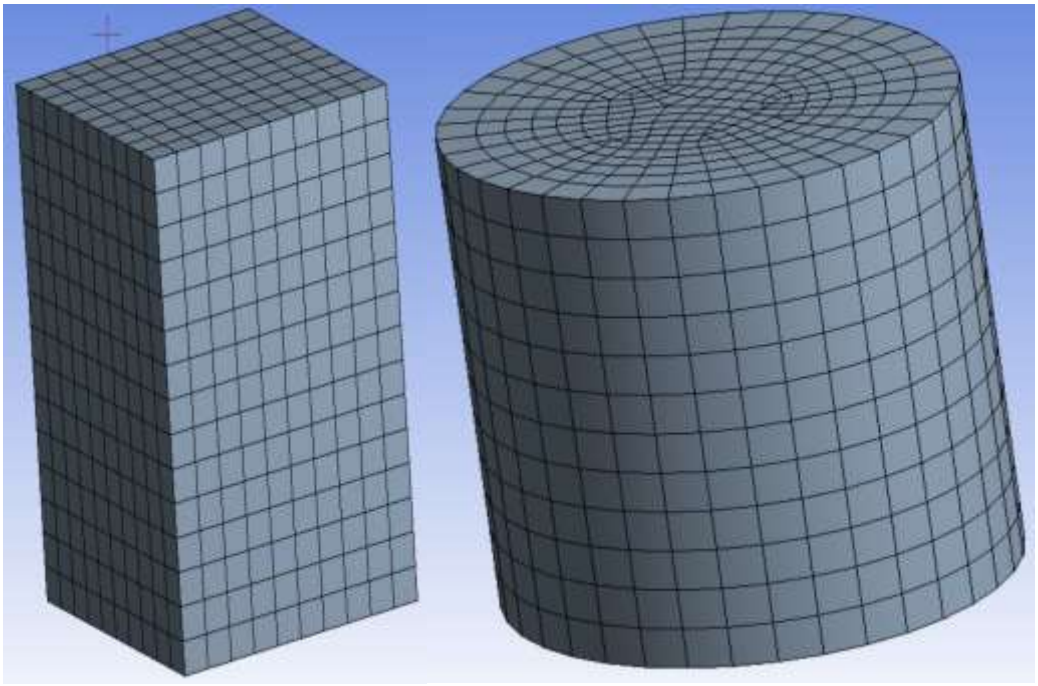

(a) One block (b) Multiple blocks

Figure 5.6: *Shows the structured mesh style*

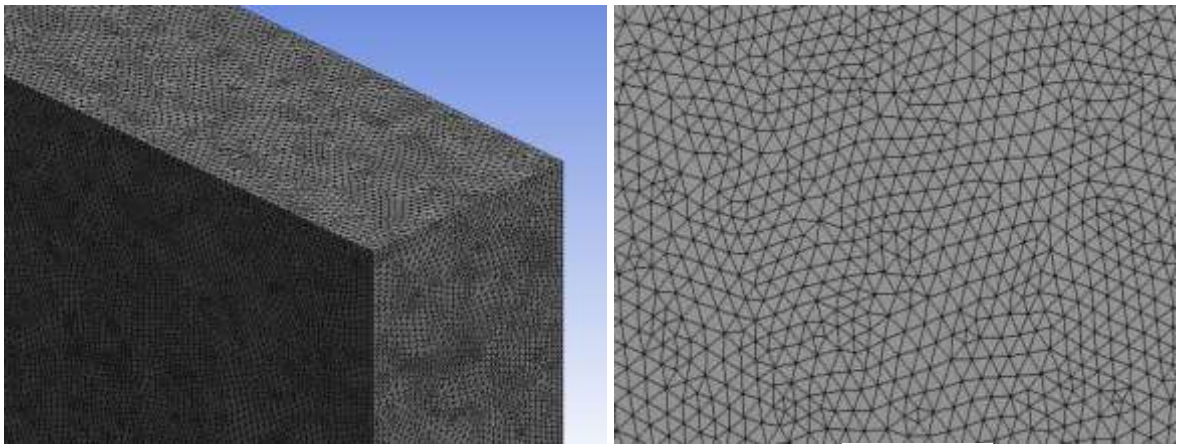

(a) (b)

Figure 5.7: *Shows the unstructured mesh style*

5.3.6 Verification of numerical methods

The verification of numerical methods involves the two important components. One is an independent study of mesh and the other is validation through comparison with other works or results. The more accurate the boundary conditions and mesh, the more accurate the converged solution will be. It is necessary to confirm that the solution is also independent of the resolution of the mesh. The process for performing a mesh independent study involves three basic steps.

The first is to run the initial simulation on the mesh and then check the convergence of the residual errors to 10^{-4}. If there is a need to refine the mesh, then there is a need to refine it. After meeting the convergence criteria, the mesh is refined overall for having finer cells throughout the geometry. Again, it must be ensured that the residual error does not drop below 10^{-4}. The solution varies because of change in mesh refinement, so mesh independent solution is still not found. Therefore, for a mesh independent study, the mesh will be refined repeatedly until a solution is achieved that is independent of mesh.

For the validation step, the experimental results and the analytical results that are already available in the literature are used for comparison. In 2009, the procedure for the verification and validation (V&V) of CFD was provided by the American Society of Mechanical Engineers (ASME). Through the validation procedure, the strengths and the weaknesses of the model of the current study will be detected and then easily evaluated, verification and validation are necessary steps in computational fluid dynamics (CFD). Validation is done for the significant improvement in the CFD model, for which validation experimentation is conducted. The relative error is calculated using some equations. This shows the relative error as presented by Santos et. al. [98].

5.3.7 Numerical simulations vs. experimental results

In order to validate and test the models, the numerical results are compared with experimental observations. Therefore, the validation and verification of the numerical simulation are important in order to be certain that the results obtained through numerical simulation are in conformity with the experimental observations. This is necessary for verification of results.

5.3.7.1 Validation of the flashing jet

The experiments of flashing jet were conducted by Witlox et. al. [99,100]. The numerical simulation results were compared as illustrated Figure 5.8 below:

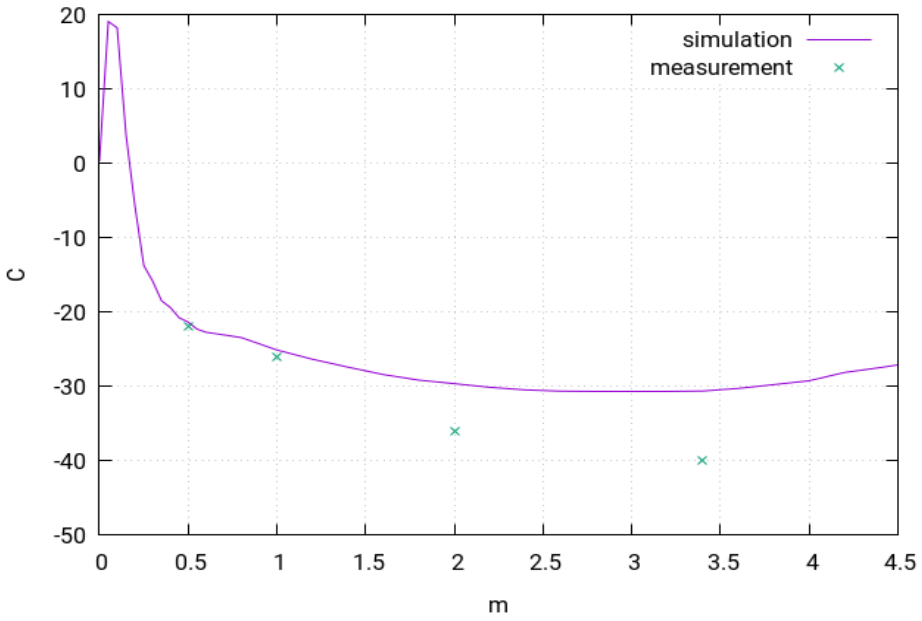

Figure 5.8: *The observations of the temperatures are indicated by the green cross points for experimental measurement and by the purple line for the numerical simulation*

Figure 5.8 shows the observations for the temperature of the flashing gas jet obtained through the numerical simulation and experimental observations. It can be seen that:

1) The purple line shows the temperature trend of the flashing jet obtained by way of the simulation. It can be seen that, as one moves away from the nozzle, the temperature first increases and then begins decreasing.

2) The green cross points show the temperature trend for the results of the flashing jet from experimental observations obtained by others for similar cases.

Hence, the temperature in Figure 5.8 is actually the temperature of the gas phase locally. It can be seen that the temperature of the gaseous mixture is almost same as the ambient temperature near the orifice since the phase change from the liquid mist to the gas just starts there. The phase change process is maintained by absorbing the ambient heat. The gas temperature is therefore quickly decreased downstream. The minimal temperature is at approximately 3.5m downstream. This is consistent with the experimental measurements.

Furthermore, the jet flow is constantly entraining the ambient air with a high temperature into the jet core. Therefore, at some point, the gas temperature must increase. The computations used in the present study find that the location after which the temperature increases is at about 3.5m. This is the reason why the temperature slowly increases from 3.5m to 4.5m.

It can be seen that the results obtained through numerical simulations match the experimental observations at the start of the nozzle. Thereafter, as the distance increases, the results of the numerical simulations deviate from the experimental results. The reasons for these deviations are:

1) In numerical simulations, the atmospheric conditions have been defined to be constant throughout the experimental domain. The temperature is set to 25°C and the pressure is 101.325 kPa.
2) In experimental observations, the temperature of the atmosphere does not remain constant, and it changes along with the distance horizontally.
3) Moreover, the pressure in the real experimental setup does not remain constant either, and it changes continuously.

This renders the temperature in experimental observations different from those in the numerical simulations. The same is the case for other parameters. However, the overall deviation is within the acceptable range of 10%.

5.3.7.2 Validation of the effect of obstacles in the heavy gas dispersion

In order to determine whether this work will be worthy of the consideration to determine the effect of obstacles in the dispersion of the heavy gas, the following graphs have been generated in this regard. They show the comparison of the calculation of concentrations for the heavy gas dispersion through both the numerical simulations performed in this work and the experimental results carried out by Ayrault et al. [101,102].

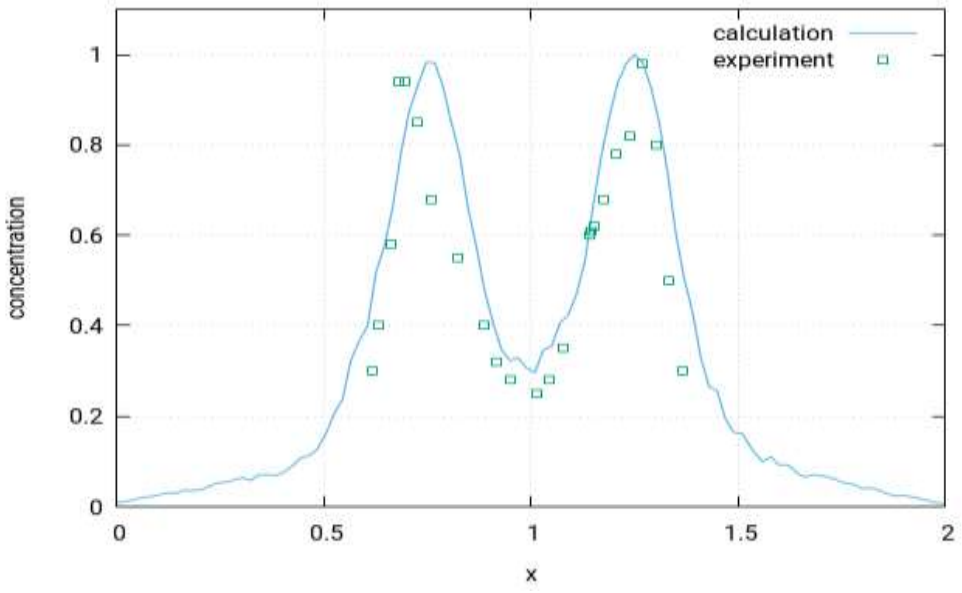

(a)

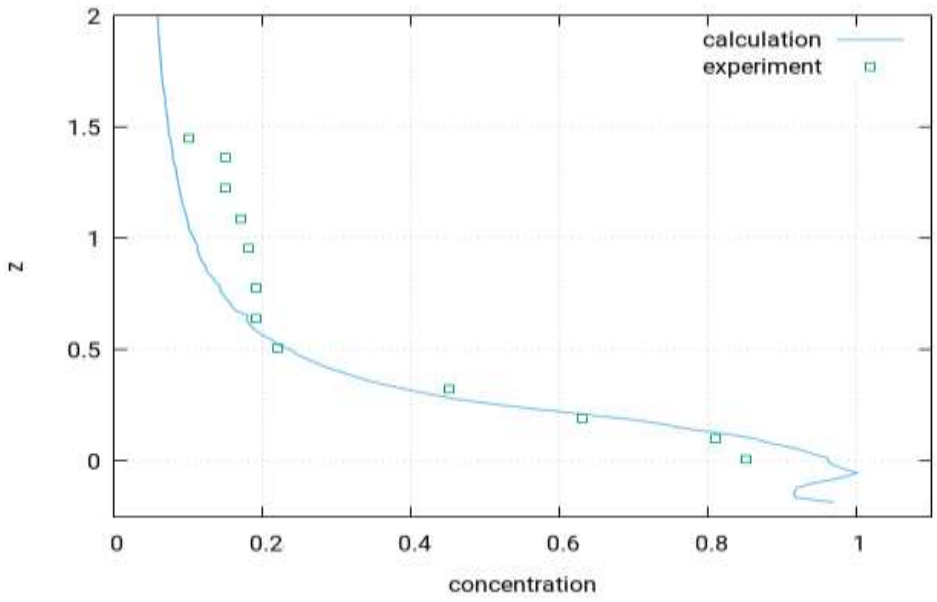

(b)

Figure 5.9: *(a) The concentration of crosswise profiles and (b) the concentration of streamwise profiles. The blue curve is for the heavy gas dispersion of numerical simulations results, while the green empty box is for the experimental results of [101,102]*

Figure (a) represents the crosswise profiles, while (b) represent the streamwise profiles. Upon analysing the Figure 5.9(a) above, it can be established that the results from the calculation for concentration for heavy gas dispersion with obstacles through numerical simulation performed in this work and the experiment performed by Ayrault et. al. [101,102] show very similar profiles and similar results. It should, therefore, be safe to say that the numerical simulations provide a particularly accurate approximation of the results.

The results from figure 5.9(b), which are the results of streamwise profiles, tell a slightly different story. The profile in the upstream region shows a difference of behaviour in the upstream region but a similar one in the downstream region.

5.3.7.3 Validation of heavy gas dispersion within a group of buildings

The following graphs validate the CFD numerical simulation approaches as the results obtained from these experiments. Before the results are described, will compare the results of experimental observations and the numerical simulations will be compared to provide an overview of the deviation of experimental data from the present study's numerical simulations. Figures 5.10(a) and (b) show the deviation of experimental values of Heidorn et. al. [103], from the numerical results.

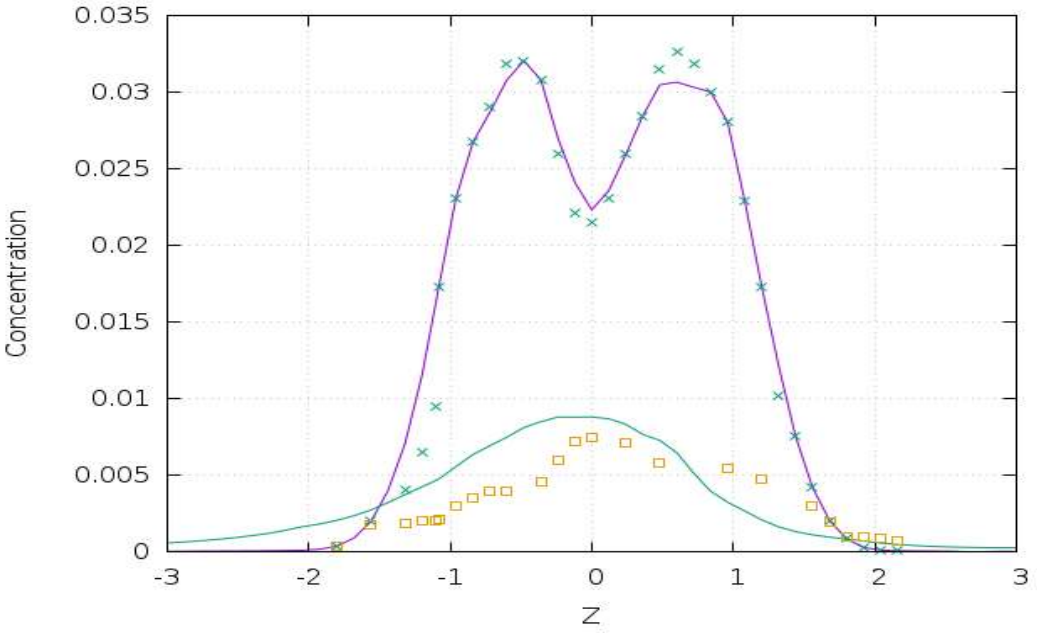

(a)

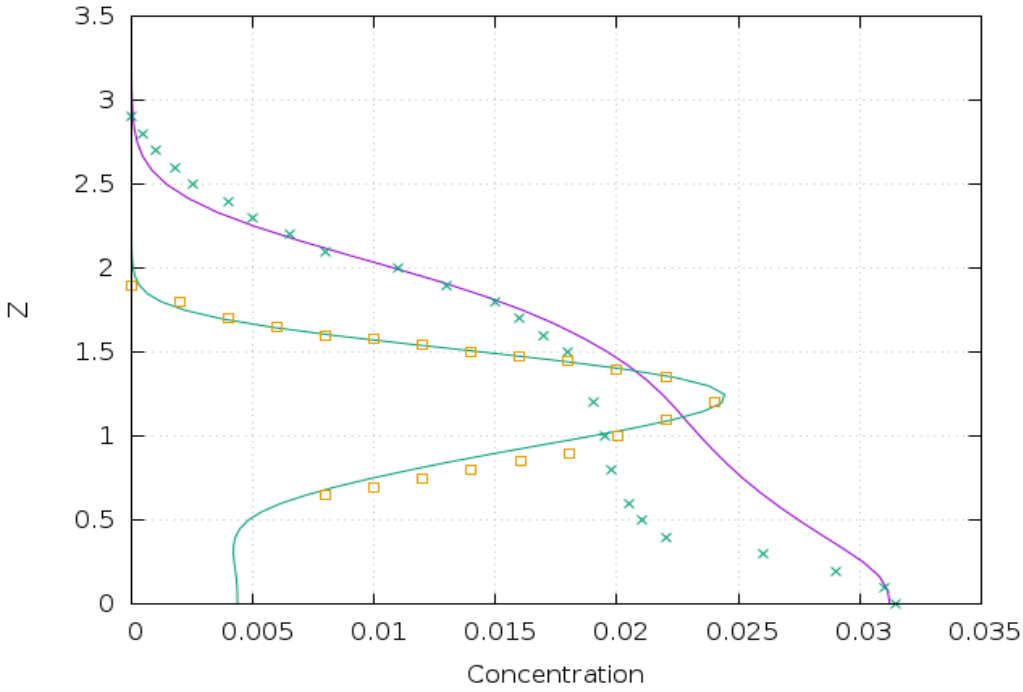

(b)

Figure 5.10: *Contrast of the numerical and experimental results for dispersion gas profiles on horizontal (a) and vertical (b) axes at 200mm behind the building. The solid purple line is for the heavy gas dispersion. The solid green line is for the neutral gas dispersion, while the square points and cross points represent for the experimental results of Heidorn et. al. [103].*

The above figures show that this deviation is the result of the following factors:

1) The ambient temperature in numerical simulation is kept constant, when, in reality, it does not remain constant. Hence, the numerical simulation results show a small deviation in results.
2) The atmospheric air velocity is also assumed to be a constant value in this study's numerical simulation calculations, when, in reality, it clearly does not remain constant.

Figure 5.10(a) shows the comparison of the numerical simulations and experimental results. The colour legend for the lines is as follow:

1) The purple solid line is for heavy gas on the horizontal profile using the numerical approach.
2) The green cross points are for heavy gas on the horizontal profile using the experimental approach.

The two lines approximately match each other and show a small deviation within 10%.

Figure 5.10(a) also shows the comparison of results for neutral gas. The colour legend for the neutral gas is:

1) The green solid line shows the results obtained using the numerical approach for neutral gas.
2) The orange squared boxes show the results obtained using the experimental study for neutral gas.

In this case, there is again a small deviation, which is within the acceptable range of 10%.

Similarly, figure 5.10(b) shows the comparison of theoretical and numerical results on the vertical profile for the dispersion of gases. In this case, there is more deviation for the heavier gas as this gas has a higher density. At high velocities, as the gas leaves the nozzle, it compresses, and the molecules of the gas move closer to each other. In theory, this effect is negligible neglected. Hence, the deviation is greater at higher velocities for heavier gas.

Chapter 6 Flashing Jets

6.1 Introduction

When heavy gases are released into the atmosphere, this causes serious environmental issues. Heavy gases stay in the atmosphere longer than other gases do Santon et. al. [104]. They are not present in the atmosphere naturally and are released due to industrial accidents in the oil and gas industry. Some accidents involve the direct release of heavy substances in gaseous form into the environment, while other accidents involve the release of heavy molecules, with a two-phase transition during the release. These two-phase releases of heavy gas are far more dangerous than single phase releases, as they also involve small droplets of heavy molecules, which remain suspended in the environment for a longer period of time.

The flashing of liquified heavy gases into the environment involves many critical factors, such as:

1) Pressure of the liquified petroleum gas
2) Ambient pressure
3) Ambient temperature
4) Diameter of the droplets
5) Diameter of the nozzle

In this study, numerical simulations of flashing jets were performed using the CFD approach. The CFD results were compared with the results obtained through experimental observations of Witlox et. al. [99,100].

6.2 CFD simulation set-up

For the simulation of the flashing jet, a simulation domain was set-up on the three-dimensions x, y and z axis - with the same set-up experiments [99,100], the properties below:

1) The computational domain is in the shape of a cuboid, which is 3.5m high, 3.5m wide and 6.5m long in the x, y and z axis, respectively.
2) The ambient air temperature is set to 298 K which is 25°C.
3) The ambient air pressure is taken as 1 atm, which, in SI units, is 101.325 kPa.

4) The whole domain is divided into meshes, which run in two directions, i.e., vertical and horizontal.
5) The resolution of the three meshes is set as 0.08m, 0.055m and 0.03m. These meshes are uniform throughout the domain (see Figure 6.7 page 111)
6) The whole lower boundary of the domain is set to zero displacement. Hence, it is regarded as the ground.
7) The other boundaries - left, right, top, front and back - are allowed to have the air flow through them with the ambient conditions set at the start, which is 298 K temperature and 101.325 kPa pressure.

After defining the computational domain, the next step is to define the flashing jets injections into the domain. This includes the following set-up:

1) For the simulation, two flashing jets are set containing different fluids having different molecular masses. One is propane and other is butane.
2) These jets are allowed to be released from a small orifice with the fixed displacement boundary condition, i.e. it cannot move with respect to the jet. The location at which the orifice is located has the coordinates of 0m, 1.5m and 2.5m in x, y and z axis, respectively.
3) When the liquified gases are released from the orifice, they become vaporised and convert into heavy gases. This is because a sudden pressure difference from very high to 101.325 K causes the liquid to be converted into gas.
4) The velocity at which the heavy gases are released depends on the thermodynamic properties of the liquid and the ambient air. These velocities are also dependent on the pipe and flow losses. If these losses are neglected, the flow velocities can be calculated from the Bernoulli's equation which states below [99,100].

$$V = \sqrt{2\frac{p_i - p_a}{\rho_p}} \tag{6.1}$$

where p_i is the pressure of the tank containing the liquified gas, p_a is the ambient pressure of the air and V is the velocity of the jet. From the above equation, the velocity can now be calculated and from the also calculate the flow rate with the following equation:

$$Flow\ Rate = Velocity\ \times Area \tag{6.2}$$

6.3 INERIS France experimental set-up

To understand the behaviour of a flashing jet released through a nozzle, a series of experiments were carried out by Witlox et. al. [99,100], using equipment containing a jet source and a tank filled with liquified heavy gas. The equipment used for the experimental observations was manufactured by INERIS. The equipment is shown in Figure 6.1.

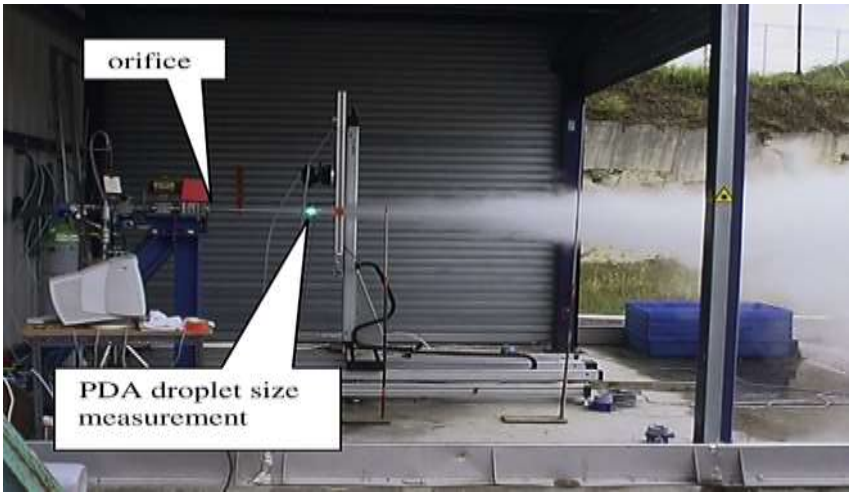

Figure 6.1: *Experimental set-up and PDA droplet size measurement*

The equipment has the following features have been used by Witlox et. al. [99,100]:

1) The equipment rig contains a helical shaped cylinder fitted with a heating element to heat the liquified gas to the set-point temperature.
2) In the cylinder, the pressure of the liquified gas is controlled by filling the tank or cylinder with an inert gas, which, in this case, is nitrogen. By changing the pressure of the overhead nitrogen, the pressure of the liquified gas can be change.
3) When the flashing heavy gas is released from the nozzle, not all of the liquified gas is vaporised at once. The flashing jet, when released through the nozzle, may be accompanied by small droplets. These droplets affect the properties of the flashing jet as the liquid droplets are suspended with the vapours and fall to the ground after some distance Witlox et. al. [10].
4) Hence, it is important to study the properties of the liquid droplets along with the flashing jet. The properties of the droplets are dependent on the diameter measurement. The diameter of the droplets is measured using the Phase Doppler Anemometry (PDA) technique. This equipment also contains a feature to measure the droplet size as shown in Figure 6.2.

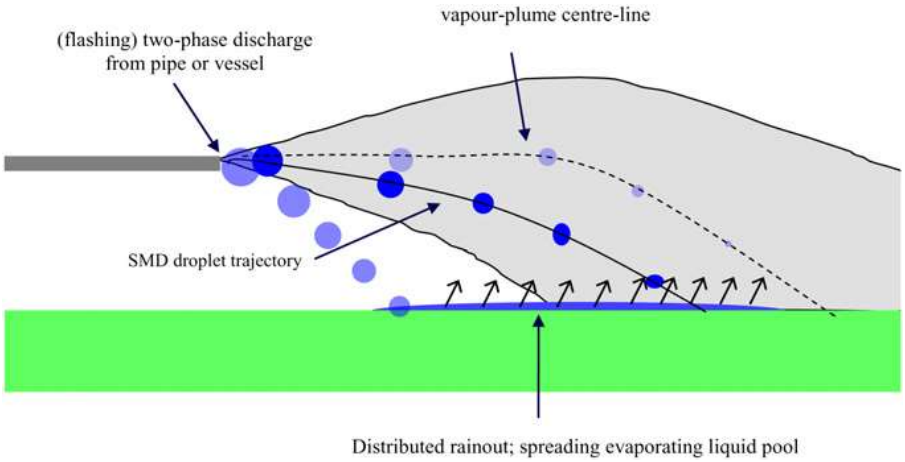

Figure 6.2: *Droplet formation in flashing jet [100]*

Figure 6.3 shows a simplified diagram for the whole experimental set-up. The liquified gas from the pressurised container is moved to the nozzle. The flow is controlled with the flow control valve at the downstream, while it is measured using a flow meter. To achieve the precise control of the jet and the flow of the liquified gas, there is an electric valve that is controlled by an electronic solenoid switch.

The flow is then moved to the nozzle, from where it is sprayed out into the atmosphere. A PDPA sensor is placed just in front of the nozzle to measure the size of the droplets.

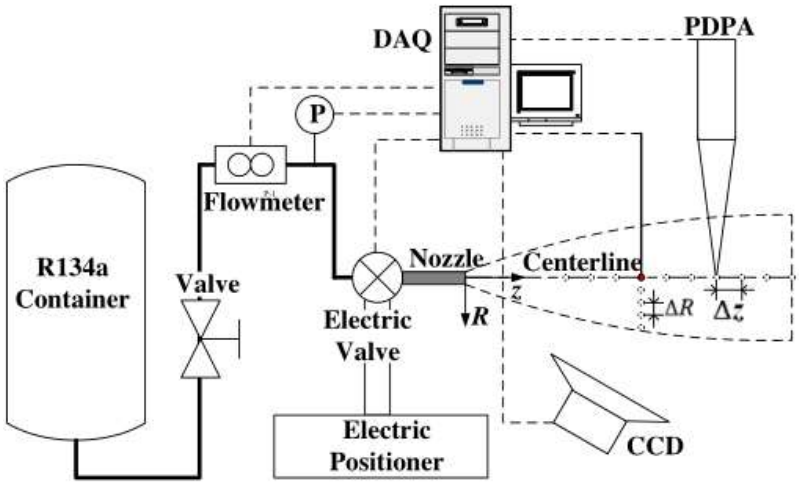

Figure 6.3: *Simplified Experimental setup diagram [106]*

Six experiments were conducted using liquified Butane. The liquid Butane used was 99.5% pure. The experiments were carried out for the study as follows:

1) The experiments were carried out using three different orifice sizes for the nozzle - 5mm, 10mm and 15mm - to understand the effect of changing nozzle size on the properties of the flashing jet i.e., velocity, temperature and pressure.

2) The release pressure was set to three different values i.e., 2 bar, 6 bar and 10 bar. The pressure of the liquified heavy gas has a direct influence on properties such as the velocity and temperature of the flashing jet.
3) Experiments were carried out and the parameters recorded. These parameters include temperature, pressure and velocity.

Table 6.1: *Experimental iterations [100]*

Number of experiment	Orifice diameter (mm)	Release pressure (barg)	Release temperature (C)	PDA axial distances (cm)	PDA resolution d_{max} (μm)
1	5	6	15–26	60	700
2	10	6	26–27	60, 85	800
3	10	10	19–22	60, 85	800
4	15	6	17–21	60, 85	750
5	10	6	9–10	40, 60, 85	750
6	10	2	7–9	40, 60, 85	750

6.4 Comparison with experiments

In this section, we will compare the results obtained through the numerical simulations and experimental observations conducted by Giannissi et. al. [107], Witlox et al. [108]. The experimental set-up used is shown in Figure 6.4(a). It can be seen that the liquefied heavy gas is released from the nozzle at some speed. Just like the present study's simulation, as soon as the jet is released, it is vaporised into a heavy gas dispersion cloud, as shown in Figure 6.4(a). Figure 6.4(b) shows the visualisation of the numerical simulation. It can be seen that the dispersion cloud of the heavy gas jet is similar to the experimental observations obtained by Giannissi et. al. [107], Witlox et al. [108].

Figure 6.4: (a) *Experimental photograph [107.108]*

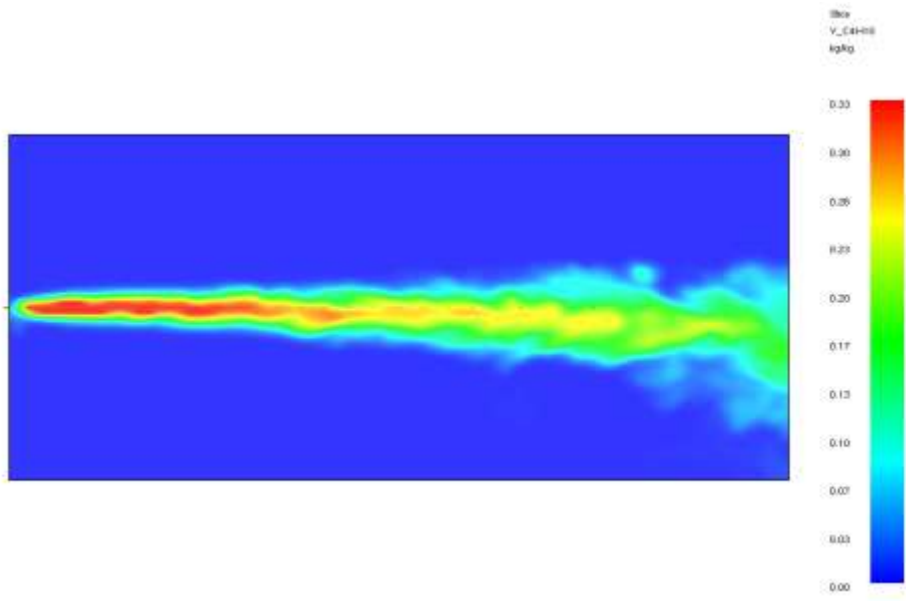

(b) *Visualisation of numerical simulations*

Figure 6.4: *Comparison of experimental observation and numerical simulations*

Now, the results for the temperature, concentration, and velocity obtained through a series of experiments carried out by Giannissi et. al. [107], Witlox et al. [108], will be compared with this study's results, which were obtained by way of numerical simulations in the previous section. The comparison of the numerical and experimental observations is explained as follows:

1) It can be seen in Figure 6.5(a) that the concentration of the flashing jet is highest at the point of release and decreases with the increase in distance from the x-axis. This is in conformity with the results from the numerical simulation, which showed that the concentration is very much dependant on the central x-axis. The red part in the results shows a concentration of 0.41 kJ/kg and the blue part shows a concentration of zero.

2) Figure 6.5(b) shows the temperature distribution in the release of heavy gas jets. It can be seen that the temperature of the jet first decreases and then increases as it moves away from the source of the release. These results also match those of the numerical approach explained in the previous section. The initial decrease in temperature is due to the evaporation of the liquified jet. Then the increase in temperature is due to the environmental effects. The red part shows the area of high temperature (20 °C), while the blue part shows the area of low temperature (-56 °C).

3) Streamwise velocity is shown in Figure 6.5(c). It can be seen that the velocity of the jet decreases as the distance from the source increases. This decrease is due to the

resistance of the surrounding air to the flow of the jet. These experimental results are in conformity with the results obtained through our numerical simulation.

4) Figure 6.5(d) shows the tangential component of the velocity, which decreases as the distance from the source increases. The red colour in the graph shows a high tangential velocity of 2.5 m/s, while the blue colour shows a low velocity of -2.5 m/s. This means that, in the blue parts, the flow is in the backward direction due to the effects of turbulence.

Hence, from the comparison of the results, it can be seen that the results we have obtained through our numerical simulations are matching with the experimental observation carried out through Giannissi and Witlox et al. [107,108].

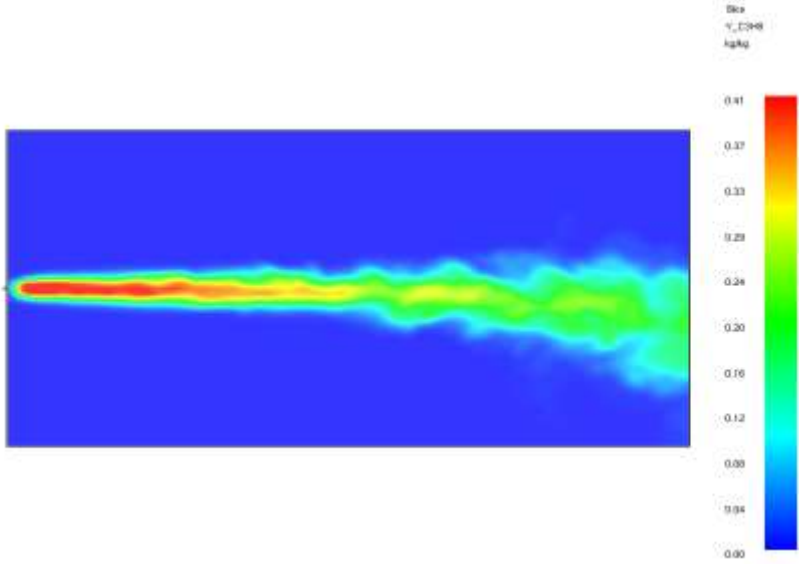

(a) *Concentration*

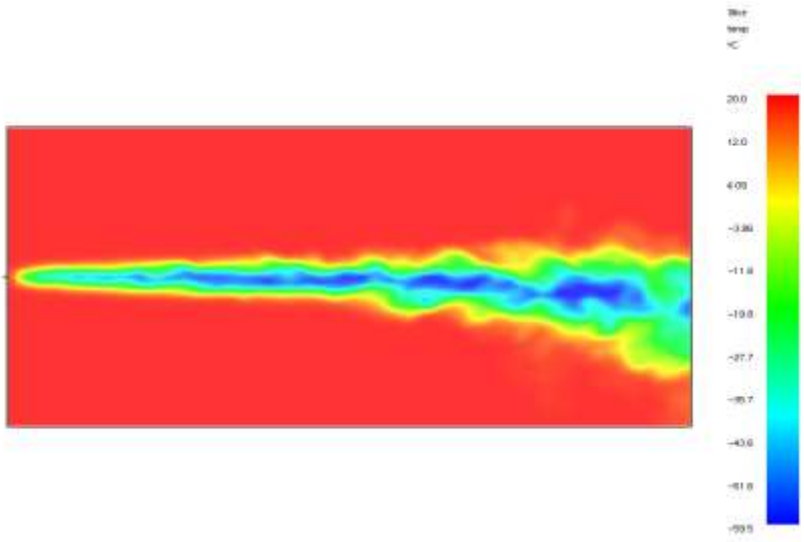

(b)*Temperature*

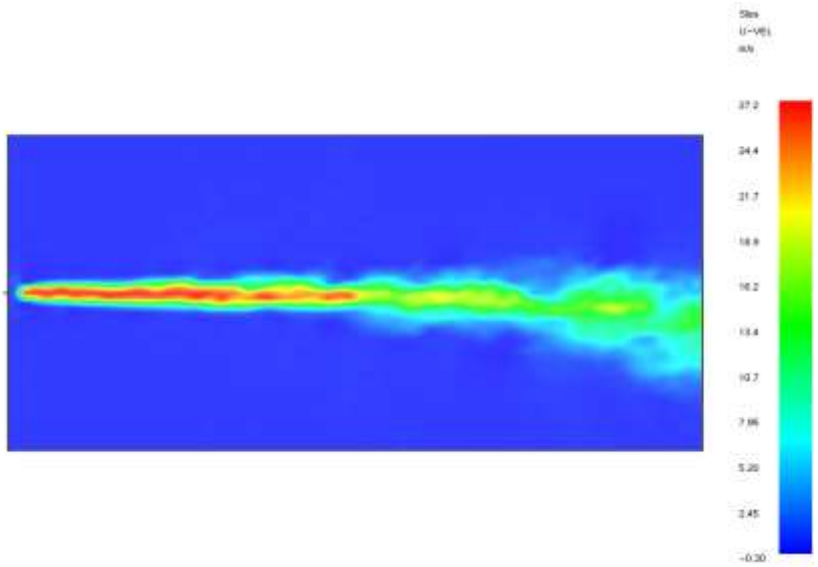

(c) *Streamwise velocity*

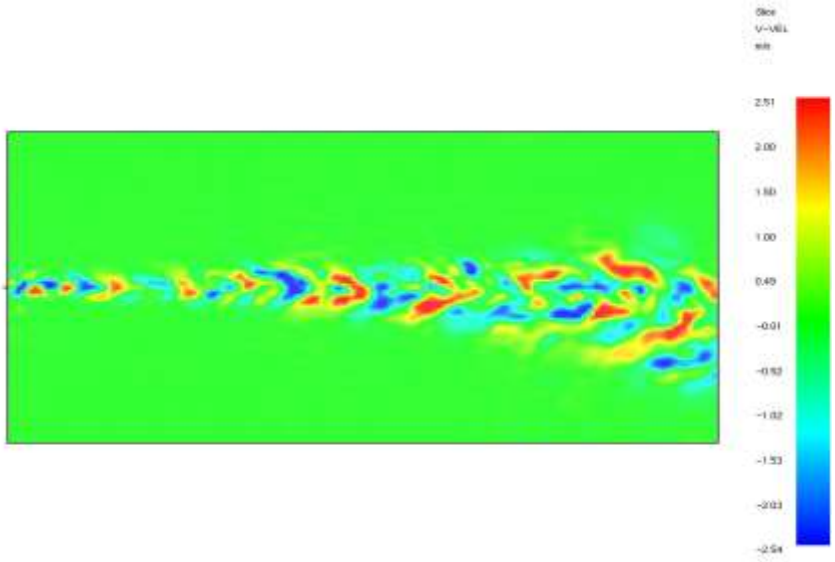

(d) *Tangent velocity*

Figure 6.5: *Visualisation of the flashing jet of propane on the central cross-section*

6.5 Results and discussions

In this section, we will discuss the results obtained from the simulations of the flashing jets released to form a cylinder. This section is divided into two parts, which are as follows:

1) In the first section, to understand the sensitivity of the numerical simulation approach, the results obtained from three mesh sizes will be discussed.
2) In the second section, there will be a detailed discussion on the results obtained using the numerical simulations.

To understand the sensitivity of this study's computational model, the simulation results will be obtained for three mesh sizes, which are taken as 7.5 cm, 5 cm and 2.5 cm. The ambient conditions are kept the same for the three mesh conditions to obtain the sensitivity of the numerical approach.

Figure 6.6. shows the average velocity and temperature for the three mesh sizes (7.5 cm, 5 cm, and 2.5 cm). Figure 6.6(a) shows the following results:

1) The light blue line shows the temperature results for the 2.5 cm mesh. The results show unsymmetrical asymmetrical behaviour of temperature with time.
2) The green line shows the temperature results for the 5 cm mesh. These results also show unsymmetrical behaviour of temperature with time. Nevertheless, this trend is consistent with that of the 2.5 cm mesh.
3) The purple line shows the temperature results for the 7.5 cm mesh. These results also show unsymmetrical behaviour of temperature with time, but this trend matches the above results.

The trend clearly shows that the results become more accurate as the mesh size decreases. However, this costs extra computational time as any increase in the number of elements means an increase in the time required to solve the elements them.

The same is the case for velocities, as shown in Figure 6.6(b), which is explained as follows:

1) The light blue line shows the velocity results for the 2.5 cm mesh. The results show unsymmetrical behaviour of velocity with time.
2) The green line shows the velocity results for the 5 cm mesh. These results also show unsymmetrical behaviour of velocity with time. Nevertheless, this trend is consistent with that of the 2.5 cm mesh.
3) The purple line shows the velocity results for the 7.5 cm mesh. These results also show unsymmetrical behaviour of velocity with time. Nevertheless, this trend is consistent with the above results.

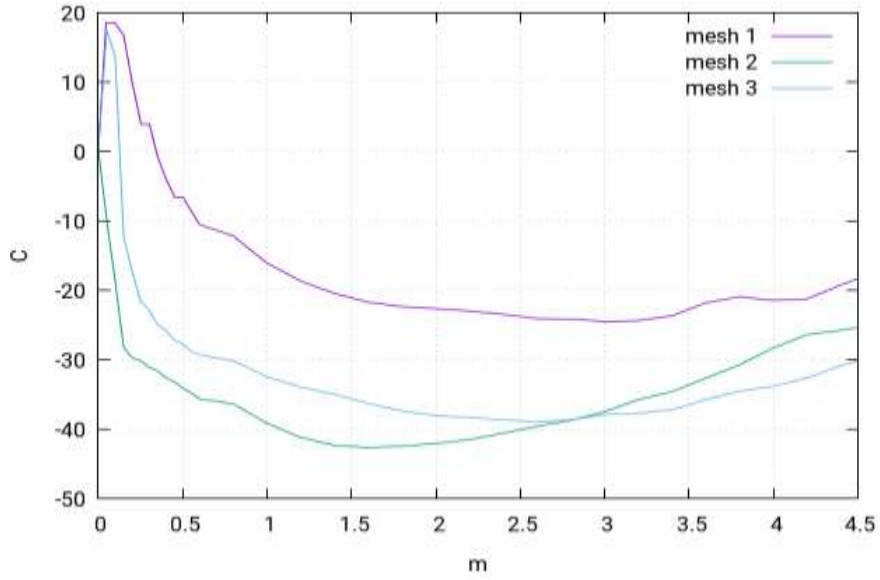

(a) *Average temperature*

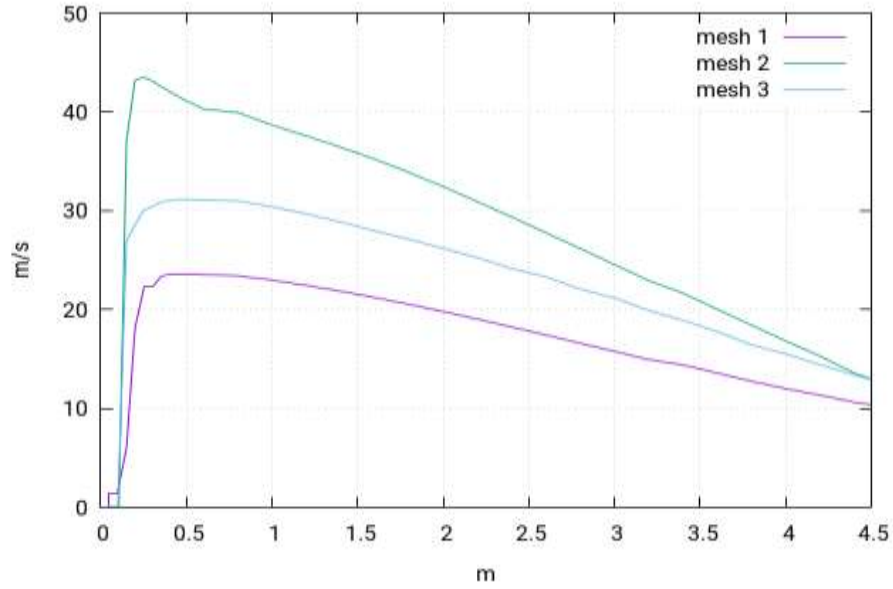

(b) *Average streamwise velocity*

Figure 6.6: *Average temperature and streamwise velocity of the gaseous mixture along the central axis of the jet, produced by three meshes with different cell lengths of 7.5cm, 5cm and 2.5cm*

Figure 6.7 shows the simulation results for the simultaneous temperature and velocity for the 7.5 cm, 5 cm and 2.5 cm meshes. The concept of simultaneous velocity and temperature is applied to somehow obtain a symmetrical pattern for the two parameters.

Figure 6.7(a) shows the simultaneous temperature with respect to time on the x-axis. The graph shows that the temperature of the flashing jet decreases with time. This is because, as the flow is established, the heat is absorbed by the flashing liquid to evaporate into the gaseous form,

and hence the temperature decreases. The same pattern is seen in the three mesh sizes. However, as shown, the results increase in accuracy as the mesh size decreases Witlox et. al. [108].

The case is similar in the case of simultaneous velocity. Simultaneous velocity first increases with time and then becomes constant. In this case too, the same pattern is seen in the three mesh sizes. However, as shown, the results increase in accuracy as the mesh size decreases.

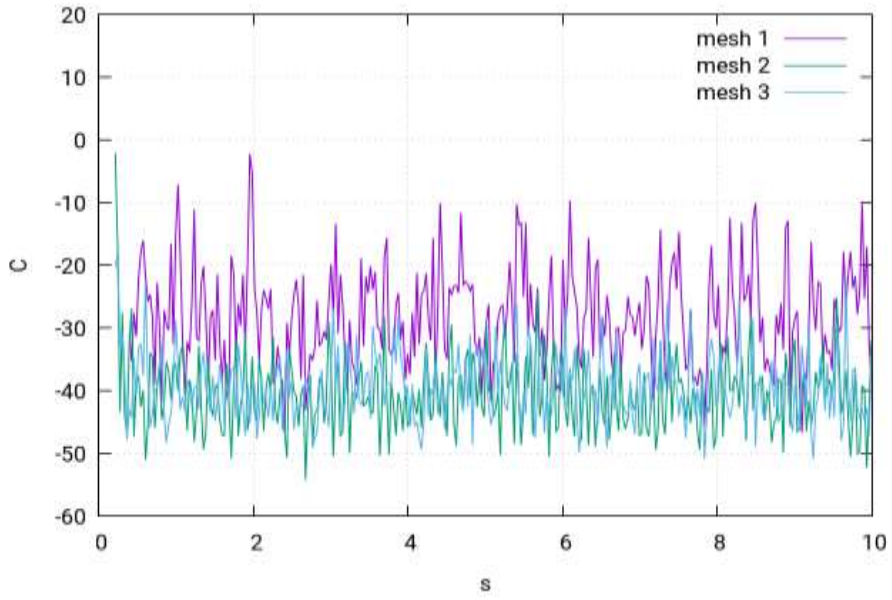

(a) *Simultaneous temperature*

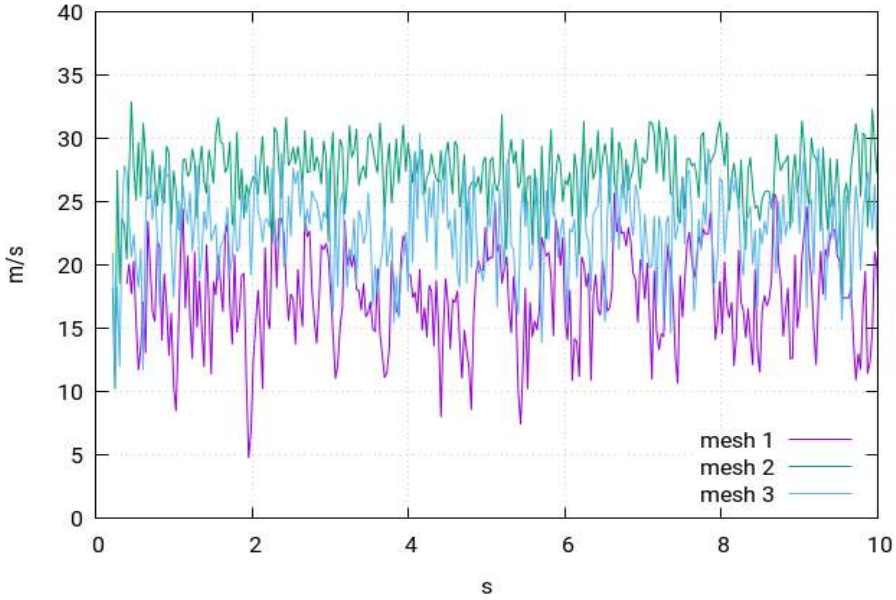

(b) *Simultaneous streamwise velocity*

Figure 6.7: *Simultaneous temperature and streamwise velocity of the gaseous mixture at a distance of 2.5m from the jet orifice produced by three meshes with different cell lengths (mesh 1 – 7.5cm, mesh 2 – 5cm and mesh 3 – 2.5cm)*

There now follows a detailed discussion of the results obtained through the simulations of flashing butane and propane. The properties of the flashing jets ejected from the nozzle are as follows in Table 6.2:

Table 6.2: *Properties of the ejected liquefied propane and butane from the nozzle*

	Propane	Butane
Volumetric flow rate (m^3/s)	22×10^{-4}	22×10^{-4}
Flow velocity (m/s)	45	45
Temperature of the jet (°C)	25	25
Sauter Mean Diameter (μm)	110, 210, 310	110, 210, 310

Sauter mean diameter is actually the mean diameter of the particles ejected from the nozzles. These particles will be explained in detail in the experimental set-up.

The two flashing jets of the liquids showed similar behaviour in terms of velocity, temperature, and concentration. Figure 6.8 shows the simulation results for the concentration, temperature, and axial velocity for the liquefied propane jet. Figure 6.8(a) shows that:

1) The graph in purple shows the concentration of the propane jet along the central domain axis. The graph shows that the concentration of the propane gas decreases as the distance from the source of the release increases on/along the central x-axis.
2) The green line shows the temperature of the propane jet. The trend also shows that the temperature of the propane gas decreases with the increase on/along the central x-axis.
3) The light blue line shows the axial velocity of the flashing propane jet. The graph shows that the velocity also decreases the distance from the source of the release increases.

Figure 6.8(b) shows the magnified version of the three parameters in the central axis range of 0 m to 1 m. The graph clearly shows that:

1) The graph in purple shows the concentration of the propane jet along the central axis of the domain. The graph shows that the concentration of the propane gas first increases with the release of the jet. Then it starts decreasing as it moves further from the source.
2) The green line shows the temperature of the propane jet. The trend also shows that the temperature of the propane gas first increases with a sudden spike and then starts decreasing.
3) The light blue line shows the axial velocity of the flashing propane jet. The graph shows that the velocity also decreases as the distance from the source of the release increases.

This behaviour remains the same. The slope of the decreasing pattern decreases as the distance from the axis increases.

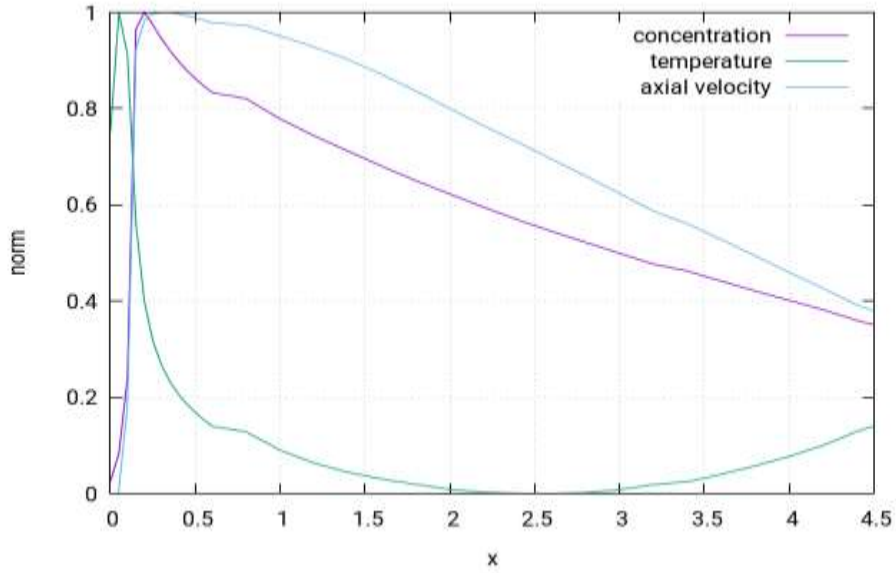

(a) *Normalised profiles of the concentration, temperature and axial direction velocity*

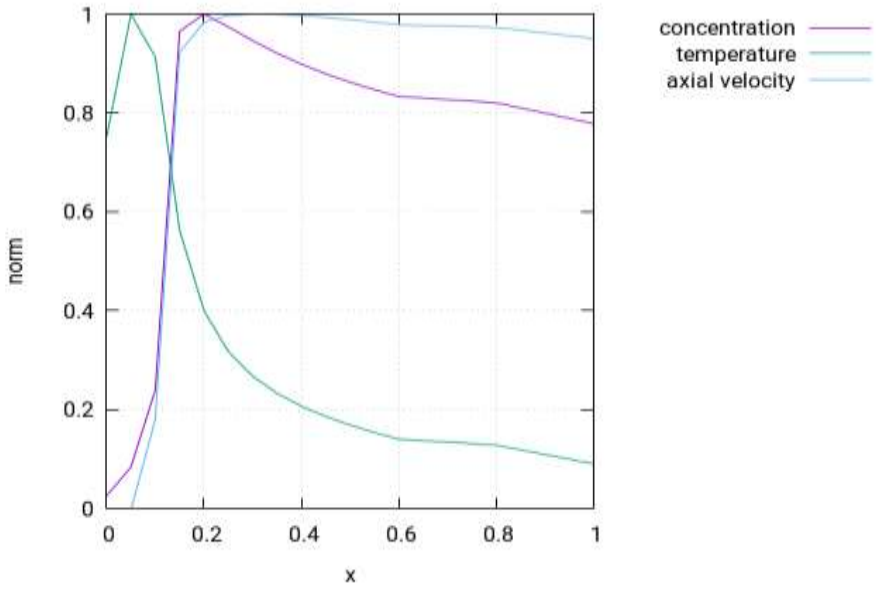

(b) *An amplified diagram to (a) of x from 0 to 1m*

Figure 6.8: *Normalized profiles of the concentration, temperature and axial direction velocity along the central axis of the liquefied propane jet.*

In the next graphs, the dependencies of the average temperature and average concentration on the mean diameter of the nozzle will be shown.

Figure 6.9 shows the graphs obtained from the simulation results, with the distance from the source or cylinder on the x-axis. The results show that:

1) Figure 6.9(a) shows the concentration obtained from the release of propane gas with the mean diameters set at 0.1mm, 0.2mm and 0.3mm.
2) The results clearly show that, as the diameter of the nozzle increases, the area of the nozzle increases and hence the volumetric flow rate of the propane gas increases.
3) This results in increased concentration of the propane gas released.
4) The overall trend of the concentration for the propane jet remains the same i.e., as the distance from the gas source increases, the concentration decreases.

Figure 6.9(b) shows that the temperature of the flashing jet changes as the diameter of the nozzle changes. The summary of the results for this case are explained as follows:

1) It can be seen that the temperature decreases as the nozzle diameter decreases. This is because, as the diameter decreases, the overall flow rate of the flashing gas decreases and hence the temperature decreases.
2) It can be seen that, as the diameter of the nozzle increases, the temperature of the jet also increases.
3) The overall trend of the average temperature is such that, as the distance from the jet source increases, the temperature first decreases and then begins increasing.
4) The first decrease in temperature is due to the flashing of the liquified gas. The increase in temperature is due to the atmospheric temperature.

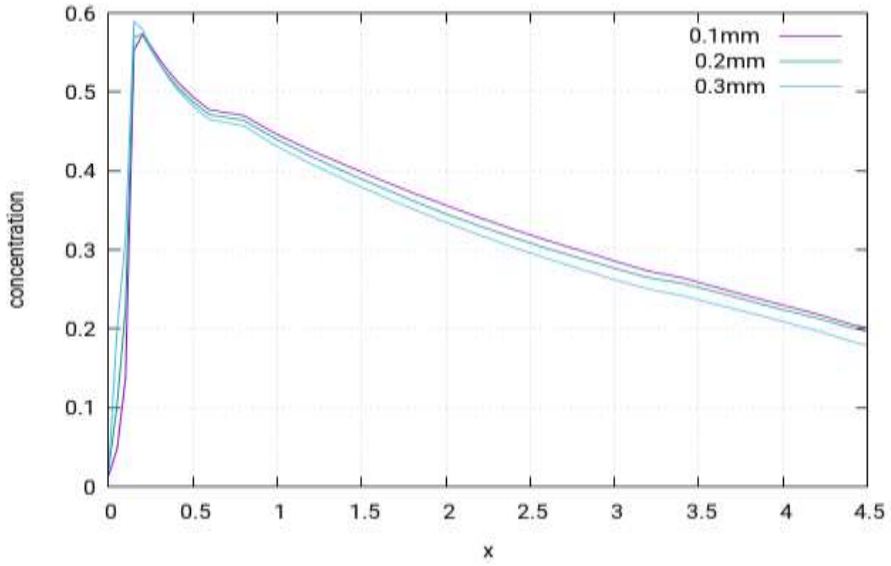

(a) *Average concentration*

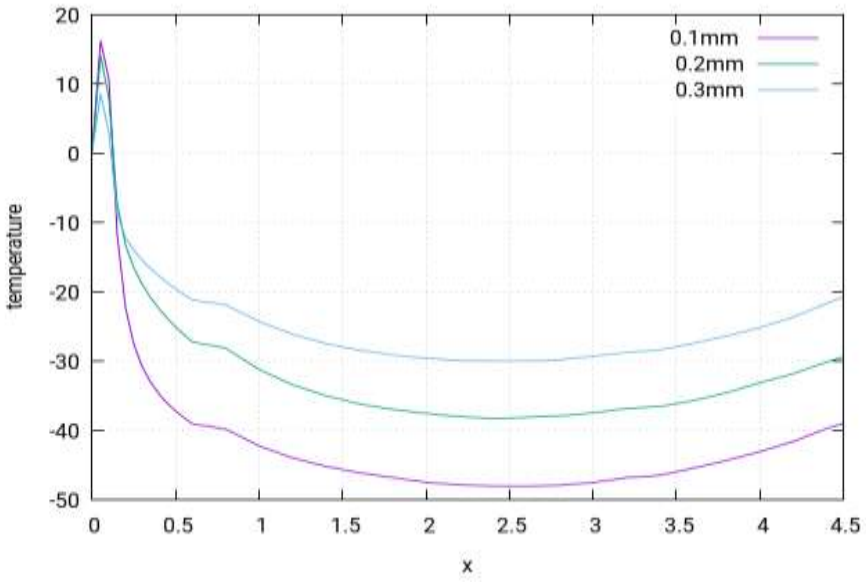

***(b)** Average temperature*

***Figure 6.9:** Comparison of the results with the SMD, 0.1mm, 0.2mm and 0.3mm. The profiles are along the jet central axis.*

Figure 6.10 shows the comparison between simulation results for propane and butane. Propane has a lower molecular mass and is lighter than butane. The molar mass of propane is 44.1 g/mol, while the molar mass of butane is 58.12 g/mol.

1) Figure 6.10(a) shows that the concentration of propane is greater than that of butane. This is because of the molar mass difference. The lighter the molecular mass, the more the evaporation. Hence, the concentration increases.
2) The trend of the concentration is the same for both gases. As the distance from the source increases, the concentration of the heavy jet first increases and then starts decreasing.
3) Figure 6.10(b) shows the temperature trend comparison for propane and butane. The graphs show that the temperature for butane is higher than that for propane. This is also due to the molecular mass of butane, which is higher and hence requires more energy to evaporate. This causes an increase in the temperature of butane.
4) The overall trend of propane and butane remains the same; with the increase in the distance from the release source, the temperature first decreases and then starts increasing.

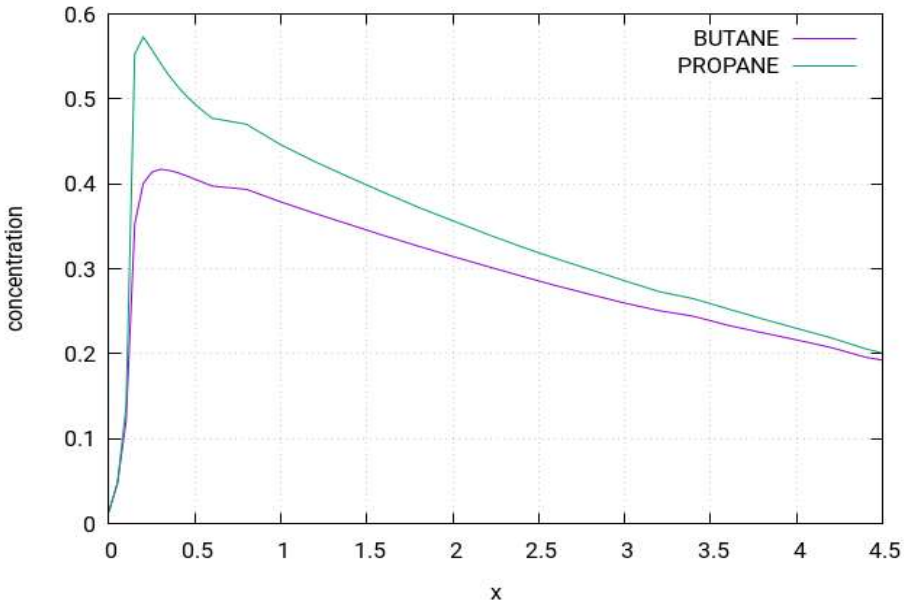

(a) *Average concentration*

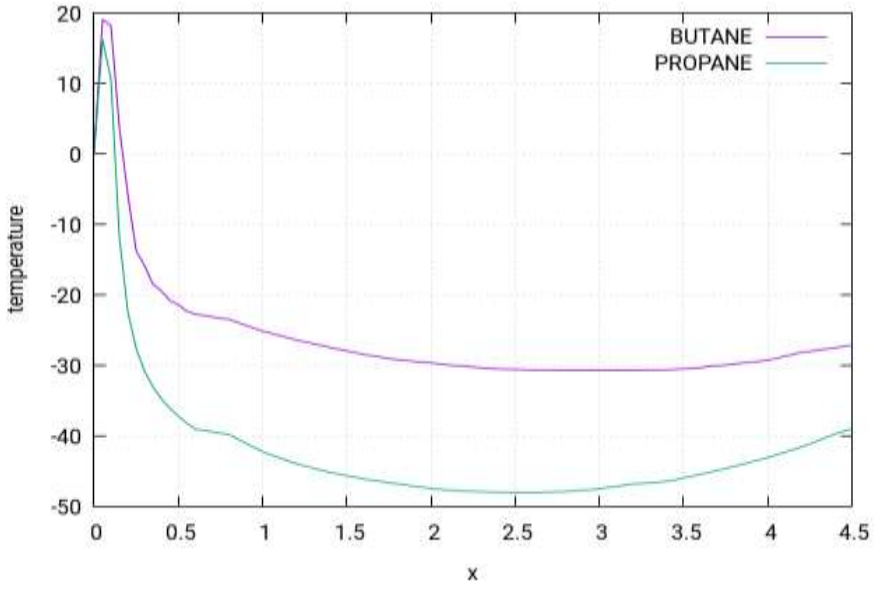

(b) *Average temperature*

Figure 6.10: *Comparison of the results of the liquefied propane and butane jets. The profiles are along the jet central axis.*

6.6 Summary

In this study, the behaviour of the flashing jet of heavy gas (butane) has been studied. A series of 5 experiments with changing parameters was conducted to understand the properties of the liquefied heavy gas released through the nozzle. It was found that the liquified gas, when flashed through the nozzle, is not completely vaporised and a small droplet of the liquid remains suspended in the vapours. These droplets may fall to the ground and form a small pool of heavy

liquid, which may evaporate over time and hence can cause greater damage and long-term damage to the environment.

The properties of the flashing jet studied in this work are as follows:

1) Concentration – It was seen that the concentration of the flashing jet is greatest at the point of release and that it decreases as the distance from the x-axis decreases.
2) Temperature – It was seen that the temperature of the flashing jet, when released from the source first, decreases due to the evaporation and then starts increasing. On page 110, it is mentioned that "1) Temperature – It is seen that the temperature of the flashing jet, when released from the source, first decreases due to evaporation and then starts increasing. This is because the jet flow is always entraining the ambient air with high temperature into the jet core. Therefore, after some point the gas temperature must increase. Our computations find that the location after which the temperature increases is at about 3.5m. This is the reason why the temperature slowly increases from 3.5m to 4.5m as shown in above figures 6.9(b) and 6.10(b).
3) Velocity – The velocity of the flashing jet gas was seen to decrease in accordance to the distance from the nozzle. This is due to the frictional effects of the atmospheric air.
4) Pressure – The pressure of the flashing jet also decreases with the distance as the flashing jet gets saturated with the atmospheric air.

These properties tend to change with changes the diameter of the nozzle of the cylinder. When the nozzle of the smaller diameter was used, the flow rate of the jet decreased. This caused the temperature to increase as there was a lower flow rate and less evaporation heat absorption. The velocity trend remained the same.

A similar study was also conducted using an advanced fire dynamic simulator (FDS) to verify these results. The study found a similar pattern in the properties. There were small deviations in the results obtained by way of the numerical simulations and experimental observations. This was due to the variable conditions of the atmosphere when experiments were performed.

Chapter 7 Effects of Obstacles on Heavy Gas Dispersion

7.1 Introduction

Flammable petroleum gas mainly consists of hydrocarbon gases. Currently, it is widely used as a fuel because of its flammable properties and other advantages, such as releasing less carbon dioxide and other pollutants per unit energy than the other solid or liquid fuels. The transportation, storage and application of the gas are critical because of its flammable properties, and any mistake in this regard could cause serious damage. It is, therefore, of great importance to take the necessary steps to avoid gas leakage, as well as the associated losses and damage in terms of the economy and human health. The name dense or heavy gas is given to petroleum gas because it is heavier than the ambient air. If the gas is leaked into the atmosphere, a heavy gas cloud, combustible in nature, will form. Such a gas cloud is at high risk of fire or explosion and producing harmful environmental pollutants. Although heavy gases are handled with extreme care, fires and explosions are a recurrent phenomenon. It is, therefore, of utmost importance to study the dispersion of leaked heavy gases and the formation of heavy gas clouds, so that a better approach can be followed to avoid these catastrophes.

The present work aims to investigate and discuss the effects of obstacles on heavy and neutral gas dispersion. Previous studies have found out that the obstacles could play an important role in the cloud shape formation of heavy gas dispersion. Therefore, in this work, simulation is performed based on a similar set-up as that of experiments and the results are analysed. After obtaining the results, the profiles are compared with previous experimental results from Zilitinkevich et. al. [109], Kevin et. al. [84]. Moreover, the major hazardous zones for the specific layouts are categorised on the basis of hazardous area classification (HAC) Standard BS EN 60079-10-1:2009 Santon el. al. [104].

7.2 CFD simulations set-up

For modelling the behaviour of obstacles on dense or heavy and neutral gases, this investigation has five scenarios for two kinds of gases, which examine five different possibilities spanning the spectrum of gas dispersion. This experiment is modelled for each condition, and the simulation is observed in ANSYS-CFX. Since these experiments have been performed in EDF-ECL atmospheric wind tunnel experiments by other researchers, the findings are not only intuitive but are also useful for gaining a deeper understanding of the behaviour of the plume

under various conditions, which are typical of real-life scenarios. The five scenarios are presented in the following sections:

In **scenario 1A,** the heavy gas leak occurs from a circular source that is 50mm in diameter. The terrain is flat, and the gas has a discharge velocity of 1 m/s. The density of the gas is 2.1, and the temperature of the gas at the source is -100°C. On the outside, the ambient temperature is 25°C. For this setting, the pressure is zero, and there are no obstacles, such as solid or semi-circular fences.

In **scenario 1B,** the neutral gas leak occurs from a circular source 50mm in diameter. The terrain is flat, and the gas has a discharge velocity of 1.7737 m/s. The density of the gas is 1.1839, and the temperature of the gas at the source is 25°C. Externally, the ambient temperature is 25°C. For this setting, the pressure is zero, and there are no obstacles, such as solid or semi-circular fences.

In **scenario 2A,** the heavy gas leaks from a circular source with a 50mm diameter. The source has a discharge velocity of 1 m/s, and the gas density is 2.1. The temperature of the gas at the source is 25°C, while the ambient temperature is 25°C. The terrain is flat, but there is a solid fence, which is 400mm downstream of the plume and has a height of 30mm.

In **scenario 2B,** the neutral gas leaks from a circular source of 50mm in diameter. The source has a discharge velocity of 1.7737 m/s, and the gas density is 1.1839. The temperature of the gas at the source is 25°C, while the ambient temperature is 25°C. The terrain is flat, but there is a solid fence, which is 400mm downstream of the plume and has a height of 30mm.

In **scenario 3A,** the heavy gas leak occurs from a circular source, which is 50mm in diameter. The discharge velocity at the source is 1 m/s and the temperature of the source gas is -100°C. The cloud has a density of 2.1. The ambient temperature is 25°C. There are two obstacles to the plume in the form of fences, which are 400mm downstream from the source. The solid fence has a height of 30mm, and the semi-circular fence has a height of 30mm.

In **scenario 3B,** the neutral gas leak occurs from a circular source, which is 50mm in diameter. The discharge velocity at the source is 1.7737 m/s and the temperature of the source gas is 25°C. The cloud has a density of 1.1839. The ambient temperature is 25°C. There are two obstacles for the plume in the form of fences, which are 400mm downstream from the source. The solid fence has a height of 30mm, and the semi-circular fence has a height of 30mm.

In **scenario 4A,** the heavy gas leak occurs from a circular source with a diameter of 50mm. The terrain is flat, and has a discharge velocity of 1 m/s. The density of the gas is 2.1, and the

temperature of the gas is -100°C. The ambient temperature is 25°C. There is one obstacle in the form of a fence, which is 400 mm downstream from the source. The solid fence is 60mm high.

In **scenario 4B,** the neutral gas leak occurs from a circular source with a diameter of 50mm. The terrain is flat, and has a discharge velocity of 1.7737 m/s. The density of the gas is 1.1839, and the temperature of the gas is 25°C. The ambient temperature is 25°C. There is one obstacle in the form of a fence, which is 400mm downstream from the source. The solid fence is 60mm high.

In **scenario 5A,** the heavy gas leak occurs from a circular opening having a 50mm diameter. The source gas has a velocity of 1 m/s, and a density of 2.1. The temperature of the gas is -100°C, while the ambient temperature is 25°C. For this case, there are two solid obstacles, which are 400mm downstream from the source. One of the solid fences stands at a height of 60mm, while the second obstacle, a semi-circular fence, has a height of 30mm.

In **scenario 5B**, the neutral gas leak occurs from a circular opening having a 50mm diameter. The source gas has a velocity of 1.7737 m/s, and a density of 1.1839. The temperature of the gas is 25°C, while the ambient temperature is 25°C. For this case, there are two solid obstacles, which are 400mm downstream from the source. One of the solid fences stands at a height of 60mm, while the second obstacle, a semi-circular fence, has a height of 30mm.

The set-up for the computational domain is as follows: The dimension is 4m × 2m × 0.6m respectively along the x, y and z coordinate axes. The numerical simulation is small-scale. The source point has the dimensions -0.25 × 1 × 0. There are two different obstacles, which are a solid fence at 400mm downstream from the source point of 2 m cross-section × 30 mm height, and a semi-circular fence of height 30 mm. In addition, the solid fence has 2 m cross-section × 60mm height. The semi-circular fence has a height of 30 mm. The fine elements have a length of 0.02m. Overall, the number of elements is under 10 million. A wind inlet boundary condition is included on the left-hand side of the domain, while the right-hand side has an outlet boundary. This configuration is the same as the experimental set-up of Ayrault et. al. [101, 102] so that the simulated results can be compared with it. To investigate the influences of obstacles on heavy gas dispersions, a computationally geometric configuration is designed as per (Figure 7.1).

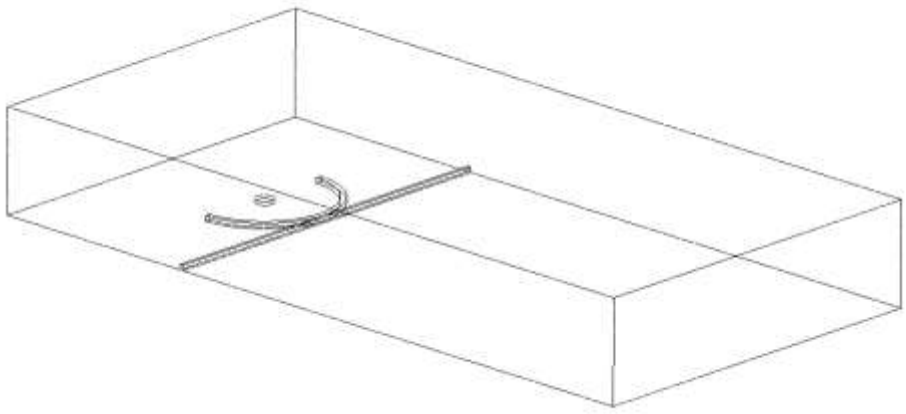

Figure 7.1: *Computational domain and obstacle arrangements*

An unstructured mesh is generated over the computational domain of Figure 7.1. This mesh is comprised of the hexahedral-dominant elements of approximately 3 million.

The ambient air has a standard atmospheric condition, i.e., its temperature is 25°C and the pressure is 101.3 kPa.

The leakage source is at the centre of the semi-circular fence. It is a small cylinder of 0.05m diameter and 0.02m height. The heavy gas leaks from its top face. The leaked gas velocity is 1.0m/s. The density and temperature of the gas are 2.1kg/m³ and -100°C.

A wind inlet boundary condition is applied on the left-hand side of the domain, while the right-hand side has an outlet boundary. The symmetrical boundary condition is applied to the other boundaries.

All the simulations were done in a HP- High Performance computer in the university lab. The computational time for 1 simulation was almost 3 days.

7.3 Ayrault et. al.'s experimental set-up

The effect of obstacles on heavy gas dispersion was studied experimentally by Ayrault et. al. [101,102]. The experimental technique used visualisations and digital image processing to study the effects of the obstacles on the dispersion of heavy gas clouds. An EDF-ECL atmospheric wind-tunnel was used to carry out the experiments. At the entrance of the wind-tunnel section, by using a porous fence, a neutrally stratified boundary layer on a flat floor was created. Laser tomography visualisations were made for both the vertical plane and the horizontal plane. The experimental set-up can be better explained with the help of the following figures:

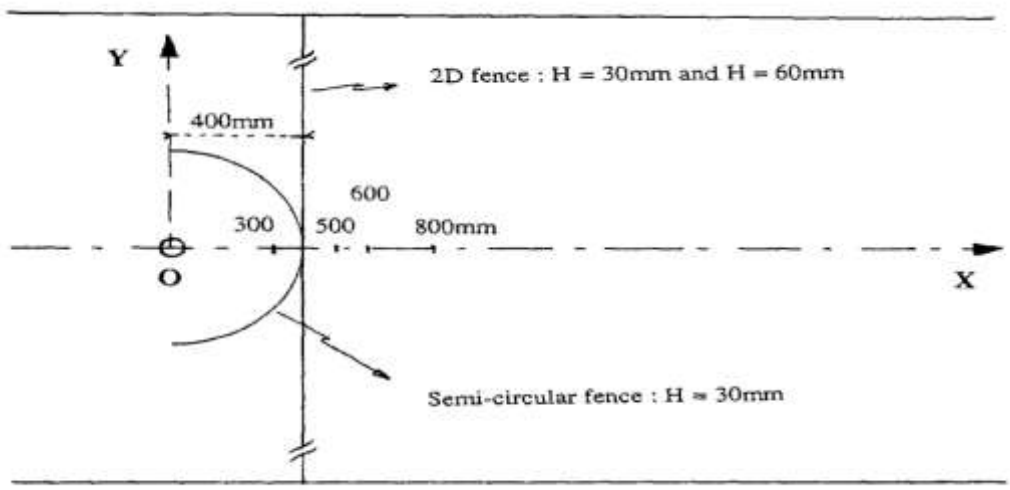

Figure 7.2: *The plane view of the source and the different fences by Ayrault et. al. [102]*

Figure 7.2 shows the schematic plan view of the source and the different fences. There is a release source at the origin at 400mm from the release source (origin) there is a solid fence as an obstacle. Since this is a two-dimensional figure, the solid fence appears as a line. The height of the fence is 30mm and is replaced by a fence of 60mm during the experiments to study the effect of the enhanced height of the solid fence as an obstacle. Beside the solid fence, there is a semi-circular fence, which appears to be tangent to the solid fence, with the centre of the fence corresponding to the area source centre. The height of the semi-circular fence is 30mm. In Figure 7.2, the longitudinal axis OX and the vertical axis is OZ. The important perimeters from the experiment to be mentioned are a volumetric gas release rate of q_0= 183 × 10 -6 m^3/s, source gas discharge velocity; w_s= 0.10m/s, a density of 2.1, modified gravity 10.8 m/s^2 and the buoyancy flux parameter of approximately 2 × 10 s m^4 s^{-3}.

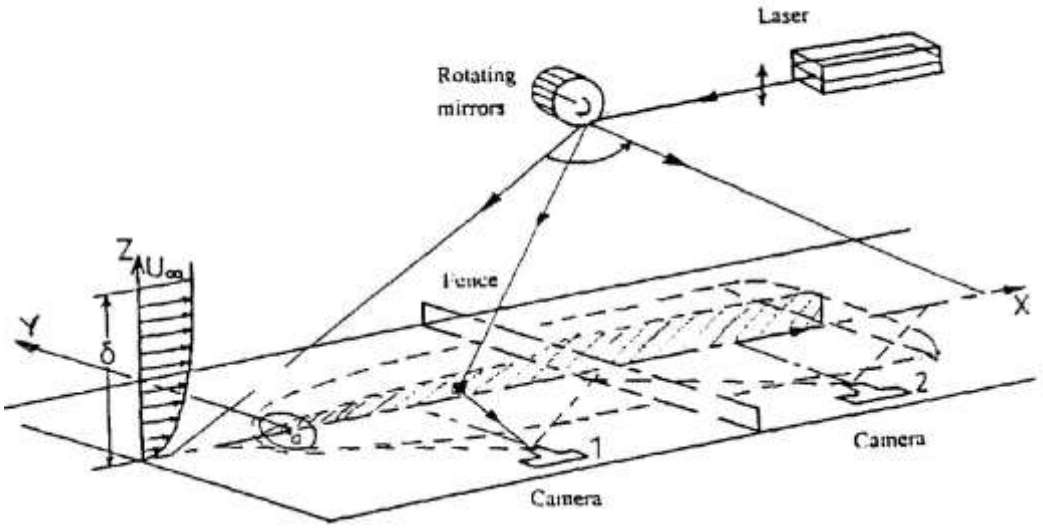

Figure 7.3: *Experimental set-up by Ayrault et. al. [102]*

Figure 7.3 shows the experimental setup for the study. For the two different planes, laser tomography visualisations were made to study the effect of the obstacles on the dispersion. The visualisations were performed for the vertical plane on the longitudinal axis (y = 0) and a horizontal plane situated 8 mm above the floor, as shown in Figure 7.2. A 5-W argon laser beam deflected by a set of 12 rotating mirrors was used to generate a 2-ram thick light plane. The mirror's rotation frequency was set to 50 Hz. Before being released into the flow, the dense gas was seeded with fine particles of incense, the mean diameter was 0.8mm and the standard deviation was 0.2 μm.

Using this experimental set-up, the effects of obstacles on heavy gas dispersions were studied and the results were captured using the cameras as shown in the experimental set-up (Figure 7.4).

7.4 Comparison with experiments

The following two figures show a comparison of the experimental and simulation results. Figure 7.4 shows the results from the simulation performed in this work, while Figure 7.5 shows the results acquired from the experiment performed by Heidorn et. al. [103].

7.4.1 CFD simulation compared with experimental results

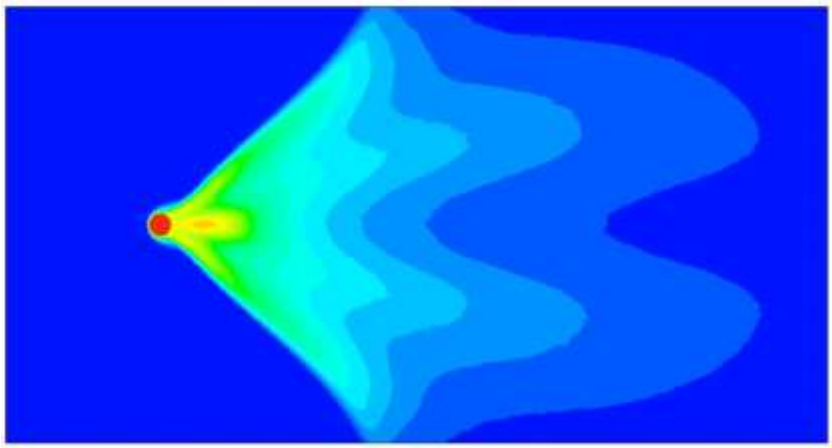

Figure 7.4: *Numerical simulation of concentration profile for heavy gas dispersion without obstacles*

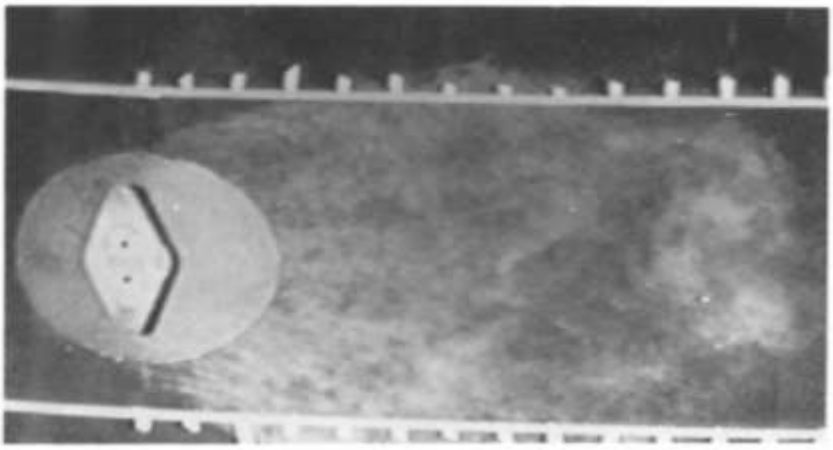

Figure 7.5: *Cloud spread without obstacles at low winds, experiment conducted by Heidorn et. al. [103]*

When both sets of results are compared, it can be seen that the present study's simulation results show a symmetric concertation of the gas cloud as seen in Figure 7.5, whereas the experimental results show asymmetrical (more concentrated lower half) behaviour of the cloud. The overall profile appears to be the same, but it is noted that, since the simulation is performed at 1m/s velocity, it has clearly influenced the cloud shape, which resulted in such a difference.

7.4.2 CFX simulation compared with FDS simulation results

Here, there is a comparison of two simulation methods used to study the dispersion of heavy gas.

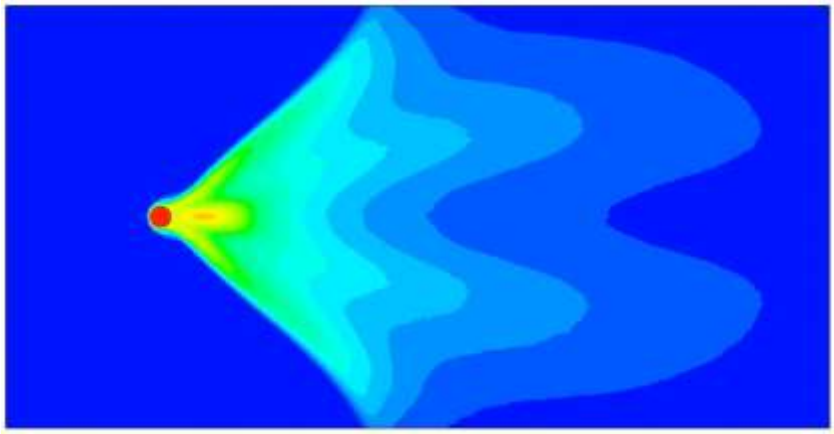

Figure 7.6: *ANSYS-CFX simulation of concentration profile for heavy gas dispersion without obstacles*

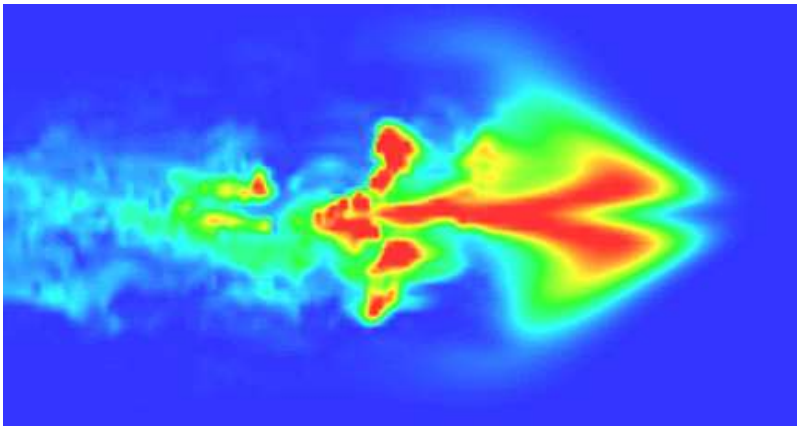

Figure 7.7: *FDS simulation of concentrations for the heavy gas dispersion*

Figure 7.7 shows the results of the simulation, which were obtained by way of the numerical simulation in the present work, while Figure 7.7 shows the results from a/the fire dynamics simulation (FDS). Both sets of results were produced by way of a computer-based simulation using Ansys-CFX tools are used. The results in Figure 7.7 were obtained through a/the fire dynamics simulation (FDS). When the results of both of these simulations are compared, it can be observed that both show that the flow in the heavy gas dispersion presents a pattern of double bubbles, but the concentration values are different. Figure 6 shows a remarkably symmetrical behaviour of the cloud spread, unlike the FDS simulation shown in Figure 7.7. In both figures, the maximum concentrations are shown in red, which leads to the second difference in the results as per the present study's results (Figure 7.6), where the maximum concentration is only at the release source. Figure 7.7, meanwhile, shows many different areas of high concentrations (shown in red). The present work shows that the concentration decreases steadily across the horizontal, but the FDS simulation produces different areas of high and low concentrations.

7.4.3 CFX simulation compared with FDS simulation results

The comparison between two computer simulations for heavy gases was discussed above. Below is a comparison of two simulation methods used to study the dispersion of neutral gas.

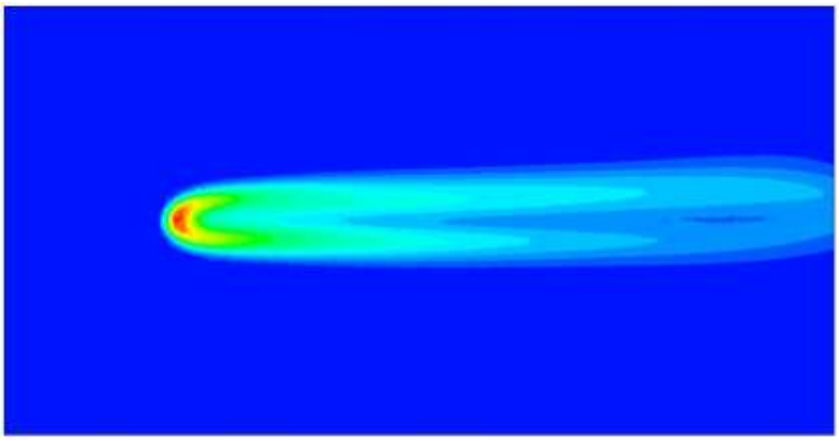

Figure 7.8: *ANSYS-CFX simulation of concentration profile for neutral gas dispersion without obstacles*

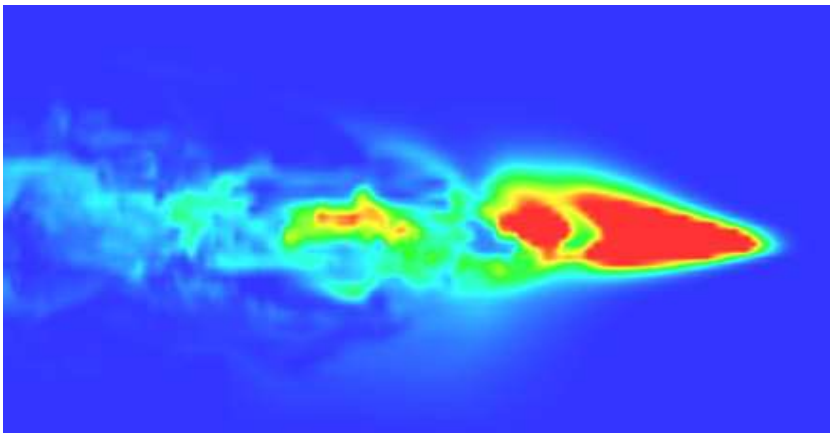

Figure 7.9: *FDS simulation of concentrations for the neutral gas dispersion*

The results obtained by way of the numerical simulation in the present work are shown in Figure 7.8, while Figure 7.9 shows the results from the FDS. Both sets of results were produced using a computer-based simulation, where Ansys-CFX tools were selected to perform the simulation. Meanwhile, the results in Figure 7.9 were obtained by way of the FDS. The first difference that can be observed in the results is that the cloud shape obtained in the present study's simulation shows a pattern of double bubbles, while that of FDS shows a pattern of a single bubble. Similar to heavy gas, the maximum concentration for neutral gas in the present work is only present at the release source, where FDS identifies the far-right end in the horizontal as the most concentrated area, also showing a couple other concentration areas. The spread of gas clouds differs between the two sets of results.

7.4.4 CFD simulation compared with experimental results

The following comparison has been carried out to compare the results of the numerical simulation and the experimental results. In the following figures, Figure 7.10 represents the numerical simulation of the concentration profile for heavy gas dispersion with a straight solid

fence at a height of 30mm as an obstacle, while Figure 7.11 represents the Cloud spread at a single solid fence downwind with a low-velocity experiment conducted by Heidorn et. al. [103].

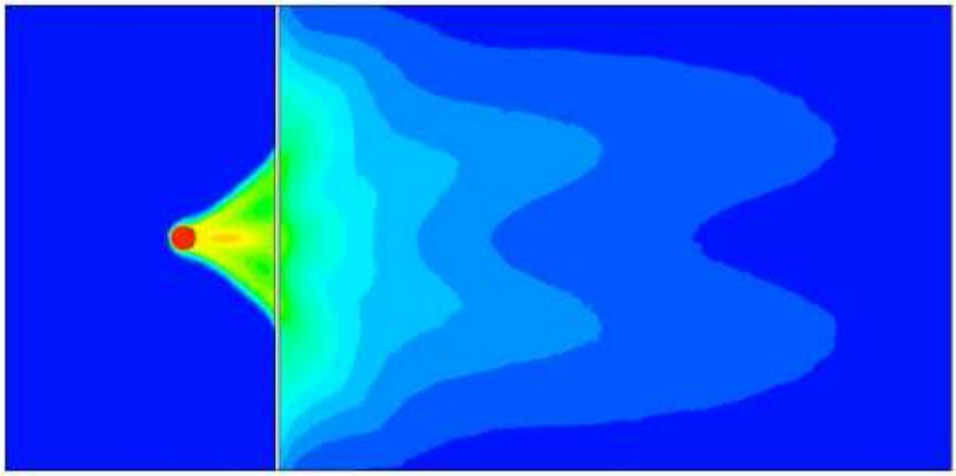

Figure 7.10: *Numerical simulation of concentration profile for heavy gas dispersion without obstacles*

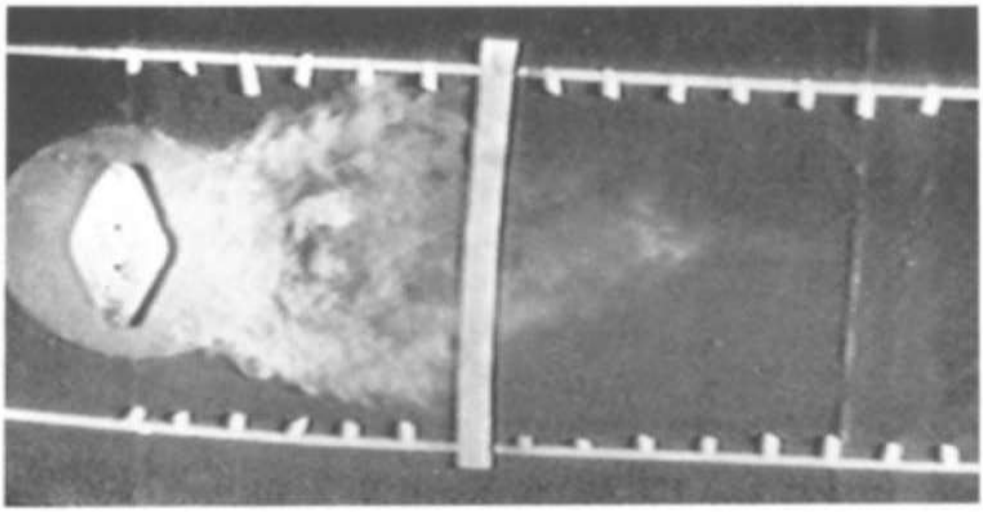

Figure 7.11: *Cloud spread without obstacles and with low winds, experiment conducted by Heidorn et. al. [103]*

In comparison between the CFD numerical simulation and the experimental results of Heidorn et al. [103]. both the numerical simulation and the experimental results were obtained with the inclusion of a 30mm solid fence as an obstacle. While this is a common aspect between the two, it should be noted that the experimental results were produced with a velocity of 7.4m/s, while the simulation was carried out at a much lower wind speed of 1m/s. Therefore, the numerical simulation shows a remarkably symmetrical profile for the concentration, while the experimental set-up shows an asymmetric profile. In Figure 7.10 it can be seen that the numerical simulation shows a highly concentrated area near the inner central area of the fence, but the experimental results show a relatively less concentrated behaviour in that area. The

difference between both may be due to the difference of the perimeters and error in the experimental implementation.

7.4.5 CFD simulation compared with experimental results

This comparison has been carried out to compare the results of the numerical simulation and the experimental results. In the following figures, Figure 7.12 represents the numerical simulation of concentration profile for heavy gas dispersion with a straight solid fence at a height of 30mm as an obstacle, while Figure 7.13 represents the cloud spread at a single solid fence in an experiment by Ayrault et. al. [101,102].

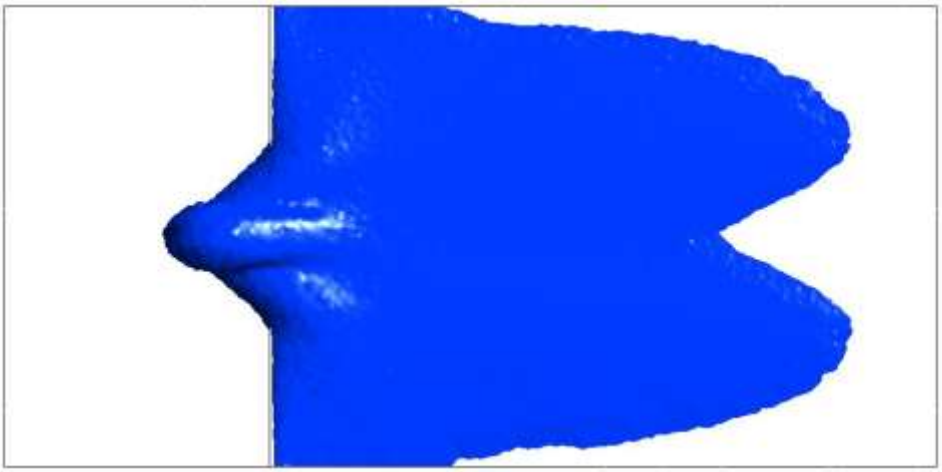

Figure 7.12: *Numerical simulation of Iso-surface concentration profile for heavy gas dispersion with a straight solid fence at a height of* ***30mm*** *as an obstacle*

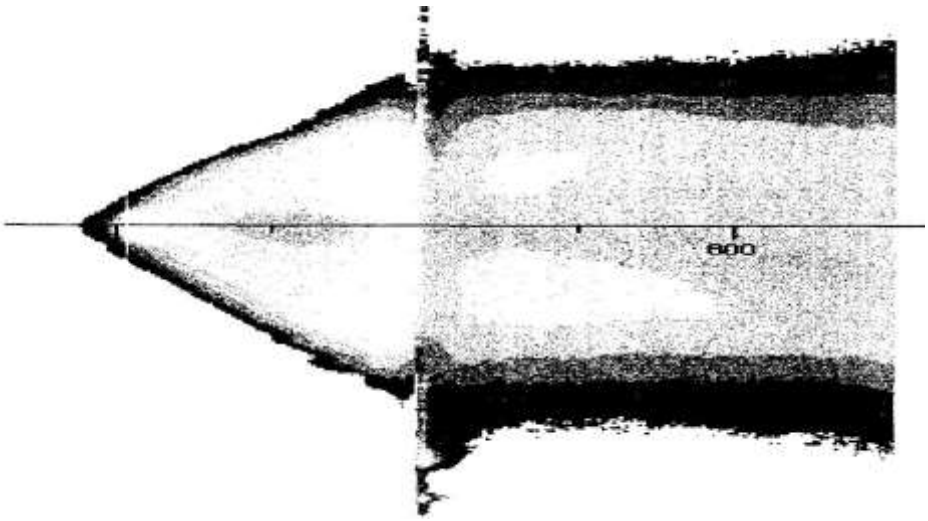

Figure 7.13: *Experiment measurement of concentration profile for heavy gas dispersion with a straight solid fence at a height of* ***30mm*** *as an obstacle Ayrault et. al. [102]*

This tells quite a different story of the comparison between the numerical simulation and the experimental results. While in the above experiments, due to the difference in perimeters and

a high-velocity difference, there was an observable difference in the concentration profile of the numerical simulation and the experimental set-up, here the numerical simulation and experimental results are largely in agreement with each other. Although the sinusoidal finishing to the profile at the right end is not visible in the experimental result, it can be seen how, in both the cases, the cloud spreads in a triangular pattern initially, and upon reaching the obstacle, it surrounds the whole obstacle and then starts a new phase of dispersion after the obstacle. This is somewhat similar to what can be seen in Figures 7.12 and 7.13 above.

7.4.6 CFX simulation compared with FDS simulation results

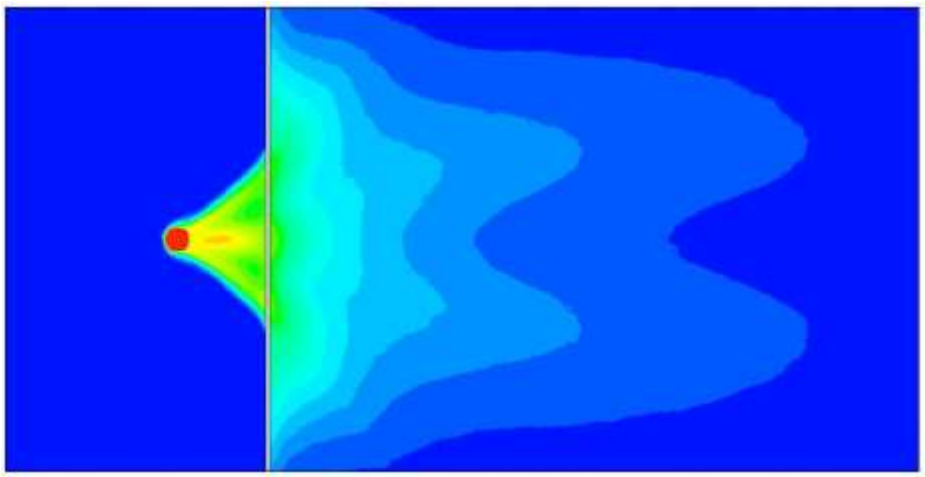

Figure 7.14: *ANSYS-CFX simulation of concentration profile for heavy gas dispersion with a straight solid fence an obstacle*

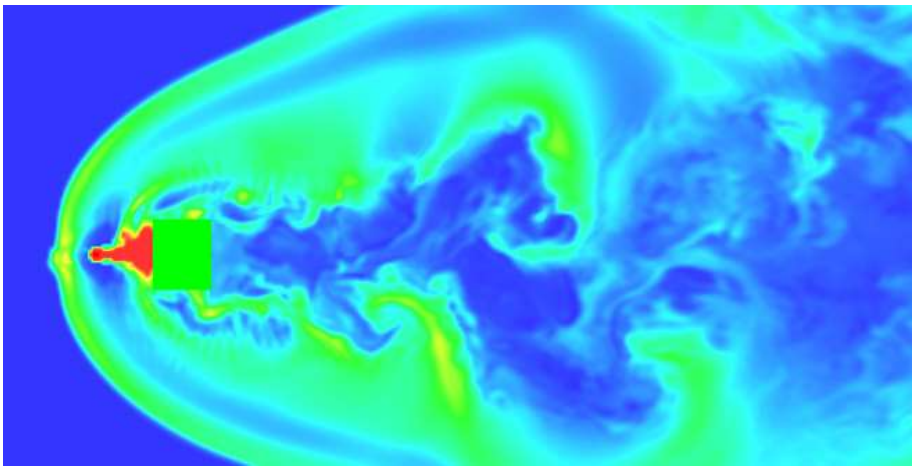

Figure 7.15: *FDS simulation of concentration profile for heavy gas dispersion around a single obstacle*

The above figures show the results of our which were obtained by way of the numerical simulation in the present work. Figure 7.15 shows the results from the FDS. Both sets of results were produced using a computer-based simulation where Ansys-CFX tools were chosen. The results in Figure 7.14 were obtained by way of the FDS. These simulations show the results of

the concentration profile for heavy gas dispersion with a straight solid fence as an obstacle. Here, the triangular shaped high concentration area from the release source to the fence is identified by both simulations. However, the FDS (Figure 7.15) treats it as an area of high concentration (shown by red), while this study's simulation (Figure 7.14) shows only the release source area as highly concentrated. The triangular shape is identified as slightly less concentrated, unlike in the FDS, which shows it as highly concentrated. The results obtained from this study's simulation show that the cloud shape is symmetrical throughout, while the FDS shows it as an asymmetric distribution. The FDS results show a very widely spread cloud dispersion of the heavy gas, while the results of this study's simulation show a very steadily distributed relatively less spread distribution.

7.4.7 CFD simulation compared with experimental results

The following comparison has been carried out to compare the results of the numerical simulation and the experimental results. In the following figures, Figure 7.16 represents the numerical simulation of concentration profile for heavy gas dispersion with a straight solid fence at a height of 30mm and a semi-circular fence with a height of 30mm as an obstacle while the Figure 7.17 shows the mean concentration image for dense or heavy plumes downwind of the semi-circular fence in the experiment conducted by Ayrault et. al. [101,102].

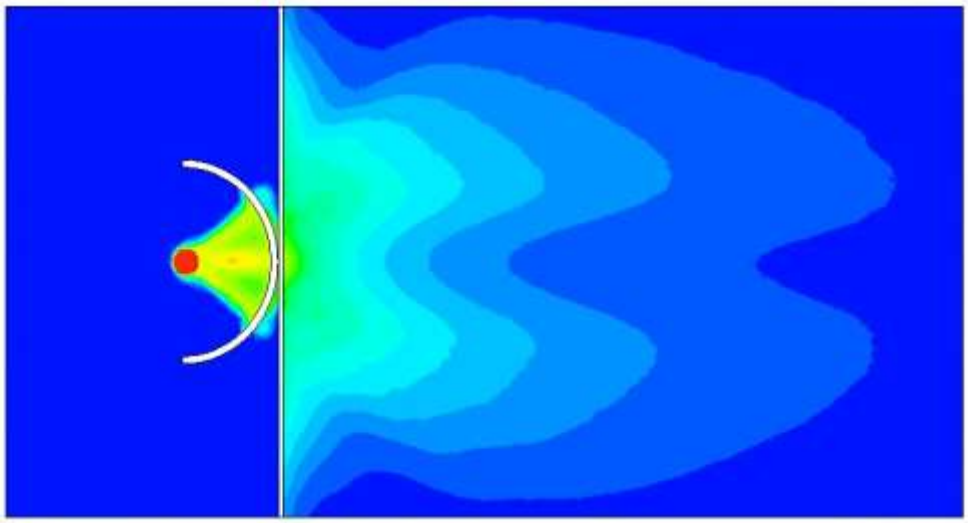

Figure 7.16: *Numerical simulation of concentration profile for heavy gas dispersion with a straight solid fence at a height of* ***30mm*** *and a semi-circular fence with height of* ***30mm*** *as an obstacle*

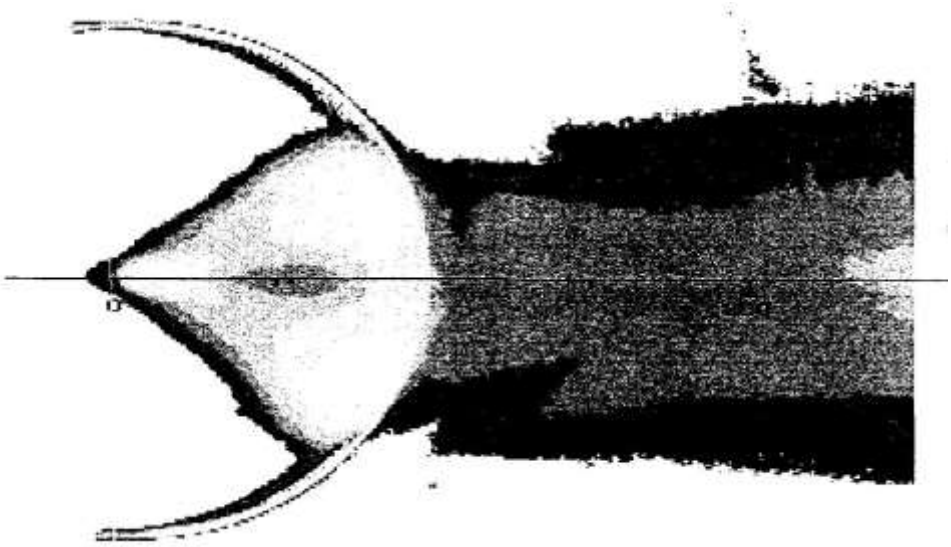

Figure 7.17: *Mean concentration image for dense or heavy plumes downwind of the semi-circular fence by Ayrault et. al. [102]*

In the above figures, the results of both the numerical simulation and the experimental set-up by Ayrault et. al. [101,102] are shown. Both the results show very similar profiles for the dispersion of the heavy gas. Although the overall view of both the profiles is very similar, there are differences as the profile in the numerical simulation is denser near the obstacle in the numerical simulation than in the experiment and shows a rectangular pattern immediately after the initial triangular-shaped pattern in the numerical simulation, which is not observed in the experimental results. This difference occurs because of the additional solid fence present in the numerical simulation which is not present in the experimental set-up. Keeping in mind the numerical simulation results from scenario 2A, it should be safe to assume that the difference in the concentration profiles in the above figures is driven by the additional solid fence of the numerical simulation.

7.4.8 CFX simulation compared with FDS simulation results

The following figures show the comparison between the results obtained from the numerical simulation and the FDS. The obstacles simulated in the numerical simulation include a solid fence, with a semi-circular fence while the FDS simulation is performed with 9 obstacles. Although the obstacles are not identical, their sizes are adjusted in such a way that they cover almost the same area in the centre.

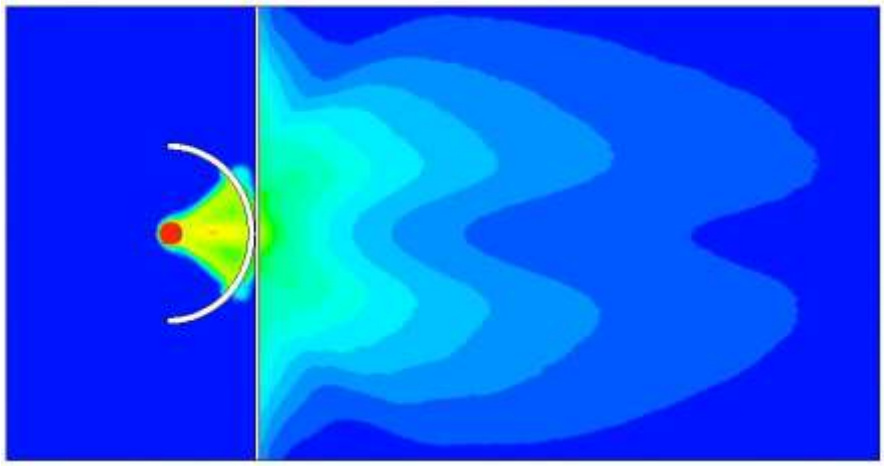

Figure 7.18: *ANSYS-CFX simulation of concentration profile for heavy gas dispersion with a solid and a semi-circular fence*

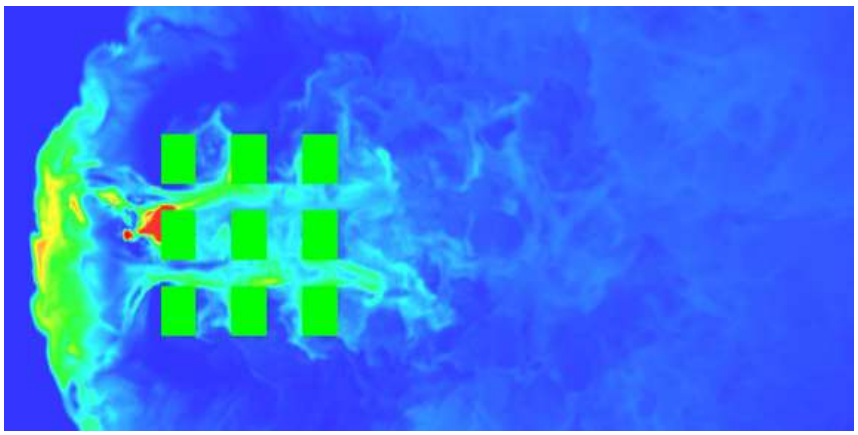

Figure 7.19: (a) *FDS simulation concentration of the heavy gas dispersion around 9 obstacles on the sections of 0.5 m above the ground*

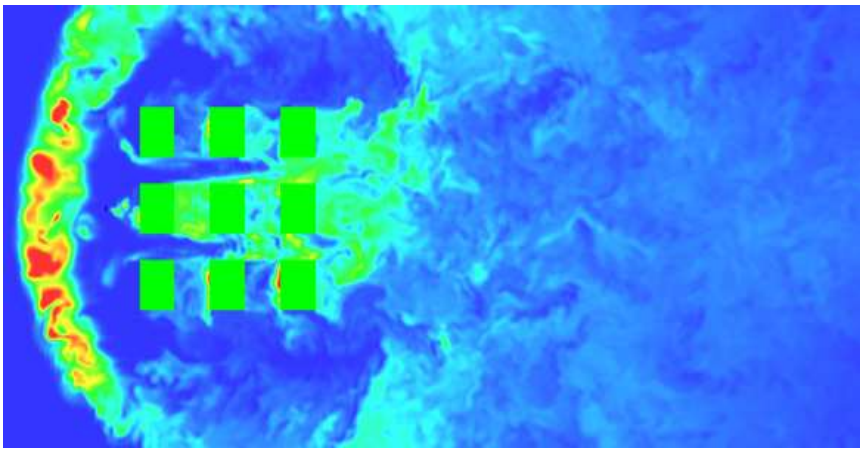

Figure 7.19: (b) *FDS simulation concentration of the heavy gas dispersion around 9 obstacles on the sections1.5 m above the ground*

The results were obtained at two different heights for FDS. Figure 7.19(a) shows the results at 0.5m height, while the Figure 7.19(b) shows the results at 1.5m. In the figures, the highest concentrations are shown in red, while blue represents the lowest concentrations. The highest

concentrated area identified in both cases is near the release source. Figures 7.19(a) and 7.19(b) are from FDS simulations that show a rather widespread distribution of highly concentrated gas clouds. The results obtained through the numerical simulation show a particularly symmetrical concentration profile, while the results from the FDS show that the concentration profile is not symmetrical either at 0.5 or 1.5m. The comparison of the figures shows that, since the obstacle shapes are quite different, very dissimilar cloud shapes are obtained, which shows the effect of obstacle shape on gas clouds. Moreover, it is noticed from Figures 7.19(a) and (b) that the concentration is more at 1.5m than at 0.5m.

7.4.9 CFX simulation compared with FDS simulation results

This comparison has been carried out to compare the results from the numerical simulation and the experimental results. Figure 7.20 represents the numerical simulation of the concentration profile for heavy gas dispersion with a straight solid fence at a height of 60mm as an obstacle, while Figure 7.21 represents the experimental measurement of the concentration profile for heavy gas dispersion with a straight solid fence at height of 60mm as an obstacle in an experiment conducted by Ayrault et. al. [101,102].

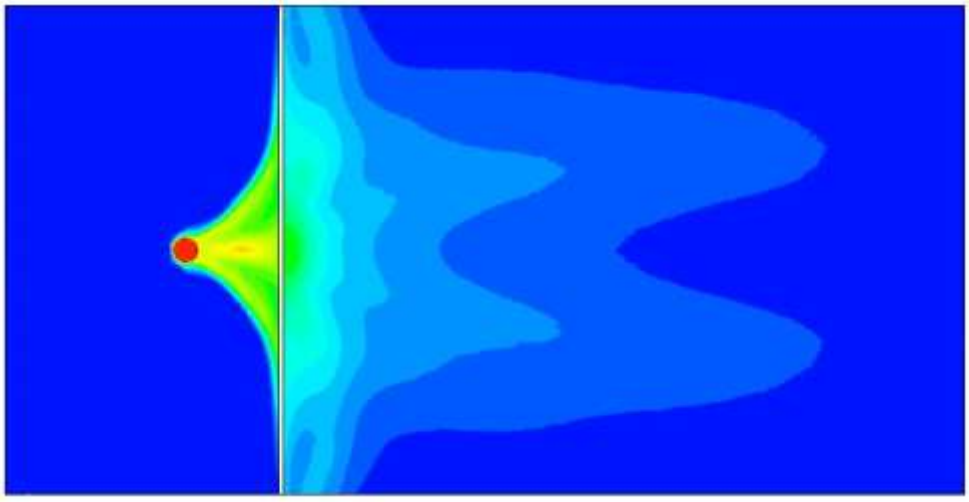

Figure 7.20: *Numerical simulation of concentration profile for heavy gas dispersion with a straight solid fence at a height of* ***60mm*** *as an obstacle.*

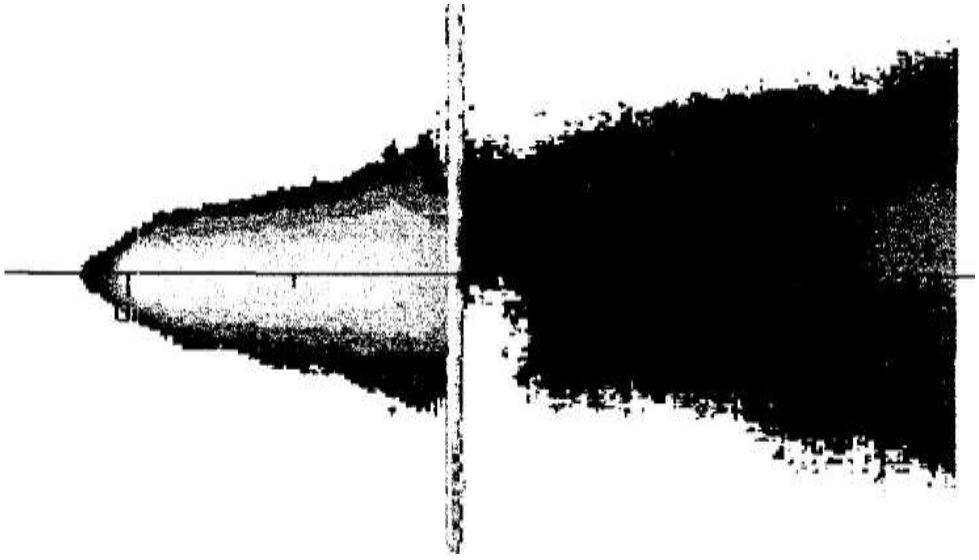

Figure 7.21: *Experiment measurement of concentration profile for heavy gas dispersion with a straight solid fence at a height of* ***60mm*** *as an obstacle by Ayrault et. al. [102]*

In the above figures, the numerical simulation and experimental results show a somewhat similar pattern of concentration profile before the obstacle, while the profile after the obstacle shows differences. The first difference is that the experimental results show that the gas cloud after the obstacle has very little presence around the obstacle and only shows the major presence in the centre, while the numerical simulations show that, although there is a major presence of the cloud around the obstacle in the centre, the cloud occupies some space throughout the obstacle and extends to each end. The second difference is that the numerical simulations show remarkably symmetrical behaviour in both the halves (before and after the obstacle), but the experimental results only show symmetrical behaviour before the obstacle, while the behaviour after the obstacle is asymmetrical.

7.4.10 CFD comparison with experimental results graphics

The following comparison for the concentration of heavy gas dispersion between the numerical simulation and the experimental set-up of Ayrault et. al. [101,102] has been shown to offer further clarity to the present work.

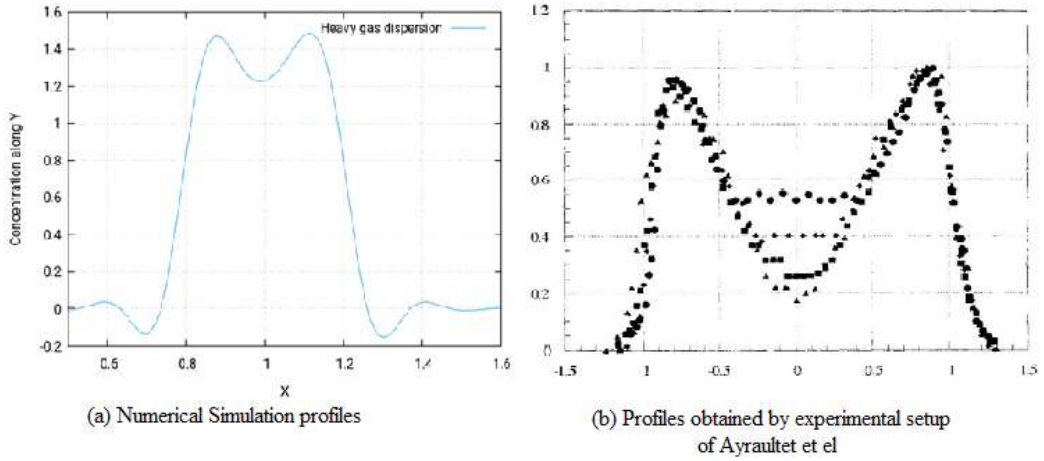

Figure 7.22: *Graphical comparison between numerical simulation and experiments of Ayrault el. al. [101,102]*

In the Figure 7.23 above, (a) represents a simple profile of heavy gas dispersion through the numerical simulation for one point, while (b) represents the 3 different profiles obtained using the experimental set-up. In Figure 7.22(b), triangles refer to section X = 300mm, squares to 500 mm, inclined squares to 600mm and circles to 800mm. A small difference in these two graphs is that the numerical simulation allows the profile to be viewed in the negative y-direction, which is not the case with the experimental one. The lowest point in the numerical simulation is -0.2, while the experimental graph starts from 0, not allowing the profile to be viewed in the negative y direction. This is why a small dip can be seen in the numerical simulation, but not the experimental results. In both graphs, the profiles show the same pattern and have only 1 peak, but the value of the peak is determined by the distance from the release source. Since the experimental graph covers 4 different profiles at 300mm, 500mm, 600mm and 800mm, as discussed above, 4 different peaks can be seen. Meanwhile, the numerical simulation shows only1 peak as it only covers 1 profile.

7.4.11 CFD comparison with experimental results graphics

The following comparison for the concentration of neutral gas dispersion between the numerical simulation and the experimental set-up of Ayrault et. al. [101,102] has been shown to offer some more clarity to the present study.

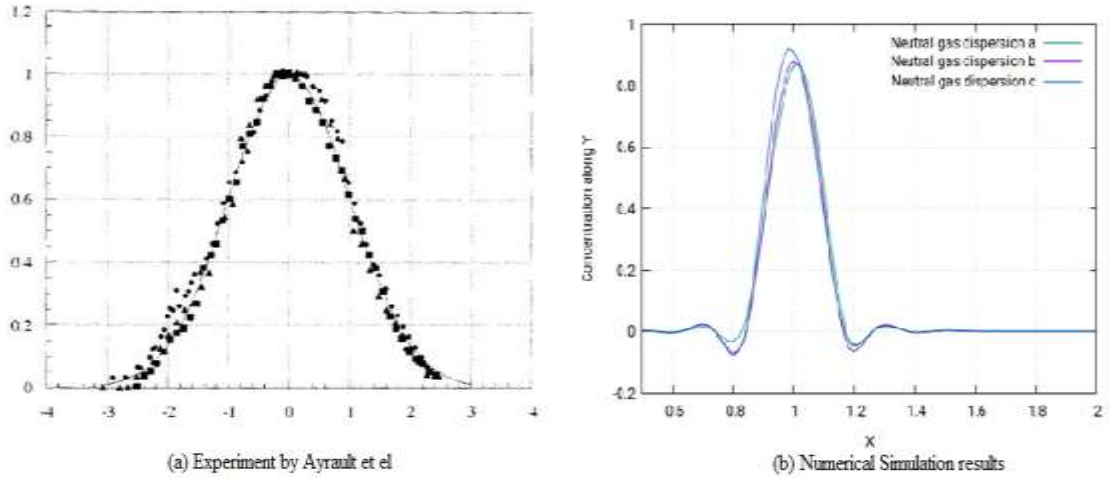

Figure 7.23: *Graphical comparison between numerical simulation and Ayrault's experiments [102]*

In the above figure, (a) represents a simple profile of neutral gas dispersion through the numerical simulation for one point, while (b) represents the 3 different profiles obtained through the experimental set-up. In figure (b), triangles refer to section X = 300mm, squares to 500 mm, inclined squares to 600mm and circles to 800mm. It is noticed that the experimental and numerical simulations are not as that similar as those for heavy gas, the results obtained from neutral gas through the experiment reveal a simple Gaussian curve, while the numerical simulation profile sees two small dips at both sides of the main gaussian curve like profile.

7.5 Results and discussions

7.5.1 Heavy gas dispersion, without obstacles

In this scenario, the heavy gas leak occurs from a circular source that is 50mm in diameter. For this setting, the pressure is zero, and there are no obstacles such as solid or semi-circular fences.

Table 7.1: *Parametric values for scenario 1A*

Density	Flow Rate	Velocity	Ambient Temperature	Release Source Temperature
2.1 kg m/s^3	1 kg/s	1 m/s	25°C	-100°C

7.5.1.1 Release source point

The following figure shows the release source for the current scenario.

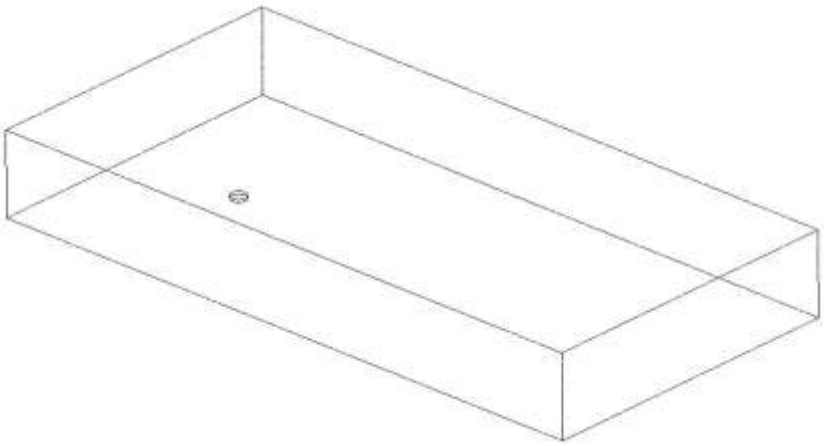

Figure 7.24: *Heavy gas release source for a flat terrain with no obstacles at* ***1m/s*** *velocity*

7.5.1.2 Concentration of heavy gas dispersion

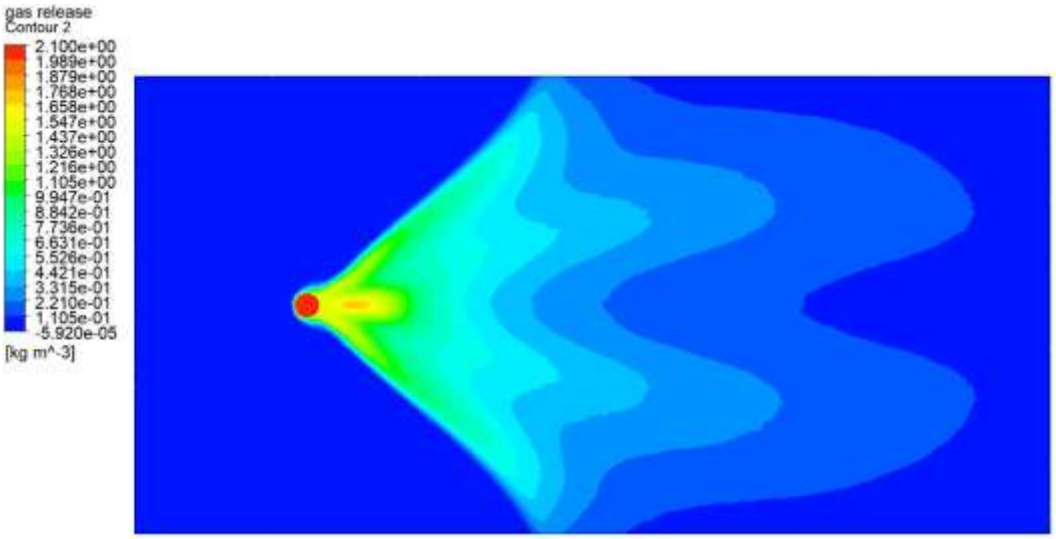

Figure 7.25: *Concentration profile of heavy gas release source for a flat terrain with* ***1m/s*** *velocity*

The concentration profile of the heavy gas for scenario 1A is shown in Figure 25 above. It shows the concentration profile for the heavy gas when released from a circular source of 50mm diameter with no obstacles. The simulation shows that, for this particular scenario, the heavy gas cloud distributes symmetrically along the horizontal axis. The concentration contour in the above figure shows the highest concentrations in red, while the lowest are in blue. The cloud shows maximum concentrations when released from the source, and it moves away taking the path of a light leaving a hand torch. The concentrations continue fading and there is a sort of layering pattern in the concentrations, with maximum concentrations in red being the layer with the highest concentrations, then the yellow ones with slightly less concentrations, followed by green with slightly less, and so on, with the final layer (blue) being the lowest

concentration. It can also be noticed that the layers make a sinusoidal curve shape at the outer surface, which is symmetrical along the horizontal axis.

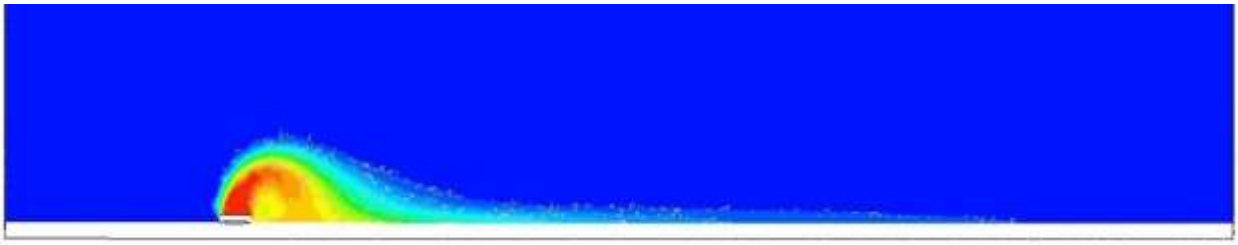

Figure 7.26: *2D view of concentration profile of heavy gas release source for a flat terrain with* ***1m/s*** *velocity*

Figure 7.26 shows the two-dimensional version of the concentration simulation. It also shows the same behaviour of the concentration for heavy gas as shown in (Figure 7.25).

7.5.1.3 Iso-surfaces of heavy gas dispersion

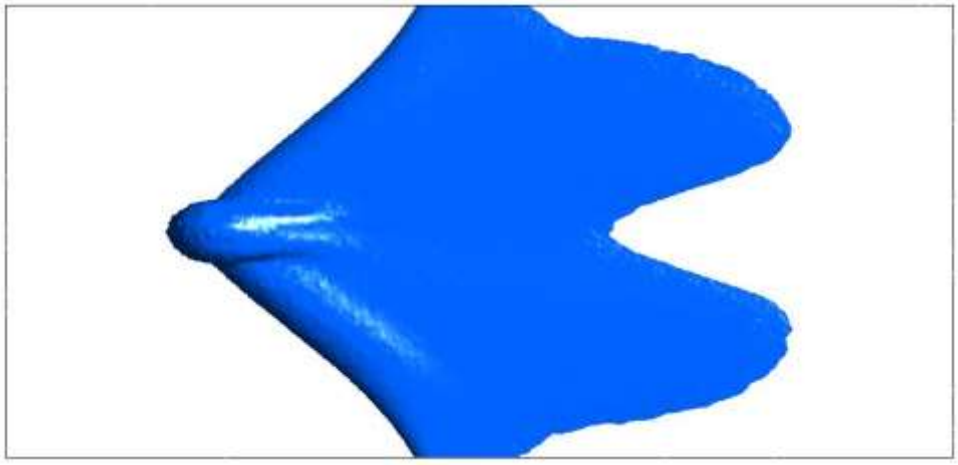

Figure 7.27: *Iso surface top view of concentration of heavy gas release source for a flat terrain with* ***1m/s*** *velocity*

Figure 7.27 shows the iso-surface of the concentration from the top view. It is noticed that the concentration is heaviest near the release source point and it is distributed symmetrically along the axis.

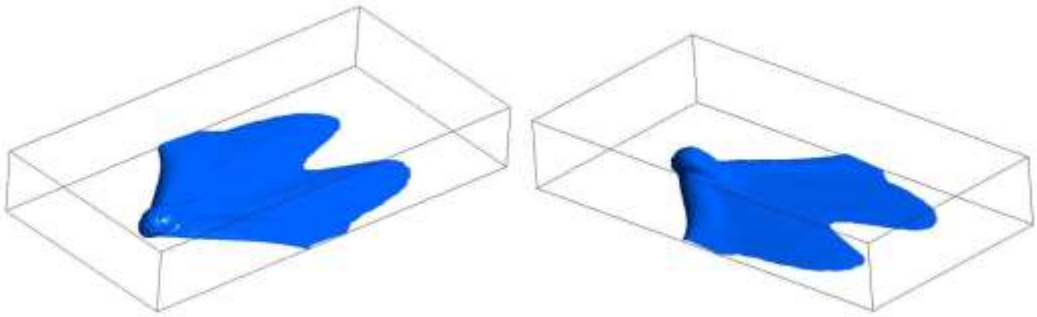

Figure 7.28: *Iso surface side and back view of concentration of heavy gas release source for a flat terrain with* ***1m/s*** *velocity*

Figure 7.28 shows the iso-surface of the concentration from the side view. It shows that the gas cloud, after showing an inclination of height near the release source, then goes on to decrease in height and is thickest near the release source, while it continues to become thinner as it moves along the horizontal axis. It also shows the iso-surface of the concentration from the back view. In this figure, although the gas cloud looks symmetrical along the horizontal axis, in the previous views, it can be observed here that the cloud density is slightly more in the upper region of the gas cloud than the lower side. Thus, along the horizontal axis, the cloud might be horizontal, but along the vertical axis, it shows deviations from symmetry.

According to Standard BS EN 60079-10-1:2009 Santon el. al.[104], the following locations can be categorised as follows:

Zone 0: The triangular-shaped area near the release source location
Zone 1: The area starting immediately after zone 0 expanding uniformly
Zone 2: All the remaining locations not categorised in zone 0 or zone 1

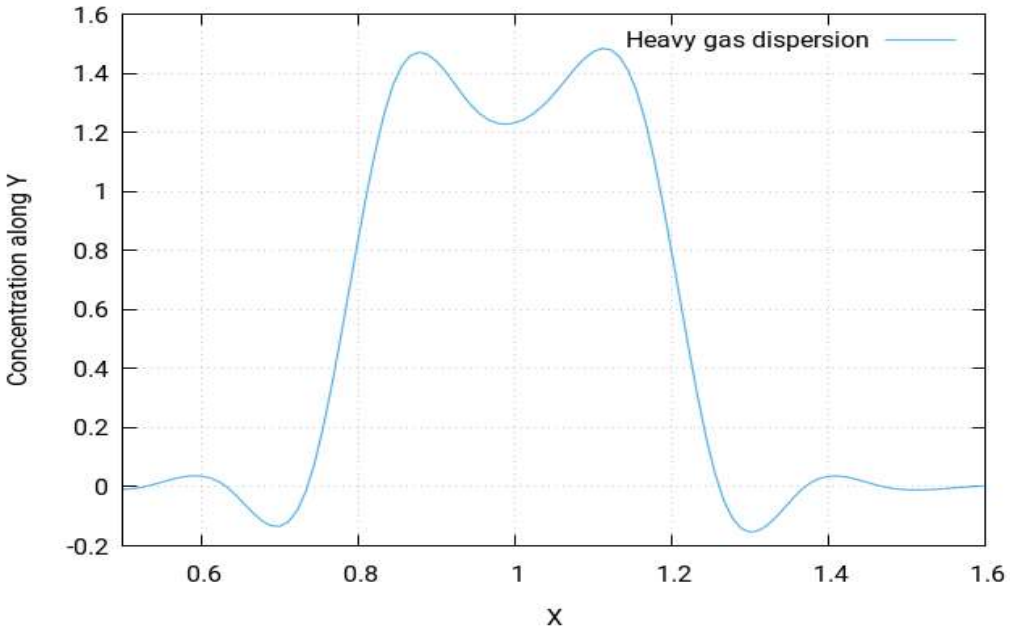

Figure 7.29: *Graphical representation for concentration of heavy gas release source for a flat terrain with* ***1m/s*** *velocity*

Figure 7.29 shows the profiles of the concentrations of the gas released. In the figure, the distance is calculated from the release source. This profile is somewhat symmetric at first but falls flat in the end.

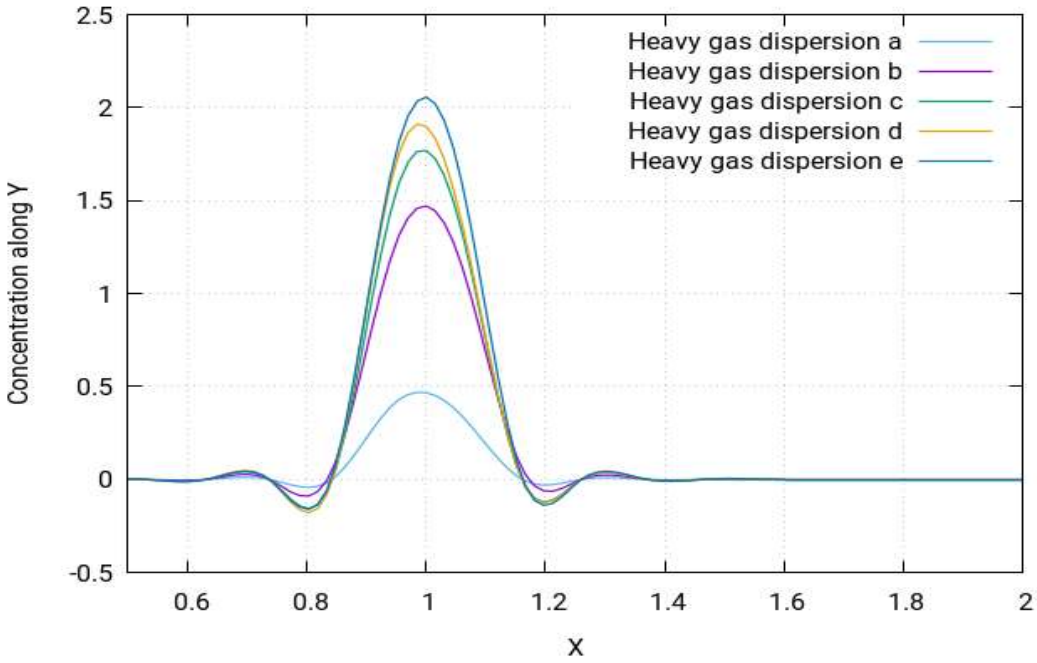

Figure 7.30: *Five different positions of heavy gas release source graphical representation of concentration at a flat terrain with* ***1m/s*** *velocity*

The concentration profiles for varying distances are shown in the figure above. From this figure, it is concluded that the concentration value of heavy gas decreases when it moves away from the source, as the (Figure 7.30) shows declining behaviour of the concentration. In the figure 7.30, the curve with the highest peak is obtained when nearest the release source and vice versa.

7.5.1.4 Density of heavy gas dispersion

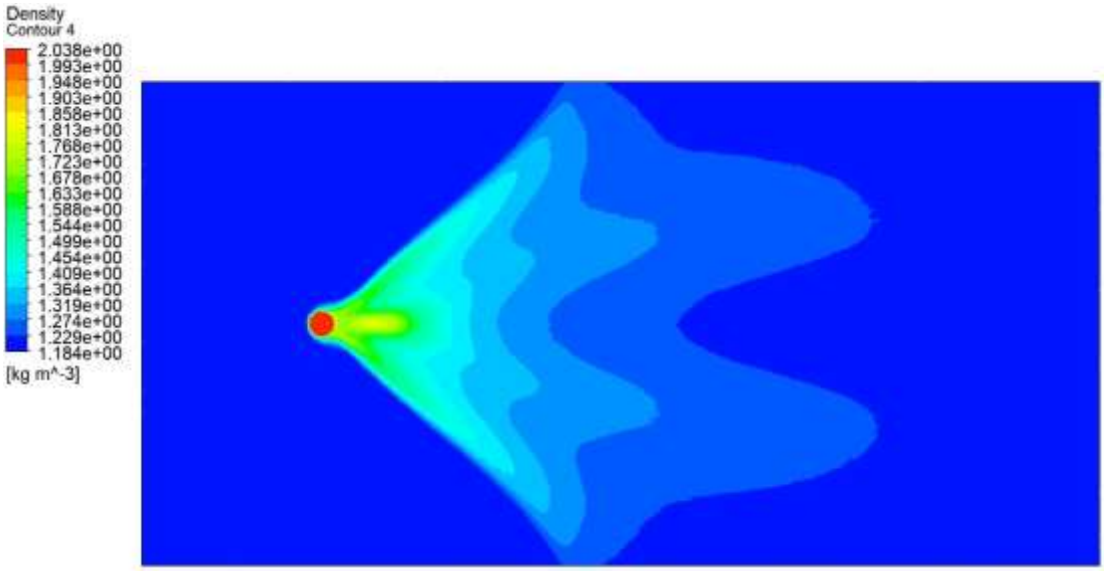

Figure 7.31: *Density of heavy gas release source for a flat terrain with* ***1m/s*** *velocity*

The density profile of the heavy gas for scenario 1A is shown in Figure 7.31 above. It shows the density profile for the heavy gas when released from a circular source of 50mm diameter with no obstacles. In the first look, it appears that the density profile also follows the same pattern as that of concentration, keeping in mind the similarity in the concentration and density profile shown in figure 7.31 and figure 7.25 respectively. However, it should be noticed that the density profile appears to be a slightly shrunken version of the concentration profile. Moreover, the concentration contour shows the value of maximum concentration to be 2.1, while the density contours show a maximum value of 2.038.

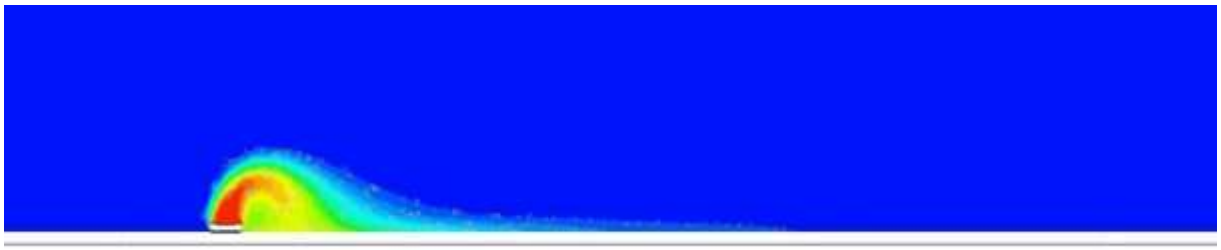

Figure 7.32: *2D-view of density of heavy gas release source for a flat terrain with* ***1m/s*** *velocity*

Figure 7.32 shows a two-dimensional view of the density profile and shows the same behaviour of the heavy gas concentration as (Figure 7.31).

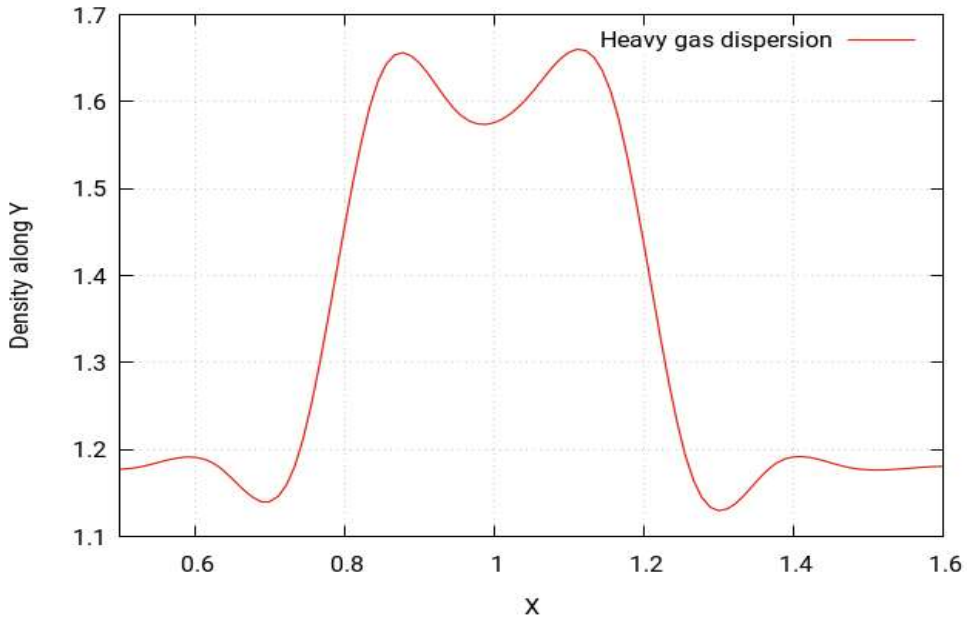

Figure 7.33: *Graphical representation of density of heavy gas release source for a flat terrain with* ***1m/s*** *velocity*

Figure 7.33 shows the profiles of the density of the gas released. In the figure, the distance is from the release source. This profile shows the same behaviour as that of the concentration profile.

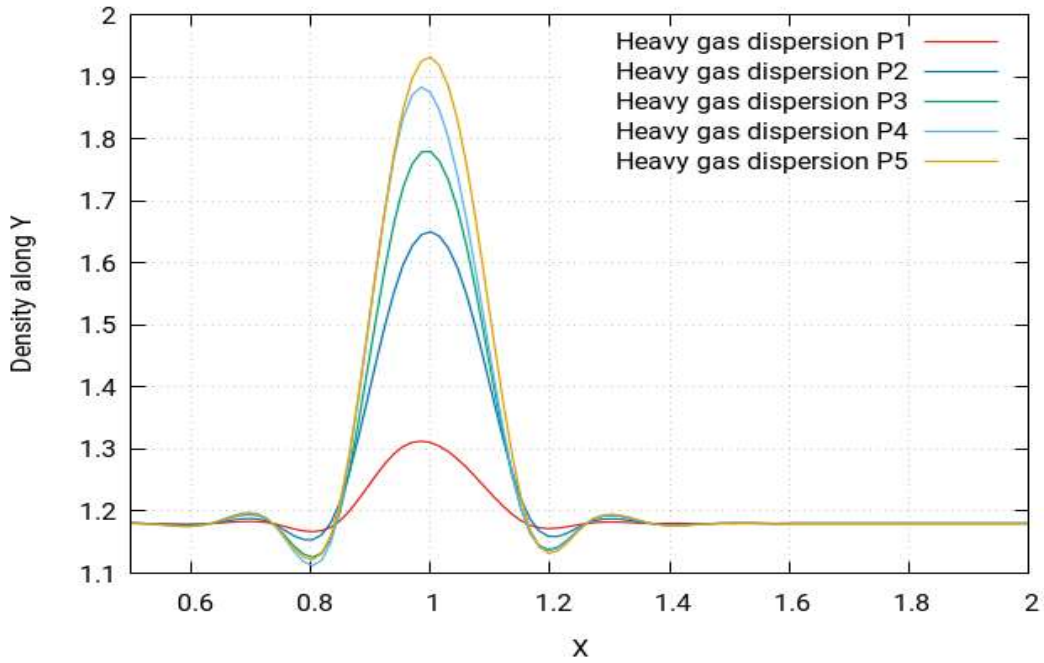

Figure 7.34: *Five different positions of heavy gas release source graphical representation of density at a flat terrain with* ***1m/s*** *velocity*

The density profiles for varying distances are shown in the figure above. These profiles show the same behaviour as that of the concentration profile.

7.5.1.5 Temperature of heavy gas dispersion

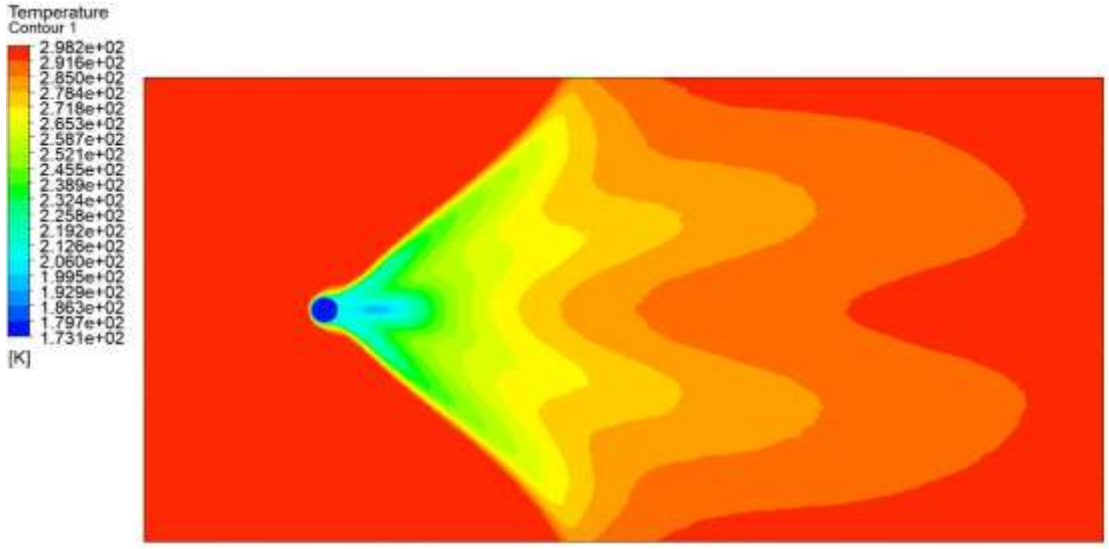

Figure 7.35: *Temperature of heavy gas release source for a flat terrain with* ***1m/s*** *velocity*

Figure 7.35 above shows the temperature simulation for this scenario. By visualising the temperature simulation, it is found out that the temperature simulation produces largely the same profile for this scenario as that of the concentration profile. However, the point to notice is that the behaviour of temperature is in fact the opposite of that of concentration. This means that the areas which were identified in the concentration simulation as highly concentrated will

in fact have the lowest temperatures, while the ones with moderate concentrations will have moderate temperatures and the least concentrated areas will have the maximum temperatures. To further simplify these findings, it should be pointed out that the concentration simulations show that the concentrations near the release source point tend to be the highest and start to fade away when moving away from the source and reach their lowest levels as they move much further away, eventually reaching the environment where the gas cloud disappears. However, the temperature is at its lowest near the release source point and tends to increase as it moves away from the source, finally achieving the maximum temperature equal to the ambient temperature of the environment.

Figure 7.36: *2D view of temperature profile of heavy gas release source for a flat terrain with* ***1m/s*** *velocity*

Figure 7.36 shows the two-dimensional version of the temperature simulation. It also shows the same behaviour of the heavy gas concentration as shown in (Figure 7.35).

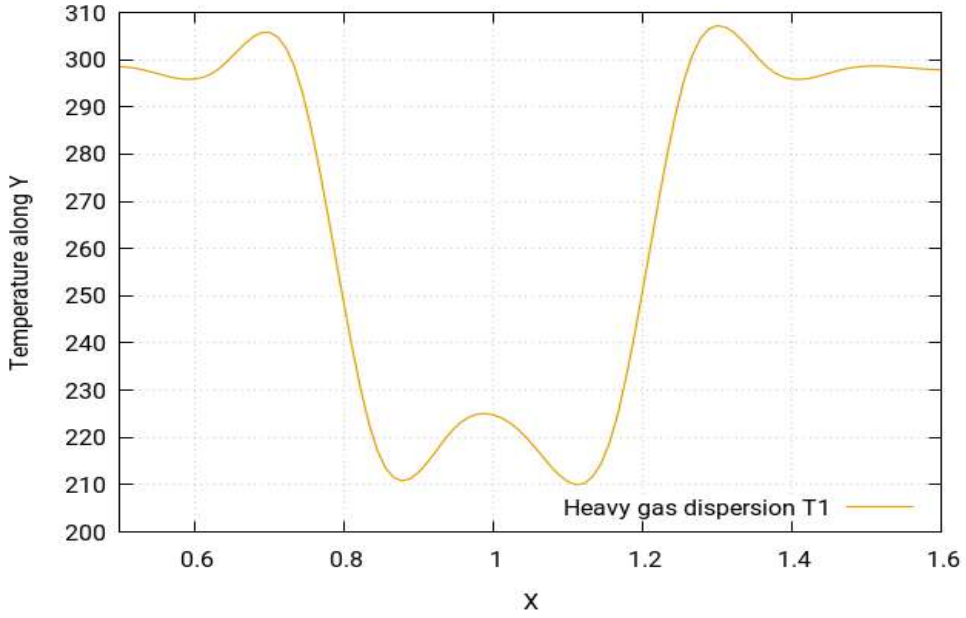

Figure 7.37: *Graphical representation of heavy gas release source for a flat terrain with* ***1m/s*** *velocity*

Figure 7.37 shows the temperature profiles of the gas released. In the figure, the distance is calculated from the release source. This profile is a mirror of the density profile.

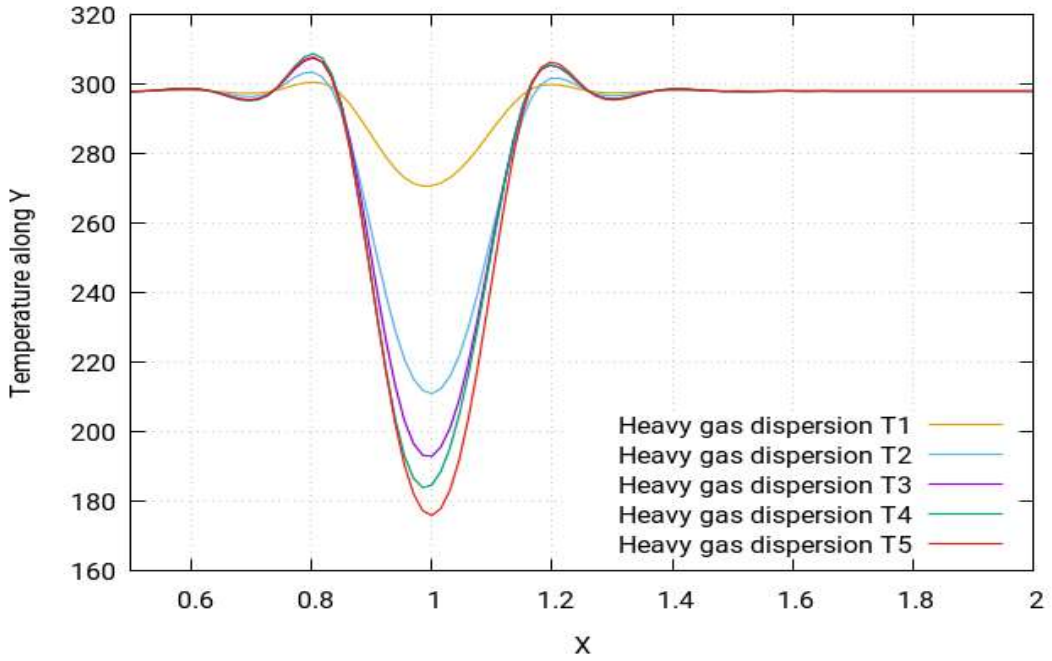

Figure 7.38: *Five different positions of heavy gas release source graphical representation of temperature at a flat terrain with* ***1m/s*** *velocity*

The temperature profiles for varying distances are shown in the figure above. These profiles show the inverse or mirrored behaviour to that of the concentration profile.

7.5.1.6 Velocity of heavy gas dispersion

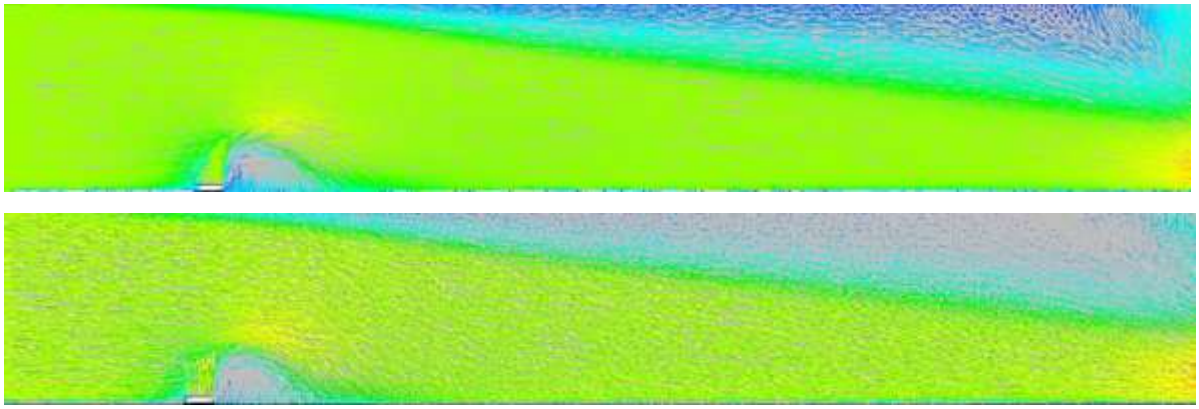

Figure 7.39: *Velocity of heavy gas release source for a flat terrain with* ***1m/s*** *velocity*

Figure 7.39 shows the velocity contours of heavy gas dispersion for this scenario. Velocity contours depict the intensity of wind or the effective wind influence at the different locations throughout the layout. Can be seen in the figure that the wind intensity is different at different points in the layout. The wind operation is smooth in this scenario and a small number of complex vertexes can be observed. The wind eddies carry the gas cloud to the nearby

environment, where a gas cloud is formed due to steady flow. This gas cloud is deemed dangerous as it is volatile and could lead to an explosion, fire, etc.

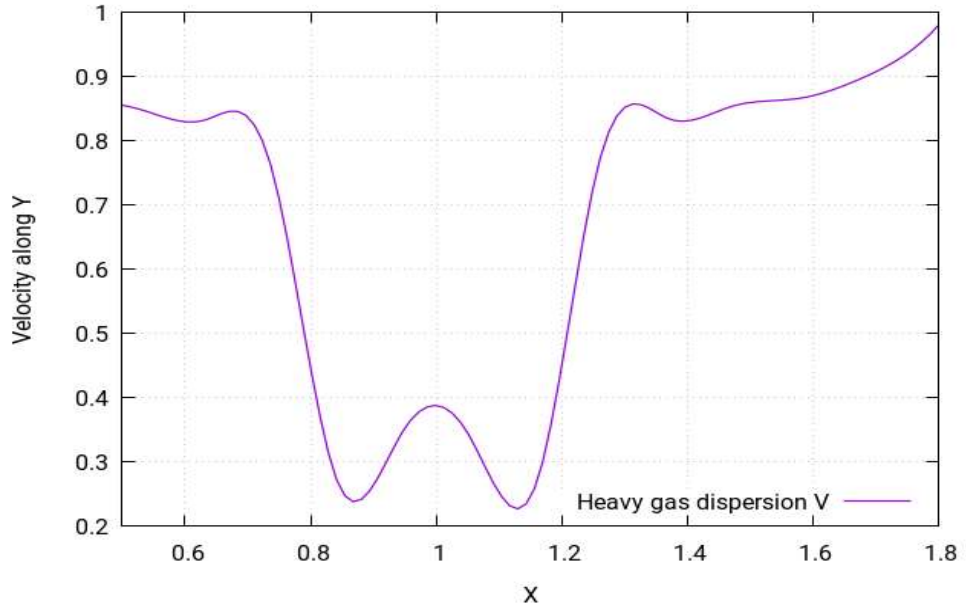

Figure 7.40: *Graphical representation of velocity heavy gas release source for a flat terrain at* ***1m/s***

Figure 7.40 shows the profile of the density of the gas released. The behaviour of the velocity profile is somewhat irregular; after a small increase there is a sharp decrease, then a brief sinusoidal behaviour followed by a sharp increase and a gradual rise.

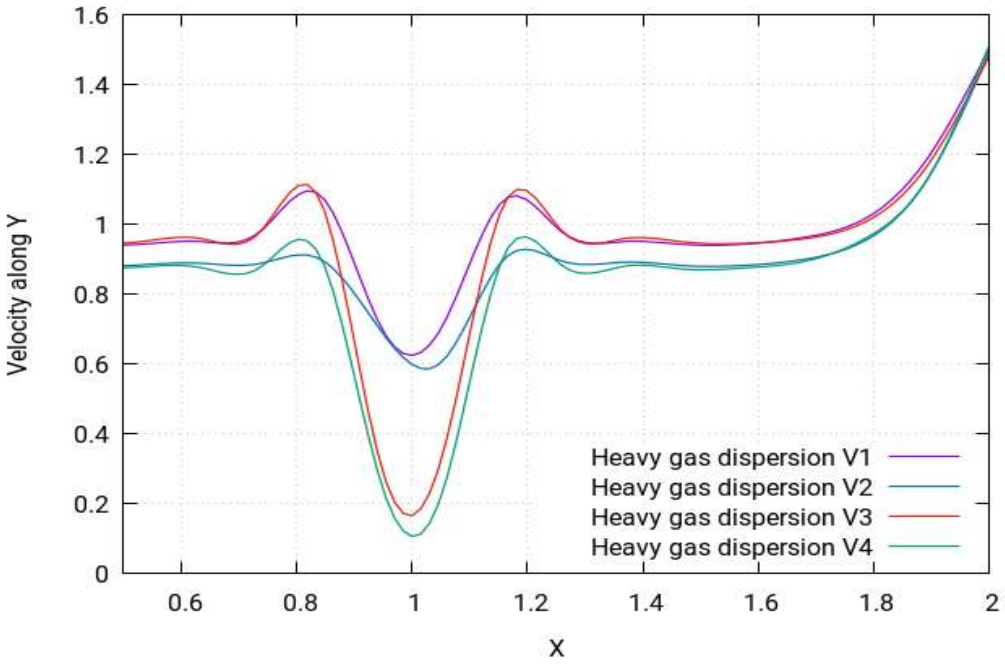

Figure 7.41: *Four different graphical representation of heavy gas release source for a flat terrain with* ***1m/s*** *velocity*

Figure 7.41 shows the varying profiles of the velocity with carrying distances. While the profiles do follow the same pattern, the values however change according to the varying distances.

7.5.2 Neutral gas dispersion, without an obstacle

In this scenario, the neutral gas leak occurs from a circular source that is 50 mm in diameter. For this setting, the pressure is zero, and there are no obstacles such as solid or semi-circular fences.

Table 7.2: *Parametric Values for Scenario 1B*

Density	Flow Rate	Velocity	Ambient Temperature	Release Source Temperature
1.1839 kg m/s^3	1.7737 kg/s	1 m/s	25°C	25°C

7.5.2.1 Release source point

The following figure shows the release source for the current scenario

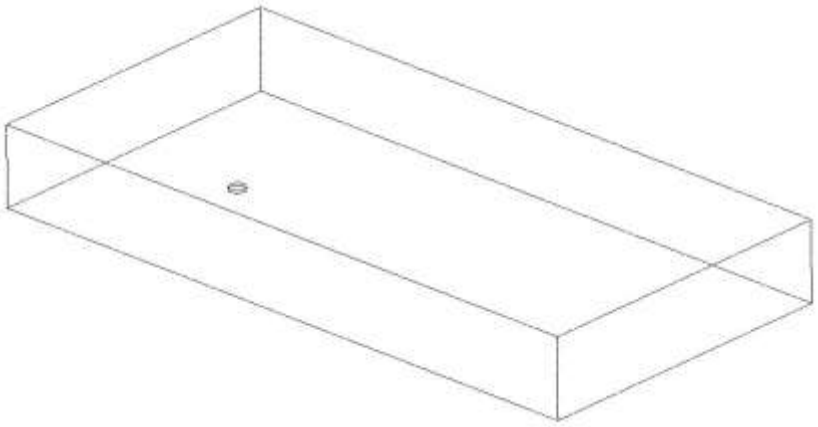

Figure 7.42: *The heavy gas release source for a flat terrain without any obstacle at* ***1m/s*** *velocity.*

7.5.2.2 Concentration of neutral gas dispersion

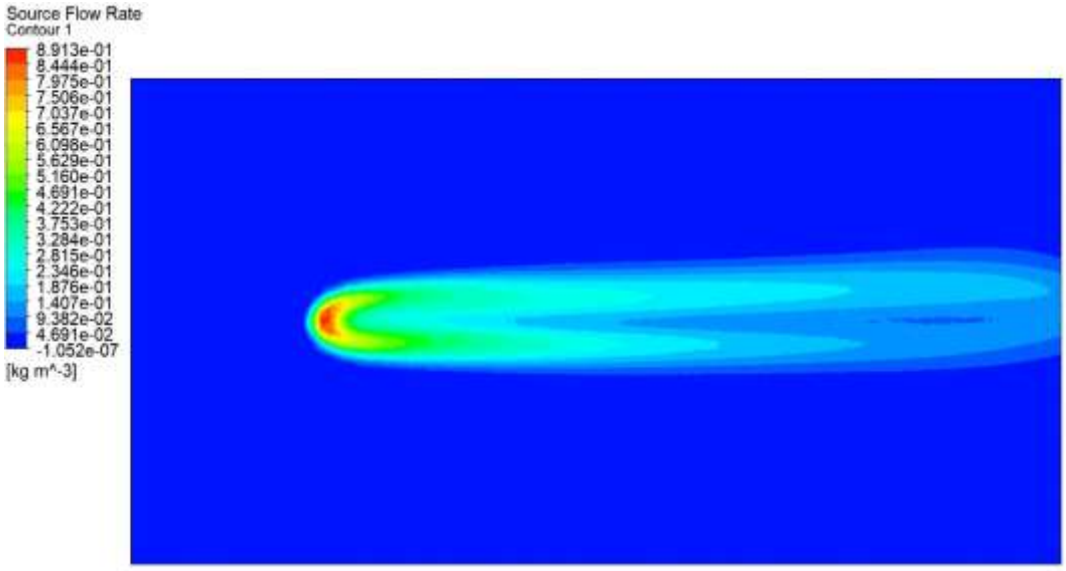

Figure 7.43: *Concentration profile of neutral gas release source for a flat terrain with* ***1m/s*** *velocity*

The concentration profile of the neutral gas for scenario 1B is shown in Figure 7.43 above. It shows the concentration profile for the neutral gas when released from a circular source of 50mm diameter with no obstacles. The cloud shape for this scenario is in the shape of an elliptical cylinder, with the top end near the release source of the cylinder being thinner than the other end. The simulation shows maximum concentrations in red near the release source. Then the concentrations begin to decrease. From the simulation, it is noticed that the concentration distribution is not symmetrical in the horizontal and that the lower half of the elliptical cylinder is more concentrated near the release source end, while the upper half extends in high concentrations at the opposite end. It can also be seen that there is a small gap in the cloud, represented by blue showing the lowest concentrations. The concentration values can be predicted using the concentration contour on the left side in the figure.

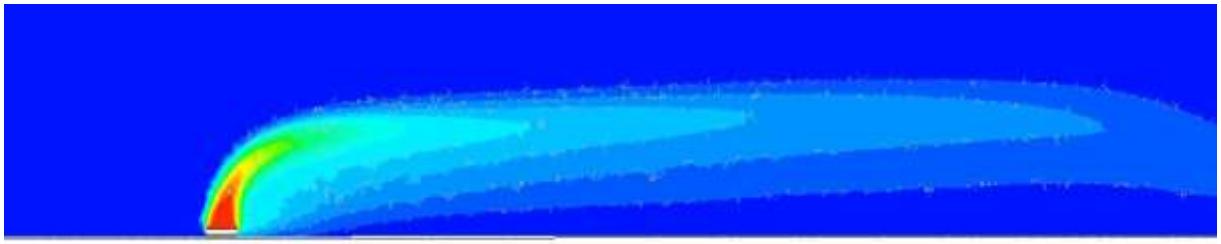

Figure 7.44: *2D view of concentration profile of neutral gas release source for a flat terrain with* ***1m/s*** *velocity*

Figure 7.44 shows the two-dimensional version of the concentration simulation. It further verifies the behaviour of the cloud shape for neutral gas studied in the previous (Figure 7.43).

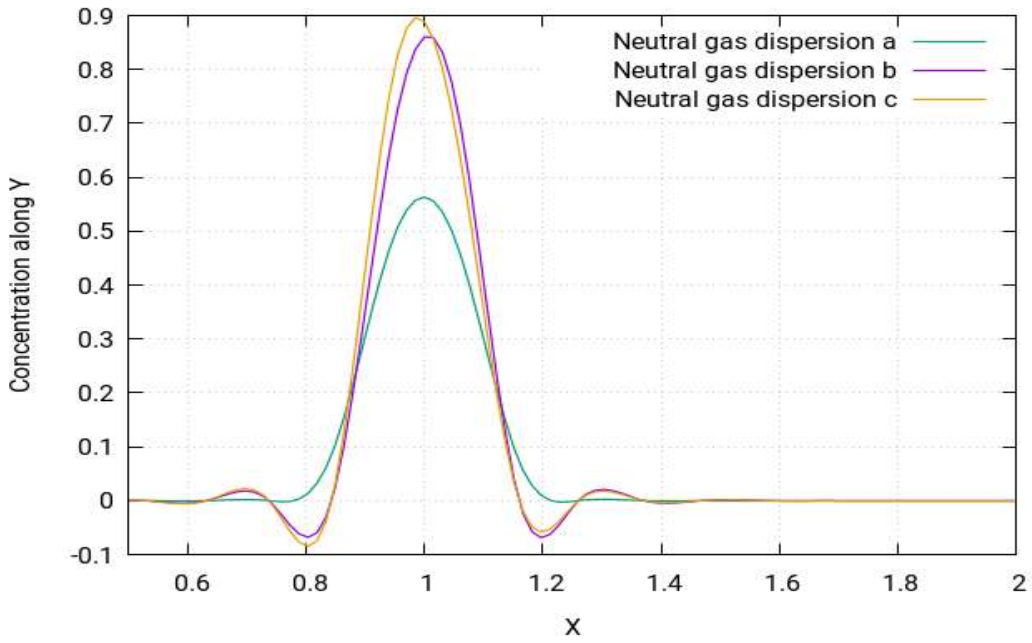

Figure 7.45: *Graphical representation of concentration profile of neutral gas release source for a flat terrain with* ***1m/s*** *velocity*

The concentration profiles for varying distances are shown in Figure 46 above. From the figure, it is concluded that the concentration value of the neutral gas decreases when it moves away from the source, as the figure shows declining behaviour of the concentration. In the figure, the curve with the highest peak is obtained when nearest to the release source and vice versa.

7.5.2.3 Iso-Surfaces of neutral gas dispersion

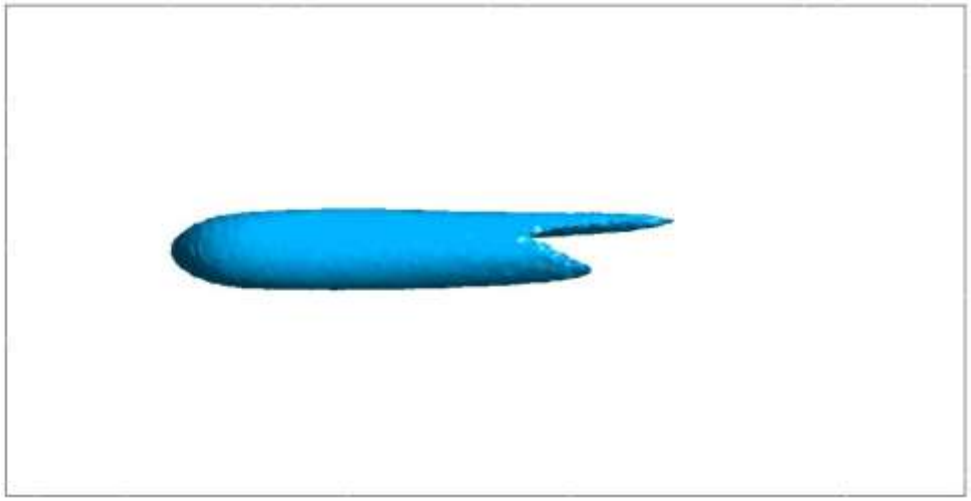

Figure 7.46: *Iso surface top view of concentration of heavy gas release source for a flat terrain with* ***1m/s*** *velocity*

Figure 7.46 shows the iso-surface of the concentration from the top view. It is observed that the upper end of the cloud is extended towards the horizontal axis showing more concentration in the upper half of the cloud than in the lower.

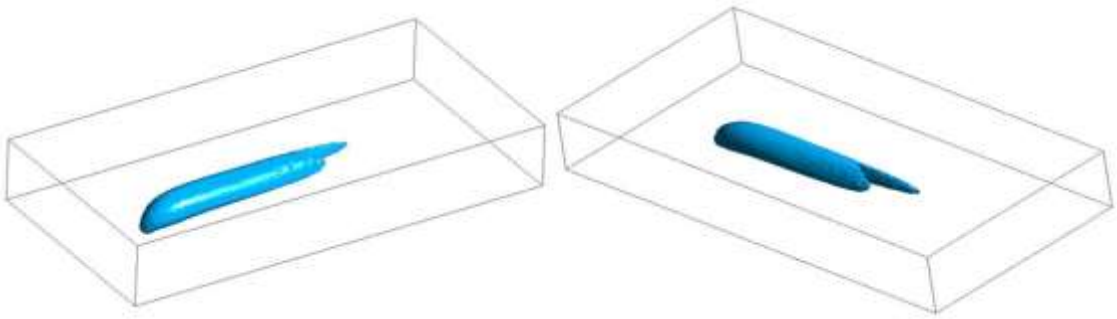

Figure 7.47: *Iso-surface side view of concentration of heavy gas release source for a flat terrain with* ***1m/s*** *velocity*

Figure 7.47 shows the iso-surface of the concentration from the side view. It shows the same results as discussed in the previous figures. It also shows the iso-surface of the concentration from the back view.

According to Standard BS EN 60079-10-1:2009 Santon el. al. [104], the following locations can be categorised:

Zone 0: The immediate surrounding of the release source
Zone 1: The split in the centre region immediate after the release source
Zone 2: All the remaining locations not categorised in zone 0 or zone 1

7.5.2.4 Velocity of neutral gas dispersion

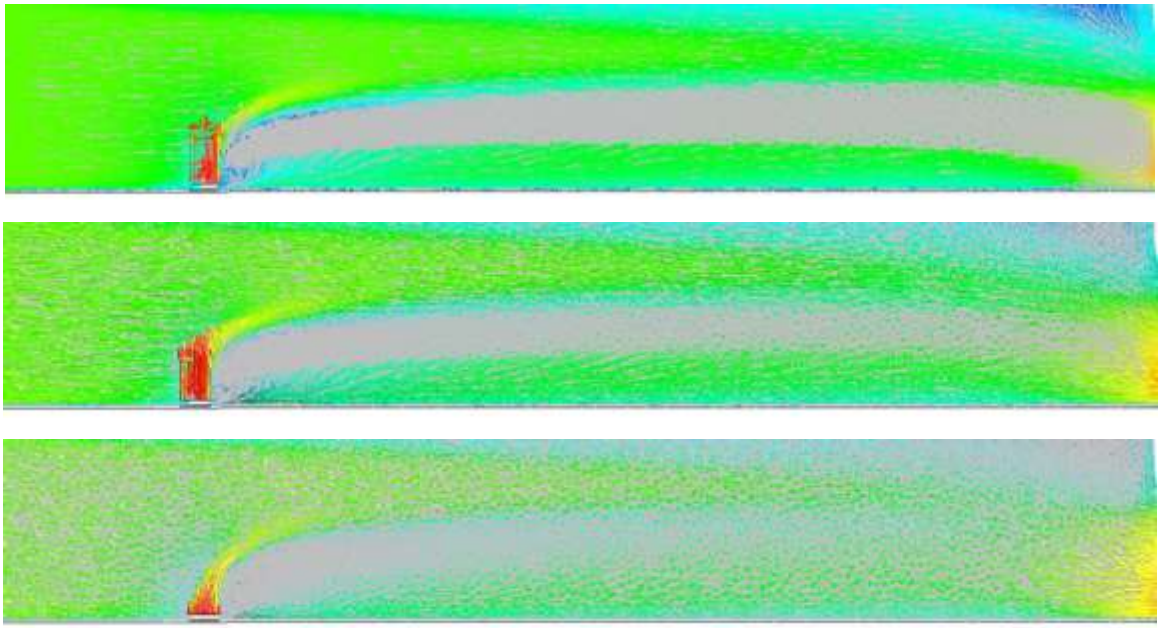

Figure 7.48: *Velocity profile of neutral gas release source for a flat terrain with* ***1m/s*** *velocity*

Figure 7.48 shows the velocity contours of heavy gas dispersion for this scenario. Velocity contours depict the intensity of wind or the effective wind influence at the different locations

throughout the layout. As can be seen in the figure, the wind intensity is different at different points in the layout. In scenario 1A, the wind operation was smooth, and not many complex vertexes were observed. However, in this scenario, it can be seen that there are many complex vertexes formed near the release source location as seen in the figure. These complex vertexes carry the gas cloud to the nearby environment, where a gas cloud is formed due to steady flow. This gas cloud is deemed dangerous as it is volatile and could lead to an explosion, fire, etc. This also causes the gas cloud to enhance in the upward direction. In the figure, the highest velocities (red) are present near the release source.

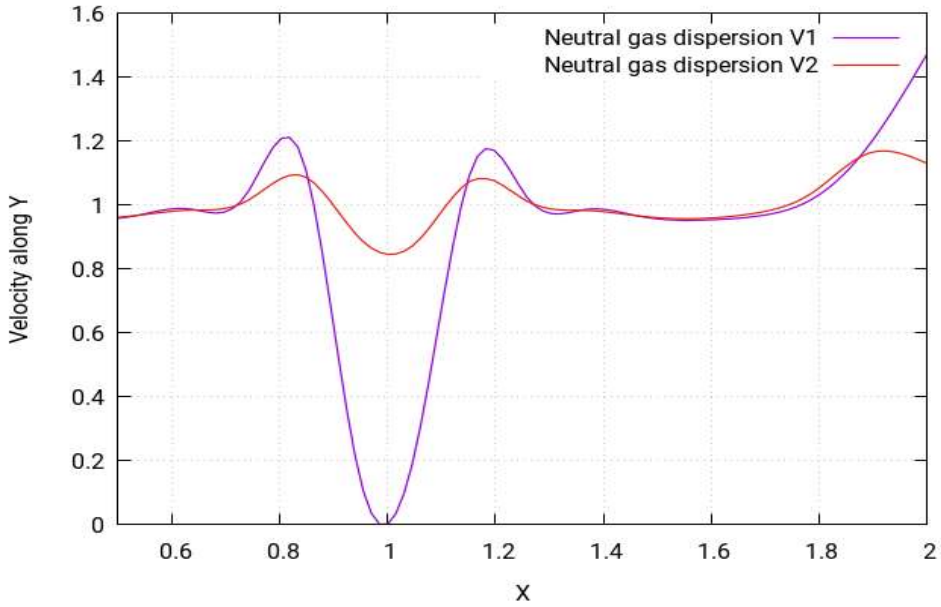

Figure 7.49: *Graphical representation of velocity of neutral gas release source for a flat terrain with* ***1m/s***

Figure 7.49 shows the profiles of the velocity of the gas released. In the figure, the distance is calculated from the release source. The purple shows the velocity values when at a distance of 0.13m and the red curve shows the velocity greater values when at a distance of 0.2m. The profile shows a huge difference in the velocity values for two different situations. It shows that values of velocity are achieved when nearer to the release source than when away from the source. This is similar to the behaviour shown in velocity contour, which shows the highest velocity values in red when nearer to the source.

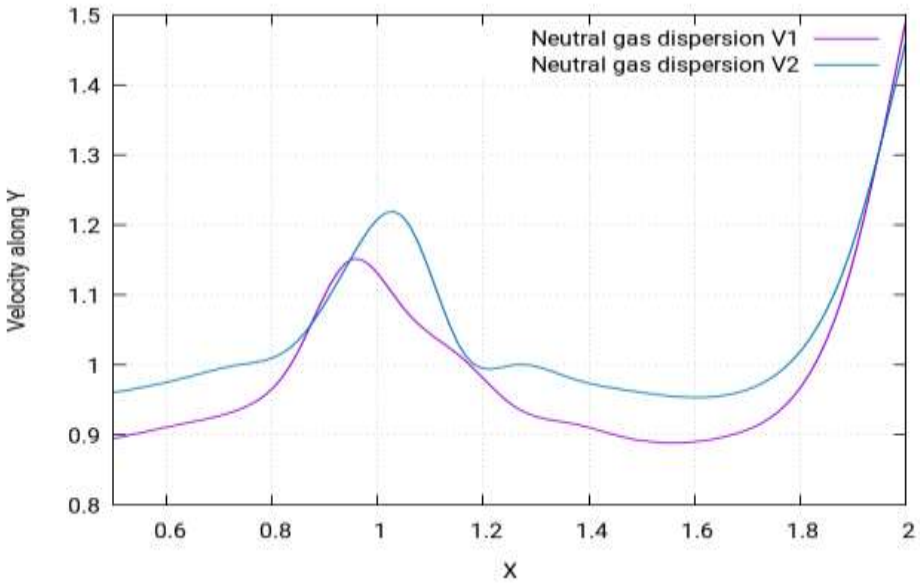

Figure 7.50: *Graphical representation of velocity of neutral gas release source for a flat terrain at* ***1m/s***

Figure 7.50 shows the profiles of the velocity of the gas released. In the figure, the distance is calculated from the release source. This figure shows another view of the velocity profiles at different points and distances from the release source. These profiles are obtained when calculated from a distance further away from the point. Unlike the previous figure, these profiles show a similar pattern but different values due to the difference of distances from the release source. These profiles the profile shows a gradual rise in concentration. Then a peak shows the presence of the obstacle, which then falls flat before a final sharp rise.

7.5.3 Heavy gas dispersion with a straight solid fence as an obstacle

The second scenario includes a heavy gas leak from a circular source of 50mm in diameter. The terrain is flat, but there is a solid fence, which is 400mm downstream of the plume and has a height of 30mm.

Table 7.3: *Parametric values of scenario 2A*

Density	Flow Rate	Velocity	Ambient Temperature	Release Source Temperature
2.1 kg m/s^3	1 kg/s	1 m/s	25°C	-100°C

7.5.3.1 Release source point

The following figure shows the release source for the current scenario:

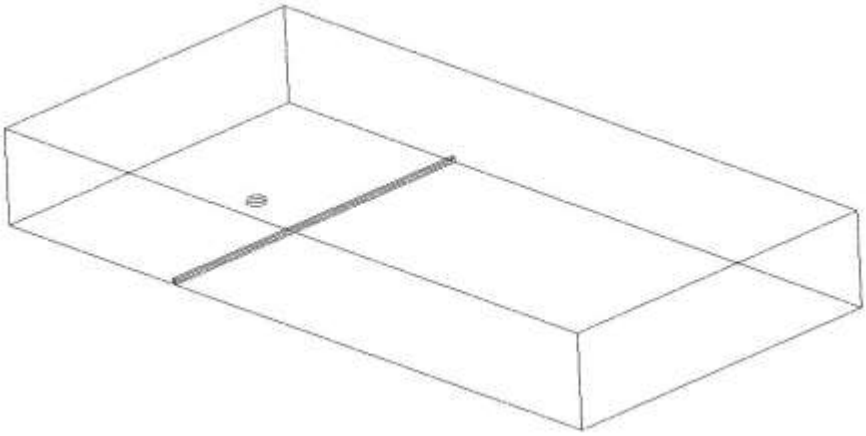

Figure 7.51: *Top View of heavy gas release source for a flat terrain with a solid fence as an obstacle at* ***1m/s*** *velocity*

7.5.3.2 Concentration of heavy gas dispersion

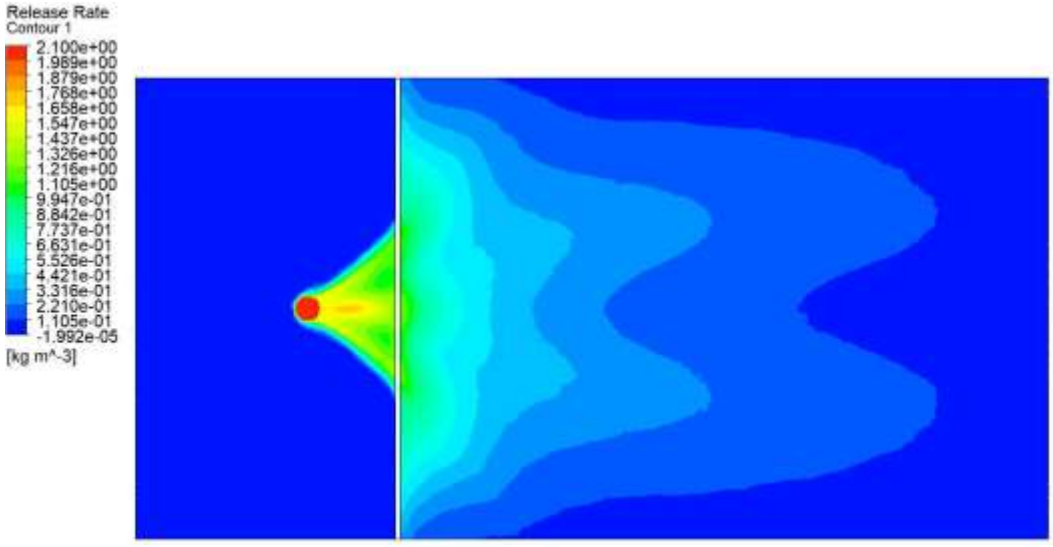

Figure 7.52: *Concentration profile of heavy gas release source for a flat terrain with a solid fence as an obstacle with* ***1m/s*** *velocity*

The concentration profile of the heavy gas for scenario 2A is shown in Figure 7.52 above. It shows the concentration profile for the heavy gas when released from a circular source with a 50mm diameter with a solid fence as an obstacle. Scenario 1A was performed in the same setting, but without the solid fence as an obstacle. It is noticed that the additional fence has affected the gas cloud in such a way that a high concentration triangle is formed from the release source to the fence and the gas cloud has widened due to the addition of the solid fence. Some additional layers of concentrations are formed in this case and the shape of the layers is not exactly sinusoidal for layers nearing the solid fence. The simulation shows that for this particular scenario the heavy gas cloud is distributed symmetrically along the horizontal axis. The concentration contour in the above figure shows the highest concentrations in red, while

the lowest are in blue. The concentrations continue to fade and there is a sort of layering pattern in the concentrations. The highest concentrations are in red , then the yellow has slightly lowered concentrations, then green with slightly lower still, and so on, with final layer (blue) being the lowest concentration.

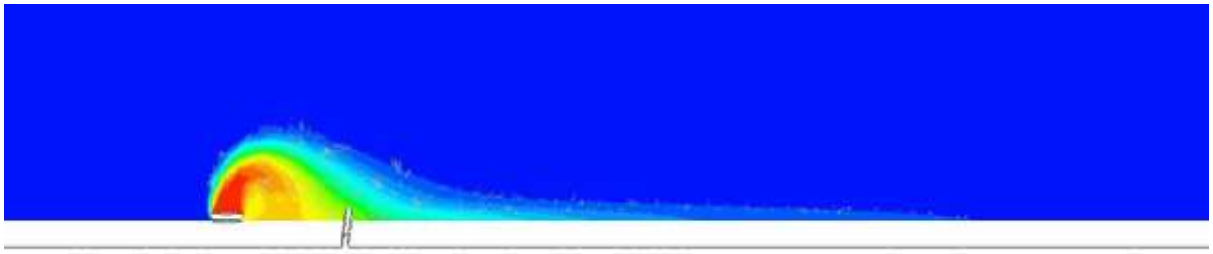

Figure 7.53: *2D view of concentration profile of heavy gas release source for a flat terrain with a solid fence as an obstacle with* ***1m/s*** *velocity.*

Figure 7.53 shows the two-dimensional version of the concentration simulation. They vary the behaviour of the cloud shape in this scenario to be the same as seen in (Figure 7.52).

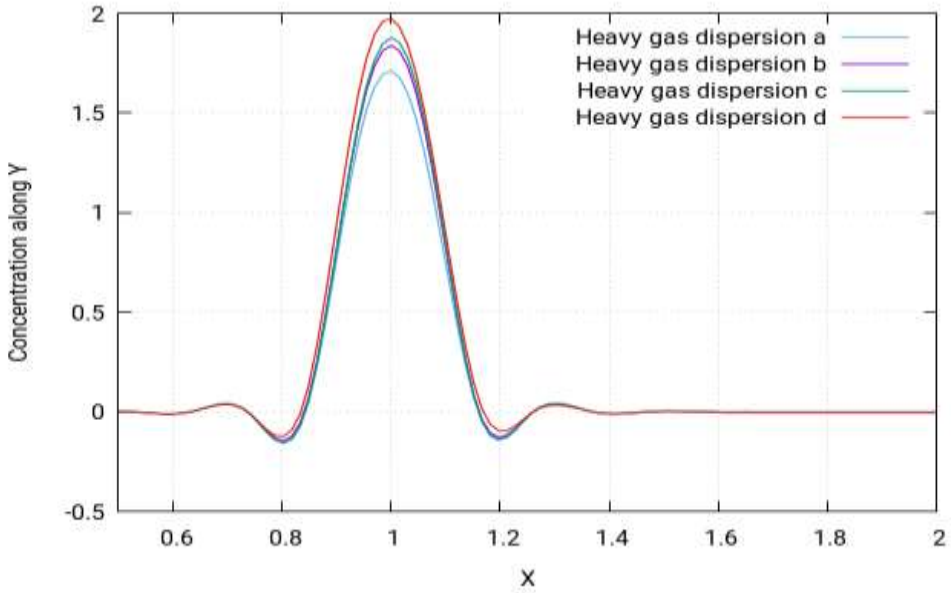

Figure 7.54: *Graphical representation for concentration of heavy gas release source for a flat terrain with* ***1m/s*** *velocity* ***before*** *a solid fence as an obstacle*

In the Figure 7.54, the concentration profiles for varying distances are shown. These are the results of the profiles before the solid fence. From the figure, it is concluded that the concentration value of the heavy gas decreases when moves away from the source as the figure shows declining behaviour of the concentration. In the figure, the curve with the highest peak is obtained when nearest to the release source and vice versa.

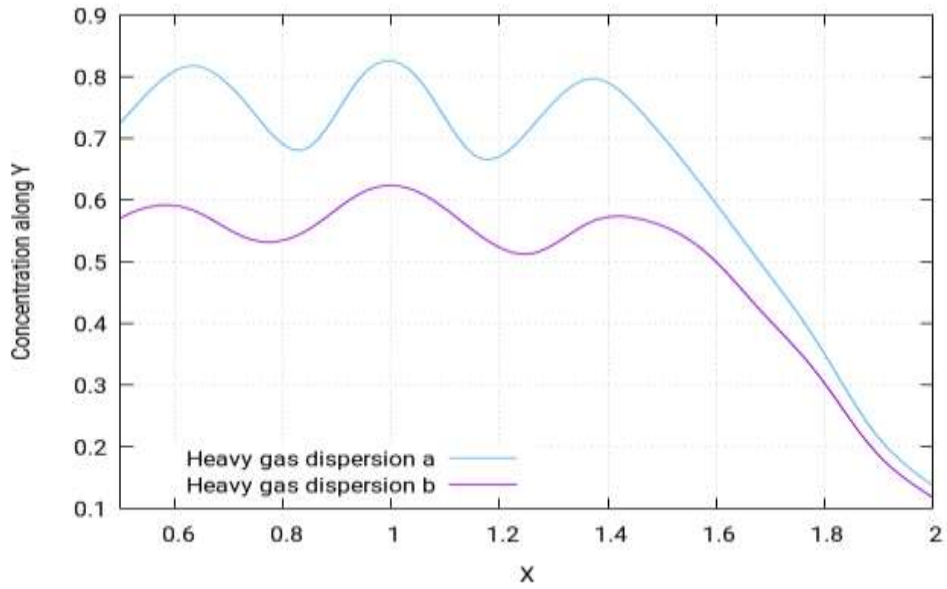

Figure 7.55: *Graphical representation for concentration of heavy gas release source for a flat terrain with **1m/s** velocity **after** a solid fence as an obstacle*

In Figure 7.55 above, the results of the concentration profiles before the fence were shown while this figure shows the results of the concentration profiles after the solid fence. "Heavy gas a" is at a distance of 0.27m, while "heavy gas b" is at a distance of 0.38m. Both the profiles follow the same pattern, but have different values of velocity, as the profile nearer to the source "heavy gas a" shows higher values of concentrations.

7.5.3.3 Density of heavy gas dispersion

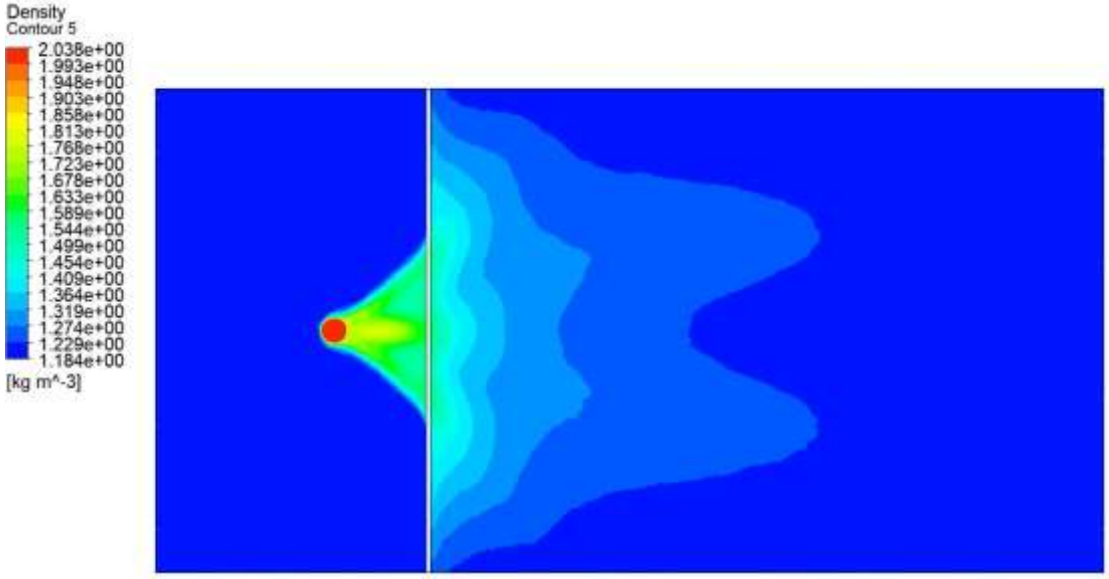

Figure 7.56: *Density profile of heavy gas release source for a flat terrain with a solid fence as an obstacle with **1m/s** velocity*

The density profile of the heavy gas for scenario 2A is shown in Figure 7.56 above. It shows the density profile for the heavy gas when released from a circular source of 50mm diameter

with a solid fence as an obstacle. In the first look, it appears that the density profile also follows the same pattern as that of concentration, keeping in mind the similarity in the concentration and density profile shown in figure 7.56 and figure 7.52 respectively. However, it should be noticed that the density profile appears to be a slightly shrunken version of the concentration profile. Moreover, the concentration contour shows the value of maximum concentration to be 2.1, while the density contours show a maximum value of 2.038.

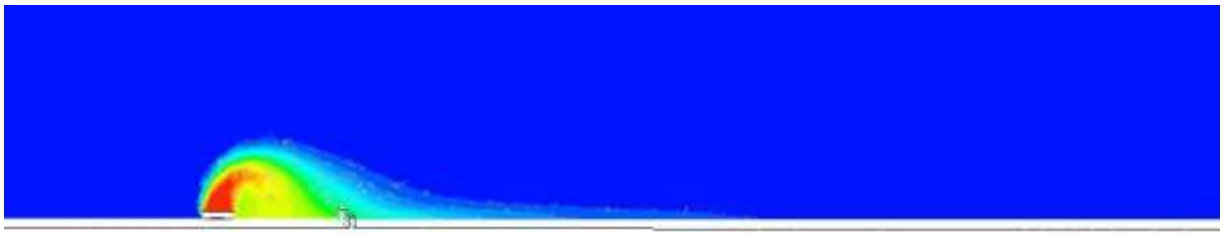

Figure 7.57: *2D-view of density profile of heavy gas release source for a flat terrain with a solid fence as an obstacle with* ***1m/s*** *velocity*

Figure 7.57 shows the two-dimensional view of the density profile. It also shows the same behaviour of the heavy gas as in (Figure 7.56).

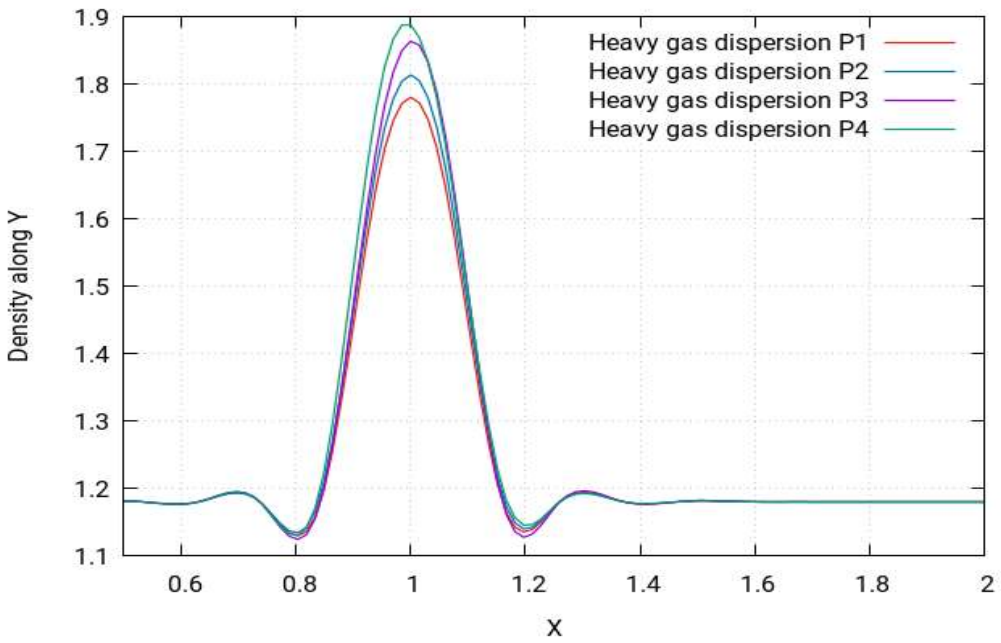

Figure 7.58: *Graphical representation for density of heavy gas release source for a flat terrain with* ***1m/s*** *velocity* ***before*** *a solid fence as an obstacle*

Figure 7.58 shows the profiles of the density of the released gas for varying distances before the solid fence. In the figure, the distance is calculated from the release source. This profile shows the same behaviour as that of the concentration profile.

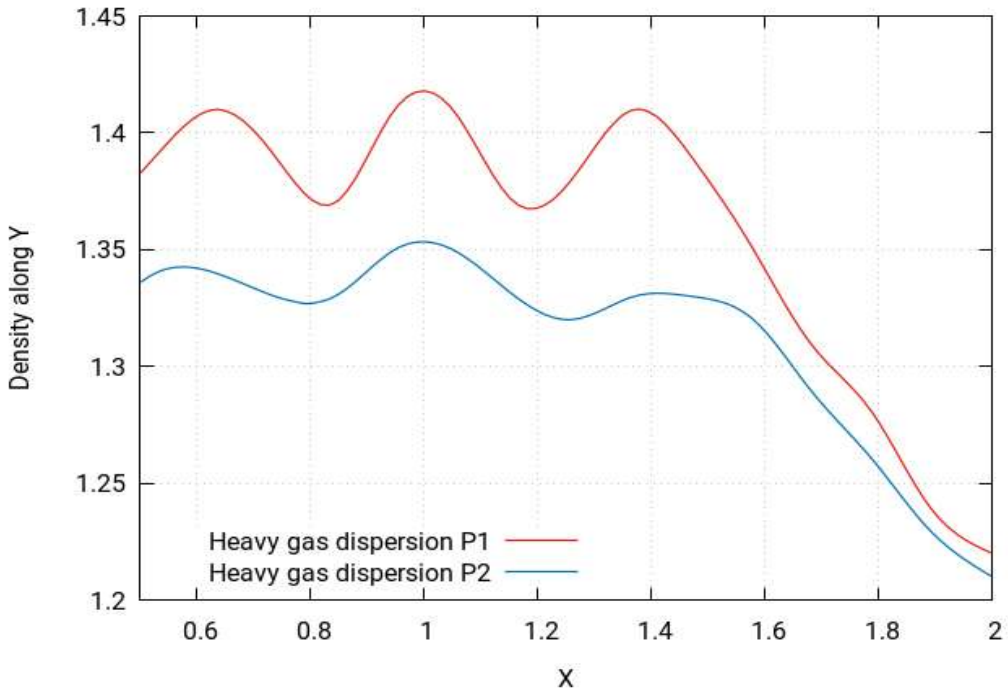

Figure 7.59: *Graphical representation for density of heavy gas release source for a flat terrain with* ***1m/s*** *velocity* ***after*** *a solid fence as an obstacle*

Figure 7.59 shows the two different profiles of the density of the gas released for varying distances after the solid fence. This profile also shows the same behaviour as that of the concentration profile.

7.5.3.4 Iso-surfaces of heavy gas dispersion

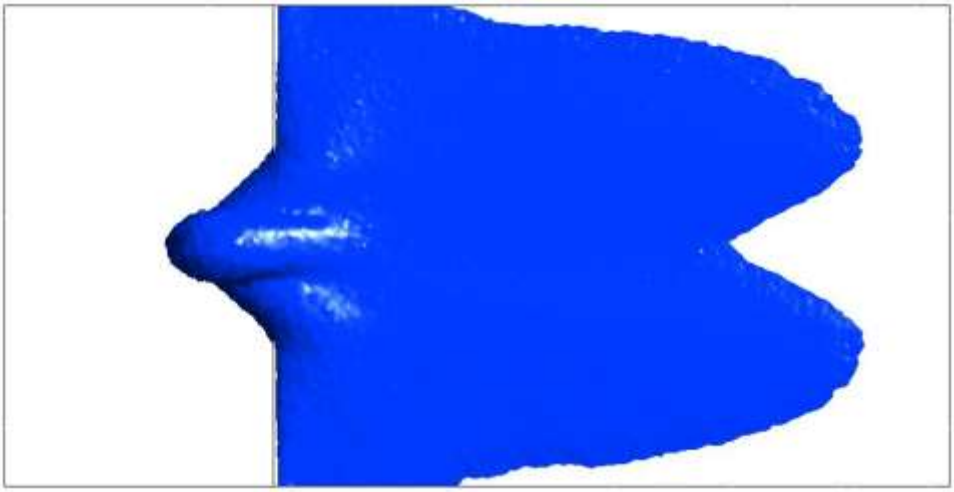

Figure 7.60: *Iso-surface top view of concentration of heavy gas release source for a flat terrain with solid fence as an obstacle* ***1m/s*** *velocity*

Figure 7.60 shows the iso-surface of the concentration from the top view. It shows the triangular-shaped distribution until the solid fence after which the distributions appear to be

uniform, before forming a sinusoidal curve at the end. It is noticed that the concentration is heaviest near the release source point and is distributed symmetrically along the axis.

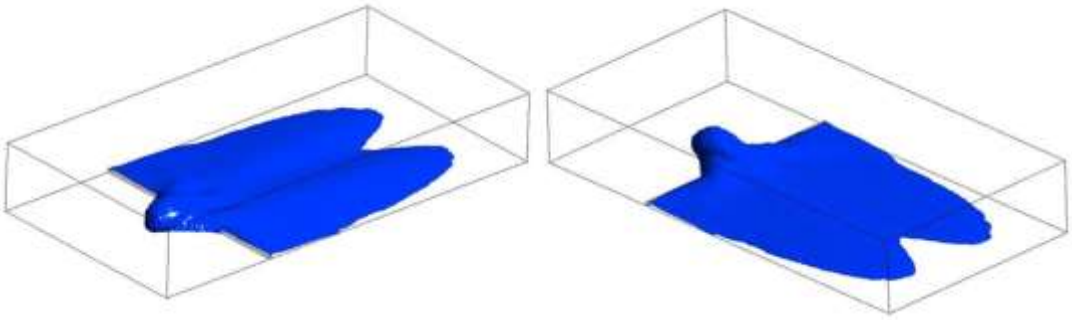

Figure 7.61: *Iso-surface side view of concentration of heavy gas release source for a flat terrain with a solid fence as an obstacle* ***1m/s*** *velocity*

Figure 7.61 shows the iso-surface of the concentration from the side view. It shows that the gas cloud, after showing an inclination of height near the release source, then goes on to decrease in height, and that it is at its thickest near the release source, whereas it continues becoming thinner as it moves along the horizontal axis. It shows the iso-surface of the concentration from the back view. In this figure, it can be seen that, although the gas cloud looks symmetrical along the horizontal axis in the previous views, the cloud density here is slightly more in the upside region of the gas cloud than the lower side. Therefore, along with the horizontal, the cloud might be horizontal but along the vertical, it shows deviations from symmetry.

According to Standard BS EN 60079-10-1:2009 Santon el. al. [104], the following locations can be categorised:

Zone 0: The triangular-shaped area near the release source location
Zone 1: The area starting immediately after zone 0 expanding uniformly
Zone 2: All the remaining locations not categorised in zone 0 and zone 1

7.5.3.5 Temperature of heavy gas dispersion

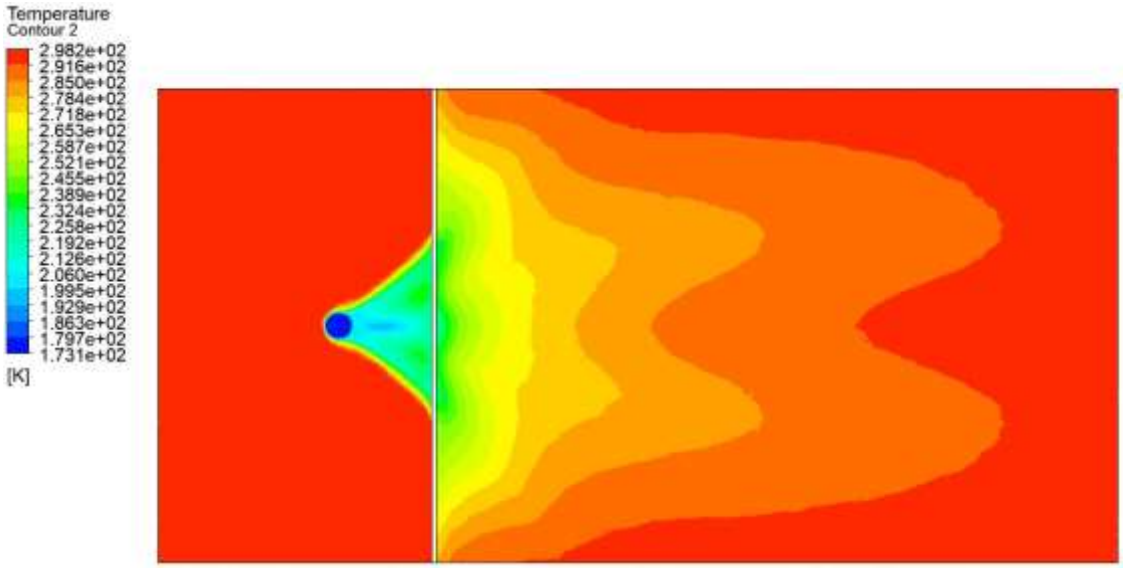

Figure 7.62: *Temperature profile of heavy gas release source for a flat terrain with a solid fence as an obstacle at* ***1m/s*** *velocity*

Figure 7.62 above shows the temperature simulation for this scenario. By visualising the temperature simulation, it is found out that it produces largely the same profile for this scenario as that of the concentration profile. However, the point to notice is that the behaviour of temperature is in fact the opposite to that of concentration. This means that the areas which were identified in the concentration simulation as highly concentrated will in fact have the lowest temperatures, while the ones with moderate concentrations will have moderate temperatures and the least concentrated areas will have the highest temperatures. To further simplify these findings, it should be pointed out that the simulations show that the concentrations near the release source point tend to be the highest, and start to fade away as they move away from the source, reaching the lowest levels when they move much further away, eventually reaching the environment where the gas cloud disappears. However, the temperature is at its lowest near the release source point and tends to increase as it moves away from the source, finally achieving the maximum temperature equal to the ambient temperature of the environment.

Figure 7.63: *2D view of temperature profile of heavy gas release source for a flat terrain with solid fence as an obstacle at* ***1m/s*** *velocity*

Figure 7.63 shows the two-dimensional version of the temperature simulation. It also shows the same behaviour of the concentration for heavy gas as shown in (Figure 7.62).

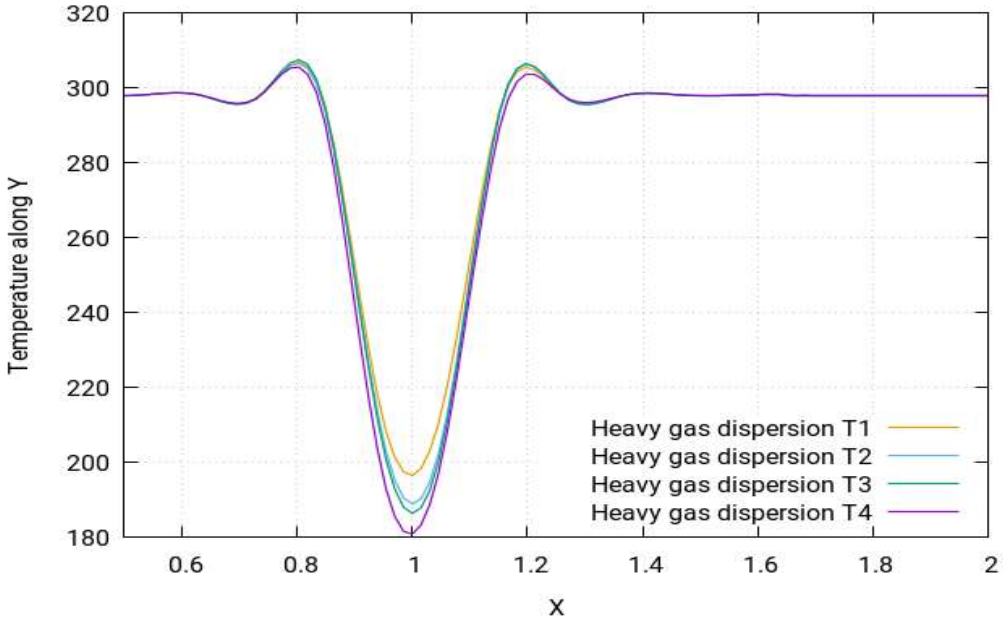

Figure 7.64: *Graphical representation of heavy gas release source temperature for a flat terrain at* ***1m/s*** *velocity* ***before*** *a solid fence*

The temperature profiles for varying distances before the obstacle (solid fence) are shown in the figure above. These profiles show the inverse or mirrored behaviour as that of the concentration profile.

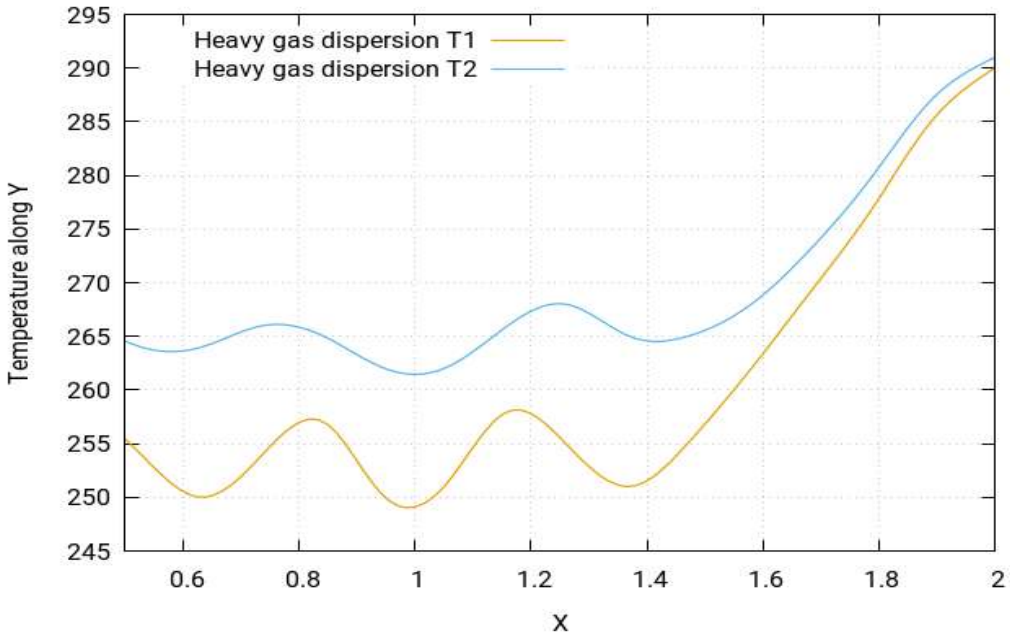

Figure 7.65: *Graphical representation of heavy gas release source temperature for a flat terrain at* ***1m/s*** *velocity* ***after*** *a solid fence*

Figure 7.65 shows the two different profiles of the temperature of the released gas for varying distances after a solid fence. This profile also shows the same behaviour as that of the concentration profile.

7.5.3.6 Velocity of heavy gas dispersion

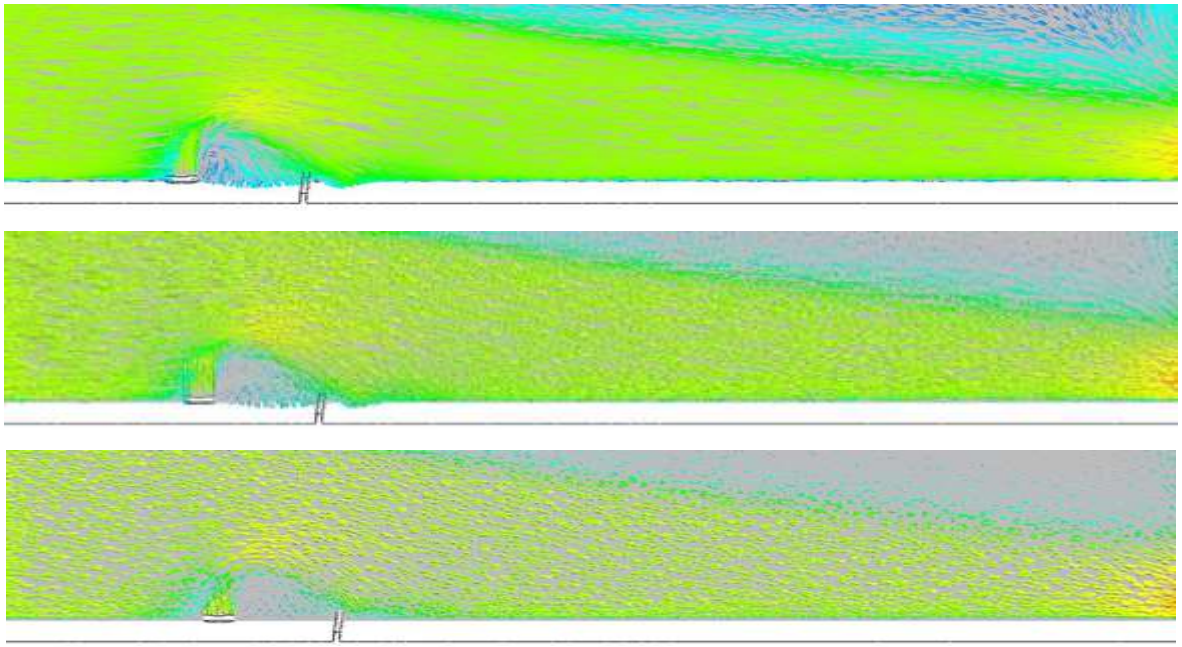

Figure 7.66: *Velocity profile of heavy gas release source for a flat terrain with a solid fence as an obstacle at* ***1m/s***

Figure 7.66 shows the velocity contours of neutral gas dispersion for this scenario. Velocity contours depict the intensity of wind or the effective wind influence at the different locations throughout the layout. As can be seen in the figure, the wind intensity is different at different points in the layout. The wind operation is smooth in this scenario and not many complex vertexes can be seen. The wind eddies carry the gas cloud to the nearby environment, where a gas cloud is formed due to steady flow. This gas cloud is deemed dangerous as it is volatile and could lead to an explosion, fire, etc.

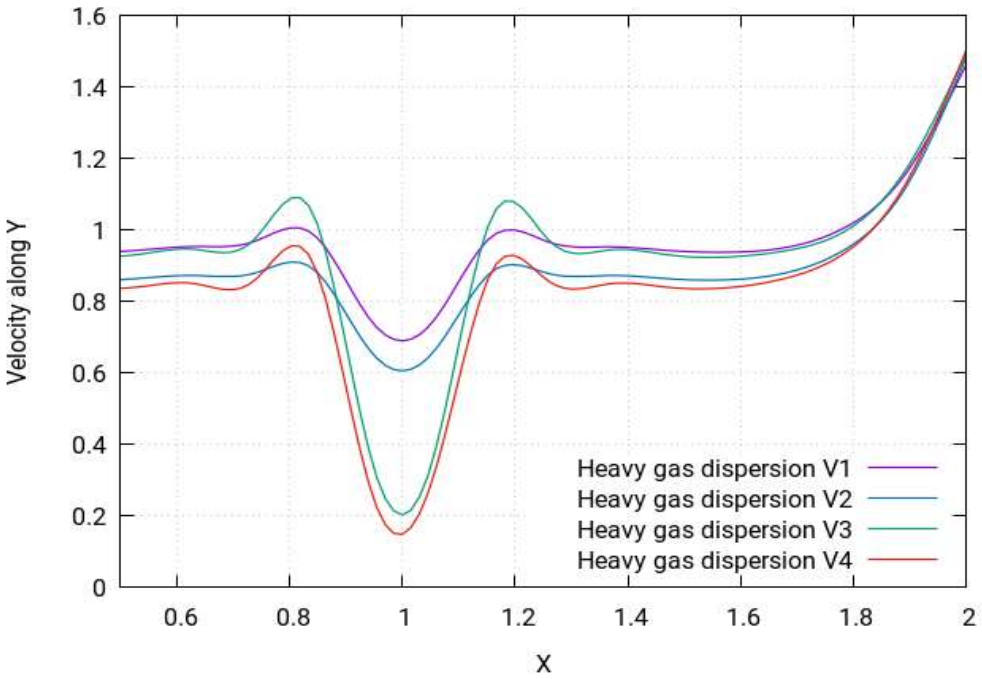

Figure 7.67: *Graphical representation of the velocity profile of heavy gas release source for a flat terrain* ***before*** *a solid fence as an obstacle at* ***1m/s***

Figure 7.67 shows the varying profiles of the velocity before the obstacle with carrying distances. While the profiles do follow a same pattern, the values change according to the varying distances.

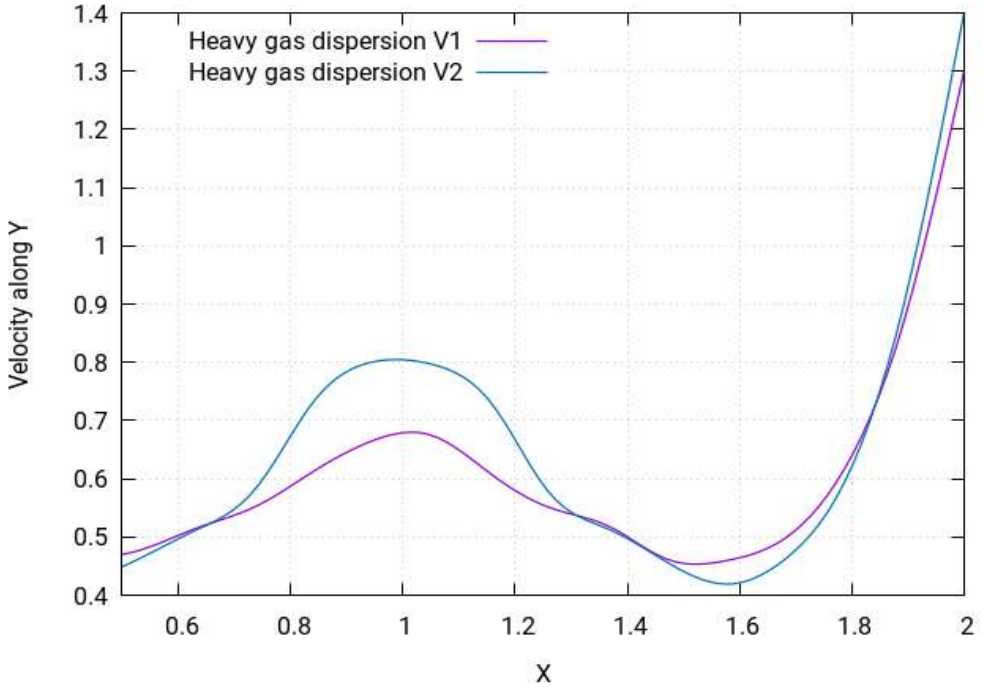

Figure 7.68: *Graphical representation of the velocity profile of heavy gas release source for a flat terrain* ***after*** *a solid fence as an obstacle at* ***1m/s***

The above shows the velocity profiles after the obstacle for this scenario. Both the curves follow the same pattern but have different values.

7.5.4 Neutral gas dispersion with a straight solid fence as an obstacle

The second scenario includes a neutral gas leak from a circular source with a 50mm diameter. The terrain is flat, but there is a solid fence, which is 400mm downstream of the plume and has a height of 30mm.

Table 7.4: *Parametric values of scenario 2B*

Density	Flow Rate	Velocity	Ambient Temperature	Release Source Temperature
1.1839 kg m/s^3	1.7737 kg/s	1 m/s	25°C	25°C

7.5.4.1 Release source point

The following figure shows the release source for the current scenario:

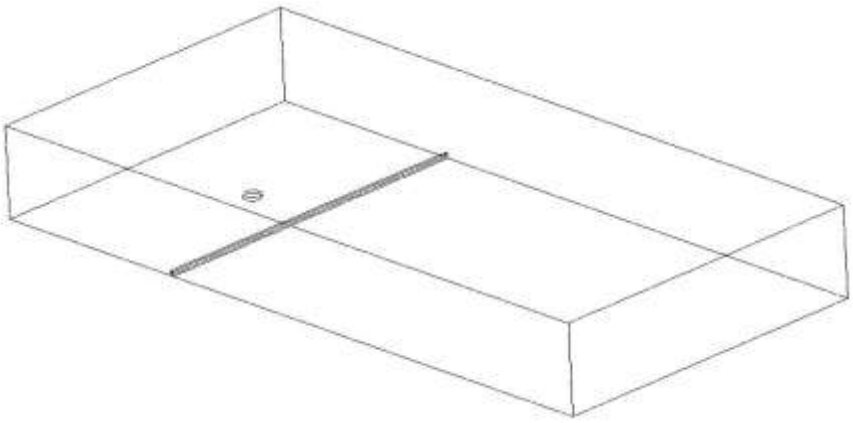

Figure 7.69: *Neutral gas release source for a flat terrain with a solid fence as an obstacle at* ***1m/s*** *velocity*

7.5.4.2 Concentration of the neutral gas dispersion

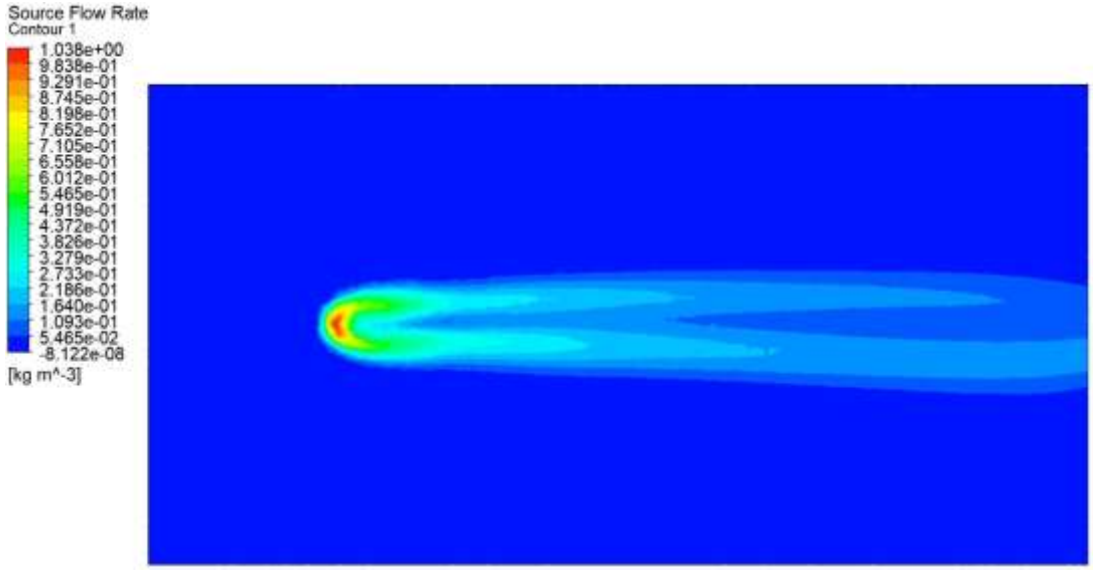

Figure 7.70: *Concentration profile of neutral gas release source for a flat terrain with a solid fence as an obstacle at* ***1m/s*** *velocity*

The concentration profile of the neutral gas for scenario 2B is shown in Figure 7.70 above. It shows the concentration profile for the neutral gas when released from a circular source of 50mm diameter with a solid fence as an obstacle. It can be seen that the cloud shape for this scenario is of the shape of an elliptical cylinder, which was also the case in scenario 1B. However, here the addition of a solid fence as an obstacle has influenced the cloud shape of the neutral gas; it is not exactly a cylinder, but has a small dent shortly after the heavily concentrated area near the release source, with the top end near the release source of the cylinder being thinner than the other end. The simulation shows the highest concentrations in red near the release source. Thereafter, the concentrations begin to decrease. From the simulation, it can be observed that the concentration distribution is not symmetrical along the horizontal axis and that the lower half of the elliptical cylinder is more concentrated.

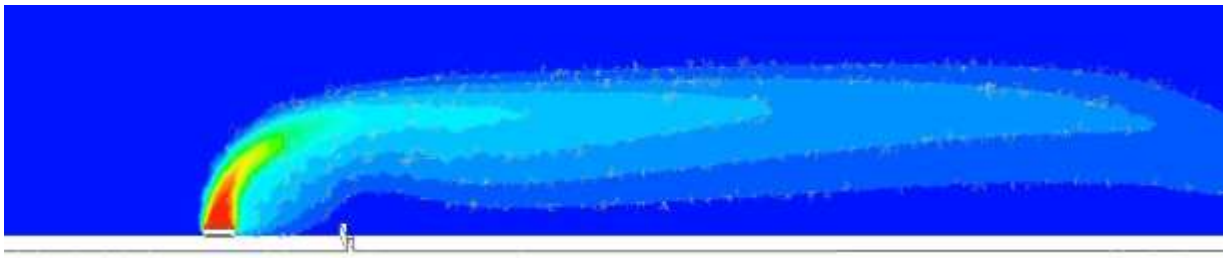

Figure 7.71: *2D view of concentration profile of neutral gas release source for a flat terrain with a solid fence as an obstacle at* ***1m/s*** *velocity*

Figure 7.71 shows the two-dimensional version of the concentration simulation. It further verifies the behaviour of the cloud shape for neutral gas discussed in the previous (Figure 7.70).

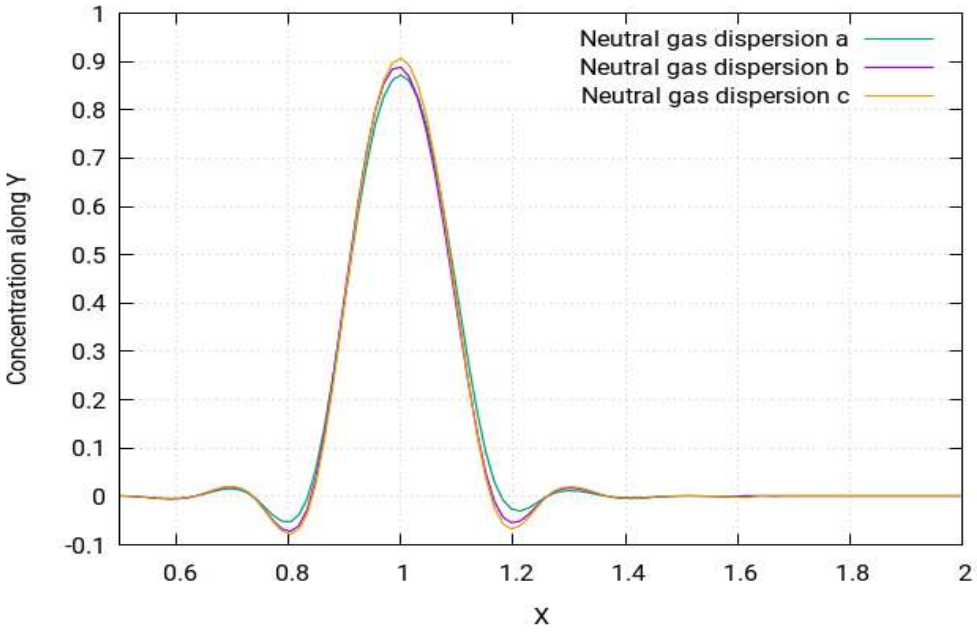

Figure 7.72: *Graphical representation of concentration profile of neutral gas release source for a flat terrain with a solid fence as an obstacle at* ***1m/s*** *velocity*

Figure 7.72 shows the concentration profiles of this scenario with varying distances. The same behaviour of the concentration profile as observed in heavy gas is also observed here. However, the difference in the concentration values is very small, like that of heavy gas.

7.5.4.3 Iso-Surfaces of the neutral gas dispersion

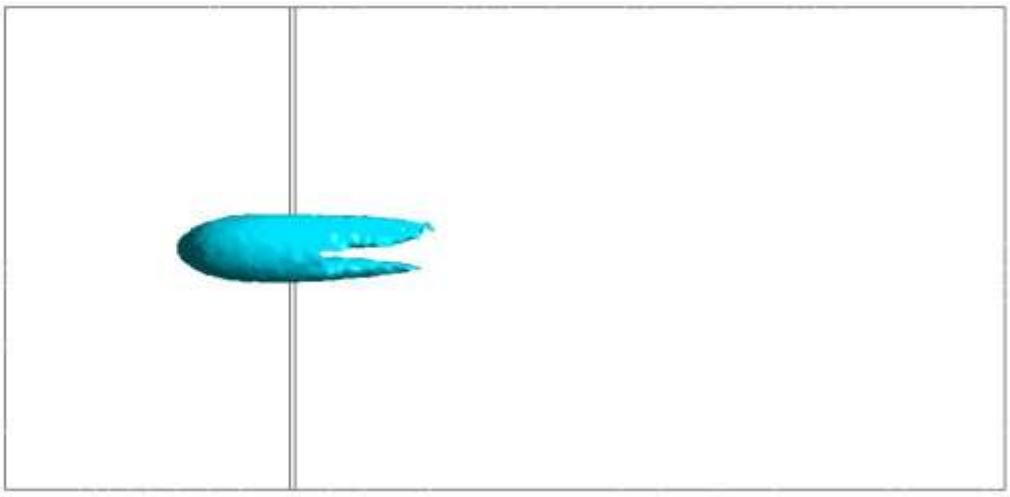

Figure 7.73*: Iso-surface top view of concentration of neutral gas release source for a flat terrain with a solid fence as an obstacle at* ***1m/s*** *velocity*

Figure 7.73 shows the iso-surface of the concentration from the top view. It is observed that the that the upper end of the cloud is thicker than the lower end and extends more the horizontal axis than the lower end, although not as much as it did in scenario 1B.

Figure 7.74: *Iso-surface side view of concentration of heavy gas release source for a flat terrain with a solid fence as an obstacle at* ***1m/s*** *velocity*

Figure 7.74 shows the iso-surface of the concentration from the side view. It shows the same results as discussed in the previous figures. It also shows the iso-surface of the concentration from the back view. It further verifies the cloud shape pattern discussed previously.

According to Standard BS EN 60079-10-1:2009 Santon el. al. [104], the following locations can be categorised:

Zone 0: The immediate surrounding of the release source

Zone 1: The area surrounding the obstacle

Zone 2: All the remaining locations not categorised in zone 0 or zone 1

7.5.4.4 Velocity of the neutral gas dispersion

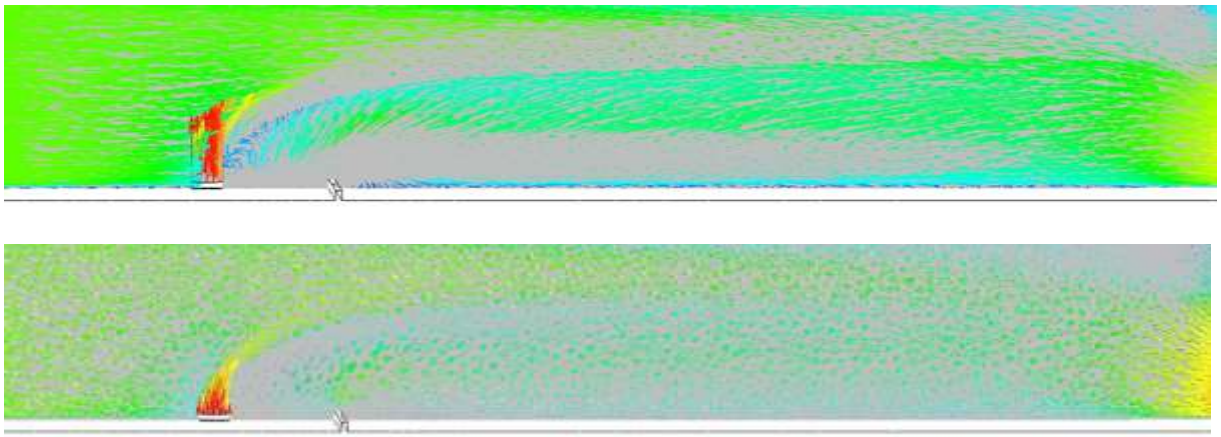

Figure 7.75: *Velocity profile of neutral gas release source for a flat terrain with a solid fence as an obstacle at* ***1m/s*** *velocity*

Figure 7.75 shows the velocity contours of neutral gas dispersion for this scenario. Velocity contours depict the intensity of wind or the effective wind influence at the different locations throughout the layout. It can be seen in the figure that the wind intensity is different at different points in the layout. In scenario 1A, the wind operation was smooth, and not many complex vertexes were observed. However, in this scenario, there are many complex vertexes formed near the release source location, as seen in the figure. These complex vertexes carry the gas

cloud to the nearby environment, where a gas cloud is formed due to steady flow. This gas cloud is deemed dangerous as it is volatile and could lead to an explosion, fire, etc. This also causes the gas cloud to enhance in the upward direction.

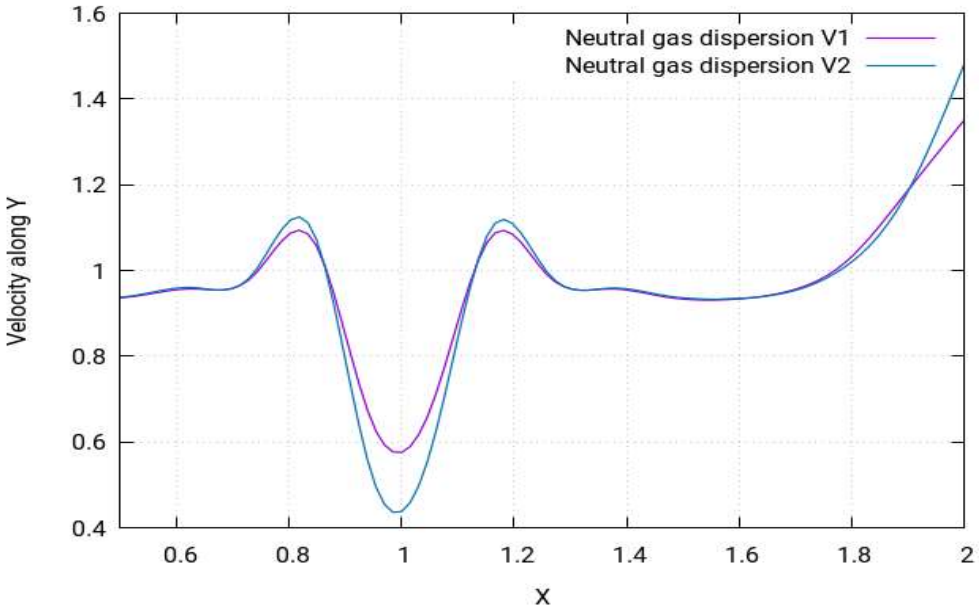

Figure 7.76: *Graphical representation of velocity of neutral gas release source for a flat terrain with a solid fence as an obstacle at* ***1m/s***

Figure 7.76 shows the varying profiles of the velocity for this scenario with varying distances. While the profiles do follow a same pattern, the values change according to the varying distances.

7.5.5 Heavy gas dispersion with a solid and a semi-circular fence

The third scenario has a heavy gas leak occurring from a circular source, which is 50mm in diameter. There are two obstacles for the plume in the form of fences, which are 400mm downstream from the source. The solid fence has a height of 30 mm, and the semi-circular fence has a height of 30mm.

Table 7.5: *Parametric values of scenario 3A*

Density	Flow Rate	Velocity	Ambient Temperature	Release Source Temperature
2.1 kg m/s^3	1 kg/s	1 m/s	25°C	-100°C

7.5.5.1 Release source

The following figure shows the release source for the current scenario.

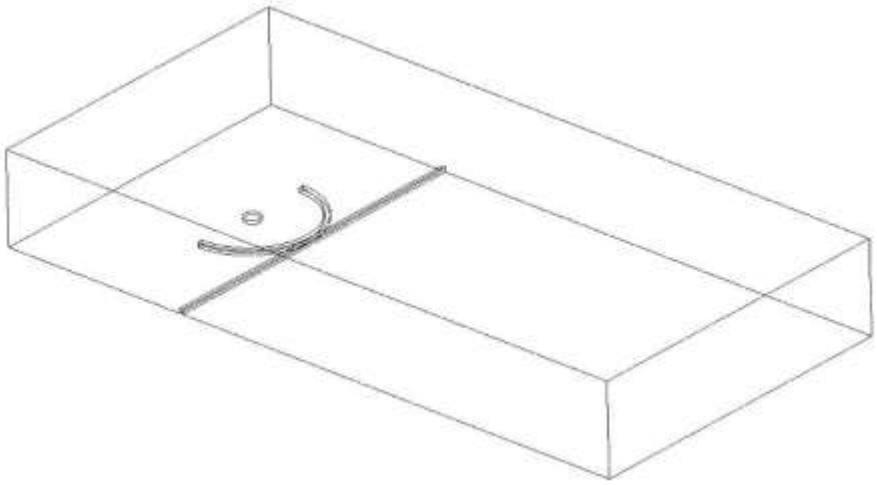

Figure 7.77: *The heavy gas release source for a flat terrain with a solid and a semi-circular fence as an obstacle at* ***1m/s*** *velocity*

7.5.5.2 Concentration of the heavy gas dispersion

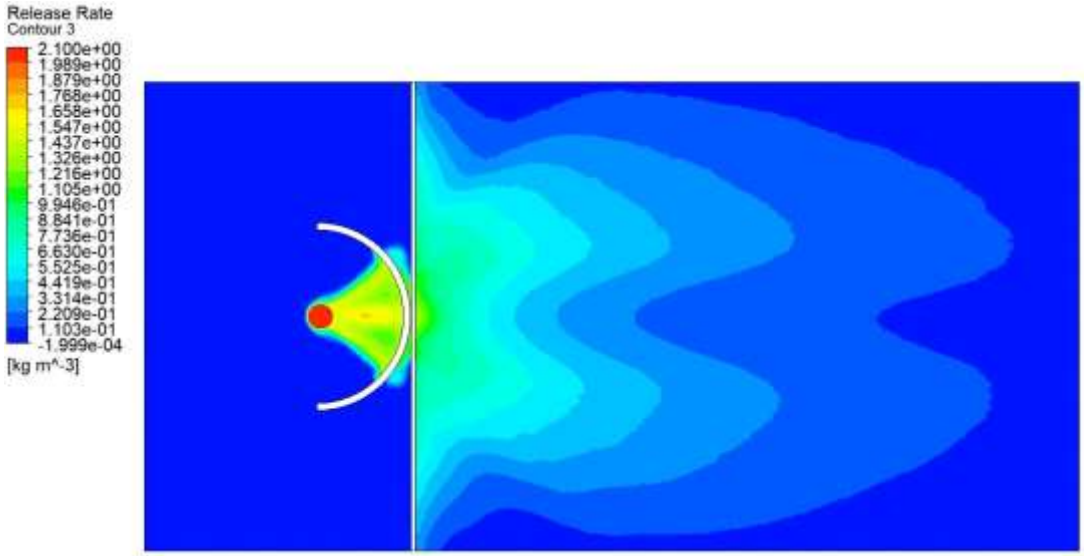

Figure 7.78: *Concentration profile of heavy gas release source for a flat terrain with a solid and a semi-circular fence as an obstacle with* ***1m/s*** *velocity*

The concentration profile of the heavy gas for scenario 3A is shown in Figure 7.78 above. It shows the concentration profile for the heavy gas when released from a circular source of 50mm diameter with a solid fence as an obstacle. Scenario 1A was performed with the same settings but without the solid and semi-circular fences as an obstacle. The additional two fences have affected the gas cloud in such a way that the high concentration triangle is now converted into a curve along the inner surface of the semi-circular fence. It can be further noticed that, with the addition of the fence, the layers of concentrations have also increased, and immediately after the solid fence, many small layers of high concentrations can be seen. The simulation shows that, for this particular scenario, the heavy gas cloud is distributed

symmetrically along the horizontal axis. The concentration contour in the figure above shows the highest concentrations in red while the lowest are in blue. The concentrations continue fading and there is a sort of layering pattern in the concentrations, with maximum concentrations in red being the layer with the highest concentrations, then the yellow ones with slightly less concentrations, followed by green with slightly less, and so on, with the final layer (blue) being the lowest concentration.

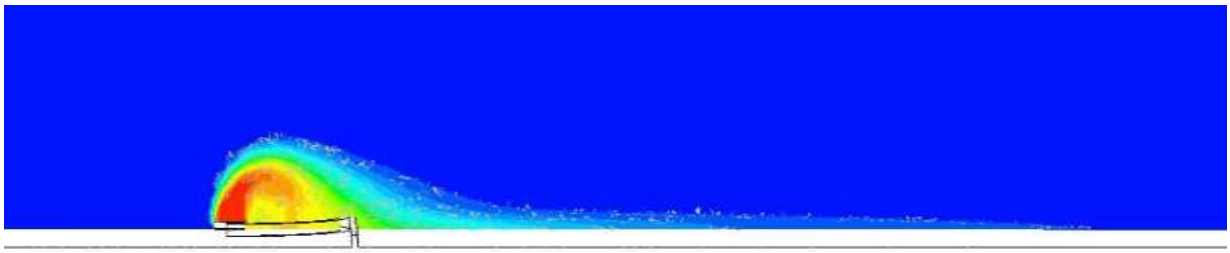

Figure 7.79: *2D view of concentration profile of heavy gas release source for a flat terrain with a solid and a semi-circular fence as an obstacle with* ***1m/s*** *velocity*

Figure 7.79 shows the two-dimensional version of the concentration simulation. They verify the behaviour of the cloud shape in this scenario as being the same as seen in (Figure 7.78).

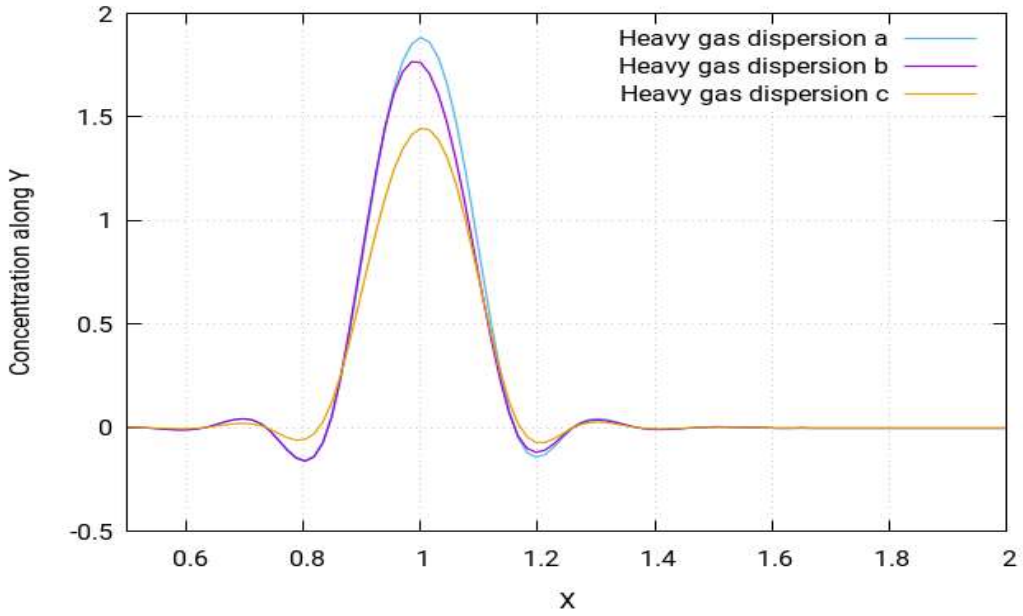

Figure 7.80: *Graphical representation for concentration of heavy gas release source for a flat terrain with* ***1m/s*** *velocity* ***before*** *the solid and the semi-circular fence as an obstacle*

The concentration profiles for this scenario before the obstacle for varying distances are shown in the figure above. The same behaviour of concentration profiles as observed in previous heavy gas scenarios 1A and 2A is also visible here.

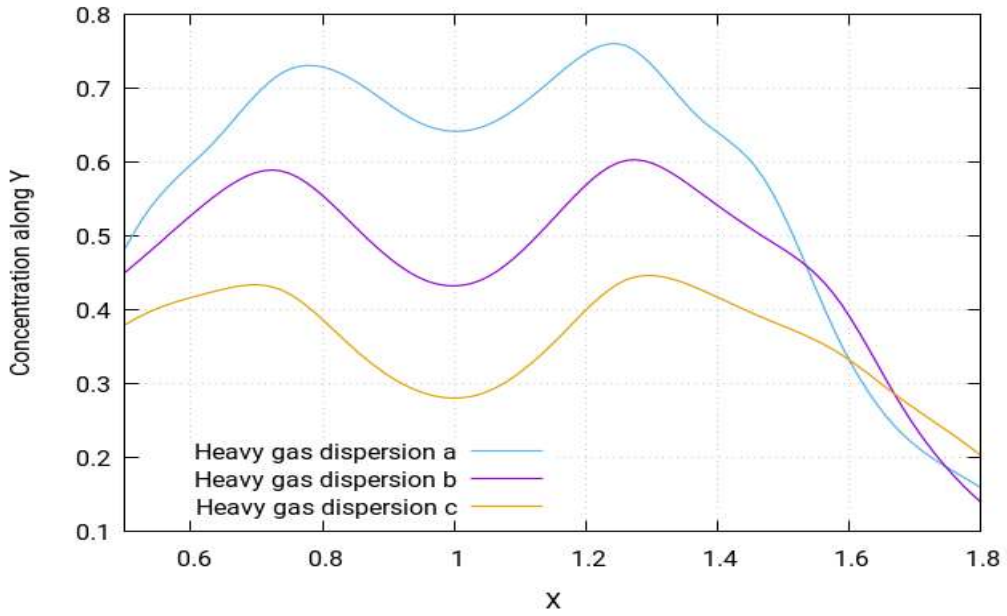

Figure 7.81: *Graphical representation for concentration of heavy gas release source for a flat terrain with **1m/s** velocity **after** a solid and the semi-circular fence as an obstacle*

The concentration profiles for this scenario after the obstacle for varying distances are shown in the above figure. While the profile of concentration shows a different pattern after the obstacle to before the obstacle, the profile at different points after the obstacle follows the same pattern and has different values to the distance from release source.

7.5.5.3 Density of the heavy gas dispersion

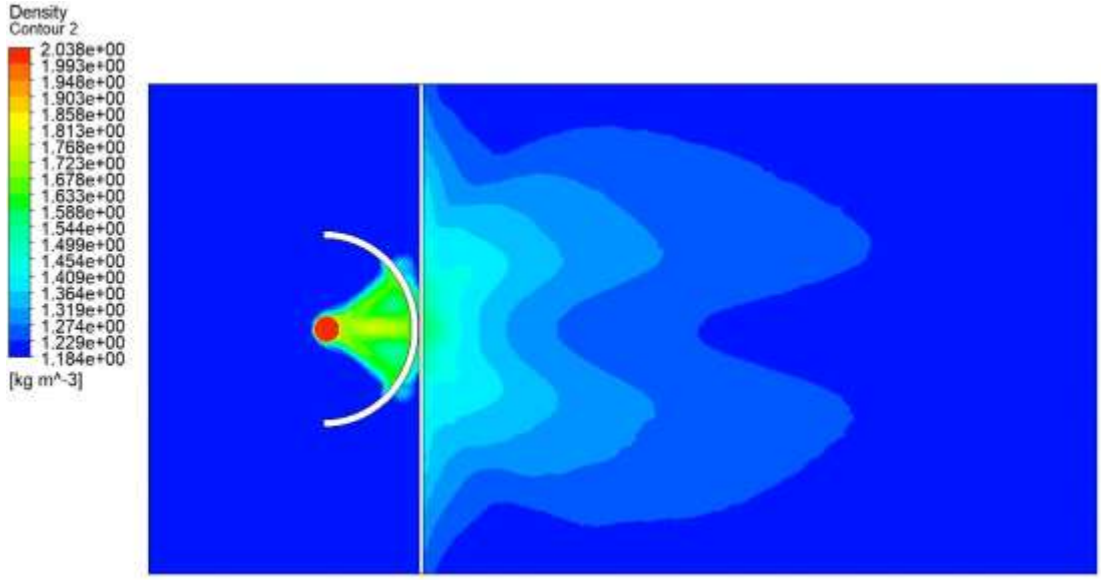

Figure 7.82: *Density profile of heavy gas release source for a flat terrain with a solid and a semi-circular fence as an obstacle with **1m/s** velocity*

The density profile of the heavy gas for scenario 3A is shown in Figure 7.82 above. It shows the density profile for the heavy gas when released from a circular source of 50mm diameter

with a solid and a semi-circular fence as an obstacle. At first glance, it appears that the density profile also follows the same pattern as that of concentration, keeping in mind the similarity in the concentration and density profile shown in Figure 7.82 and Figure 7.78, respectively. However, it must be noticed that the density profile appears to be a slightly shrunken version of the concentration profile. Moreover, the concentration contour shows the value of maximum concentration to be 2.1, while the density contours show a maximum value of 2.038.

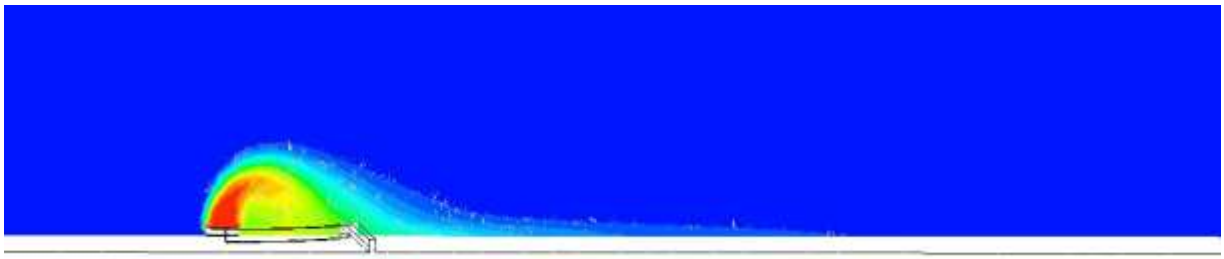

Figure 7.83: *2D view of density profile of heavy gas release source for a flat terrain with a solid and a semi-circular fence as an obstacle with* ***1m/s*** *velocity*

Figure 7.83 shows the two-dimensional view of the density profile and shows the same behaviour of the heavy gas as (Figure 7.82).

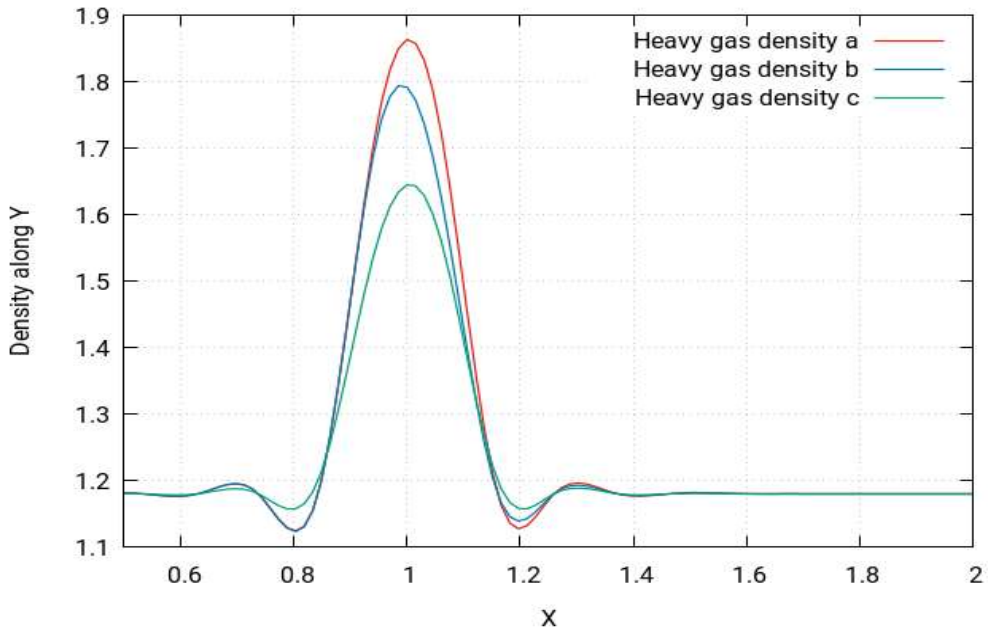

Figure 7.84: *Graphical representation of density profile of heavy gas release source for a flat terrain* ***before*** *a solid and a semi-circular fence as an obstacle with* ***1m/s*** *velocity.*

Figure 7.84 shows the profiles of the density before the obstacle of the released gas with varying distances. In the figure, the distance is calculated from the release source. This profile shows the same behaviour as that of the concentration profile.

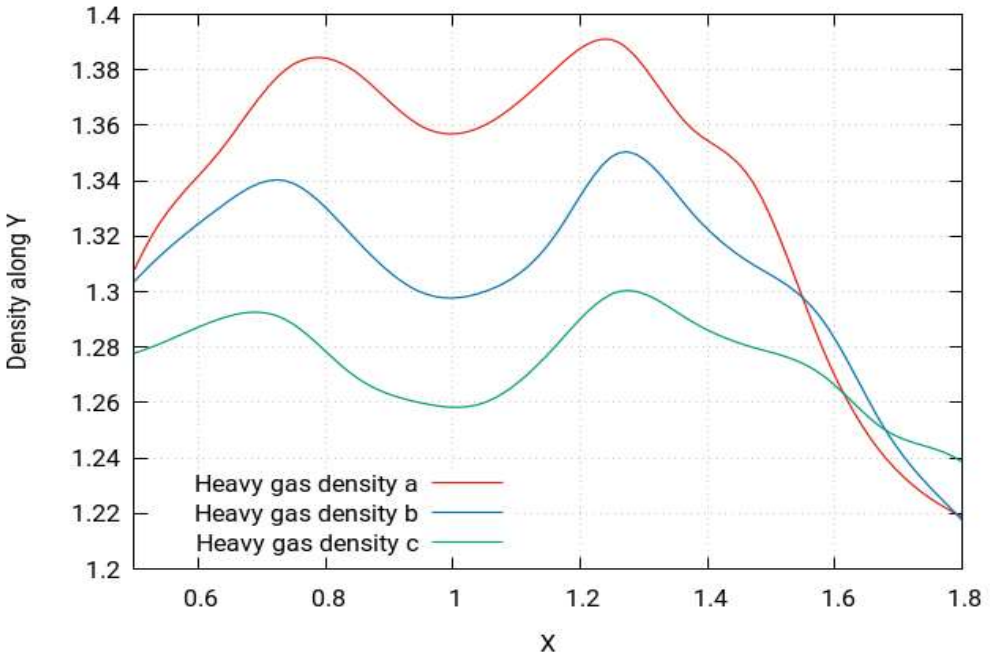

Figure 7.85: *Graphical representation of density profile of heavy gas release source for a flat terrain* ***after*** *a solid and a semi-circular fence as an obstacle with* ***1m/s*** *velocity*

Figure 7.85 shows the profiles of the density after the obstacle of the released gas with varying distances. In the figure, the distance is calculated from the release source. This profile shows the same behaviour as that of the concentration profile.

7.5.5.4 Temperature of the heavy gas dispersion

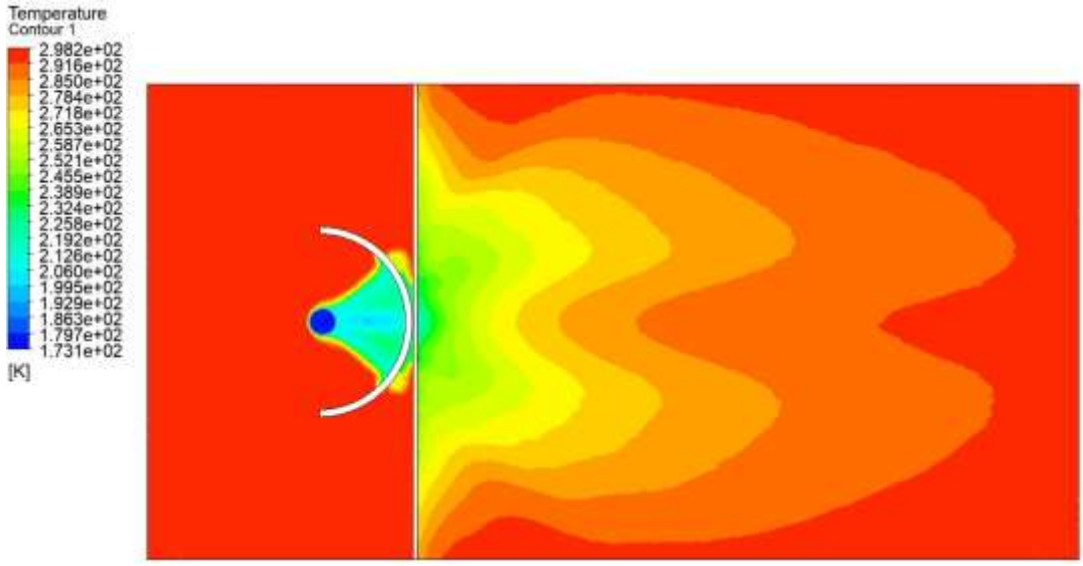

Figure 7.86: *Temperature profile of heavy gas release source for a flat terrain with a solid and a semi-circular fence as an obstacle with* ***1m/s*** *velocity*

Figure 7.86 above shows the temperature simulation for this scenario. By visualising the temperature simulation, it is found out that the temperature simulation produces largely the same profile for this scenario as that of the concentration profile. However, it should be noticed

that the behaviour of temperature is in fact the opposite to that of concentration. This means that the areas which were identified in the concentration simulation as highly concentrated will in fact have the lowest temperatures, while ones with moderate concentrations will have moderate temperatures and the least concentrated areas will have the highest temperatures. To further simplify these findings, it should be pointed out that the simulations show that the concentrations near the release source point tend to be the highest and start to fade away as they move away from the source, reaching the lowest levels when they move much further away, eventually reaching the environment where the gas cloud disappears. However, the temperature is at its lowest near the release source point and tends to increase as it moves away from the source, finally achieving its highest temperature equal to the ambient temperature of the environment.

Figure 7.87: *2D view of temperature profile of heavy gas release source for a flat terrain with a solid and a semi-circular fence as an obstacle with* ***1m/s*** *velocity*

Figure 7.87 shows the two-dimensional view of the temperature profile and shows the same behaviour of the heavy gas as (Figure 7.86).

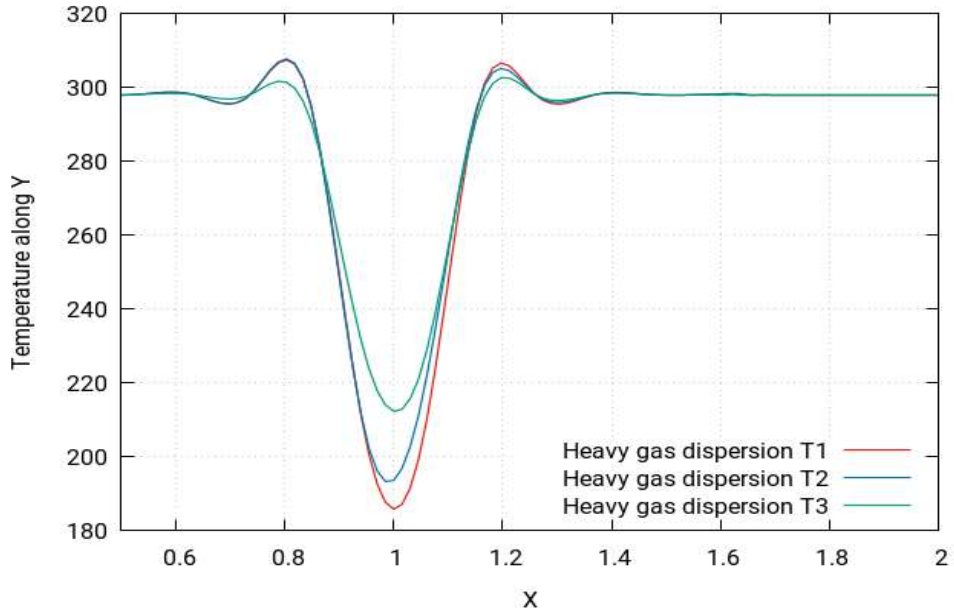

Figure 7.88: *Graphical representation of temperature profile of heavy gas release source for a flat terrain* ***before*** *solid and a semi-circular fence as an obstacle with* ***1m/s*** *velocity*

Figure 7.88 shows the profiles of the temperature of the released gas before the obstacle for varying distances. In the figure, the distance is calculated from the release source. These profiles are a mirror of the density profile.

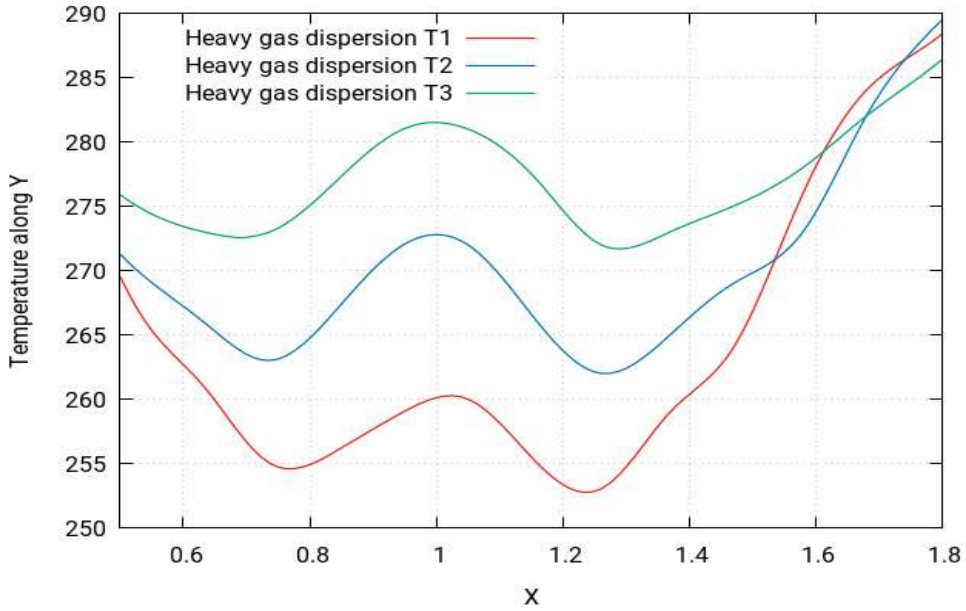

Figure 7.89: *Graphical representation of temperature profile of heavy gas release source for a flat terrain* ***after*** *a solid and a semi-circular fence as an obstacle with* ***1m/s*** *velocity*

Figure 7.89 shows the profiles of the temperature after the obstacle of the released gas with varying temperatures. In the figure, the temperature is calculated from the release source. This profile shows the same behaviour as that of the concentration profile.

7.5.5.5 Iso-surfaces of the heavy gas dispersion

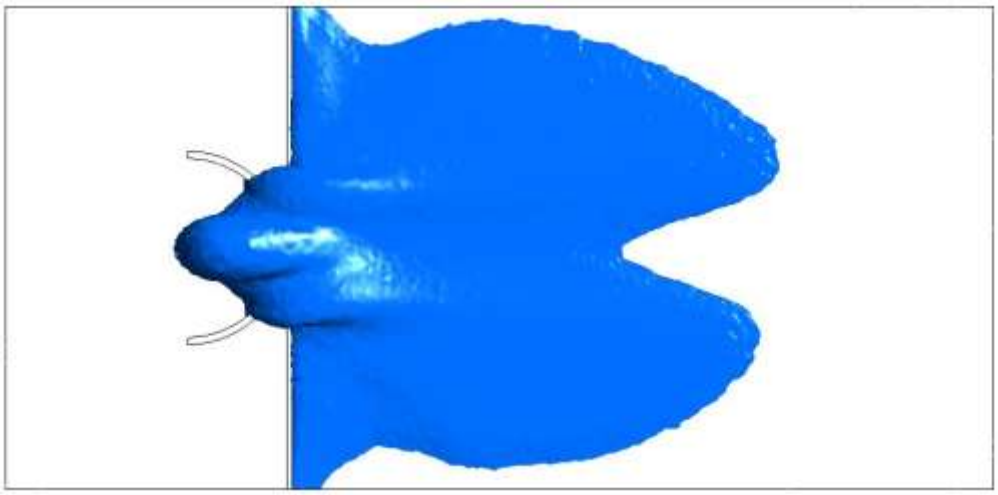

Figure 7.90: *Iso-surface top view of concentration of heavy gas release source for a flat terrain with a solid and a semi-circular fence as an obstacle* ***1m/s*** *velocity*

Figure 7.90 shows the iso-surface of the concentration from the top view. It shows the triangular shaped distribution converted into curve shaped distribution along the inner wall of

the semi-circular fence until the solid fence after which the distributions appear to be uniform and then form a sinusoidal curve at the end. The concentration is heaviest near the release source point and is distributed symmetrically along the axis.

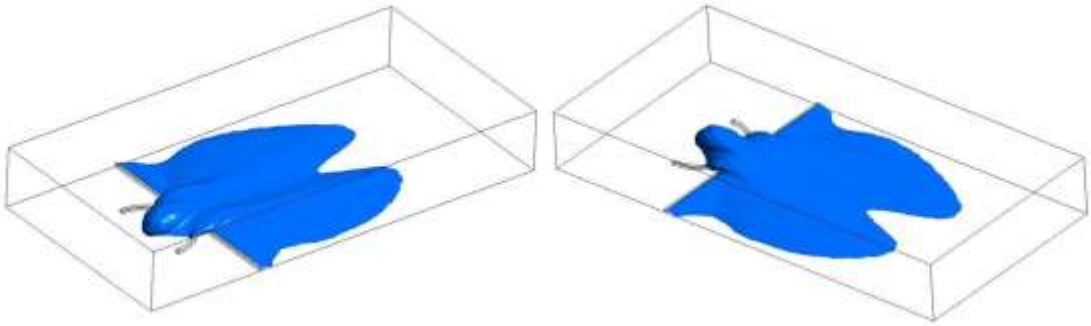

Figure 7.91: *Iso-surface back and side view of concentration of heavy gas release source for a flat terrain with a solid and a semi-circular fence as an obstacle* ***1m/s*** *velocity*

Figure 7.91 shows the iso-surface of the concentration from the side view. It shows that the gas cloud, after showing an inclination of height near the release source, then goes on to decreased in height, and that it is at its thickest near the release source, whereas it continues becoming thinner as it moves along the horizontal axis. It shows the iso-surface of the concentration from the back view. In this figure, it can be seen that, although the gas cloud looked symmetrical along the horizontal axis in the previous views, the cloud density here is slightly more in the upside region of the gas cloud than the lower side. So, along the horizontal axis, the cloud might be, symmetrical, but along the vertical, it shows deviations from symmetry.

According to Standard BS EN 60079-10-1:2009 Santon el. al. [104], the following locations can be categorised:

Zone 0: The triangular shaped area near the release source location

Zone 1: The inner surface of the semi-circular obstacle

Zone 2: All the remaining locations not categorised in zone 0 or zone 1

7.5.5.6 Velocity of the heavy gas dispersion

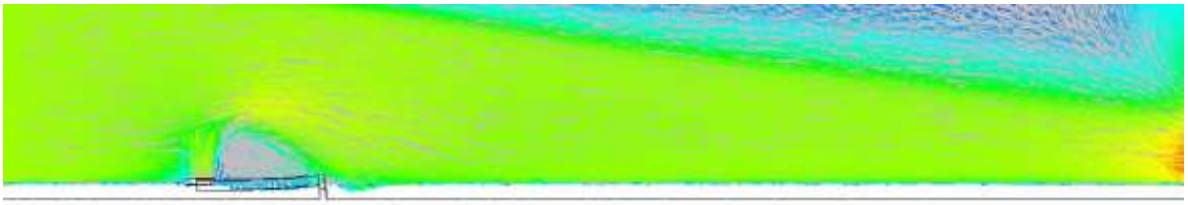

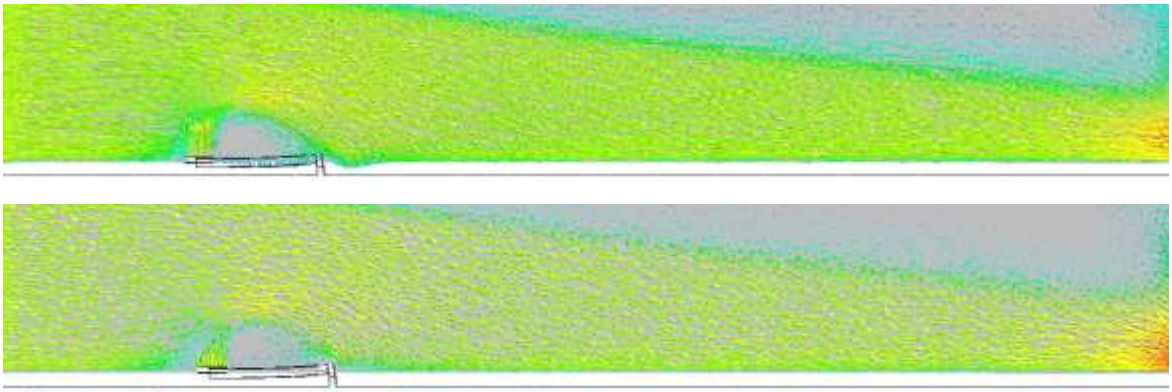

Figure 7.92: *Velocity profile of heavy gas release source for a flat terrain with a solid and a semi-circular fence as an obstacle* ***1m/s*** *velocity*

Figure 7.92 shows the velocity contours of heavy gas dispersion for this scenario. Velocity contours depict the intensity of wind or - or the effective wind influence - at the different locations throughout the layout. As can be seen in the figure, the wind intensity is different at different points in the layout. The wind operation is smooth in this scenario and not many complex vertexes can be seen. The wind eddies carry the gas cloud to the nearby environment, where a gas cloud is formed due to steady flow. This gas cloud is deemed dangerous as it is volatile and could lead to an explosion, fire, etc.

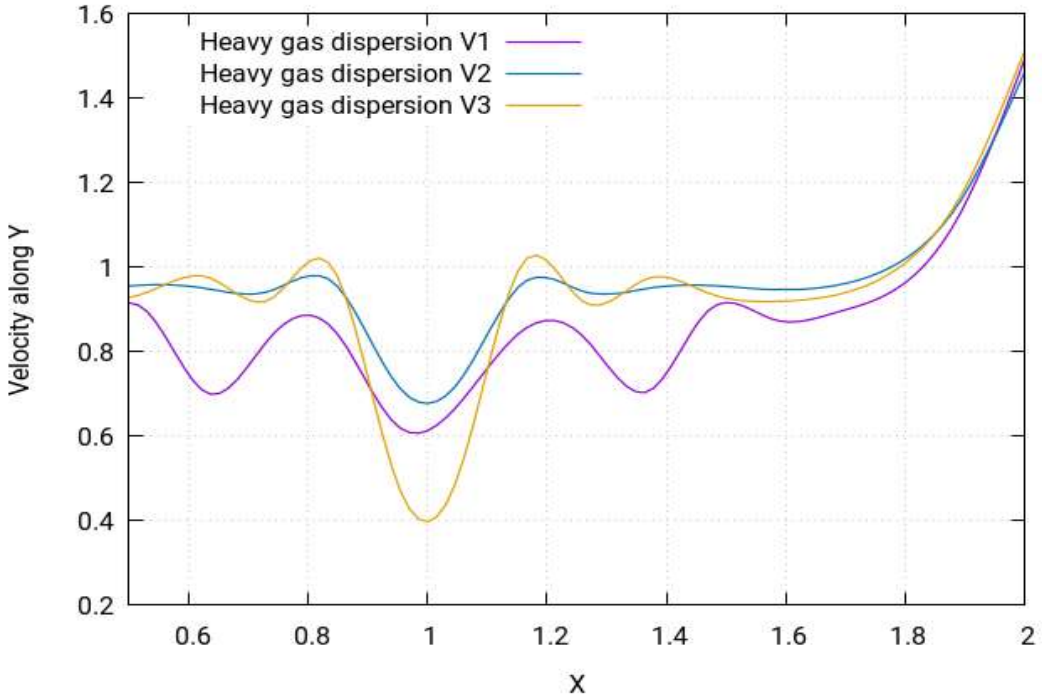

Figure 7.93: *Graphical representation of velocity profile of heavy gas release source for a flat terrain* ***before*** *a solid and a semi-circular fence as an obstacle at* ***1m/s***

Figure 7.93 shows the profile of the density of the released gas for this scenario before the obstacle. The profiles show a sinusoidal behaviour initially, but a sharp increase at the end. All

the profiles follow a similar pattern, but have different in values due to differences in distance from the released source.

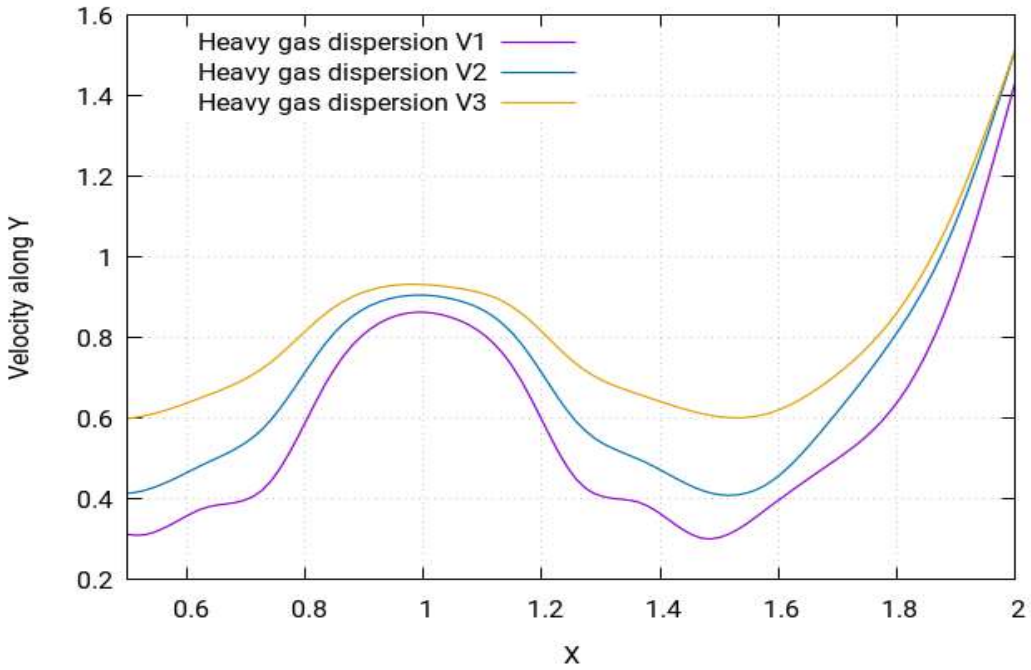

Figure 7.94: *Graphical representation of velocity profile of heavy gas release source for a flat terrain* ***after*** *a solid and a semi-circular fence as an obstacle at* ***1m/s***

Figure 7.94 shows the varying profiles of the velocity after the obstacle with varying distances. While the profiles do follow a same pattern, the values change according to the varying distances.

7.5.6 Neutral gas dispersion with a straight solid and semi-circular fence

The third (B) scenario has a neutral gas leak occurring from a circular source, which is 50mm in diameter. There are two obstacles for the plume in the form of fences, which are 400mm downstream from the source. The solid fence has a height of 30mm, and the semi-circular fence has a height of 30mm.

Table 7.6: *Parametric values of scenario 3B*

Density	Flow Rate	Velocity	Ambient Temperature	Release Source Temperature
1.1839 kg m/s^3	1.7737 kg/s	1 m/s	25°C	25°C

7.5.6.1 Release source

The following figure shows the release source for the current scenario:

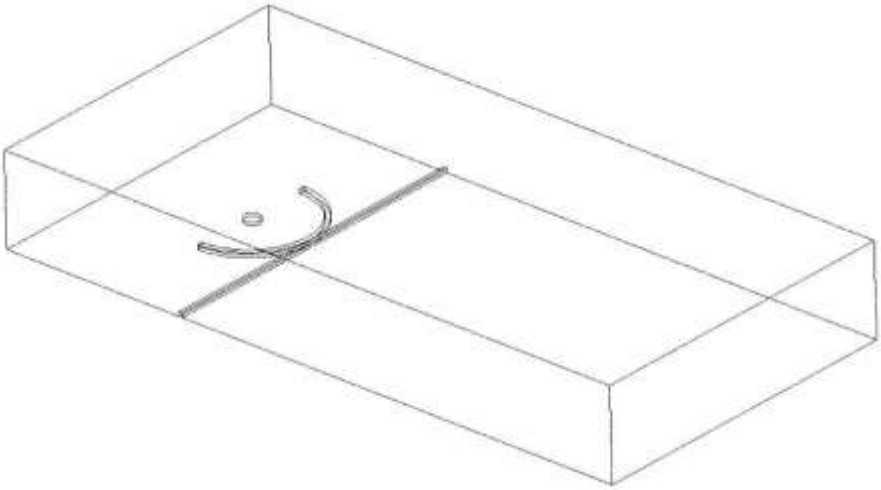

Figure 7.95: *The neutral gas release source for a flat terrain with a solid and a semi-circular fence as an obstacle at* ***1m/s*** *velocity*

7.5.6.2 Concentration of the neutral gas dispersion

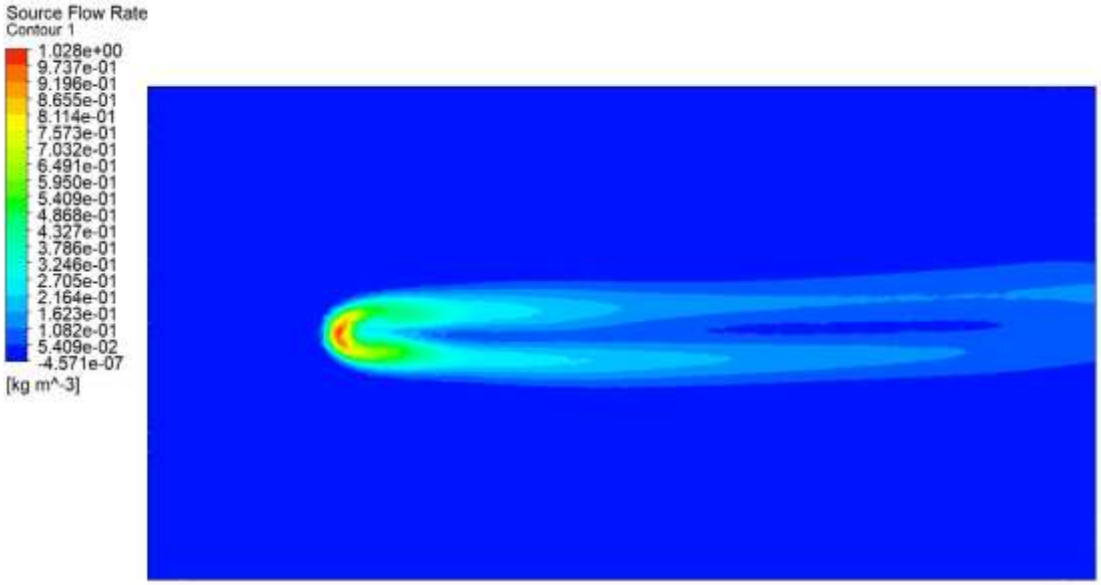

Figure 7.96: *Concentration profile of neutral gas release source for a flat terrain with a solid and a semi-circular fence as an obstacle at* ***1m/s*** *velocity*

The concentration profile of the neutral gas for scenario 3B is shown in Figure 7.96 above. It shows the concentration profile for the neutral gas when released from a circular source of 50mm diameter with a solid and a semi-circular fence as an obstacle. It can be that the cloud shape for this scenario is of the shape of an elliptical cylinder, which was also the case in scenario 1B and 2B, as here the addition of a solid and a semi-circular fence as an obstacle has influenced the cloud shape of the neutral gas. It resembles that of an elliptical cylinder, but the shape of the cylinder has been changed by the obstacles as it can be in the shape of a curved shaped boundary of the upper surface of the elliptical cylinder. The simulation shows the highest concentrations in red near the release source and then the concentrations start to

decrease. From the simulation, it can be observed that the concentration distribution is not symmetrical in the horizontal and that the upper half of the elliptical cylinder is more concentrated than the lower. The pattern in the upper layers is that after the hierarchal distribution of concentration layers; the concentrations first fade away in the third half and then increase a slightly again.

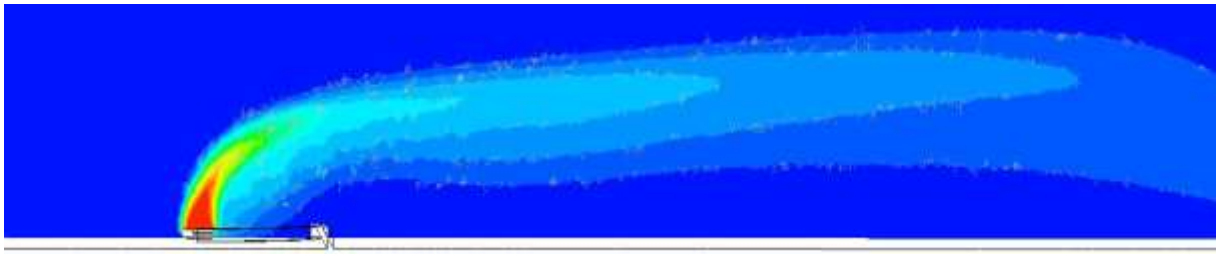

Figure 7.97: *2D view of concentration profile of neutral gas release source for a flat terrain with a solid and a semi-circular fence as an obstacle at* ***1m/s*** *velocity*

Figure 7.97 shows the two-dimensional version of the concentration simulation. It further verifies the behaviour of the cloud shape for neutral gas studied in the previous (Figure 7.96).

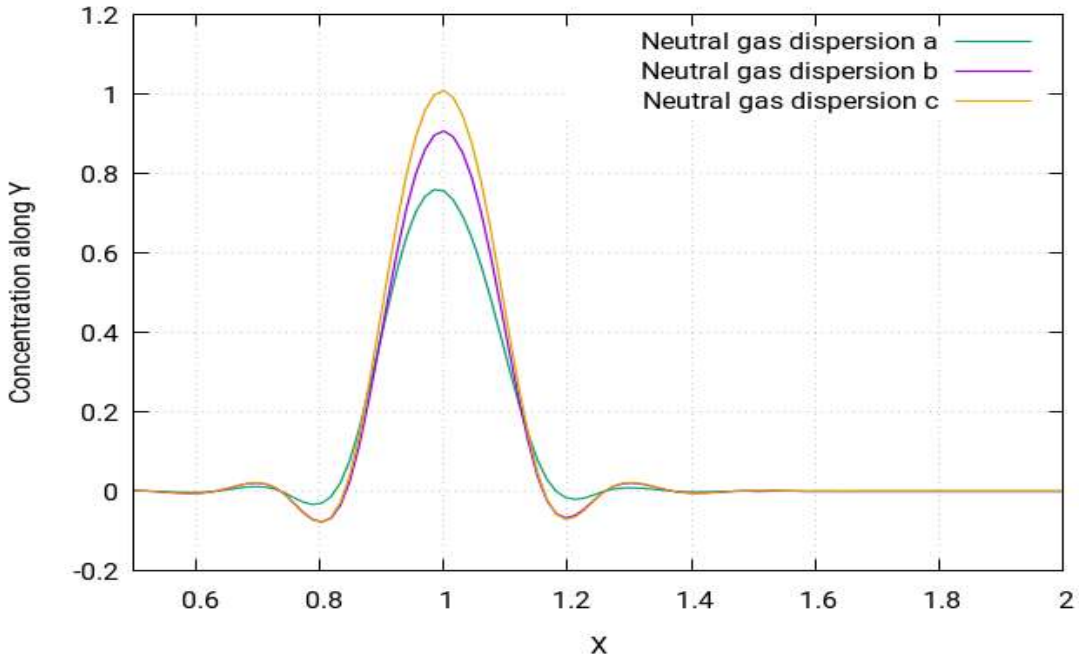

Figure 7.98: *Graphical representation of concentration profile of neutral gas release source for a flat terrain with a solid and a semi-circular fence as an obstacle at* ***1m/s*** *velocity*

Figure 7.98 above shows concentration profiles for this scenario before the obstacle for varying distances. The same behaviour of concentration profiles as observed in previous neutral gas scenarios 1B and 2B is also visible here.

7.5.6.3 Iso-surfaces of the neutral gas dispersion

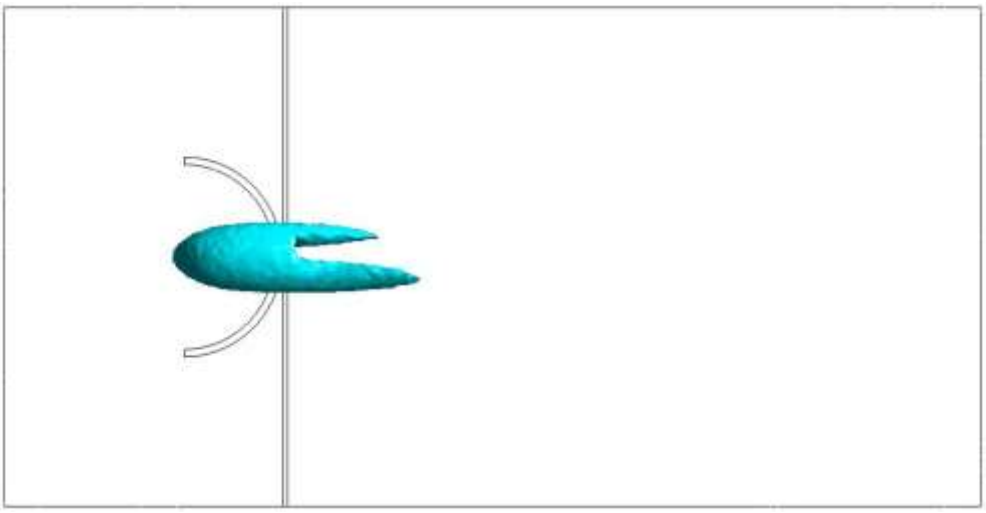

Figure 7.99: *Iso-surface top view of concentration of neutral gas release source for a flat terrain with a solid and a semi-circular fence as an obstacle at* ***1m/s*** *velocity*

Figure 7.99 shows the iso-surface of the concentration from the top view. It can be observed that the lower end of the cloud is thicker than the lower end and extends slightly more along the horizontal than the lower end.

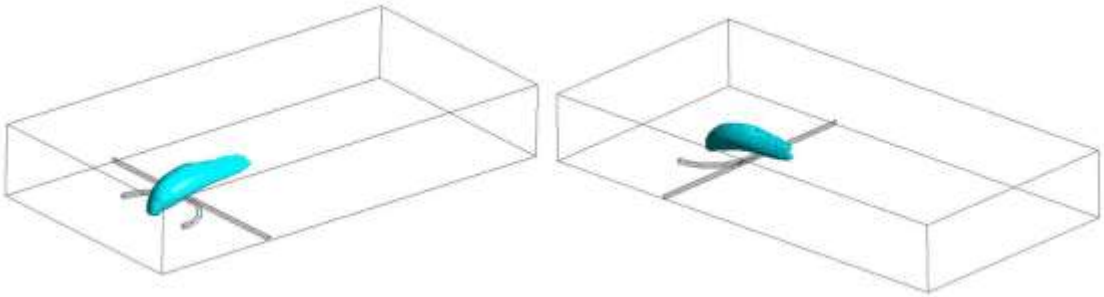

Figure 7.100: *Iso-surface side view of concentration of neutral gas release source for a flat terrain with a solid and a semi-circular fence as an obstacle at* ***1m/s*** *velocity*

Figure 7.100 shows the iso-surface of the concentration from the side view. It shows the same results as discussed in the previous figures. It also shows the iso-surface of the concentration from the back view. It further verifies the cloud shape pattern discussed previously.

According to Standard BS EN 60079-10-1:2009 Santon el. al. [104], the following locations can be categorised:

Zone 0: The immediate surrounding of the release source

Zone 1: The immediate surrounding of the obstacles

Zone 2: All the remaining locations not categorised in zone 0 or zone 1

7.5.6.4 Velocity of the neutral gas dispersion

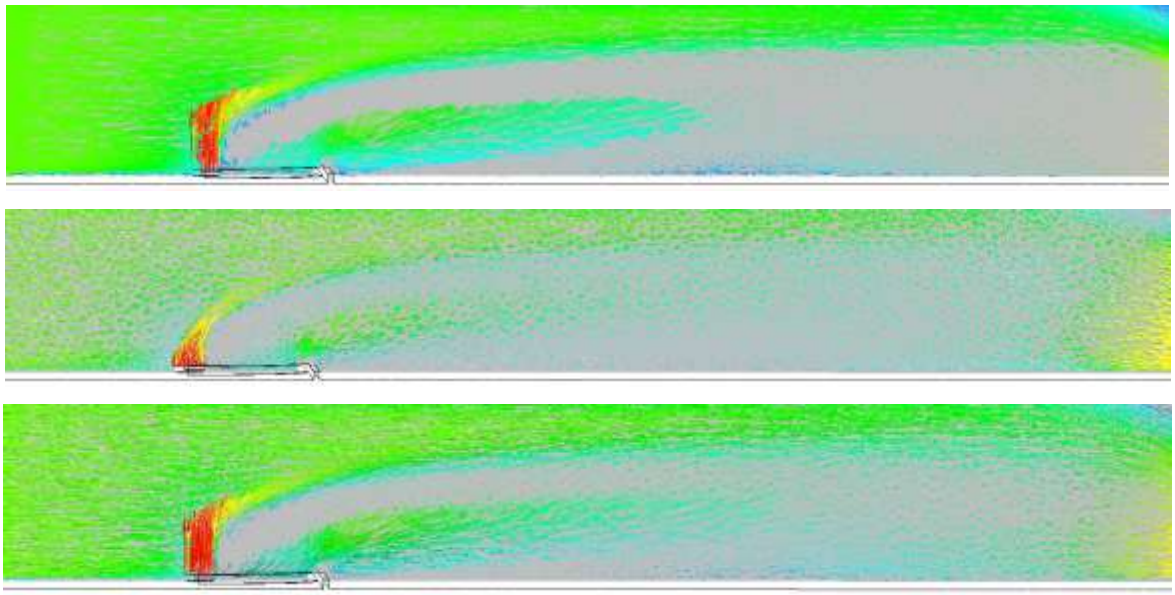

Figure 7.101: *Velocity profile of neutral gas release source for a flat terrain with a solid and a semi-circular fence as an obstacle* ***at 1m/s*** *velocity*

Figure 7.101 shows the velocity contours of neutral gas dispersion for this scenario. Velocity contours depict the intensity of wind - or the effective wind influence - at the different locations throughout the layout. In the figure, the wind intensity is different at different points in the layout. In scenario 1A, the wind operation was smooth, and not many complex vertexes were seen. However, in this scenario, many complex vertexes are formed near the release source location, as seen in the figure. These complex vertexes carry the gas cloud to the nearby environment, where a gas cloud is formed due to steady flow. This gas cloud is deemed dangerous as it is volatile and could lead to an explosion, fire, etc. This also causes the gas cloud to advance in the upward direction.

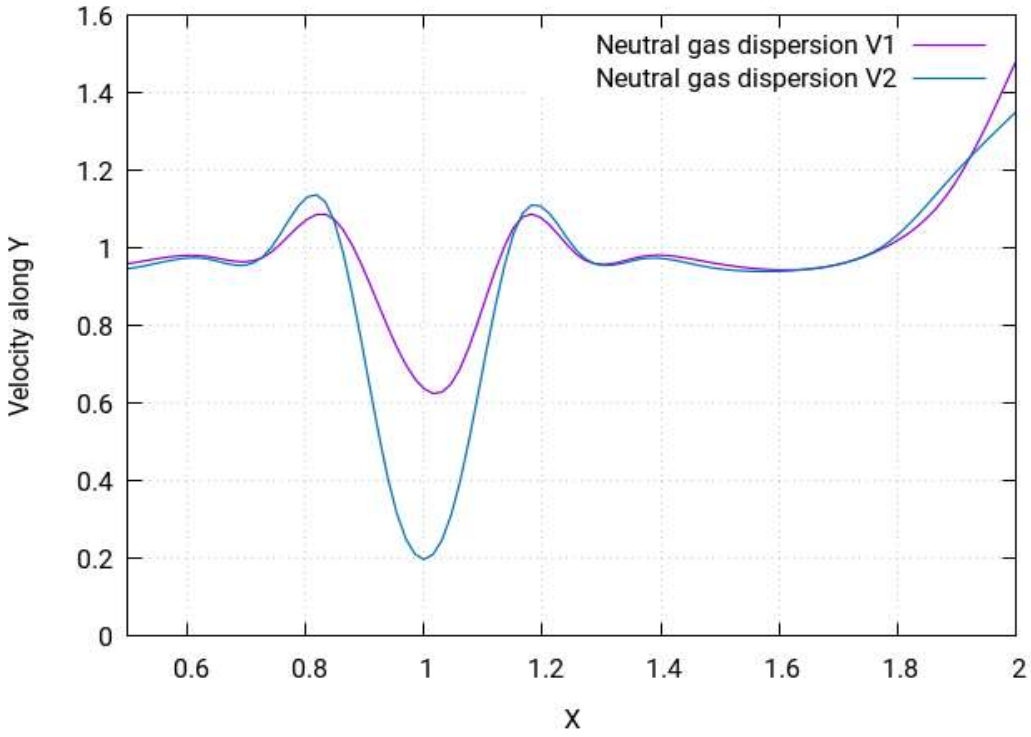

Figure 7.102: *Graphical representation of velocity of neutral gas release source for a flat terrain with a solid and a semi-circular fence as an obstacle at* ***1m/s*** *velocity*

Figure 7.102 shows the varying profiles of the velocity after the obstacle with varying distances. While the profiles do follow a same pattern, the values change according to the varying distances.

7.5.7 Heavy gas dispersion with a straight solid fence as an obstacle

In this case, the gas leak occurs from a circular source with a diameter of 50mm. There is one obstacle in the form of a fence, which is 400mm downstream from the source. The solid fence is 60mm high

Table 7.7: *Parametric values of scenario 4A*

Density	Flow Rate	Velocity	Ambient Temperature	Release Source Temperature
2.1 kg m/s^3	1 kg/s	1 m/s	25°C	-100°C

7.5.7.1 Release source

The following figure shows the release source for the current scenario:

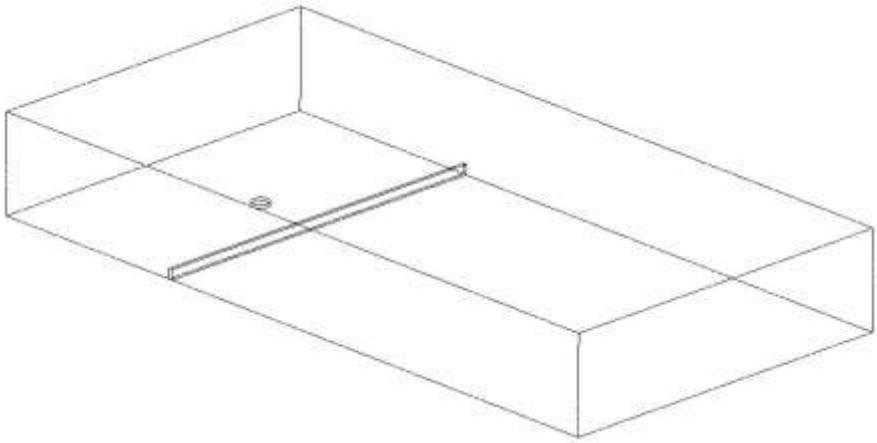

Figure 7.103: *The heavy gas release source for a flat terrain with a* ***600mm*** *solid fence as an obstacle at* ***1m/s*** *velocity*

7.5.7.2 Concentration of the heavy gas dispersion

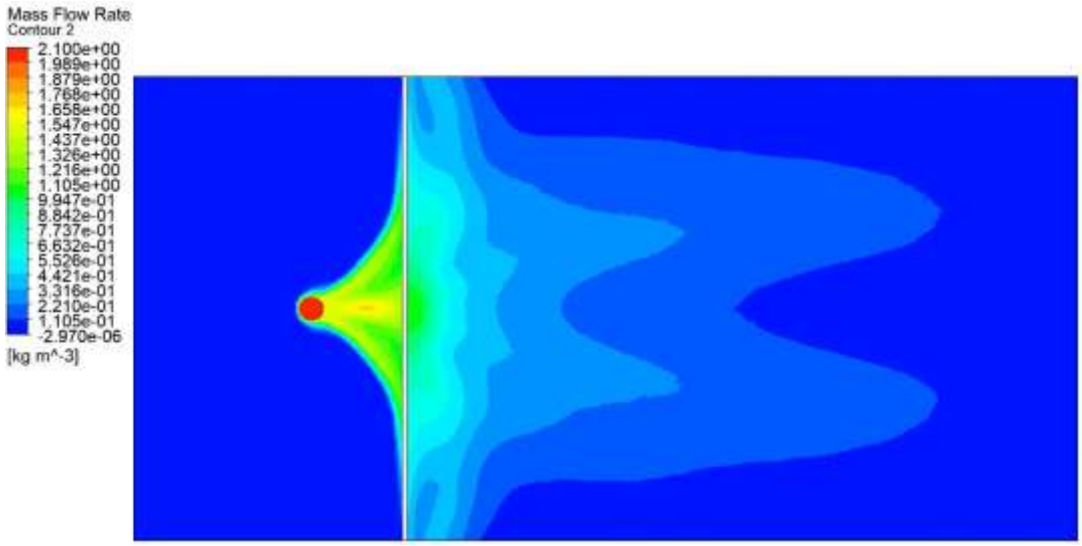

Figure 7.104: *Concentration profile of heavy gas release source for a flat terrain with a* ***600mm*** *solid fence as an obstacle with* ***1m/s*** *velocity*

The concentration profile of the heavy gas for scenario 4A is shown in the Figure 7.104 above. It shows the concentration profile for the heavy gas when released from a circular source of 50mm diameter with a solid fence of 600mm as an obstacle. The scenario 2A was performed with the same setting, but in that scenario, the solid fence was 300mm, which means this scenario is simulated with twice the size of the solid fence as that of scenario 2A. Therefore, Figure 7.104 appears to be a scaled-up version of the same simulation shown in scenario 2A. In scenario 2A, it was observed that the additional fence had affected the gas cloud in such a way that a high concentration triangle was formed from the release source to the fence and the gas cloud was widened by the addition of the solid fence. In this scenario, the same phenomenon occurs, but on a larger scale. This means that the high concentration triangle is larger in size and the layers are more concentrated, as in scenario 2A. Some additional layers

of concentrations are also formed in this case and the layers' shape is not exactly sinusoidal for layers near the solid fence. The simulation shows that, for this particular scenario, the heavy gas cloud distributes symmetrically along the horizontal axis. The concentration contour in the above figure shows the highest concentrations in red while the lowest are in blue. The concentrations go on fading and there is a sort of layering pattern in the concentrations, with red being the layer with highest concentrations, followed by the yellow ones with slightly lower concentrations, then green with slightly less and so on, with the final layer (blue) being the lowest concentration.

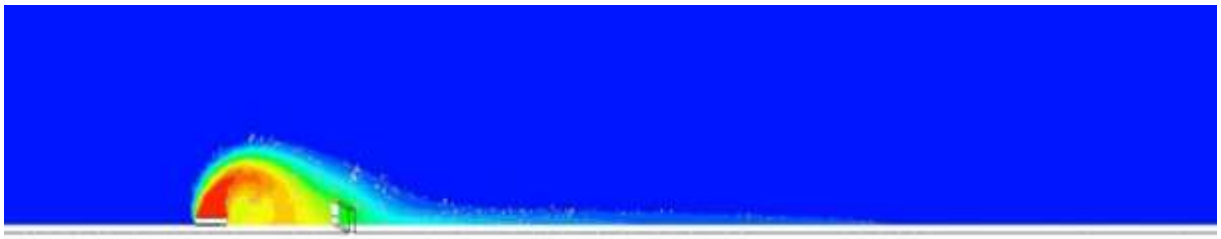

Figure 7.105: *2D view of concentration profile of heavy gas release source for a flat terrain with a solid fence as an obstacle with* ***1m/s*** *velocity.*

Figure 7.105 shows the two-dimensional version of the concentration simulation. They are similar to the behaviour of the cloud shape in this scenario to be the same as seen in (Figure 7.104).

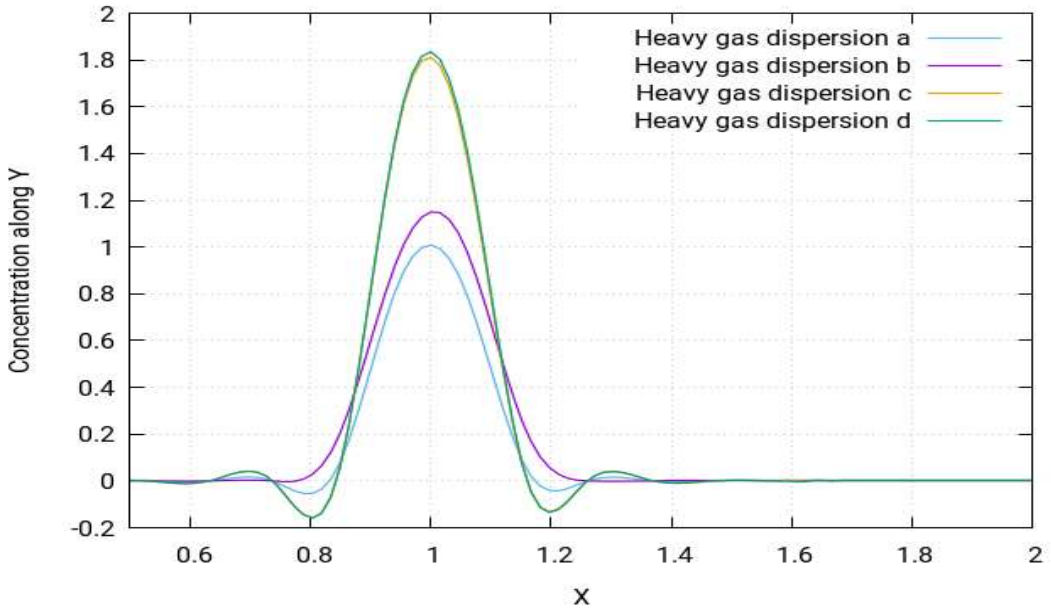

Figure 7.106: *Graphical representation for concentration of heavy gas release source for a flat terrain with* ***1m/s*** *velocity* ***before*** *the solid fence as an obstacle*

Figure 7.106 above shows concentration profiles for this scenario before the obstacle for varying distances. The same behaviour of concentration profiles as observed in previous heavy gas scenarios 1A, 2A and 3A is also visible here.

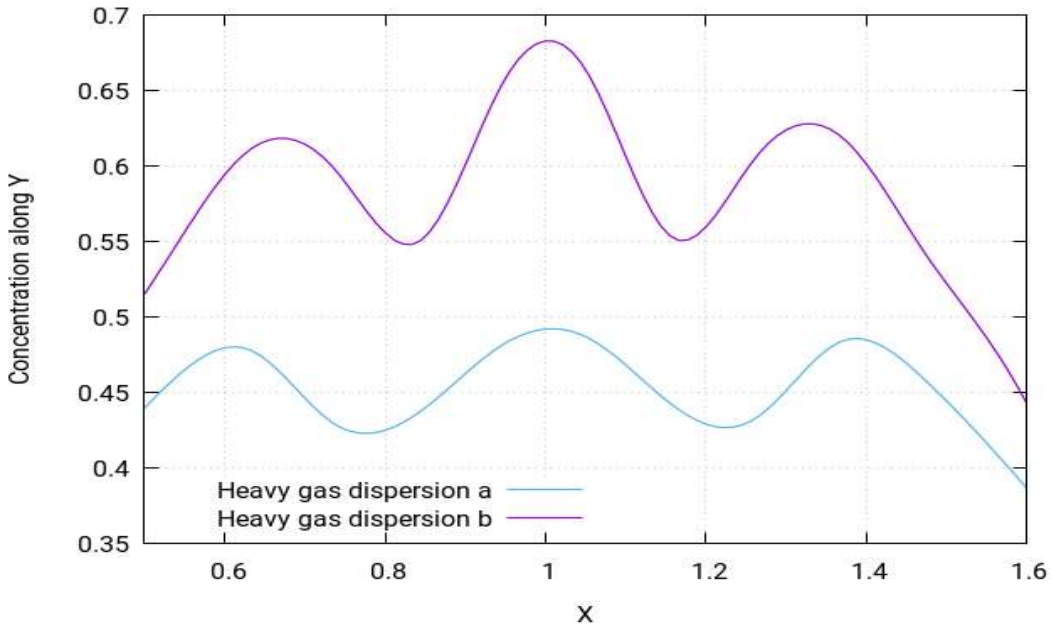

Figure 7.107: *Graphical representation for concentration of heavy gas release source for a flat terrain with **1m/s** velocity **after** the solid fence as an obstacle*

The concentration profiles for this scenario after the obstacle for varying distances are shown in the Figure 7.107 above. While the profile of concentration shows a different pattern after the obstacle to before the obstacle, the profile at different points after the obstacle follows the same pattern and have different values to the distance from release source.

7.5.7.3 Density of the heavy gas dispersion

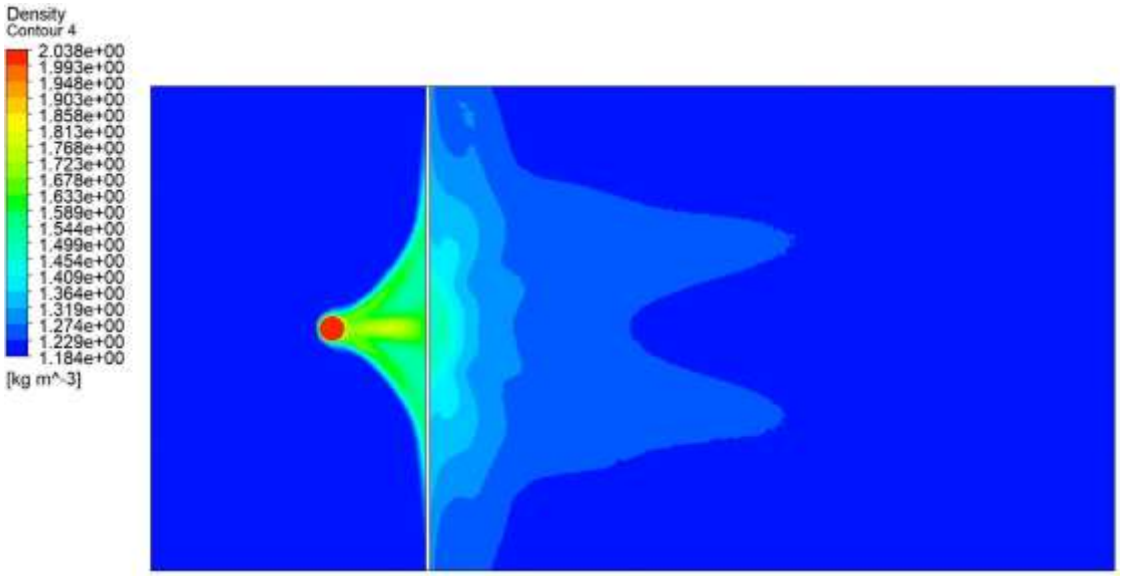

Figure 7.108: *Density profile of heavy gas release source for a flat terrain with a solid fence as an obstacle with **1m/s** velocity*

The density profile of the heavy gas for scenario 4A is shown in Figure 7.108 above. It shows the density profile for the heavy gas when released from a circular source of 50mm diameter

with a solid fence as an obstacle. At first glance, it appears that the density profile also follows the same pattern as that of concentration, keeping in mind the similarity in the concentration and density profile shown in Figure 7.108 and Figure 7.104 respectively. However, it must be noticed that the density profile appears to be a slightly shrunken version of the concentration profile. Moreover, the concentration contour shows the value of maximum concentration to be 2.1, while the density contours show a maximum value of 2.038.

Figure 7.109: *2D-view of density profile of heavy gas release source for a flat terrain with a solid fence as an obstacle with* ***1m/s*** *velocity*

Figure 7.109 shows the two-dimensional view of the density profile and shows the same behaviour of the heavy gas as (Figure 7.108).

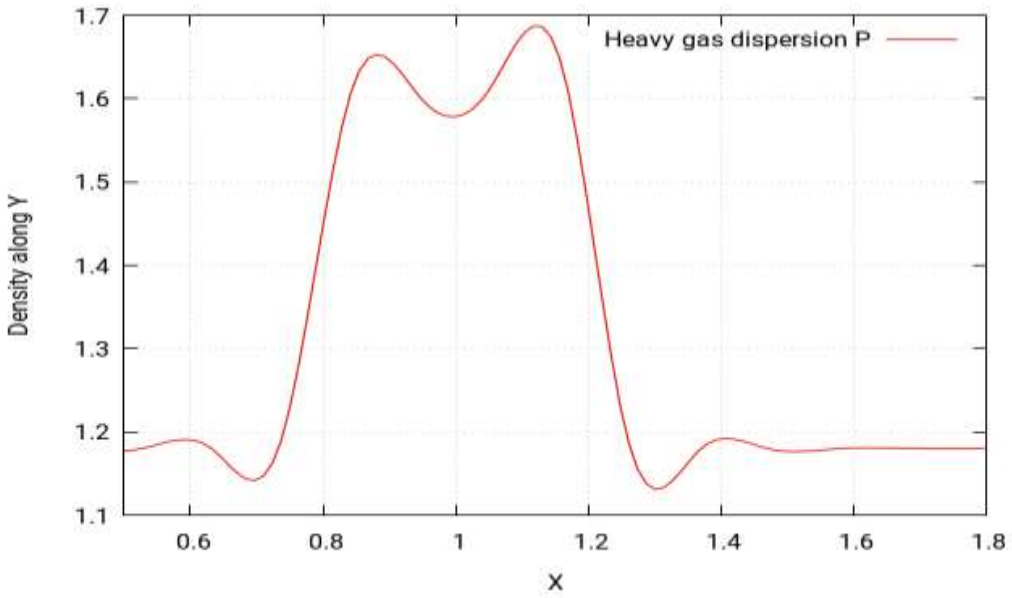

Figure 7.110: *Graphical representation for density of heavy gas release source for a flat terrain with* ***1m/s*** *velocity* ***before*** *the solid fence as an obstacle*

Figure 7.110 shows the density profile before the obstacle for this scenario. In the figure, the distance is calculated from the release source. The profile shows a sinusoidal pattern. It should be noticed that the profiled pattern as seen in the figure is not exactly symmetrical, as it shows an increase in value at greater distances away.

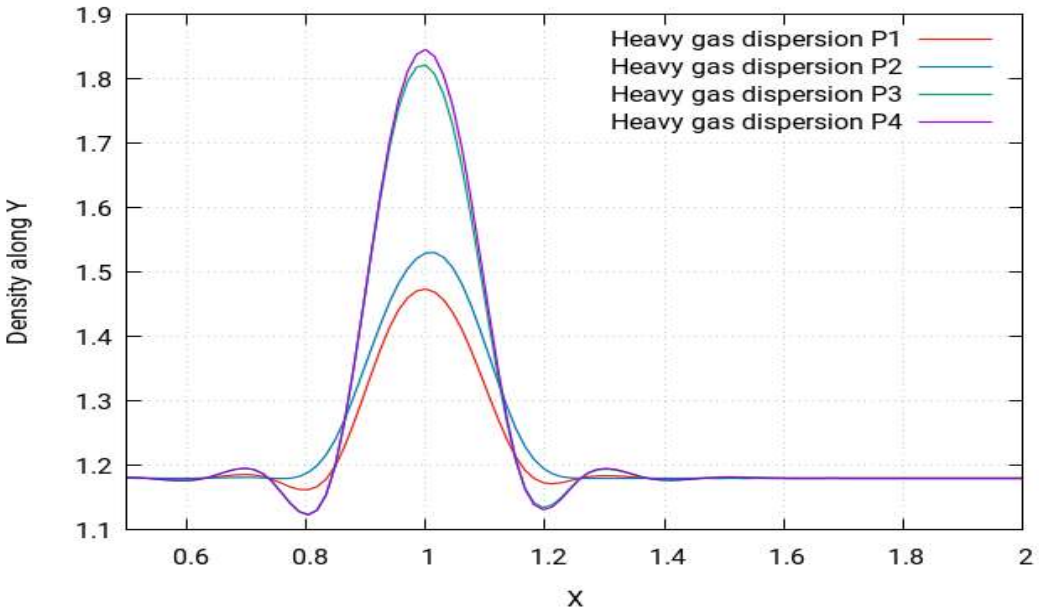

Figure 7.111: *Graphical representation for density of heavy gas release source for a flat terrain with* ***1m/s*** *velocity* ***before*** *the solid fence as an obstacle*

Figure 7.111 shows the profiles of the density before the obstacle of the released gas with varying distances. In the figure, the distance is calculated from the release source. This profile shows the same behaviour as that of the concentration profile.

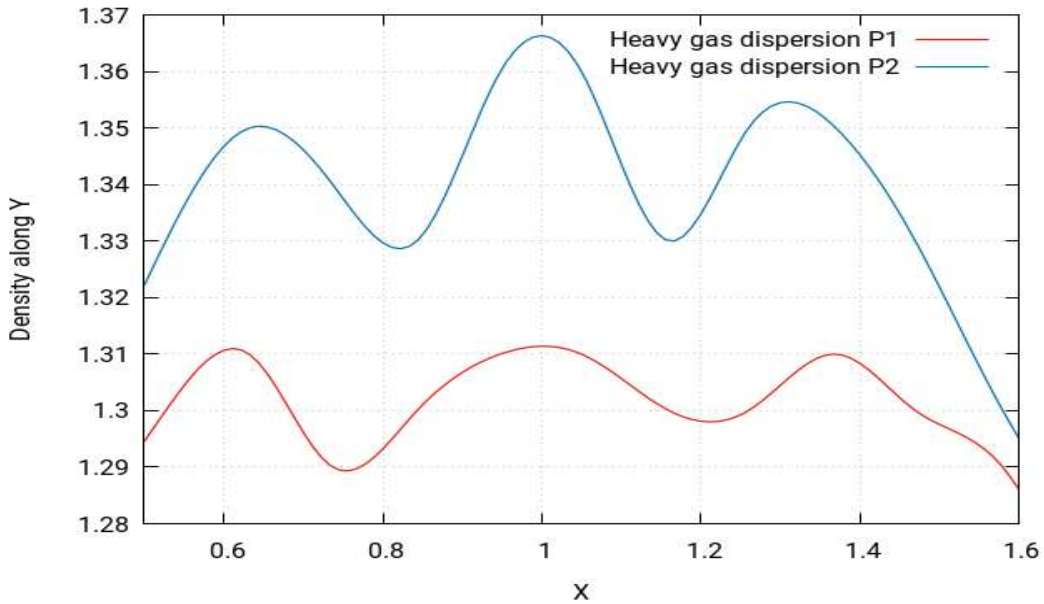

Figure 7.112: *Graphical representation for density of heavy gas release source for a flat terrain with* ***1m/s*** *velocity* ***after*** *the solid fence as an obstacle*

The profiles of the density after the obstacle of the gas released, with varying distances are shown in Figure 7.112 above. These profiles show the same behaviour as that of the concentration profile.

7.5.7.4 Temperature of the heavy gas dispersion

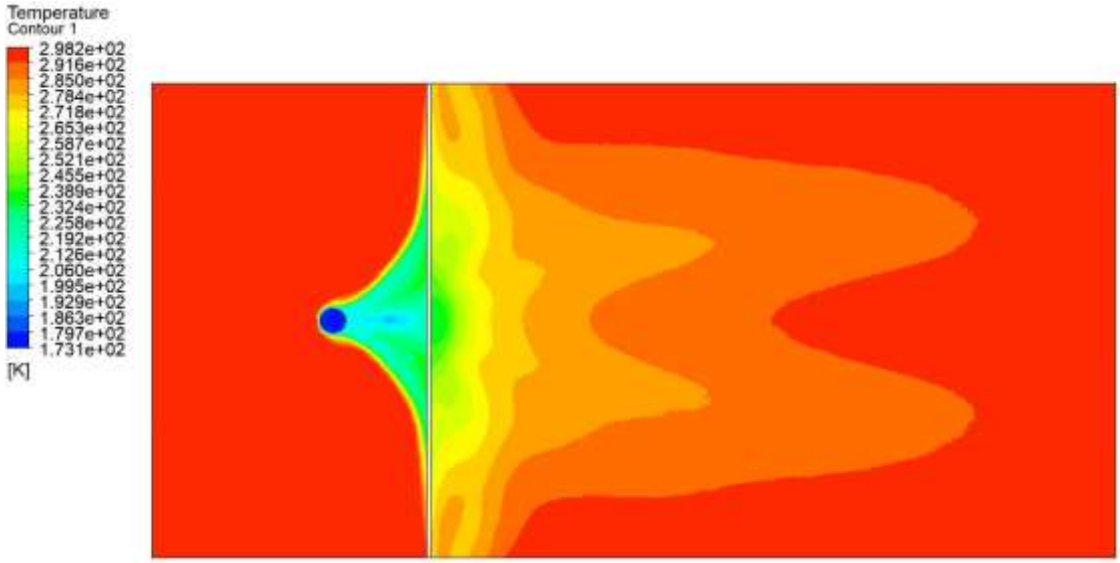

Figure 7.113: *Temperature profile of heavy gas release source for a flat terrain with a solid fence as an obstacle at* ***1m/s*** *velocity*

The above Figure 7.113 shows the temperature simulation for this scenario. By visualising the temperature simulation, it is found out that the temperature simulation produces quite the same profile for this scenario as that of the concentration profile. However, the thing to notice is that the behaviour of temperature is in fact the opposite to that of concentration. It means that the areas which were identified in the concentration simulation as highly concentrated will in fact have the lowest temperatures, the ones with moderate concentrations will have moderate temperatures and the least concentrated areas will have the maximum temperatures. To further simplify these findings, we should point out that the simulations show that the concentrations near the release source point tend to be the highest, and start to fade away as they move away from the source, reaching the lowest levels as they move much further away, eventually reaching the environment where the gas cloud disappears. However, the temperature is at its lowest near the release source point and tends to increase as it moves away from the source, finally achieving the maximum temperature equal to the ambient temperature of the environment.

Figure 7.114: *2D view of temperature profile of heavy gas release source for a flat terrain with a solid fence as an obstacle at* ***1m/s*** *velocity*

Figure 7.114 shows the two-dimensional view of the temperature profile and shows the same behaviour of the heavy gas as (Figure 7.113).

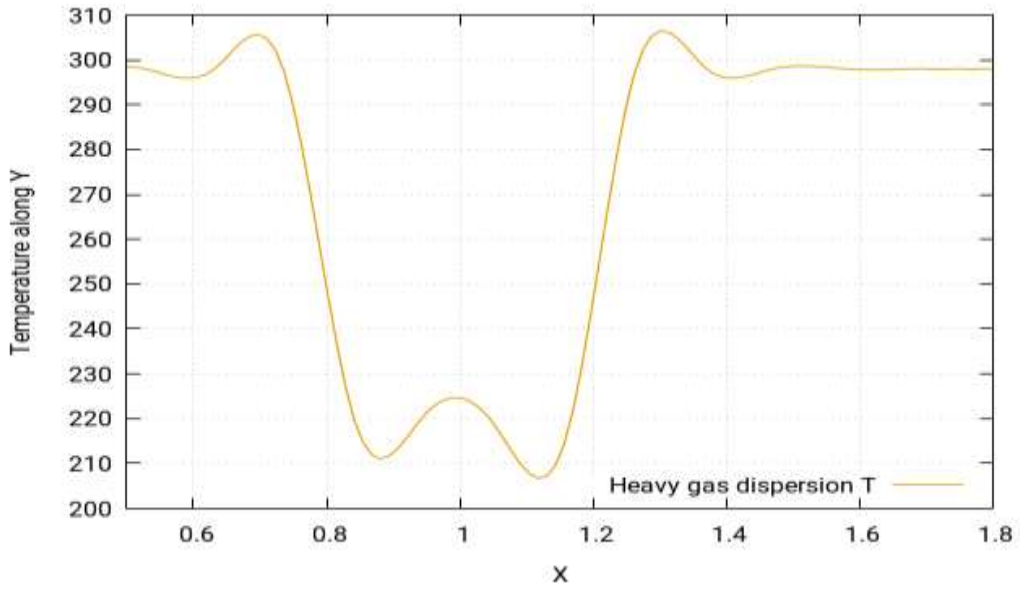

Figure 7.115: *Graphical representation of temperature of heavy gas release source for a flat terrain at* ***1m/s*** *velocity* ***before*** *the solid fence*

Figure 7.115 shows the temperature profile before the obstacle for this scenario. In the figure, the distance is calculated from the release source. This profile is a mirrored image of the concentration profile.

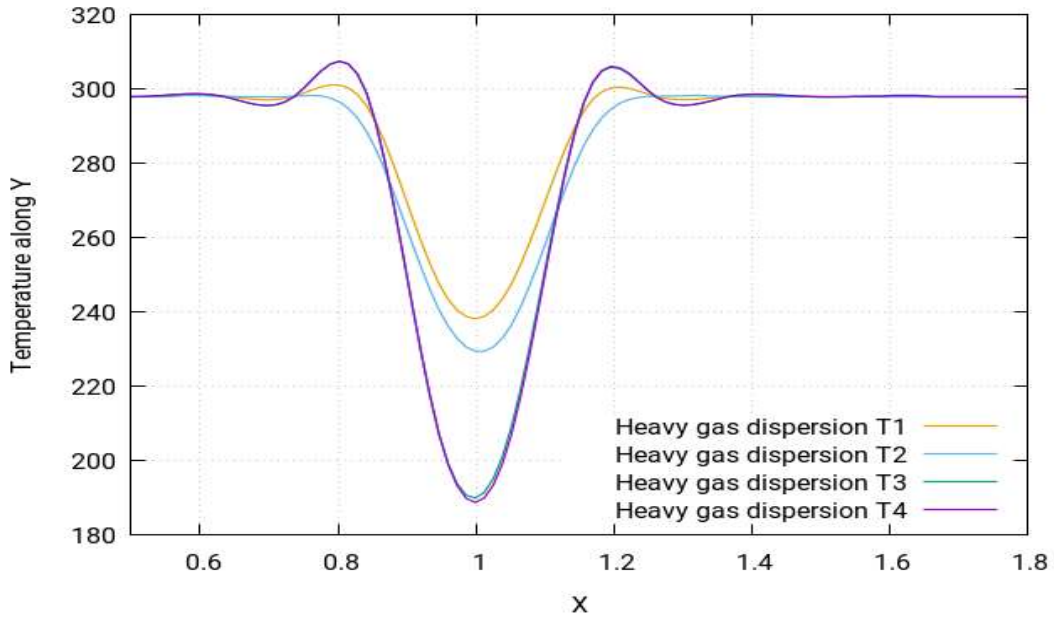

Figure 7.116: *Graphical representation of temperature of heavy gas release source for a flat terrain at* ***1m/s*** *velocity* ***before*** *the solid fence*

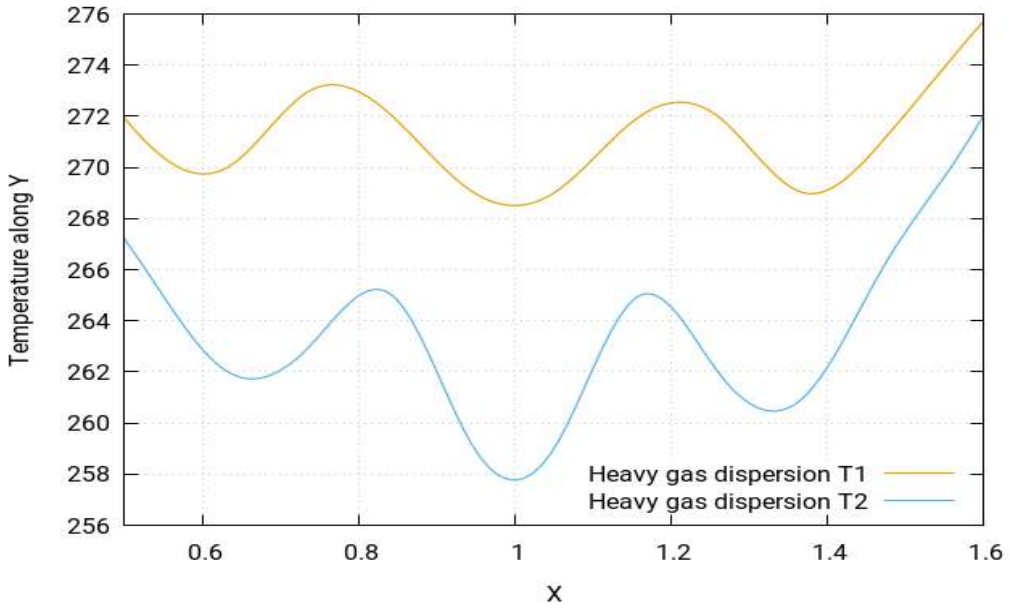

Figure 7.117: *Graphical representation of temperature of heavy gas release source for a flat terrain at **1m/s** velocity **after** the solid fence*

The temperature profiles for this scenario for varying distances and after the obstacle have been shown in the above figure. Similar to the profile before the obstacle, these profiles show the inverse - or mirrored - behaviour as that of the concentration profile after the obstacle.

7.5.7.5 Iso-surfaces of the heavy gas dispersion

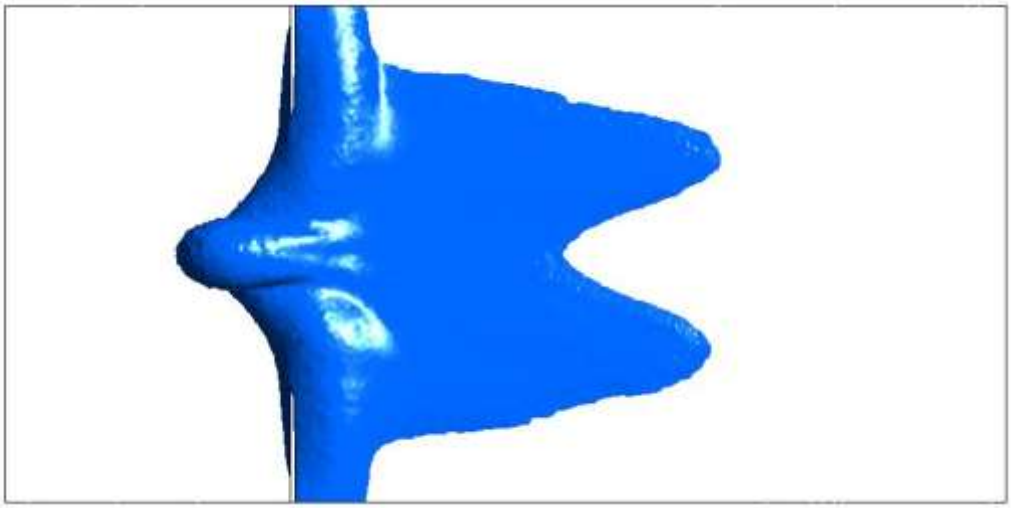

Figure 7.118: *Iso-surface top view of concentration of heavy gas release source for a flat terrain with a solid fence as an obstacle **1m/s** velocity*

Figure 7.118 shows the iso-surface of the concentration from the top view. It shows the triangular shaped distribution until the solid fence, after which the distributions appear to be uniform and then form a sinusoidal curve at the end. The concentration is heaviest near the release source point and is distributed symmetrically along the axis.

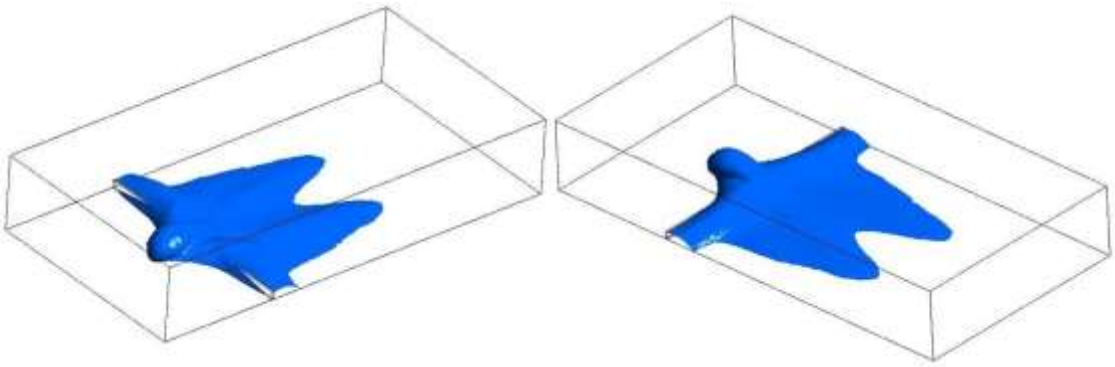

Figure 7.119: *Iso surface side view of concentration of heavy gas release source for a flat terrain with a solid fence as an obstacle* ***1m/s*** *velocity*

Figure 7.119 shows the iso-surface of the concentration from the side view. It shows that the gas cloud, after showing an inclination of height near the release source, goes on to decrease in height and is thickest near the release source, whereas it continues becoming thinner as moves along the horizontal axis. It shows the iso-surface of the concentration from the side view. It shows that the gas cloud, after showing an inclination of height near the release source, goes on to decrease in height and is thickest near the release source, whereas it continues becoming thinner as it moves along the horizontal axis.

According to Standard BS EN 60079-10-1:2009 Santon el. al. [104], the following locations can be categorised:

Zone 0: The triangular shaped area near the release source location

Zone 1: The areas immediately surrounding obstacles

Zone 2: All the remaining locations not categorised in zone 0 or zone 1

7.5.7.6 Velocity of the heavy gas dispersion

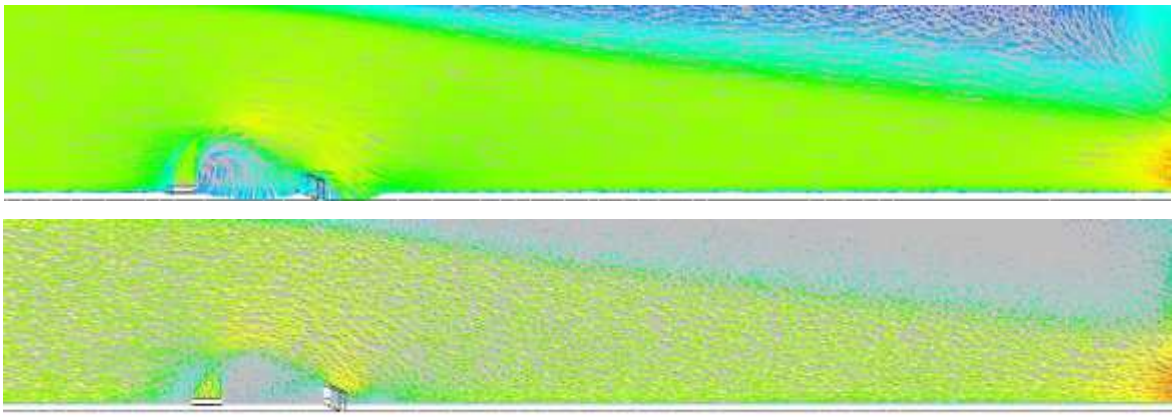

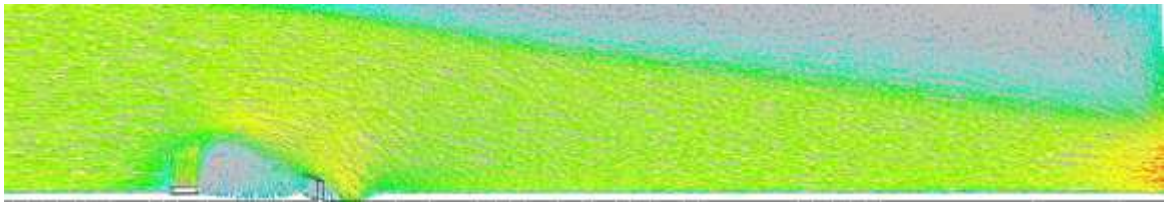

Figure 7.120: *Velocity profile of heavy gas release source for a flat terrain with a solid fence as an obstacle at* ***1m/s***

Figure 7.120 shows the velocity contours of heavy gas dispersion for this scenario. Velocity contours depict the intensity of wind - or the effective wind influence - at the different locations throughout the layout. As can be seen in the figure, the wind intensity is different at different points in the layout. The wind operation is smooth in this scenario and not many complex vertexes can be seen. The wind eddies carry the gas cloud to the nearby environment, where a gas cloud is formed due to steady flow. This gas cloud is deemed dangerous as it is volatile and could lead to an explosion, fire, etc.

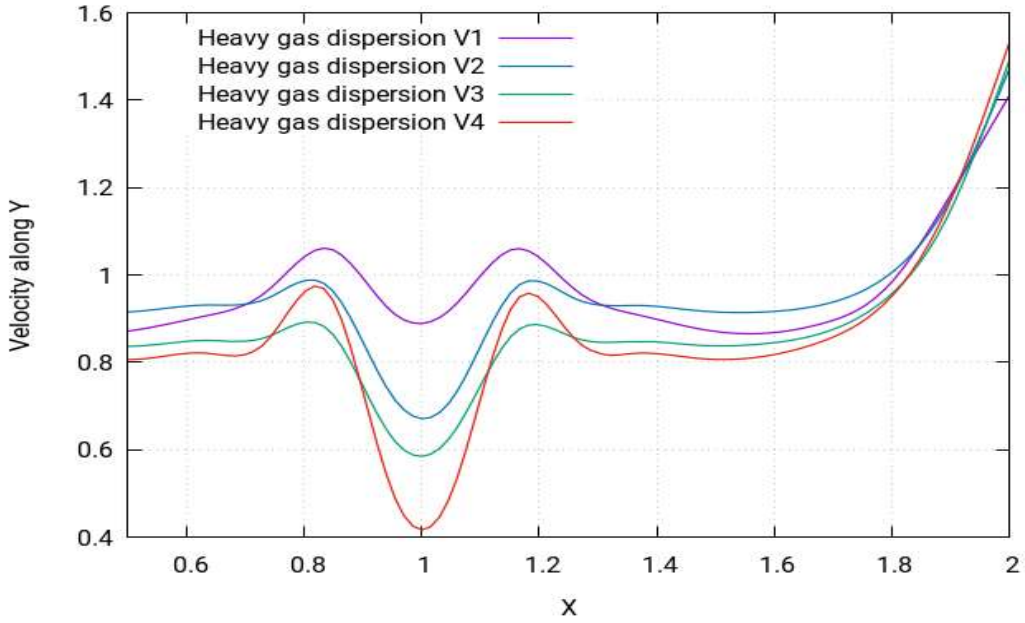

Figure 7.121: *Graphical representation of the velocity profile of heavy gas release source for a flat terrain* ***after*** *a solid fence as an obstacle at* ***1m/s***

Figure 7.121 shows the profile of the velocity of the gas released for this scenario before the obstacle. The profiles show sinusoidal behaviour initially, but a sharp increase at the end. All the profiles follow a similar pattern but have difference in values due to difference of distance from the release source.

7.5.8 Neutral gas dispersion with a straight solid fence as an obstacle

In this case, the gas leak occurs from a circular source with a diameter of 50mm. The ambient temperature is 25°C. There is one obstacle, in the form of a fence, which is 400 mm downstream from the source. The solid fence is 60mm high.

Table 7.8: *Parametric values of scenario 4B*

Density	Flow Rate	Velocity	Ambient Temperature	Release Source Temperature
1.1839 kg m/s^3	1.7737 kg/s	1 m/s	25°C	25°C

7.5.8.1 Release source

The following figure shows the release source for the current scenario:

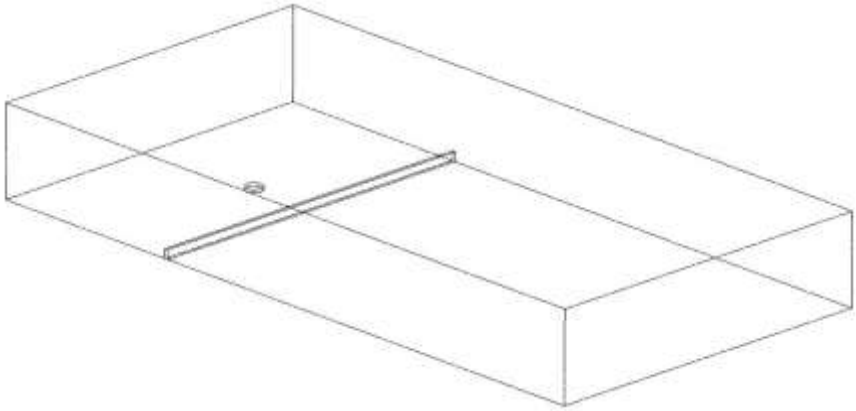

Figure 7.122: *The neutral gas release source for a flat terrain with a* ***60mm*** *solid fence as an obstacle at* ***1m/s*** *velocity*

7.5.8.2 Concentration of the neutral gas dispersion

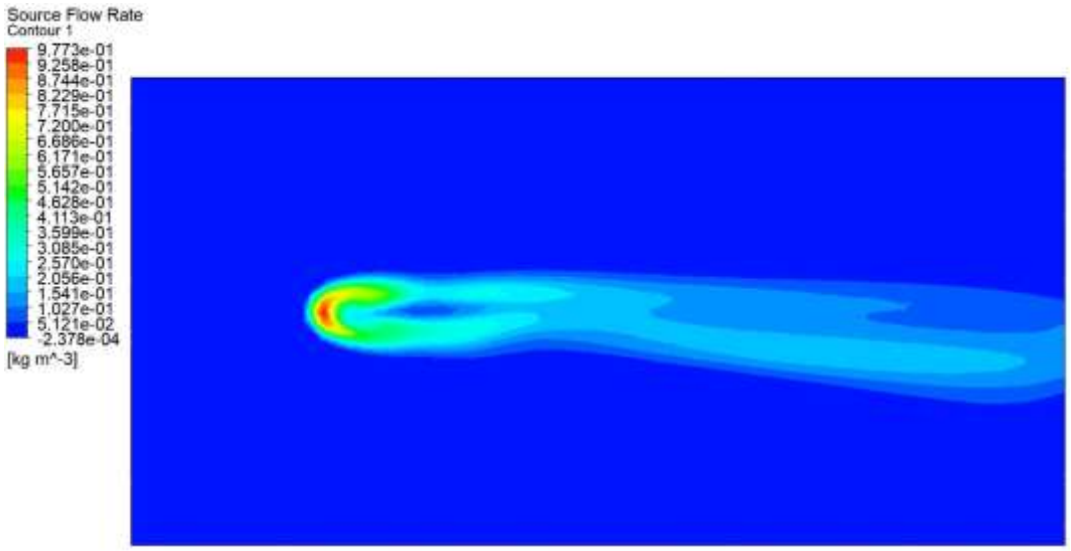

Figure 7.123: *Concentration profile of neutral gas release source for a flat terrain with a* ***60mm*** *solid fence as an obstacle at* ***1m/s*** *velocity*

The concentration profile of the neutral gas for scenario 4B is shown in Figure 7.123 above. It shows the concentration profile for the neutral gas when released from a circular source of 50mm diameter with a solid fence of 60mm as an obstacle. The usual elliptical cylinder cloud shape as seen in scenario 2B and 3B is not seen in this scenario. The deviation from the usual elliptical cylinder-shaped cloud is such that there is a bend in the cloud after first the high concentration end of the cloud, which is likely due to the 60mm fence. The fence influences the cloud shape in such a way that, after striking the obstacle (60mm fence), the cloud goes off declining and expanding more on the lower side than on the upper side. The simulation shows maximum concentrations in red near the release source. Thereafter the concentrations begin to be decreased. From the simulation, we notice that the concentration distribution is not symmetrical in the horizontal and that the lower half of the elliptical cylinder is more concentrated.

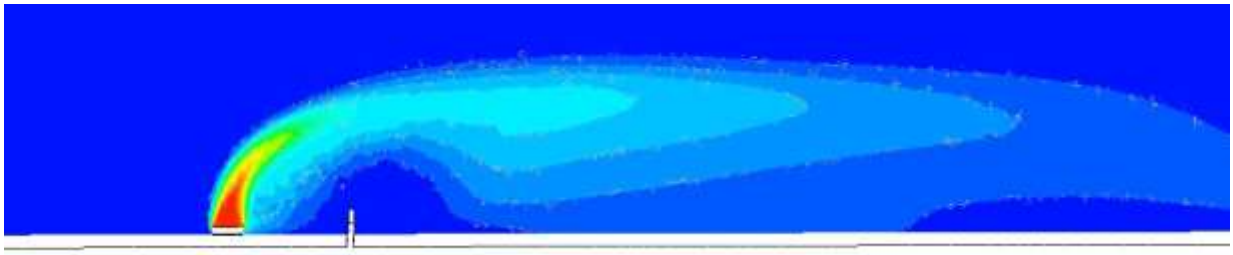

Figure 7.124: *2D view of concentration profile of neutral gas release source for a flat terrain with a* ***60mm*** *solid fence as an obstacle at* ***1m/s*** *velocity*

Figure 7.124 shows the two-dimensional version of the concentration simulation. It further verifies the behaviour of the cloud shape for neutral gas discussed in (Figure 7.123) previously.

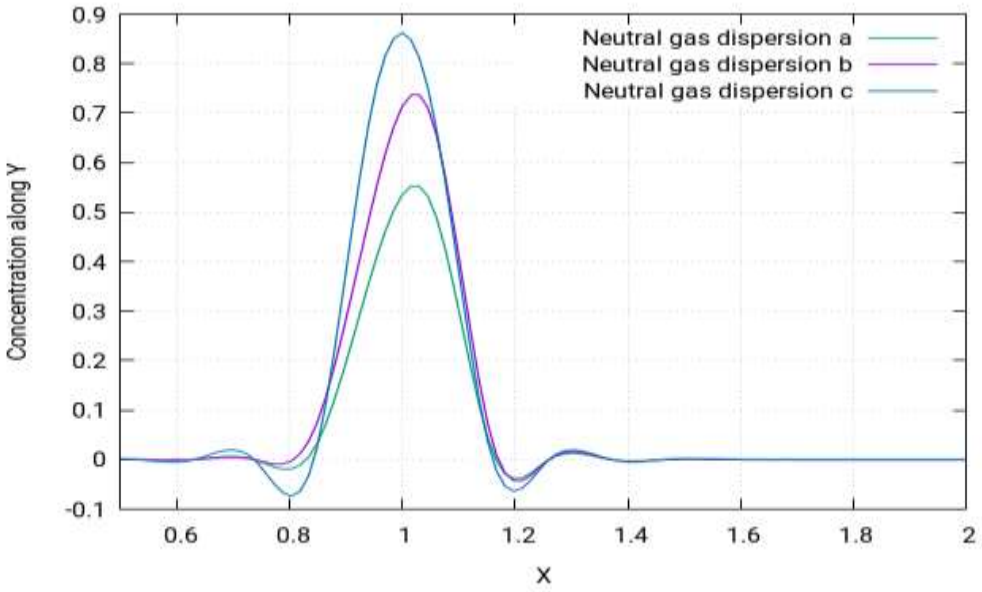

Figure 7.125: *Graphical representation of concentration profile of neutral gas release source for a flat terrain with a* ***60mm*** *solid fence as an obstacle at* ***1m/s*** *velocity*

Figure 7.125 above shows concentration profiles for this scenario for varying distances. The same behaviour of concentration profiles as observed in previous neutral gas scenarios 1B, 2B and 3B is also visible here.

7.5.8.3 Iso-surfaces of the neutral gas dispersion

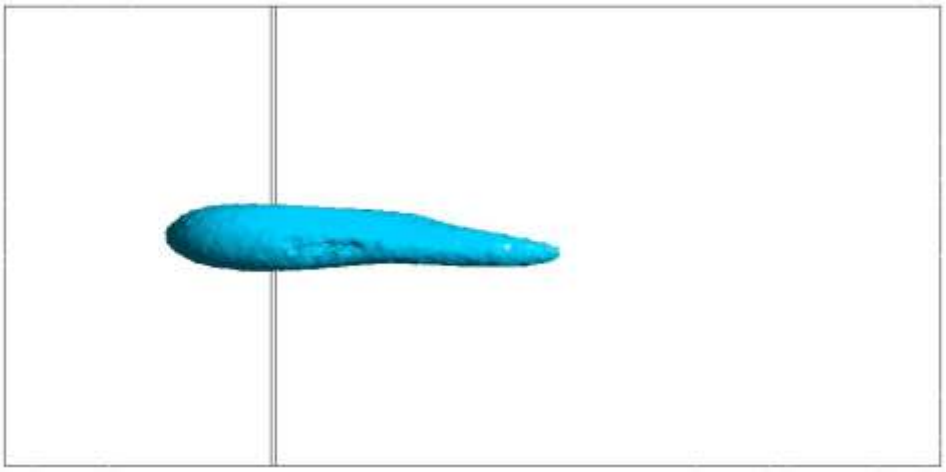

Figure 7.126*: Iso-surface top view of concentration of neutral gas release source for a flat terrain with a* ***60mm*** *solid fence as an obstacle at* ***1m/s*** *velocity*

Figure 7.126 shows the iso-surface of the concentration from the top view. It can be seen that the release source end of the gas cloud is thicker than the other end and the cloud moves with a declining pattern from the thicker towards the thinner end.

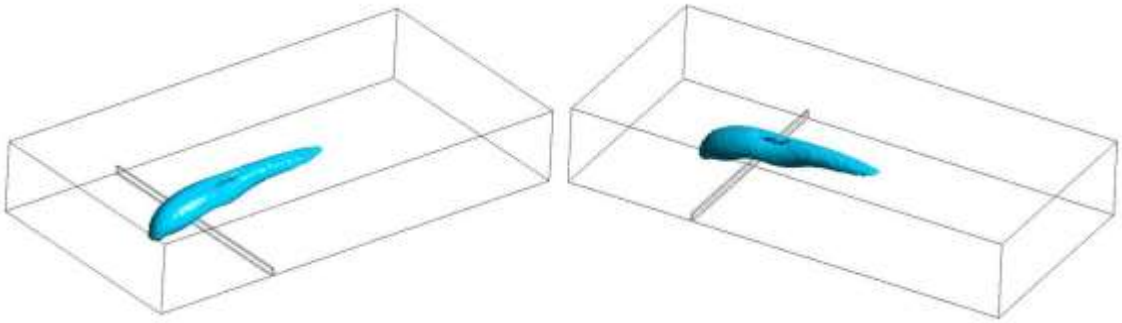

Figure 7.127: *Iso-surface side view of concentration of heavy gas release source for a flat terrain with a* ***60mm*** *solid fence as an obstacle at* ***1m/s*** *velocity*

Figure 7.127 shows the iso-surface of the concentration from the side view. The same results can be seen as those discussed in the previous figure. It also shows the iso-surface of the concentration from the back view. It further verifies the cloud shape pattern discussed previously.

According to Standard BS EN 60079-10-1:2009 Santon el. al. [104], the following locations can be categorised:

Zone 0: The areas near the release source

Zone 1: The area after the release source up to obstacle

Zone 2: All the remaining locations not categorised in zone 0 or zone 1

7.5.8.4 Velocity of the neutral gas dispersion

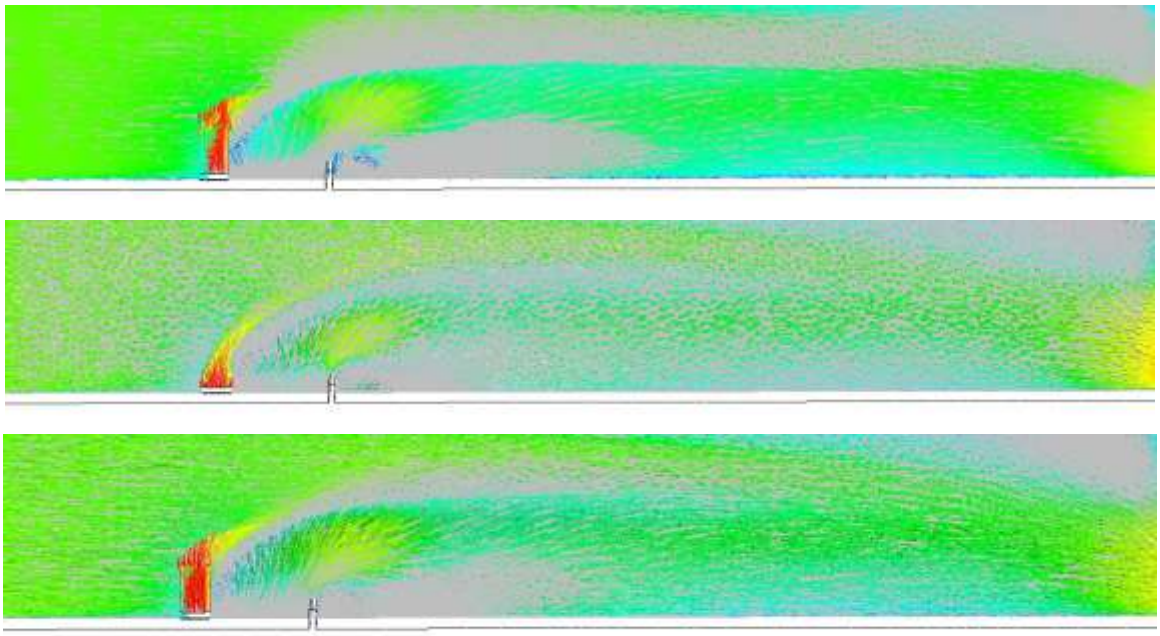

Figure 7.128: *Velocity profile of neutral gas release source for a flat terrain with a **60mm** solid fence as an obstacle at **1m/s***

Figure 7.128 shows the velocity contours of neutral gas dispersion for this scenario. Velocity contours depict the intensity of wind - or the effective wind influence - at the different locations throughout the layout. As can be seen in the figure, the wind intensity is different at different points in the layout. In scenario 1A, the wind operation was smooth, and not many complex vertexes were seen. However, in this scenario, many complex vertexes are formed near the release source location, as seen in the figure. These complex vertexes carry the gas cloud to the nearby environment, where a gas cloud is formed due to steady flow. This gas cloud is deemed dangerous as it is volatile and could lead to an explosion, fire, etc. This also causes the gas cloud to enhance in the upward direction.

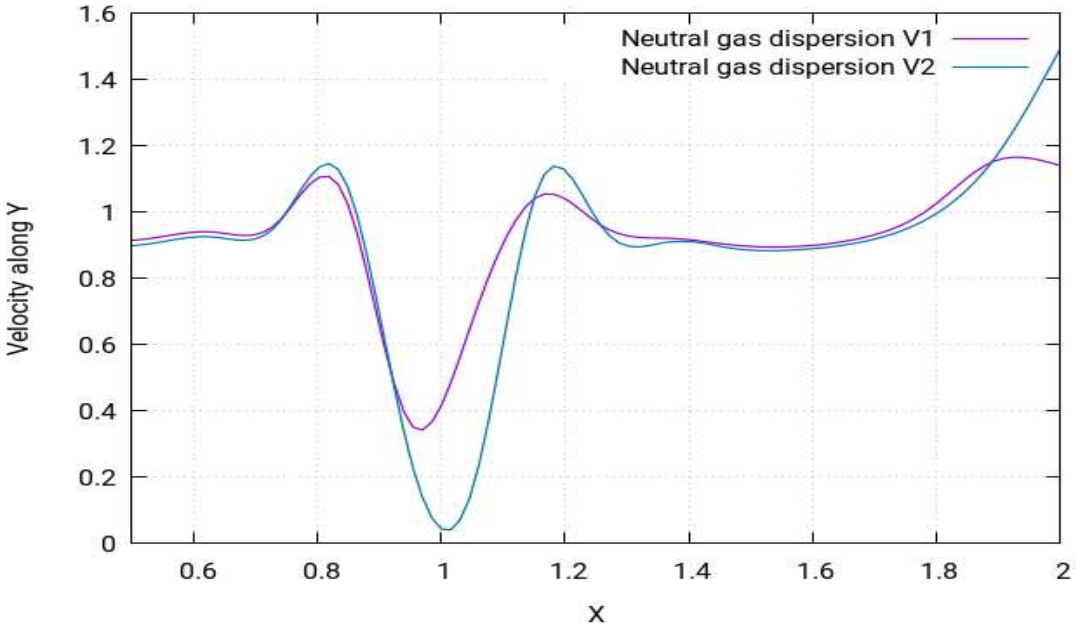

Figure 7.129: *Graphical representation of velocity of neutral gas release source for a flat terrain with a* ***600mm*** *solid fence as an obstacle at* ***1m/s***

Figure 7.129 shows the varying profiles of the velocity with varying distances. While the profiles do follow a same pattern, the values change according to the varying distances.

7.5.9 Heavy gas dispersion with a solid and semi-circular fence as an obstacle

In this scenario, the heavy gas leak occurs from a circular opening having a 50mm diameter. For this case, there are two solid obstacles, which are 400mm downstream from the source. One of the solid fences stands at a height of 60mm, while the second obstacle, a semi-circular fence, has a height of 30mm.

Table 7.9: *Parametric values of scenario 5A*

Density	Flow Rate	Velocity	Ambient Temperature	Release Source Temperature
2.1 kg m/s^3	1 kg/s	1 m/s	25°C	-100°C

7.5.9.1 Release source

The following figure shows the release source for the current scenario:

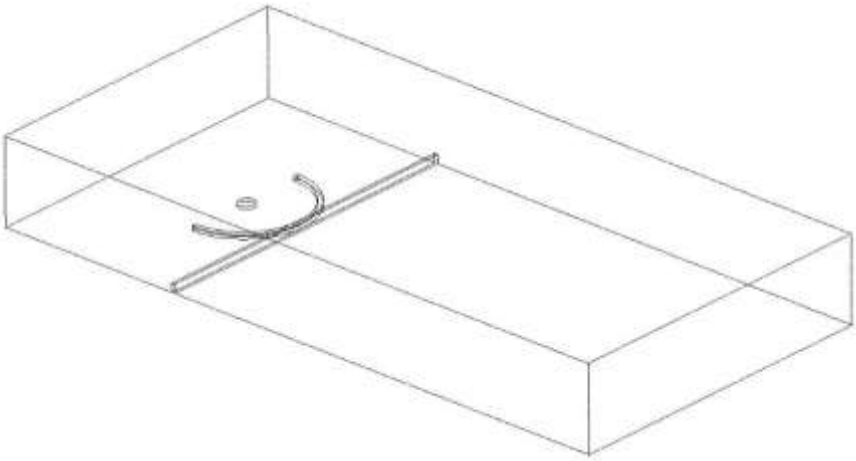

Figure 7.130: *The heavy gas release source for a flat terrain with a solid and a semi-circular as an obstacle at* ***1m/s*** *velocity*

7.5.9.2 Concentration of the heavy gas dispersion

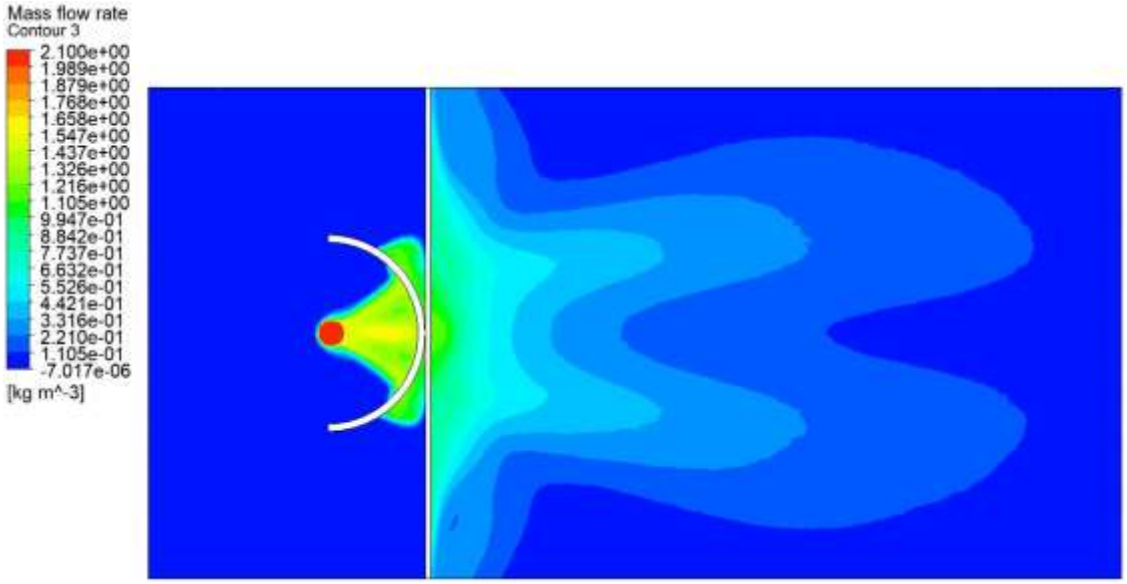

Figure 7.131: *Flow rate profile of heavy gas release source for a flat terrain with a solid and a semi-circular fence as an obstacle with* ***1m/s*** *velocity*

The concentration profile of the heavy gas for scenario 4A is shown in Figure 7.131 above. It shows the concentration profile for the heavy gas when released from a circular source of 50mm diameter with a solid 60mm high fence and a 30mm semi-circular fence as an obstacle. Scenario 3A was performed with the same settings, but the solid fence was 30mm, while in this case, the solid fence is 60mm. It is noticed that, after the release source, there is a high concentration triangle in the beginning, then a slightly lower concentration rectangle and a curve shaped area alongside the inner surface of the solid face. While the areas near the release source are highly concentrated, it can be seen that the same effect is followed when the cloud strikes an obstacle. Similarly, it is further noticed that, with the addition of the fence, the layers

of concentrations have also increased and, immediately after the solid fence, many small layers of high concentrations can be seen. The simulation shows that, for this particular scenario, the heavy gas cloud distributes symmetrically along the horizontal axis. The concentration contour in the above figure shows the highest concentrations red, while the lowest are in blue. The concentrations go on fading and there is a sort of layering pattern in the concentrations, with red being the layer with highest concentrations, then the yellow ones with slightly lower concentrations, then green with slightly less and so on, with the final layer (blue) being the lowest concentration.

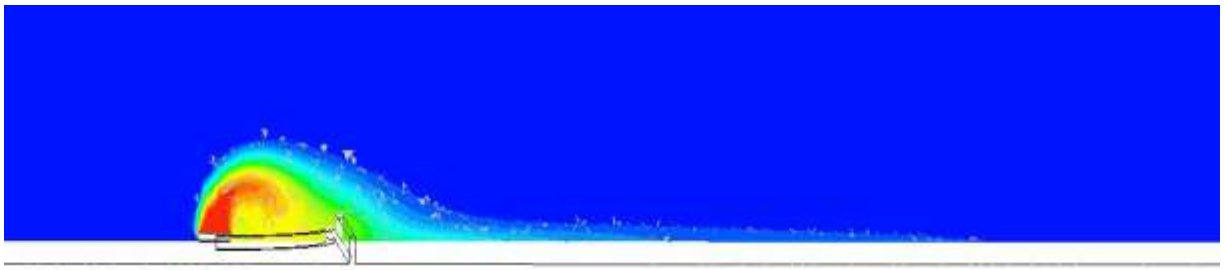

Figure 7.132: *2D view of flow rate profile of heavy gas release source for a flat terrain with a solid and a semi-circular fence as an obstacle with* ***1m/s*** *velocity*

Figure 7.132 shows the two-dimensional version of the concentration simulation. They similar to the behaviour of the cloud shape in this scenario to be the same as that seen in (Figure 7.131).

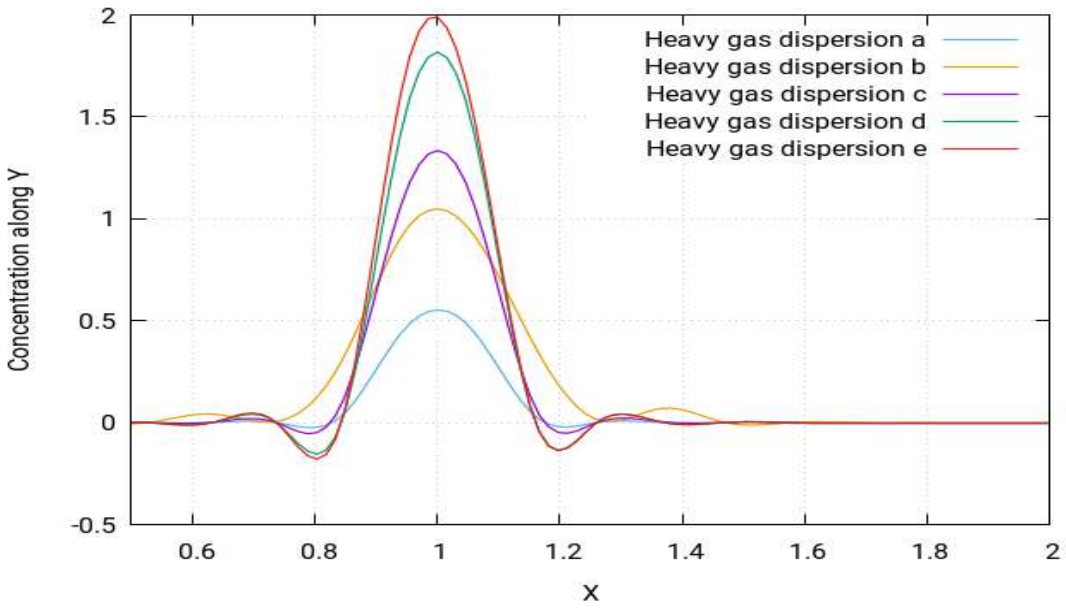

Figure 7.133: *Graphical representation for concentration of heavy gas release source for a flat terrain with* ***1m/s*** *velocity* ***before*** *the solid and the semi-circular fence as an obstacle*

In Figure 7.133 above, concentration profiles for this scenario before the obstacle for varying distances are shown. The same behaviour of concentration profiles as observed in previous heavy gas scenarios 1A, 2A, 3A and 4A is also visible here.

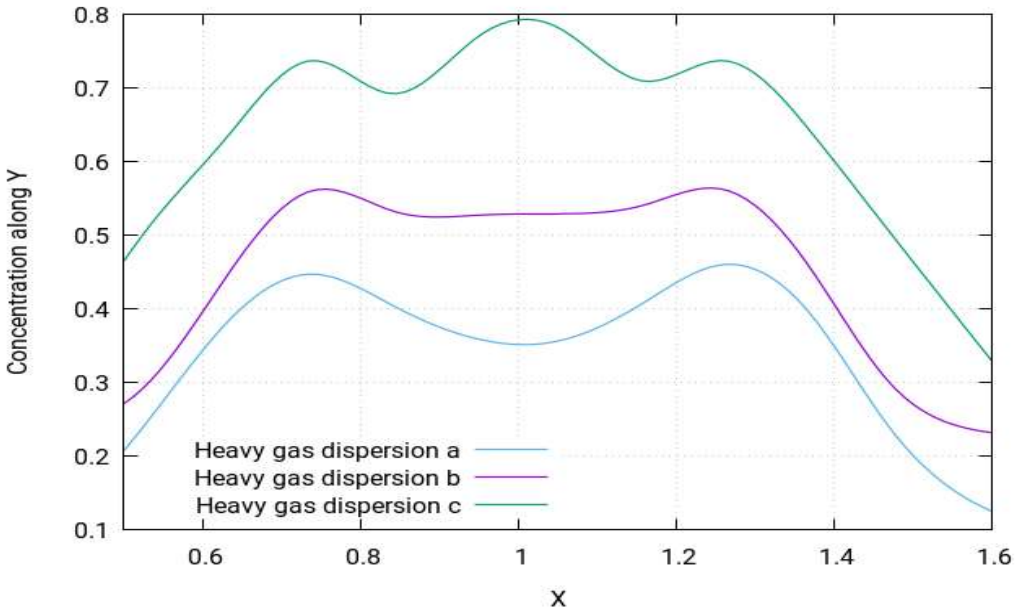

Figure 7.134: *Graphical representation for concentration of heavy gas release source for a flat terrain with **1m/s** velocity **after** the solid and the semi-circular fence as an obstacle*

The concentration profiles for this scenario after the obstacle for varying distances are shown in Figure 7.134 above. While the profile of concentration shows a different pattern after the obstacle to before the obstacle, the profile at different points after the obstacle follows the same pattern and has different values to the distance from release source.

7.5.9.3 Density of the heavy gas dispersion

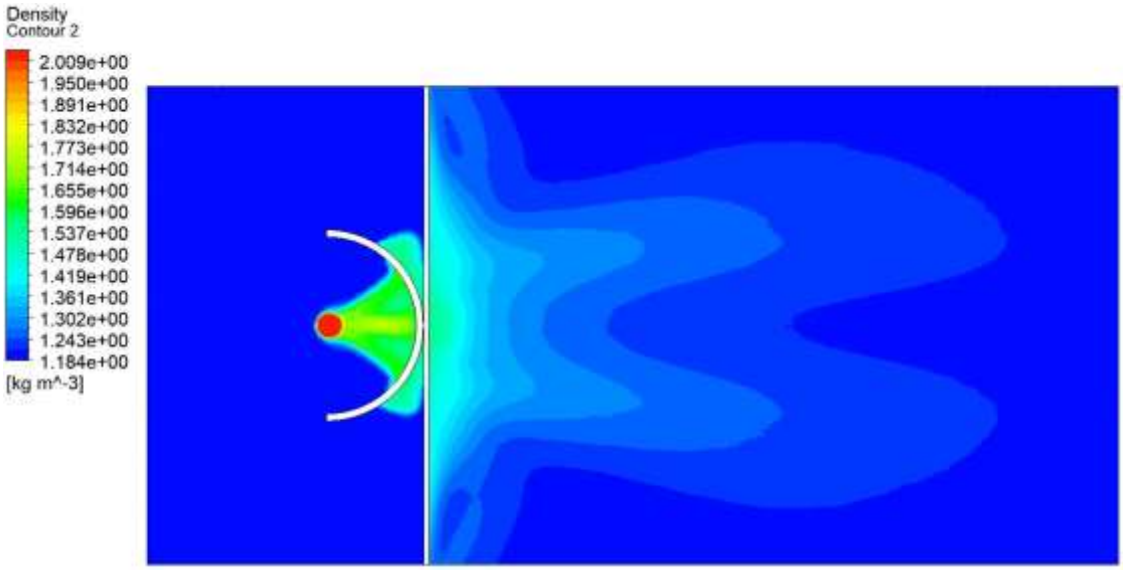

Figure 7.135: *Density profile of heavy gas release source for a flat terrain with a solid and a semi-circular fence as an obstacle with **1m/s** velocity*

The density profile of the heavy gas for scenario 4A is shown in Figure 7.135 above. It shows the density profile for the heavy gas when released from a circular source of 50mm diameter with a solid fence of 60mm and a semi-circular fence of 30mm as an obstacle. At first glance,

it appears that the density profile also follows the same pattern as that of concentration, keeping in mind the similarity in the concentration and density profile shown in Figure 7.135 and Figure 7.131 respectively. However, it should be noted that the density profile appears to be a slightly shrunken version of the concentration profile. Moreover, the concentration contour showed the value of maximum concentration to be 2.1, but the density contours show a maximum value of 2.038.

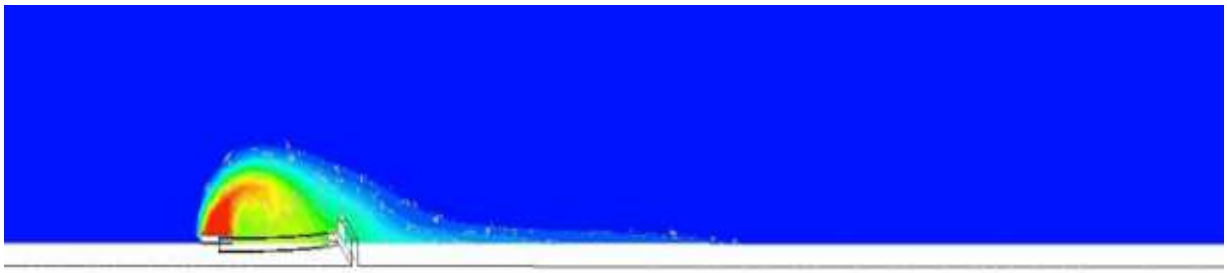

Figure 7.136:*2D view of flow rate profile of heavy gas release source for a flat terrain with a solid and a semi-circular fence as an obstacle with* ***1m/s*** *velocity*

Figure 7.136 shows the two-dimensional view of the density profile and it shows the same behaviour of the heavy gas as (Figure 7.135).

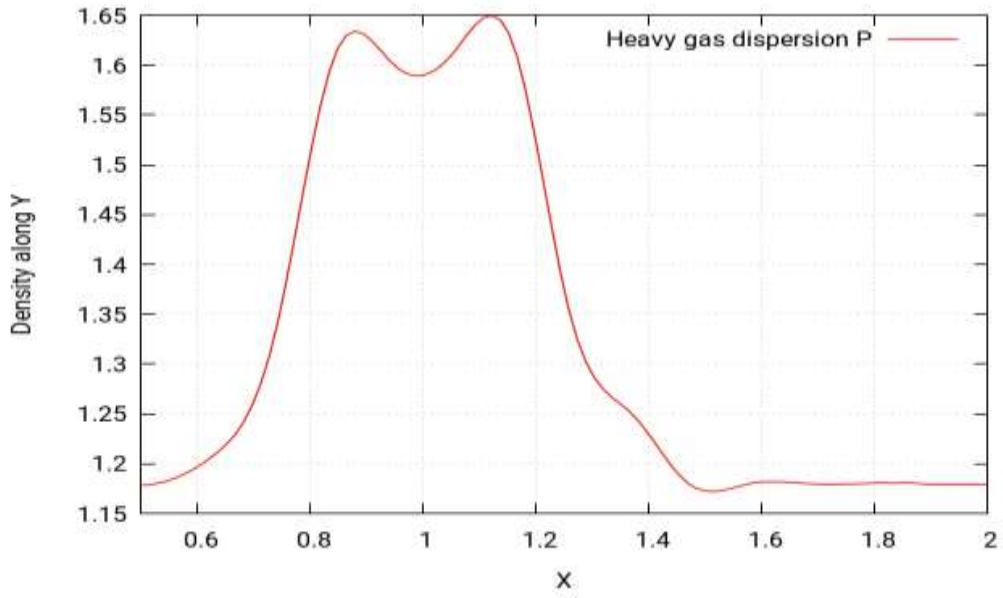

Figure 7.137: *Graphical representation for density of heavy gas release source for a flat terrain with* ***1m/s*** *velocity* ***before*** *a solid and the semi-circular fence as an obstacle*

Figure 7.137 shows density profile before the obstacle of the released gas for this scenario. In the figure, the distance is calculated from the release source. The same pattern of density observed in scenario 4A previously is also visible here.

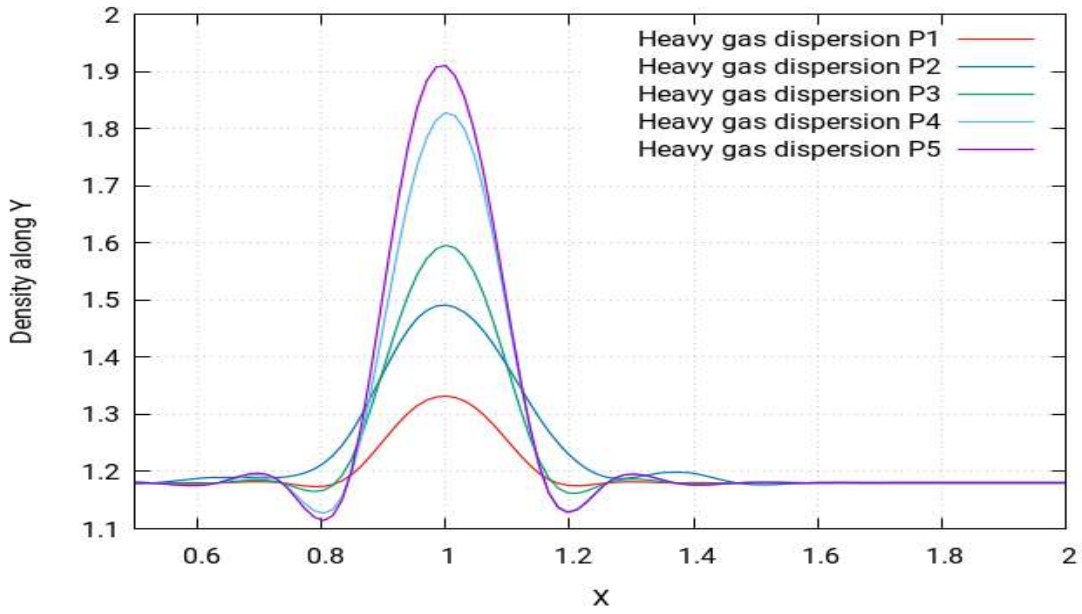

Figure 7.138: *Graphical representation for density of heavy gas release source for a flat terrain with* ***1m/s*** *velocity* ***before*** *the solid and the semi-circular fence as an obstacle.*

Figure 7.138 shows the profiles of the density before the obstacle of the released gas with varying distances. In the figure, the distance is calculated from the release source. This profile shows the same behaviour as that of the concentration profile.

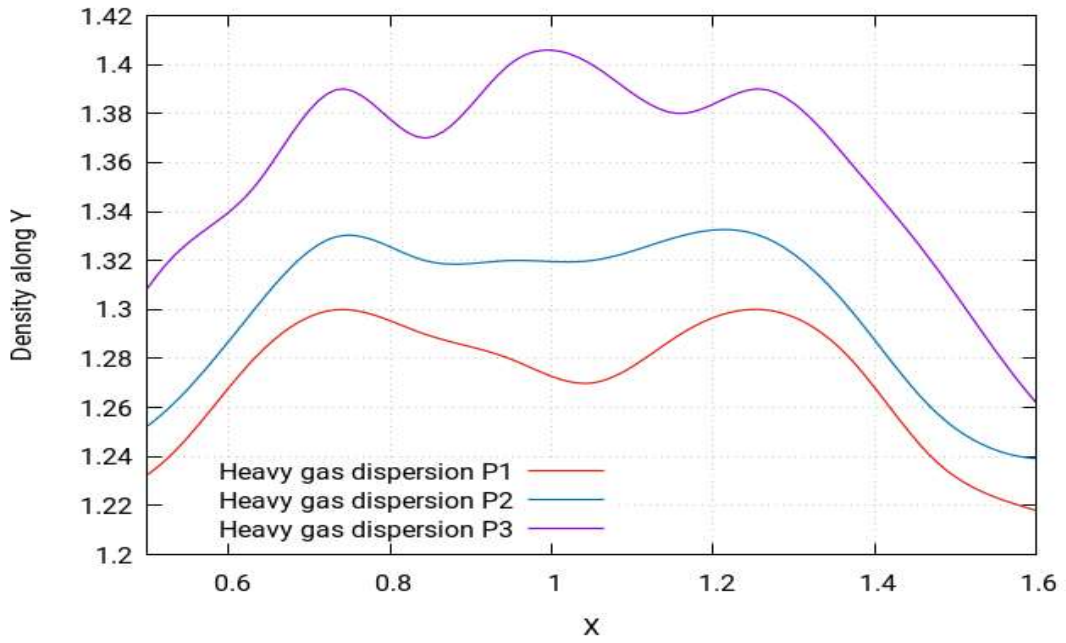

Figure 7.139: *Graphical representation for density of heavy gas release source for a flat terrain with* ***1m/s*** *velocity* ***after*** *the solid and the semi-circular fence as an obstacle*

7.5.9.4 Temperature of the heavy gas dispersion

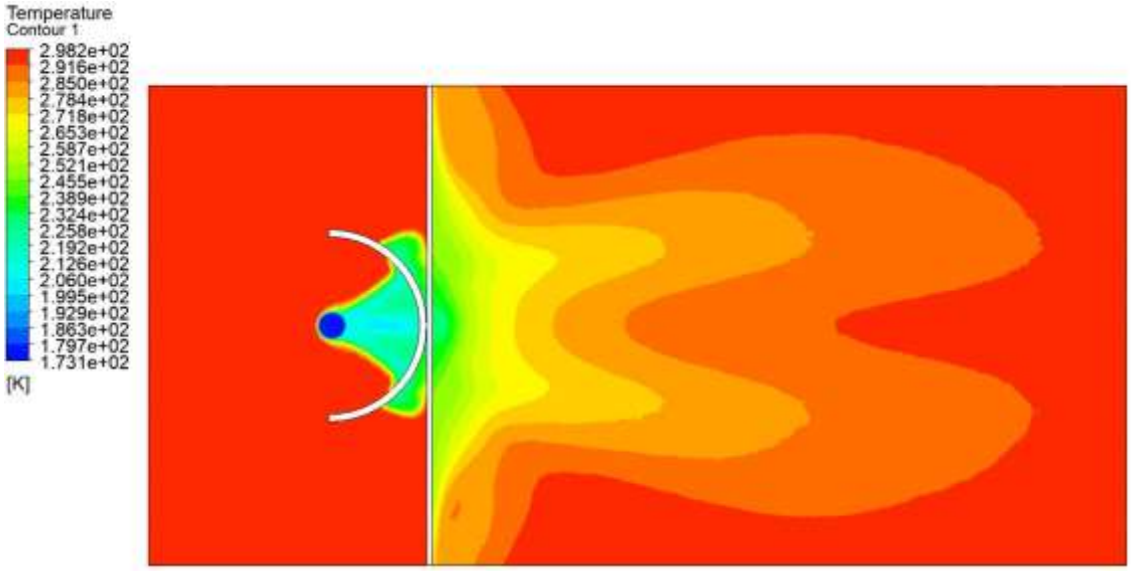

Figure 7.140: *Temperature profile of heavy gas release source for a flat terrain with a solid and a semi-circular fence as an obstacle with* ***1m/s*** *velocity*

Figure 7.140 above shows the temperature simulation for this scenario. Looking at the temperature simulation produces quite the same profile for this scenario as that of the concentration profile. However, the point to notice is that the behaviour of temperature is in fact the opposite to that of concentration. This means that the areas identified in the concentration simulation as being highly concentrated will have the lowest temperatures, the ones with moderate concentrations will have moderate temperatures and the least concentrated areas will have the highest temperatures. To further simplify these findings, it should be pointed out that the concentrations simulations show that the concentrations near the release source point tend to be the highest, and start to fade away as they move away from the source, reaching the lowest levels when they move much further away, eventually reaching the environment where the gas cloud disappears. However, the temperature is at its lowest near the release source point and tends to increase as it moves away from the source, finally achieving the maximum temperature equal to the ambient temperature of the environment.

Figure 7.141: *2D view of temperature profile of heavy gas release source for a flat terrain with a solid and a semi-circular fence as an obstacle with* ***1m/s*** *velocity*

Figure 7.141 shows a two-dimensional view of the temperature profile and it shows the same behaviour of the heavy gas as (Figure 7.140).

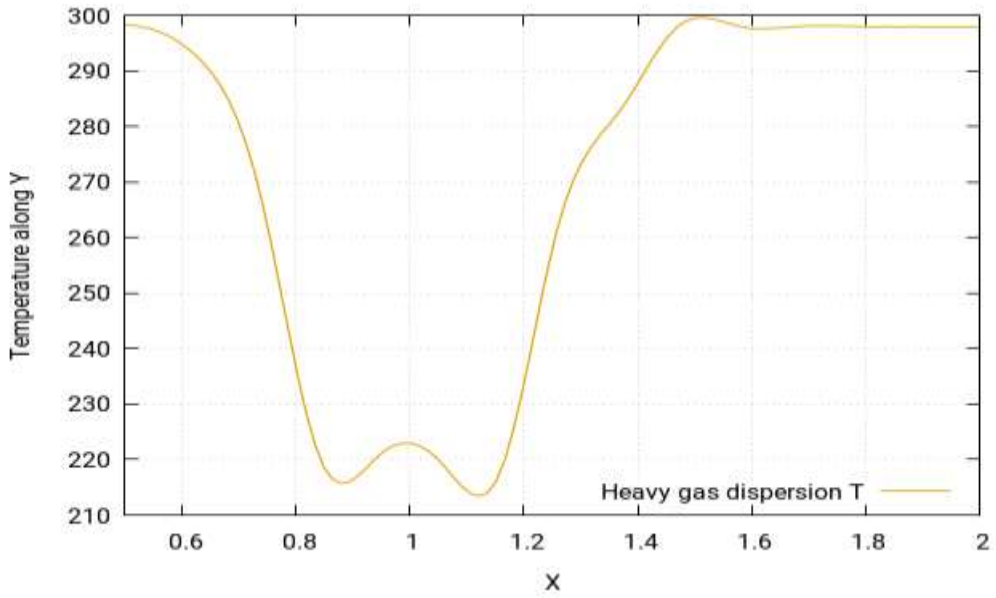

Figure 7.142: *Graphical representation for temperature of heavy gas release source for a flat terrain with **1m/s** velocity **before** the solid and the semi-circular fence as an obstacle*

Figure 7.142 shows temperature profile before the obstacle of the gas released for this scenario. In the figure, the distance is calculated from the release source. This same pattern of temperature as observed in previous scenario 4A is also visible here.

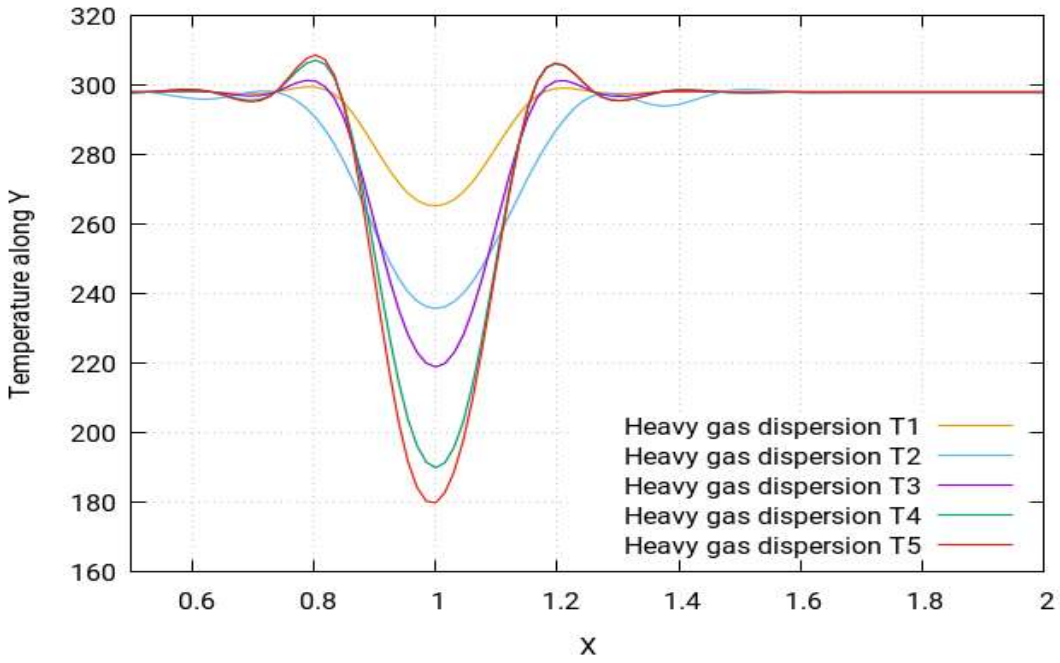

Figure 7.143: *Graphical representation for temperature of heavy gas release source for a flat terrain with **1m/s** velocity **before** the solid and the semi-circular fence as an obstacle*

Figure 7.143 shows the profiles of the temperature of the gas released before the obstacle for varying distances. In the figure, the distance is calculated from the release source. These profiles are inverse of the density profile.

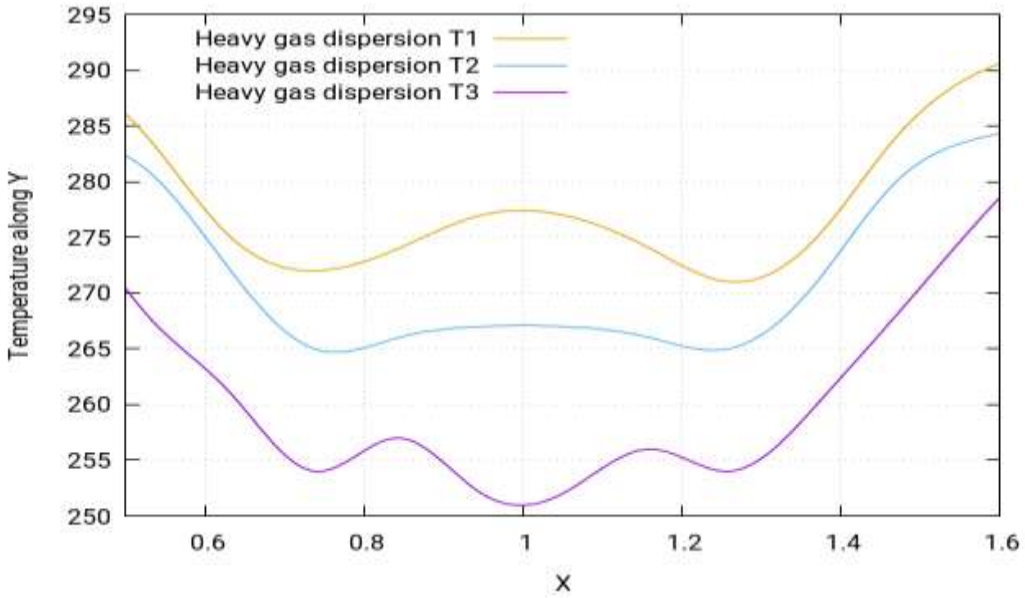

Figure 7.144: *Graphical representation for density of heavy gas release source for a flat terrain with* ***1m/s*** *velocity* ***after*** *the solid and the semi-circular fence as an obstacle*

The temperature profiles for this scenario for varying distances and after the obstacle are shown in the figure above. Similar to the profile before the obstacle, these profiles show the inverse - or mirrored - behaviour to that of the concentration profile after the obstacle.

7.5.9.5 Iso-surface of the heavy gas dispersion

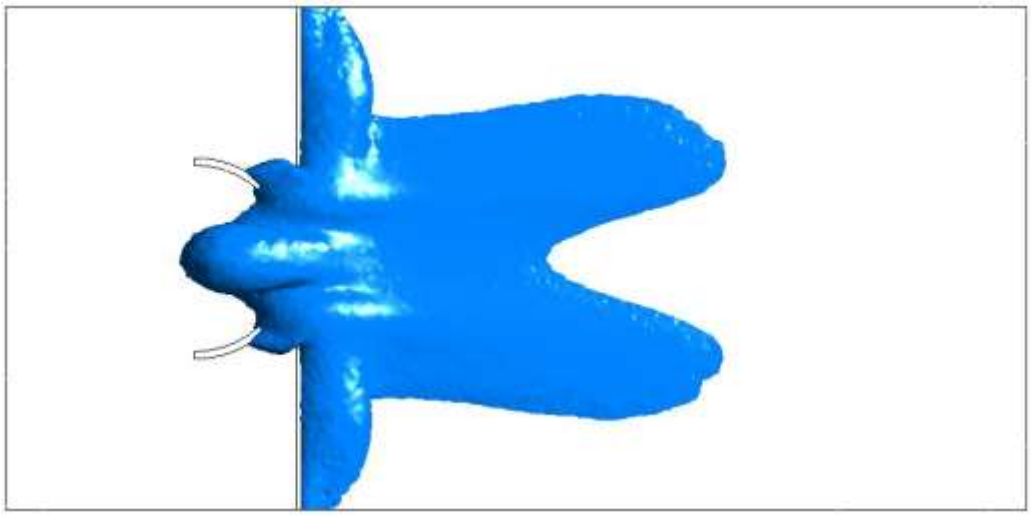

Figure 7.145: *Iso-surface top view of concentration of heavy gas release source for a flat terrain with a solid and a semi-circular fence as an obstacle* ***1m/s*** *velocity*

Figure 7.145 shows the iso-surface of the concentration from the top view. It shows us the triangular shaped distribution converted into curved shaped distribution along the inner wall of

the semi-circular fence until the solid fence after which the distributions appear to be uniform and then form a sinusoidal curve at the end. The concentration is heaviest near the release source point and is distributed symmetrically along the axis.

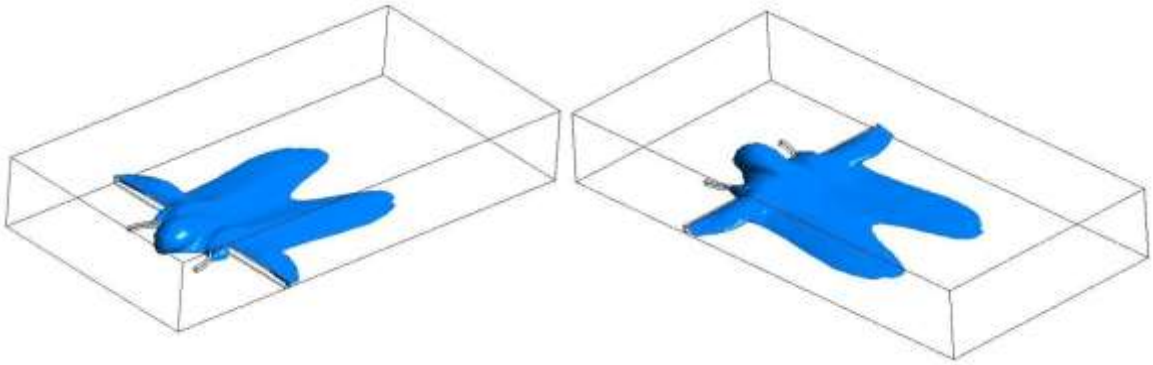

Figure 7.146: *Iso-surface side view of concentration of heavy gas release source for a flat terrain with a solid and a semi-circular fence as an obstacle* ***1m/s*** *velocity*

Figure 7.146 shows the iso-surface of the concentration from the side view. It shows that the gas cloud, after showing an inclination of height near the release source, then goes on to decrease in height and is thickest near the release source, whereas it continues to become thinner as it moves along the horizontal axis. It also shows the iso-surface of the concentration from the rear view. In this figure, although the gas cloud looked symmetrical along the horizontal in the previous views, it can be noticed here that the cloud density is a slightly more in the upside region of the gas cloud than the lower side. So, along the horizontal axis, the cloud might be horizontal, but along the vertical axis, it shows deviations from symmetry.

According to Standard BS EN 60079-10-1:2009 Santon el. al. [104], the following locations can be categorised:

Zone 0: The triangular plus rectangular shaped area near the release source location
Zone 1: The area beginning immediately after zone 0 expanding uniformly
Zone 2: All the remaining locations not categorised in zone 0 or zone 1

7.5.9.6 Velocity of the heavy gas dispersion

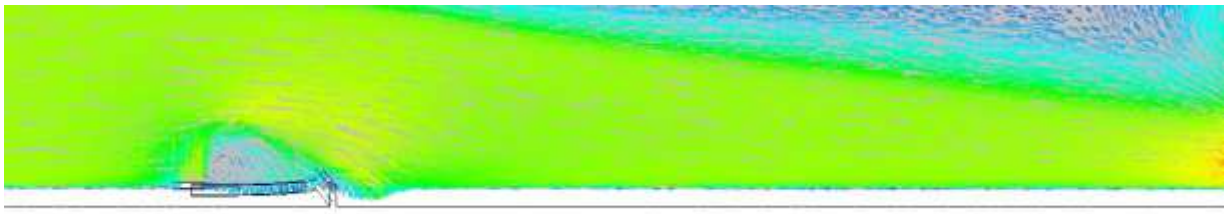

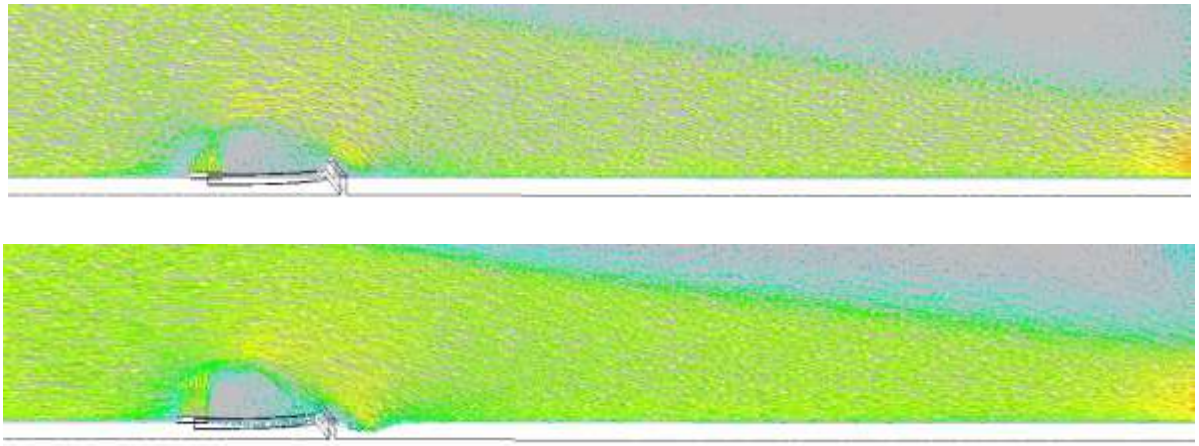

Figure 7.147: *Velocity profile of heavy gas release source for a flat terrain with a solid and a semi-circular fence as an obstacle with* ***1m/s*** *velocity*

Figure 7.147 shows the velocity contours of heavy gas dispersion for this scenario. Velocity contours depict the intensity of wind - or the effective wind influence - at the different locations throughout the layout. It can be seen in the figure that the wind intensity is different at different points in the layout. The wind operation is smooth in this scenario and not many complex vertexes are seen. The wind eddies carry the gas cloud to the nearby environment, where a gas cloud is formed due to steady flow. This gas cloud is deemed dangerous as it is volatile and could lead to an explosion, fire, etc.

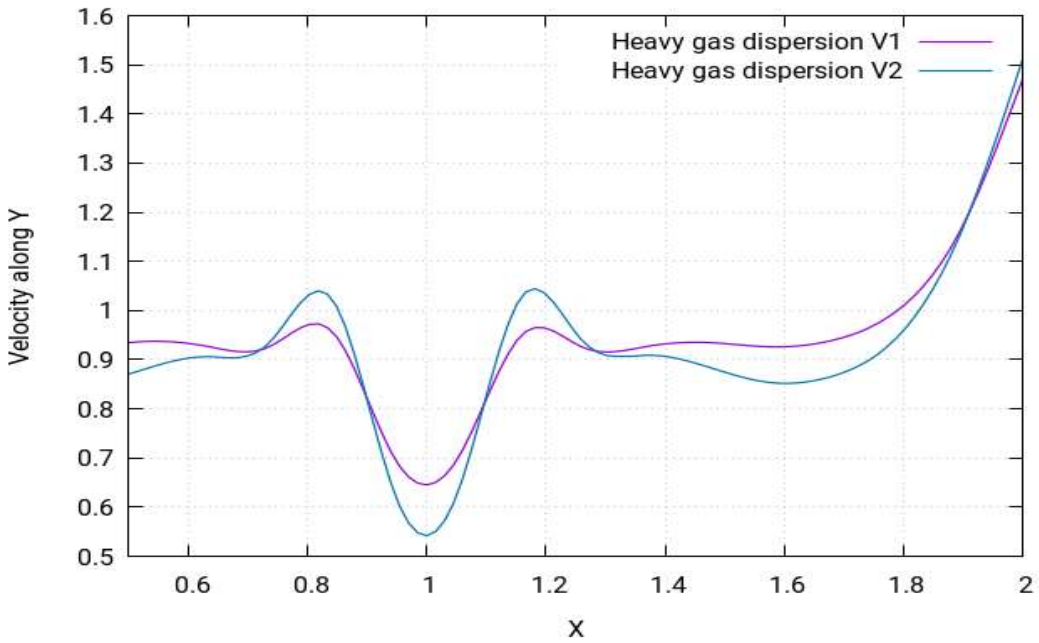

Figure 7.148: *Graphical representation of velocity profile of heavy gas release source for a flat terrain* ***before*** *a solid and a semi-circular fence as an obstacle at* ***1m/s***

Figure 7.148 shows the profile of the velocity of the released gas for this scenario before the obstacle. The profiles show a sinusoidal behaviour initially, but show a sharp increase at the

end. All the profiles follow a similar pattern, but have differences in values due to difference of distance from the release source.

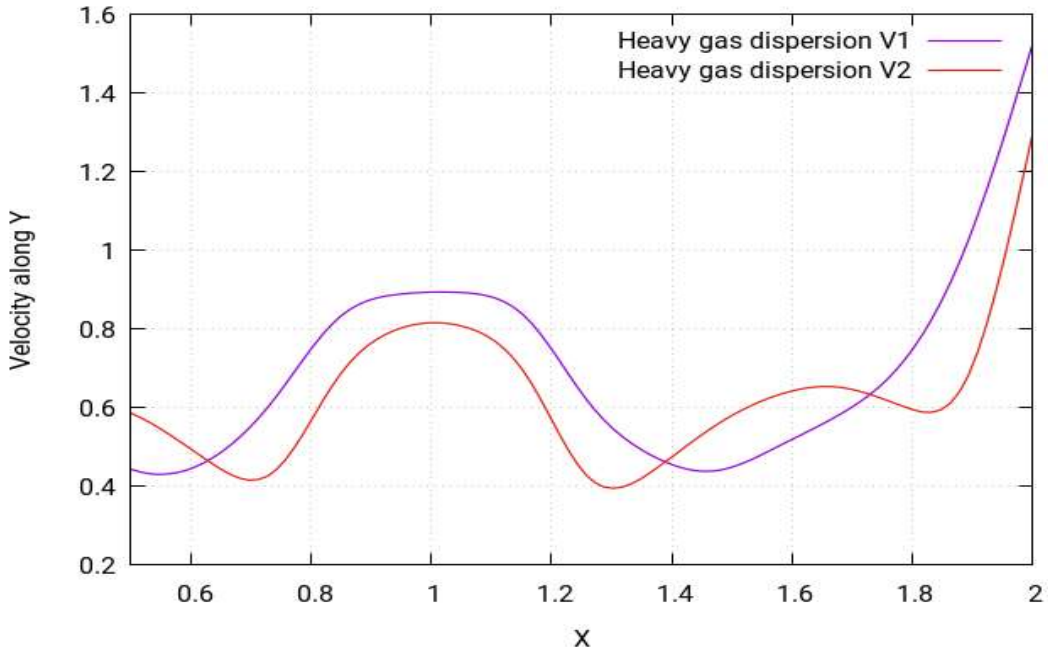

Figure 7.149: *Graphical representation of velocity profile of heavy gas release source for a flat terrain* ***after*** *a solid and a semi-circular fence as an obstacle at* ***1m/s***

Figure 7.149 shows the varying profiles of the velocity after the obstacle with varying distances. While the profiles do follow the same pattern, the values change according to the varying distances.

7.5.10 Neutral gas dispersion with a solid and a semi-circular fence as an obstacle

In this scenario, the neutral gas leak occurs from a circular opening having a 50mm diameter. For this case, there are two solid obstacles, which are 400mm downstream from the source. One of the solid fences is at a height of 60mm, while the second obstacle, a semi-circular fence, has a height of 30mm.

Table 7.10: *Parametric values of scenario 5B*

Density	Flow Rate	Velocity	Ambient Temperature	Release Source Temperature
1.1839 kg m/s^3	1.7737 kg/s	1 m/s	25°C	25°C

7.5.10.1 Release source

The following figure shows the release source for the current scenario:

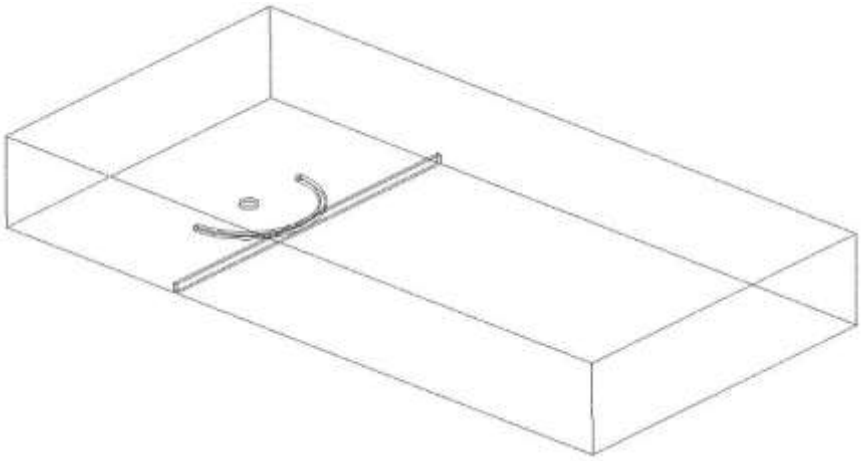

Figure 7.150: *Top view of neutral gas release source for a flat terrain with a solid and a semi-circular fence as an obstacle at* ***1m/s*** *velocity*

7.5.10.2 Concentration of the neutral gas dispersion

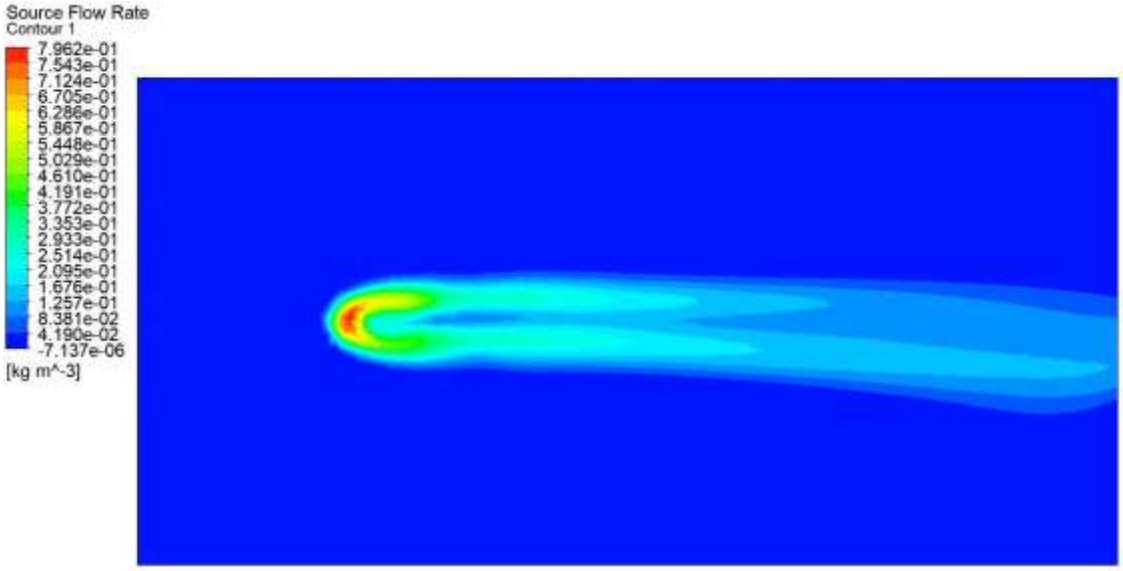

Figure 7.151: *Concentration profile of neutral gas release source for a flat terrain with a 60mm solid fence and a 30mm semi-circular fence as an obstacle at* ***1m/s*** *velocity*

The concentration profile of the neutral gas for scenario 5B is shown in Figure 7.151 above. It shows the concentration profile for the neutral gas when released from a circular source of 50mm diameter with a solid fence of 60mm and a semi-circular fence of 30mm as an obstacle. It was noticed in scenario 4B that the usual elliptical cylinder cloud shape was the same as seen in scenario 2B and 3B was not seen. A deviation from the usual elliptical cylinder-shaped cloud is observed such that there is a bend in the cloud after first high concentration end of the cloud which was likely due to the 60mm fence. The same behaviour has been extended in this scenario. Here, it can be observed that there is an extra cloud split layer in the cloud shape. In this case, as there is another obstacle in the form of a 30mm high fence in this scenario. Similar

to scenario 4B, the fence influences the cloud shape in such a way that, after striking the obstacle (60mm solid and 30mm semi-circular fence), the cloud goes off declining and expanding more in the lower side than in the upper side. The simulation shows maximum concentrations in red near the release source. Thereafter, the concentrations begin to decrease. From the simulation, it can be observed that the concentration distribution is not symmetrical on the horizontal axis and that the lower half of the elliptical cylinder is more concentrated.

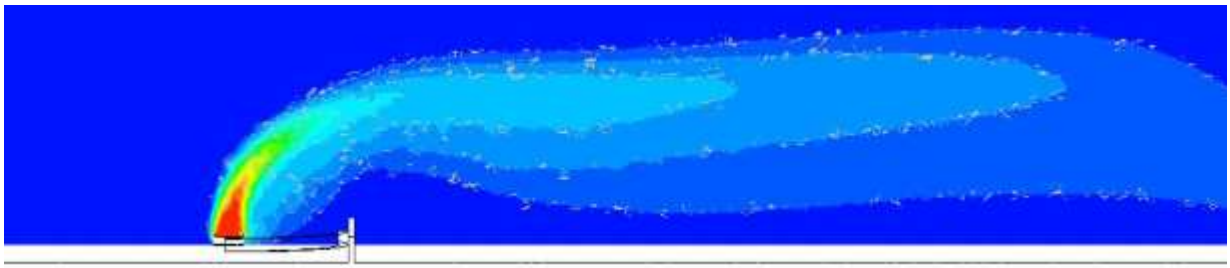

Figure 7.152: *2D view of concentration profile of neutral gas release source for a flat terrain with a 60mm solid fence and a 30mm semi-circular fence as an obstacle at* ***1m/s*** *velocity*

Figure 7.152 shows the two-dimensional version of the concentration simulation. It further verifies the behaviour of the cloud shape for neutral gas studied in the (Figure 7.151) previously.

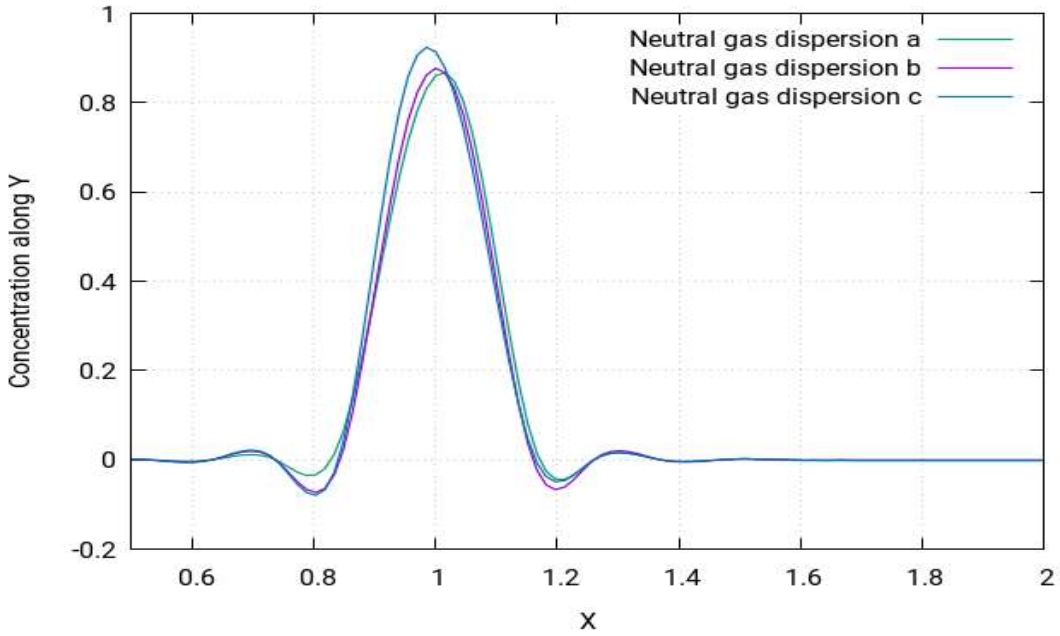

Figure 7.153: *Graphical representation of concentration profile of neutral gas release source for a flat terrain with a 60mm solid fence and a 30mm semi-circular fence as an obstacle at* ***1m/s*** *velocity*

In Figure 7.153 above, concentration profiles for this scenario before the obstacle for varying distances are shown. The same behaviour of concentration profiles as observed in previous neutral gas scenarios 1B, 2B, 3B and 4B is also visible here.

7.5.10.3 Iso-surface of the neutral gas dispersion

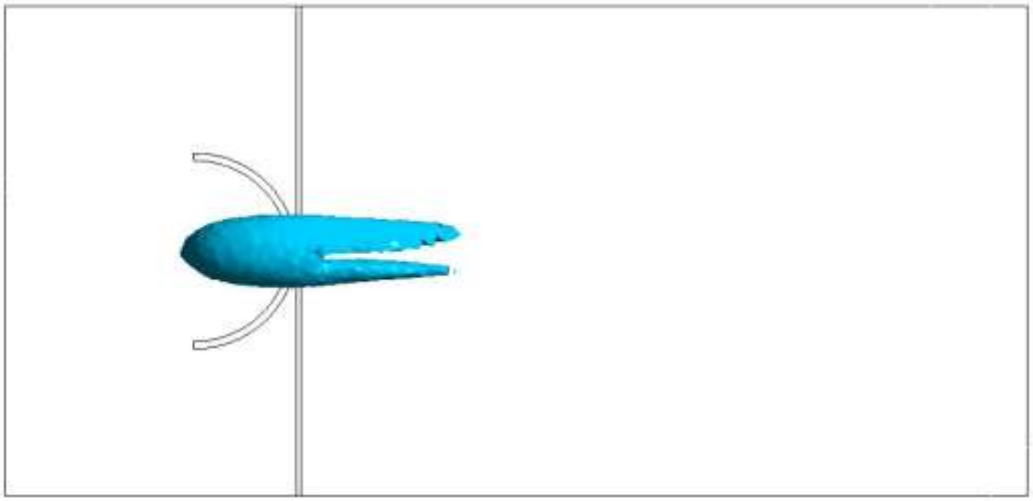

Figure 7.154: *Iso-surface top view of concentration of neutral gas release source for a flat terrain with a 60mm solid fence and a 30mm semi-circular fence as an obstacle at* ***1m/s*** *velocity*

Figure 7.154 shows the iso-surface of the concentration from the top view. The split from centre cloud pattern, like that in scenario 3B, is also present here, but the cloud lengths in both parts are almost equal, while the upper part of the cloud is more concentrated.

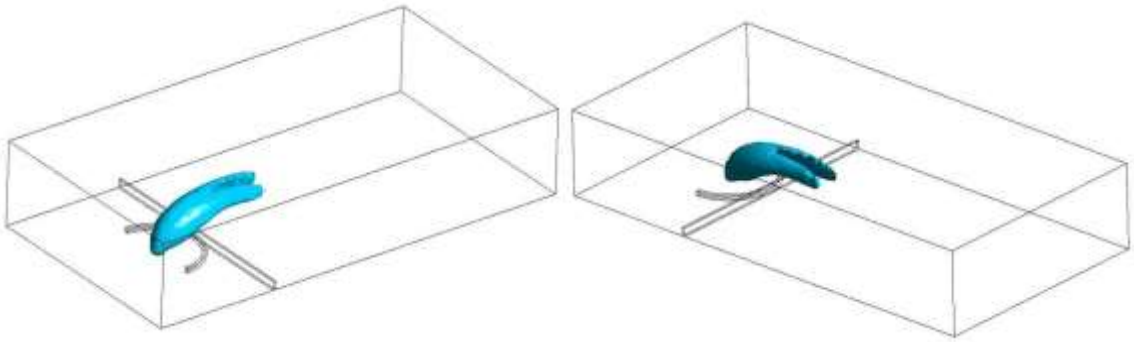

Figure 7.155: *Iso-surface side and back view of concentration of heavy gas release source for a flat terrain with a 60mm solid fence and a 30mm semi-circular fence as an obstacle at* ***1m/s*** *velocity*

Figure 7.155 shows the iso-surface of the concentration from the side view. It shows the same results as discussed in the previous figure. It also shows the iso-surface of the concentration from the back view. It further verifies the cloud shape pattern discussed previously.

According to Standard BS EN 60079-10-1:2009 Santon el. al. [104], the following locations can be categorised:

Zone 0: The area near the release source

Zone 1: The area beginning immediately after release source up to the obstacle

Zone 2: All the remaining locations not categorised in zone 0 or zone 1

7.5.10.4 Velocity of the neutral gas dispersion

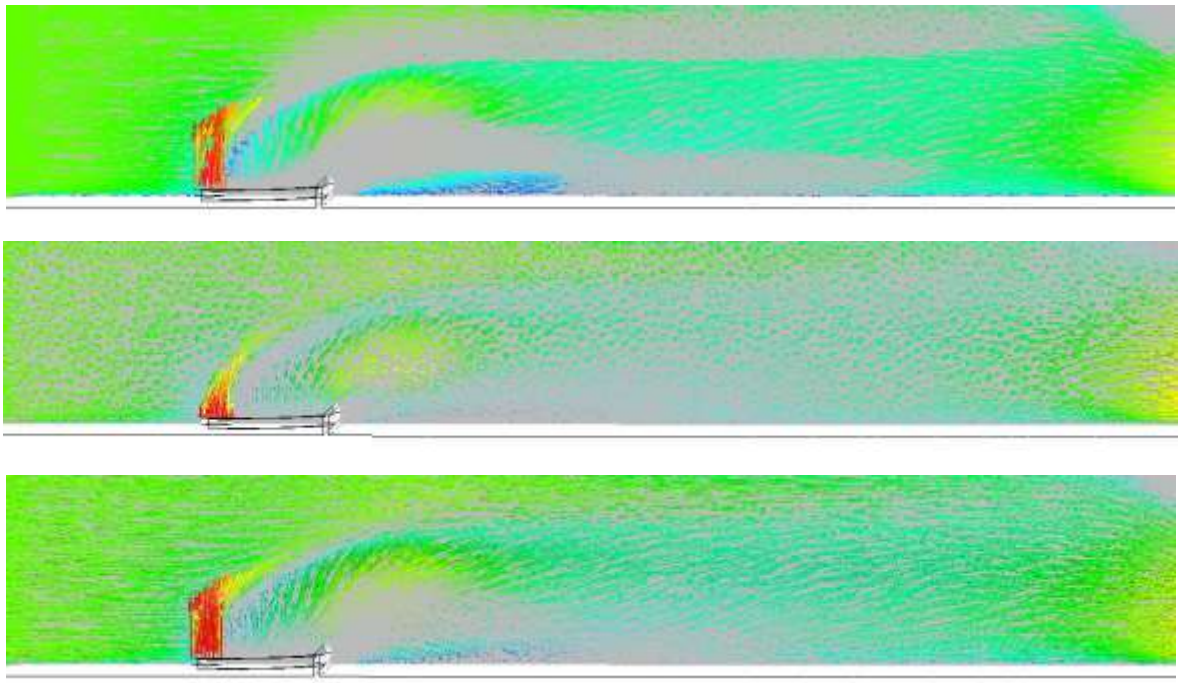

Figure 7.156: *Velocity profile of neutral gas release source for a flat terrain with a 60mm solid fence and a 30mm semi-circular fence as an obstacle at* ***1m/s***

Figure 7.156 shows the velocity contours of neutral gas dispersion for this scenario. Velocity contours depict the intensity of wind - or the effective wind influence - at the different locations throughout the layout. It can be seen in the figure that the wind intensity is different at different points in the layout. In scenario 1A, the wind operation is smooth, and not many complex vertexes are seen. However, in this scenario, there are many complex vertexes formed near the release source location, as seen in the figure. These complex vertexes carry the gas cloud to the nearby environment, where a gas cloud is formed due to steady flow. This gas cloud is deemed dangerous as it is volatile and could lead to an explosion, fire, etc. This also causes the gas cloud to advance in the move further in an upward direction.

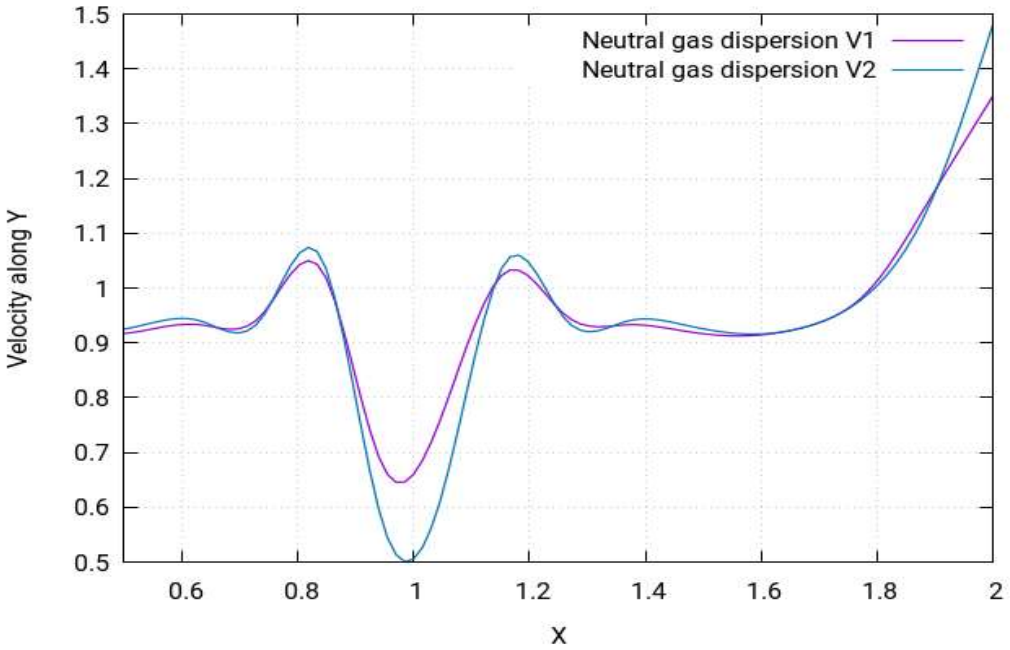

Figure 7.157: *Velocity profile of neutral gas release source for a flat terrain with a 60mm solid fence as an obstacle at* ***1m/s***

Figure 7.157 shows the varying profiles of the velocity after the obstacle with varying distances. While the profiles do follow a same pattern, the values change according to the varying distances.

7.6 Summary

The results of this work provide critical and in-depth analysis of the behaviour of heavy and dense plumes and how the dispersion is affected by obstacles. After a detailed analysis and different experimentation to the set-up using no obstacles, as well as one and two obstacles, to see how the gas dispersion is affected by obstacles, it is found out that two-dimensional obstacles have a very significant effect of the dispersion of heavy gas, while they have some effect on the neutral gas cloud, but not as significant as the heavy gas clouds. This proves that heavy gas plumes are very sensitive to obstacles. Moreover, it is found out that the obstacle shape also plays a key role in defining the shape of the gas cloud, as the solid fence had a more significant effect on the gas clouds compared to the semi-circular fence. The findings of the results are also compared with other experimental results, such as [57,58] and [59]. A remarkably close relationship can be seen in the profiles. This leads to the assumption that numerical simulations can be particularly useful for analysing the behaviour of the gas cloud.

Chapter 8 Heavy gas dispersion within a group of buildings

8.1 Introduction

Petroleum gas is heavier than ambient air and, when leaked to the atmosphere, it is also called dense or heavy gas. If leaked into the atmosphere, heavy gas tends to make a combustible gas cloud after mixing with the surrounding air. This combustible gas is at a high risk of fire or explosion and producing harmful environmental pollutants. Even though great care is taken when handling heavy gas, incidents of fire and explosions continue to occur around the world. Therefore, it is of paramount importance to study the dispersion of leaked heavy gases and the formation of heavy gas clouds so that a better approach can be adopted to avoid these catastrophes.

In this chapter, heavy gas dispersion in three groups of buildings or structures is studied using the CFD approach. The buildings and structures are cuboid-shaped, cylinder-shaped and sphere-shaped. In each group, these buildings have collocated and staggered layouts. The perimeters are varied along with the release source location, and the effect of the difference in the values of these parameters is analysed. The results obtained from these numerical simulations are also compared with the experimental results of Heidorn et. al. [103].

The zones for gases, vapours or mists are currently defined in the relevant Standard BS EN 60079-10-1:2009 Santon el. al. [104] as:

Zone 0 – a place in which an explosive gas atmosphere is present continuously, for long periods or frequently

Zone 1 – a place in which an explosive atmosphere is likely to occur in normal operation

Zone 2 – a place in which an explosive atmosphere is not likely to occur occasionally in normal operation, but if it does occur, it will persist for a short time only

8.2 CFD simulation set-up

CFD simulations can provide very detailed and accurate results but require a great deal of computation for accurate results. The greater the number of nodes, the greater the computation time. ANSYS-CFX and fire dynamic simulator (FDS) are used to model the fluid flows, which are fire-driven using advanced computational fluid dynamics (CFD) based on the Navier-Stokes's equations and large eddy simulations. CFD uses advanced numerical methods to

perform the iterations and compute the results. These results can provide accurate information regarding the dispersion of heavy gases. The numerical computations for the flow dispersions are based on the Navier-Stokes's equations. The dispersion of the heavy gas is influenced by many factors, like turbulence, nature of the gas and properties of the atmosphere. All these factors play an important role in determining the nature of dispersion. CFD analysis is better for predicting properties. It uses Reynold's Averaged Navier-Stokes (RANS) equations to predict the Reynold's number which gives information regarding the turbulence of the flow Scargiali et. al. [24], Pontiggia et. al. [41].

The numerical display is set up with a similar set-up to the examinations. The computational space has a component of 2 x 3 x 0.32 (in meters) in an/the x, y and z coordinate system. The overall area is divided into several cells of sizes 2.5 x 2 x 2 (mm). As the CFD requires the boundary conditions to be specified, the surfaces of the solid and the ground are taken as no-slip boundary limits. The CFD also demands some initial conditions to be specified. In the present study, the calculations were begun with uniform initial conditions and the procedures were coordinated up to 300seconds.

The CFX total number of elements for the simulation was kept under 25 million to reduce the computation time. Each computation took approximately 3,600 seconds to complete.

8.3 Heidorn et. al's experimental set-up

The following experiment is a wind tunnel simulation using the parameters shown in Table 8.1 below.

Table 8.1: *Simulation design parameters of Heidorn et. al.[103]*

Simulation design parameters

Parameter	Scale[a]									
	Full	1:50		1:100		1:300		1:500		
Release height (m)	13	0.26		0.13		0.043		0.026		
Release width (m)	14	0.28		0.14		0.047		0.028		
Release volume (m^3)	2000	0.016		0.002		7.4×10^{-5}		1.6×10^{-5}		
Release volume (L)	2×10^6	16		2		0.074		0.016		
Richardson number	2.1	2.1		2.1		2.1		2.1		
Reference height (m)	10	0.2		0.1		0.033		0.02		
Gradient height (m)	600[b]	12		6		2		1.2		
Density ratio (ρ_g/ρ_a)	1.96	1.96	4.19	1.96	4.19	1.96	4.19	1.96	4.19	
Wind velocity at reference height (m/s)	7.5	1.08	1.97	0.75	1.37	0.44	0.80	0.34	0.62	
Wind velocity at pilot height (m/s)[c]		1.45	2.65	1.01	1.85	0.59	1.08	0.46	0.84	

To achieve more accurate results, the model scale of the wind tunnel must be chosen according to velocities and densities of the gases. The gases in the present experiment were kept under a

velocity of 2 m/s. Considering the densities, the wind tunnel scale was kept at ratios 1/50 and 1/100.

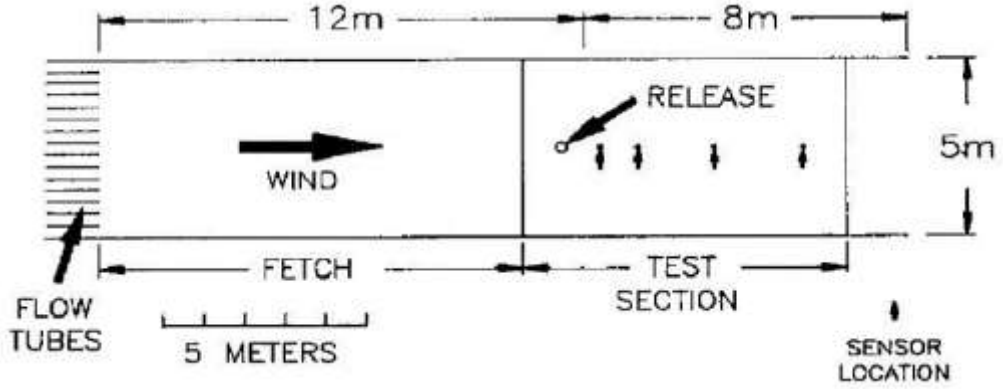

Figure 8.1: *Experimental set-up of Heidorn et. al. [103]*

These were conducted using Thorney Island Theory for simulations of heavy gases inside the wind tunnel. This theory states that there should be an instantaneous release of heavy gases inside the wind tunnel model to decrease the chances of affecting the density of the gas. For this purpose, in the experiment, they used a can containing a nozzle at the front, which is closed. The nozzle was operated by an electronic solenoid switch for an instantaneous on and off operation.

Furthermore, to prevent any alterations in the density values, it was arranged in such a way that the can fell as soon as it released the gas. The properties, including the dimensions of the can, are shown in Table 8.2.

Table 8.2: *Heavy gas cans dimensions of Heidorn et. al. [103]*

Parameter	Scale[a]		
	Full	1:50 scale	1:100 scale
Height, H (m)	13	0.276	0.126
Diameter, D (m)	14	0.251	0.142
Volume (L)	2,000,000	13.63	2.0
Aspect ratio, H/D	0.93	1.10	0.89

Heidorn et. al. [103], experimental study carried out to understand the dispersion behaviour of heavy gases consisted of the following steps:

1) A wind tunnel is used in the experiment, in which a source of a heavy gas is placed at the place in the room where the velocity of the surrounding air is lowest.
2) The heavy gas is released from the nozzle, which is placed at the centre of the obstacles at ground level.

3) The velocity of the heavy gas dispersion is kept at 1 m/s, which is controlled by the nozzle.
4) The gases released are placed in a straight line with the obstacles. These obstacles are actually the cubic blocks.

The obstacles in the form of cubic blocks are placed in three different arrangements which are shown as:

1) With spacing of 0.3:1
2) With spacing of 1:1
3) With spacing of 3:1

These blocks are placed in two different settings or arrangements:

1) Staggered
2) Equally spaced

8.3.1 Methods of visualising the flow

For the visualisation of flow, cameras are used. These high-resolution cameras are placed at different places to cover the whole experimental area.

Two cameras are also placed at the top of the set-up to obtain a bird's eye view of the whole setup. These motion-sensitive cameras provide real-time feedback on the monitors of the heavy gases to obtain the flow simulation.

8.3.2 Measuring the concentration

The concentration of the gas is measured by measuring the volume of the gas released and volume of the testing tunnel. The two tunnels used for the simulation, i.e., 1/50 and 1/100, have different dimensions as shown in (Table 8.2).

The concentration can also be measured using the FID i.e., flame ionization detector, which detects the number of ions present in the gas and measuring the concentration on the basis of it.

8.3.3 Visualisations of flow

Visualisations of the flows obtained from the overhead cameras for different cases are explained as follows:

8.3.3.1 Visualisation of flow for 1:1 block for still air

The pictures of the flow obtained from cameras reveal a more uniform flow of the heavy gases for the 1:1 obstacle placed equally. The flow distribution is diagonal with 45° angles along with the corners. The distribution of the flow is in the circular pattern as shown in Figure 8.2.

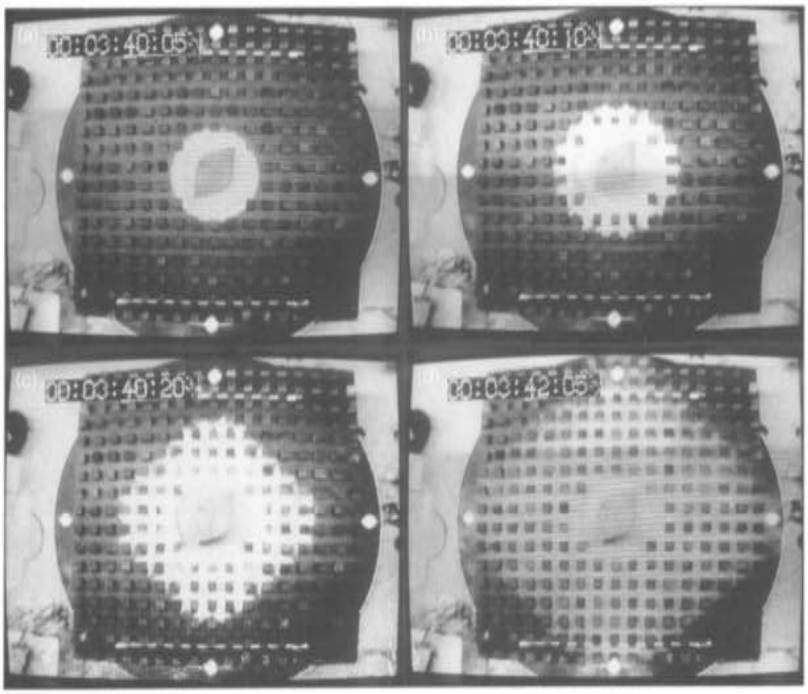

Figure 8.2: *Visualisation of flow for 1:1 of Heidorn et. al. [103]*

8.3.3.2 Visualisation of flow for 3:1 block for still air

The pictures obtained of the flow for 3:1 block is shown as follows in Figures 8.3 and 8.4. The pattern obtained for this gas is again diagonal. The pattern is mostly in the form of a diamond.

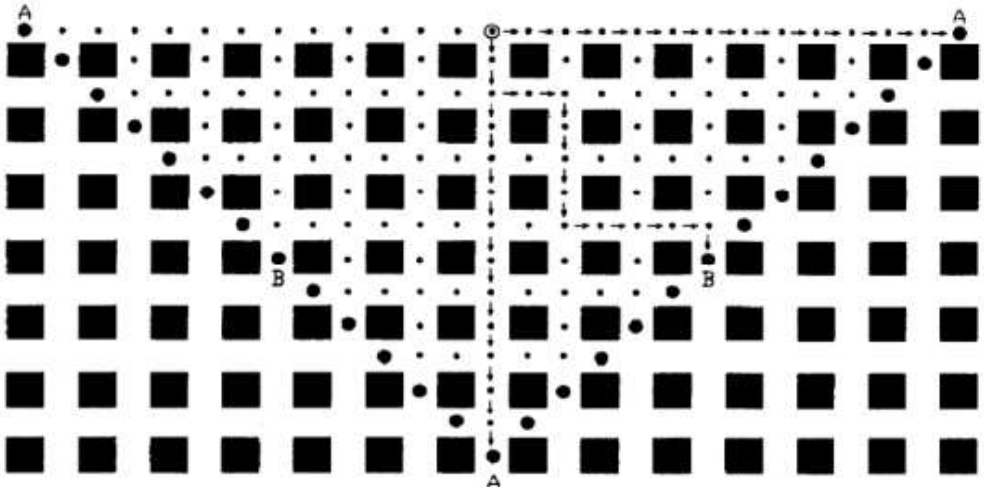

Figure 8.3: *Visualisation of flow for 3:1 for uniform array of Heidorn et. al. [103]*

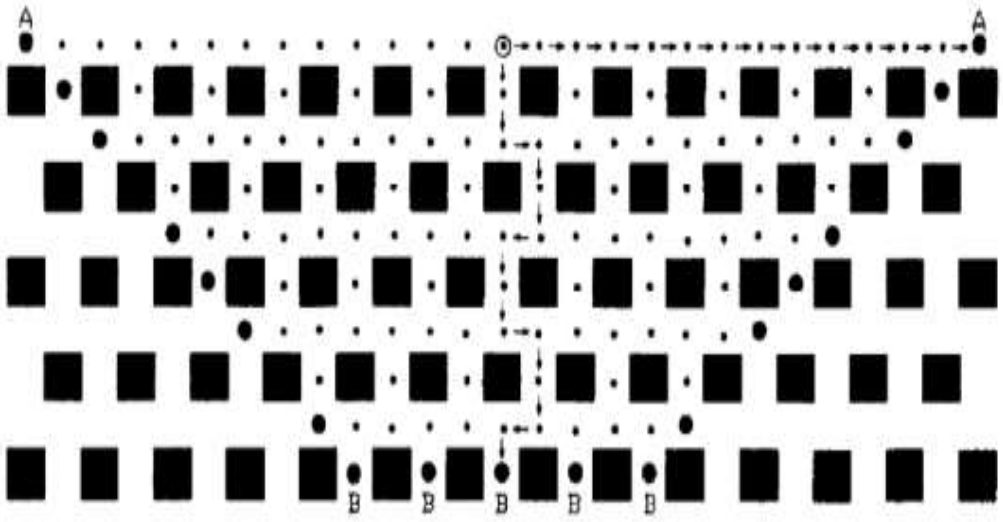

Figure 8.4: *Visualisation of flow for 3:1 for staggered array Heidorn et. al.[103]*

8.3.3.3 Visualisation of flow for staggered block for still air

The flow is the same as that for the 1:1 arranged block; however, in this case the distribution is not at 45° but at another angle, as shown in the figure 8.5.

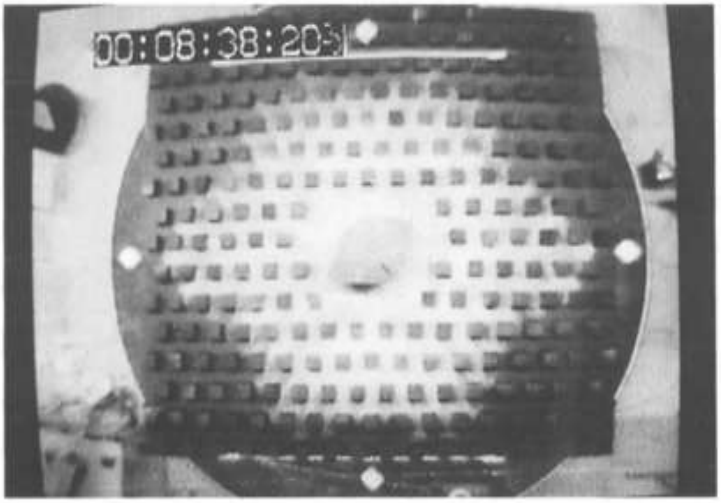

Figure 8.5: *Visualisation of flow for 1:1 for Staggered array of Heidorn et. al.[103]*

8.4 Heavy gas dispersion within cuboid-shaped buildings or structures

In this section, the results are analysed for gas cloud dispersion of both heavy gas and neutral gas within cuboid-shaped buildings. It also features a discussion of the effects of the building layouts on the heavy and neutral gas dispersion clouds. There are some other parameters that also affect the dispersion of heavy and neutral gas clouds. These parameters include (1) flow rate of release source, (2) gas density release source location, (3) wind velocity, (4) release source temperature and (5) ambient temperature. The effects of these parameters are also addressed.

8.4.1 Building layout

Two building layouts, namely collocated and staggered layouts, are explored in this study. The purpose of the study is to examine the behaviour of gas clouds under different building layouts so that it can be examined how the cloud of a heavy or neutral gas behave in different conditions. This would mean that the results of this study could be used for necessary steps required to be taken to avoid accidents and explosions caused by gas dispersion clouds.

8.4.2 Flow rate

The flow rate of the release source was also considered as a driving parameter and the effects of flow rate on the dispersions of the gas cloud for both heavy gas and neutral gas were also analysed. The flow rates used in the study for heavy and neutral gas are as follows:

Table 8.3: *Flow rate values*

Gas type	Flow rate for case one	Flow rate for case two
Heavy	1 kg/s	5 kg/s
Neutral	1.7737 kg/s	1.7737 kg/s

8.4.3 Gas density

As gas density is a very important factor in the dispersion of gas clouds, the influence of gas density was also taken into consideration for the studying of gas dispersion clouds in this study. The gas densities used in the present study are as follows:

Table 8.4: *Density values*

Gas type	Density
Heavy	2.1 kg m/s^3
Neutral	1.1839 kg m/s^3

8.4.4 Release source temperature

The effect of the release source temperature on the gas cloud dispersion was also analysed. The following temperatures were used in this study of dispersion of gas clouds for heavy and neutral gas.

Table 8.5: *Temperature values*

Gas type	Release source temperature
Heavy	-100°C
Neutral	25°C

8.4.5 Ambient temperature

An ambient temperature of 25°C was used for both heavy and neutral gas.

8.4.6 Wind velocity

Wind velocity plays a major role in the dispersion of gas clouds, so the effect of wind velocity was also studied. The values of wind velocity for both the heavy and neutral gas is given below.

Table 8.6: *Wind speed*

Gas type	Velocity for case one	Velocity for case two
Heavy	1 m/s	0.25 m/s
Neutral	1 m/s	0.25 m/s

8.4.7 Release source location

Clearly, the release source location would also affect the gas cloud dispersion. So, the behaviour of gas cloud dispersion for different release source locations should also be analysed. Different positions of the release sources point were explored in this study. The location of the release source will be specified with each case study in this work.

Now that the necessary information has been delivered, there now follows an attempt to analyse and understand the results with the help of case studies. First, the patterns of the cloud dispersion of the collocated type layouts will be analysed, followed by the staggered ones.

Note: The following case studies will be done for a fixed gas release source location. Their results will then be analysed and discussed thoroughly.

8.5 CFD comparison with experimental results

The case studies performed in the present study provide highly valuable information. However, the authenticity of these case studies could be challenged if the actual results are not accordance with those of this case study. For this purpose, it is necessary to validate the results of these numerical simulations with those of experimental results.

The dispersion of gases is very much dependent on their buoyancy and the density of the surrounding fluid. Buoyancy is the upward force or thrust that acts on a body by the fluid in which it is placed. It is given by the Archimedes' Principle as below Tominaga et.al. [110]:

$$F_b = -\rho g V \tag{8.1}$$

In the above equation, F_b is the buoyant force acting on the gas due to the surrounding air, ρ is the density and V is the volume of the air displaced by the gas.

Although the buoyancy and the velocity of the gas dispersed are not related, the vertical component of the velocity is responsible for creating the wake regions around obstacles. The experiments have shown that the value for the turbulent kinetic energy 'k' is different for different gases around obstacles i.e., it is negative for heavy gas, positive for neutral gas and much larger for lighter gas. This means that for the heavy gas, the wake region is much larger Tominaga et.al. [110].

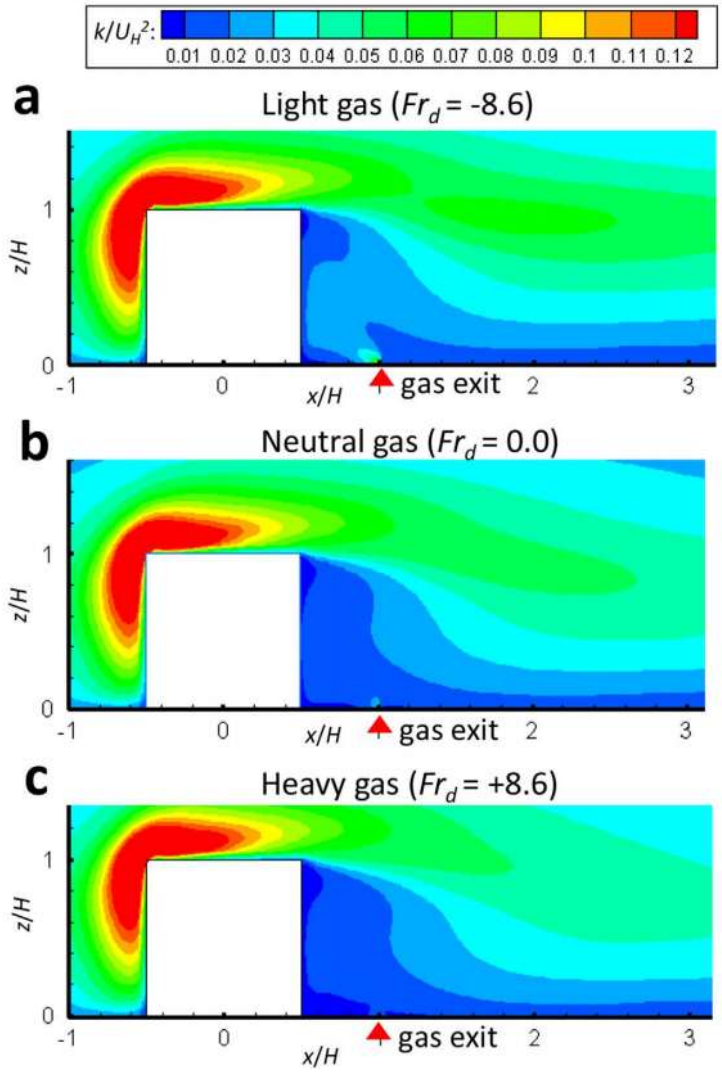

Figure 8.6: *The white region showing an obstacle that is placed in front of the gas flow. The x-axis shows the turbulent kinetic energy 'k'* ***(a)*** *Smaller wake region for the light gas* ***(b)*** *Neutral gas having much smaller wake region* ***(c)*** *Very large wake region in case of heavy gas [110]*

Figure 8.6 shows the effect of a rectangular obstacle placed in front of the heavy gas flow on the turbulence of the gas. Figure 8.6(a) shows the turbulence resulting from the light gas. It is clear that in case of light gas case, the wake region (shown in dark blue) produced is significantly less. This is because the density of the light gas is low, which in turn results in

low turbulence around the obstacle. In contrast to this, Figure 8.6(b) shows a low wake region as, in this case, neutral gas is used. Similarly, for Figure 8.6(c), in which heavy gas is used, the wake region produced is very large, owing to the large quantity of turbulence produced.

To validate the results of the case studies, the following comparison is made between the results from case studies and the experimental results of Heidorn et. al. [103]. The experiment and the numerical simulations are based upon same perimeters, with the exception that the experimental results were produced without any wind influence, while the following chosen case study was simulated at a wind speed of approximately 1m/s and a low velocity of 0.25m/s. Moreover, gas release is a continuous process in the numerical simulations but in the experimental setup, it is instantaneous. Despite the fact that these two differences are present in the numerical simulations and experimental setup, the results still show a similarity in the features, as shown in the figures below.

8.5.1 CFX comparison with FDS simulation

The following figures show the comparison between the results obtained from the CFX numerical simulation and the fire dynamics simulation (FDS) performed in the present work. Both simulations are performed for the collocated layout of buildings. Figure 8.7(a) shows the CFX simulation of concentrations, while (b) and (c) show the results of FDS simulation of concentrations of heavy gas at 0m and 0.2m over the ground respectively. This comparison will help to understand the effect of height on gas cloud dispersion. In the real world, these results will help to identify the safe floors of buildings. The inlet velocity of the gas was set at 0.25 m/s and 1 m/s at the temperature of 25°C, with the gas composition constant throughout the experiment.

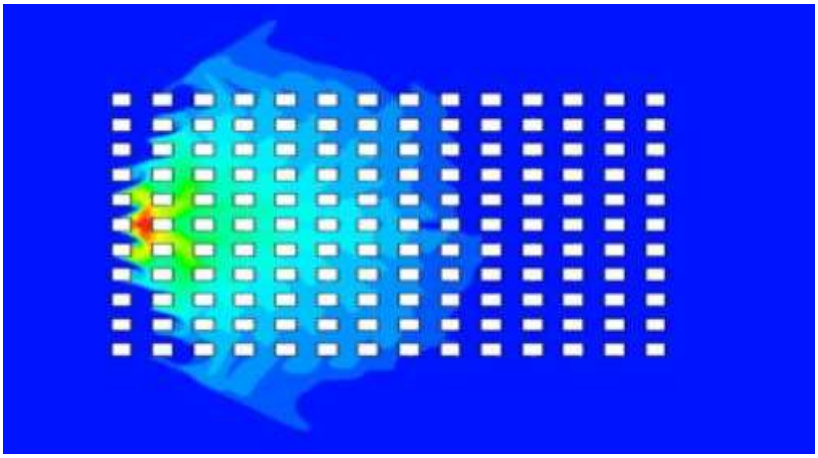

Figure 8.7(a): *CFX simulation of concentrations of heavy gas for the collocated distribution of buildings*

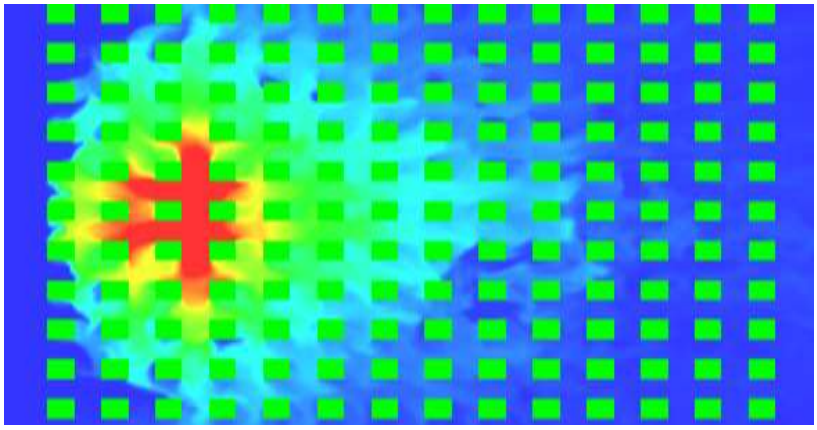

(b): *FDS simulation of concentrations of heavy gas for the collocated distribution of buildings at height = 0.0 m, on the ground*

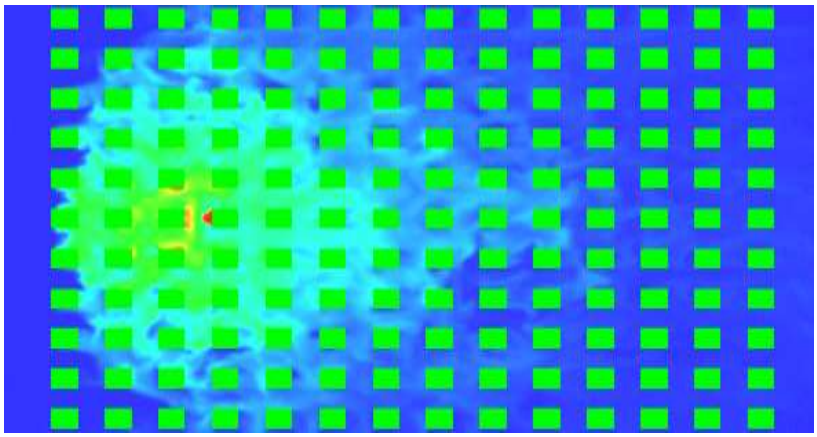

(c): *FDS simulation of concentrations of heavy gas for the collocated distribution of buildings at h = 0.2 m above the ground*

When all three figures are analysed, it is observed that a basic high concentration prismatic shaped pattern is evident in all three figures, which solves the major application of the work i.e., to identify the areas of major hazards in terms of highest concentration. The cloud shape obtained from both simulations is somewhat similar to CFX, except that it shows a greater spread of the cloud in the building layout compared to FDS. In the CFX simulation, slight edges of clouds can be seen creeping out of the building layout, while the FDS simulation reveals no such phenomenon. The phenomenon can be explained with the help of the no slip condition of the heavy gas around the obstacles and separation of the boundary layer Scargiali et. al. [24]. The heavy gas strikes the obstacles, flows around them because of the no-slip condition and becomes separated at the back, causing the generation of the wake region behind the obstacles. The concentration is symmetric in all three figures. As the only difference between (b) and (c) is that (b) is performed at 0m, while (c) is performed at 0.2m above the ground. This enables the behaviour of concentration across the height to be determined. It is observed that concentration is greater nearer the ground than at an elevated height.

The velocity of the heavy gas was set at 0.5 m/s as the gas was released at the centre of the simulation. One more small difference between CFX and FDS simulations is that the FDS simulation shows that the cloud covers more distance in the horizontal as compared to the CFX simulation.

There are many factors that influence heavy gas dispersion. These include the height of the release source from the ground, the flow rate of the gas, the position of the source in the plane and the temperature of the atmosphere and the gas Liu et. al. [111]. In this analysis, the only factor changed was the height from the ground. The first simulation was done by placing the source at the ground level and the second simulation by moving the source gas to a height of 0.2 m from the ground. It is clear from the simulation results that, for both cases, dispersion of the gas was different. The concentration of the gases is greater around the obstacles in case of a 0 m height as compared to the other case.

8.5.2 CFD comparison with experimental results

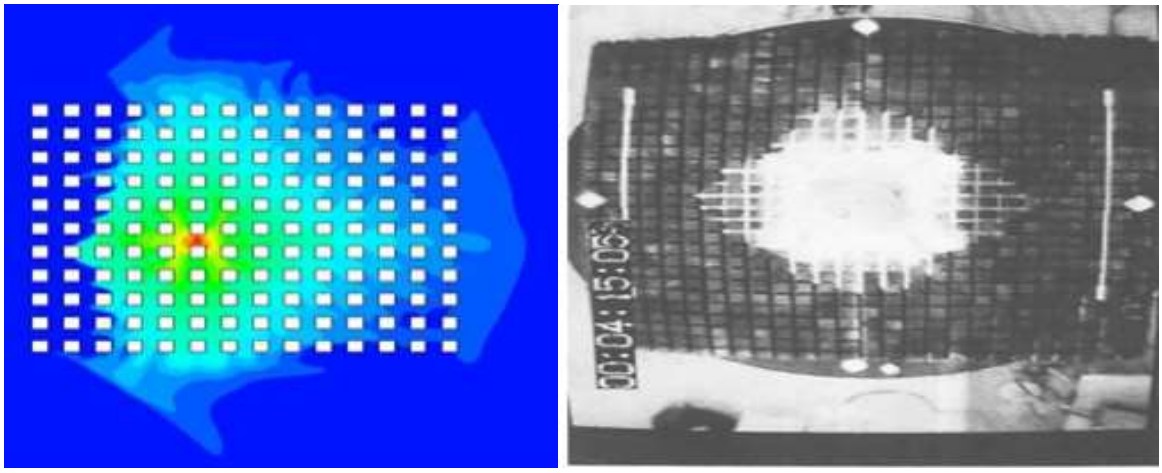

(a) (b)

Figure 8.8: (a) *Concentration of numerical simulation for collocated distribution of a building layout and* ***(b)*** *Concentration of experimental observation for collocated distribution of a building layout obtained by Heidorn et. al. [103]*

Figure 8.8(a) shows the results from the numerical simulation from one of the case studies performed in the present work. Figure 8.8(b) shows results from the experimental observation of Heidorn et. al. [103]. It can be seen noticed that, in both cases, the release source is almost at the centre of the building layout. Both sets of results show a certain similarity in terms of cloud shape, as in both cases the prismatic shape of high concentrations can be observed.

The resemblance is uncanny in the downstream part; however, the upstream part has differences. It is well known that the wind has significant effects on the upstream part of the

gas cloud. While no wind was available in the experimental set-up, a wind with a speed of 1m/s was present in the numerical simulations. It can, therefore, be argued that due to the wind acting on the upstream part of the numerical simulation, the upstream part shows a flatter cloud shape in the numerical simulations than those of the experimental set-up.

The flow of the heavy gas is also very much dependent on the wind direction. From the simulation results, it is evident that the gas cloud is flatter and thinner in the wind direction at axis x. Scargiali et. al. [24] performed a dispersion analysis on a chlorine gas cloud and obtained similar results.

In this case, the dispersion of heavy gas is very much dependent on wind velocity. In this case, wind was introduced flowing from left to right at a velocity of 0.5 m/s. The turbulence produced by the wind velocity maintained the high concentration of the heavy gas even at greater distance from the release source. The results obtained from the experiment of Heidorn et. al. [103] verify that, the greater the wind, the greater the turbulence around the obstacles. This results in the accumulation of heavy gases Pontiggia et. al. [41].

8.5.3 CFX comparison with FDS simulation

The following figure shows the comparison between the results obtained from the numerical simulation and the fire dynamics simulation (FDS) performed in the present work. Both the simulations are modelled for the collocated layout of buildings. Figure 8.9(a) shows the CFX simulation of concentrations, while 8.9(b) shows the results of FDS simulation of concentrations of the heavy gas.

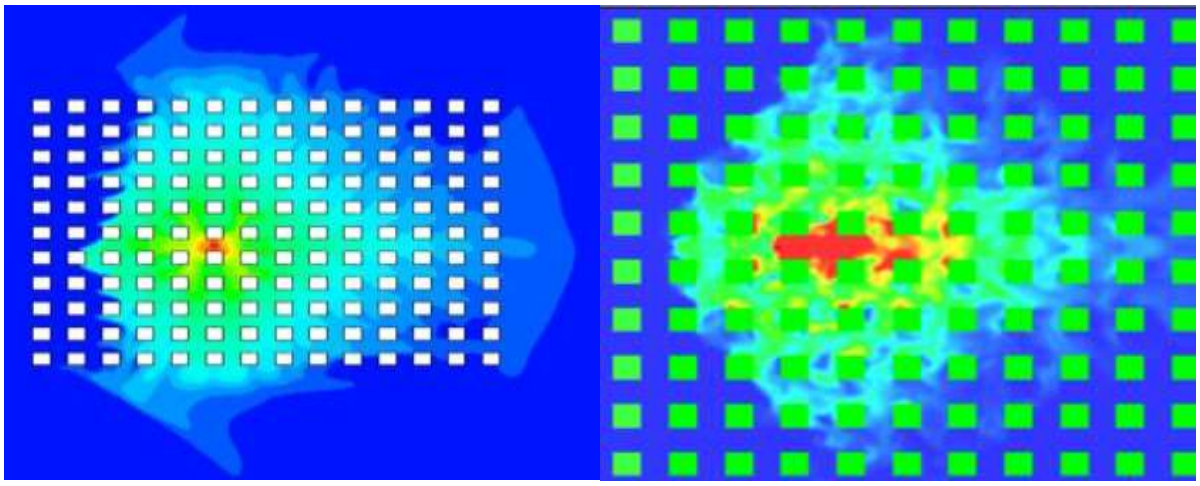

(a) (b)

Figure 8.9: (a) *CFX simulation of concentrations of the heavy gas for the collocated distribution of buildings, and* ***(b)*** *FDS simulation of concentrations of the heavy gas for the collocated distribution of buildings.*

The comparisons of both the simulations show the release source locations to be the most concentrated area. However, in CFX simulations a very small area of high concentrations can be seen occupying just one column compared to three of FDS. The prismatic high concentration pattern is also visible in this case. The spread of cloud in CFX simulation is slightly more than that of the FDS simulation. The FDS simulation appears to be related more to the experimental results of Heidorn et. al. [103] shown in the previous comparison.

In this comparison, the turbulence effect of the wind on heavy gas dispersion is analysed with the help of both CFX and FDS techniques. Both the techniques show large distances of heavy gas cloud formation that cover most of the area due to the influence of the wind velocity. FDS and CFX employs Averaged Navier-Stokes equations to calculate the effect of the wind velocity and other boundary conditions, such as temperature on the dispersion of the heavy gas Pontiggia et. al. [41].

8.5.4 CFD comparison with experimental results in a different geometry

The following figure shows a comparison between the results obtained from the numerical simulation performed in the present work and the experimental results of Heidorn et. al. [103]. Figure 8.10(a) shows the CFX simulation of concentrations, while Figure 8.10(b) shows the experimental results of concentrations of heavy gas. The reason for this comparison is to investigate the effect of structural shape on heavy gas dispersion and how the cloud forms. These results will be useful for designing building structures which cause minimal accumulation of the heavy gas leakage in the surrounding area.

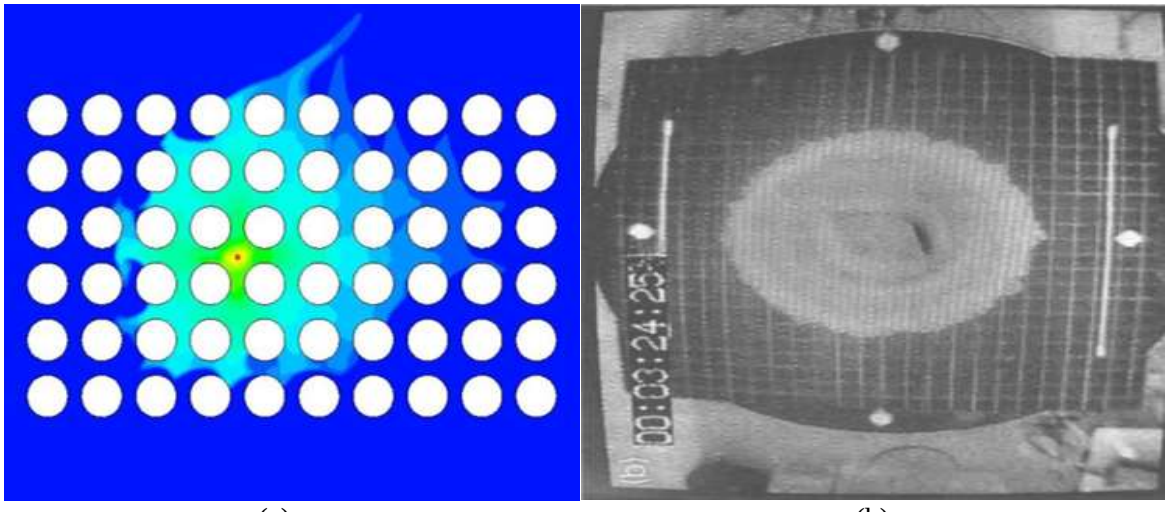

(a) (b)

Figure 8.10: (a) *Concentration of numerical simulation for a/the collocated distribution of a cylindrical building layout and* ***(b)*** *Concentration of experimental observation of Heidorn et. al. [103]*

In the case of these comparison was made for the results of the experimental observation by Heidorn et. al. [103] for the rectangular structures with the numerical simulations of the present case studies for the circular structures. A certain degree of similarity was found in the features of the cloud shape in the experimental setup and the numerical simulations. The purpose of this comparison is to understand the effect of the structural shape on the heavy gas dispersion and how the cloud forms. These results will be useful for designing building structures to cause minimal accumulation of heavy gas leakage in the surrounding area. However, one comparison is not sufficient for the validation of the numerical solutions, it will require further validate.

Figure 8.10(a) shows the results for the numerical simulation from one of the case studies performed in the work for the present study, while Figure 8.10(b) shows results from the experimental set-up of Heidorn et. al. [103]. Both figures show the same pattern for the development of the gas cloud i.e., a very uniform circular spreading pattern of the gas cloud with the radius increasing with time. It should now be noticed that the circular spread of the gas cloud in the numerical simulation is not quite symmetrical, while that the one in the experimental setup is remarkably symmetrical. Again, the reason is that the wind in the upstream region disturbs the symmetry of the gas cloud in the numerical simulations. As a result, a deviation of symmetry in the shape of the gas cloud can be seen. At the beginning of the gas dispersion, a cloud is formed and spreads out uniformly in all directions. Upstream of the cloud, wind is introduced to understand the effect of the wind on the wake region around the obstacles and to visualise the concentration of the heavy gas dispersion Atkinson et. al. [8]. It can be seen that the concentration of the gaseous cloud in the wind direction is lower, but the spread area is larger.

8.5.5 CFX comparison with FDS simulation in a different geometry

The following figures show the comparison between the results obtained from the CFX numerical simulation and fire dynamics simulation (FDS) performed in the work for the present study. Figure 8.11(a) shows the CFX simulation of concentrations, while (b) shows the results of FDS simulation of concentrations of heavy gas dispersion.

This comparison is to understand the differences between the two simulation techniques i.e., FDS and CFX. Both techniques are powerful and provide a complete, detailed understanding for the dispersion of gases. For this case, different geometries were used to add another comparison for the simulations. The reason for this comparison is to investigate the effect of structural shape on heavy gas dispersion and how the cloud forms. These results will be useful

for designing building structures which cause minimal accumulation of heavy gas leakage in the surrounding area.

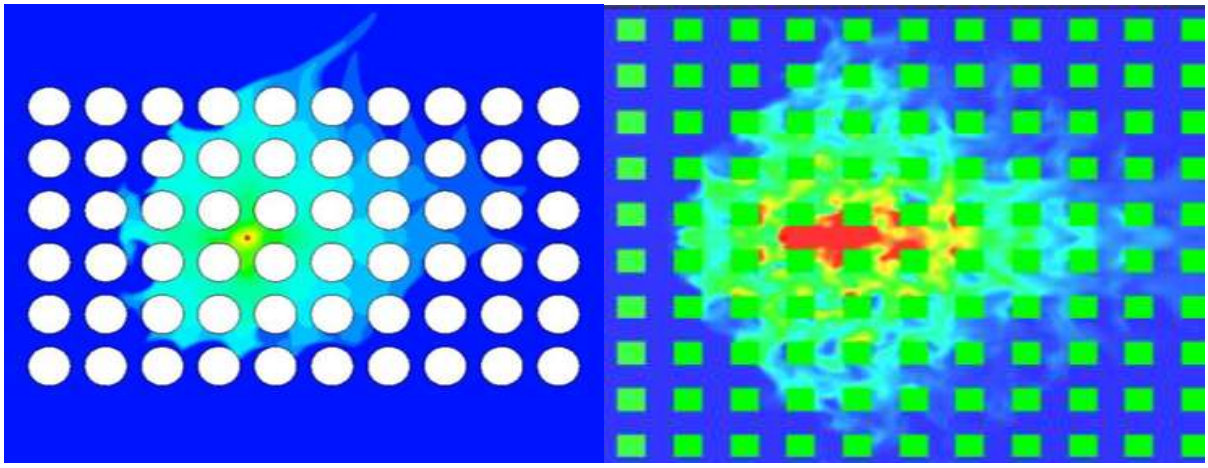

(a) (b)

Figure 8.11: (a) *CFX simulation of concentrations of the heavy gas for the collocated distribution of cylindrical building layout, and* ***(b)*** *FDS simulation of concentrations of the heavy gas for collocated distribution of buildings.*

The comparison of both the results shows an overall different picture, but there are some similarities. First of all, it should be stated that the CFX simulation is performed for the circular layout of buildings, while FDS simulation is performed for the cube-shaped building of collocated layout, so it is expected that there will be differences in the results. Nevertheless, it is noticed that the release source area is the area of maximum concentrations. The highest concentrations in CFX simulation make a circular pattern, while those of FDS make a prismatic pattern. The shape of the obstacles also affects the dispersion of the heavy gases. In this analysis, the dispersion of the heavy gas is studied for the circular and rectangular shaped buildings [103]. It is evident from the results that the turbulence of the wind around the sharp corners of the rectangular structures results in the accumulation of heavy gases [41]. This contrasts with the circular shaped structures which have laminar flow around them owing to the geometry.

This leads to the conclusion that building shape plays an important role in defining the shape of gas clouds.

8.5.6 CFD comparison with experimental results

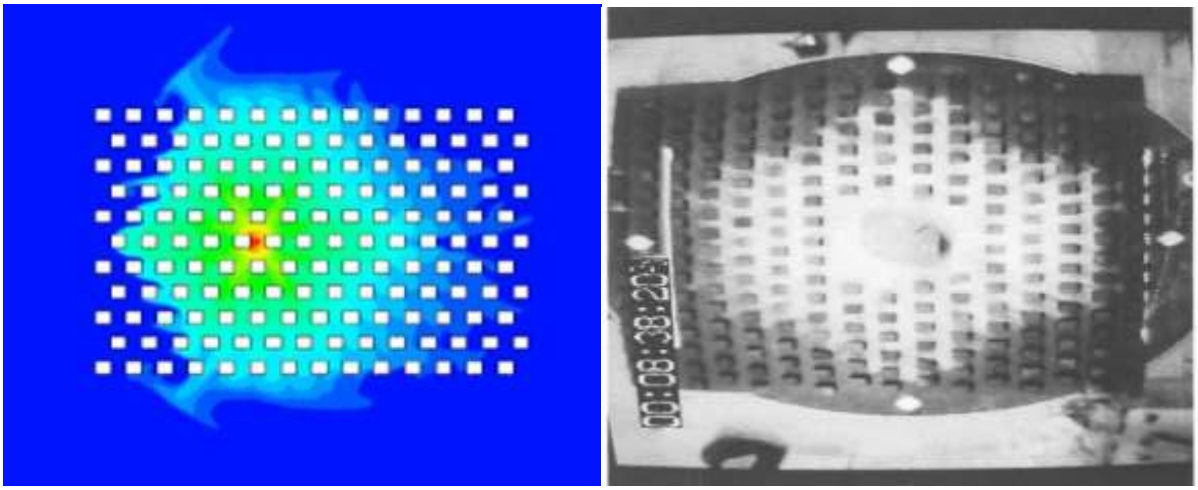

(a) (b)

Figure 8.12: (a) *Concentration of numerical simulation for a/the staggered distribution of a cylindrical building layout and* ***(b)*** *Concentration of the experimental observations from a/the staggered building layout of Heidorn et. al. [103]*

This case deals with the comparison between the results for the CFX numerical simulation and the experimental results of the staggered layout of the buildings. Figure 8.12(a) shows the results from the CFX numerical simulation from one of the case studies performed in the work for the present study, while Figure 8.12(b) shows results from the experiment carried out by Heidorn et, al. [103].

Like the collocated layout, the staggered layout simulations also produced somewhat similar results to the experimental setup. The same pattern can be seen as that followed in the previous cases i.e., the shape features truly match downstream but differ upstream due to the wind. This demonstrates that the wind plays an important role in breaking the symmetry of the cloud shape.

Moreover, the layout or the arrangement of the structures is also of great importance. For the collocated arrangements, the obstacles are placed in such a way that there is no obstacle in the middle of two obstacles [110]. This results in a smooth flow of the gas through the structures. This contrasts with the staggered arrangement in which an obstacle is placed in the middle entrance of every two obstacles. This results in accumulation and very turbulent dispersion of the heavy gas, as shown in the simulation results.

Heavy gases are characterised by high-density molecules which cannot be easily carried away by diffusion only. The change in temperature and wind velocity are the two main factors that result in the dispersion of the gas. In the case of the collocated arrangement, the wind has less resistance to flow; hence, the dispersion of the gas is high and at large distances, as is evident

from the results [41]. In case of the staggered arrangement, greater resistance is faced by the wind due to the obstacles, resulting in accumulation of the heavy gas around the buildings.

8.5.7 CFX comparison with FDS simulations

The following figures show the comparison between the results obtained from the CFX numerical simulation and FDS numerical simulation, both of which were performed in the work for the present study. Figure 8.13(a) shows the CFX simulation of concentrations, while Figure 8.13(b) shows the FDS simulation of the concentrations of the heavy gas dispersion.

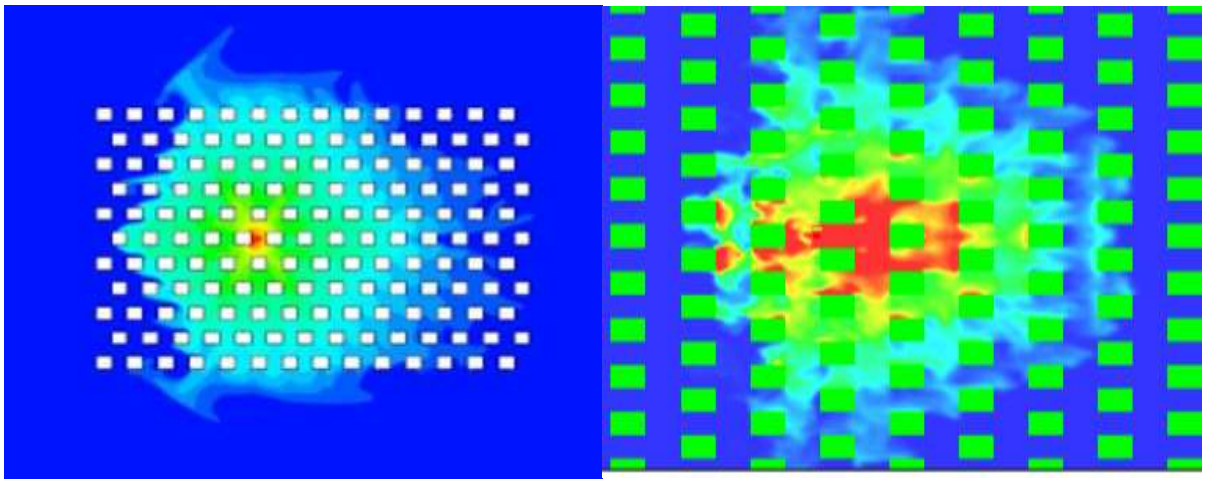

(a) (b)

Figure 8.13: (a) *CFX simulation of the concentrations of the heavy gas for the staggered distribution of buildings and* ***(b)*** *FDS simulation of the concentrations of the heavy gas for the staggered distribution of buildings*

Both the CFX numerical simulation and FDS numerical simulation were performed for the staggered layout of buildings by showing some similarities and differences at the same time; the main similarity being the typical prismatic shape of the gas clouds for cuboidal shaped buildings, and the main difference between the scale of maximum concentration areas. The maximum concentration area in FDS simulations remains within the bounds of 1 column only, but the spread reaches approximately 5 columns in the building layout. Moreover, the overall spread of the gas cloud shape in both simulations is symmetric, regardless of the zoom in at the FDS modelling results.

The effect of the wind on the dispersion in the case of the staggered arrangement of obstacles is observed in this study. As expected, the dispersion of the gases is not high because resistance to the wind flow is greater, resulting in high turbulence dissipation rate and low turbulent kinetic energy. As a result, the heavy gas accumulate around the staggered obstacles [41].

8.5.8 CFX comparison with FDS simulation in a different geometry

The following figures show the comparison between the results obtained from the CFX numerical simulation and the FDS numerical simulation performed in this study. Figure 8.14(a) shows the CFX simulation of concentrations, while Figure 8.14(b) shows the results for the FDS simulation of concentrations of heavy gas dispersion. The purpose of this comparison is to investigate the effect of structural shape on heavy gas dispersion and how the cloud forms. These results will be useful for designing building structures to cause minimal accumulation of heavy gas leakage in the surrounding area.

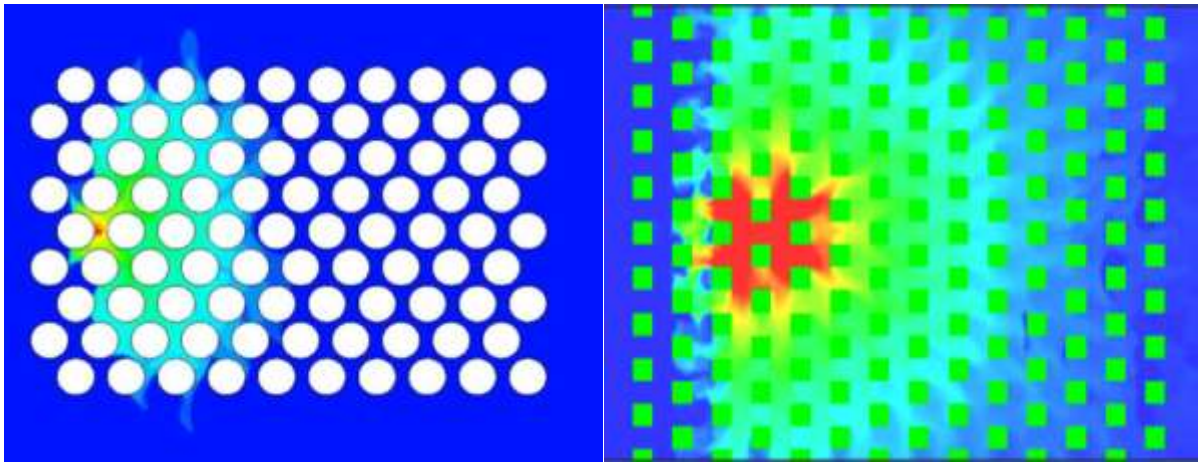

(a) *(b)*

Figure 8.14: (a) *CFX simulation of concentrations of heavy gas for the staggered distribution of cylindrical building layout and* ***(b)*** *FDS simulation of concentrations of heavy gas for the staggered distribution of buildings.*

The results obtained from these simulations show the same similarities and differences as observed in previous comparisons in terms of the spread area and the span of maximum concentrations.

In this case, the spread area in FDS simulations is significantly high as compared to the CFX simulation. When both figures are analysed closely, it can be said that, apart from the maximum concentration area part, the FDS simulation is a scaled version of CFX simulation itself. For the circular shaped and staggered arrangement, the dispersion results are different. The heavy gas has a buoyancy value which is negative. This means that the heavy gas tends to settle on the ground if there is no wind or temperature difference. In the presence of wind, the molecules of heavy gas are carried away by the wind velocity. For the circular shaped staggered arrangement, the resistance is less owing to the smooth geometry and hence the accumulation of the heavy gas is less.

8.5.9 CFX comparison with FDS simulation graphs

The previous comparisons sought to compare the results of the present study's CFX simulation with those of experimental results and other simulations such as the FDS simulations. The various different results of the comparisons have already been discussed; however, to obtain a deeper comparison, here it features a comparison of the graphical results for the concentrations across the wind direction.

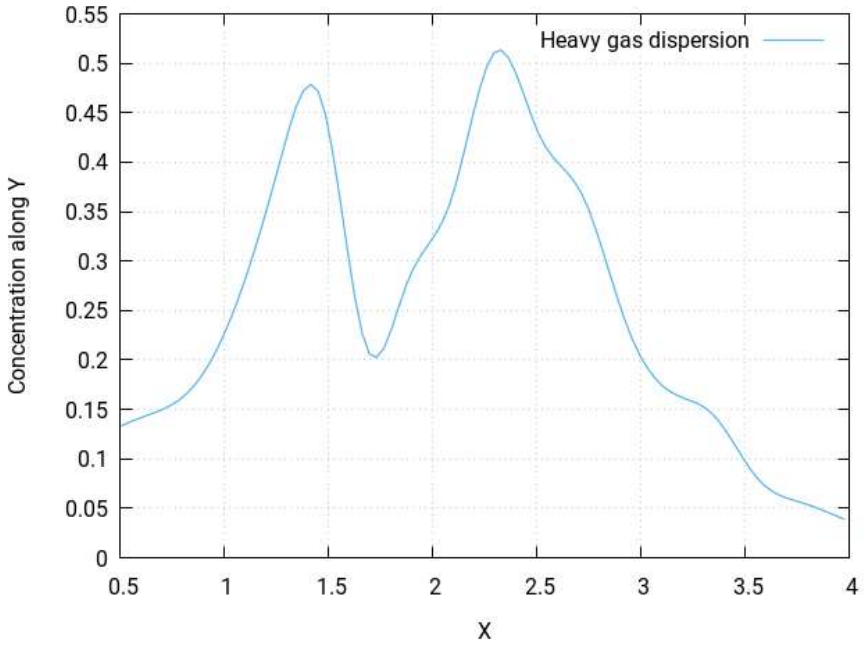

Figure 8.15: (a) *CFX simulation concentration profile of the heavy gas dispersion across the wind direction*

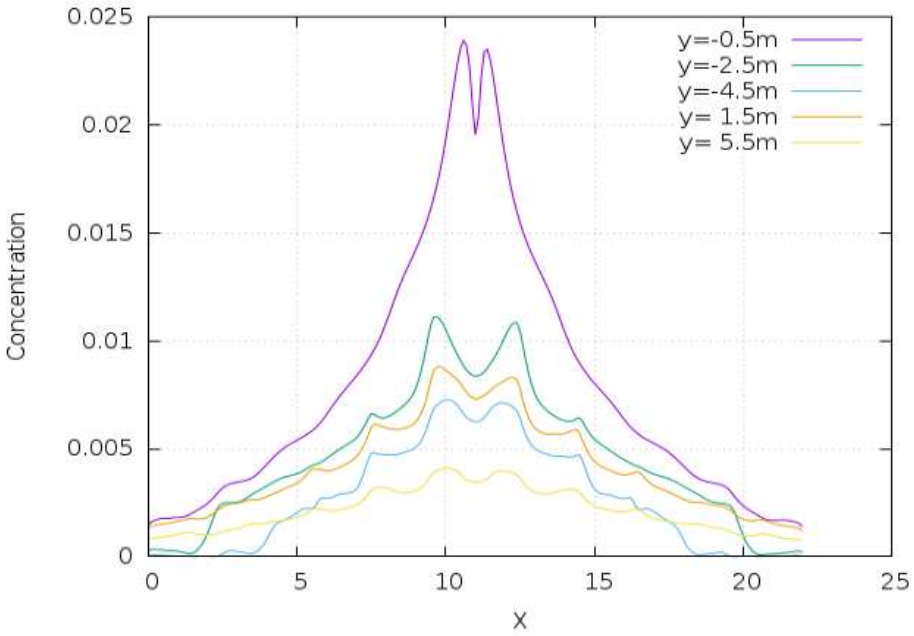

(b) *FDS simulation concentration profile of the heavy gas dispersion across the wind direction*

According to the above results, both the simulations show the same pattern for the concentration profile of heavy gas across the wind direction, as it can be seen that both Figures (a) and (b) show a pattern of double peaks. Moreover, the CFX simulation is performed for study flow but the FDS simulation is performed for unsteady flow. As a result, it can be seen that the double peak pattern at greater distances in Figure (b) is disturbed. Therefore, some extra small peaks can be seen at the distances for the curve of 1.5m and 5.5m. Moreover, it can be observed in both figures that the concentration profiles are not symmetrical. The reason for this is that the wind affects the symmetry of the profiles across the wind direction. Another important point to note is that both the graphical results obtained from the CFX and FDS simulations showed double peaks at different distances from the source gas. This shows that the heavy gas concertation is maximum at two points in the axis. This is true for all the heights. The effect of wind is that it tends to increase the length of the along its direction. As a result, the length of the cloud across the wind direction is reduced. The wind effect across the wind direction tends to disturb the symmetry. The concentration values depend upon the distance from the release source and are proved from the figure (b) that the closer the distance to the release source, the higher the concentration values.

8.5.10 A summary of all the results for the comparisons is presented

First comparison results:

Just above ground height, the concentration of the gas is maximum at the point of release source. This means that the heavy gas does not rise above the ground. At a height of 2 m above the ground, the concentration of the gas is very low as compared to that at ground level.

Second comparison results:

In this section, there is a comparison of the heavy gas dispersion for a collocated distribution of the structures with the results obtained from the similar study done by Heidorn et al. [103].

In the collocated arrangement, the concentration of the gas is greater around the buildings. The CFX numerical simulation results obtained are similar to those of the experiments carried out by the Heidorn et al. [103].

Third comparison results:

In this category, a comparison was made between different modelling techniques i.e., CFX and FDS simulations. The comparisons of both the simulations show the release source locations

to be the maximum concentrated area but in CFX simulations there is a very small area of high concentrations occupying just one compared to three columns of FDS. The prismatic high concentration pattern is also visible in this case. The spread of the cloud in the CFX simulations is a slightly more as compared to the FDS simulation.

Fourth comparison results:

This featured a comparison of the results of gas dispersion in cylindrical structure with those of Heidorn et. al. [103]. A degree of similarity was found between the features of the cloud shape in the experimental set-up and the numerical simulations.

Fifth comparison results:

For the fifth comparison, the heavy gas dispersion it was noticed that the release source area is the area of maximum concentration. Moreover, for the circular structures, the distribution is more uniform.

Sixth comparison results:

In this section, a comparison was made between the numerical simulation of the heavy gas dispersion in staggered arrangement and results were compared with a similar approach top that adapted by Heidorn et. al. [103].

The same pattern that was followed in the previous cases can be seen i.e., the shape features truly match in the downstream but differ in the upstream due to the wind.

Seventh comparison results:

In this section, a comparison was made between the FDS simulation of the heavy gas and the (You cannot use 'similar' here as you have just used the word 'comparison', making it a redundancy.)results obtained from the CFX simulation performed in our work.

Eighth comparison results:

In this section, a comparison was carried out between the CFX simulation of heavy gas dispersion in circular and staggered arrangement (if these are two different arrangements: 'rectangular and staggered arrangement'. If it is one: 'a rectangular, staggered arrangement') of structure with the FDS simulation in rectangular and staggered arrangement.

The spread area in FDS simulations is significantly higher than in the CFX simulation.

Ninth comparison results:

In this section, a graphical comparison of the heavy gas dispersion of the FDS and CFX simulations was carried out.

It can be noticed in both the figures that the concentration profiles are not symmetric. The reason for this is that the wind influences the symmetry of the profiles across the wind direction. The effect of wind is that it tends to increase the length concentration the along its direction. As a result, the length of the cloud across the wind direction is reduced. The wind effect across the wind direction tends to disturb the symmetry.

8.6 Results and discussions

8.6.1 Location 1: Heavy gas dispersion

8.6.1.1 Building layout

The type of layout adopted for this case study is a collocated layout. A layout of 154 buildings of cubic shape will be created as collocated layouts and the release source will be located in different positions. The behaviour of the heavy gas dispersion or clouds will then be studied.

8.6.1.2 Release source location

The release source location (1) of the heavy gas dispersion in this case study was at the upwind front of the group of buildings between the first and second column at the sixth row.

Table 8.7: *Parametric values for heavy gas simulation (location 1)*

Density	Flow Rate	Velocity	Ambient Temperature	Release Source Temperature
2.1 kg m/s^3	1 kg/s	1 m/s	25°C	-100°C

8.6.1.3 Concentration of the heavy gas dispersion

With the parameters described above, the simulation was performed for the concentration of the heavy gas dispersion. The results of the simulation are shown in Figure 8.16 below:

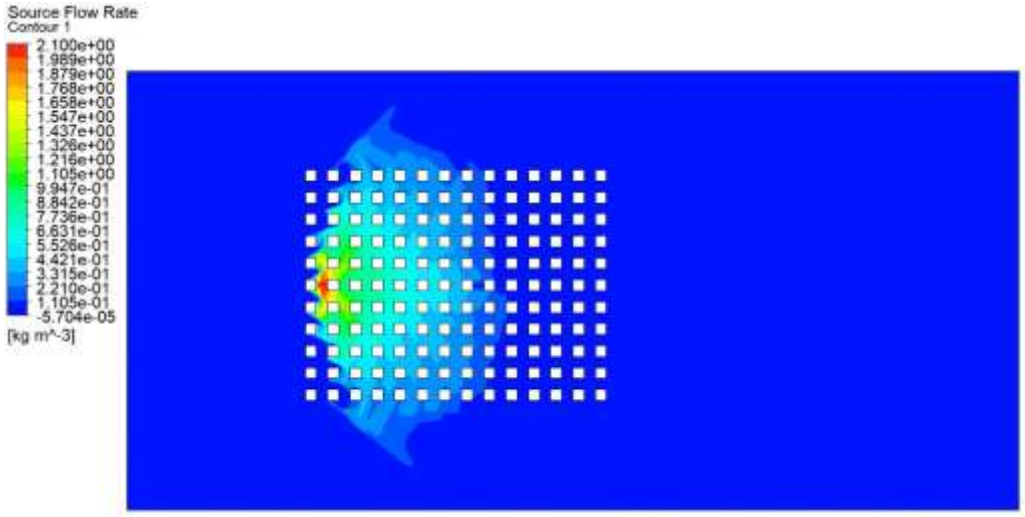

Figure 8.16: *Concentration of heavy gas dispersion for a/the collocated layout with release source located at the upwind front of the group buildings between the first and second column in the sixth row.*

Figure 8.16 shows the concentration of the heavy gas cloud when the release source is placed at the upwind front of the group of buildings between the first and second columns in the sixth row. In the figure, red represents the maximum concentration, and blue represents the minimum concentration. It can be easily noted that, under these particular conditions as those of case study 1, the shape of the gas cloud for heavy gas is largely symmetrical. Critically analysing the shape of the cloud, it can be said that the shape of the cloud resembles that of a prism. The concentrations are maximum near the release point. Thereafter, it follows a somewhat a decreasing degree of concentration as it moves away from the source.

The focus now moves to the simulation of the mean temperature of the heavy gas dispersion under the same conditions. Figure 8.17 (below) shows a picture of the simulation of the mean temperature of the heavy gas dispersion.

8.6.1.4 Temperature of the heavy gas dispersion

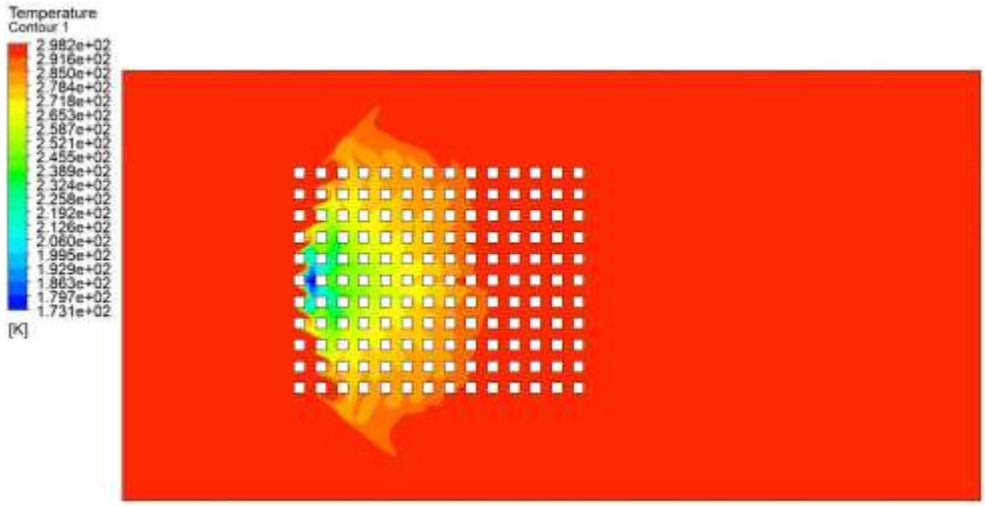

Figure 8.17: *Mean temperature of the heavy gas dispersion for a/the collocated layout with the release source located at the upwind front of the group buildings between the first and second columns in the sixth row.*

In Figure 8.17, red represents the maximum mean temperature, while blue represents the minimum temperature. It can be easily noted that, under the same parametric conditions, although the simulation of mean temperature shows similarity in terms of cloud shape to that of gas concentrations, the effect is actually the opposite. Unlike the case of the gas concentrations, the mean temperature is lowest nearer the source and continues increasing as it moves away from the source, until it approaches the maximum ambient temperature of the environment. Similar to the gas concentrations, critically analysing the shape of the cloud, it can be said that the shape of the cloud resembles that of a prism.

8.6.1.5 Iso-surface of the heavy gas dispersion

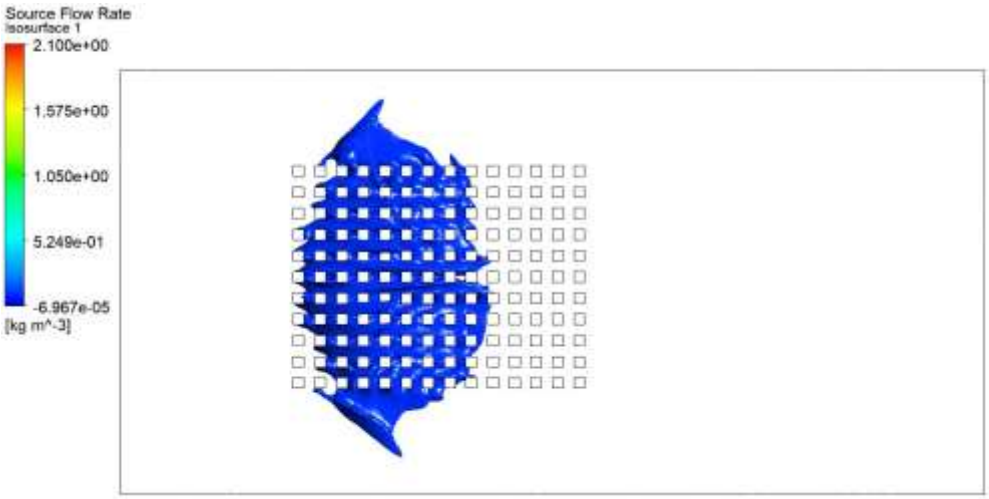

Figure 8.18: *Top view of the mean concentration of the heavy gas dispersion for collocated layout with release source located at upwind front of the building group between the first and second column at the sixth row. Green is the highest concentrations, sky-blue a slightly less and blue the least concentrated space.*

Figure 8.18 presents the top view of the mean concentration of the gas cloud. It can be seen in this figure that the gas cloud tends to move more along the x-direction and then takes a very symmetric shape with a uniformly spread behaviour the gas cloud tends to move more along the x-direction and then takes a very symmetric shape with a uniformly spread behaviour approximately more than the half of the buildings. The gas cloud tends to take an almost rectangular shape within the buildings with an edge creeping out along the z-axis in both directions. This was already shown in Figure 8.16.

The blue in Figure 8.18 represents the points of low concentration. This result is consistent with that of Figure 8.16, which means that Figure 8.18 further supports he findings of Figure 8.16. If the entire cloud were to resemble in the form of shape names, Figure 8.16 would be perfect to describe them and it could be said say that the cloud is of a rectangular shape in the centre with slight edges creeping in the z-direction at both ends, with the highest concentrations being in the form of a prism.

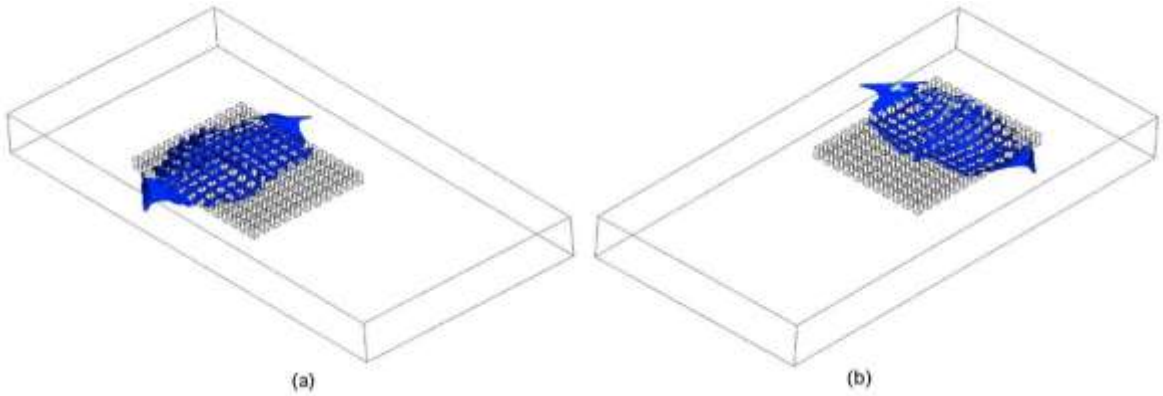

Figure 8.19: *Side and back view of the mean concentration of the heavy gas dispersion for a/the collocated layout with the release source located at the upwind front of the group buildings between the first and second column in the sixth row*

Figure 8.19 is the side and back view of the mean concentration of the gas cloud. It is added here simply to give a dynamic point of view for the analysis of cloud shape. The results obtained from Figures 8.16 and 8.19 are the same as can be in this figure. Although at first, both the figures appear to be identical in shape, with the only difference being in the angle, there is a certain significance to this. Figure 8.19(a) helps to determine the behaviour of gas cloud aloud along the axis y direction. Although Figure 8.19(a) very precisely determines the shape of the cloud along the axis x and axis z direction, the determination of the cloud along the axis y direction is difficult to ascertain from it. Figure 8.19(b) clearly shows the spread of the cloud in the y-direction. After critically analysing Figure 8.19(b) it can now be seen that

the creeping edge along the z-direction as discussed above is nearer to the ground. The places of higher concentration (the prism) tend to be upwards along the y-direction.

Temperature is a particularly important factor and is responsible for the dispersion of the heavy gases. If all the factors; height, flow rate, release velocity and location are kept constant, the dispersion of the heavy gas is dependent on the turbulence of the wind, the temperature difference of the gas and the atmosphere, which produces the buoyancy effect [111]. The wind in the atmosphere creates a turbulent pattern that carries the heavy gas particles. The difference in the temperatures of the gas and atmosphere creates a density difference; the gas which has high temperature has lower density and rises. In this way, the temperature and turbulence of the wind is responsible for the dispersion of the gases [111].

According to Standard BS EN 60079-10-1:2009 Santon el. al. [104], the following locations can be categorised:

Zone 0: All the buildings from the 2nd to 5th rows in the building layout
Zone 1: The buildings from the fifth row up to middle front
Zone 2: All the remaining locations not categorised in zone 0 or zone 1

8.6.1.6 Velocity of the heavy gas dispersion

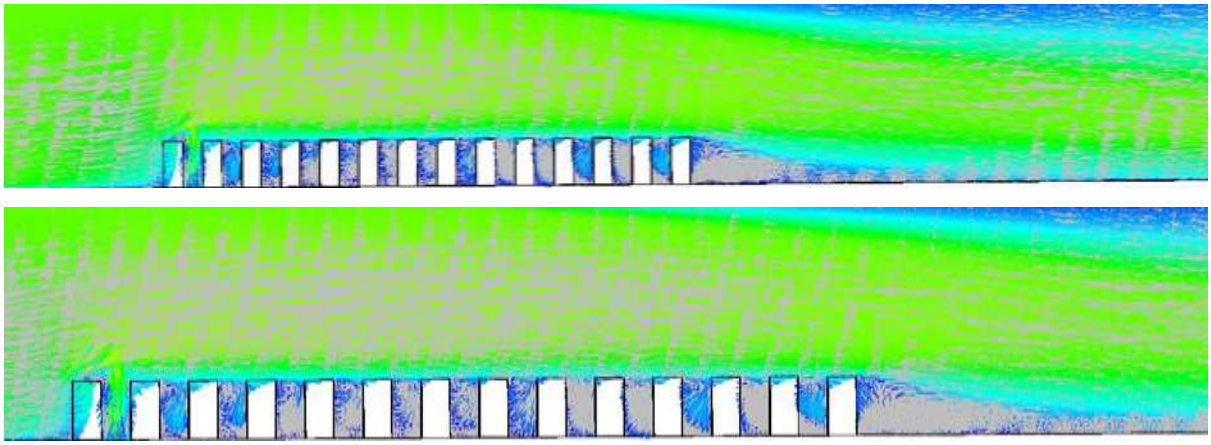

Figure 8.20: *Velocity vectors (Line arrow) of the heavy gas dispersion for a/the collocated layout with the release source located at the upwind front of the group of buildings between the first and second columns in the sixth row. Green is the highest velocity, sky-blue slightly lower and blue the lowest velocity.*

Figure 8.20 shows the velocity vectors simulation for this case study with zoomed in and zoomed out views. It can be seen in the figure that the velocity above the ground is significantly higher. This was expected because higher winds tend to be found at higher altitudes. At the ground level, the layout of the building causes hindrance in the flow of the wind, which causes

a slight blockage of wind. For this reason, the gas when released from the source tends to move more in the vertical y-direction.

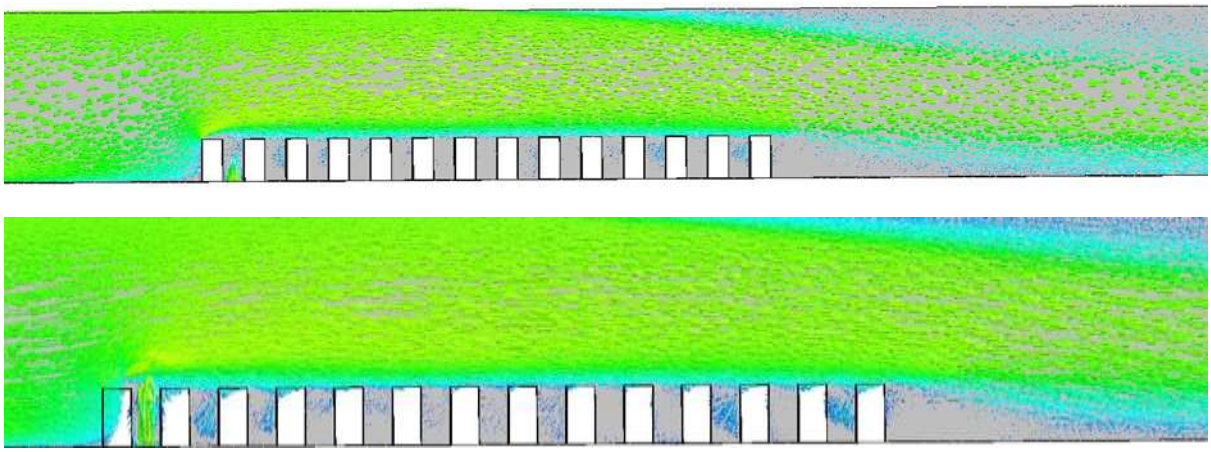

Figure 8.21: *Velocity vectors (Arrowhead3D view) of the heavy gas dispersion for a/the collocated layout with the release source located at the upwind front of the group of buildings between the first and second columns in the sixth row. Green is the highest velocity, sky-blue slightly lower and blue the lowest velocity.*

Figure 8.21 features the zoomed in and zoomed out the representations of the same simulation from another view i.e., the Arrowhead3D view. The simulation shows the same behaviour as that of Figure 8.20, with the exception that, in this figure, the highest intensity can be seen near the gas release source location.

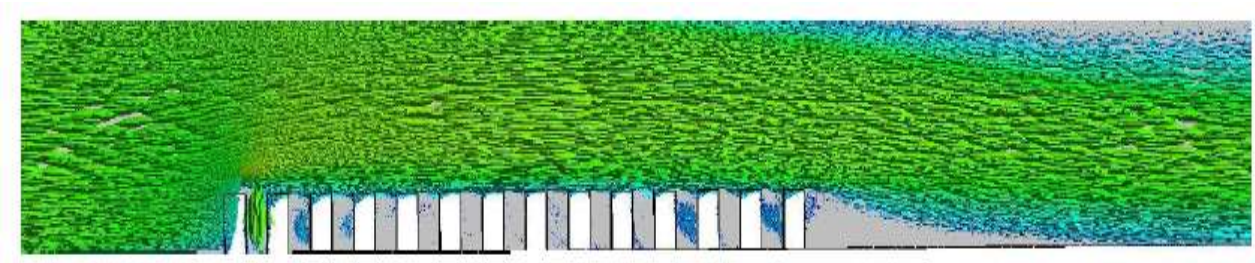

Figure 8.22: *Velocity vectors (Fish 3D view) of the heavy gas dispersion for a/the collocated layout with the release source located at the upwind front of the group of buildings between the first and second column at the sixth row. Green is the highest velocity, sky-blue slightly lower and blue the lowest velocity.*

Again, another form of representation of the velocity vectors was selected; this time, the Fish3D view. The same behaviour as observed in the previous figures is also found here. Although, the Fish3D view does not show any changes in the behaviour, it does present an aesthetically better representation of the same behaviour.

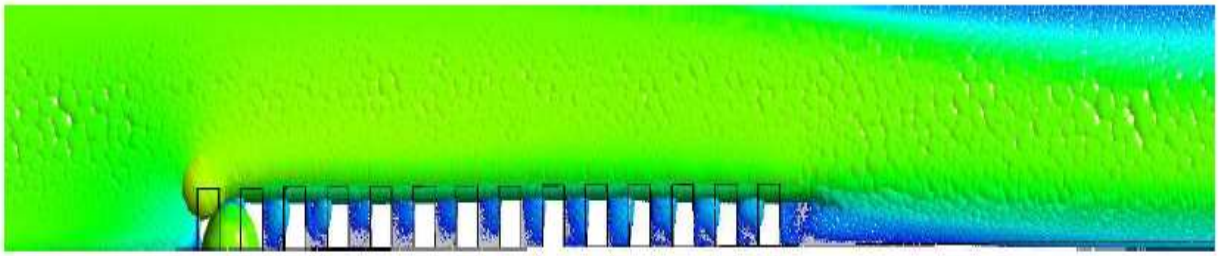

Figure 8.23: *Velocity vectors (Ball view) of the heavy gas dispersion for collocated layout with release source located at upwind front of the group of buildings between the first and second column in the sixth row. Green is the highest velocity, sky-blue a slightly lower and blue the lowest velocity.*

The final figure for the representation of the results for this case study is unique as the gas cloud can now be seen forming near the release source location. The hindrance resulting from the buildings in the flow of the wind causes the gases to flow over the ground with more intensity, as seen in (Figure 8.23). The heavy gas released from the source causes these results in an enhanced concentration of the gas cloud in the upward direction near the release source, which mixes with the nearby cloud. This ultimately results in the formation of a hazardous zone, which can cause an explosion if subjected to a high-temperature source.

8.6.1.7 Graphical representation

The results for the dispersion for heavy gas have already been analysed with the help of the figures of the simulations performed. Nevertheless, representing the results with the help of graphs is always helpful as it gives a clear picture of the behaviour of the perimeters. With the help of graphs, this section seeks to determine the behaviour of various perimeters, such as concentration, temperature and velocity of the heavy gas dispersion, when released from a certain source. The values of the perimeters have already been mentioned in the case studies. Therefore, the graphs generated for the data can now be examined.

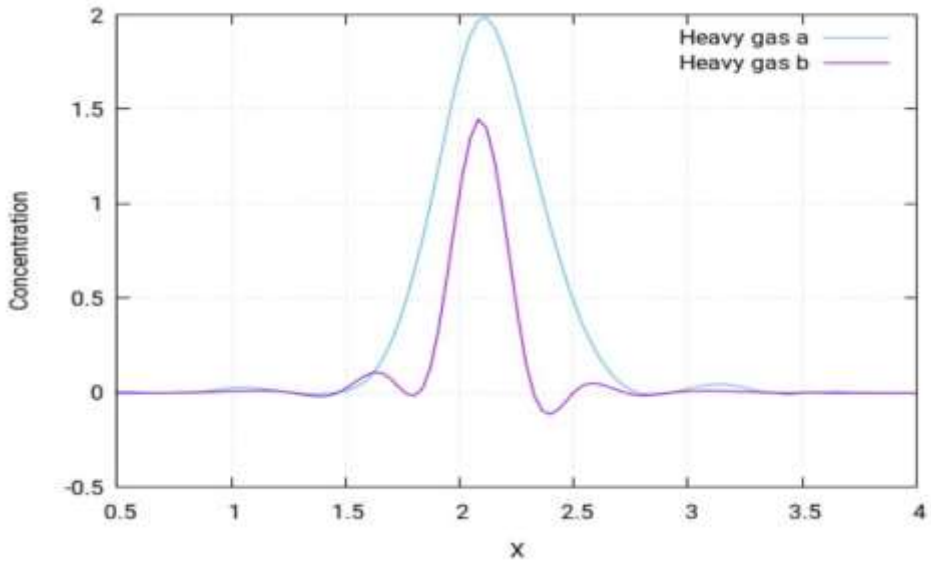

Figure 8.24: *Graphical representation of the concentration of the heavy gas dispersion profile along the y-direction at different points of (a) x=1.75m, y=-1m, z=7.20m (b)x=1.75m, y=-1m, and z=9.84*

Figure 8.24 compares the results of the heavy gas concentration simulation at two different locations. The blue curve shows the results of the concentration of heavy gas at a location of 7.20m in the z-direction, while the purple is for the location of z at 9.84m. The concentration profile in both cases follows the same trend. The only difference is that the concentration peak in case a is higher than that in case b. This simply means that the concentrations of the heavy gas cloud are largely the same near the edges, but that the most concentrated region of the concentrations (high concentrations) will be nearer towards the source, as 7.20m location is closer to the source than the 9.84m one.

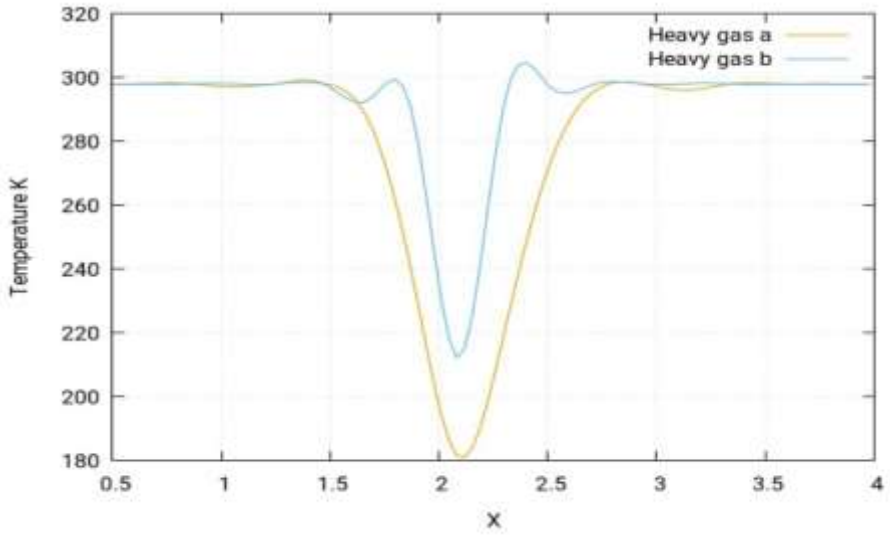

Figure 8.25: *Graphical representation of the temperature of the heavy gas dispersion profile along the y-direction at different points of (a) x=1.75m, y=-1m, z=7.20m (b)x=1.75m, y=-1m and z=9.84*

Figure 8.25 compares the results of the heavy gas temperature simulation at two different locations. The blue curve shows the results of the temperature simulation of the heavy gas at a location of 7.20m in the z-direction, while the orange is for the location of z at 9.84m. The figure shows that the temperature profile in both cases follows the same trend, with the difference being that temperature in case b approaches a lower value than that of case a. When both the concentration and temperature profile of Figure 8.24 and Figure 8.25 are compared, it can be seen that both profiles are a mirror of each other.

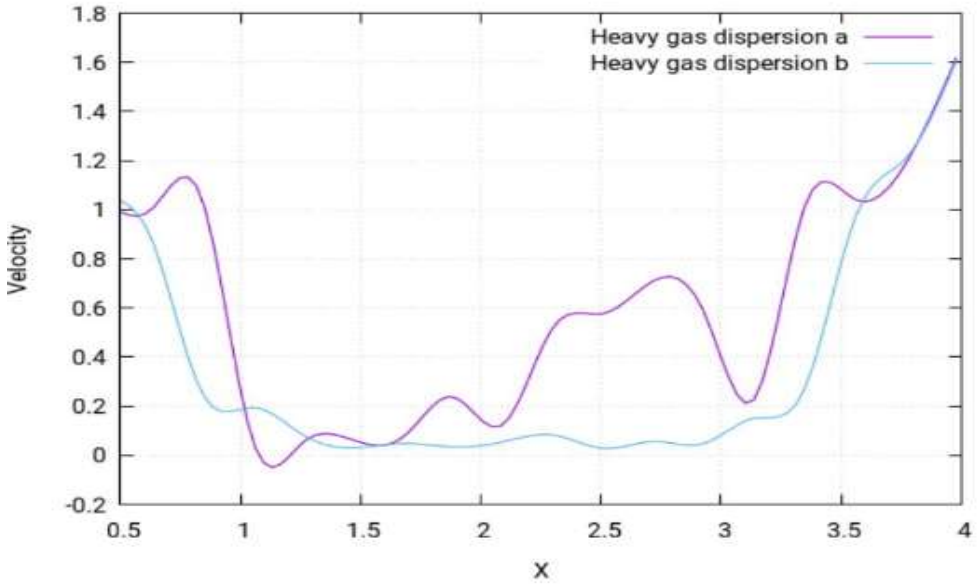

Figure 8.26: *Graphical representation of the velocity of the heavy gas dispersion profile along the y-direction at different points of (a)x=1.75m, y=-1m, z=7.20m (b)x=1.75m, y=-1m and z=9.84*

Figure 8.26 compares the results of the heavy gas velocity simulation at two different locations. The purple curve shows the results for the velocity simulation of the heavy gas at a location of 7.20m in the z-direction, while the blue is for the location of z at 9.84m. It is noticed that the velocity profile in both cases follows a very irregular pattern of behaviour. The velocity is quite different throughout the layout, which is what causes this difference. If the purple curve is observed for 7.20m in the z-direction, it is noticed that the velocity first increases, then sees a rapid decrease. After fluctuating behaviour for some time, it sees another sizeable decrease, after which it rises steadily. On the other hand, the blue curve for 6.84m in the z-direction shows that the velocity first rapidly decreases and then sees a rapid increase in the profile. Thus, the velocity profile for 9.84m is more stable than for the 7.20m. This could mean that, at the 7.20m location, more turbulence occurs than at the 9.84m location.

8.6.1.8 Summary of results for case study (1)

The simulations for heavy gas (density = 2.1kg m/s^3) cloud dispersion in the collocated layouts, when subjected to a wind speed of 1m/s with the release source located at the upwind front of the group of buildings between the first and second column in the sixth row, show that the concentrations are greater near the gas release source and tend to move more along the wind direction and also in the upward direction and high concentration cloud (hazardous area) is in the form takes the form of a prism for these particular conditions. However, the temperature is lower near the source and increases as it moved away from the source.

The behaviour of the gas cloud dispersion in spreading uniformly can be explained in terms of gas buoyancy and density of both the gas and the atmosphere. The buoyancy of the gas is dependent on various factors, such as concentration, volume and temperature [110]. The greater the volume occupied by the gas, the larger the buoyant force, which causes the gas to rise upward. Hence, as the gas is released, it spreads uniformly in the x-direction and as it occupies greater volume. The buoyant force increases and causes the gas to rise upward in the z-direction. This results in the formation of a peculiar cloud shape which is very much dependent on density and temperature [110].

8.6.2 Location 1: Heavy gas dispersion at low velocity

This case study will be performed with different perimeters so that the difference in the cloud shape can be analysed and compared with the previous case study (case study1) to determine how different perimeters effect the cloud shape. The selected perimeters for this case study given below.

8.6.2.1 Building layout

The type of layout adopted for this case study is also a/the collocated layout. A layout of 154 buildings of cubic shape as collocated layouts was created and the release source was placed in the same position as in (case study1).

8.6.2.2 Release source location

The release source location (1) of the heavy gas dispersion in this case study was also the same as that in case study 1 i.e., at the upwind front of the group of buildings between the first and second column in the sixth row.

Table 8.8: *Parametric values of the heavy gas simulation (location 1)*

Density	Flow Rate	Velocity	Ambient Temperature	Release Source Temperature
2.1 kg m/s^3	5 kg/s	0.25 m/s	25°C	-100°C

A comparison of the perimeters of both case studies reveals that all the perimeters are the same except the flow rate and the inlet velocity of the wind. The inlet velocity in the previous case study was 1m/s and the flow rate was 1kg/s; however, in this case study, the velocity is 0.25m/s and the flow rate is 5kg/s.

Now that the difference in the perimeters has been stated, the behaviour of the cloud will be analysed.

8.6.2.3 Concentration of the heavy gas dispersion at low velocity

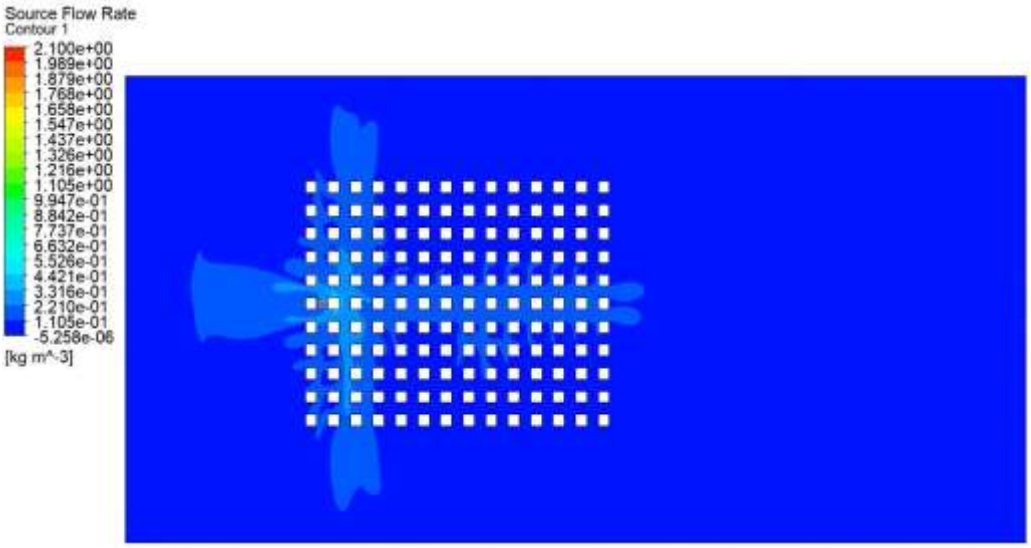

Figure 8.27: *Concentration profile of the heavy gas dispersion for a/the collocated layout with the release source located at the upwind front of the group of buildings between the first and second columns in the sixth row at* ***0.25m/s***

Figure 8.27 shows the concentration of the heavy gas cloud with 0.25m/s inlet velocity and 5kg/s flow rate. It can be seen that the shape of the gas cloud is different to that in (case study1). The gas cloud travelled more in the horizontal x-direction and the width of the cloud is less than that of the previous case. Moreover, since the inlet velocity is 4 times less in this case, the cloud also managed to travel in the direction against the wind because the reduced wind is not affecting the spread of the cloud now. The shape of the cloud resembles a sleeve and a caudal fin on a fish. At this point, it can be said that the concentration is more in the x-direction. However, more views of the simulation could help define the concentration better.

8.6.2.4 Temperature of the heavy gas dispersion at low velocity

Figure 8.28: *Mean temperature of the heavy gas dispersion for a/the collocated layout with the release source located at the upwind front of the group of buildings between the first and second columns in the sixth row at* ***0.25m/s***

Figure 8.28 shows the temperature profile for the heavy gas cloud with 0.25m/s inlet velocity flow rate. The shape of the gas cloud is different to that in case study 1. The shape of the temperature profile is similar to that of the concentration profile, but the trend of the temperature is same as that in case study 1 i.e., it is minimum near the release source location and tends to decrease as it moves away from the source.

8.6.2.5 Iso-surface of the heavy gas dispersion at low velocity

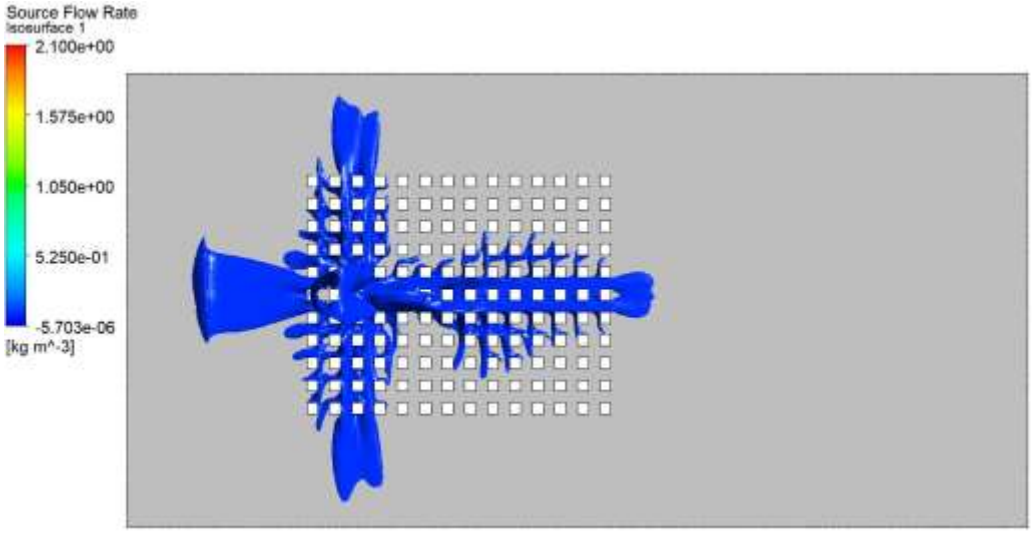

Figure 8.29: *Top view/horizontal cross-section of the cloud shape for the concentration of the heavy gas dispersion for a/the collocated layout with the release source located at the upwind front of the group of buildings between the first and second columns in the sixth row.*

Figure 8.29 shows the top view of the cloud shape for the concentration of the heavy gas dispersion for a collocated layout with the release source located at the upwind front of the

group of buildings between the first and second column in the sixth row at 0.25m/s and 5m/s. It shows us that the gas cloud is intensely concentrated near the gas release source and clouds the two entire rows in both directions, while trying to creep away from the same buildings and enlarging is spread in the nearby environment. It also shows that the gas cloud moves centrally along the x-direction, covering three columns entirely and two columns partially. The cloud also manages to travel in the direction against the wind because the reduction in wind does not affect the spread of the cloud, as is evident through this figure.

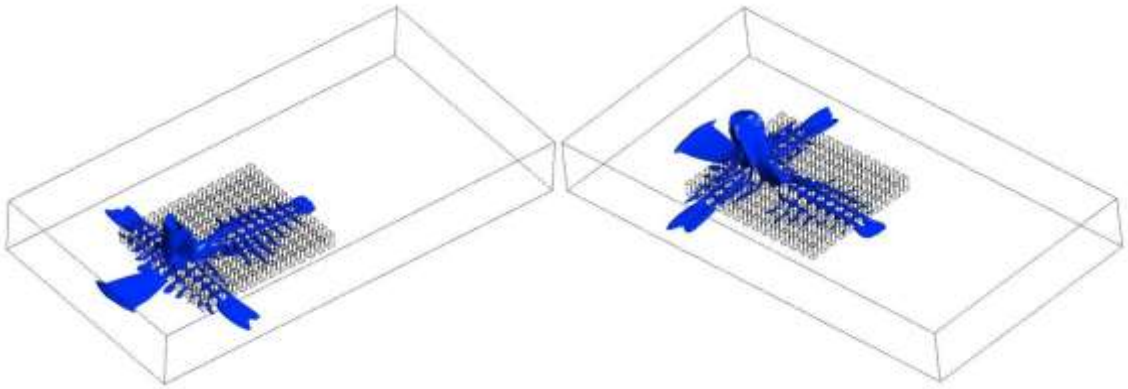

(a) (b)

Figure 8.30: *Side and back view of the cloud shape for the concentration of the heavy gas dispersion for a/the collocated layout with the release source located at the upwind front of the group of buildings between the first and second columns in the sixth row.*

Figure 8.30 is an isometric representation of the concentration of the gas cloud at 0.25m/s. It shows us that, under these conditions, the gas cloud is highly concentrated near the release source location in the upward direction and resembles that of a bowtie, while a good part of the gas cloud also travels in the opposite x-direction and resembles to that of a baseball bat handle. Figure 8.30(b) is the rotated view of the previous figure (8.30(a)). The previous figure helped determine a great deal about the concentration of the gas cloud, but the spread of cloud in the vertical direction is determined by this figure (8.30(b)). It demonstrates that the concentrations of cloud in the building layout are somewhat uniformly spread out in the vertical direction, but that the part of the cloud which creeps out of the building layout in both directions tends to be nearer to the ground. Meanwhile, the heavy gas cloud near the gas release source travels a great deal more in the vertical direction as compared to other directions.

According to Standard BS EN 60079-10-1:2009 [104], the following locations can be categorised:

Zone 0: The central surrounding the area up to 2 rows on each side and the negative x-direction and vertical y-direction

Zone 1: The central 3 columns and the sideways of the 2 rows each side of release source rows

Zone 2: All the remaining locations not categorised in zone 0 or zone 1

8.6.2.6 Low velocity of the heavy gas dispersion

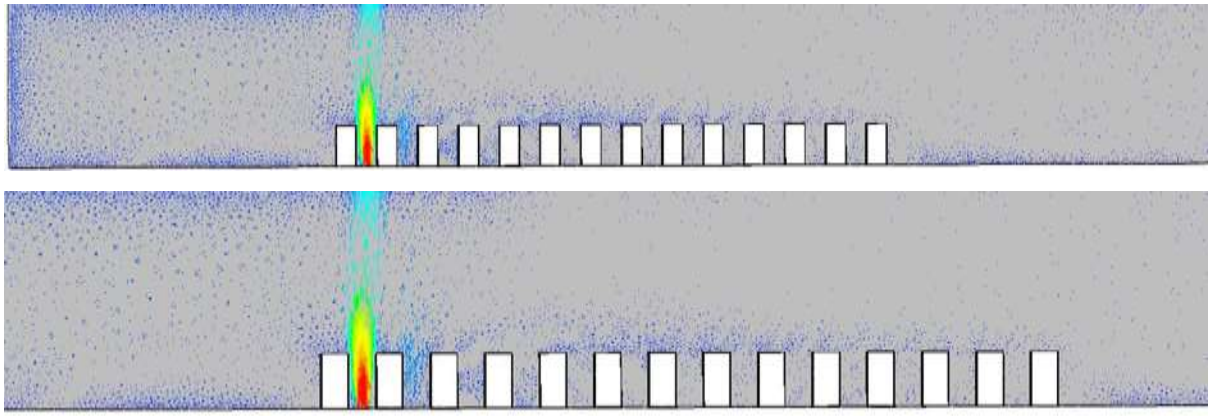

Figure 8.31: *Velocity vectors of the mean concentration of the heavy gas dispersion for a/the collocated layout with release source located at the upwind front of the group of buildings between the first and second columns in the sixth row at* ***0.25m/s****. Red is the highest velocity and blue is the lowest velocity.*

Figure 8.31 is the representation of velocity vectors of the mean concentration of the heavy gas dispersion for collocated layout with the release source located at the upwind front of the group of buildings between the first and second column in the sixth row at 0.25m/s. These results differ to those of (case study1) as, in this case study, various complex vertexes are formed within the buildings near the release source. The heavy gas release from the source is carried by these vertexes to the nearby mixture of the gas cloud, which then moves smoothly away from the source. Moreover, the hindrance in the wind flow caused by the buildings results in the vertexes moving in the upward direction, which enhances the shape of the cloud in the upward direction.

8.6.2.7 Summary of results for case study (2)

This case study shows that, for increase flow rate and reduced speed, the shape of the cloud is more spread along the horizontal x-direction and that the symmetrically is in the z-direction. The reduced wind speed allows the cloud to spread in the negative x-direction. The overall cloud resembles a sleeve with tiny fin-shaped clouds creeping towards the side, while a small portion spread in the negative x-direction takes the shape of the handle of a baseball bat.

In this case, the heavy gas is released at the low velocity and at low temperature. Since the gas is heavy and the velocity is low, it would theoretically not have dispersed; however, the delta between the temperatures of the heavy gas and atmosphere is very high i.e., 125 °. This results

in a density difference and, as a result of buoyancy, the heavy gas is dispersed in all directions, as shown in the simulation results above.

8.6.3 Location 1: Neutral gas dispersion

8.6.3.1 Building layout

The type of layout adopted for this case study is the collocated layout. A layout of 154 buildings of cubic shape as collocated layouts will create and the release source will be put in different positions, then the behaviour of the gas clouds will be studied.

8.6.3.2 Release source location

The release source location (1) of the neutral gas dispersion in this case study was at the upwind front of the group of building between the first and second columns in the sixth row.

Table 8.9: *Parametric values of the neutral gas simulation (location 1)*

Density	Flow Rate	Velocity	Ambient Temperature	Release Source Temperature
1.1839 kg m/s^3	1.7737 kg/s	1 m/s	25°C	25°C

8.6.3.3 Concentration of the neutral gas dispersion

With the parameters described above, the simulation was performed for the concentration of the neutral gas dispersion. The results of the simulation have been shown in the following (Figure 8.32).

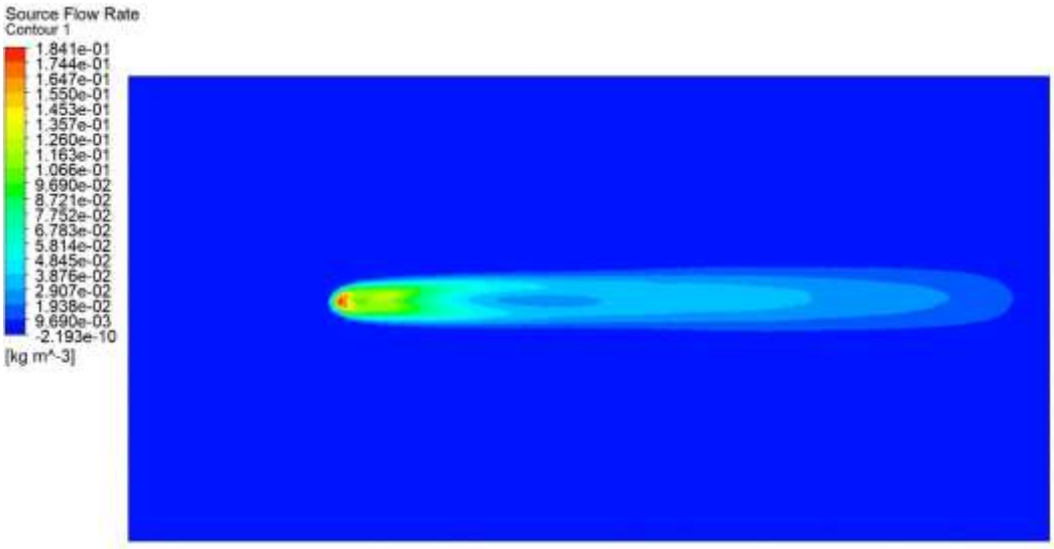

Figure 8.32: *Concentration profile of the neutral gas dispersion for a/the collocated layout with the release source located at the upwind front of the group of building between the first and second columns in the sixth row at* ***0.25 m/s***

Figure 8.32 shows the concentration of neutral gas cloud when the release source is placed at the upwind front of the group of buildings between the first and second columns in the sixth row. In the figure, red represents the highest concentration, while blue represents the lowest concentration. It can be clearly seen that, under these particular conditions, the shape of the neutral gas cloud resembles an elliptical cylinder.

The planar distance is increased from the ground to reveal the shape of the neutral gas cloud as the neutral gas cloud spreads in the upward direction, unlike the heavy gas dispersion and neutral gas shape is one peak or single bubble.

However, there is a similarity in the trend as the concentrations are highest near the release point and then follow a decreasing degree of concentration as the cloud moves away from the source. The shape of the cloud is entirely different in this case and hence the distribution of the gas cloud.

8.6.3.4 Iso-surface of the neutral gas dispersion

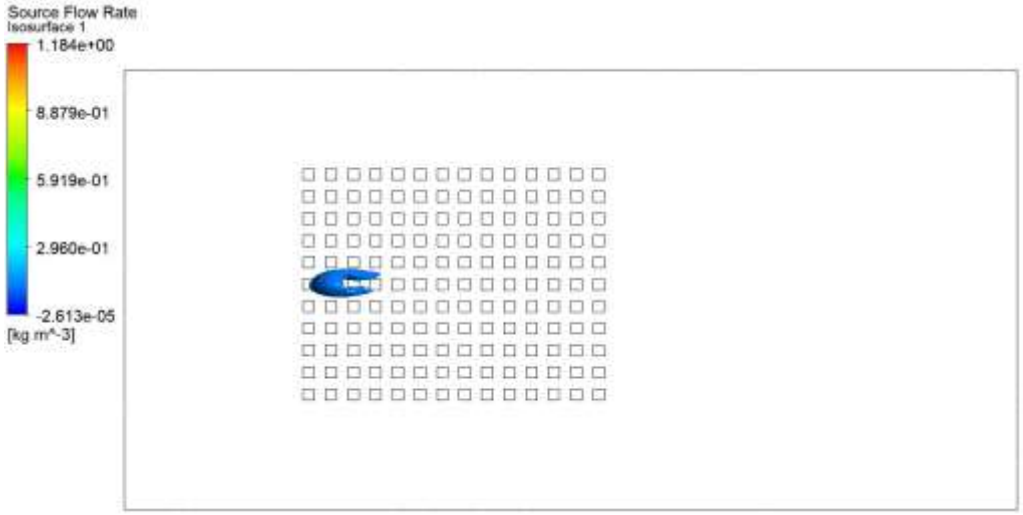

Figure 8.33: *Top view of the concentration profile of the neutral gas dispersion for a/the collocated layout with the release source located at the upwind front of the group of buildings between the first and second columns in the sixth row at* ***1 m/s***

Figure 8.33 features a representation of the mean concentration of the neutral gas cloud in the form of a/the horizontal cross-section/top view. It reflects the behaviour of the cloud along the x and z-directions. In the figure, the gas cloud tends to move more along the x-direction and takes a very concentrated near the gas release source. The concentration distributes uniformly initially but then distributes into two portions from the centre, resembling that of the flukes of a dolphin. As compared to the heavy gas cloud, the neutral gas cloud looks very small. Similar to the heavy cloud case i.e., case study 1, the cloud does not travel in the opposite x-direction due to the wind coming from that direction.

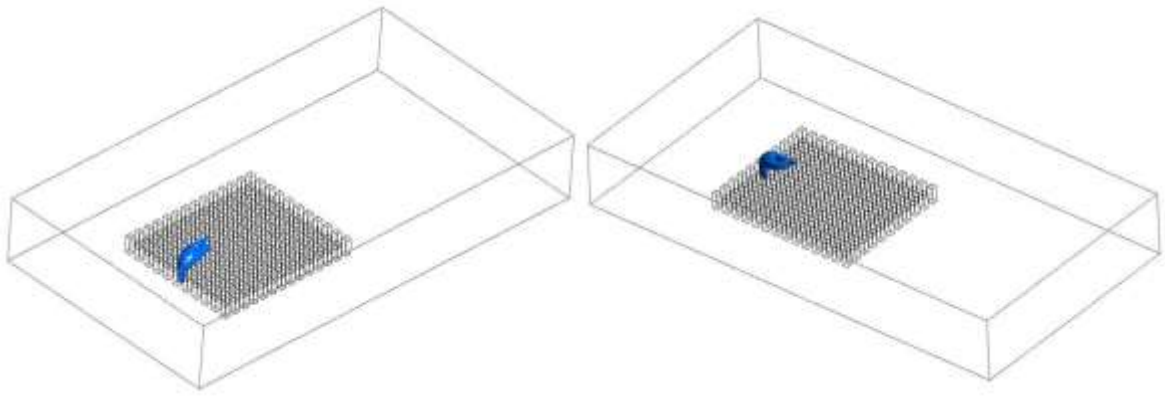

(a) (b)

Figure 8.34: *Side and back view of the concentration profile of the neutral gas dispersion for a/the collocated layout with the release source located at the upwind front of the group of buildings between the first and second column in the sixth row at* ***1 m/s***

Figure 8.34(a) represents an isometric view of the concentration profile of neutral gas dispersion for a collocated layout with the release source located at the upwind front of the group of buildings between the first and second columns in the sixth row at 1 m/s. It shows that, in the case of neutral gas, the gas cloud does not tend to go towards the ground and moves in the upward direction, forming a curve like profile. This could be because of the low density of the neutral gas. The observation that concentration distributes uniformly initially but then distributes into two portions from the centre, resembling that of the flukes of a dolphin, is also evident through this figure. Figure 8.34(b) presents a rotated view of the previous figure and also shows the concentration profile of neutral gas dispersion for a collocated layout with the release source located at the upwind front of the group of buildings between the first and second columns in the sixth row at 0.25 m/s. This figure provides another perspective of the cloud shape and provides an insight into the distribution of the cloud concentration in the vertical direction. This shows that a good part of the cloud does travel in the upward direction and the gas cloud is above the ground.

According to Standard BS EN 60079-10-1:2009 [104], the following locations can be categorised:

Zone 0: The release source location of the gas

Zone 1: The central 3 columns up until the midway point of the building layout

Zone 2: All the remaining locations not categorised in zone 0 or zone 1

8.6.3.5 Velocity of the neutral gas dispersion

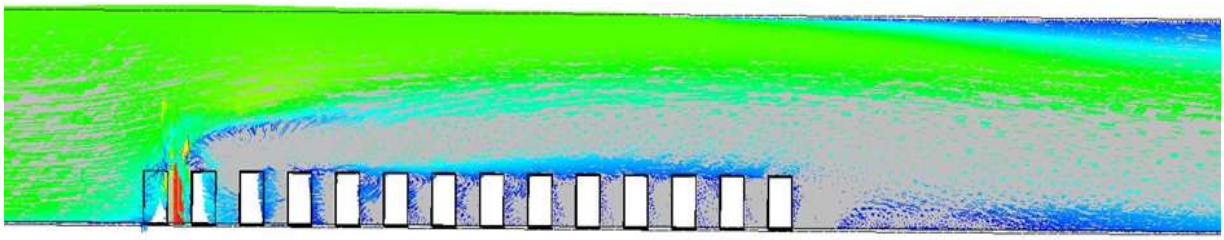

Figure 8.35: *Velocity vectors (Line arrow) of the neutral gas dispersion for a/the collocated layout with the release source located at the upwind front of the group of buildings between the first and second columns in the sixth row. Green is the highest velocity, sky-blue slightly lower and blue the lowest velocity.*

Figure 8.35 shows the velocity vectors simulation for this case study with zoomed in and zoomed out views. Since the wind speed in this case study and case study 1 are similar, almost the same effects are observed. It can be seen in the figure that the velocity above the ground is much more, which is expected because higher winds tend to be found at higher altitudes. At the ground level, the layout of the building causes a hindrance to the wind flow, which results in a slight blockage of wind. For this reason, the gas, when released from the source, tends to move more in the vertical y-direction. This is all remarkably similar to (case study 1).

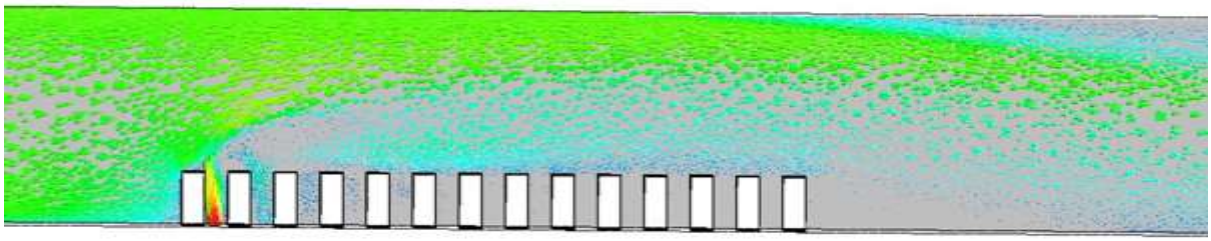

Figure 8.36: *Velocity vectors (Arrowhead 3D view) of the neutral gas dispersion for a/the collocated layout with the release source located at the upwind front of the group of buildings between the first and second columns in the sixth row. Green is the highest velocity, sky-blue slightly lower and blue the lowest velocity.*

Figure 8.36 shows another view i.e., Arrowhead 3D view, of the velocity vectors of the neutral gas dispersion for a collocated layout with the release source located at the upwind front of the group of buildings between the first and second columns in the sixth row. The figure shows the intense vertexes near the release source in red. This means that the neutral gas released from the source at that point is being carried upwards in the vertical direction by the vertical eddies of the wind.

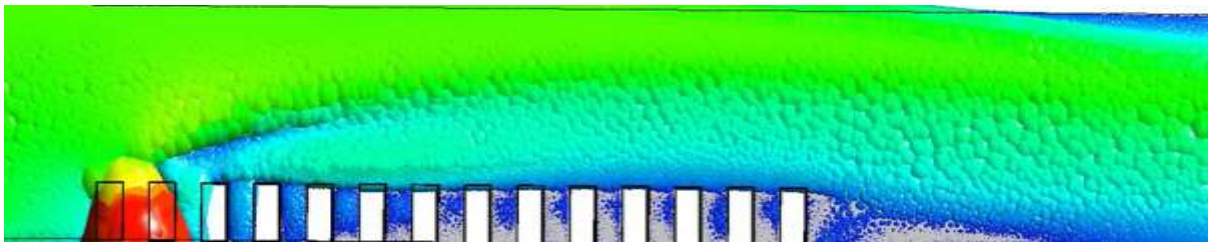

Figure 8.37: *Velocity vectors (Ball view) of the neutral gas dispersion for a/the collocated layout with the release source located at the upwind front of the group of buildings between the first and second columns in the sixth row. Green is the highest velocity, sky-blue slightly lower and blue the lowest velocity.*

This final figure (Figure 8.37) for presenting the results for this case study enables a very clear visualisation of the hazardous area of the gas cloud formation near the release gas source. It identifies that the release source location is a critical point in the building layout and that a certain exposure to the high-temperature source can have devastating effects.

8.6.3.6 Summary of results for case study (3)

This case study was performed for neutral gas with a density of 1.1839kg/m^3 for a wind speed of 1 m/s and flow rate of 1.7837 kg/s. It has shown that the neutral gas tends to move quickly upwards in the vertical direction when released from the source. The behaviour of the cloud is very different, and the cloud of the neutral gas is mostly above ground level.

The dispersion of the neutral gas is maximum in the z or upward direction, which is due to the low buoyancy resulting from the very low density of the gas.

8.6.4 Location 1: Neutral gas dispersion at low velocity

8.6.4.1 Building layout

The type of layout adopted for this case study is a collocated layout. A layout of 154 buildings of cubic shape will be created as collocated layouts and the release source will be located in different positions. The behaviour of the heavy gas dispersion or clouds will then be studied.

8.6.4.2 Release source location

The release source location (1) of the neutral gas dispersion in this case study is at the upwind front of the group of buildings between the first and second columns in the sixth row.

Table 8.10: *Parametric values for the neutral gas simulation at low speed (location1)*

Density	Flow Rate	Velocity	Ambient Temperature	Release Source Temperature
1.1839 kg m/s^3	1.7737 kg/s	0.25 m/s	25°C	25°C

8.6.4.3 Concentration of the neutral gas dispersion

With the parameters described above, the simulation was performed for the concentration of the neutral gas dispersion. The results of the simulation are shown in Figure 8.38 below:

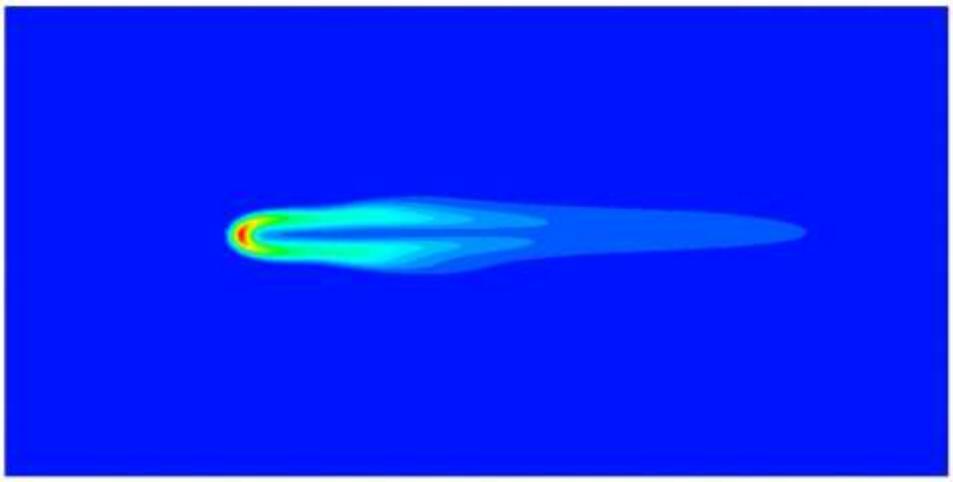

Figure 8.38: *Concentration profile of the neutral gas dispersion for a/the collocated layout with the release source located at the upwind front of the group of buildings between the first and second columns in the sixth row* ***0.25 m/s***

Figure 8.38 shows the concentration of neutral gas cloud when the release source is placed at the upwind front of the group of buildings between the first and second columns in the sixth row. In the figure, red represents the highest concentration, and blue represents the lowest concentration. It can be clearly seen that, under these particular conditions, the shape of the gas cloud for the neutral gas cloud appears not to be similar to case study 3 where it looked like an elliptic cylinder. In case study 3, there was only 1 cloud, while in this case, the cloud splits into two symmetrical parts.

The planar distance in this case is increased to visualise the neutral gas rise in the upward direction. The neutral gas shape is one peak or a single bubble. However, there is a similarity in the trend as the concentrations are highest near the release point. There is then a decreasing degree of concentration as it moves away from the source. However, the shape of the cloud is entirely different in this case and hence the distribution on the gas cloud.

8.6.4.4 Iso-surface of the neutral gas dispersion

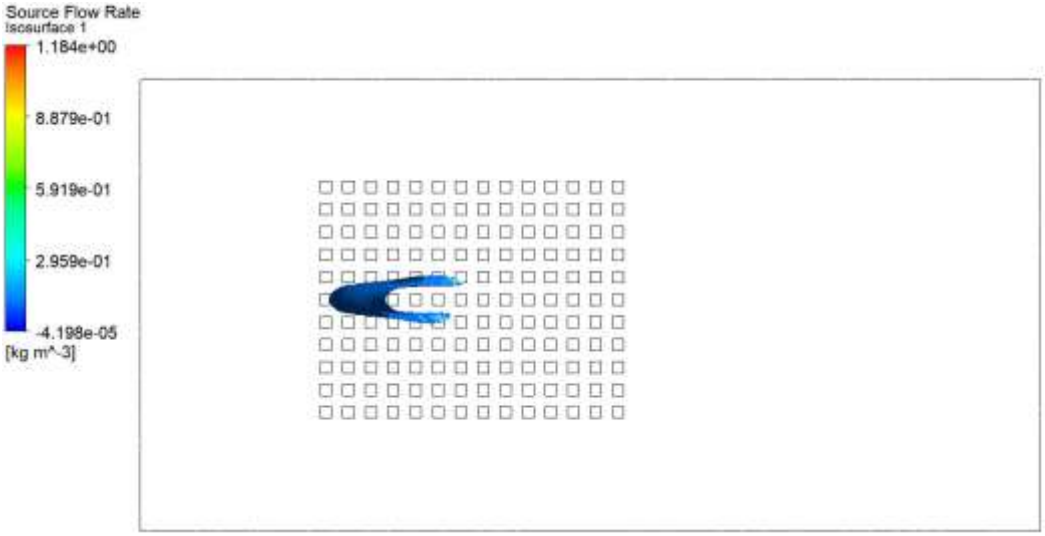

Figure 8.39: *Top view of the concentration profile of the neutral gas dispersion for a/the collocated layout with the release source located at the upwind front of the group of buildings between the first and second columns in the sixth row* ***0.25 m/s****. Blue is the least concentrated space.*

Figure 8.39 is the representation of the mean concentration of the neutral gas cloud in the form of a horizontal cross-section/top view. It reflects the behaviour of the cloud along the x and z-directions. As we can see in the figure, the gas cloud tends to move more along the x-direction and takes a very concentrated near the gas release source. The concentration distributes uniformly initially, but then splits into two portions from the centre, resembling that of the flukes of a dolphin. However, the difference compared to case study 3 is that, in this case, the gas is more flattened and covers a greater span of the building layout. Similar to (case study 3), as compared to the heavy gas cloud, the neutral gas cloud looks very small. Moreover, the cloud does not travel in the opposite x-direction due to the wind coming from that direction.

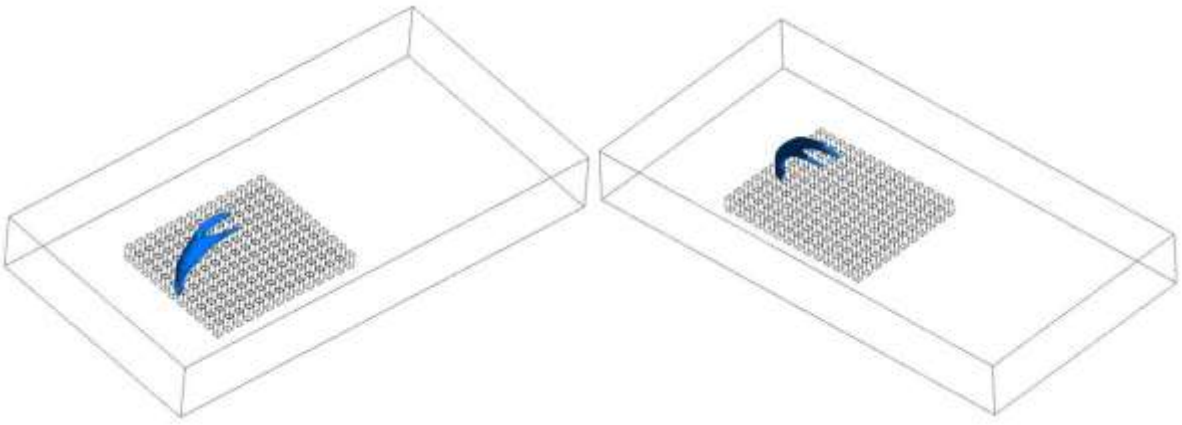

(a) (b)

Figure 8.40: *Side and back of the concentration profile of the neutral gas dispersion for a/the collocated layout with the release source located at the upwind front of the group of buildings between the first and second columns in the sixth row* ***0.25 m/s****. Blue represents the least concentrated space.*

Figure 8.40(a) represents the isometric view of the concentration profile of neutral gas dispersion for a collocated layout with the release source located at the upwind front of the group of buildings between the first and second columns in the sixth row at 0.25 m/s. Although it shows a similar trend similar to that of case study 3 i.e., in the case of neutral gas, the gas cloud does not tend to go towards the ground and moves in the upward direction, forming a curve like profile. As discussed earlier, this could be due to the low density of the neutral gas. This figure reveals that concentration distributes uniformly initially but then separates into two portions from the centre resembling that of the flukes of a dolphin. Moreover, the span of the cloud in the building layout is bigger than that of case study 3. This is similar to the trend observed in the previous figure. Figure 8.40(b) is a rotated view of the previous figure and represents the concentration profile of neutral gas dispersion for a collocated layout with the release source located at the upwind front of the group of buildings between the first and second columns in the sixth row at 0.25 m/s. This figure provides another perception of the cloud shape and offers an understanding of the distribution of the cloud concentration in the vertical direction, which shows that a large portion of the cloud does travel in the upward direction and the gas cloud is above the ground.

According to Standard BS EN 60079-10-1:2009 [104], the following locations can be categorised:

Zone 0: The release source location of the gas

Zone 1: The central 3 columns up until the midway point of the building layout

Zone 2: All the remaining locations not categorised in zone 0 or zone 1

8.6.4.5 Low velocity of the neutral gas dispersion

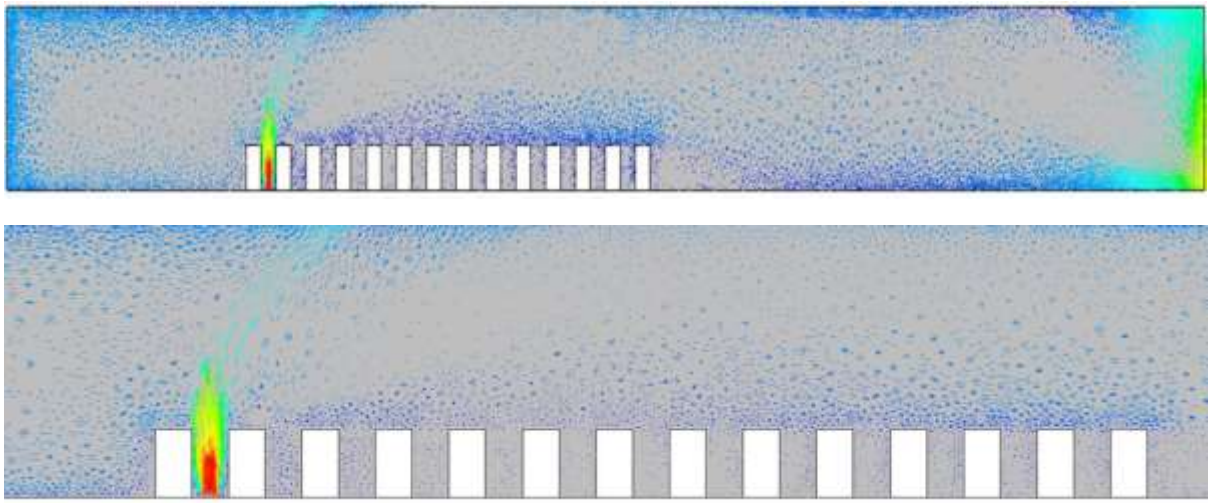

Figure 8.41: *Velocity vectors profile of the neutral gas dispersion for a/the collocated layout with the release source located at the upwind front of the group of buildings between the first and second columns in the sixth row* ***0.25 m/s***

Figure 8.41 shows the zoomed in and zoomed out view of the velocity vectors of neutral gas for a collocated layout with the release source located at the upwind front of the group of buildings between the first and second columns in the sixth row 0.25 m/s. The two views are presented for the sake of offering clarity and analysing the details of the simulation. As seen in the figure, the simulation of the velocity vectors shows the complex vertexes forming near the release source location. Since the buildings block the wind, the wind feels a hindrance due to the building layout and the vertical eddies of the wind vertexes force the gas cloud to travel in the upward direction. As a result, the cloud is above the ground.

8.6.4.6 Summary of results for case study (4)

This case study was performed for neutral gas with a density of 1.1839kg/m^3 for a wind speed of 0.25 m/s and a flow rate of 1.7837 kg/s and similar to Case Study 3. It shows that the neutral gas tends to quickly move upwards in the vertical direction when released from the source. The behaviour of the cloud is quite similar to Case Study 3, but in this case study, it is observed the cloud cover a greater span of the building's layout than that of (case study 3).

In this case, the temperature difference between the neutral gas and atmosphere is zero, which results in no density difference between the two. Hence, the buoyancy is zero. This results in less dispersion of the neutral gases, which is also evident from the simulation.

Note: The location was fixed for the gas release source. The results from simulations of concentration, temperature and velocity were studied in detail. Since there were the initial case studies, analysing them in detail was absolutely necessary. However, now that their results have been thoroughly analysed, they can be used as a reference and case studied can be discussed briefly for the rest of the locations.

8.6.5 Location 2: Heavy gas dispersion at high and low velocities

8.6.5.1 Building layout

The type of layout undertaken for these two case studies is a collocated layout. A layout of 154 buildings of cubic shape will be created as collocated layouts and the release source with be place in the same positions. The behaviour of the gas clouds will then be studied.

8.6.5.2 Release source location

Release source location (2) of the heavy gas dispersion in these case studies was at the upwind front of the group of buildings between the first and second columns in the middle between the fifth and sixth rows. The perimeters selected for this case study are stated below:

Table 8.11: *(A) Parametric values for the heavy gas simulation at high-speed (location 2)*

Density	Flow Rate	Velocity	Ambient Temperature	Release Source Temperature
2.1 kg m/s^3	1 kg/s	1 m/s	25°C	-100°C

Table 8.12: *(B) Parametric values for the heavy gas simulation at low speed (location 2)*

Density	Flow Rate	Velocity	Ambient Temperature	Release Source Temperature
2.1 kg m/s^3	5 kg/s	0.25 m/s	25°C	-100°C

8.6.5.3 Concentration of the heavy gas dispersion at different velocities

The following figure shows the concentration behaviour of the heavy gas at location 2. The whereabouts of location 2 is stated at the beginning of the passage.

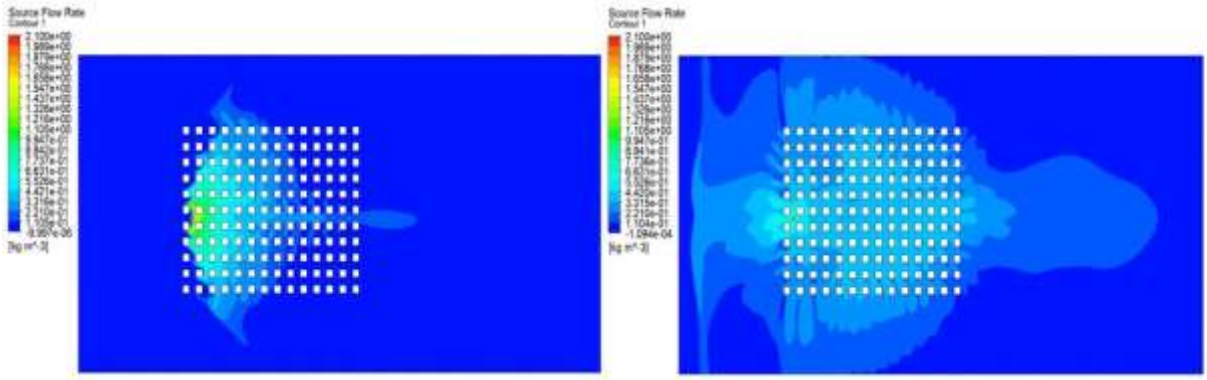

Figure 8.42: **(a)** *Concentration profile of the heavy gas dispersion for a/the collocated layout with the release source located at the upwind front of the group of buildings between the first and second columns in the middle between the fifth and sixth rows at 1m/s.* ***(b)*** *At 0.25m/s*

The concentration profile of the heavy gas at location 2 is shown in Figure 8.42(a). Figure 8.42(b) represents the concentration behaviour of the heavy gas when the release gas source is placed between the first and the second columns in the middle between the 5th and 6th rows. In the above figure, the part labelled (a) is at high speed, while the one labelled (b) is at low speed. The simulations show that, since the release source is now exposed to the air, it does affect the shape of the associate cloud of the heavy gas, which is now more spread in the horizontal direction. The change of location has affected the cloud shape in such a way that, at high speed, it now makes an extended knobhead shape in the horizontal direction creeping out of the last column of the layout, as shown in Figure 8.42(a). The affect is more extended when

at a low speed of 0.25m/s, as shown in Figure 8.42(b). The simulations for location 1 had shown that the cloud shape is of the form of a prism. The same can also be seen for this case, but it should be noticed that the prism shape in this case is not as noteworthy as that of case 1. Moreover, in this case, it can be seen that the cloud creeps out of the building layout from the horizontal side, which was not the case in the previous location.

The low-speed simulation (Figure 8.42(b)) presents an entirely different cloud shape. As discussed in the previous paragraph, the cloud shape now makes an extended knobhead shape in the horizontal section of the building layout. In the case of low speed, the shape is more exaggerated than when the speed is high.

8.6.5.4 Iso-surface of the heavy gas dispersion at different velocities

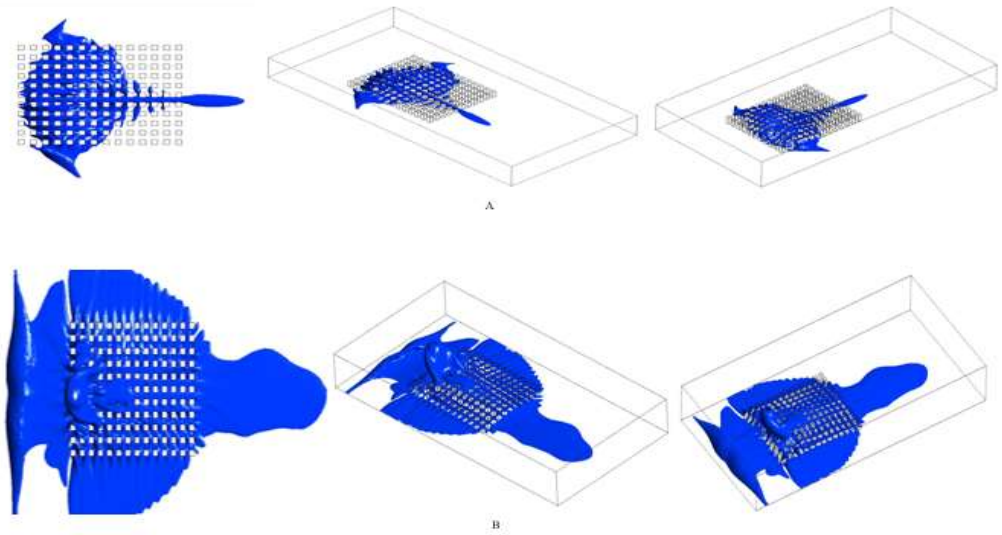

Figure 8.43: (a) *Iso-surfaces of the concentration profile of the heavy gas dispersion for a/the collocated layout with the release source located at the upwind front of the group of buildings between the first and second column in the middle between fifth and sixth rows at 1m/s.* ***(b)*** *At 0.25m/s*

Figure 8.43 shows the iso-surfaces of the concentration profile of heavy gas dispersion for a collocated layout with the release source located at the upwind front of the group of buildings between the first and second columns in the middle between the fifth and sixth rows at both low and high speeds. At low speeds, the shape of cloud changes by a scale of approximately three. The iso-surfaces play an important role in helping us determine the shape of the cloud as, with the help of these iso-surfaces, it can be seen how the cloud is distributed along the three dimensions of space. The above iso-surfaces illustrate that the gas cloud at low speed covers not only the entire building of the layout but also its surroundings. This is in contradiction to the high-speed case, which only covers approximately half of the building

layout and the central rows. The iso-surfaces also help determine that, at the release source point, the gas cloud is more concentrated in the vertical direction.

According to Standard BS EN 60079-10-1:2009 [104], the following locations can be categorised:

High speed:

Zone 0: The immediate areas surrounding the release source in all directions, especially the middle rows and the extreme areas of the middle and final front

Zone 1: The central 2 two rows starting from the middle front right up to the final front

Zone 2: All the remaining locations not categorised in zone 0 or zone 1

Low speed:

Zone 0: The central upwind front of the building layout

Zone 1: The immediate surrounding of the building layout and areas not categorised in zone 0

Zone 2: All the remaining locations not categorised in zone 0 or zone 1

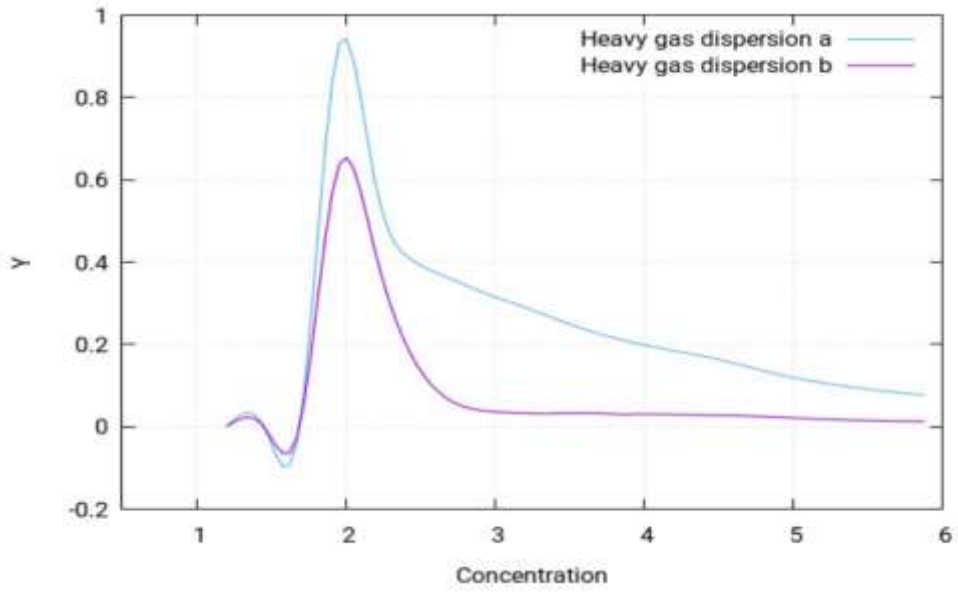

Figure 8.44: *Concentration of heavy gas dispersion profile along the* ***x****-direction at* ***1m/s*** *at different points of (a) x=1.20m, y=1.95m and z=7.20m (b)x=1.20m, y=1.95m and z=1.55m*

In Figure 8.44 (above), two different curves for the concentration profiles are shown. They show the pattern of the concentration profile along the x-direction when the wind speed for the simulation is 1m/s. The two different curves are obtained for two different distances from the release source. Both curves follow the same pattern but have different values due to differences in distances. From the figure, it can be concluded that the concentration value of the heavy gas decreases as it moves away from the source. In the figure, the curve with the highest peak is obtained when nearest to the release source and vice versa.

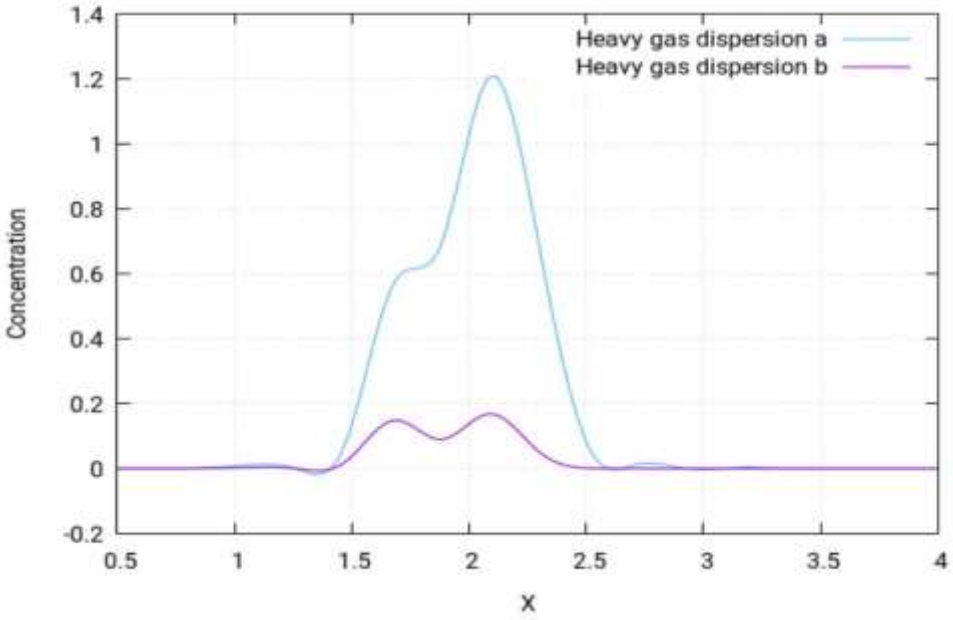

Figure 8.45: *Concentration of heavy gas dispersion profile along the* ***y****-direction at* ***1m/s*** *at different points of (a) x=1.75m, y=-1m and z=7.20m (b)x=1.75m, y=-1m and z=9.50m*

In Figure 8.45 (above), two different curves for the concentration profiles are shown. They show the pattern of the concentration profile along the y-direction when the wind speed for the simulation is 1m/s. The two different curves are obtained for two different distances from the release source. It can be seen that, along the y-direction, the profiles do not follow the same pattern, unlike the x-direction, where they followed the same pattern. This is because the wind makes a significant effect in the y-direction.

8.6.5.5 Temperature of heavy gas dispersion at different velocities

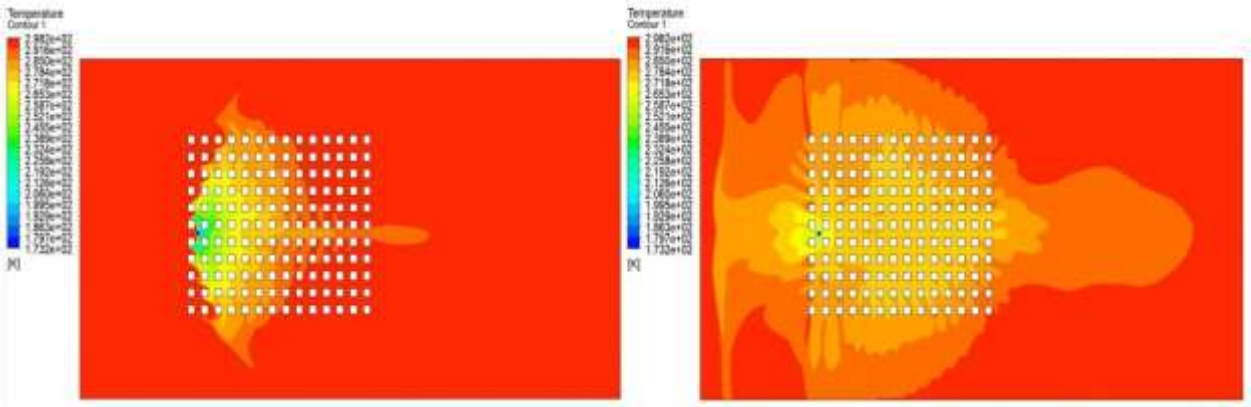

Figure 8.46: (a) *Temperature profile of the heavy gas dispersion for a/the collocated layout with the release source located at the upwind front of the group of buildings between the first and second columns in the middle between the fifth and sixth rows at 1m/s.* ***(b)*** *At 0.25m/s*

The temperature simulation shows the same cloud shape that is achieved from concentration 1.So, it is unnecessary to discuss the cloud shape again. However, the trend of temperature

starts from its lowest at the release source and slowly increases until it approaches the atmosphere and attains the ambient temperature. The temperature simulation is shown in Figure 8.46(a) for high speed and Figure 8.46(b) for low speed.

Figure 8.46(a) for high speed and Figure 8.46(b) for low speed (both above) shows the temperature simulation for this study. By visualising the temperature simulation, it is found out that the temperature simulation produces largely the same profile for the case study as that of the concentration profile. However, the behaviour of temperature is in fact the opposite to that of concentration. This means that the areas identified in the concentration simulation as the highly concentrated will in fact have the lowest temperatures, while the ones with moderate concentrations will have moderate temperatures and the least concentrated areas will have the maximum temperatures. To further simply these findings, it should be pointed out that the simulations show that the concentrations near the release source point tend to be the highest and start to fade away as they move away from the source, reaching their lowest when they move much further away in the layout, ultimately reaching the environment where the gas cloud disappears. However, the temperature is at its lowest near the release source point and tends to increase as it moves away from the source, finally achieving its highest temperature equal to the ambient temperature of the environment.

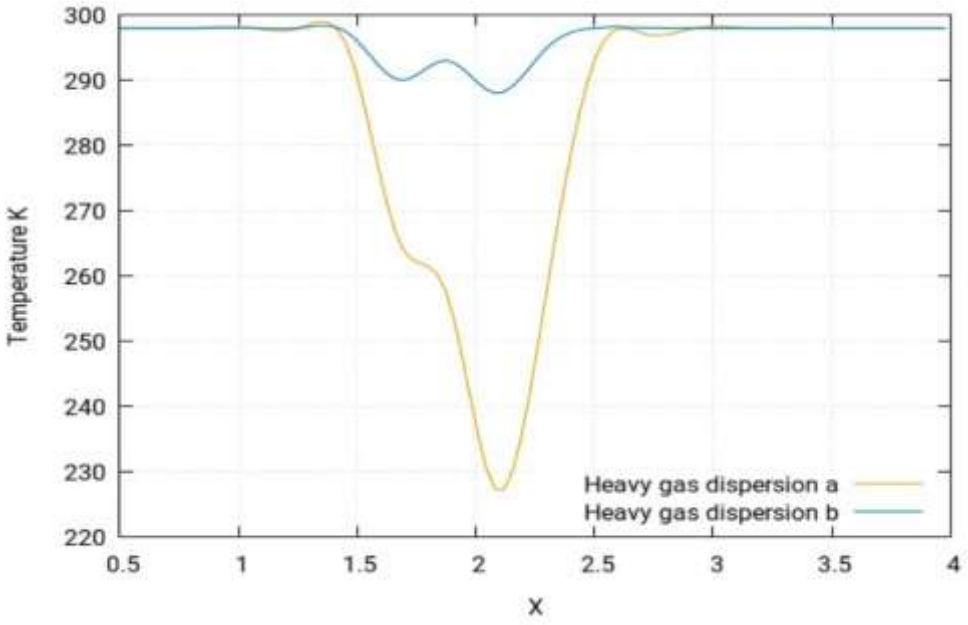

Figure 8.47: *Temperature of the heavy gas dispersion profile along the y-axis at* ***1m/s*** *direction at different points of (a) x=1.75m, y=-1m, z=7.20m (b)x=1.75m, y=-1m and z=9.50m*

In Figure 8.47 (above), two different curves for the temperature profiles are shown. They show the pattern of the temperature profile along the y-direction when the wind speed for the simulation is 1m/s. The two different curves are obtained for two different distances from the

release source. These results show that, at a speed of 1m/s, temperature profiles are a mirror of concentration profile.

8.6.5.6 Heavy gas dispersion at different velocities

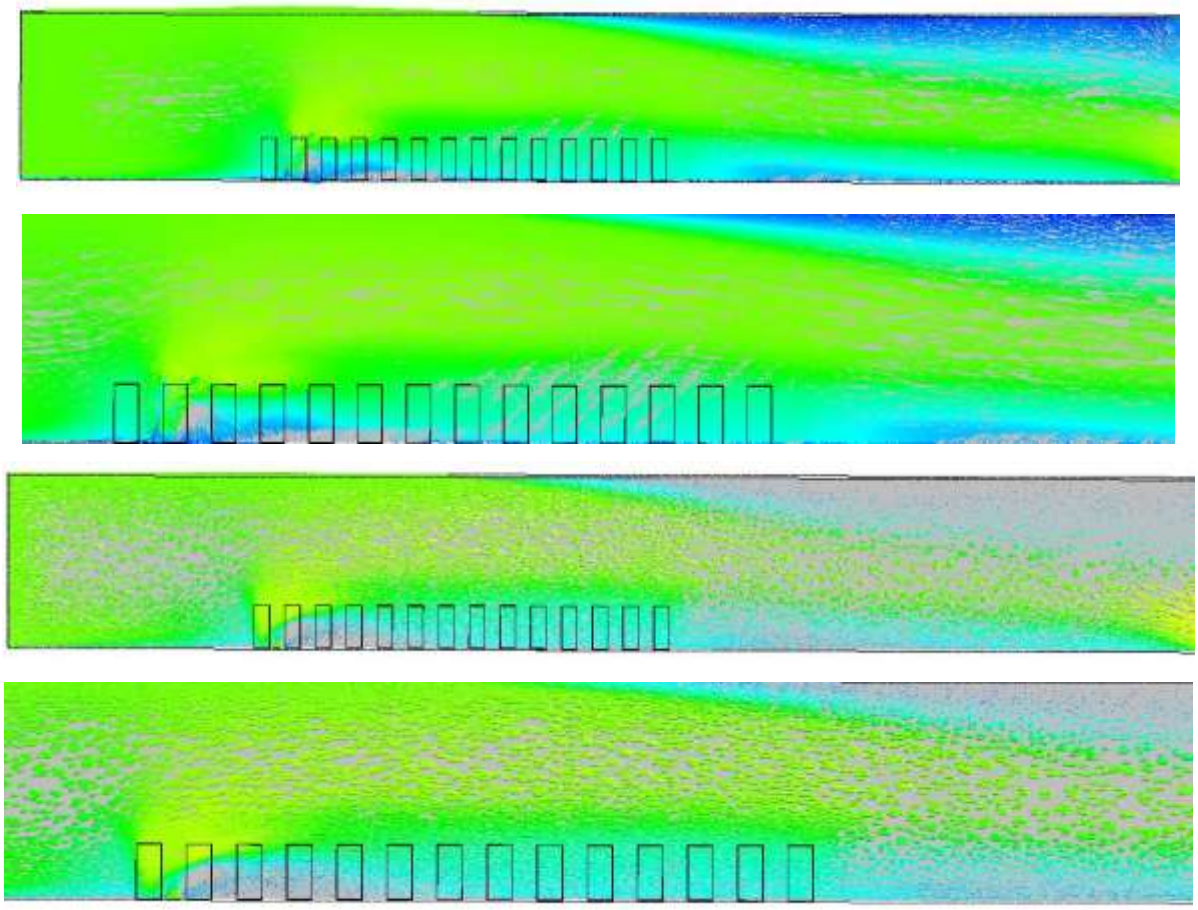

Figure 8.48: (a) *Velocity contours of the heavy gas dispersion for a collocated layout with the release source located at the upwind front of the group of buildings between the first and second columns in the middle between the fifth and sixth rows at* ***1m/s***

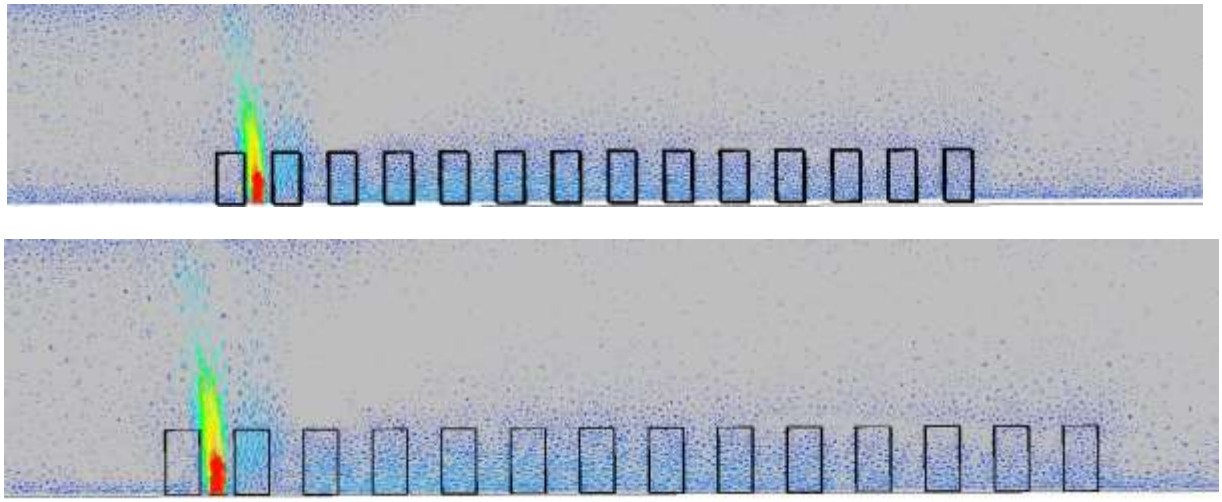

Figure 8.49: (b) *Velocity contours of heavy gas dispersion for a collocated layout with the release source located at the upwind front of the group of buildings between the first and second columns in the middle between the fifth and sixth rows at* ***0.25m/s***

The above figures show the velocity contours for both high speed (1m/s) and low speed (0.25m/s) of heavy gas dispersion for this case study with the release source located at the upwind front of the group of buildings between the first and second columns in the middle between fifth and sixth rows. Velocity contours depict the intensity of wind - or the effective wind influence - at the different locations throughout the layout. As can be seen in the figure, the wind intensity is different at different points in the layout; it is a commonly known effect that at greater altitudes, enhanced wind speeds are experienced. This is because the objects at the lower altitudes create resistance to the flow of wind. As there is resistance caused by the buildings in the flow of gas in the opposite direction to the wind the wind flowing from left to right fails to indict the same motion of flow. Instead, various complex vertexes are formed within the buildings near the release source location, as can be seen in the figures above. The heavy gas released from the source is carried by these vertexes to the nearby mixture of the gas cloud and then moves smoothly away from the source. Moreover, the hindrance in the wind flow caused by the buildings results in the vertexes moving in the upward direction, which enhances the shape of the cloud in the upward direction.

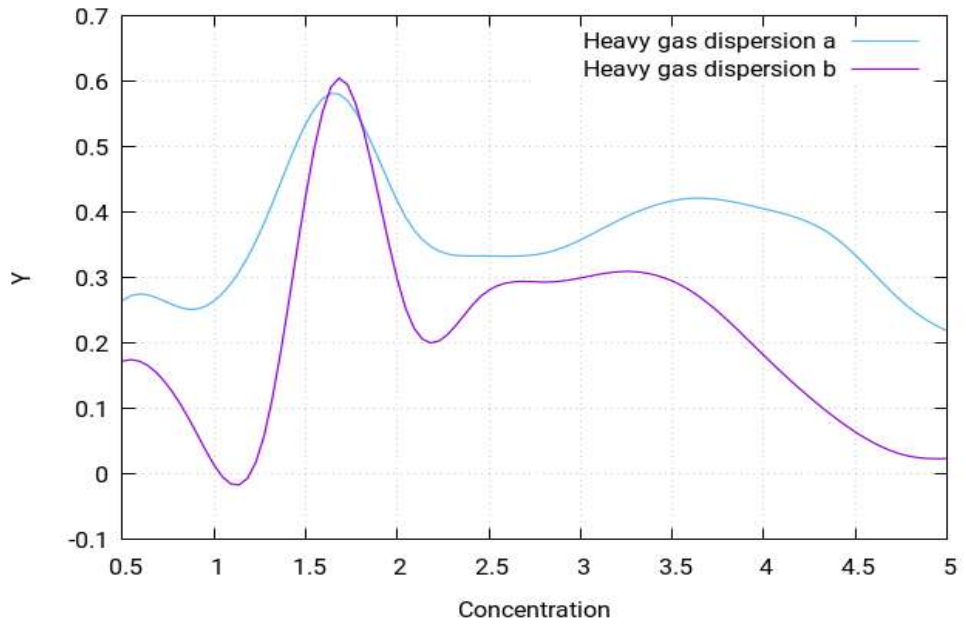

Figure 8.50: *The concentration of the heavy gas dispersion profile with a low velocity of* ***0.25 m/s*** *along the* ***x****-direction at different points of (a) x=1m, y=1.95m and z=7.20m (b)x=1m, y=1.95m and z=9.84m*

The above figure shows the concentration profiles for two of the gas dispersions at two different locations along the x-axis at 0.25m/s wind speed depending on distance from release source. Both curves follow the same pattern but have different values.

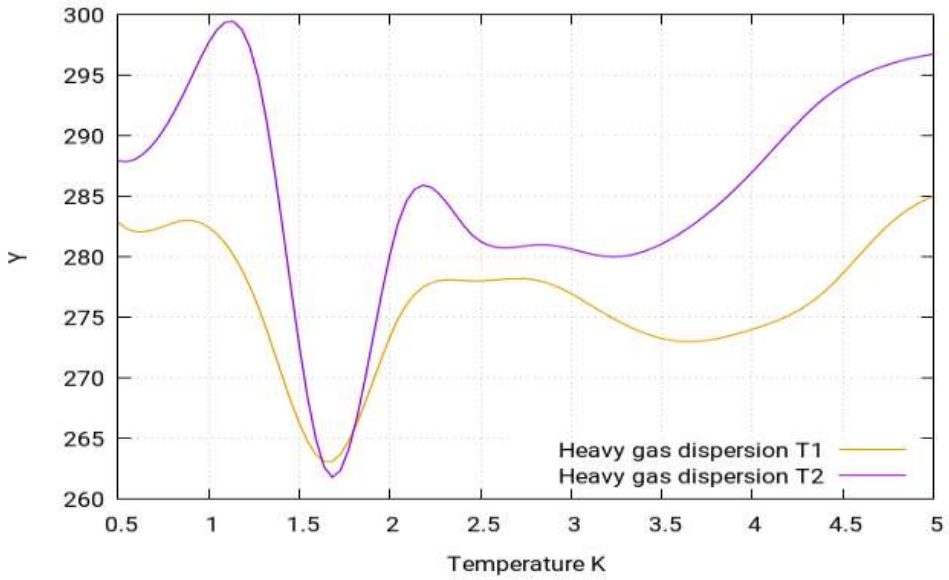

Figure 8.51: *Temperature of the heavy gas dispersion profile with a low velocity of* ***0.25 m/s*** *along the* ***x-*** *direction at different points of (T1) x=1m, y=1.95m and z=7.20m (T2) x=1m, y=1.95m and z=9.84m*

In Figure 8.51, two different curves for the temperature profiles are shown. They show the pattern of the temperature profile along the x-direction when the wind speed for the simulation is 0.25m/s. The two different curves are obtained for two different distances from the release source. These results show that at speed of 1m/s, temperature profiles are a mirror of concentration profile.

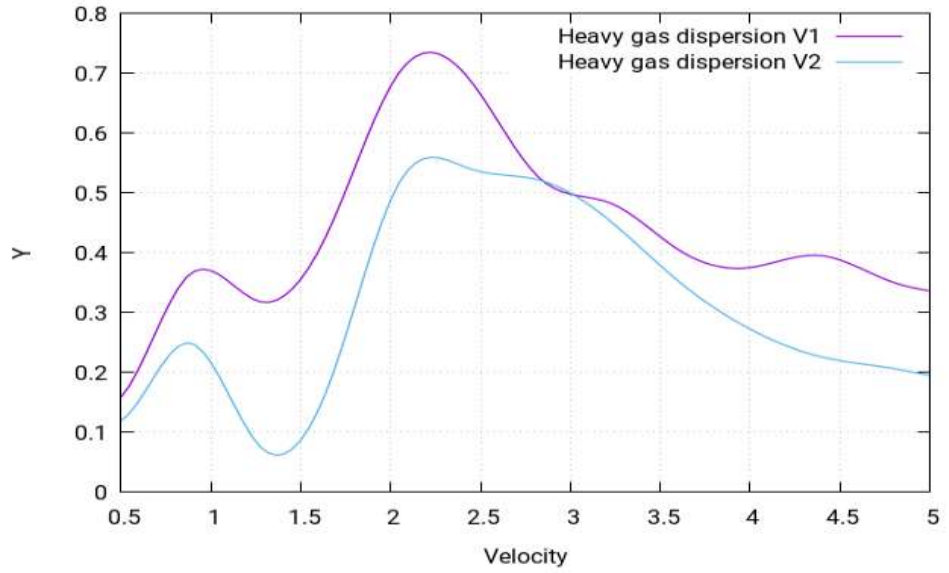

Figure 8.52: *Velocity of the heavy gas dispersion profile with a low velocity of* ***0.25 m/s*** *along the* ***x-*** *direction at different points of (V1) x=1m, y=1.95m and z=7.20m (V2) x=1m, y=1.95m and z=9.84*

The above figure shows the velocity profiles for different locations for the gas dispersion at two different locations depending on distance from release source. Both curves follow the same pattern but have different values.

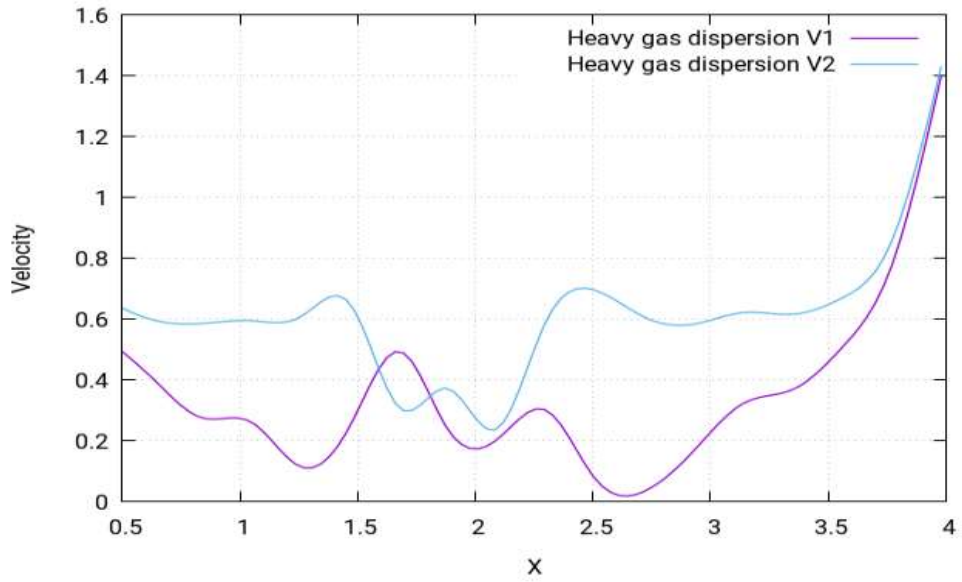

Figure 8.53: *Velocity of the heavy gas dispersion profile with a low velocity of* ***0.25 m/s*** *along the* ***y****-direction at different points of (V1) x=1.75m, y=-1m, z=7.20m (V2) x=1.96m, y=-1m and z=7.20m*

Similar to previous figure, Figure 8.53 shows the velocity profiles for different locations for the gas dispersion at two different locations depending on distance from release source. Both curves follow the same pattern but have different values.

In this case, a comparison was carried out to understand the effect of velocity on the dispersion of heavy gas. In the first case, in which the heavy gas was released at a velocity of 1 m/s, there was greater dispersion due to the turbulent behaviour of the gas. In the second case, in which the velocity is 0.25 m/s, there was less dispersion due to the laminar flow of the gas around the obstacles. Moreover, in both cases, the temperature difference between the gas and atmosphere was kept the same i.e., 125°C.

8.6.6 Location 2: Neutral gas dispersion

8.6.6.1 Building layout

The type of layout adopted for this case study is a collocated layout. A layout of 154 buildings of cubic shape will be created as collocated layouts and the release source will be placed in the same positions. Thereafter, the behaviour of the gas clouds will be studied.

8.6.6.2 Release source location

Release source location (2) for the neutral gas dispersion in this case study is at the upwind front of the group of buildings between the first and second column in the middle between the fifth and sixth rows. The perimeters selected for this case study are stated below:

Table 8.13: *Parametric values for the neutral gas simulation at high speed (location2)*

Density	Flow Rate	Velocity	Ambient Temperature	Release Source Temperature
1.1839 kg m/s^3	1.7737 kg/s	1 m/s	25°C	25°C

8.6.6.3 Concentration of the neutral gas dispersion

The following figure shows the concentration behaviour of the neutral gas at location (2). The whereabouts of location 2 have been stated at the beginning of the passage.

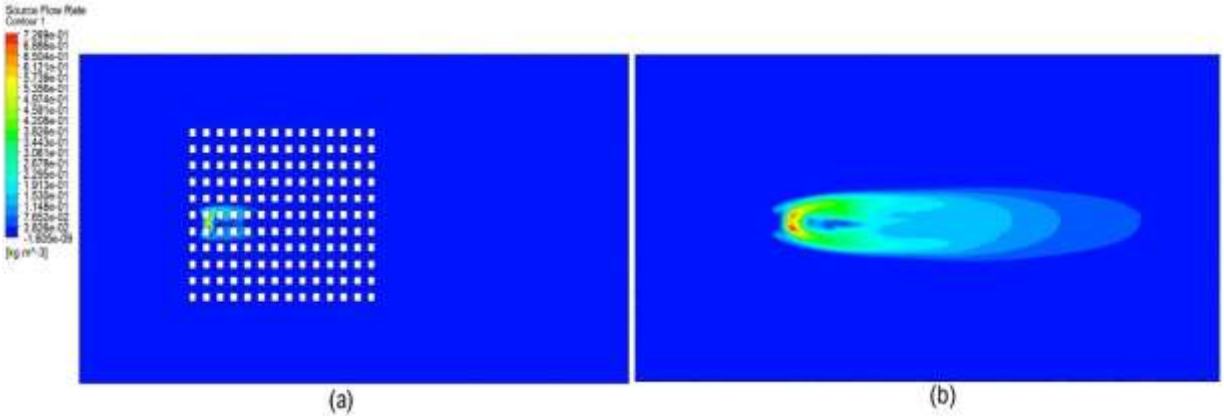

Figure 8.54: *concentration profile of the neutral gas dispersion for a collocated layout with the release source located at the upwind front of the group of buildings between the first and second columns in the middle between the fifth and sixth rows at* ***1m/s***

In Figure 8.54, the concentration of the neutral gas cloud can be seen when the release source is placed at the upwind front of the group of buildings between the first and second columns in the middle between the fifth and sixth rows. In the previous case study for the neutral gas, the release source was not exposed to the air because it was placed behind one of the buildings in the layout in row six. However, in the present case, it is placed in the middle, which makes it exposed to the air; therefore, the cloud shape is different. In Figure 8.54(a), the plane is placed on the ground and it can be seen that the neutral gas dispersion is very small in the x-direction but very large in the upward direction. For that reason, the planar distance from the ground is increased in Figure 8.54(b) and the neutral gas dispersion can be seen in the form of a cloud. Nevertheless, there is a similarity in the trend, as the concentrations are maximum near the release point. However, if the plane distance from the ground floor up was increased, to visualise the shape of the neutral gas as shown in above figures that it is going up not spread at the ground like the heavy gas. The neutral gas shape is one peak or a single bubble. The following plane is then placed on the ground and the concentration can be seen as it moves away from the source. The iso-surfaces should better explain the shape of the cloud.

8.6.6.4 Iso-surface for the neutral gas dispersion

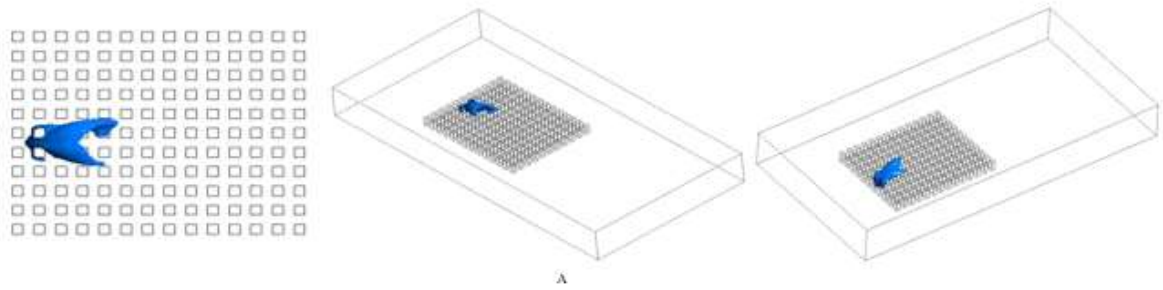

Figure 8.55*:** *Iso-surfaces of the density profile of the neutral gas dispersion for a collocated layout with the release source located at the upwind front of the group of buildings between the first and second columns in the middle between the fifth and sixth rows at* ***1m/s

In Figure 8.55, the iso-surfaces can be seen for the concentration profile of the neutral gas cloud when the release source is placed at the upwind front of the group of buildings between the first and second column in the middle between the fifth and sixth rows. These iso-surfaces help identify that the shape of the cloud is somewhat shrunken in this case and only occupies a few of the building blocks of the layout resembling the shape of a/the symmetrical opening in the horizontal direction.

According to Standard BS EN 60079-10-1:2009 [104], the following locations can be categorised:

Zone 0: The central upwind front of the building layout from the 2nd to 4th row

Zone 1: The immediate surroundings of the building layout and areas categorised in zone 0

Zone 2: All the remaining locations not categorised in zone 0 or zone 1

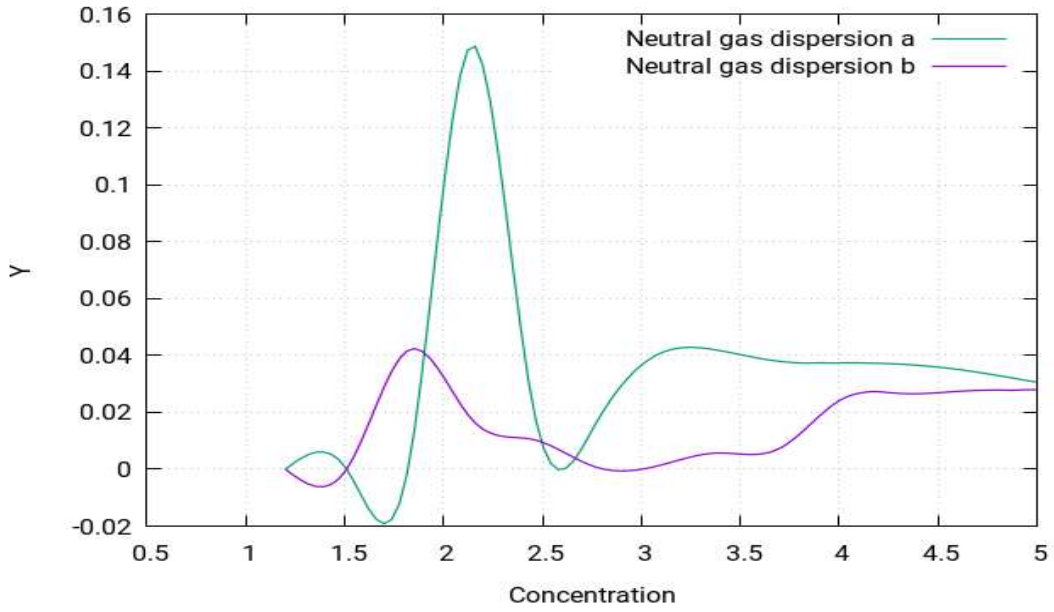

Figure 8.56: *The concentration of the neutral gas dispersion profile along the* ***x****-direction at* ***1m/s*** *at different points of (a) x=1.20m, y=1.95m, z=7.20m (b) x=1.20m, y=1.95m, and z=3.04m*

The above figure shows the concentration profiles for two of the gas dispersions at two different locations along the x-direction at a 1m/s wind speed depending on distance from release source. Both the curves follow the same pattern but have different values.

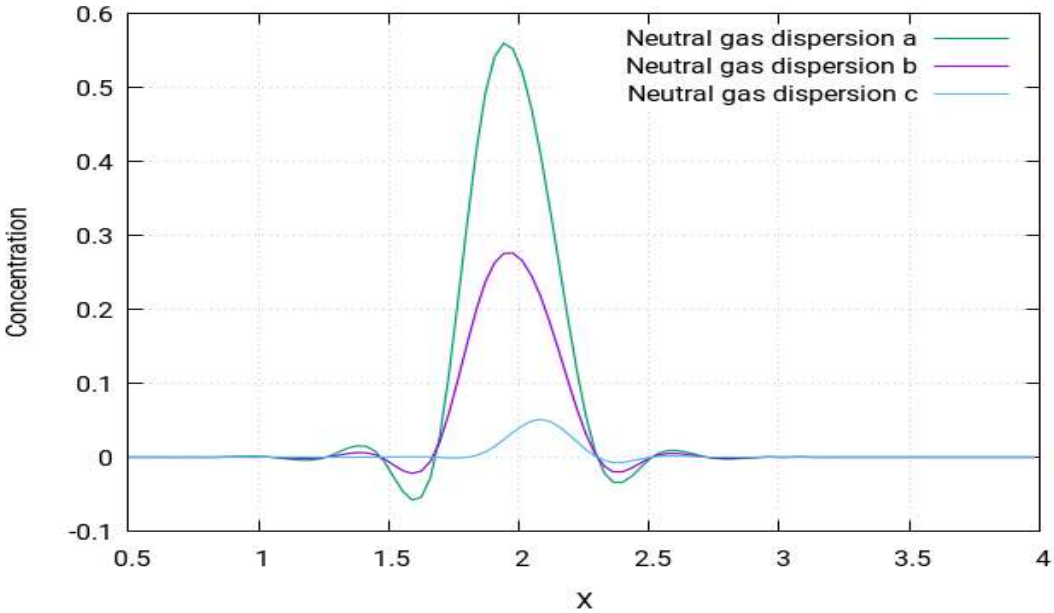

Figure 8.57: *The concentration of neutral gas dispersion profile along the* ***y****-direction at* ***1m/s*** *at different points of (a) x=1.75m, y=-1m, z=7.20m (b) x=1.80m, y=-1m, z=1.33m, and (c) x=2.05m, y=-1m, z=2.42m*

In Figure 8.57 (above), three different curves for the concentration profiles are shown. They show the pattern of the concentration profile along the y-direction when the wind speed for the simulation is 1m/s. The curves are obtained for three different distances from the release

source. All the curves follow the same pattern but have different values due to differences in distances. From the figure, it is concluded that the concentration value of the concentration of heavy gas decreases as it moves away from the source shows declining behaviour.

Note: No temperature profile for neutral gas because temperature is constant in neutral gas dispersion.

8.6.6.5 Velocity of the neutral gas dispersion

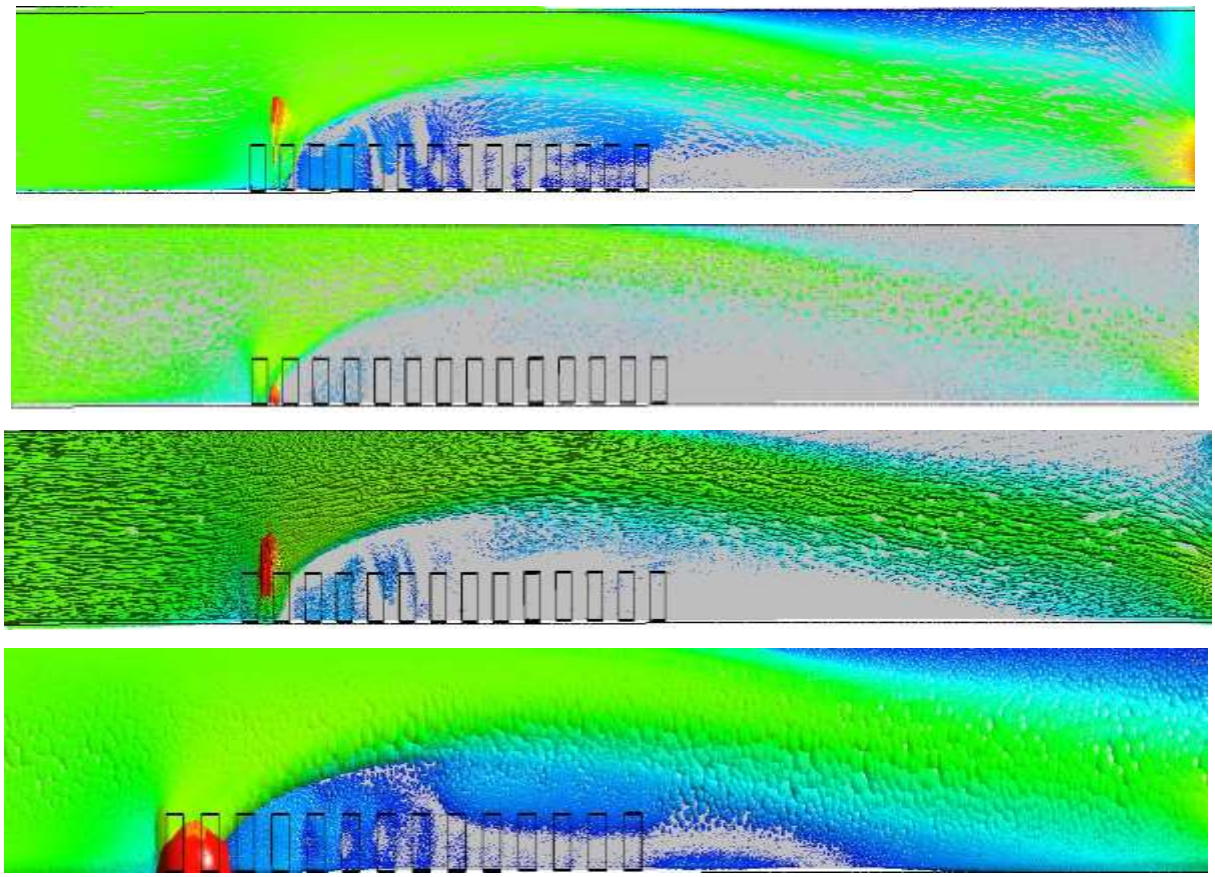

Figure 8.58: *The velocities profile of the neutral gas dispersion for a/the collocated layout with the release source located at the upwind front of the group of buildings between the first and second columns in the middle between the fifth and sixth rows at* ***1m/s***

Figure 8.58 shows the velocity contours of neutral gas dispersion for this case study with the release source located at the upwind front of the group of buildings between the first and second columns in the middle between the fifth and sixth rows at 1m/s. The velocity contours depict the intensity of wind - or the effective wind influence - at the different locations throughout the layout. In the figure, red represents the maximum velocity of 1m/s and blue is for zero velocity. A large cloud of red can be seen at the release source, showing that there are many complex vertexes of maximum velocity being formed near the release source. It can be noticed that, immediately after the heavy red portion near the release source in the building layout, there is a continuous blue in the rest of the building layout. This proves that the heavy gas, when the

neutral gas was released from the source, created complex vertexes of the maximum velocity near the release source. These vertexes carried the neutral gas towards the upward direction due to the low density of the neutral gas compared to the ambient air. As a result, the neutral gas flew over the building layout rather than within the building layout. Therefore, a continuous blue portion can be seen in the building layout after the release source, showing the void left behind, representing zero velocities by the blue colour of the velocity contours.

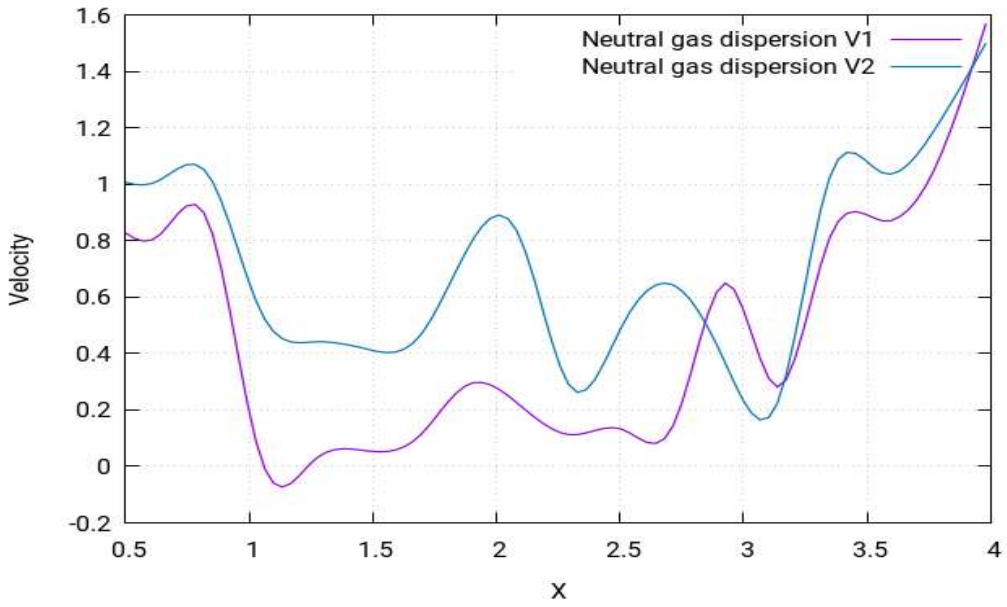

Figure 8.59: *The velocity of the neutral gas dispersion profile along the* ***y****-direction at* ***1m/s*** *at different points of (V1) x=1.75m, y=-1m, z=7.20m, (V2) x=1.80m, y=-1m, and z=1.33m*

The above figure shows the velocity profiles for two different locations for the gas dispersion at two different locations depending on distance from release source. Both curves follow the same pattern but have different values.

In this case, the dispersion of the neutral gas was observed for no temperature difference between the gas and the atmosphere at different locations. At 1 m/s, the turbulence occurs only at around the corners of the obstacles near the source location, which results in dispersion of the neutral gases. For neutral gas, the dispersion is maximum in the z-direction because of the low densities.

8.6.7 Location 3: Heavy gas dispersion at high and low velocity

8.6.7.1 Building layout

The type of layout undertaken for these two case studies is a collocated layout. a layout of 154 buildings of cubic shape will be created as collocated layouts and the release source will be placed in the same positions. The behaviour of the gas clouds will then be studied.

8.6.7.2 Release source location

The release source position (3) of the heavy gas dispersion in these case studies was at the upwind front of the group of buildings between the first and sixth rows in the sixth column. The perimeters selected for this case study are stated below:

Table 8.14: *(A) Parametric values of the heavy gas dispersion at high-speed (location 3)*

Density	Flow Rate	Velocity	Ambient Temperature	Release Source Temperature
2.1 kg m/s^3	1 kg/s	1 m/s	25°C	-100°C

Table 8.15: *(B) Parametric values of the heavy gas dispersion at low speed (location 3)*

Density	Flow Rate	Velocity	Ambient Temperature	Release Source Temperature
2.1 kg m/s^3	5 kg/s	0.25 m/s	25°C	-100°C

8.6.7.3 Concentration of the heavy gas dispersion at different velocities

The following two figures show the concentration behaviour of the heavy gas at location 3. The whereabouts of location 3 has stated at the beginning of the passage.

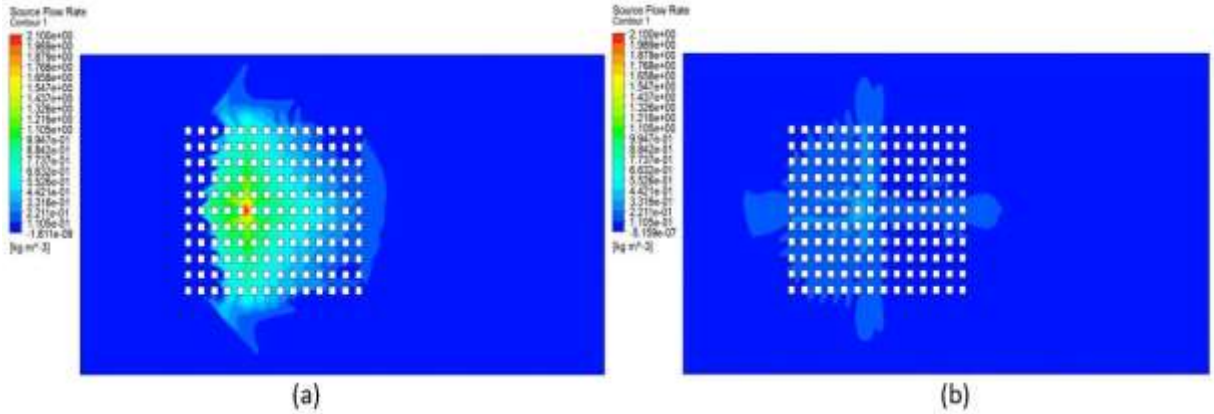

Figure 8.60: (a) *Concentration profile of the heavy gas dispersion for a/the collocated layout with the release source located at the upwind front of the group of buildings between the first and sixth rows in the sixth column at 1m/s.* ***(b)*** *At 0.25m/s*

8.6.7.4 Iso-surface of the heavy gas dispersion at different velocities

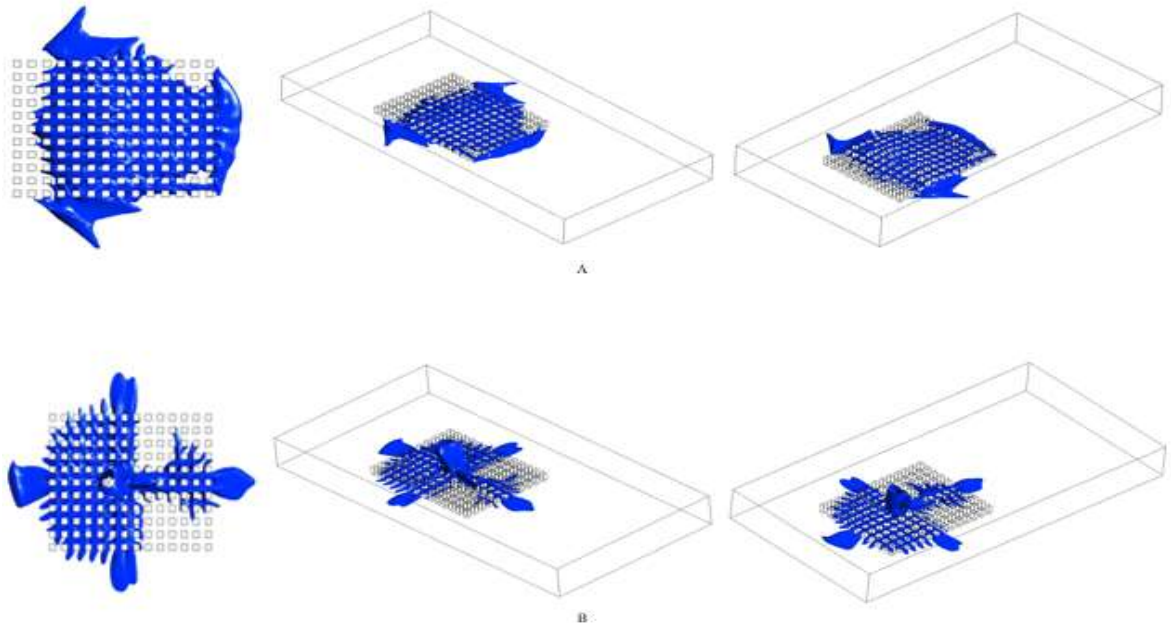

Figure 8.61: (a) *Iso-surfaces of the concentration profile of the Heavy Gas Dispersion for a collocated layout with the release source located at the upwind front of the group of buildings between the first and sixth rows in the sixth column at 1m/s.* ***(b)*** *At 0.25m/s*

The concentration profile of the heavy gas at location 3 is shown in Figures 8.60 and 8.61 (above). These figures represent the concentration behaviour of the heavy gas when the release gas source is placed at the upwind front of the group of buildings between the first and sixth rows in the sixth column. In the above two figures, parts labelled (A) are at high speed and those labelled (B) are at low speed. These simulations show that, for this particular setting of the perimeters and the release source location, the gas cloud takes the shape of the cloud which resembles that of case study 1 i.e., location 1 of the release source. Although the resemblance is uncanny to a certain extent, the cloud has shifted towards the right side or, perhaps more accurately, it has leaned forward towards the right side. It could be argued that the shifting of the release source towards the right side has, as a result, shifted the cloud in the same direction. The spread of the cloud in other directions also resembles that of (location 1).

According to Standard BS EN 60079-10-1:2009 [104], the following locations can be categorised:

High speed:

Zone 0: The central most region of the middle front surrounding the release source

Zone 1: The extreme boundaries of the middle front

Zone 2: All the remaining locations not categorised in zone 0 or zone 1

Low speed:

Zone 0: The central region of the middle front

Zone 1: The sleeve shaped region of the central columns and the 2nd and 3rd rows

Zone 2: All the remaining locations not categorised in zone 0 or zone 1

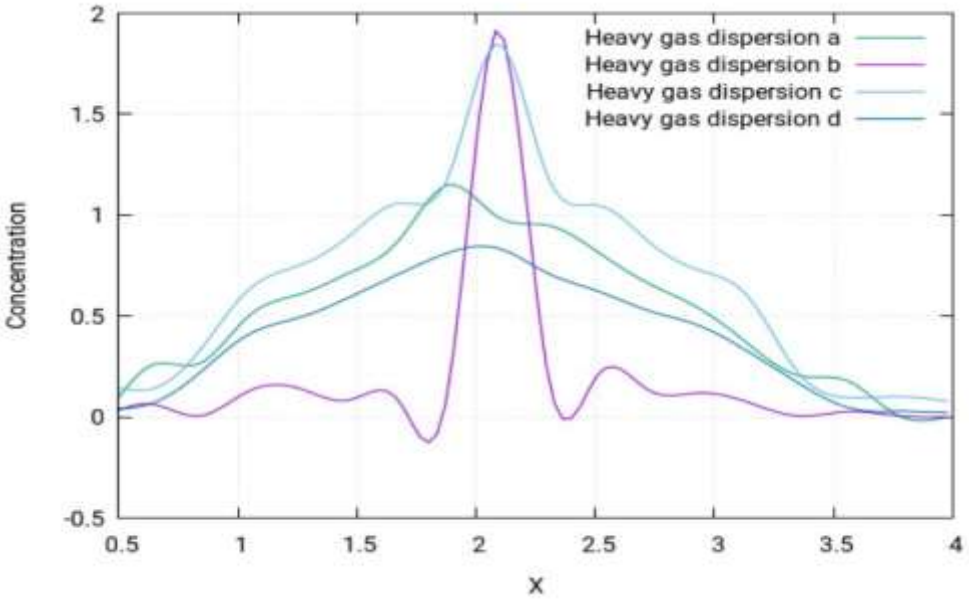

Figure 8.62: *Concentration of the heavy gas dispersion profile along the* ***y****-direction at* ***1m/s*** *at different points of (a) x=2.35m, y=-1m and z=7.20m, (b) x=2.55m, y=-1m and z=7.20m, (c) x=2.55m, y=-1m, z=9.84m (d) x=2.95, y=-1m and z=5.06m*

In Figure 8.62 (above), four different curves for the concentration profiles are shown. They show the pattern of the concentration profile along the x-direction when the wind speed for the simulation is 1m/s. The four different curves are obtained for two different distances from the release source. Both the curves follow the same pattern but have different values due to differences in distances. From the figure, it is concluded that the concentration value of the concentration of heavy gas decreases as it moves away from the source. In the figure, the curve with the highest peak is obtained when nearest to the release source and vice versa.

8.6.7.5 Temperature of heavy gas dispersion at different velocities

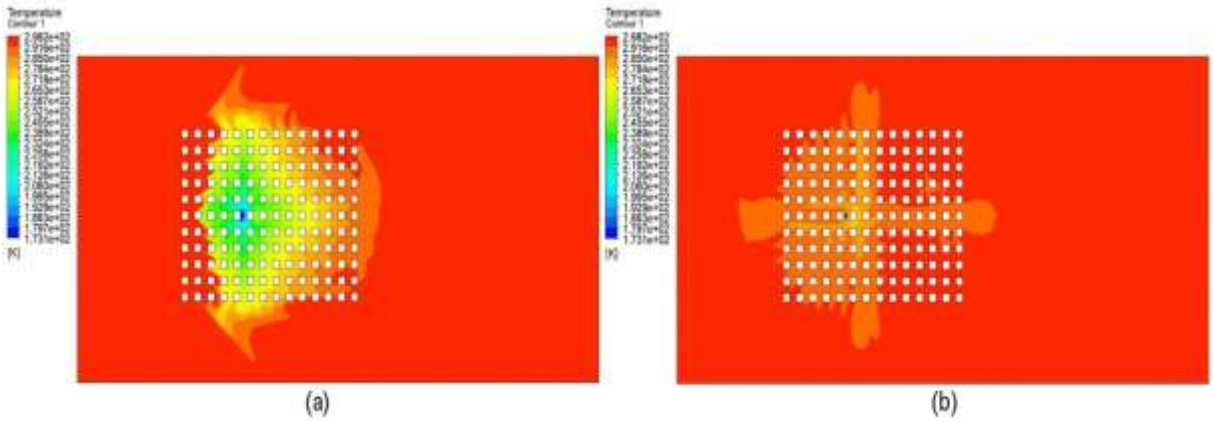

Figure 8.63: (a) *Temperature profile of the concentration profile of the Heavy Gas Dispersion for a collocated layout with the release source located at the upwind front of the group of buildings between the first and sixth rows in the sixth column at 1m/s.* ***(b)****At 0.25m/s*

Figure 8.63(a) for high speed and Figure 8.63(b) for low speed show the temperature simulation for this study. By visualising the temperature simulation, it is found out that it produces largely the same profile for the case study as that of the concentration profile. However, the behaviour of temperature is in fact the opposite to that of concentration. This means that the areas which were identified in the concentration simulation as highly concentrated will in fact have the lowest temperatures, the ones with moderate concentrations will have moderate temperatures and the least concentrated areas will have the highest temperatures. To further simply these findings, it should be pointed out that the simulations show that the concentrations near the release source point tend to be the highest and start to fade away as they move away from the source, and are the lowest as move much further away in the layout, eventually reaching the environment where the gas cloud disappears. However, the temperature is at its lowest near the release source point and tends to increase as it is that moves away from source and finally achieves its highest temperature, which is equal to the ambient temperature of the environment.

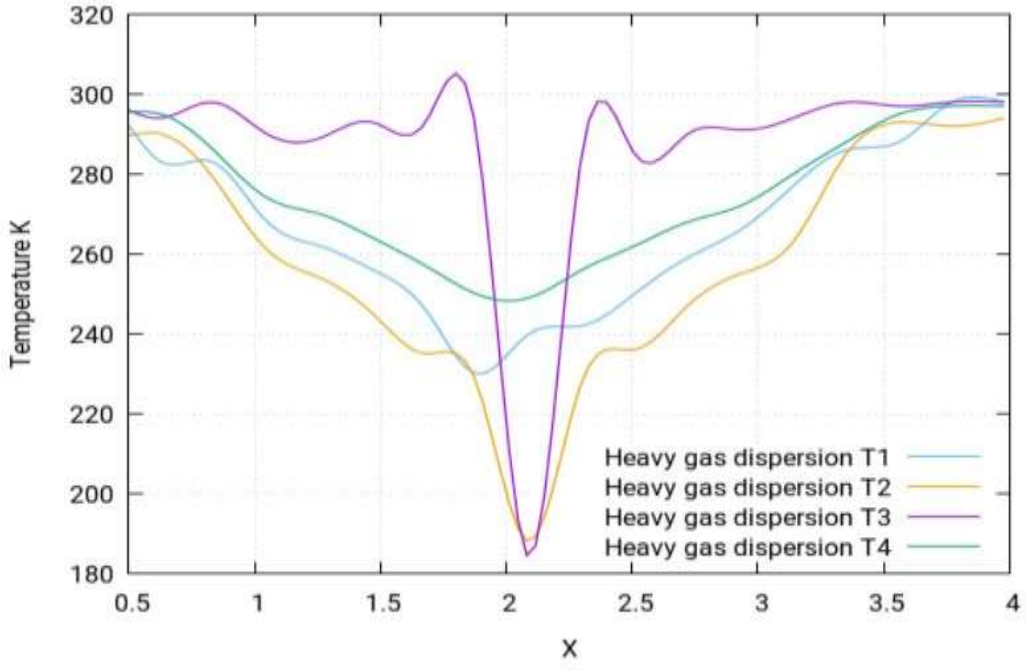

Figure 8.64: *Temperature of the heavy gas dispersion profile along the* ***y****-direction at* ***1m/s*** *different points of (T1) x=2.35m, y=-1m, z=7.20m, (T2) x=2.55m, y=-1m, z=7.20m, (T3) x=2.55m, y=-1m, z=9.84m (T4) x=2.95, y=-1m and z=7.20m*

Figure 8.64 (above) shows the concentration profiles for the gas dispersions at different locations along the y-direction at 1m/s wind speed depending on distance from release source.

The curves follow the same pattern but have different values. The lowest value of temperature is identified by the highest inverted peak at almost 2.1m.

8.6.7.6 Velocity of heavy gas dispersion at different velocities

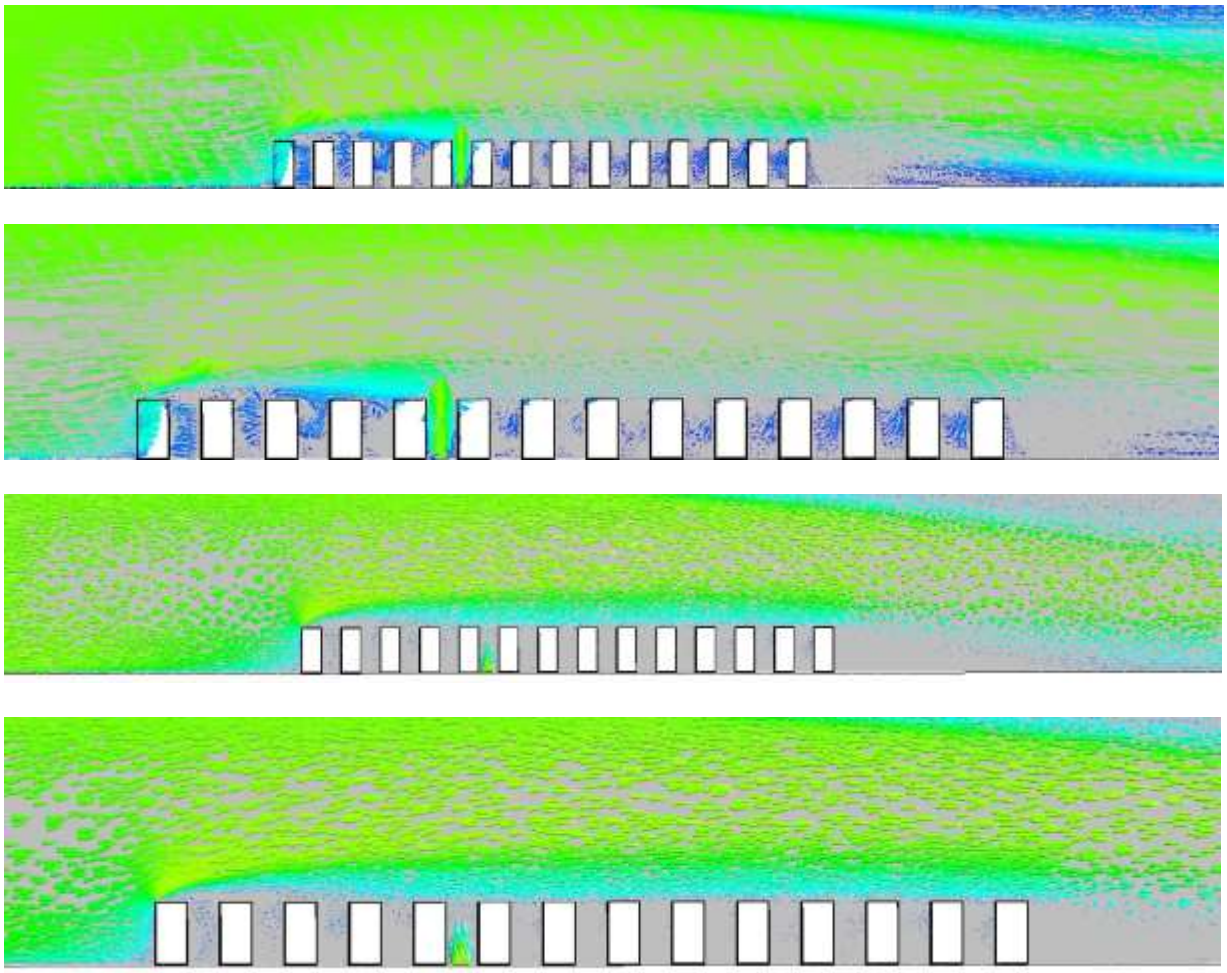

Figure 8.65: (a) *Velocity contours of the concentration profile of the Heavy Gas Dispersion for a collocated layout with the release source located at the upwind front of the group of buildings between the first and sixth rows in the sixth column at* ***1m/s***

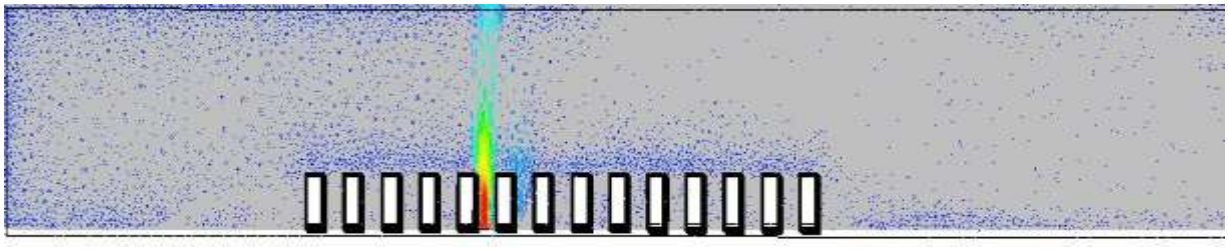

Figure 8.66: (b) *Velocity contours of the concentration profile of the Heavy Gas Dispersion for a collocated layout with the release source located at the upwind front of the group of buildings between the first and sixth rows in the sixth column at* ***0.25m/s***

The above figures show the velocity contours of heavy gas dispersion for this case study with the release source located at the upwind front of the group of buildings between first and sixth

rows in the sixth column. Velocity contours depict the intensity of wind - or the effective wind influence - at the different locations throughout the layout. As can be seen in the figure, the wind intensity is different at different points in the layout. It is a commonly known effect that, with enhanced altitudes, wind speeds increase. This is because the objects at the lower altitudes create resistance to the wind flow. As resistance is caused by the buildings in the flow of gas towards the direction opposite of wind, the wind flowing from left to right fails to indict the same motion of flow. Instead, various complex vertexes are formed within the buildings near the release source location, as can be seen in the above figures. The heavy gas released from the source is carried by these vertexes to the nearby mixture of the gas cloud, which then moves smoothly away from the source. Moreover, the hindrance in the wind flow caused by the buildings results in the vertexes moving in the upward direction, which enhances the shape of cloud in the upward direction.

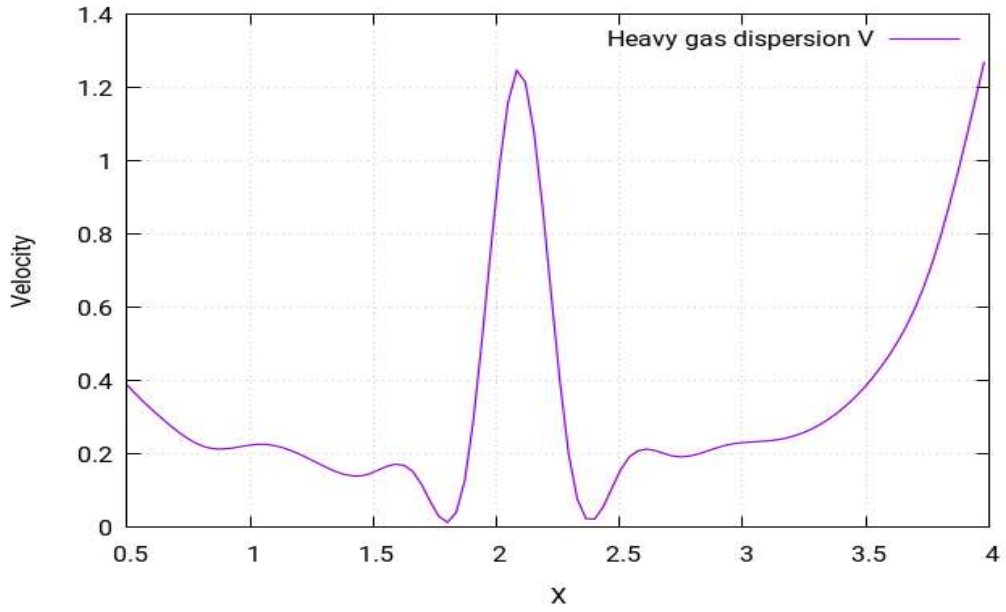

Figure 8.67: *The velocity of heavy gas dispersion profile along the* ***y****-direction at* ***0.25m/s*** *different points of x=2.55m, y=-1m, and z=2.05m*

The above figure shows the velocity profiles for the dispersion of heavy gas at 0.25m/s. The profile is an asymmetric curve with one big peak at almost 2m.

At a different location i.e., location no. 3, the effect of the release velocity of the gas on the dispersion is observed. The same results are observed as those obtained for other locations. In the case in which the velocity of the gas is high, the turbulence around the corners of the buildings is highest due to the no-slip boundary conditions and air resistance.

8.6.8 Location 3: Neutral gas dispersion at high and low velocity

8.6.8.1 Building layout

The type of layout adopted for these two case studies is a collocated layout. A layout of 154 buildings of cubic shape will be created as collocated layouts and the release source will be placed in same positions. The behaviour of the gas clouds will then be studied.

8.6.8.2 Release source location

Release source position (3) of the neutral gas dispersion in these case studies was placed in the 6^{th} row between the 5^{th} and 6^{th} columns. The perimeters selected for this case study are stated below:

Table 8.16: *(A) Parametric values of the neutral gas simulation at high velocity (location 3)*

Density	Flow Rate	Velocity	Ambient Temperature	Release Source Temperature
1.1839 kg m/s^3	1.7737 kg/s	1 m/s	25°C	25°C

Table 8.17: *(B) Parametric values of the neutral gas simulation at low velocity (location 3)*

Density	Flow Rate	Velocity	Ambient Temperature	Release Source Temperature
1.1839 kg m/s^3	1.7737 kg/s	0.25 m/s	25°C	25°C

8.6.8.3 Concentration of the neutral gas dispersion at different velocities

The following two figures show the concentration behaviour of the neutral gas at location 3. The whereabouts of location 3 has been stated at the beginning of the passage.

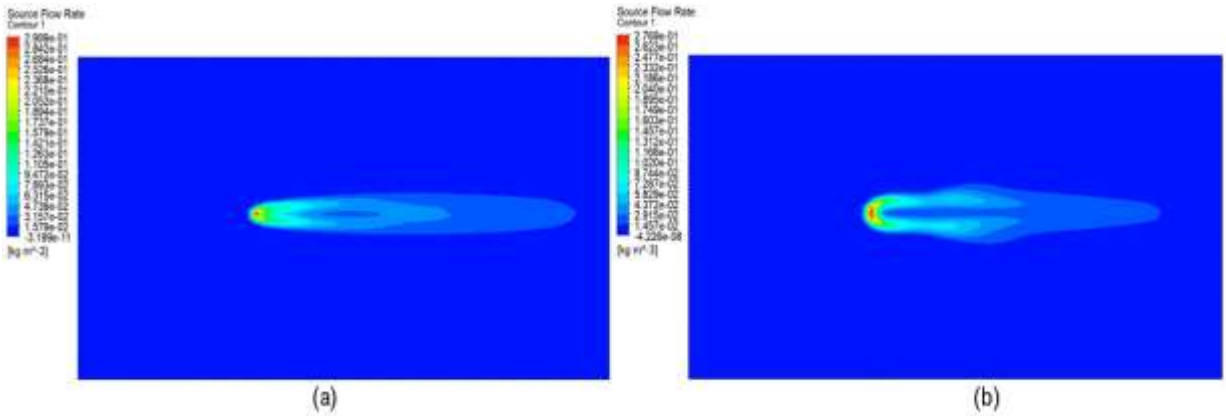

Figure 8.68: (a) *Concentration profile of the neutral gas dispersion for a/the collocated layout the with the release source located at the upwind front of the group of buildings between the fifth and sixth rows in the sixth column at 1m/s.* ***(b)*** *At 0.25m/***s**

8.6.8.4 Iso-surface of the neutral gas dispersion at different velocities

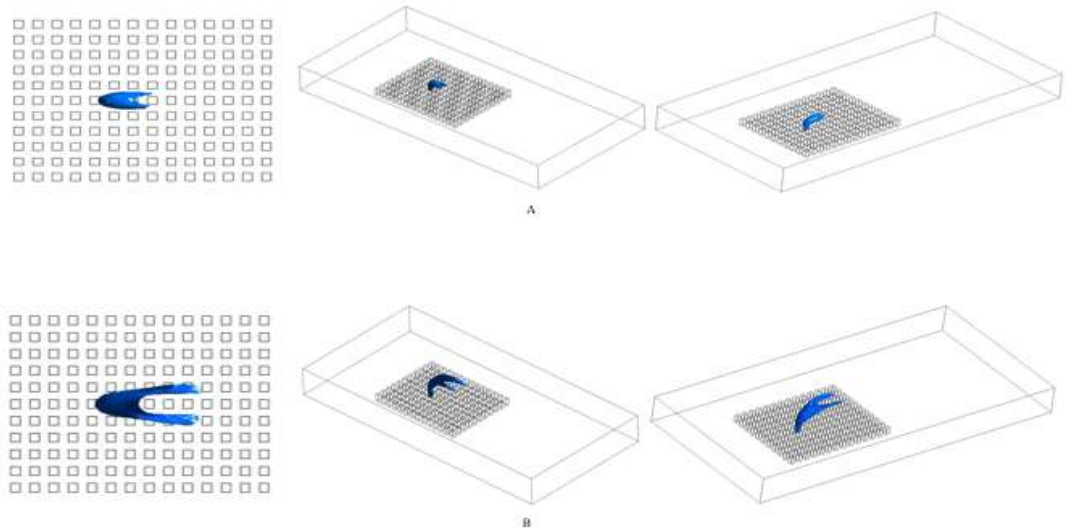

Figure 8.69: (a) *Iso-surfaces of the concentration profile of the Neutral Gas Dispersion for a collocated layout with the release source located at the upwind front of the group of buildings between the fifth and sixth rows in the sixth column at 1m/s.* ***(b)*** *At 0.25m/s*

For Figures 8.69(a) and 8.69(b), the planar distance is increased to observe the dispersion of the neutral gas. This is because the dispersion of the neutral gas is in the upward direction, in contrast to the heavy gas dispersion. The concentration profile of the neutral gas at location 3 has been shown in Figure 8.69(a) and Figure 8.69(b) (both above). The figures represent the concentration behaviour of the neutral gas when the release gas source is placed at the upwind front of the group of buildings between the fifth and sixth rows in the sixth column. In both figures, the plane distance from the ground floor up has been increased to visualise the shape of the neutral gas. It was noticed that it was going up not spreading at ground level like the heavy gas. The neutral gas shape appears in both figures as one peak or a single bubble.

In the two figures above 8.69(a) and 8.69(b), parts labelled (A) are at a high speed and those labelled (B) are at a low speed. Similar to the case of heavy gas, these simulations show that, for this particular setting of the perimeters and the release source location, the gas cloud takes the shape of the cloud, which resembles that of case study 1 i.e., location 1 of the release source. The resemblance is again extremely similar to the case of location 1 and the cloud has shifted towards the horizontal side or, perhaps more accurately, it has leaned forward towards the right side. The shifting of release source towards the right side can be said to have shifted the cloud in the same direction. The spread of the cloud in other directions also resembles that of location 1.

According to Standard BS EN 60079-10-1:2009 [104], the following locations can be categorised:

Zone 0: The central middle front of the building layout from the 5th to 8th row

Zone 1: The immediate surrounding of the building layout and areas categorised in zone 0

Zone 2: All the remaining locations not categorised in zone 0 or zone 1

.

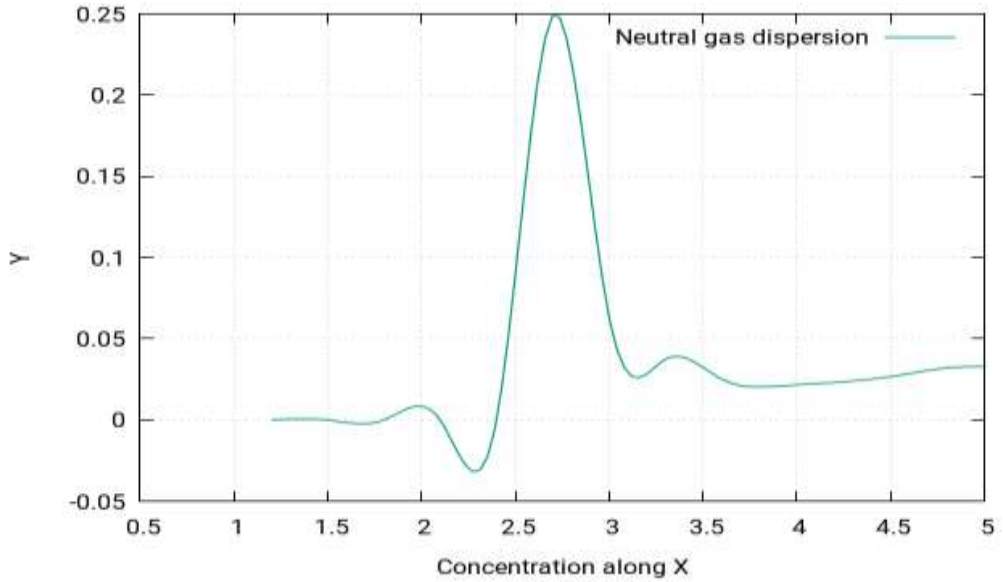

Figure 8.70: *Concentration of the neutral gas dispersion profile along the* ***x****-direction at* ***1m/s*** *at different points of x=1.20m, y=2.05m, and z=3.49m*

The above figure shows the velocity concentration profile curve for this case study along the x-direction at 1m/s. The profile shows asymmetric behaviour along the horizontal unlike the previous cases.

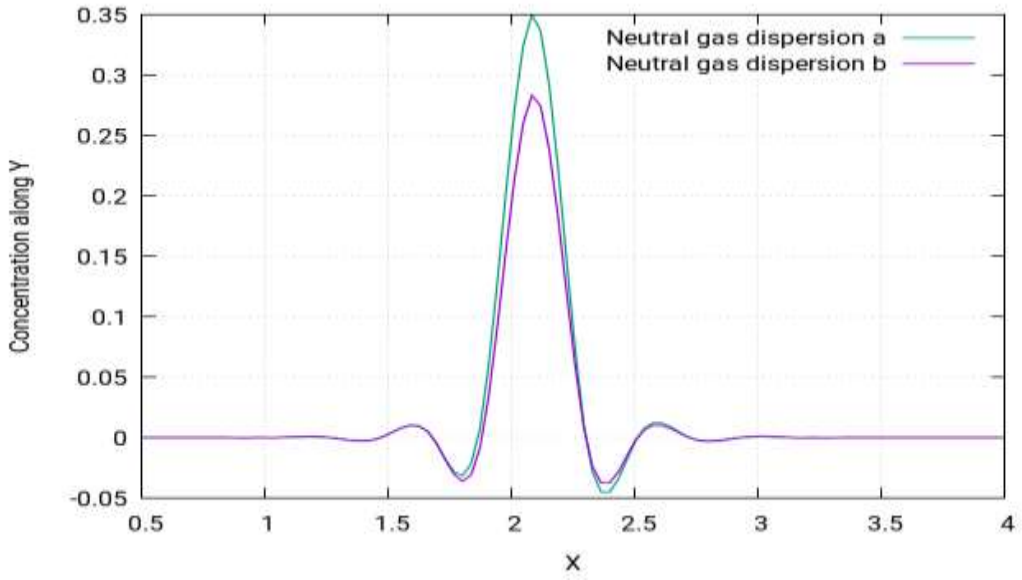

Figure 8.71: *Concentration of the neutral gas dispersion profile along the* ***y****-direction at* ***0.25m/s*** *at different points of (a) x=2.62m, y=-1m, z=4.40m (b) x=2.55m, y=-1m and, z=2.20m*

In Figure 8.71 (above), two different curves for the concentration profiles are shown. They show the pattern of the concentration profile along the y-direction when the wind speed for the simulation is 0.25m/s. The two different curves are obtained for two different distances from the release source. The profiles show somewhat symmetric behaviour in this case. This is probably because the lower wind speed of 0.25m/s does not make as much impact as that of a wind speed of 1m/s.

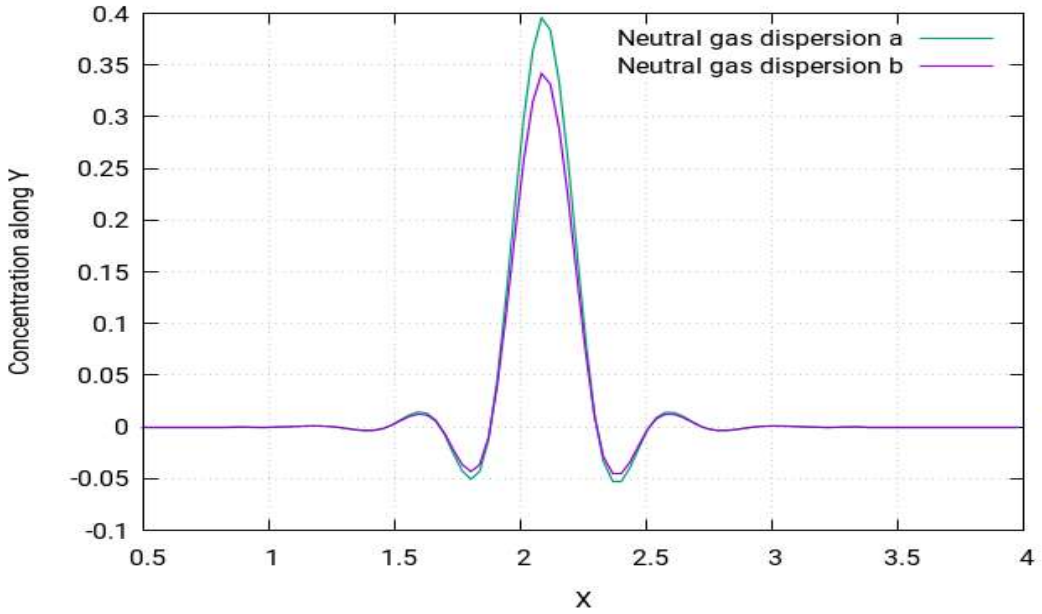

Figure 8.72: *Concentration of the neutral gas dispersion profile along the* ***y****-direction at* ***1m/s*** *at different points of (a) x=2.55m, y=-1m, z=2.20m (b)x=2.63m, y=-1m and, z=2.88m*

The above figure shows the velocity profiles for the gas dispersion at two different locations depending on distance from release source. Both the curves follow the same pattern of symmetric behaviour but have different values.

8.6.8.5 Velocity of the neutral gas dispersion at different velocities

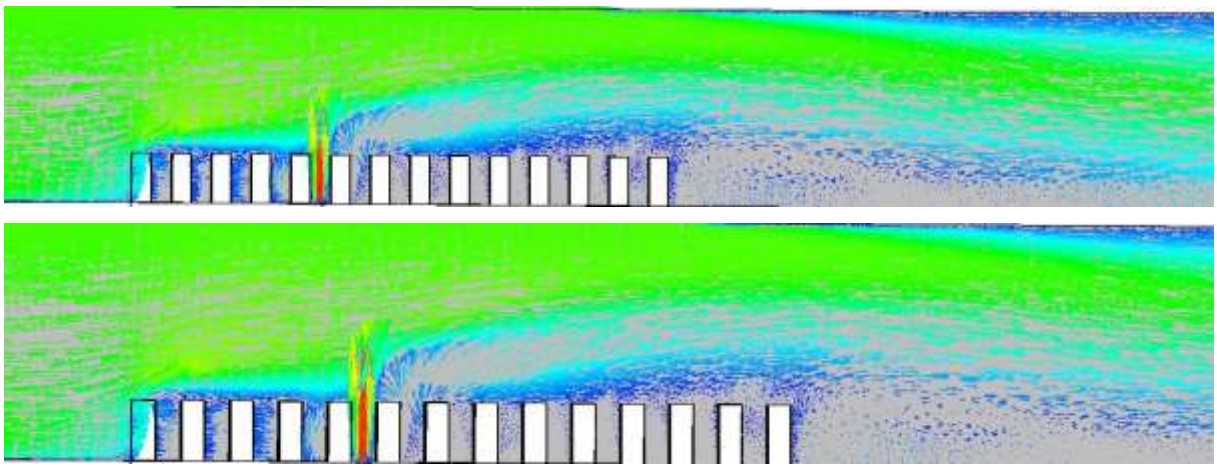

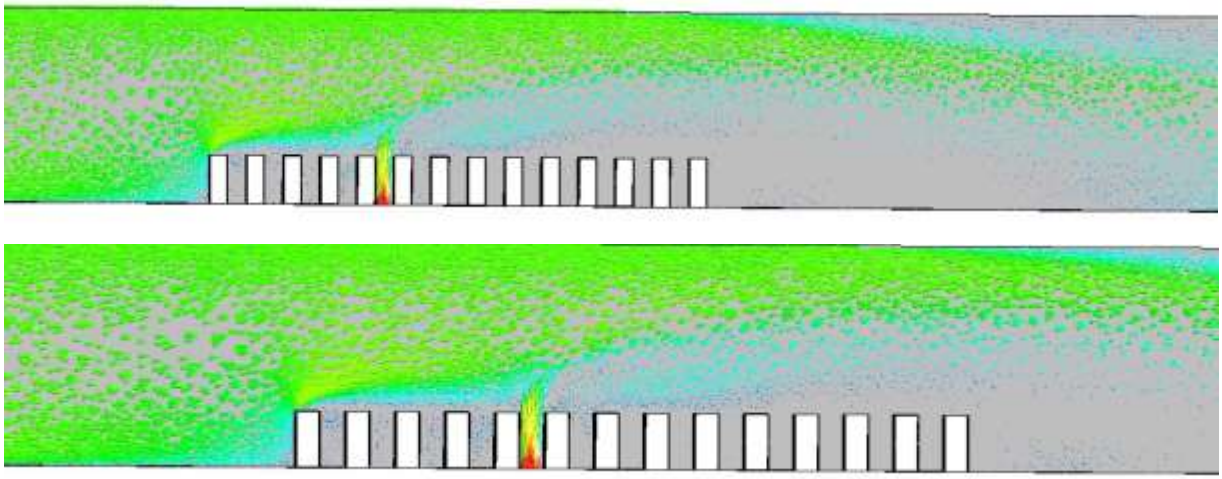

Figure 8.73: (a) *Velocity contours of the Neutral Gas Dispersion for a collocated layout with the release source located at the upwind front of the group of buildings between the fifth and sixth rows in the sixth column at* ***1m/s***

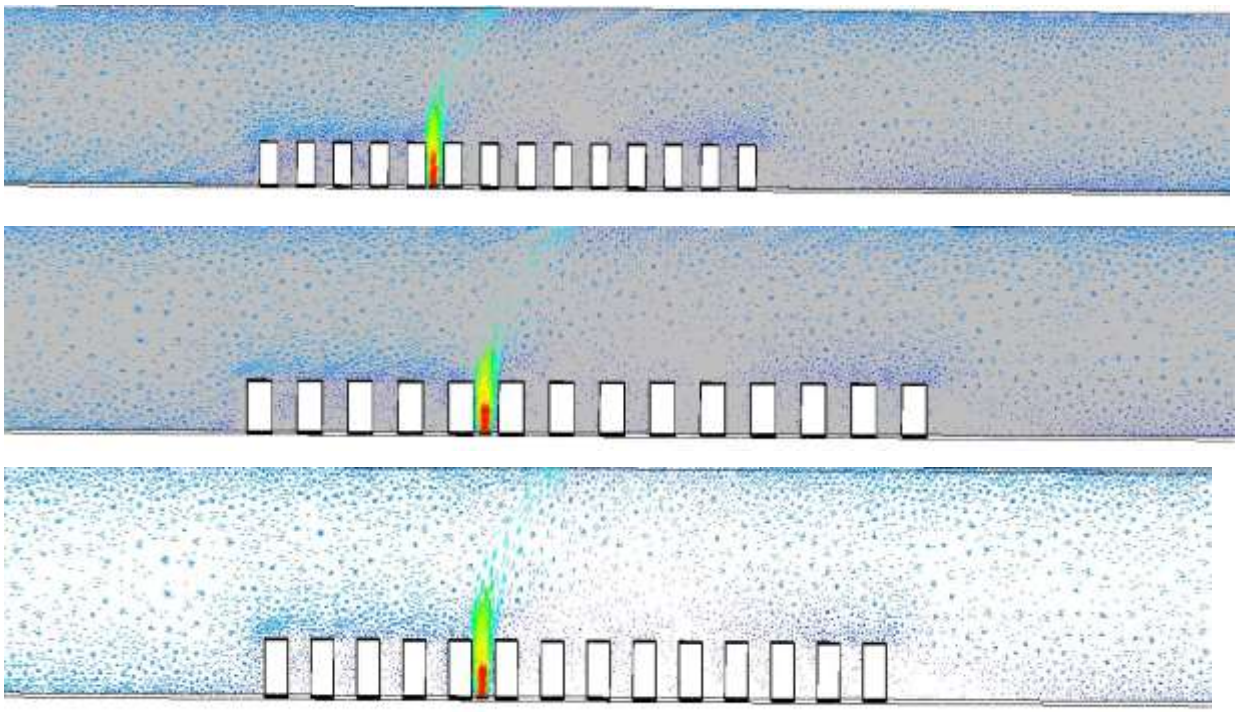

Figure 8.74: (b) *Velocity contours of the Neutral Gas Dispersion for a collocated layout with the release source located at the upwind front of the group of buildings between the fifth and sixth rows in the sixth column at* ***0.25m/s***

The above figures show the velocity contours of neutral gas dispersion for this case study with the release source located at the upwind front of the group of buildings between the fifth and sixth rows in the sixth column at both 1m/s and 0.25m/s. Velocity contours depict the intensity of wind - or the effective wind influence - at the different locations throughout the layout. In the figure, red represents the maximum velocity of 1m/s and blue is for zero velocity. Similar to previous cases, a large cloud of red can be seen at the release source, showing that there are many complex vertexes of maximum velocity being formed near the release source. It can be

noticed that, immediately after the heavy red portion near the release source in the building layout, there is continuous blue in the rest of the building layout. This proves that, when the neutral gas was released from the source, the heavy gas created complex vertexes of the maximum velocity near the release source. These vertexes carried the neutral gas towards the upward direction due to the density of the neutral gas being lower than the ambient air. As a result, the neutral gas flew over the building layout, rather than within it. Therefore, a continuous blue portion can be seen in the building layout after the release source, showing the void left behind, representing zero velocities by the blue colour of the velocity contours.

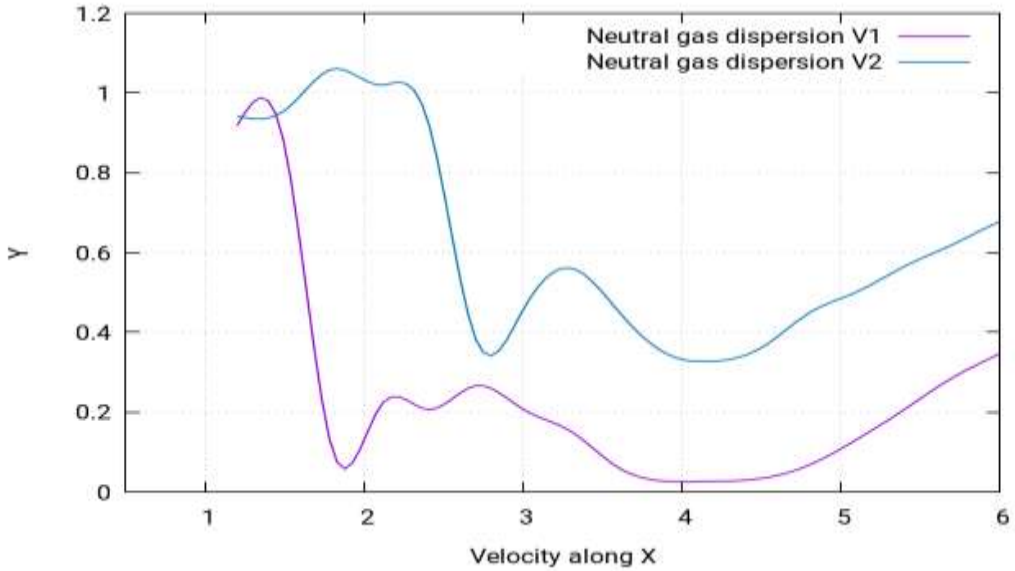

Figure 8.75: *Velocity of neutral gas dispersion profile along the* ***x****-direction at* ***1m/s*** *different points of (V1) x=1.20m, y=2.05m, z=2.20m (V2) x=1.20m, y=2.05m, and z=3.49m*

The above figure shows the velocity profiles for the gas dispersion along the x-direction at two different locations depending on distance from release source. The curves show somewhat different patterns, unlike previous cases where they showed the same pattern but difference in values.

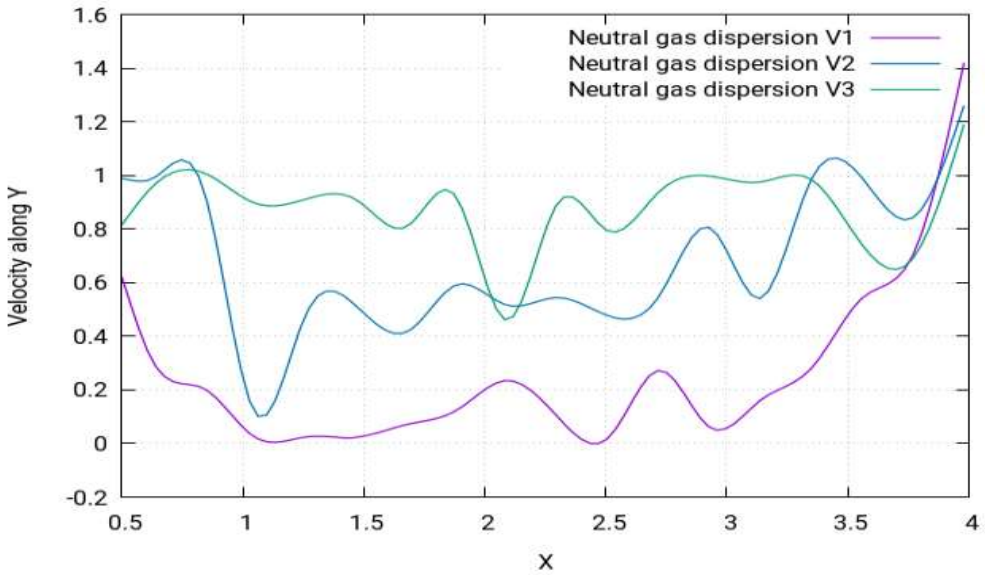

Figure 8.76: *Velocity of the neutral gas dispersion profile along the* ***y****-direction at* ***1m/s*** *at different points of (V1) x=2.55m, y=-1m, z=7.20m (V2) x=2.55m, y=-1m, z=2.20m (V3) x=2.63m, y=-1m and, z=2.88m*

Figure 8.76 shows the curves for the velocity profile along the y-direction. The curves follow a slightly dissimilar and asymmetrical pattern. There are several peaks with the highest peak, being at approximately 3.5m. As the neutral gas moves upward, the concertation of the gas decreases along with the increase in the density of the air. The combined effect of these two factors causes the abnormal behaviour of the neutral gas velocity.

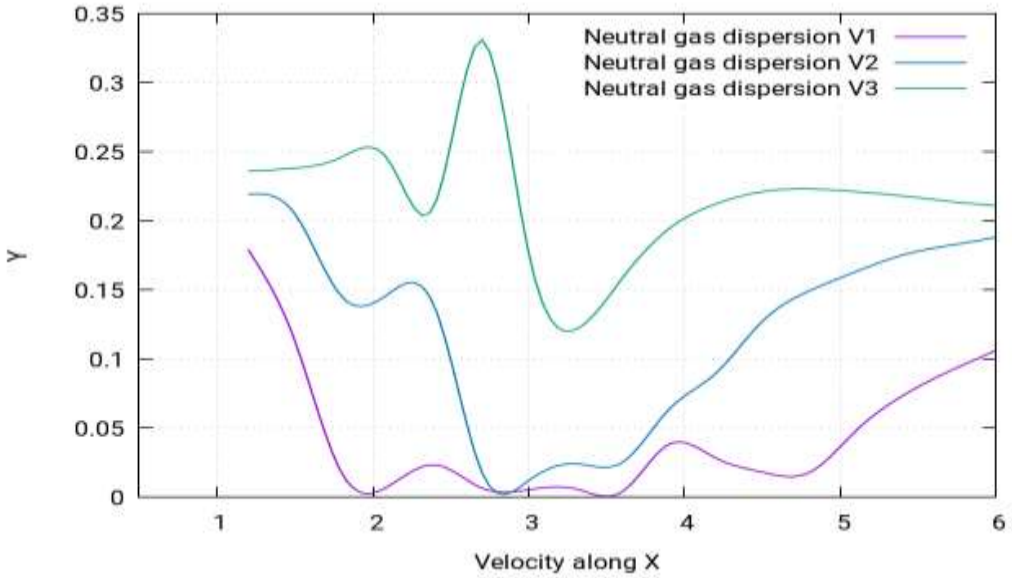

Figure 8.77: *Velocity of the neutral gas dispersion profile along the* ***x****-direction with a low velocity of* ***0.25 m/s*** *at different points of (V1) x=1.20m, y=2.05m, z=7.20m (V2) x=1.20m, y=2.05m and z=2.20m*

Figure 8.77 shows the velocity profiles for the gas dispersion along the x-direction at three different locations depending on distance from release source. The curves show somewhat

different patterns, unlike previous cases where they showed the same pattern but had differences in values.

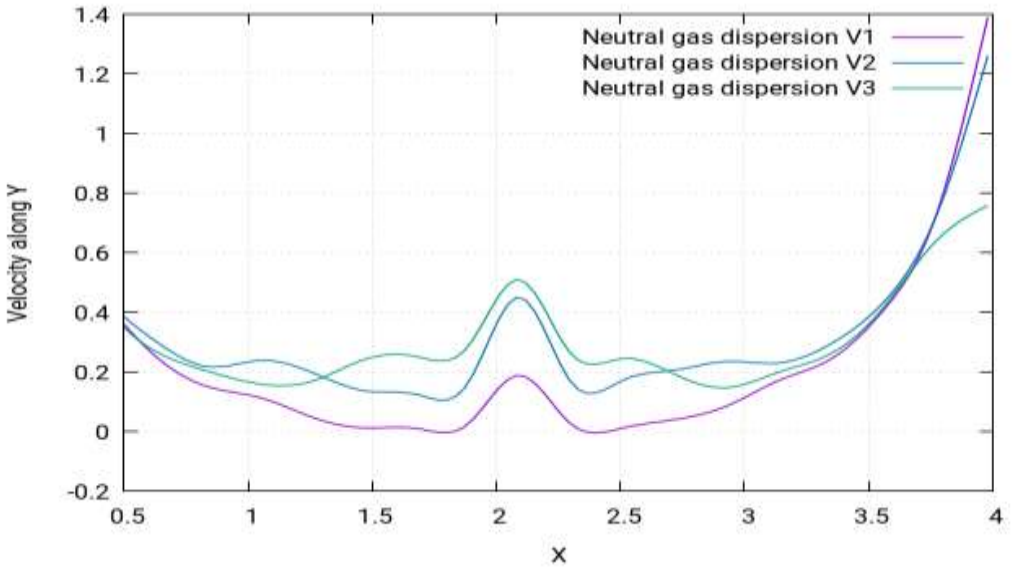

Figure 8.78: *Velocity of the neutral gas dispersion profile along the* ***y****-direction with a low velocity of* ***0.25 m/s*** *at different points of (V1) x=2.55m, y=-1m, z=7.20m, (V2) x=2.55m, y=-1m, z=2.20m (V3) x=2.62m, y=-1m and z=4.40m*

Figure 8.78 shows the velocity profiles for the gas dispersion along the x-direction at three different locations depending on distance from release source. The curves show a somewhat similar pattern. For location 3, the dispersion of the neutral gas is observed for different velocities. It is evident from the results that the horizontal distribution is greater for the neutral gas, which is released at high velocity because of the turbulence, but the upward dispersion is reduced. This is because the neutral gas is now more inclined towards the x-direction instead of the upward direction.

8.6.9 Location 1: Heavy gas dispersion at high and low velocity

8.6.9.1 Building layout

The type of layout undertaken for these two case studies is a staggered layout. A layout of 154 buildings of cubic shape will be created as a staggered layout and the release source will be placed in the same positions. The behaviour of the gas clouds will then be studied.

8.6.9.2 Release source location

The release source location (1) of the heavy gas dispersion in these case studies was at the upwind front of the group of buildings in the middle between the sixth and seventh rows. The perimeters selected for this case study are stated below:

Table 8.18: *(A) Parametric values of the heavy gas simulation at high velocity (location 1)*

Density	Flow Rate	Velocity	Ambient Temperature	Release Source Temperature
2.1 kg m/s^3	1 kg/s	1 m/s	25°C	-100°C

Table 8.19: *(B) Parametric values of the heavy has simulation at low velocity (location 1)*

Density	Flow Rate	Velocity	Ambient Temperature	Release Source Temperature
2.1 kg m/s^3	5 kg/s	0.25 m/s	25°C	-100°C

8.6.9.3 Concentration of heavy gas dispersion at different velocities

The following two figures show the concentration behaviour of the heavy gas at location 1 for staggered layouts. The whereabouts of location 1 has been stated at the beginning of the passage.

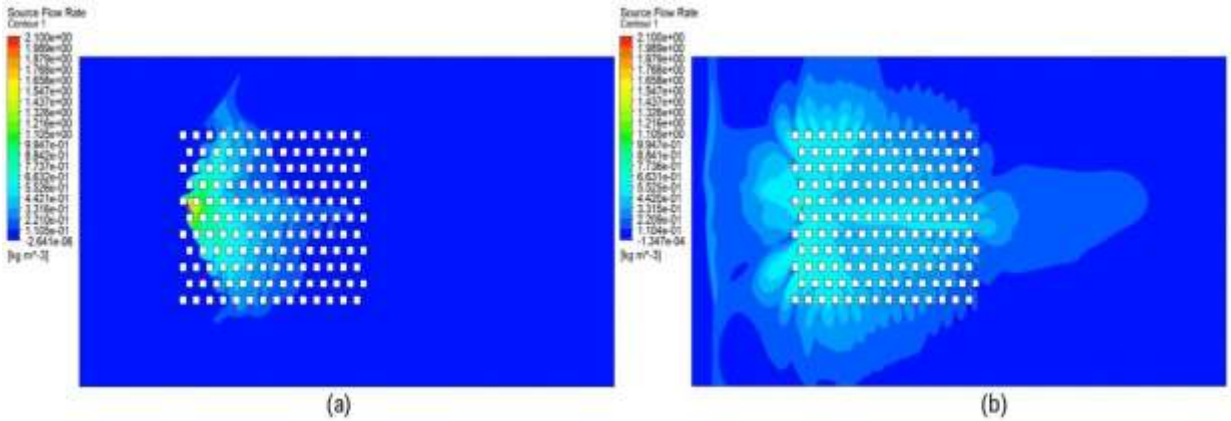

Figure 8.79: (a) *Concentration profile of the heavy gas dispersion for a/the staggered layout with the release source located in the middle between the sixth and seventh rows at 1m/s.* ***(b)*** *At 0.25m/s*

The concentration profile of the heavy gas at location 1 for a/the staggered layout is shown in Figures 8.79(a) and 8.79(b) (both above). These figures represent the concentration behaviour of the heavy gas when the release gas source is placed between the first and the second column in the middle between the 5th and 6th rows. In the above two figures, parts labelled (a) are at high speed, while those labelled (b) are at low speed. The same study was also performed for collocated layouts under the same parameters and release source location. The cloud shape for this particular study has been discussed in collocated sections of these results (refer to location 2 in collocated layouts). The simulations show that the release source is exposed to the air, which affects the gas coming out of the release source directly. As a result, the gas cloud adopts a more spread pattern, unlike if the gas source was not exposed to the air. The change of location has affected the cloud shape in such a way that, at high speeds, it now makes an

extended knobhead in the horizontal direction, creeping out of the last column of the layout, as shown in Figure 8.79(a). The same was also observed for collocated layouts; however, in this case, the head of the cloud in the horizontal portion has faded away due to the change in the layout. Moreover, in the collocated layout, the cloud shape had a certain symmetry, which cannot be observed in the present case of the staggered layout. Moreover, the cloud shape in the collocated layout crept out of the last column, while no such observation can be made from Figure 8.79(a). The affect is more extended at a low speed of 0.25m/s, as shown in Figure 8.79(b). The same was observed in collocated layouts, but it can be seen here that there are some differences between the cloud shapes in collocated and staggered layouts. The cloud shape in the collocated layout showed a showed a more spread-out concentration in the entire middle front of the layout, while in the case of staggered layouts, the high concentrations point march across the central rows of the layout.

8.6.9.4 Iso-surface of heavy gas dispersion at different velocities

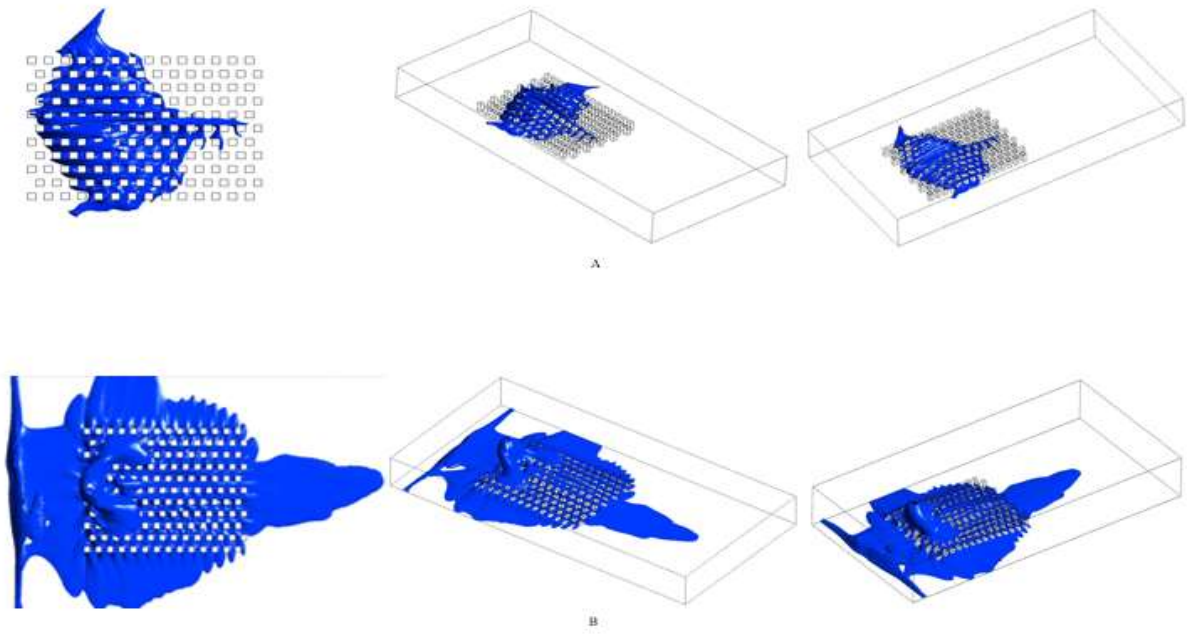

Figure 8.80: (a) *Iso-surfaces of the concentration profile of the heavy gas dispersion for a/the staggered layout with the release source located between the sixth and seventh rows at 1m/s and* ***(b)*** *At 0.25m/s*

In Figures 8.80(a) and 8.80(b), the iso-surfaces can be seen for the concentration profile of heavy gas dispersion for a staggered layout with the release source located at the upwind front of the group of buildings between the first and second columns in the middle between the fifth and sixth rows at both low and high speeds. It can be said that, at low speed, the shape of cloud changes by a scale of approximately three.

According to Standard BS EN 60079-10-1:2009 [104], the following locations can be categorised:

High speed:

Zone 0: The upwind front of the building block right up to 3 to 4 columns excluding the triangular shape of buildings in the initial few columns

Zone 1: The right middle front of the building layout and a third size of the same on the opposite side with some building in the immediate front of the central rows

Zone 2: All the remaining locations not categorised in zone 0 or zone 1.

Low speed:

Zone 0: The immediate c-shaped area of the release source covering two to three columns and the central rows

Zone 1: All the areas not categorised in zone 0, including the immediate surroundings of the building layout

Zone 2: All the remaining locations not categorised in zone 0 or zone 1

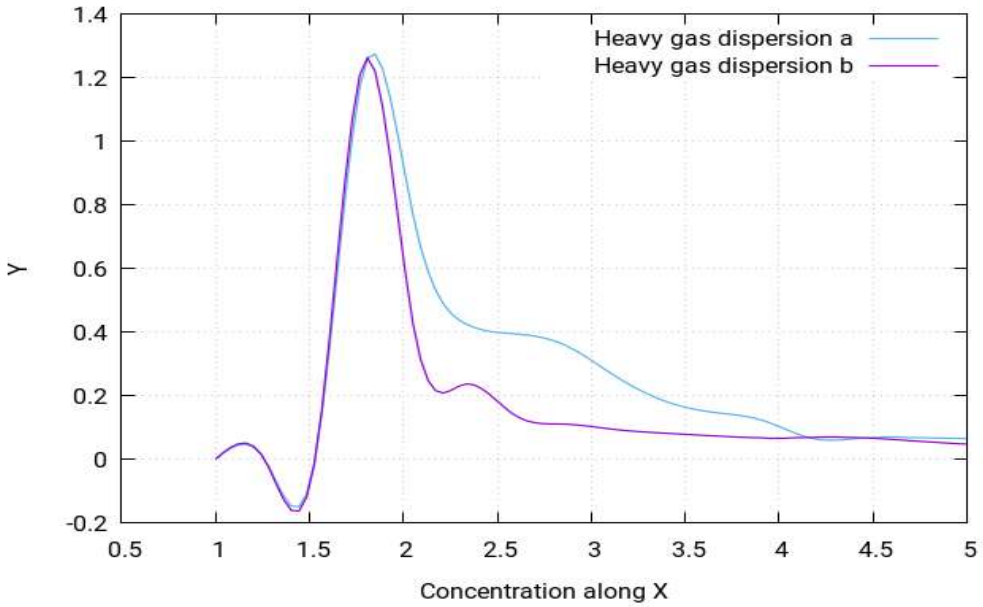

Figure 8.81: *Concentration of the heavy gas dispersion profile along the **x**-direction at **1m/s** different points of (a) x=1m, y=2.16m, z=7.20m (b) x=1m, y=1.16m and z=9.84m*

In Figure 8.81 (above), two different curves for the concentration profiles are shown. They show the pattern of the concentration profile along the x-direction when the wind speed for the simulation is 1m/s. The two different curves are obtained for two different distances from the release source. Both curves follow the same pattern but have different values due to differences in distances. From the figure, it can be concluded that the concentration value of the heavy gas

decreases as it moves away from the source. In the figure, the curve with the highest peak is obtained when nearest the release source and vice versa.

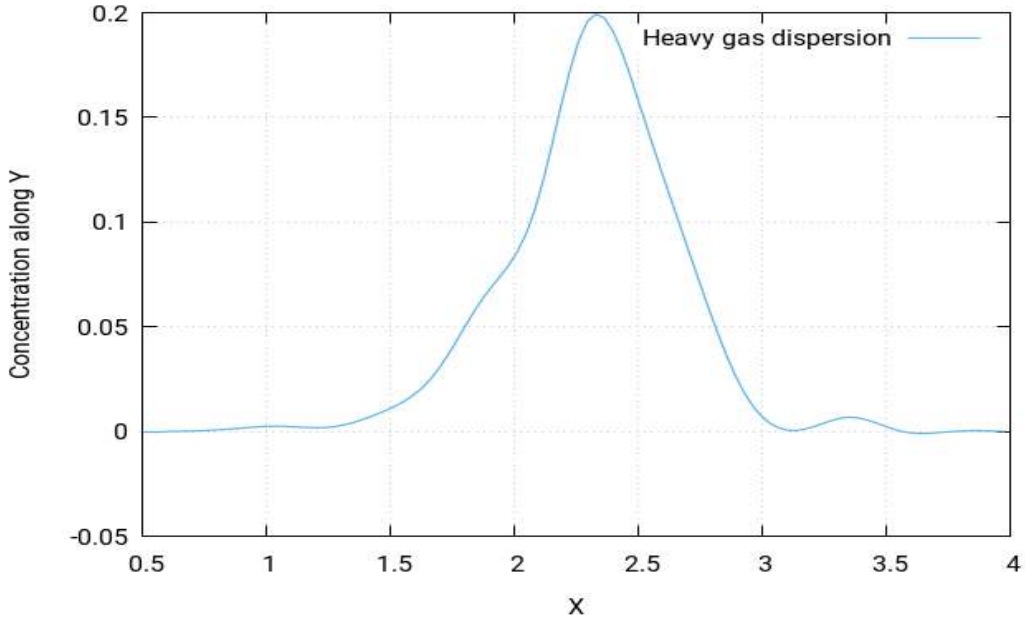

Figure 8.82: *Concentration of heavy gas dispersion profile along the **y**-direction at **1m/s** different points of (a) x=2.25m, y=-1m and z=2.10m*

The above figure shows the concentration profile for the gas dispersions along the y-direction at 1m/s. It can be seen that the curve here follows the pattern of a simple gaussian curve.

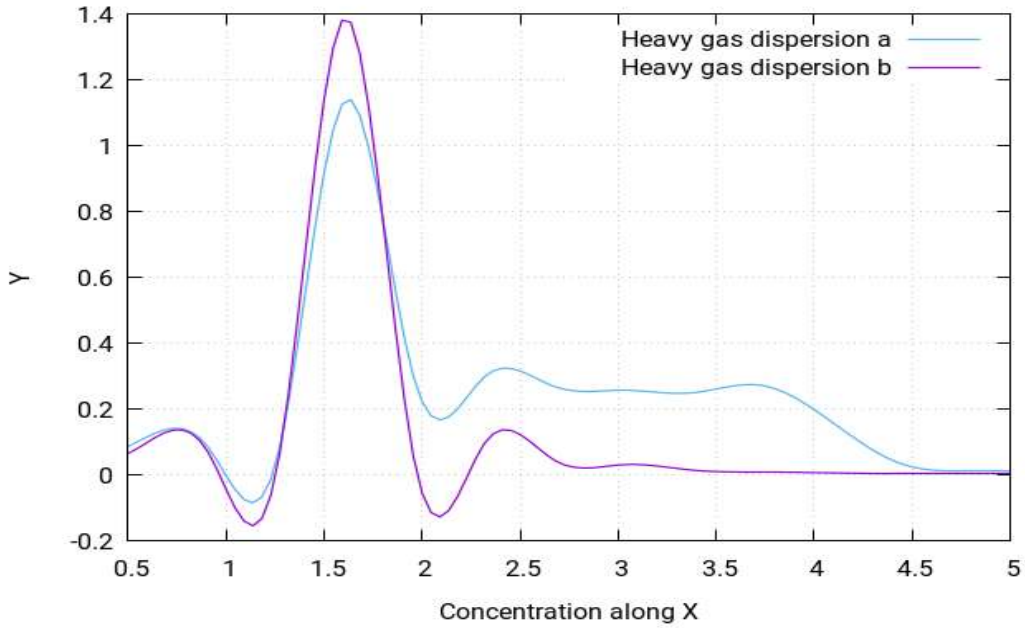

Figure 8.83: *Concentration of the heavy gas dispersion profile along the **x**-direction at **0.25m/s** different points of (a) x=2m, y=2.16m and z=9.84m, and (b) x=2m, y=1.16m and z=2.88m*

The above figure shows the concentration profiles for two of the gas dispersions at two different locations along the x-direction at a wind speed of 0.25m/s depending on distance from release source. Both curves follow the same pattern but have different values.

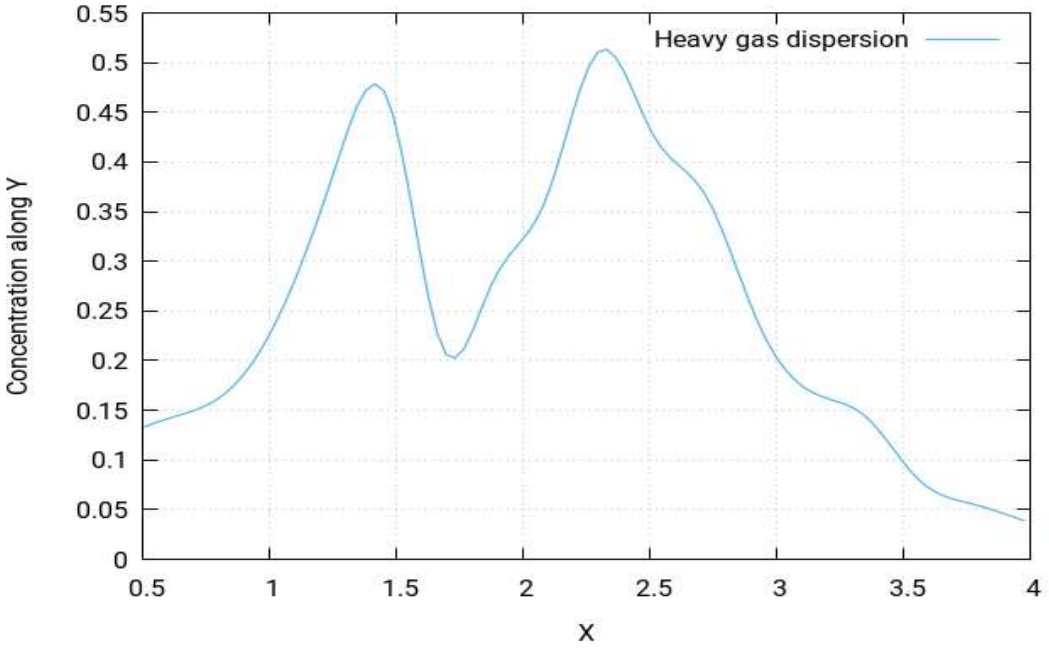

Figure 8.84: *Concentration of the heavy gas dispersion profile along the* ***y****-direction at* ***0.25m/s*** *points of x=1.22m, y=-1m and z=7.20m*

The above figure shows the concentration profile for the gas dispersions along the y-direction at 0.25m/s. It can be seen that the curve here has two peaks compared to a single peak for the dispersion at 1m/s. The curve is also asymmetrical.

8.6.9.5 Temperature of heavy gas dispersion at different velocities

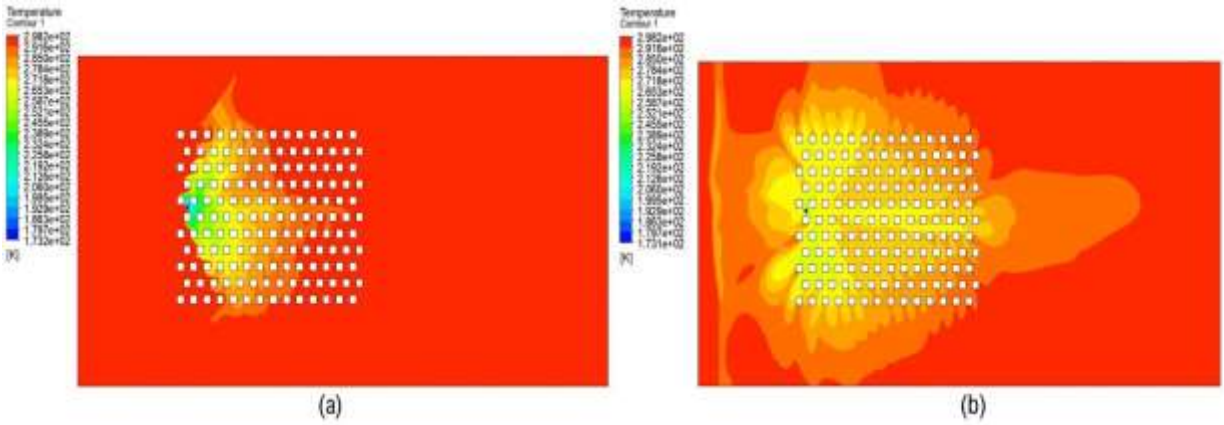

Figure 8.85: (a) *Temperature profile of the heavy gas dispersion for a/the staggered layout with the release source located between the sixth and seventh rows at 1m/s.* ***(b)*** *At 0.25m/s*

Figure 8.85(a) for high speed and Figure 8.85(b) for low speed (both above) show the temperature simulation for the present study. By visualising the temperature simulation, it is

found out that the temperature simulation produces largely the same profile for the case study as that of the concentration profile. However, the behaviour of temperature is in fact the opposite to that of concentration. This means that the areas which were identified in the concentration simulation as being highly concentrated will in fact have the lowest temperatures, while the ones with moderate concentrations will have moderate temperatures and the least concentrated areas will have the highest temperatures. To further simply these findings, it should be pointed out that the simulations show that the concentrations near the release source point tend to be the highest and start to fade away as they move away from the source and are at their lowest as they move much further away in the layout, eventually reaching the environment where the gas cloud disappears. However, the temperature is at its lowest near the release source point and tends to increase as it moves away from source and finally achieves its highest temperature equal to the ambient temperature of the environment. Figure 8.85(a) for high speed and Figure 8.85(b) (both above) have been added in order to depict this temperature behaviour.

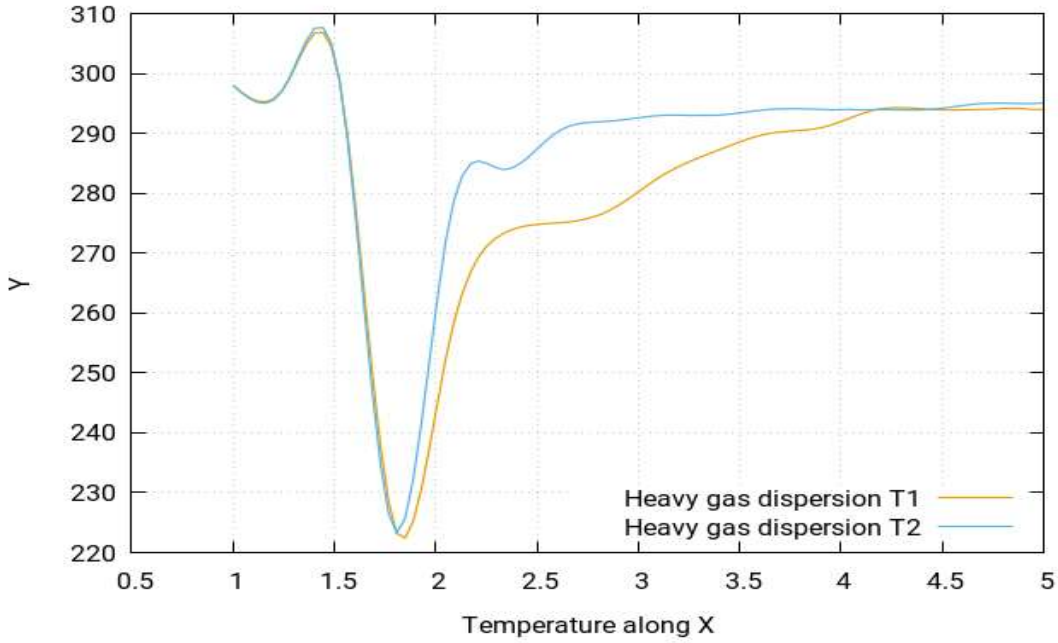

Figure 8.86: *Temperature of the heavy gas dispersion profile along the* ***x****-direction at* ***1m/s at*** *different points of (T1) x=1m, y=2.16m, z=7.20m (T2) x=1m, y=2.16m and z=9.84m*

In Figure 8.86, two different curves for the temperature profiles are shown. They show the pattern of the temperature profile along the x-direction when the wind speed for the simulation is 1m/s. The two different curves are obtained for two different distances from the release source. These results show that at speed of 1m/s, temperature profiles are a mirror of the concentration profile.

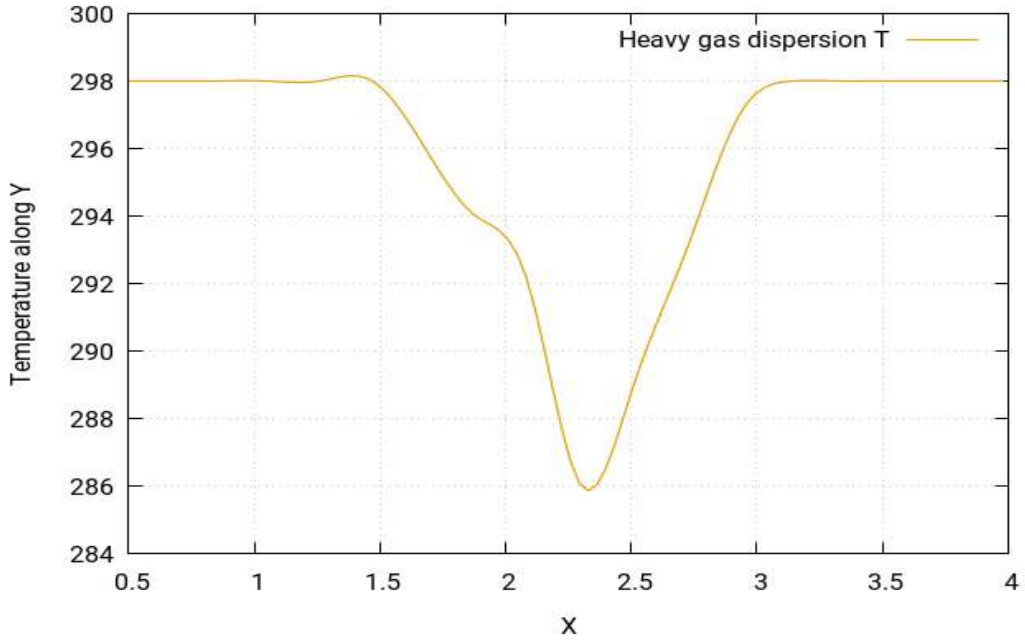

Figure 8.87: *Temperature of the heavy gas dispersion profile along the* ***y****-direction at* ***1m/s*** *points of (T)x=2.25m, y=-1m and z=2.10m*

Figure 8.87 shows the curve for temperature profile along the y-direction at 1m/s. The curve follows a symmetrical pattern and has a single inverted peak at almost 2.3m.

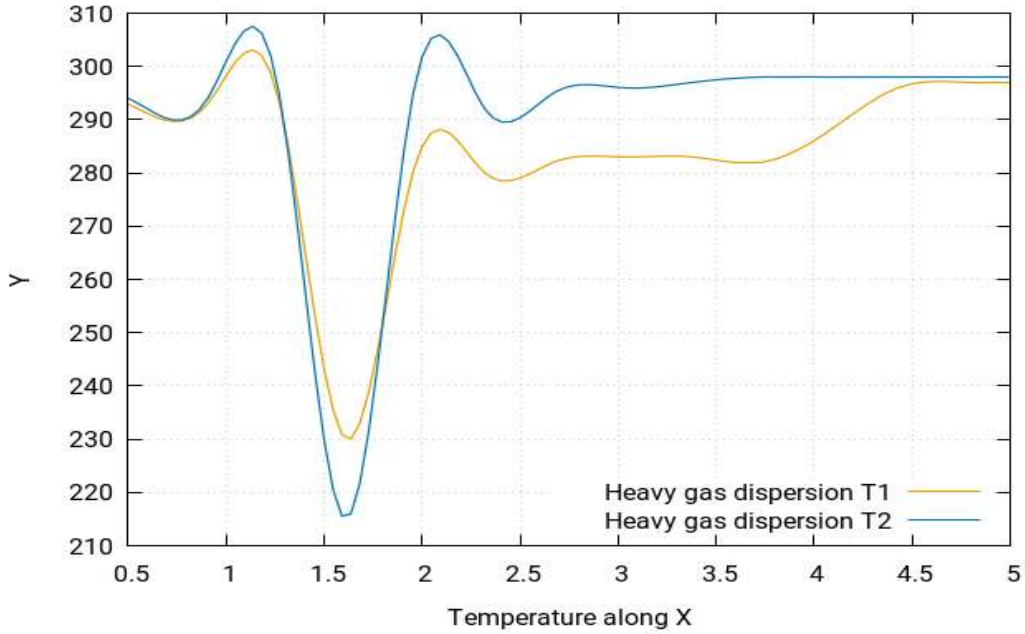

Figure 8.88: *Temperature of the heavy gas dispersion profile along the* ***x****-direction at* ***0.25m/s*** *different points of (T1) x=2m, y=2.16m and z=9.84m (T2) x=2m, y=2.16m and z=2.88m*

The above figure shows the temperature profiles for two of the gas dispersions at two different locations along the x-direction at a 0.25m/s wind speed depending on distance from release source. Both curves follow the same pattern but have different values.

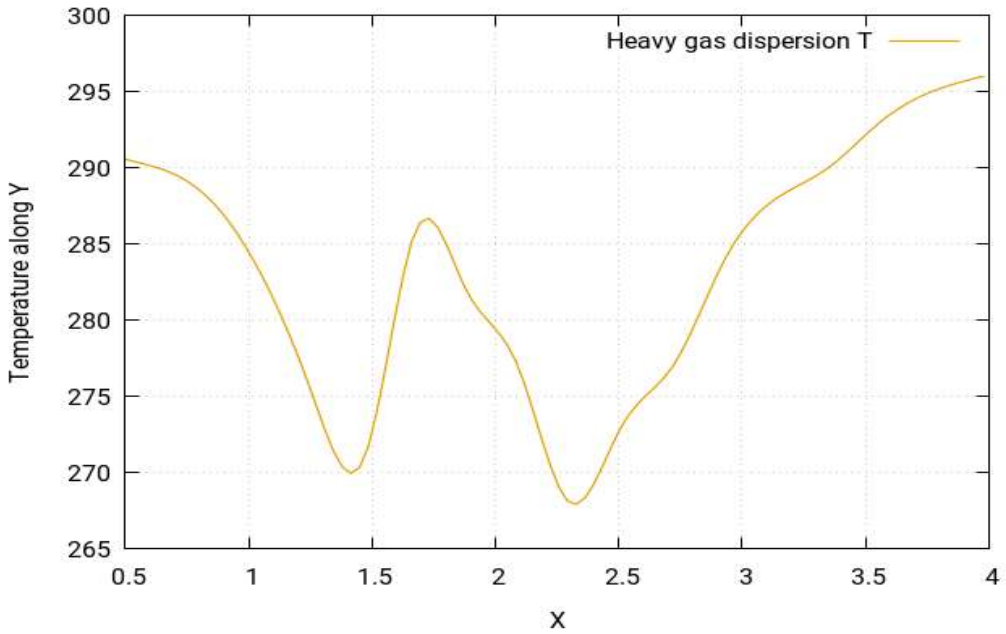

Figure 8.89: *Temperature of the heavy gas dispersion profile along the* ***y****-direction at* ***0.25m/s*** *points of (T)x=1.22m, y=-1m and z=7.20m*

Figure 8.89 shows the curve for the temperature profile along the y-direction at 0.25m/s. The curve follows an asymmetrical pattern and has two peaks, with the highest peak at almost 2.3m.

8.6.9.6 Velocity of heavy gas dispersion at different velocities

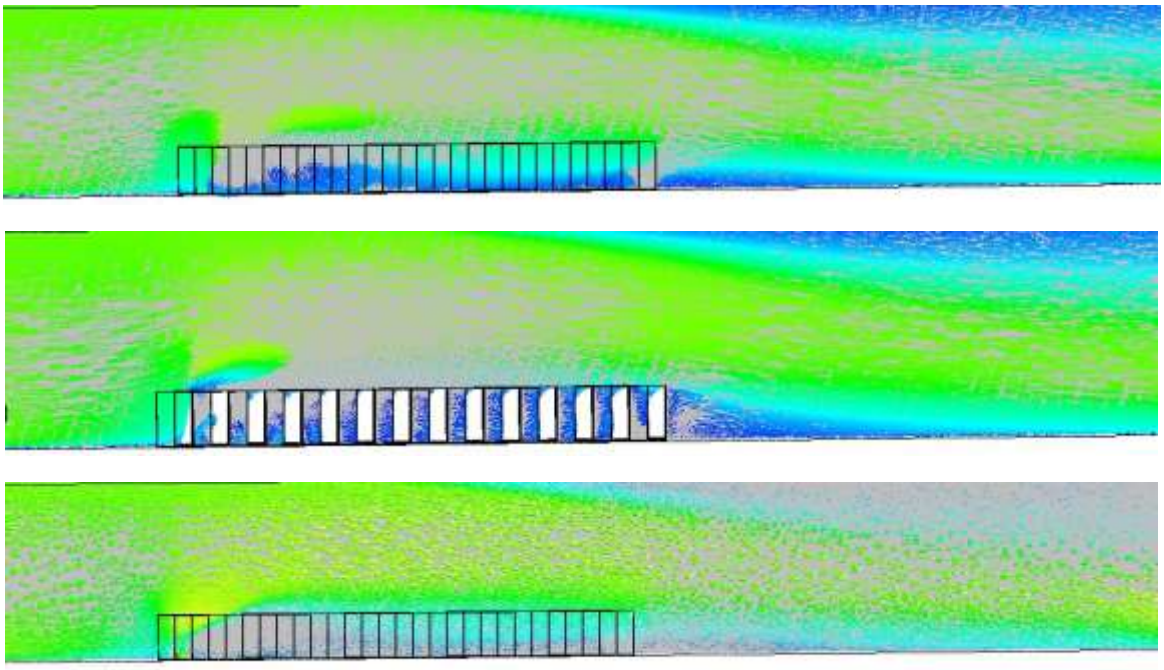

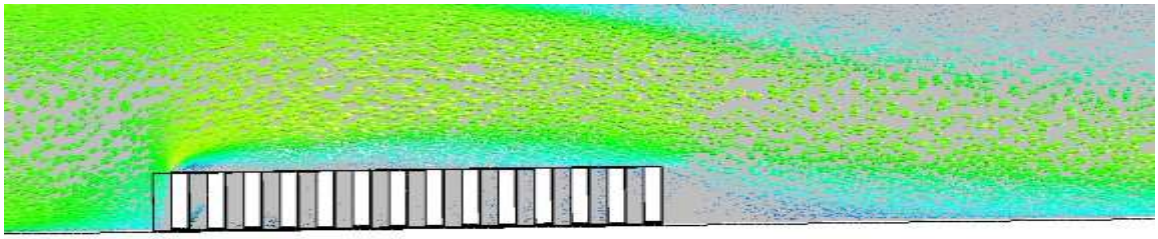

Figure 8.90: (a) *Velocity contours of the heavy gas dispersion for a/the staggered layout with the release source located between the sixth and seventh rows at* ***1m/s***

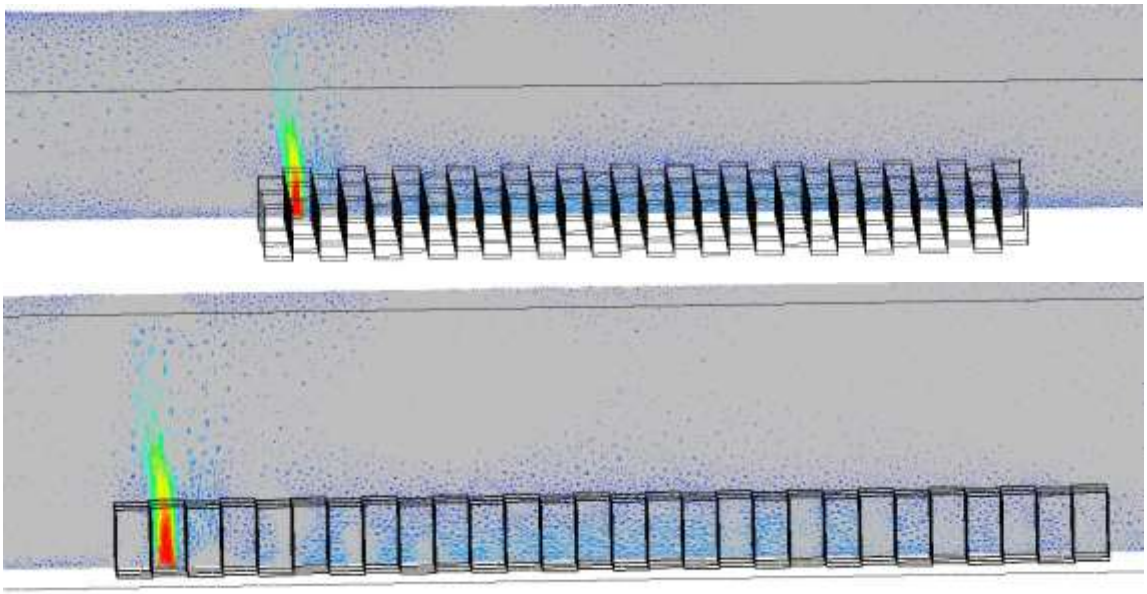

Figure 8.91: (b) *Velocity contours of the heavy gas dispersion for a/the staggered layout with the release source located between the sixth and seventh rows at* ***0.25m/s***

The above figures show the velocity contours of heavy gas dispersion for this case study with the release source located at the upwind front of the group of buildings between the first and second columns in the middle between the sixth and seventh rows. Velocity contours depict the intensity of wind - or the effective wind influence - at the different locations throughout the layout. As can be seen in the figure, the wind intensity is different at different points in the layout. It is a commonly known effect that, with enhanced altitudes, wind speeds increase. This is because the objects at lower altitudes create resistance to the flow of wind. As resistance is caused by the buildings in the flow of gas towards the direction opposite of wind, the wind flowing from left to right fails to indict the same motion of flow. Instead, various complex vertexes are formed within the buildings near the release source location, as can be seen in the above figures. The heavy gas release from the source is carried by these vertexes to the nearby mixture of the gas cloud, which them moves smoothly away from the source. Moreover, the hindrance in the wind flow caused by the buildings results in the vertexes moving in the upward direction, which enhances the shape of cloud in the upward direction.

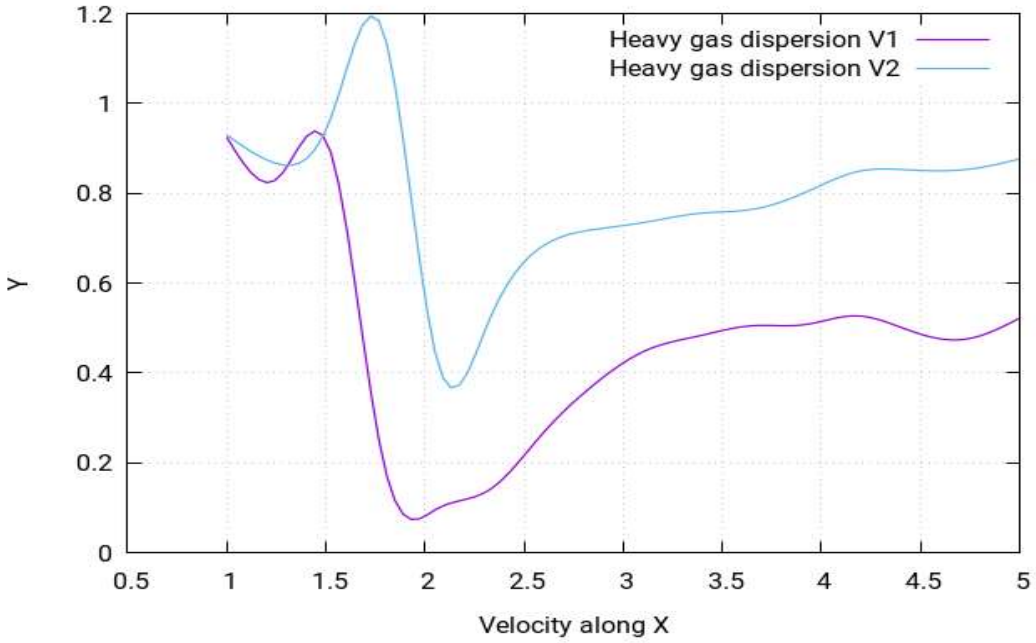

Figure 8.92: *Velocity of the heavy gas dispersion profile along the* ***x-*** *direction at* ***1m/s*** *different points of (V1) x=1m, y=2.16m, z=9.84m (V2) x=1m, y=2.16m and z=2m*

The above figure shows the velocity profiles for two of the gas dispersions at two different locations depending on distance from release source. Both curves follow the same pattern but have different values.

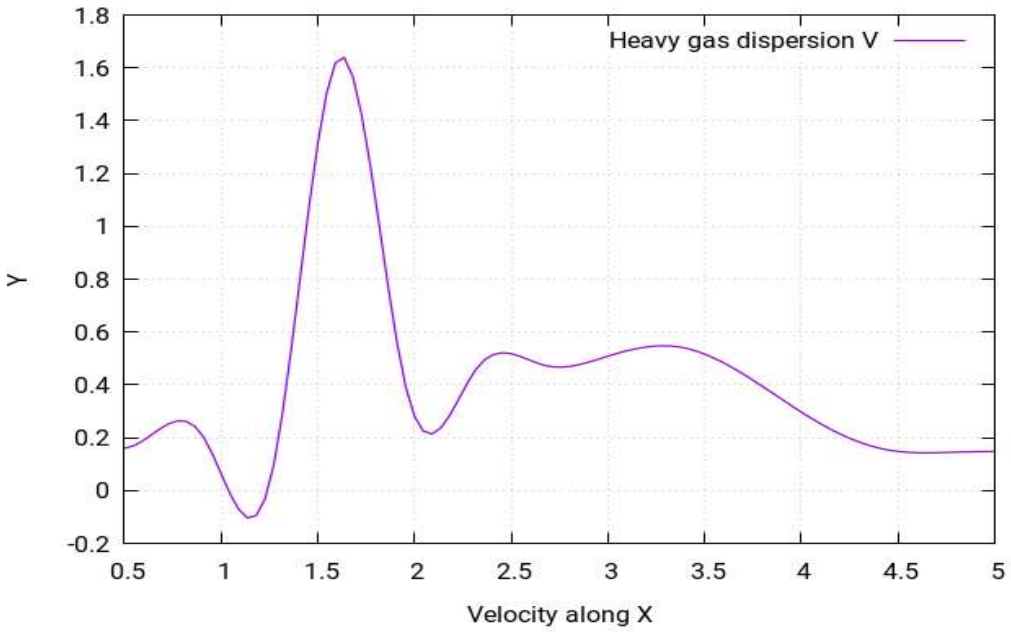

Figure 8.93: *Velocity of the heavy gas dispersion profile along the* ***x-****direction at* ***0.25m/s*** *points of (V) x=2m, y=2.16m and z=9.84m*

Figure 8.93 (above) shows the pattern of the velocity profile along the x-direction at 0.25m/s. There is only 1 peak in the curve and the curve is asymmetrical. For the staggered arrangement, the dispersion of the heavy gas is observed for different discharge velocities i.e., 1 m/s and 0.25

m/s. The results show the staggered arrangement of the buildings or obstacles causes more turbulence at high velocities. This results in a higher concentration of the heavy gas around them.

8.6.10 Location 1: Neutral gas dispersion

8.6.10.1 Building layout

The type of layout adopted for these two case studies is a staggered layout. A layout of 154 buildings of cubic shape will be created as a staggered layout and the release source will be placed in the same positions (1). The behaviour of the gas clouds will then be studied.

8.6.10.2 Release source location

The release source location (1) of the neutral gas dispersion in this case study was at the upwind front of the building group at the middle between sixth and seventh row**.**The perimeters selected for this case study are stated below:

Table 8.20: *Parametric values of the neutral gas simulation at high speed (location 1)*

Density	Flow Rate	Velocity	Ambient Temperature	Release Source Temperature
1.1839 kg m/s^3	1.7737 kg/s	1 m/s	25°C	25°C

8.6.10.3 Concentration of the neutral gas dispersion

The following figures show the concentration behaviour of the neutral gas at location 1 for staggered layouts. The whereabouts of location 1 has been stated at the beginning of the passage.

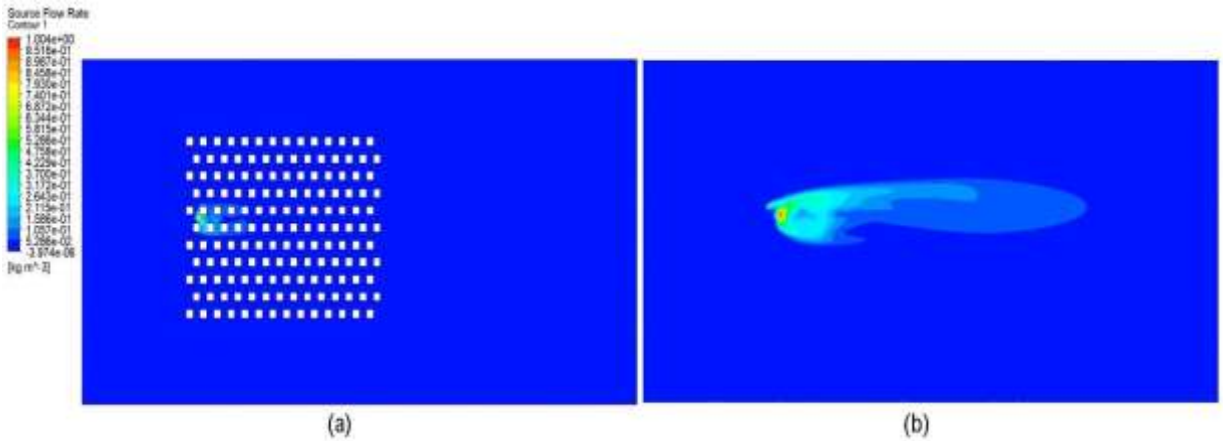

Figure 8.94: *Concentration of the neutral gas dispersion for a/the staggered layout with the release source located between the sixth and seventh row at* ***1m/s***

In Figure 8.94 (above) shows the concentration of a/the neutral gas cloud when the release source is placed at the upwind front of the group of buildings between the first and second columns in the sixth row.

In Figure 8.94(a), the plane is placed on the floor to observe the dispersion of the neutral gas in a/the staggered arrangement. It is clear that the dispersion is weak in the x-direction of the arrangement. In Figure 8.94(b), the plane is increased to move upward from the ground floor to observe the neutral gas dispersion in the y-axis and visualise the shape of the neutral gas which always manifests itself as one peak or single bubble which is going up to disperse.

8.6.10.4 Iso-surfaces of the neutral gas dispersion

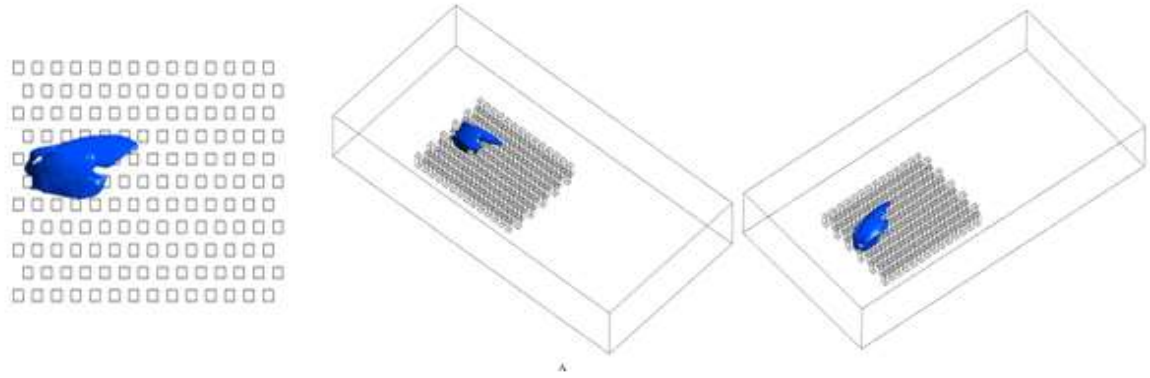

Figure 8.95: *Iso-surfaces of the neutral gas dispersion for a/the staggered layout with the release source located between the sixth and seventh rows at* ***1m/s***

The concentration profile of the neutral gas at location 1 for a/the staggered layout is shown in Figure 8.95 above. It shows the concentration behaviour of the neutral gas when the release gas source is placed at the upwind front of the group of buildings between the sixth and seventh rows in the sixth column. Similar to the case of heavy gas, these simulations show that, for this particular setting of the perimeters and the release source location, the gas cloud also resembles one of the shapes of the cloud of a/the previous case study, namely a/the collocated layout at location 2. The resemblance is again extremely similar to the case in location 1. Moreover, the cloud has shifted towards the horizontal side or, perhaps more accurately, it has leaned forward towards the right side. There is only a small deviation in the cloud shape as the symmetry is vacated. This was also seen in the case of the collocated layout in (location 2). The gas cloud looks more deviated in the lateral direction and appears to be smaller in size as compared to that case.

According to Standard BS EN 60079-10-1:2009 [104], the following locations can be categorised:

Zone 0: The central upwind front of the building layout

Zone 1: The immediate surrounding of the building layout and areas categorised in zone 0

Zone 2: All the remaining locations not categorised in zone 0 or zone 1

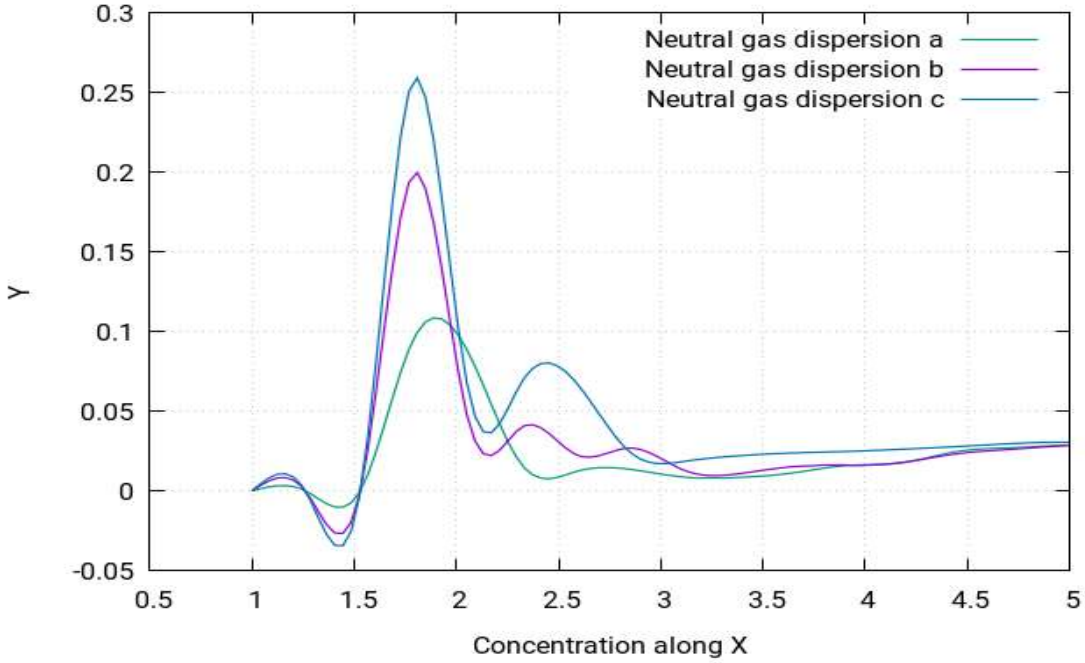

Figure 8.96: *Concentration of the neutral gas dispersion profile along the* ***x****-direction at* ***1m/s*** *different points of (a) x=1m, y=2.16m, z=7.20m (b) x=1m, y=1.16m, z=9.84m, (c)x=1m, y=2.16m and z=2.20m*

In Figure 8.96 (above), two different curves for the concentration profiles are shown. They show the pattern of the concentration profile along the **x-**direction when the wind speed for the simulation is 1m/s. The two different curves are obtained for two different distances from the release source. Both curves follow the same pattern but have different values due to differences in distances. From the figure, it can be concluded that the concentration value of the concentration of heavy gas decreases as it moves away from the source. The curve with the highest peak is obtained when nearest to the release source and vice versa.

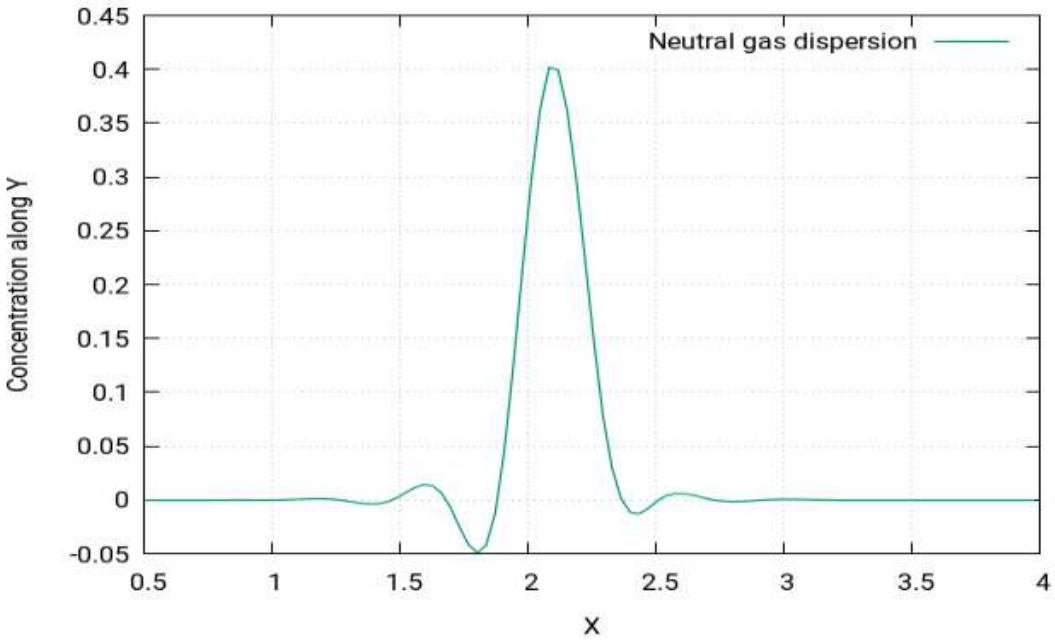

Figure 8.97: *Concentration of neutral gas dispersion profile along the* ***y****-direction at* ***1m/s*** *at different points of x=1.85m, y=-1m and z=2.20m*

Figure 8.97 shows the concentration curves along the y-direction for this case study when the wind speed is 1m/s. The curve shows an asymmetrical pattern and has a single peak at almost 2m.

8.6.10.5 Velocity of the neutral gas dispersion

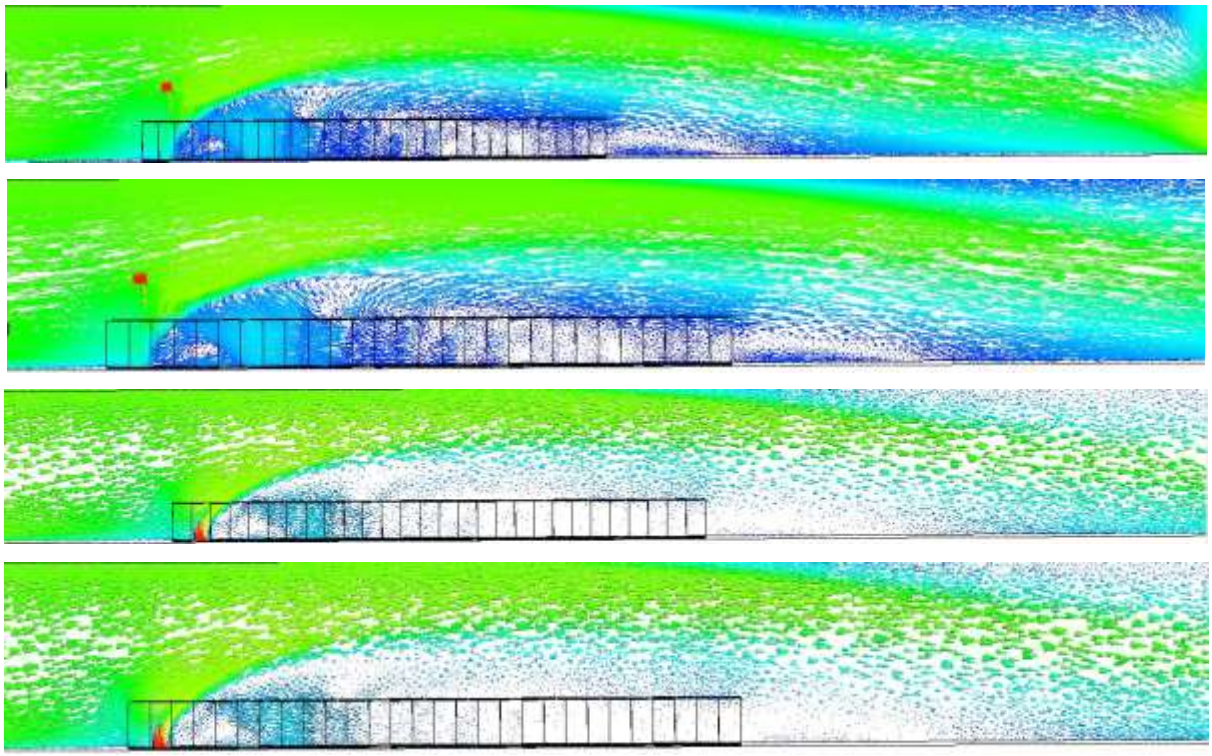

Figure 8.98: *Velocity contours of the neutral gas dispersion for a/the staggered layout with the release source located between the sixth and seventh rows at* ***1m/s***

Figure 8.98 shows the velocity contours of neutral gas dispersion for this case study with release source located between the sixth and seventh rows. Velocity contours depict the intensity of wind - or the effective wind influence - at the different locations throughout the layout. As seen in the figure, the wind intensity is different at different points in the layout. It is a commonly known effect that, with enhanced altitudes, enhanced wind speeds are experienced. This is because the objects at the lower altitudes create resistance in the wind flow. As resistance is caused by the buildings in the flow of gas towards the direction opposite of wind, the wind flowing from left to right fails to indict the same motion of flow. Instead, various complex vertexes are formed within the buildings near the release source location, as can be seen in the (Figure 8.98). The heavy gas release from the source is carried by these vertexes to the nearby mixture of the gas cloud, which then moves smoothly away from the source. Moreover, the hindrance in the wind flow caused by the buildings results in the vertexes moving in the upward direction, which enhances the shape of the cloud in the upward direction.

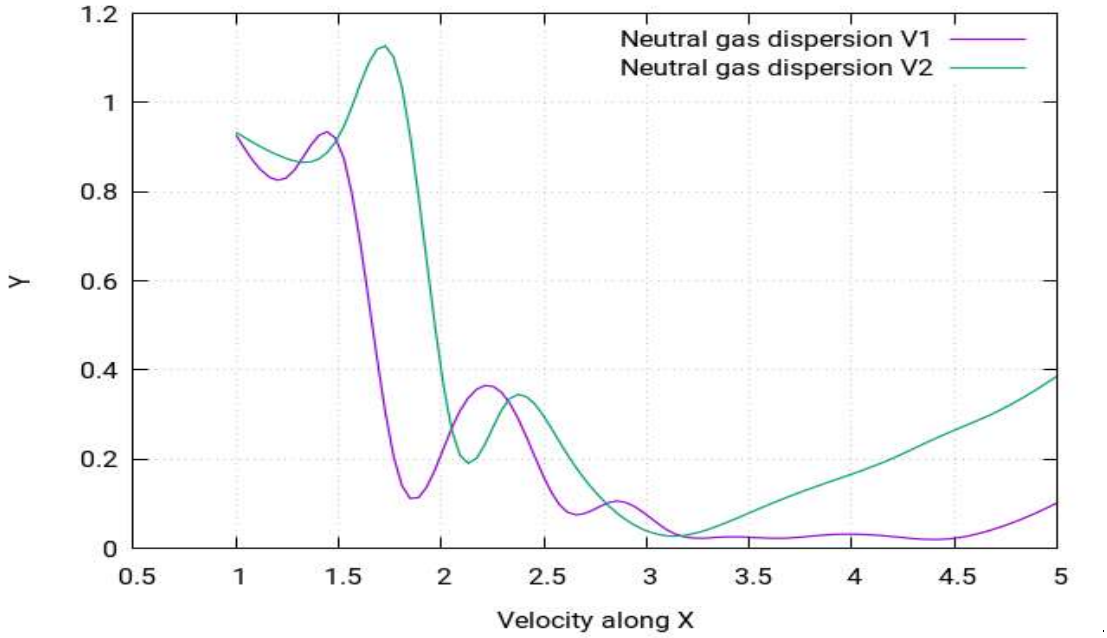

Figure 8.99: *Velocity of the neutral gas dispersion profile along the* ***x****-direction at* ***1m/s*** *at different points of (V1) x=1m, y=2.16m and z=9.84m (V2) x=1m, y=2.16m and z=2.20m*

The above figure shows the velocity profiles for two of the gas dispersions at two different locations depending on distance from release source. Both curves follow the same pattern but have different values. For the staggered arrangement, the dispersion of the neutral gas is observed at location 1. It is seen that, due to low density, the dispersion of the neutral gas is the same for the collocated arrangement i.e., in the upward direction.

8.6.11 Location 2: Heavy gas dispersion

8.6.11.1 Building layout

The type of layout adopted for this case study for a staggered layout. A layout of 154 buildings of cubic shape will be created as a staggered layout and the release source will be placed in positions. Then the behaviour of the gas clouds will be studied.

8.6.11.2 Release source location

The release source location (2) of the heavy gas dispersion in this case study was at the upwind front of the group of buildings in the sixth row. The perimeters selected for this case study is stated below:

Table 8.21: *Parametric values of the heavy gas simulation at high velocity (location 2)*

Density	Flow Rate	Velocity	Ambient Temperature	Release Source Temperature
2.1 kg m/s^3	1 kg/s	1 m/s	25°C	-100°C

8.6.11.3 Concentration of the heavy gas dispersion

The following figure shows the concentration behaviour of the heavy gas at location 1 for a/the staggered layouts. The whereabouts of location 2 has been stated at the beginning of the passage.

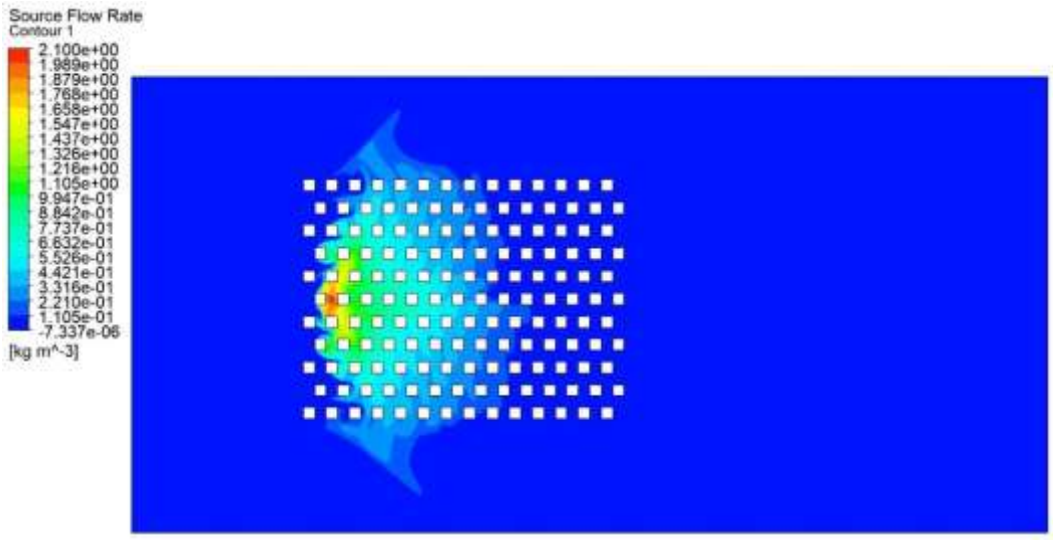

Figure 8.100: *Concentration of the heavy gas dispersion for a/the staggered layout with the release source located at the upwind front of the group of buildings in the sixth row at* ***1m/s***

The concentration profile of the heavy gas at location 2 for a/the staggered layout is shown in Figure 8.100 (above), which represents the concentration behaviour of the heavy gas when the release gas source is placed between the first and second columns at the middle between the

5th and 6th row. The above figure, shows at velocity of 1 m/s. The same study was also performed for collocated layouts under the same parameters and release source location. The cloud shape for this particular study has been discussed in collocated sections of these results (refer TO location 2 in collocated layouts). The simulations show that the release source is exposed to the air, which affects the gas coming out of the release source directly. As a result, the gas cloud shape takes a more spread pattern, unlike if the gas source was not exposed to the air. The change of location has affected the cloud shape in such a way that, at high speed, it now forms an extended knobhead in the horizontal direction, creeping out of the last column of the layout, as shown in (Figure 8.100). The same was also observed for collocated layouts. However, in this case, the head of the cloud in the horizontal portion has faded away due to the change in the layout. Moreover, in a/the collocated layout, the cloud shape had a certain symmetry, which cannot be observed in this case for the staggered layout. The cloud shape in the collocated layout showed a more spread-out concentration in the entire middle front of the layout, while in the case of staggered layouts, the high concentrations point runs across the central rows of the layout.

8.6.11.4 Iso-surfaces of the heavy gas dispersion

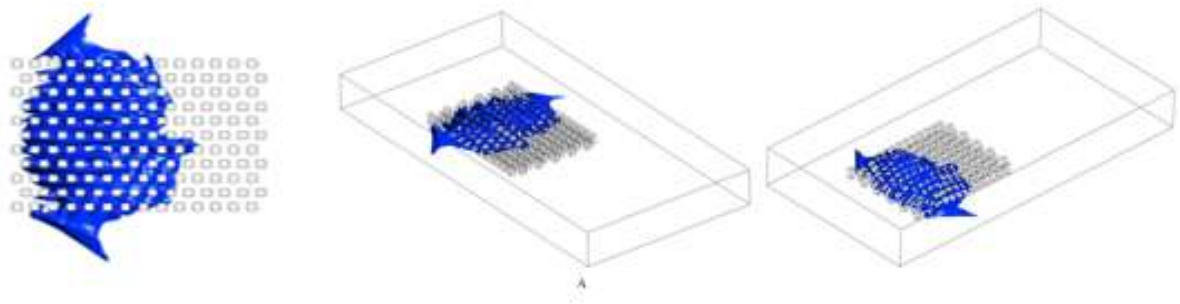

Figure 8.101: *Iso-surfaces concentration of the heavy gas dispersion for a/the staggered layout with the release source located at the upwind front of the group of buildings in the sixth row at* ***1m/s***

Figure 8.101, shows the iso-surfaces of the concentration profile of heavy gas dispersion for a/the staggered layout with the release source located at the upwind front of the group of buildings in the sixth row. It can be said that, at low speed, the shape of the cloud changes by a scale of three approximately.

According to Standard BS EN 60079-10-1:2009 [104], the following locations can be categorised:

Zone 0: The upwind front of the building block all the way to the middle front, excluding the triangular shape of buildings of the initial few columns

Zone 1: The central portion of the middle front and the immediate surrounding of first few blocks of the upwind front

Zone 2: All the remaining locations not categorised in zone 0 or zone 1

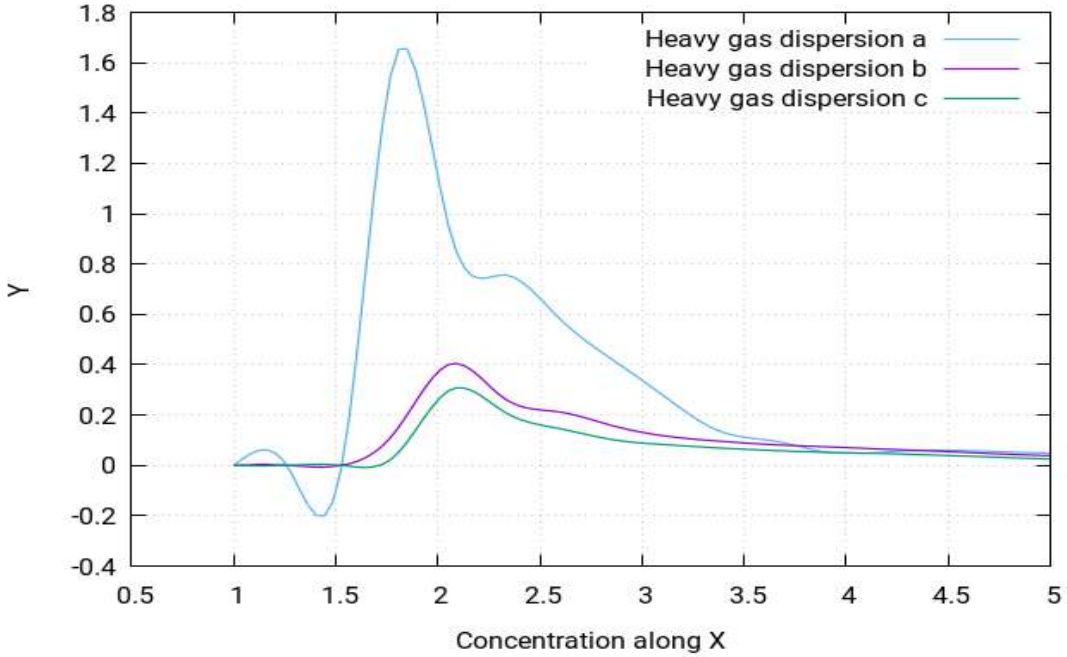

Figure 8.102: *Concentration of the heavy gas dispersion profile along the* ***x****-direction at* ***1m/s*** *different points of (a) x=1m, y=1.95m, z=7.20m (b) x=1m, y=1.95m, z=9.84m (c) x=1m, y=1.95 and z=1.50m*

In Figure 8.102 (above), three different curves for the concentration profiles are shown. They show the pattern of the concentration profile along the X-direction when the wind speed for the simulation is 1m/s. The two different curves are obtained for two different distances from the release source. Both curves follow the same pattern but have different values due to difference of distances. From the figure, it can be concluded that the concentration value of the concentration of heavy gas decreases when moved away from the source. The curve with the highest peak is obtained when nearest the release source and vice versa.

8.6.11.5 Temperature of the heavy gas dispersion

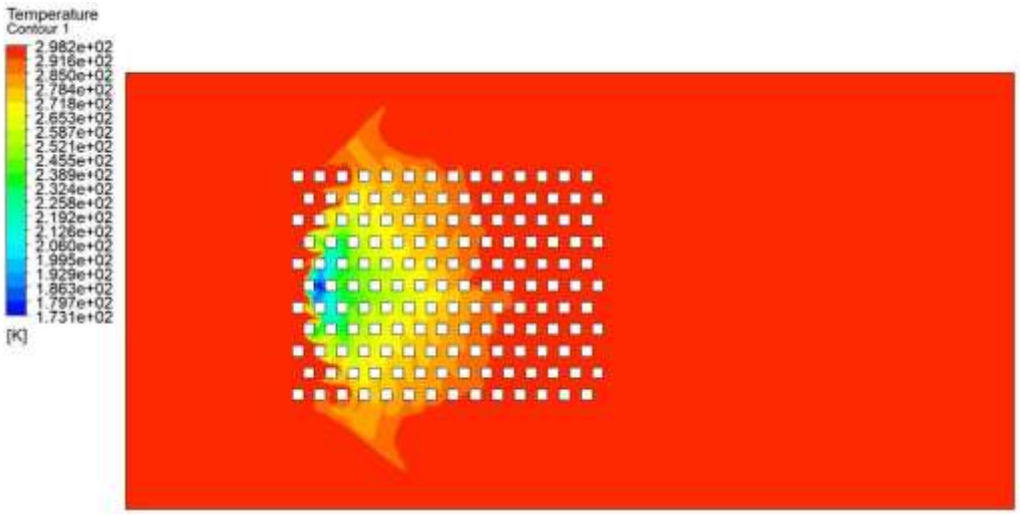

Figure 8.103: *Temperature profile of the heavy gas dispersion for a/the staggered layout with the release source located at the upwind front of the group of building in the sixth row at* ***1m/s***

The above figure shows the temperature simulation for this study. By visualising the temperature simulation, it is found out that the temperature simulation produces largely the same profile for the case study as that of the concentration profile. However, the behaviour of temperature is in fact the opposite to that of concentration. This means that the areas which were identified in the concentration simulation as highly concentrated will in fact have the lowest temperatures, while ones with moderate concentrations will have moderate temperatures and the least concentrated areas will have the maximum temperatures. To further simplify these findings, it should be pointed out that the simulations show that the concentrations near the release source point tend to be the highest and start to fade away as it moves away from the source, being at its lowest as it moves much further away in the layout, eventually reaching the environment where the gas cloud disappears. However, the temperature reaches its lowest near the release source point and tends to increase as it moves away from source, finally achieving its highest temperature equal to the ambient temperature of the environment.

8.6.11.6 Velocity of the heavy gas dispersion

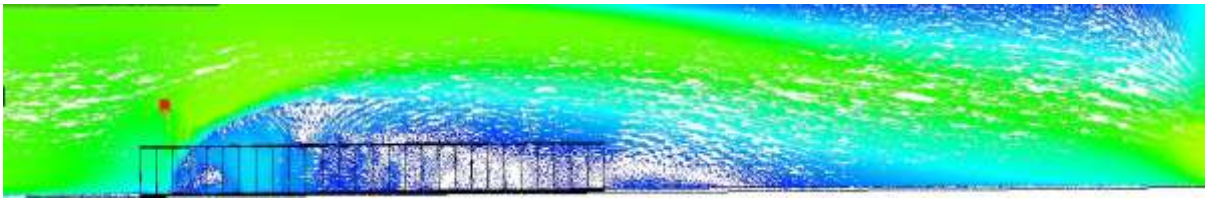

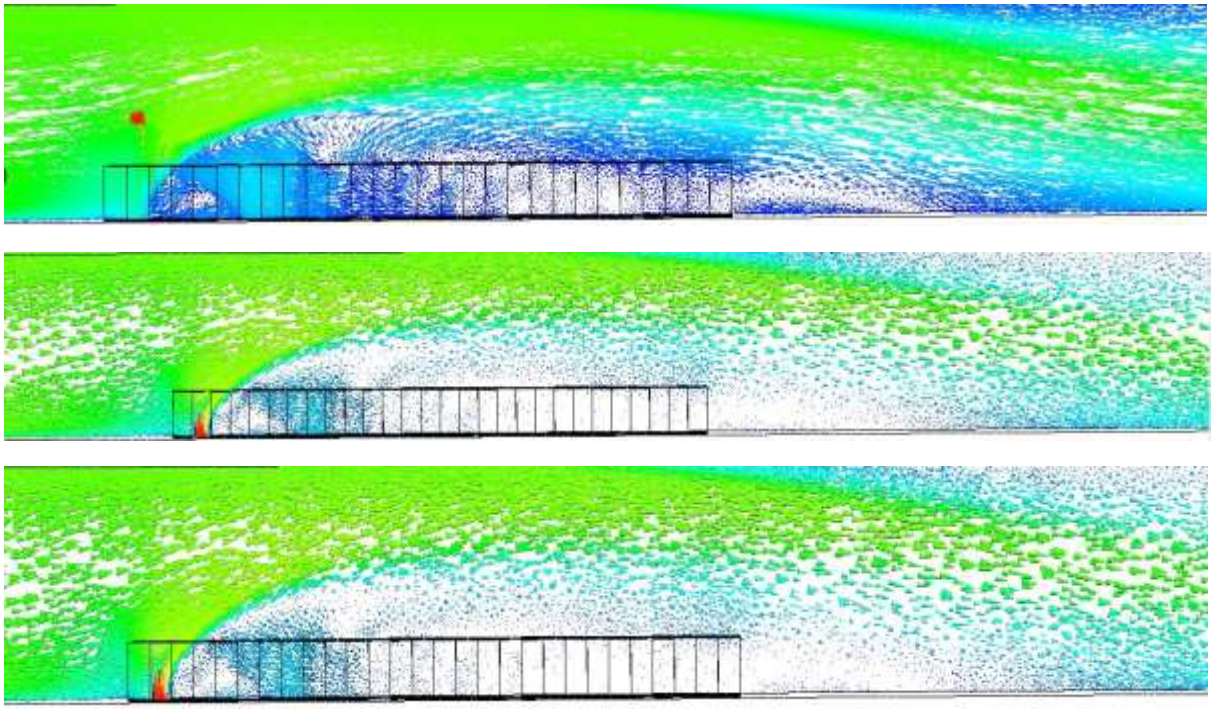

Figure 8.104: *Velocity contours of the heavy gas dispersion for a/the staggered layout with the release source located at the upwind front of the group of buildings in the sixth row at* ***1m/s***

Figure 8.104 shows the velocity contours of heavy gas dispersion for this case study with the release source located at the upwind front of the group of buildings in the sixth row. The velocity contours depict the intensity of wind - or the effective wind influence - at the different locations throughout the layout. According to the figure, the wind intensity is different at different points in the layout. It is a commonly known effect that, with enhanced altitudes, enhanced wind speeds are experienced. This is because the objects at the lower altitudes create resistance to wind flow. As there is resistance caused by the buildings in the flow of gas towards the direction opposite of wind, the wind flowing from left to right fails to indict the same motion of flow. Instead, various complex vertexes are formed within the buildings near the release source location, as can be seen in (Figure 8.104). The heavy gas release from the source is carried by these vertexes to the nearby mixture of the gas cloud, which then moves smoothly away from the source. Moreover, the hindrance in the wind flow caused by the buildings results in the vertexes moving in the upward direction, which enhances the shape of cloud in the upward direction.

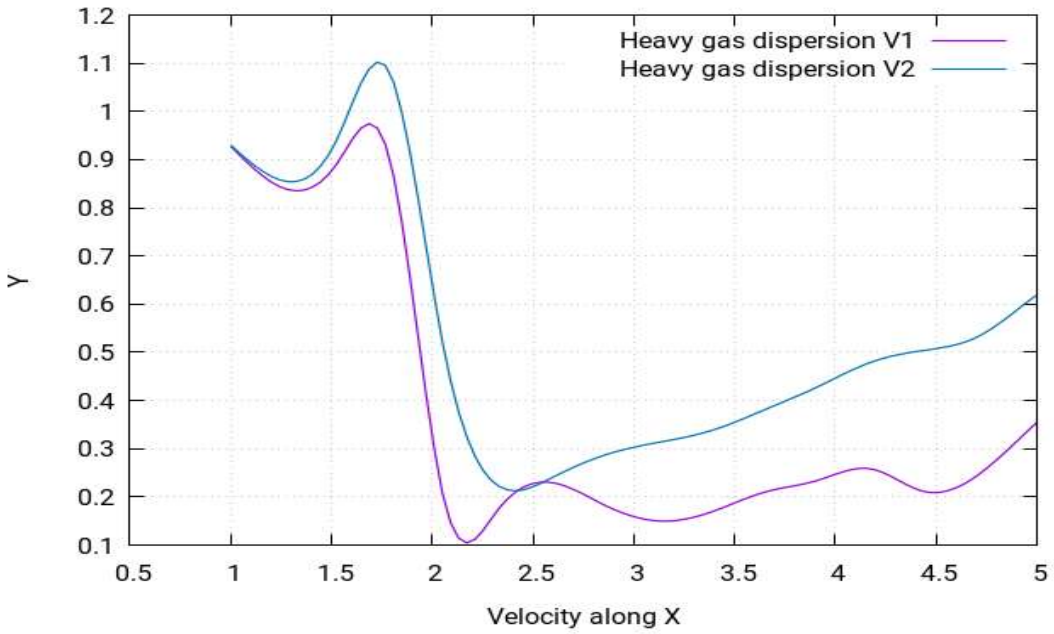

Figure 8.105: *Velocity of the heavy gas dispersion profile along the* ***x****-direction at* ***1m/s*** *different points of (V1) x=1m, y=1.95m, z=9.84m (V2) x=1m, y=1.95m and z=1.50m*

The above figure shows the velocity profiles for two of the gas dispersions at two different locations depending on distance from release source. The curves show the same pattern initially but tend to show a different pattern at the end.

For the staggered arrangement, the dispersion of the heavy gas is now observed at location 2. The results show that the concentration of the heavy gas is maximum around the obstacles which are near the source. This is because the turbulence of the wind near these obstacles is high, which is what causes the accumulation of the heavy gas.

8.6.12 Location 2: Neutral gas dispersion

8.6.12.1 Building layout

The type of layout adopted for this case study for the staggered layout. A layout of 154 buildings of cubic shape will be created as staggered layouts and the release source will be placed in positions. Then, the behaviour of the gas clouds will be studied.

10.6.12.2 Release source location

The release source location (2) of the neutral gas dispersion in this case study was at the upwind front of the group of buildings the sixth row. The perimeters selected for this case study is stated below:

Table 8.22: *Parametric values of the neutral gas simulation at high speed (location 2)*

Density	Flow Rate	Velocity	Ambient Temperature	Release Source Temperature
1.1839 kg m/s^3	1.7737 kg/s	1 m/s	25°C	25°C

8.6.12.3 Concentration of the neutral gas dispersion

The following figure shows the concentration behaviour of the neutral gas at location 2 for staggered layouts. The whereabouts of location 2 has been stated at the beginning of the passage.

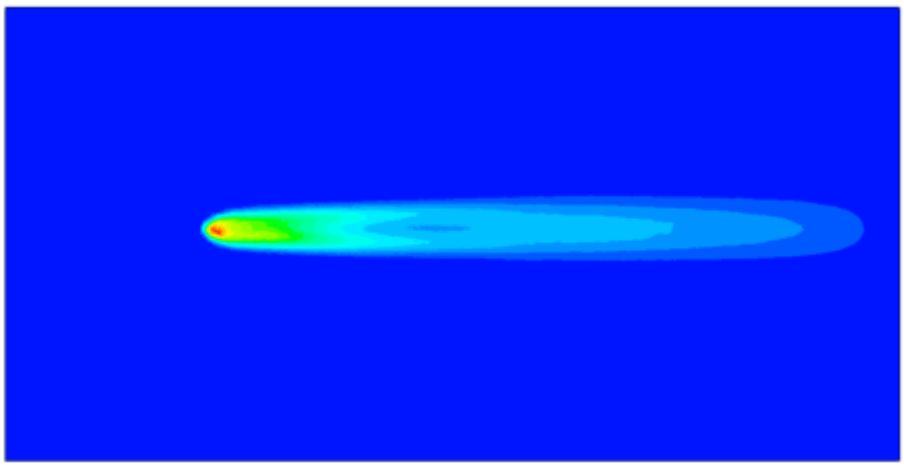

Figure 8.106: *Concentration of the neutral gas dispersion for a/the staggered layout with the release source located at the upwind front of the group of buildings in the sixth row at* ***1m/s***

The concentration of neutral gas cloud can be seen when the release source is placed at the upwind front of the group of buildings between the first and second columns in the sixth row, as per Figure 8.106. Red represents maximum concentration, while blue represents the minimum concentration. In the above figure, the plane is increased to moved upward from the ground floor to observe the neutral gas dispersion in the y-axis to visualise the shape of the neutral gas in a/the staggered arrangement, as always shown as one peak or single bubble which is going up to disperse. When the cloud shape is observed, a similar cloud shape is found to the one that was identified in the case of collocated layouts at location 1 for neutral gas. However, a small difference is that, in that case, the high concentration part of the cloud looked like an elliptical cylinder, while this one looks like a reverse nozzle. Although there is a similarity in the trend, as the concentrations are maximum near the release point and then follow a decreasing degree of concentration when moved away from the source, the shape of the cloud

is entirely different in this case and hence the distribution of the gas cloud. These results point to the fact that the change of layout does not affect the cloud shape in the case of neutral gas.

8.6.12.4 Iso-surface of the neutral gas dispersion

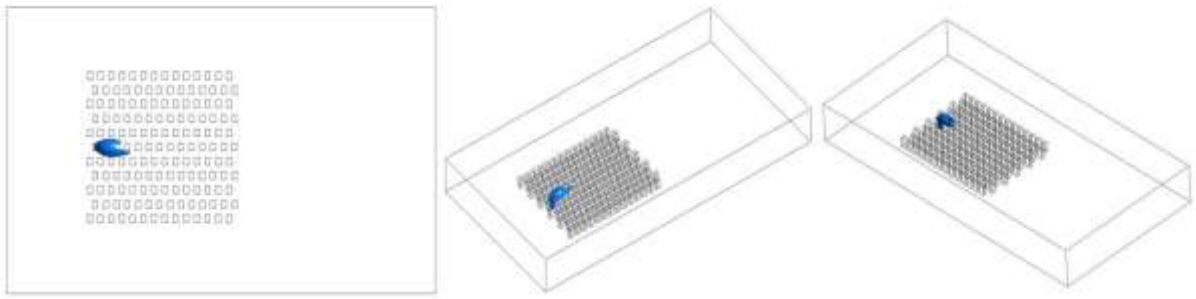

Figure 8.107: *Iso-surfaces of the concentration of the neutral gas dispersion for a/the staggered layout with the release source located at the upwind front of the group of buildings in the sixth row at* ***1m/s***

In Figure 8.107, the iso-surfaces of the concentration profile of neutral gas cloud can be seen when the release source is placed at the upwind front of the group of buildings in the sixth row. These iso-surfaces help determine that the shape of the cloud is somewhat shrunken in this case and only occupies a few of the building blocks of the layout, resembling the shape of symmetrical opening in the horizontal direction. This is identical to the results of the neutral gas case study at (location 2).

According to Standard BS EN 60079-10-1:2009 [104], the following locations can be categorised:

Zone 0: The central upwind front of the building layout
Zone 1: The immediate surrounding of the building layout and areas categorised in zone 0
Zone 2: All the remaining locations not categorised in zone 0 or zone 1

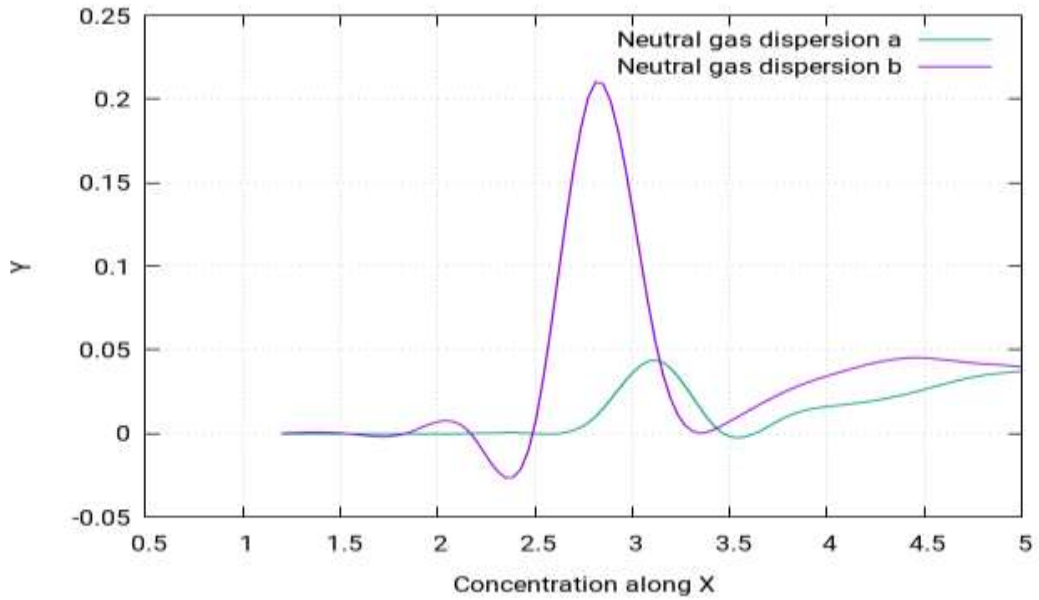

Figure 8.108: *Concentration of the neutral gas dispersion profile along the* ***x****-direction at* ***1m/s*** *different points of (a) x=1m, y=2.05m, z=3.00m (b) x=1m, y=2.05m and z=3.55m*

In Figure 8.108 (above), two different curves for the concentration profiles are shown. They show the pattern of the concentration profile along the x-direction when the wind speed for the simulation is 1m/s. The two different curves are obtained for two different distances from the release source. Both curves follow the same pattern but have different values due to difference in distances. From the figure, it can be concluded that the concentration value of the heavy gas decreases as it moves away from the source. In the figure, the curve with the highest peak is obtained when nearest to the release source and vice versa.

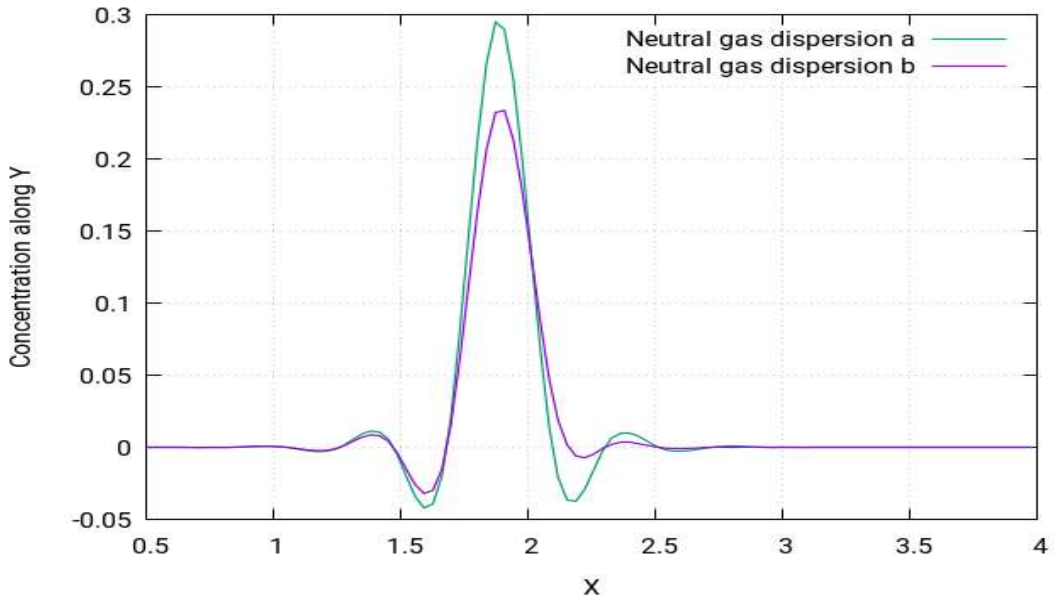

Figure 8.109: *Concentration of the neutral gas dispersion profile along the* ***y****-direction at* ***1m/s*** *different points of (a) x=1.85m, y=-1m and z=2.65m, and (b) x=1.95m, y=-1m and z=3.20m*

In Figure 8.109 (above), two different curves for the concentration profiles are shown. They show the pattern of the concentration profile along the y-direction when the wind speed for the simulation is 1m/s. The two different curves are obtained for two different distances from the release source. It can be seen that, along the y-direction, the profiles show a remarkably symmetrical pattern.

8.6.12.5 Velocity of the neutral gas dispersion

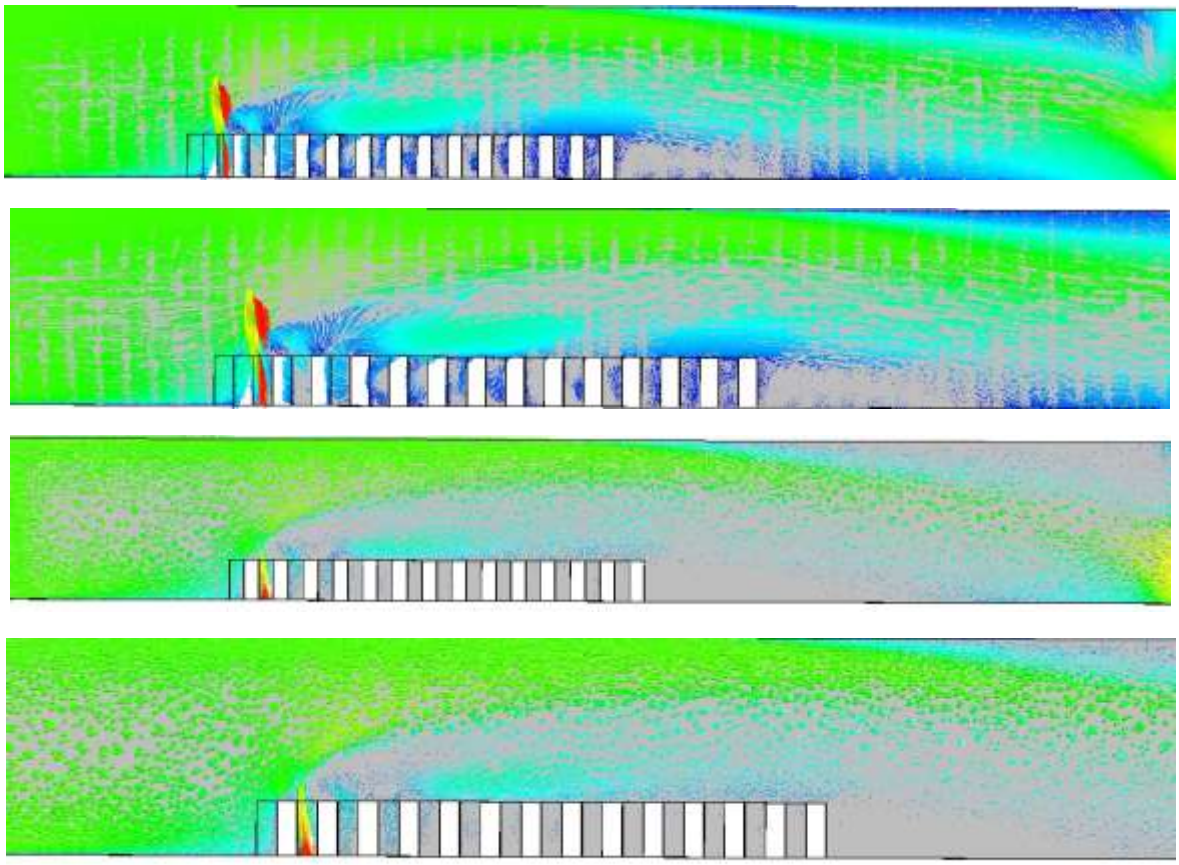

Figure 8.110: *Iso-surfaces of concentration of the neutral gas dispersion for a/the staggered layout with the release source located at the upwind front of the group of buildings in the sixth row at* ***1m/s***

Figure 8.110 shows the velocity contours of neutral gas dispersion for this case study with the release source located at the upwind front of the group of buildings in the sixth row. Velocity contours depict the intensity of wind - or the effective wind influence - at the different locations throughout the layout. As can be seen in the figure, the wind intensity is different at different points in the layout. It is a commonly known effect that, with enhanced altitudes, enhanced wind speeds are encountered. This is because the objects at the lower altitudes create resistance to the wind flow. As there is resistance caused by the buildings in the flow of gas towards the direction opposite of wind, the wind flowing from left to right fails to indict the same motion of flow. Instead, various complex vertexes are formed within the buildings near the release

source location, as can be seen in (Figure 8.110). The heavy gas release from the source is carried by these vertexes to the nearby mixture of the gas cloud, which then moves smoothly away from the source. Moreover, the hindrance in the wind flow caused by the buildings results in the vertexes moving in the upward direction, which enhances the shape of cloud in the upward direction.

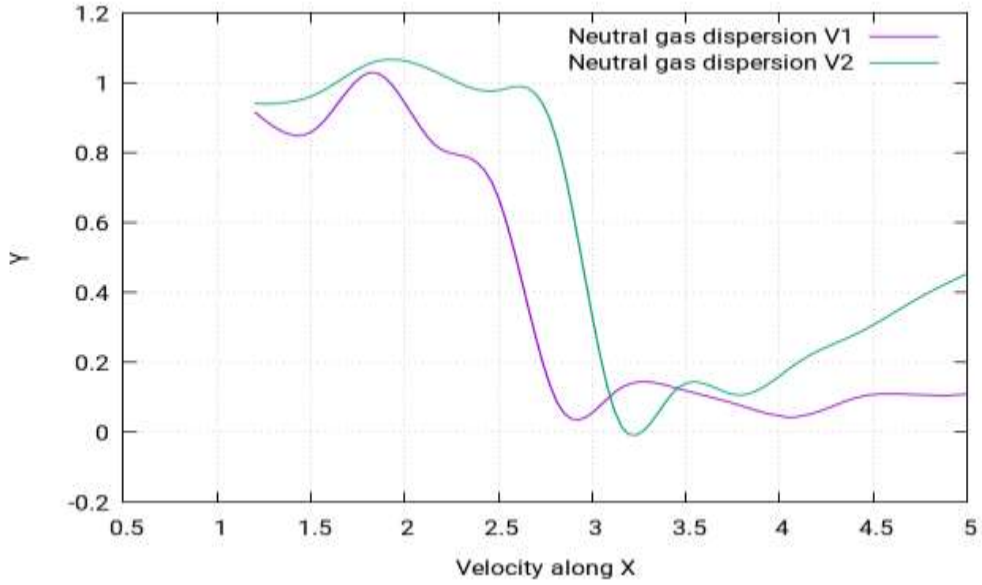

Figure 8.111: *Velocity of the neutral gas dispersion profile along the* ***x****-direction at* ***1m/s*** *different points of (V1) x=1m, y=2.05m, z=3m (V2) x=1m, y=2.05m and z=3.55m*

The above figure shows the velocity profiles for two of the gas dispersions at two different locations depending on distance from release source. Both the curves show a somewhat similar pattern but have different values.

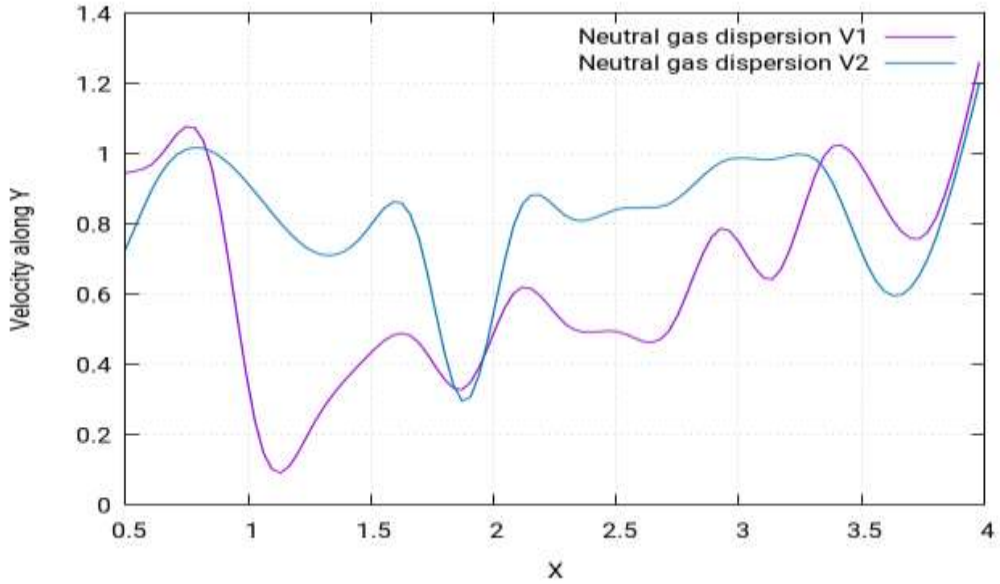

Figure 8.112: *The velocity of neutral gas dispersion profile along the* ***y****-direction at* ***1m/s*** *different points of (V1) x=1.85m, y=-1m z=2.65m (V2) x=1.95m, y=-1m and z=3.20m*

The above figure shows the velocity profiles for two of the gas dispersions at two different locations depending on distance from release source. Both curves show a somewhat similar pattern but have different values.

8.6.13 Location 3: Heavy gas dispersion at different velocities

8.6.13.1 Building layout

The type of layout undertaken for these two case studies the staggered layout. A layout of 154 buildings of cubic shape will be created as staggered layouts and the release source will be placed in the same positions. Then the behaviour of the gas clouds will be studied.

8.6.13.2 Release source location

The release source location (3) of the heavy gas dispersion in these case studies was at the middle front of the group of buildings in the sixth row. The perimeters selected for this case study are stated below:

Table 8.23: *(A) Parametric values of the heavy gas simulation at high speed (location 3)*

Density	Flow Rate	Velocity	Ambient Temperature	Release Source Temperature
2.1 kg m/s^3	1 kg/s	1 m/s	25°C	-100°C

Table 8.24: *(B) Parametric values of the heavy gas simulation at low speed (location 3)*

Density	Flow Rate	Velocity	Ambient Temperature	Release Source Temperature
2.1 kg m/s^3	5 kg/s	0.25 m/s	25°C	-100°C

8.6.13.3 Concentration of the heavy gas dispersion at different velocities

The following figure shows the concentration behaviour of the heavy gas at location (3) for a/the staggered layout. The whereabouts of location 3 has been stated at the beginning of the passage.

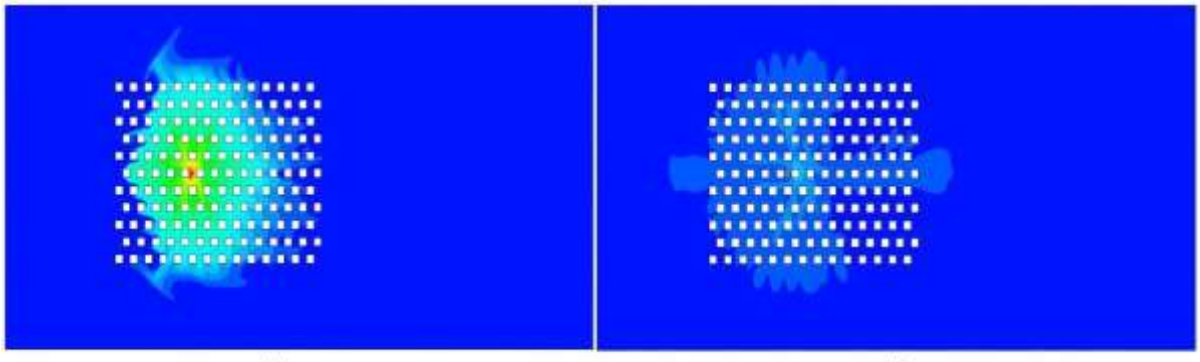

Figure 8.113: (a) *Concentration profile of the heavy gas dispersion for a/the staggered layout with the release source located in the middle of the group of buildings in the sixth row at 1m/s* ***(b)*** *At 0.25m/s*

The concentration profile of the heavy gas dispersion at location 3 for staggered layout is shown in Figure 8.113 above. It represents the concentration behaviour of the heavy gas when the release gas source is placed at the middle of the group of buildings in the sixth row. In the above figure, parts labelled (a) are at high speed and those labelled (b) are at low speed. The same study was also performed for collocated layouts under the same parameters and at a slightly different release source location. The simulations show that, since the release source is now not exposed to the air, the gas coming out of the release source is therefore not directly affected. As a result, the gas cloud shape takes a more concentrated pattern, unlike if the gas source was exposed to the air. The change of location has affected the cloud shape in such a way that, at high speed, it now makes a concentrated prism like shape, starting from the second column right up to the final third half of the layout, out as shown in Figure 8.113(a). The cloud shape is largely symmetrical. It should be noted that the same parameter settings were also adopted for location 2, with the only difference being that location 2 was at the upwind front of the building layout and location 3 is at the middle front of the building layout.

The cloud shape for low speed is shown in Figure 8.113(b). It shows a certain similarity in the cloud shape in the cases of collocated layout in location 1 and staggered layout in location 3. The difference again is that the location 1 was at the upwind front, while location 3 is at the middle front of the building layout. Moreover, the change of layout disturbs the symmetry of the cloud shape, as can be seen in (Figure 8.113). Moreover, it should also be stressed that, in the staggered layouts, the cloud shaped kind of fade up a little.

8.6.13.4 Iso-surface of the heavy gas dispersion at different velocities

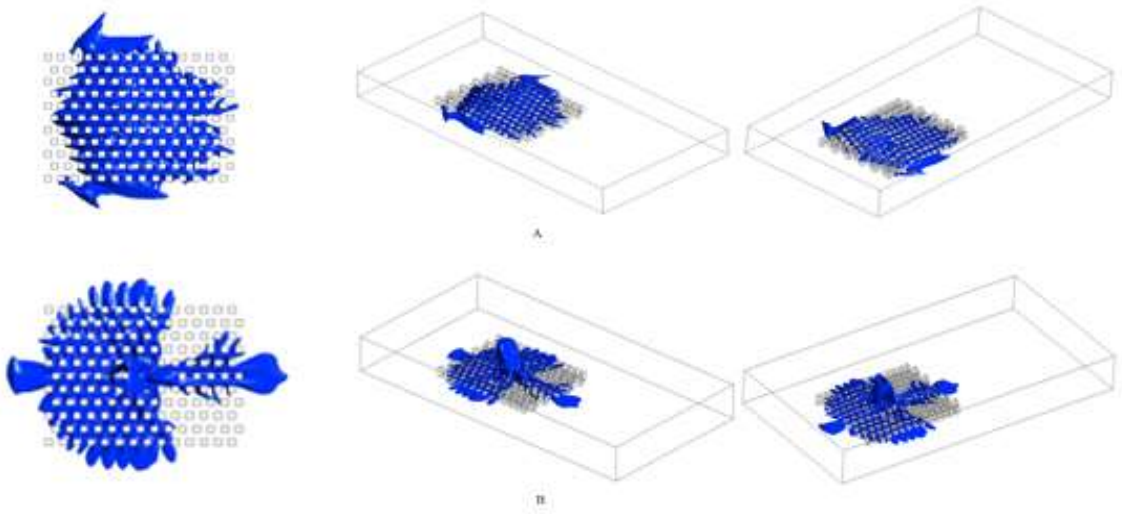

Figure 8.114: (a) *Iso-surfaces of concentration profile of Heavy Gas Dispersion for a/the staggered layout with the release source located in the middle of the group of buildings in the sixth row at 1m/s.* ***(b)*** *At 0.25m/s*

In Figure 8.114, the iso-surfaces of the concentration profile of heavy gas dispersion can be seen for a/the staggered layout with the release source located at the middle of the group of buildings in the sixth row at both low and high speeds. This helps identify the spread of the cloud in each dimension. It can be seen that the cloud is concentrated at the release source location and takes a rather higher portion of the vertical direction, while at other locations, it tends to remain at lower altitudes. The iso-surfaces also help visualise the accumulated areas of the gas cloud in the case of low speed in Figure 8.114(b).

According to Standard BS EN 60079-10-1:2009 [104], the following locations can be categorised:

High speed:

Zone 0: An X-shaped building pattern near the release source, covering almost five central rows and the columns near the release source

Zone 1: The prism shaped portion of the building layout, starting from the upwind front, extending to the third half of the building layout

Zone 2: All the remaining locations not categorised in zone 0 or zone 1

Low speed:

Zone 0: The central portion of the middle front

Zone 1: The rectangular-cross shape portion of the building layout, with one part of the cross being the central rows and the other being the central columns

Zone 2: All the remaining locations not categorised in zone 0 and zone 1

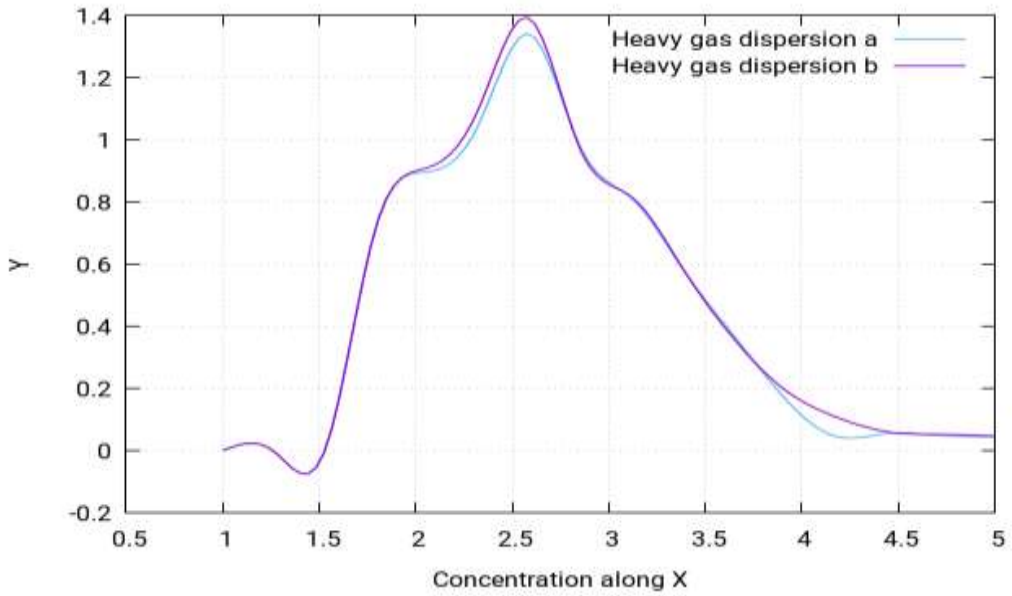

Figure 8.115: *Concentration of the heavy gas dispersion profile along the* ***x****-direction at* ***1m/s*** *different points of (a) x=1m, y=1.95m, z=2m (b) x=1m, y=2.15m and z=2m*

In Figure 8.115 (above), two different curves for the concentration profiles are shown. They show the pattern of the concentration profile along the x-direction when the wind speed for the simulation is 1m/s. The two different curves are obtained for two different distances from the release source. Both the curves follow the same pattern but have different values due to difference in distance. From the figure, it can be concluded that the concentration value of heavy gas decreases as it moves away from the source. The curve with the highest peak is obtained when nearest to the release source and vice versa.

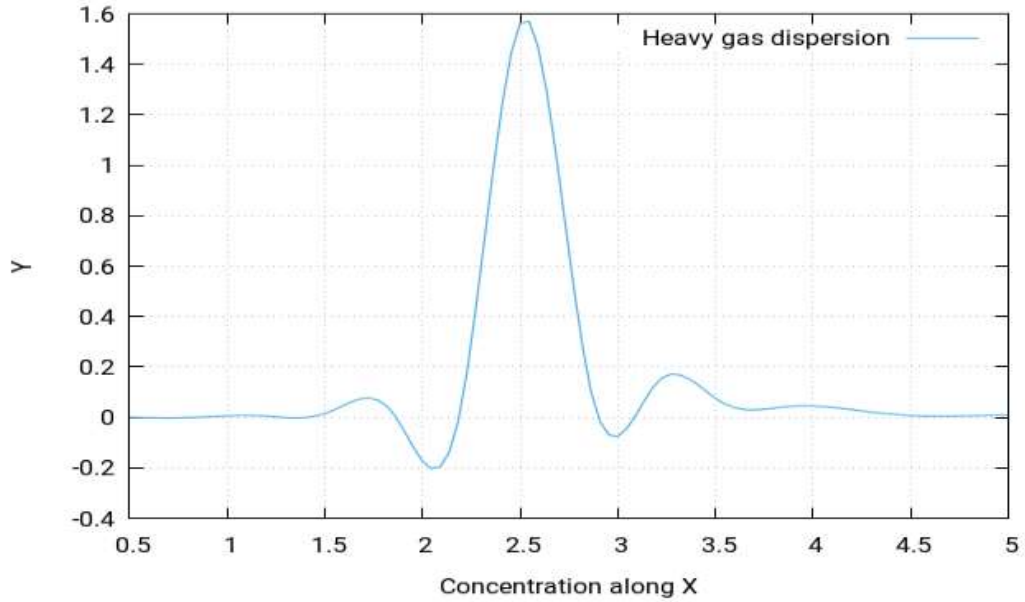

Figure 8.116: *Concentration of the heavy gas dispersion profile along the* ***x****-direction at* ***0.25m/s*** *points of x=5m, y=2.05m and z=2.12m*

Figure 8.116 shows the concentration curves along the x-direction for this case study when the wind speed is 0.25m/s. The curve shows a remarkably symmetrical pattern and has a single peak at almost 2.5m.

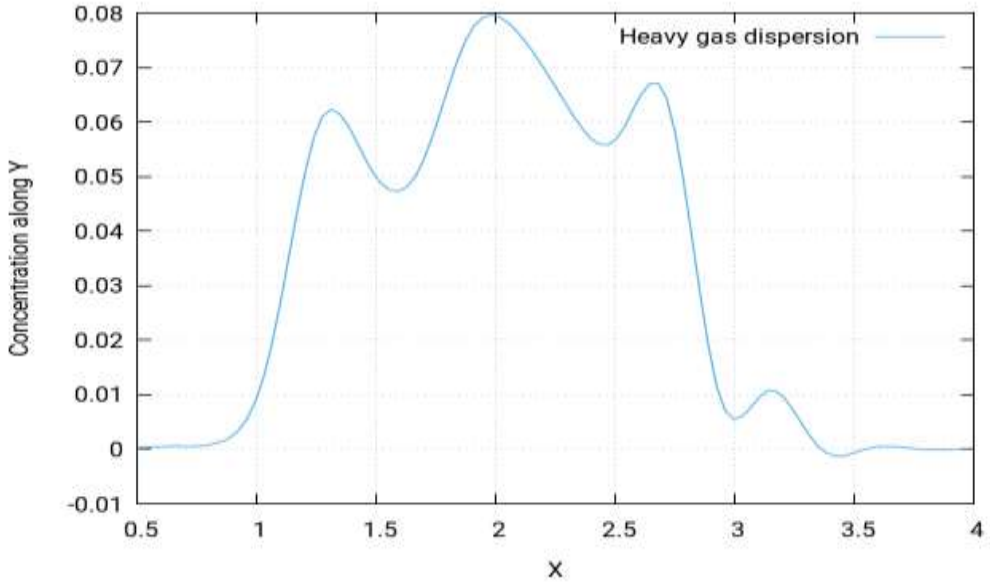

Figure 8.117: *Concentration of the heavy gas dispersion profile along the* ***y****-direction at* ***1m/s*** *different points of (a) x=2.86m, y=-1m and z=2m*

Figure 8.117 shows the concentration curves along the y-direction for this case study when the wind speed is 1m/s. The curve shows an asymmetric pattern and has a single peak at almost 2m.

8.6.13.5 Temperature of the heavy gas dispersion at different velocities

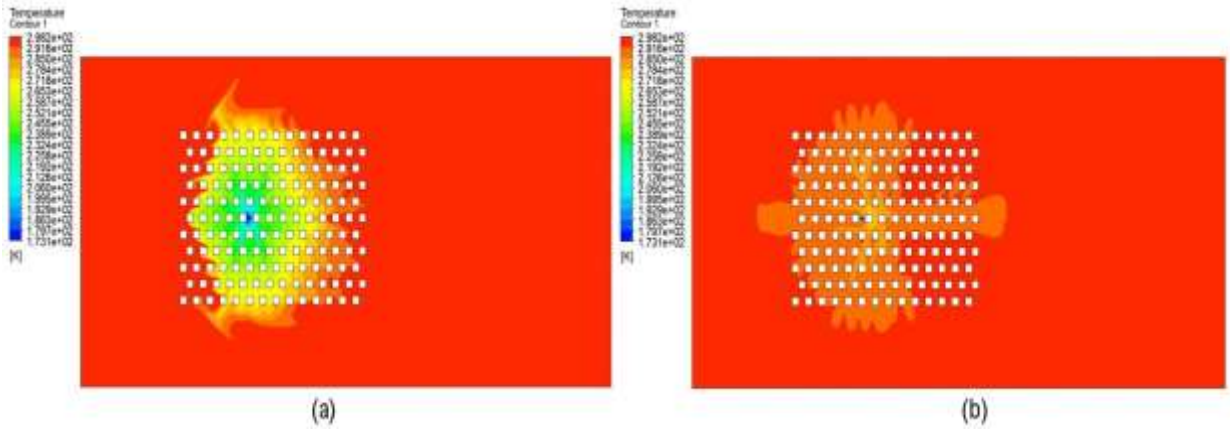

Figure 8.118: (a) *Temperature profile of the heavy gas dispersion for a/the staggered layout with the release source located in the middle of the group of buildings in the sixth row at 1m/s.* ***(b)*** *At 0.25m/s*

Figure 8.118(a) for high speed and Figure 8.118(b) for low speed show the temperature simulation for this study. By visualising the temperature simulation, it is found out that the temperature simulation produces quite the same profile for the case study as that of the

concentration profile. However, the behaviour of temperature is in fact the opposite to that of concentration. This means that the areas which were identified in the concentration simulation as the highly concentrated will in fact have the lowest temperatures, while the ones with moderate concentrations will have moderate temperatures and the least concentrated areas will have the highest temperatures. To further simply these findings, it should be pointed out that the simulations showed that the concentrations near the release source point tend to be the highest and start to fade away as the gas cloud moves away from the source and are at their lowest when as it moves much further away in the layout, reaching the environment where the gas cloud eventually disappears. However, the temperature is at its lowest near the release source point and tends to increase as the gas cloud moves away from source, achieving its highest temperature equal to the ambient temperature of the environment.

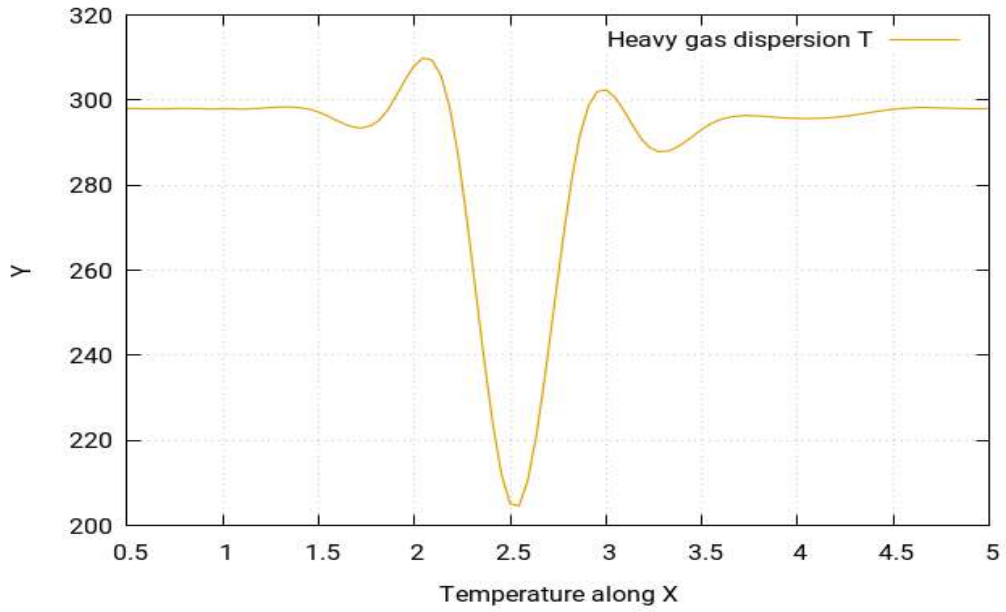

Figure 8.119: *Temperature of the heavy gas dispersion profile along the* ***x****-direction at* ***0.25m/s*** *points of (T) x=2.54m, y=-1m and z=2.12m*

Figure 8.119 shows the temperature curve along the x-direction for this case study when the wind speed 0.25m/s. The temperature curve is a mirror of the concentration curve.

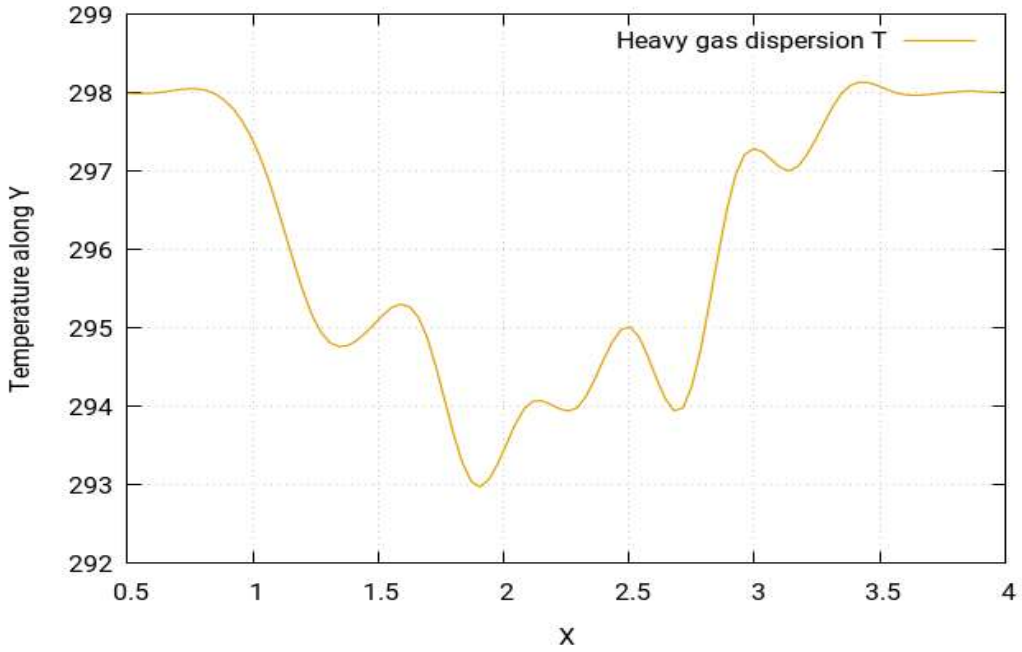

Figure 8.120: *Temperature of the heavy gas dispersion profile along the **y**-direction at **1m/s** points of (T) x=2.86m, y=-1m and z=2m*

Figure 8.120 shows the temperature curve along the y-direction for this case study when the wind speed is 1m/s. It can be seen that the curve shows an asymmetrical pattern and has a multiple peak with the highest peak at almost 1.8m.

8.6.13.6 Heavy gas dispersion with different velocities

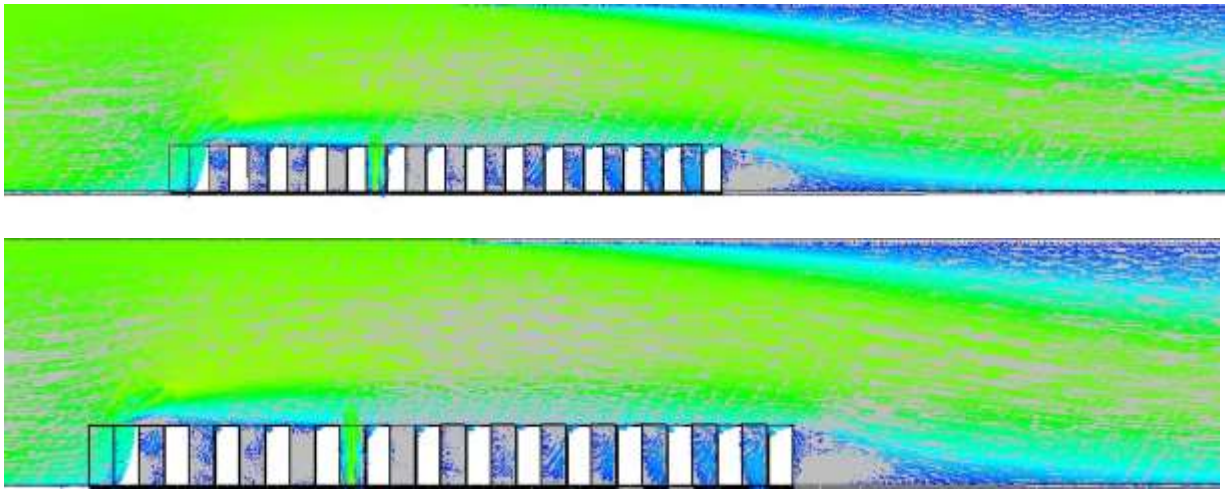

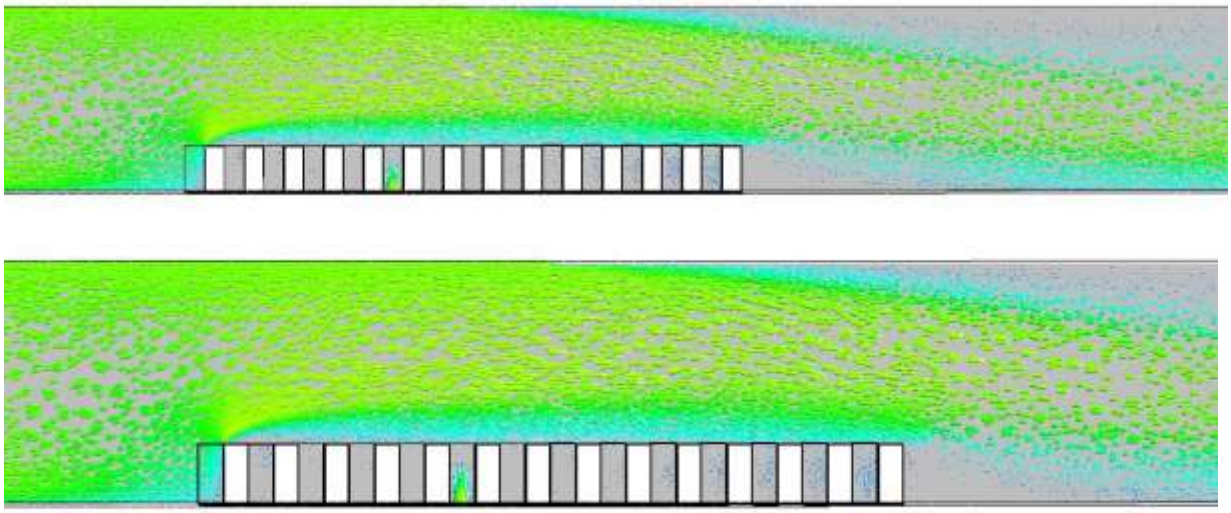

Figure 8.121: (a) *Velocity contours of the heavy gas dispersion for a/the staggered layout with the release source located in the middle of the group of buildings in the sixth row at 1m/s*

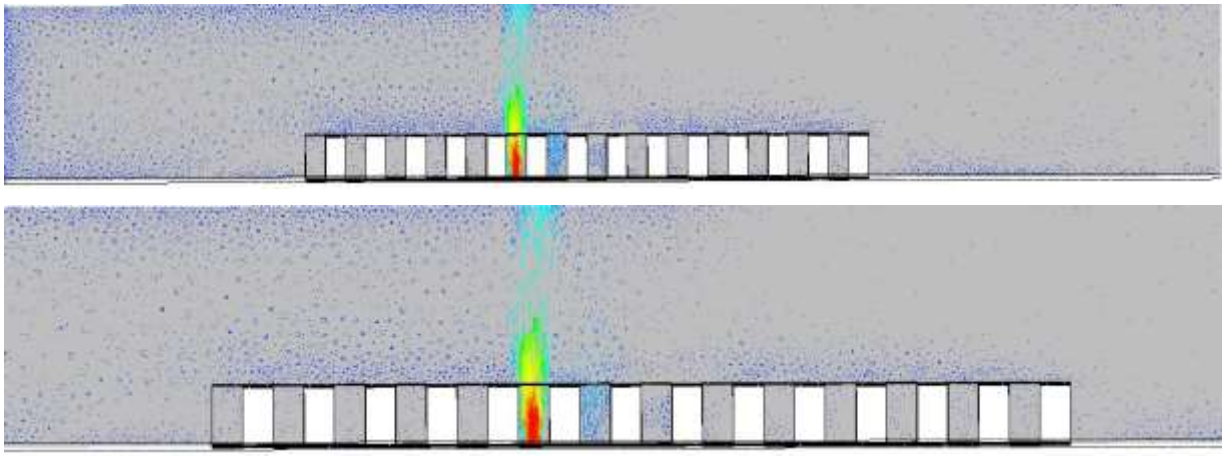

Figure 8.122: (b) *Velocity contours of the heavy gas dispersion for a/the staggered layout with the release source located in the middle of the group of buildings in the sixth row at* ***0.25m/s***

The above figures show the velocity contours of heavy gas dispersion for this case study with the release source located in the middle of the group of buildings in the sixth row. Velocity contours depict the intensity of wind - or the effective wind influence - at the different locations throughout the layout. As can be seen in the figure, the wind intensity is different at different points in the layout. It is a commonly known effect that, with enhanced altitudes, enhanced wind speeds are encountered. This is because the objects at the lower altitudes create resistance to the wind flow. As resistance is caused by the buildings in the flow of gas towards the direction opposite of wind, the wind flowing from left to right fails to indict the same motion of flow. Instead, various complex vertexes are formed within the buildings near the release source location, as can be seen in the above figures. The heavy gas release from the source is carried by these vertexes to the nearby mixture of the gas cloud, which them moves smoothly

away from the source. Moreover, the hindrance to the wind flow caused by the buildings results in the vertexes moving in the upward direction, which enhances the shape of cloud in the upward direction.

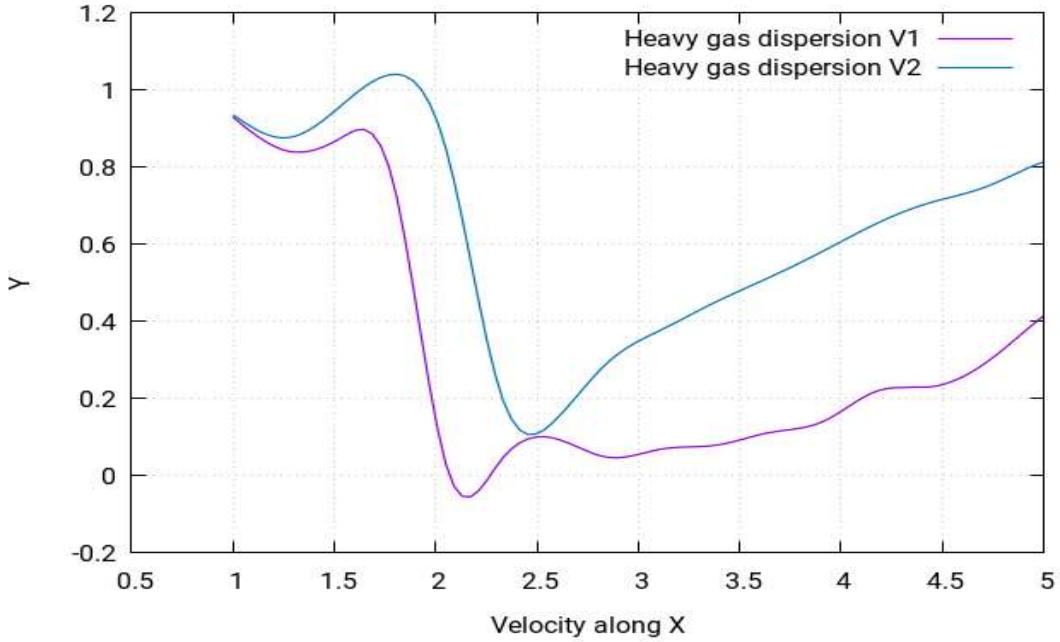

Figure 8.123: *Velocity of the heavy gas dispersion profile along the* ***x****-direction at* ***1m/s*** *different points of (V1) x=1m, y=1.95m z=9.84m (V2) x=1m, y=2.15m and z=2m*

The above figure shows the velocity profiles for two of the gas dispersions along the x-direction at two different locations depending on distance from release source. Both curves follow the same pattern but have different values.

8.6.14 Location 3: Neutral gas dispersion

8.6.14.1 Building layout

The type of layout undertaken for this case study is for the staggered layout. A layout of 154 buildings of cubic shape will be created as staggered layouts and the release source will be placed in positions. The behaviour of the gas clouds will then be studied.

8.6.14.2 Release source location

The release source location (3) of the neutral gas dispersion in this case study was at the middle front of the group of buildings in the sixth row. The perimeters selected for this case study is stated below:

Table 8.25: *Parametric values of the high-speed neutral gas simulation (location 3)*

Density	Flow Rate	Velocity	Ambient Temperature	Release Source Temperature

1.1839 kg m/s^3	1.7737 kg/s	1 m/s	25°C	25°C

8.6.14.3 Concentration of the neutral gas dispersion

The following figure shows the concentration behaviour of the neutral gas at location 3 for a/the staggered layout. The whereabouts of location 3 has been stated at the beginning of the passage.

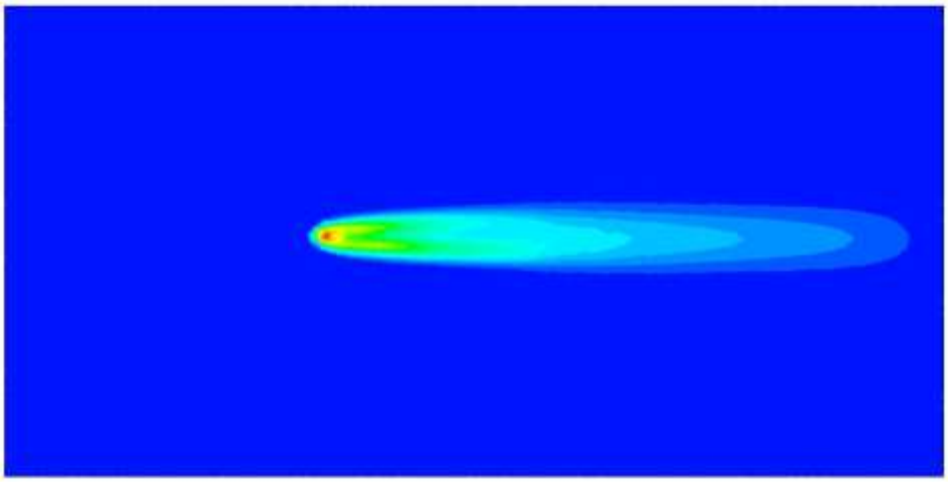

Figure 8.124: *Concentration of the neutral gas dispersion for a/the staggered layout with the release source located at the middle of the group of buildings in sixth row at* ***1m/s***

The planar distance is increased from the ground floor to observe the overall dispersion of the neutral gas. This is because the neutral gas moves in the upward direction, unlike the heavy gas which moves in the horizontal direction.

The concentration of the neutral gas cloud when the release source is placed at the upwind front of the group of buildings in the sixth row can be seen in Figure 8.124 (above). In the figure, red represents the highest concentration, while blue represents the lowest concentration. When the cloud shape is studied, a similar cloud shape can be seen as that seen in the case of the collocated layouts at location 2 for neutral gas. However, there is a small difference in that, in that case, the high concentration part of the cloud looked like an elliptical cylinder, while this one looks like a reversed nozzle. Although there is a similarity in the trend, as the concentrations are maximum near the release point and then follow a decreasing degree of concentration as the cloud moves away from the source, the shape of the cloud is entirely different in this case and hence the distribution on the gas cloud is also different. These results point to the fact that the change of layout does not affect the cloud shape in the case of neutral gas dispersion.

8.6.14.4 Iso-surface of the neutral gas dispersion

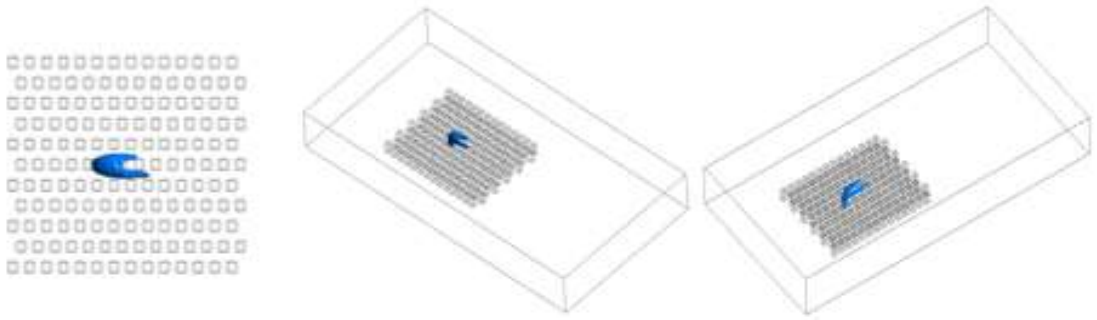

Figure 8.125: *Iso-surfaces of the concentration of neutral gas dispersion for a/the staggered layout with the release source located in the middle of the group of buildings in the sixth row at* ***1m/s***

Figure 8.125 presents the iso-surfaces of the concentration profile of a/the neutral gas cloud when the release source is placed at the upwind front of the group of buildings in sixth row. These iso-surfaces help determine that the shape of the cloud is somewhat shrunken in this case and only occupies a few of the building blocks in the layout, resembling the shape of the symmetrical opening in the horizontal direction. This is identical to the results of the neutral gas case study at (location 1).

According to Standard BS EN 60079-10-1:2009 [104], the following locations can be categorised:

Zone 0: The central middle front of the building layout

Zone 1: The immediate surrounding of the building layout and areas categorised in zone 0

Zone 2: All the remaining locations not categorised in zone 0 or zone 1

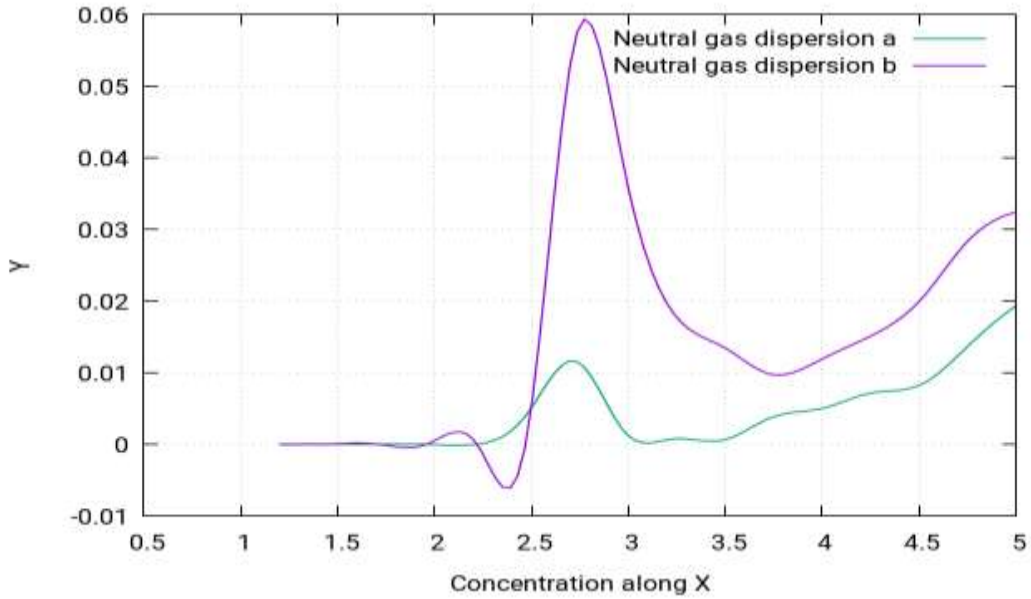

Figure 8.126: *Concentration of the neutral gas dispersion profile along the* ***x-*** *direction at* ***1m/s*** *different points of (a) x=1.20m, y=2.05m, z=2m (b) x=1.20m, y=2.05m and z=3.03m*

In Figure 8.126 (above), two different curves for the concentration profiles are shown. They show the pattern of the concentration profile along the x-direction when the wind speed for the simulation is 1m/s. The two different curves are obtained for two different distances from the release source. Both curves follow the same pattern but have different values due to a difference of distances. From the figure, it is concluded that the concentration value of the concentration of heavy gas decreases as it moves away from the source. In the figure, the curve with highest peak is obtained when nearest to the release source and vice versa.

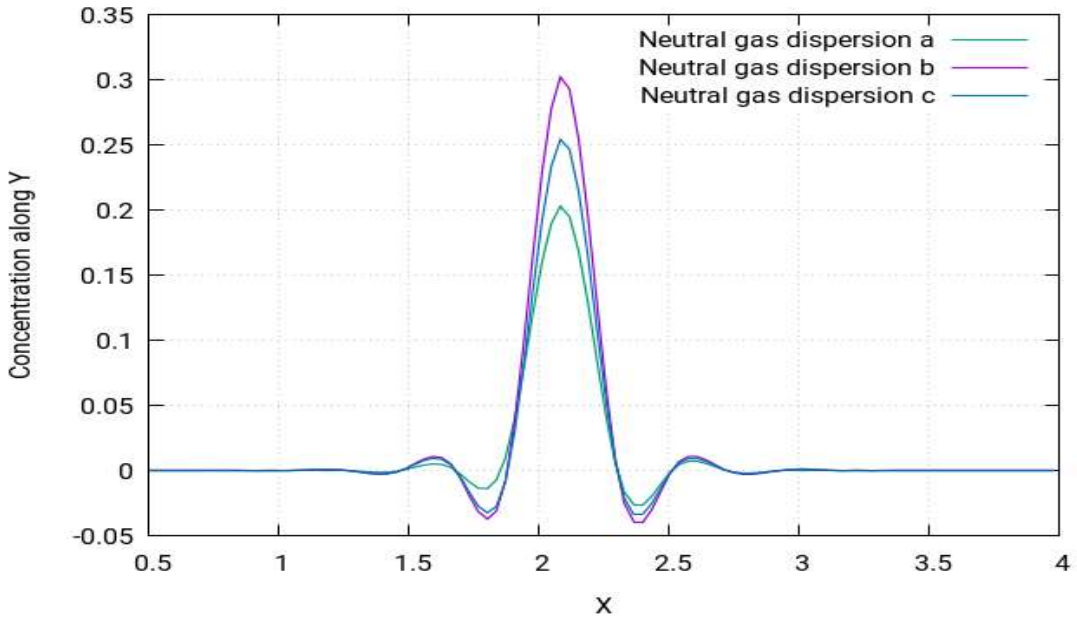

Figure 8.127: *Concentration of the neutral gas dispersion profile along the **y**-direction at **1m/s** different points of (a) x=2.75m, y=-1m, z=3.30m, (b) x=2.65m, y=-1m, z=2.85m (c)x=2.55m and y=-1m, z=2m*

In Figure 8.127 (above), two different curves for the concentration profiles are shown. They show the pattern of the concentration profile along the y-direction when the wind speed for the simulation is 1m/s. The two different curves are obtained for two different distances from the release source. Along the y-direction, the profiles show a remarkably symmetric and similar pattern with a single peaked curve.

8.6.14.5 Velocity of the neutral gas dispersion

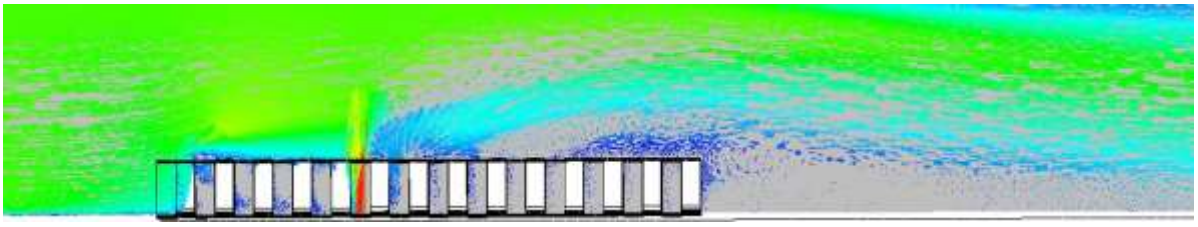

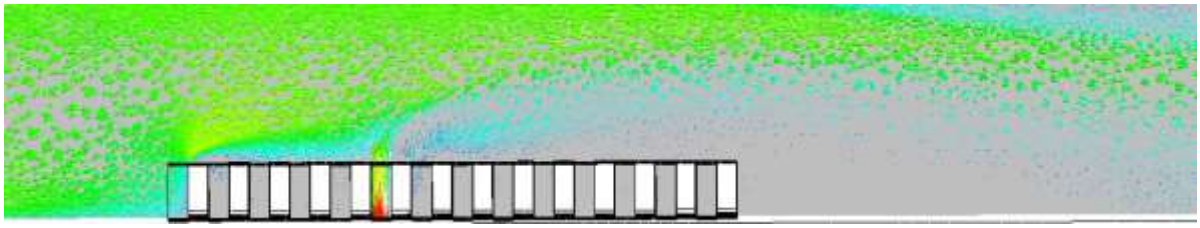

Figure 8.128: *Velocity contours of the concentration of neutral gas dispersion for a/the staggered layout with the release source located at the middle of the group of buildings in the sixth row at* ***1m/s***

Figure 8.128 shows the velocity contours of the neutral gas dispersion for this case study, with the release source located in the middle of the group of buildings in the sixth row. The velocity contours depict the intensity of wind - or the effective wind influence - at the different locations throughout the layout. As can be seen in the figure, the wind intensity is different at different points in the layout. It is a commonly known effect that, with enhanced altitudes, enhanced wind speeds are encountered. This is because the objects at the lower altitudes create resistance to the wind flow. As resistance is caused by the buildings in the flow of gas towards the direction opposite of wind, the wind flowing from left to right fails to indict the same motion of flow. Instead, there are various complex vertexes formed within the buildings near the release source location, as can be seen in (Figure 8.128). The heavy gas released from the source is carried by these vertexes to the nearby mixture of the gas cloud, which then moves smoothly away from the source. Moreover, the hindrance in the wind flow caused by the buildings results in the vertexes moving in the upward direction, which enhances the shape of cloud in the upward direction.

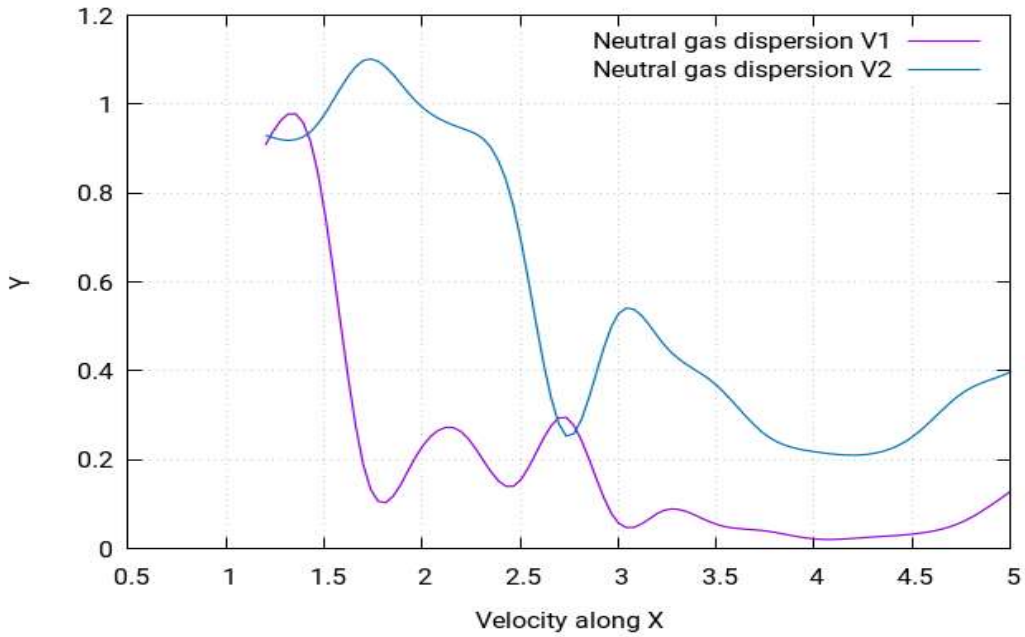

Figure 8.129: *Velocity of neutral gas dispersion profile along the* ***x****-direction at* ***1m/s*** *different points of (V1) x=1.20m, y=2.05m, z=2m (V2) x=1.20m, y=-1m and z=3.03m*

The above figure shows the velocity profiles for two of the gas dispersions at two different locations depending on distance from release source. The curves show a very different pattern when compared to each other.

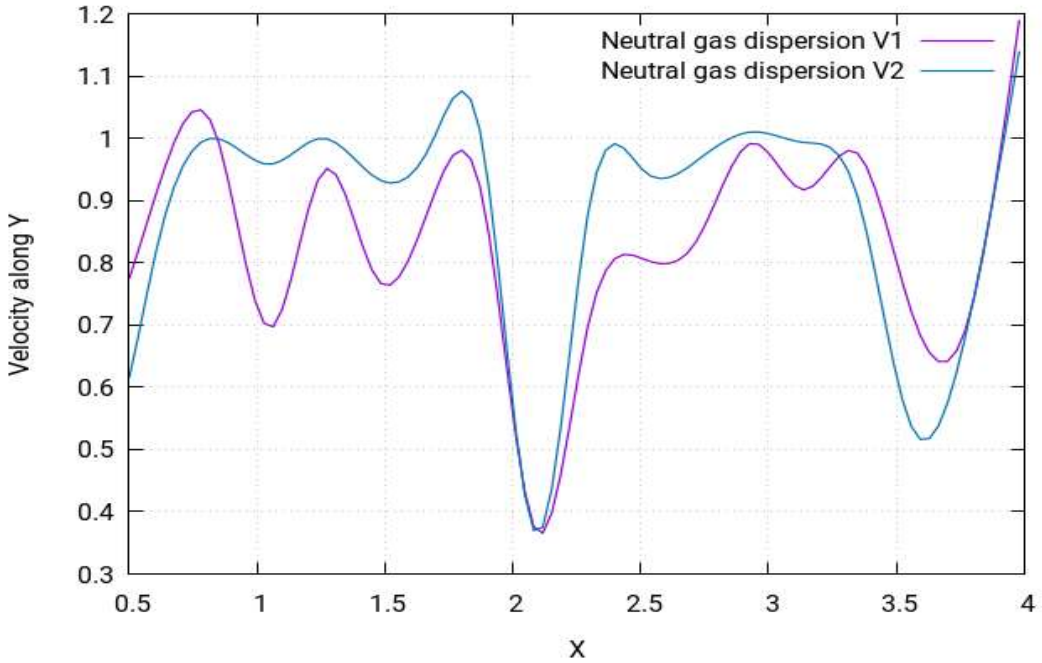

Figure 8.130: *Velocity of the neutral gas dispersion profile along the* ***y****-direction at* ***1m/s*** *different points of (V1) x=2.65m, y=-1m, z=2.85m (V2) x=2.75m, y=-1m and z=3.30m*

Figure 8.130 shows the curves for the velocity profile along the x-direction. The curves follow an asymmetrical pattern and have several peaks, with the highest peak being at approximately 2.1m.

The dispersion of the neutral gas for location 3 can be seen in this figure. It is seen that the dispersion of the neutral gases remains the same i.e., in the upward direction independent of the location.

8.6.15 Location 1: Heavy gas dispersion at different velocities

8.6.15.1 Structure of layout

The type of layout adopted for these two case studies the collocated layout. A layout of 6 Oil storage tanks group will be created, as will a cylinder shape distribution, and the release source will be placed in the same positions. The behaviour of the gas clouds will then be studied.

8.6.15.2 Release source location

The release source point was located (1) at the upwind front of the group of gas storage tanks between the first and second column in the middle between the third and fourth rows. The perimeters selected for this case study are stated below:

Table 8.26: *(A) Parametric values for the high-speed heavy gas simulation (location 1)*

Density	Flow Rate	Velocity	Ambient Temperature	Release Source Temperature
2.1 kg m/s^3	1 kg/s	1 m/s	25°C	-100°C

Table 8.27: *(B) Parametric values for the high-speed heavy gas simulation (location 1)*

Density	Flow Rate	Velocity	Ambient Temperature	Release Source Temperature
2.1 kg m/s^3	5 kg/s	0.25 m/s	25°C	-100°C

8.6.15.3 Concentration of the heavy gas dispersion at different velocities

The following figure shows the concentration behaviour of the heavy gas at location 1. The whereabouts of location 1 has been stated at the beginning of the passage.

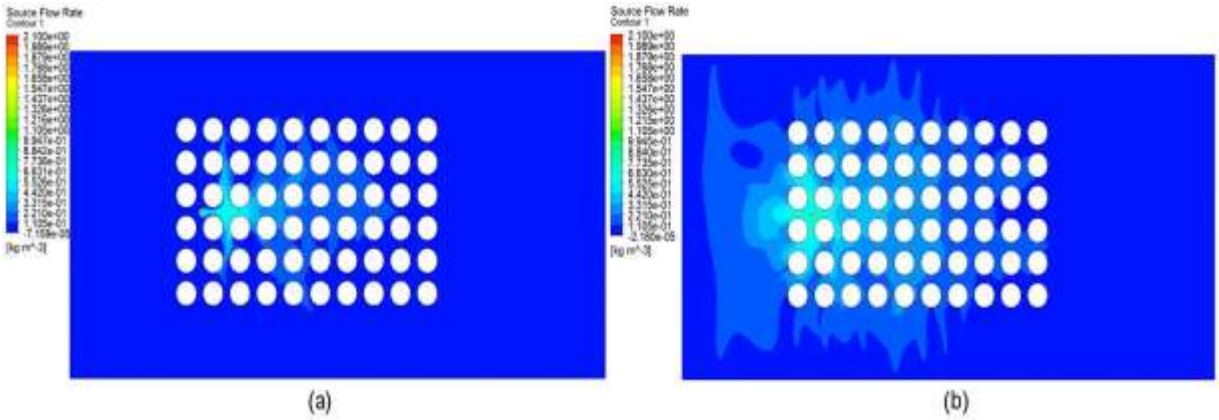

Figure 8.131: (a) *Concentration profile of the heavy gas dispersion with the release source located at the upwind front of the group of gas storage tanks between the first and second columns in the middle between the third and fourth rows at 1m/s.* ***(b)****At 0.25m/s*

The concentration profile of the heavy gas at location 1 is shown in Figure 8.131 above. It represents the concentration behaviour of the heavy gas when the release gas source is placed at the upwind front of the group of gas storage tanks between the first and second column in the middle between the third and fourth rows. In the above figure, parts labelled (a) are at high speed and those labelled (b) are at low speed. In the figure, the cloud shape for high-speed heavy gas shows that the gas cloud looks like a rectangle stretched from the horizontal edges. Another thing to note is that the cloud shape is case of low speed (0.25m/s) seems to show the

same pattern but in a very broad region. Moreover, in case of high speed, the gas cloud is prevented from moving in the direction opposite to wind, while in the low-speed case, it does move in the direction opposite to wind i.e., the negative horizontal direction.

8.6.15.4 Iso-surface of the concentration heavy gas dispersion different velocities

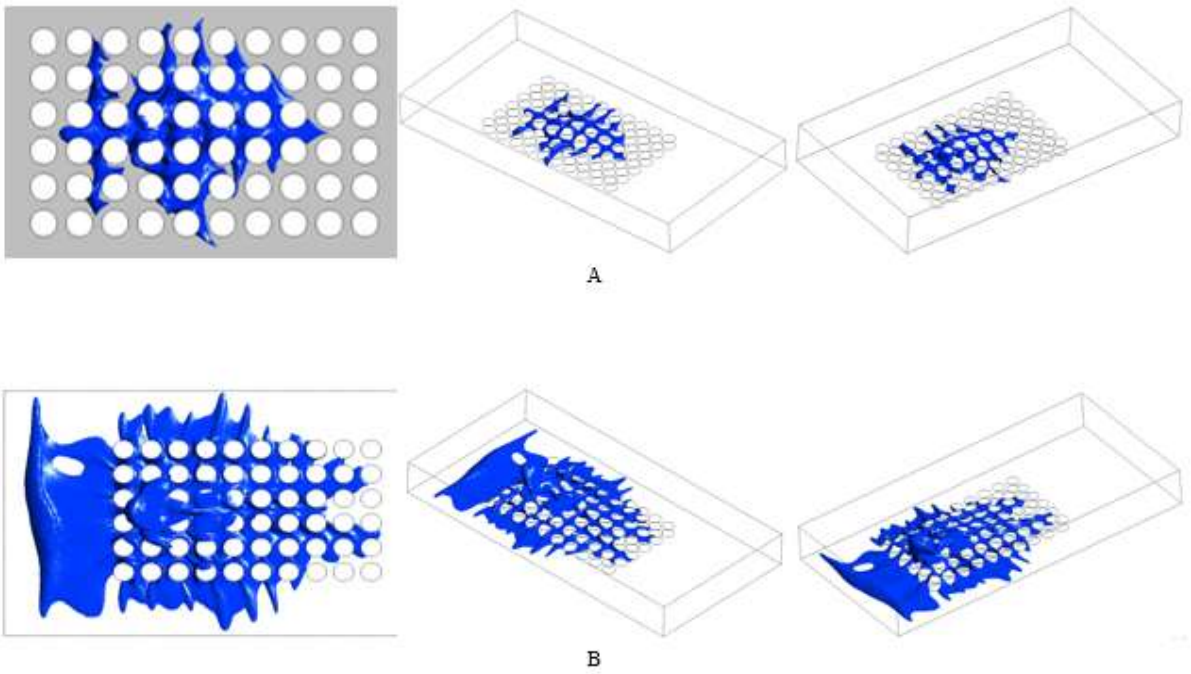

Figure 8.132: (a) *Iso-surfaces of the concentration profile of the heavy gas dispersion with the release source located at the upwind front of the gas storage tanks group between the first and second columns in the middle between the third and fourth rows at 1m/s.* ***(b)****At 0.25m/s*

Figure 8.132(a) presents the iso-surfaces of the concentration profile of the heavy gas dispersion for a/the staggered layout with release source located at the upwind front of the gas storage tanks group between the first and second columns in the middle between the third and fourth rows. This helps identify the spread of the cloud in each dimension; it can be seen that the cloud is concentrated at the release source location and takes a rather higher portion of the vertical direction, while at other locations, it tends to stay at lower altitudes. The iso-surfaces also help visualise the accumulated areas of the gas cloud in the case of low speed as in Figure 8.132(b).

According to Standard BS EN 60079-10-1:2009 [104], the following locations can be categorised:

High speed:

Zone 0: The central two rows of the building layout containing the release source

Zone 1: The middle symmetrical central portion of the building layout

Zone 2: All the remaining locations not categorised in zone 0 or zone 1

Low speed:

Zone 0: The central two rows of the building layout containing the release source area and the upwind front of the building layout

Zone 1: The remaining portions of the building layout mentioned in zone 0, excluding a small triangle of buildings in the last front

Zone 2: All the remaining locations not categorised in zone 0 or zone 1

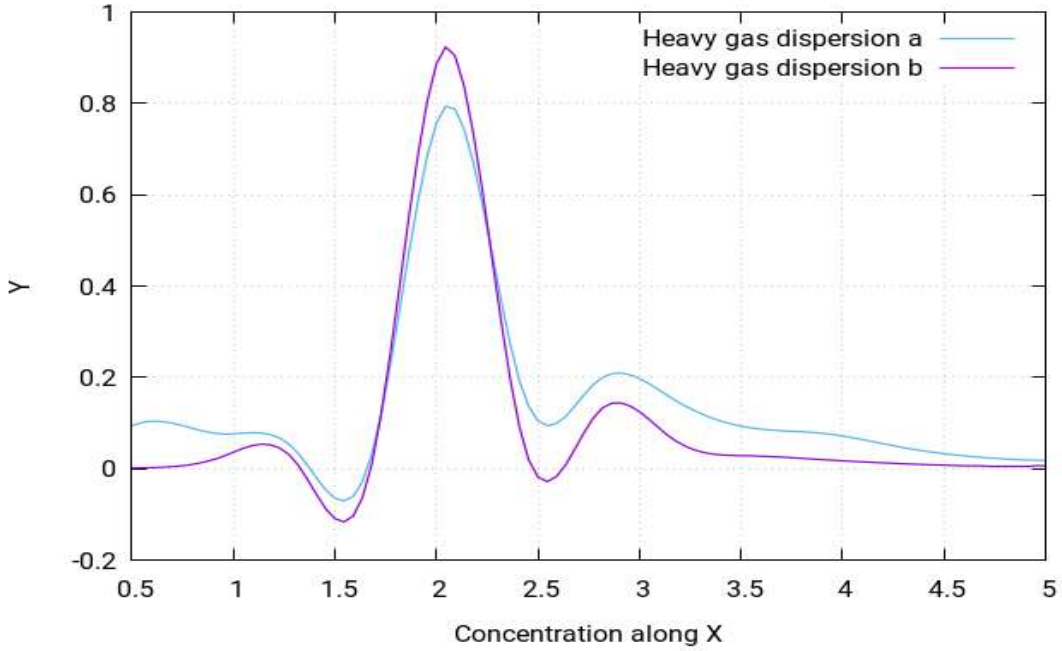

Figure 8.133: *Concentration of the heavy gas dispersion profile with a low velocity of* ***0.25 m/s*** *along the* ***x****-direction at different points of (a) x=2.00m, y=2.03m, z=1.50m (b)x=2.00m, y=2.03m and z=1.50m*

The above figure shows the velocity profiles for two of the gas dispersions at two different locations depending on distance from release source. Both curves follow the same pattern but have different values.

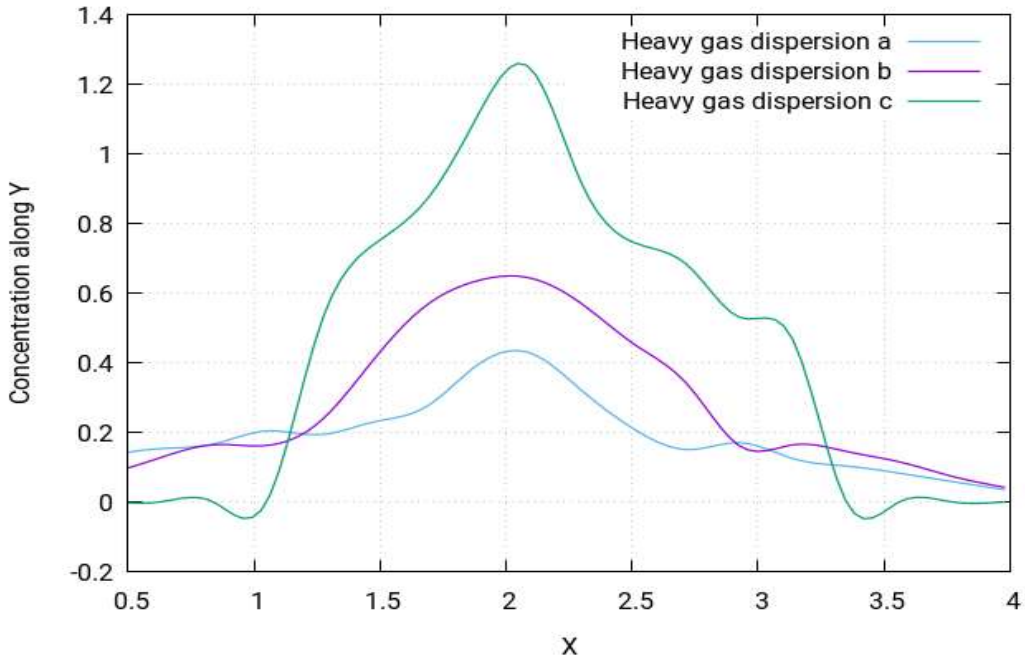

Figure 8.134: *Concentration of the heavy gas dispersion profile with a low velocity of* ***0.25 m/s*** *along the* ***y****-direction at different points of (a) x=1.30m, y=-1m, z=7.20m (b)x=1.94m, y=-1m, z=97.20m (c) x=1.94m, y=-1m and z= 1.52m*

The above figure shows the velocity profiles for three of the gas dispersions at three different locations depending on distance from release source. The curves follow the same pattern but have different values.

8.6.16.5 Temperature of heavy gas dispersion with different velocities

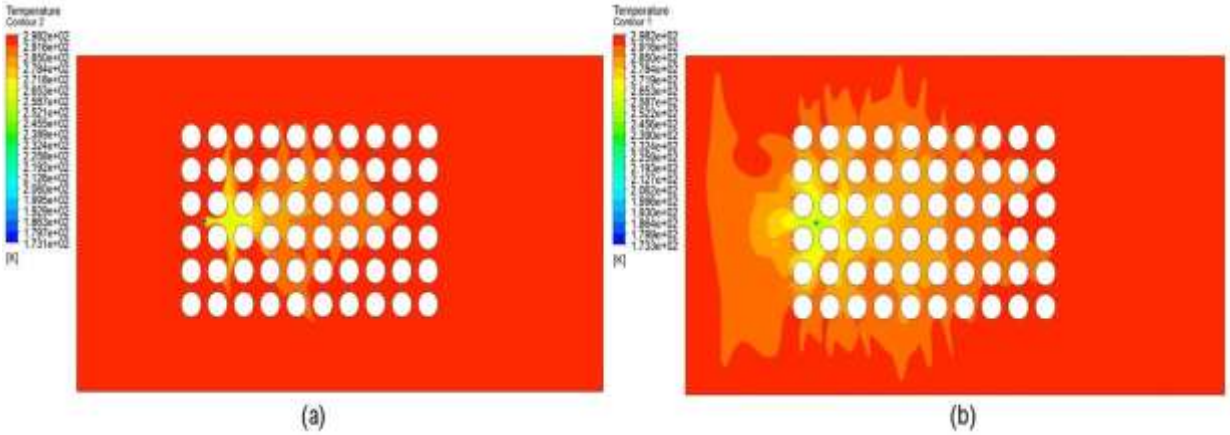

Figure 8.135: (a) *Temperature profile of the concentration profile of the heavy gas dispersion with the release source located at the upwind front of the gas storage tanks group between the first and second columns in the middle between the third and fourth rows at 1m/s.* ***(b)*** *At 0.25m/s*

Figure 8.135(a) for high speed and Figure 8.135(b) for low speed (both above) show the temperature simulation for this study. By visualising the temperature simulation, it is found out that the temperature simulation produces largely the same profile for the case study as that of the concentration profile. However, the behaviour of temperature is in fact the opposite to that

of concentration. This means that the areas which were identified in the concentration simulation as highly concentrated will in fact have the lowest temperatures, while the ones with moderate concentrations will have moderate temperatures and the least concentrated areas will have the highest temperatures. To further simply these findings, it should be pointed out that the simulations show that the concentrations near the release source point tend to be the highest and start to fade away as the gas cloud moves away from the source and end to be the lowest when it moves much further away in the layout reaching the environment where the gas cloud eventually disappears. However, the temperature is at its lowest near the release source point and tends to increase as the gas cloud moves away from source, finally achieves the highest temperature equal to the ambient temperature of the environment. Figure 8.135(a) for high speed and Figure 8.135(b) have been added in order to depict this behaviour of the temperature.

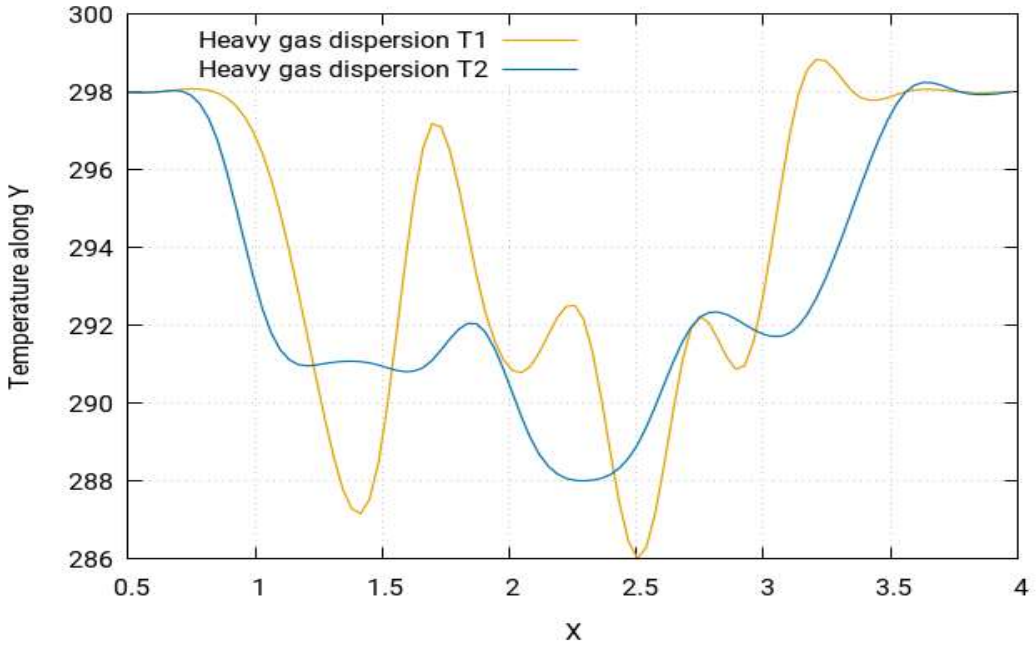

Figure 8.136: *Temperature of the heavy gas dispersion profile along the* ***y****-direction at* ***1m/s*** *different points of (T1) x=2.35m, y=-1m, z=7.00m (T2) x=3.50m, y=-1m and z=6.00m*

The above figure shows the temperature profiles for two of the gas dispersions at two different locations depending on distance from release source. The curves show distinctly different patterns from each other.

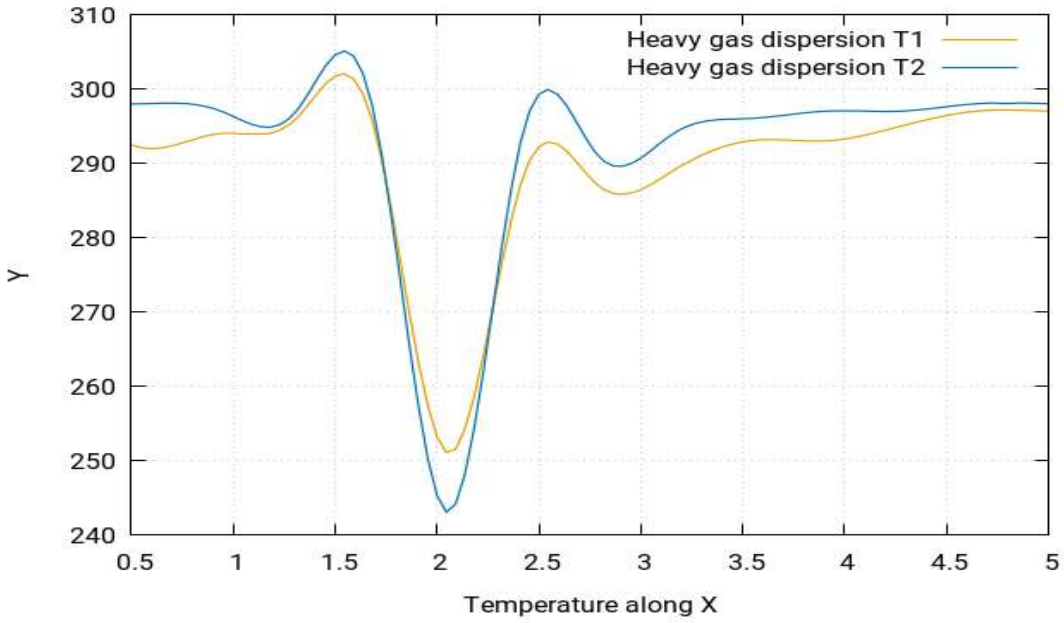

Figure 8.137: *Temperature of the heavy gas dispersion profile with a low velocity of* ***0.25 m/s*** *along the* ***x****-direction at different points of (T1) x=2.00m, y=2.03m, z=1.50m (T2) x=2.00m, y=2.03m and z=2.88m*

In Figure 8.137 (above), two different curves for the temperature profiles are shown. They show the pattern of the temperature profile along the x-direction when the wind speed for the simulation is 0.25m/s. The two different curves are obtained for two different distances from the release source. These results show that, at speed of 0.25m/s, temperature profiles are a mirror of the concentration profile.

8.6.16.6 Heavy gas dispersion at different velocities

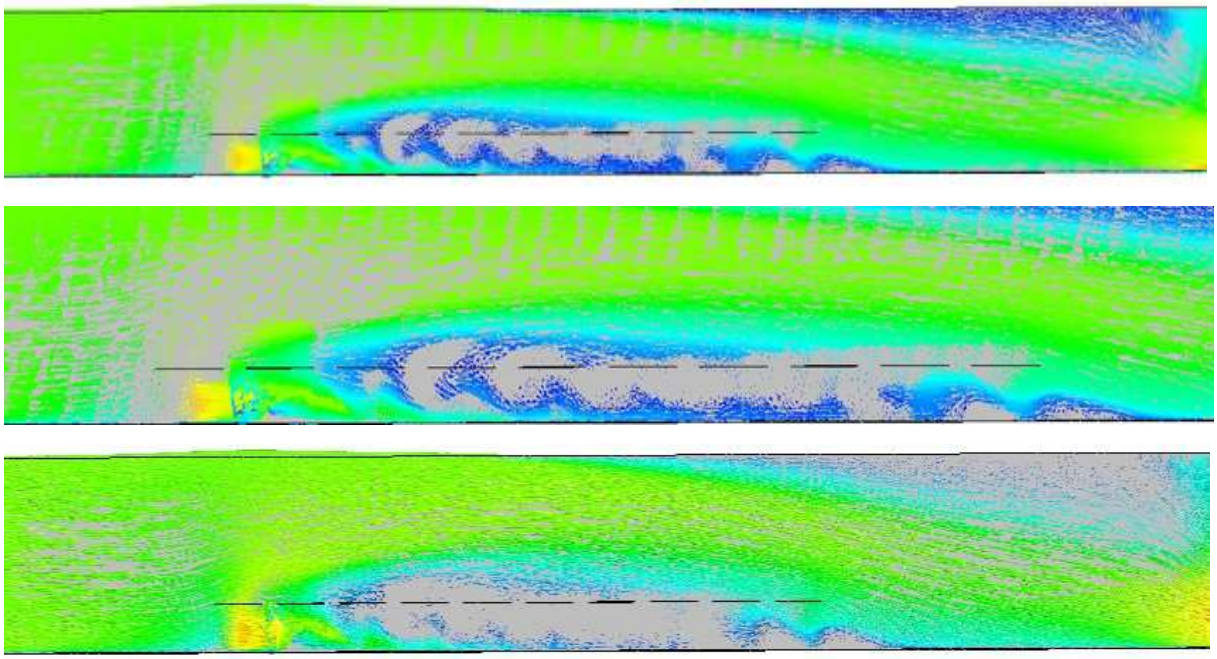

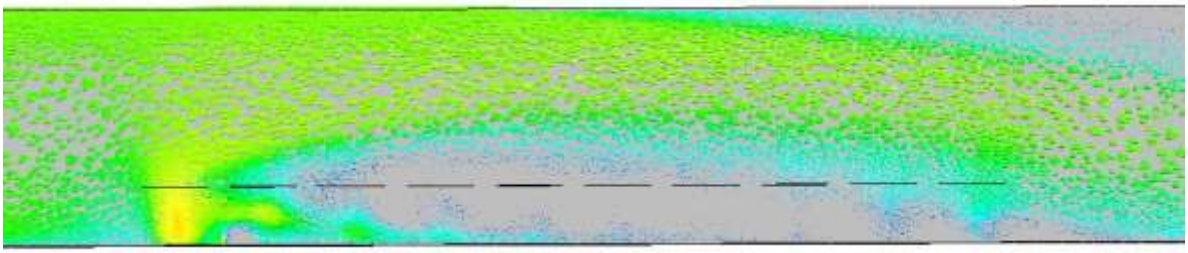

Figure 8.138: (a) *Velocity contours of the heavy gas dispersion with the release source located at the upwind front of the group of gas storage tanks between the first and second columns in the middle between the third and fourth rows at* ***1m/s***

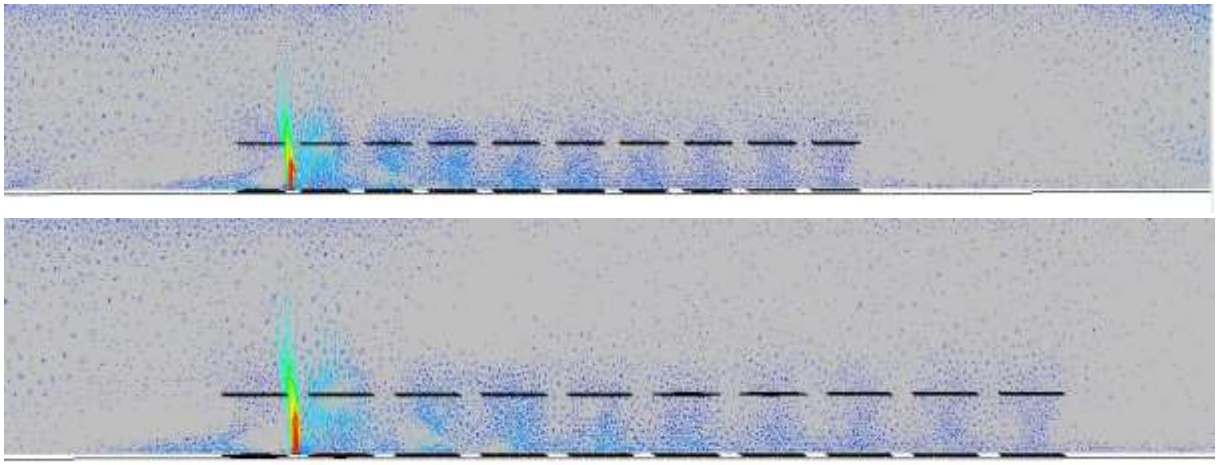

Figure 8.139: (b) *Velocity contours of the heavy gas dispersion with the release source located at the upwind front of the group of gas storage tanks between the first and second columns in the middle between third and fourth rows at* ***0.25m/s***

The above figures show the velocity contours of the heavy gas dispersion for this case study, with the release source located at the upwind front of the group of gas storage tanks between the first and second columns in the middle between the third and fourth rows. Velocity contours depict the intensity of wind - or the effective wind influence - at the different locations throughout the layout. In the figure, the wind intensity is different at different points in the layout. It is a commonly known effect that, with enhanced altitudes, enhanced wind speeds are encountered. This is because the objects at the lower altitudes create resistance to the wind flow. As resistance caused by the buildings in the flow of gas towards the direction opposite of wind, the wind flowing from left to right fails to indict the same motion of flow. Instead, various complex vertexes are formed within the buildings near the release source location, as can be seen in the above figures. The heavy gas released from the source is carried by these vertexes to the nearby mixture of the gas cloud, which then moves smoothly away from the source. Moreover, the hindrance to the wind flow caused by the buildings results in the vertexes moving in the upward direction, which enhances the shape of cloud in the upward direction.

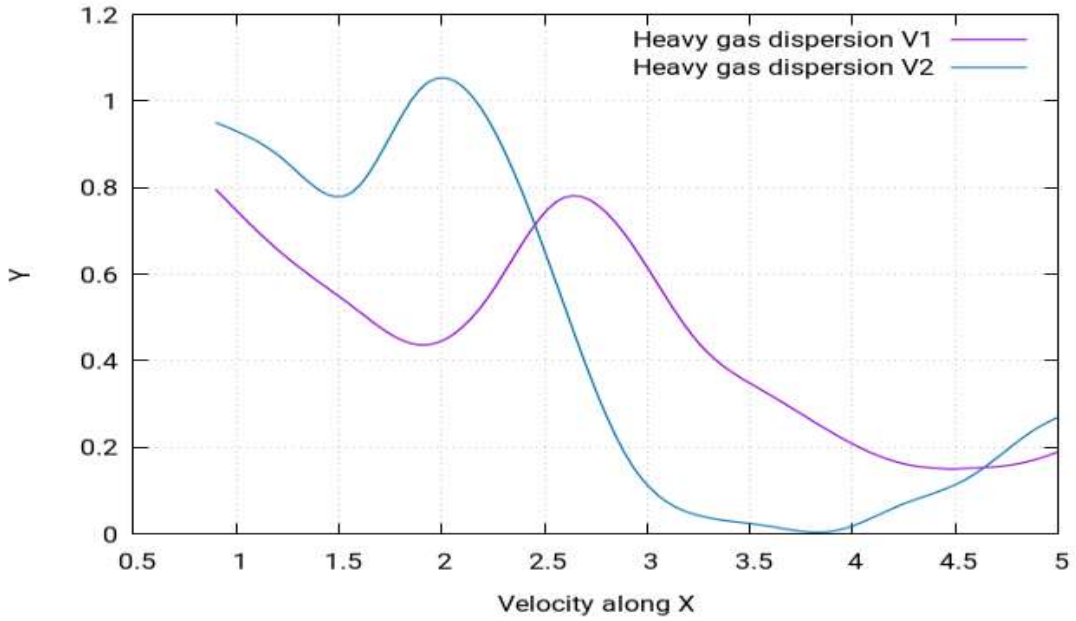

Figure 8.140: *Velocity of the heavy gas dispersion profile along the **x**-direction at **1m/s** different points of (V1) x=9.00m, y=2.03m, z=7.20m (b) x=9.00m, y=2.03m and z=9.84m*

The above figure shows the velocity profiles for two of the gas dispersions at two different locations depending on distance from release source. Both curves follow the same pattern but have different values.

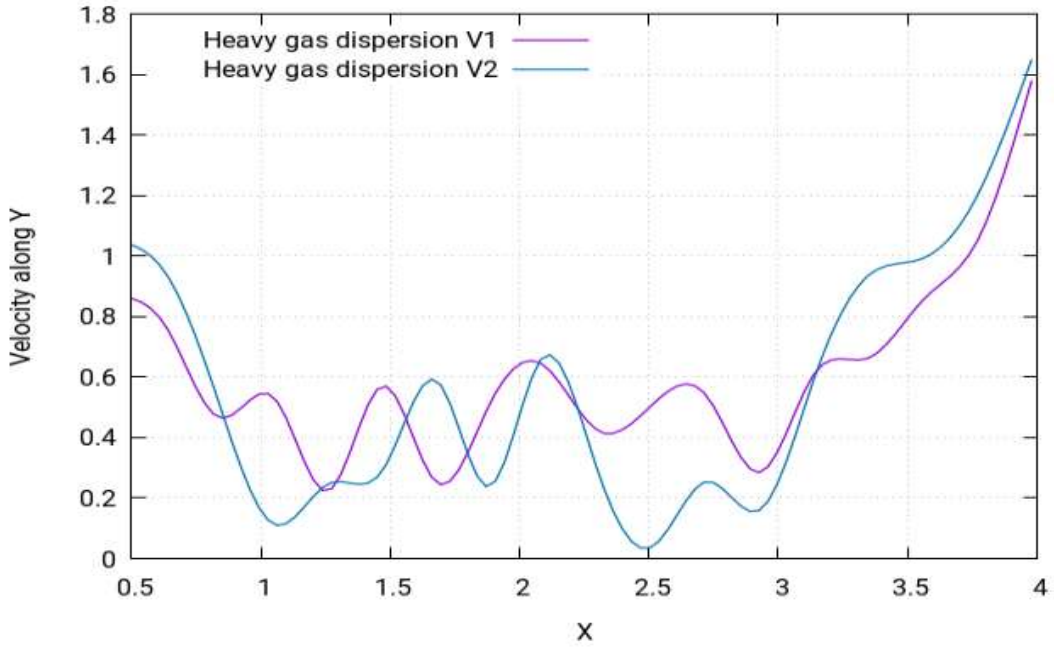

Figure 8.141: *Velocity of the heavy gas dispersion profile along the **y**-direction at **1m/s** different points of (V1) x=1.94m, y=-1m, z=7.20m (V2) x=2.35m, y=-1m and z=7.00m*

Figure 8.141 shows the curves for the velocity profile along the y-direction. The curves follow an asymmetrical pattern and have several peaks, with the highest peak being at approximately 2.5m.

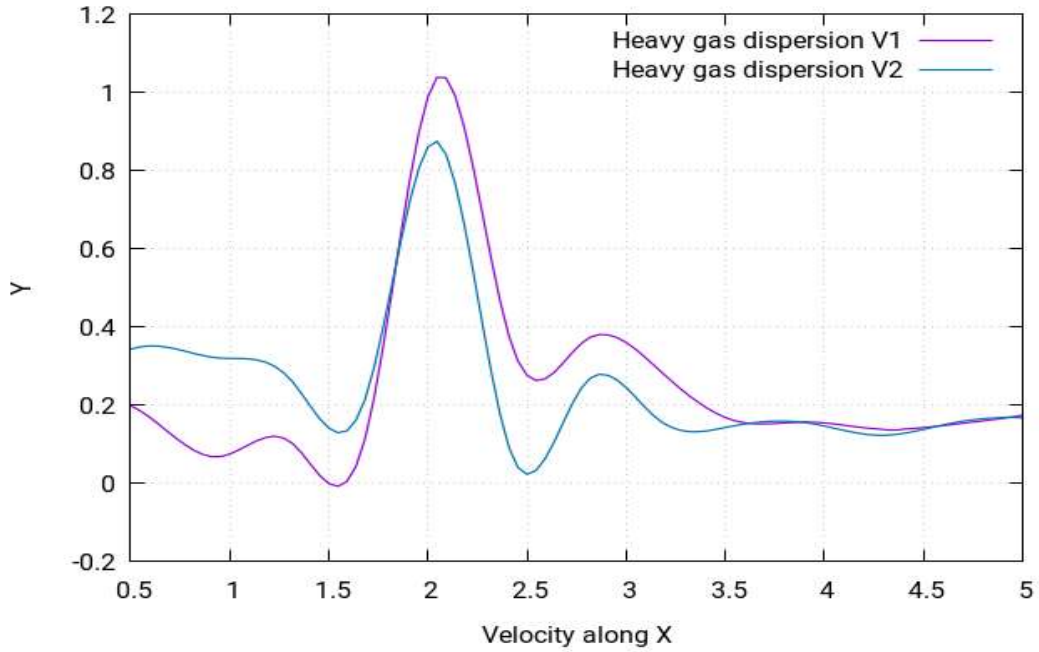

Figure 8.142: *Velocity of the heavy gas dispersion profile with a low velocity of* ***0.25 m/s*** *along the* ***x****-direction at different points of (V1) x=2.00m, y=2.03m z=1.50m (V2) x=2m, y=2.03m and z=2.88m*

The above figure shows the velocity profiles for two of the gas dispersions at two different locations depending on distance from release source. Both curves follow the same pattern but have different values.

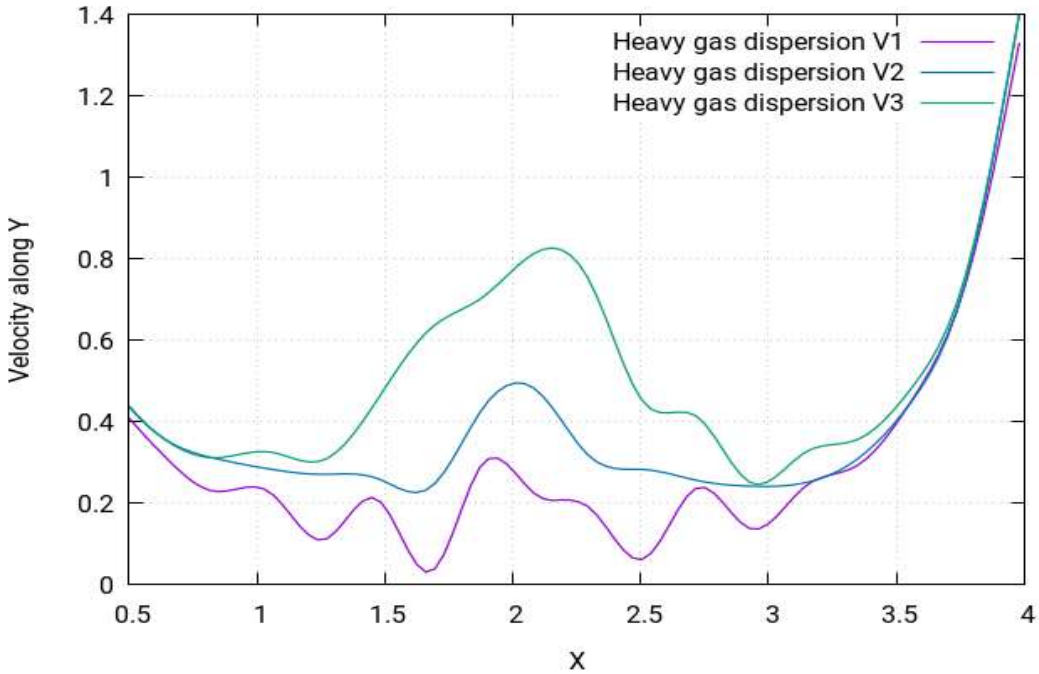

Figure 8.143: *Velocity of the heavy gas dispersion profile with a low velocity of* ***0.25 m/s*** *along the* ***y****-direction at different points of (V1) x=1.94m, y=-1m, z=1.52m, (V2) x=1.30m, y=-1m, z=7.20m (V3) x=1.94m, y=-1m and z=7.20m*

The above figure shows the velocity profiles for three of the gas dispersions at three different locations depending on distance from release source. The curves follow the same pattern but have different values.

For the circular shaped obstacles, the dispersion of the heavy gas is observed at different velocities of 1 m/s and 0.25 m/s. It is seen that, in the case of circular shaped obstacles, the dispersion of the gas is smooth around the obstacles with no accumulation of the heavy gas. However, the dispersion area increases in case of high velocity of the heavy gas due to low turbulence.

8.6.17 Location 1: Neutral gas dispersion

8.6.17.1 Structure of layout

The type of layout adopted for this case study is for the collocated layout. A layout of 60 oil storage tanks group will be created with a cylinder-shaped distribution and the release source will be place in position. The behaviour of the gas clouds will then be studied.

8.6.17.2 Release source location

The release source point (1) was located at the upwind front of the group of gas storage tanks between the first and second columns in the middle between the third and fourth rows. The perimeters selected for this case study is stated below:

Table 8.28: *Parametric values for high-speed neutral gas simulation (location 1)*

Density	Flow Rate	Velocity	Ambient Temperature	Release Source Temperature
1.1839 kg m/s^3	1.7737 kg/s	1 m/s	25°C	25°C

8.6.17.3 Concentration of the neutral gas dispersion

The following figure shows the concentration behaviour of the neutral gas at location 1. The whereabouts of location 1 has been stated at the beginning of the passage.

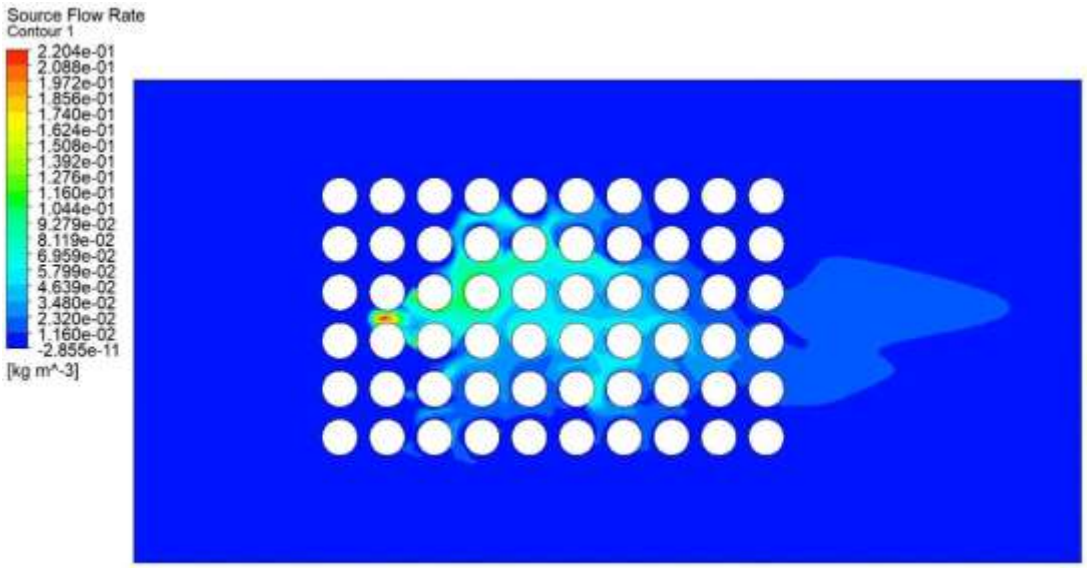

Figure 8.144: *Concentration profile of the neutral gas dispersion with the release source located in the upwind front of the group of gas storage tanks between the first and second columns in the middle between the third and fourth rows at* ***1m/s***

The concentration profile of the neutral gas at location 1 is shown in Figure 8.144 (above). It represents the concentration behaviour of the neutral gas when the release gas source is placed at the middle front of the group of buildings in the middle between the third and fourth row. It can be seen in the figure that the cloud shape in this case is of a zig-zagged form. The cloud first tends to move towards the upward edge of the layout and then leans towards the downward edge, hence forming zig-zagged pattern. The gas source is placed at the upwind front and the study is conducted at high speed so no concentrations in the negative horizontal directions are noticed.

8.6.17.4 Iso-surfaces of the neutral gas dispersion

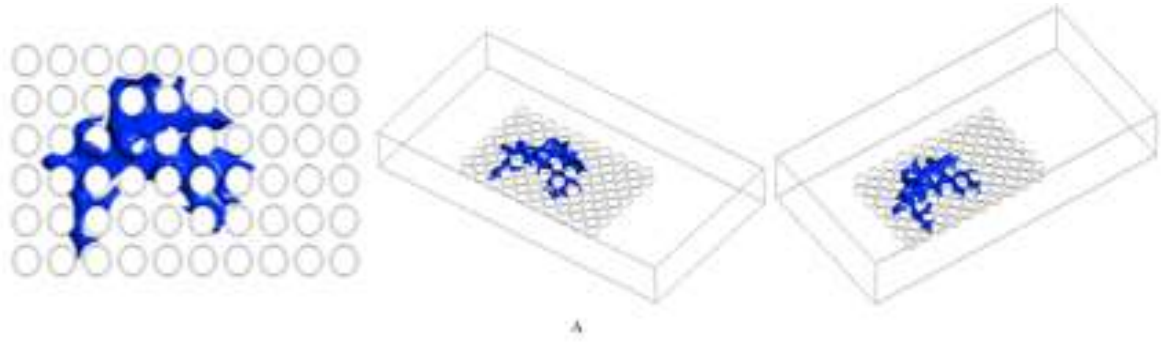

Figure 8.145: *Iso-surfaces of the concentration profile of the neutral gas dispersion with the release source located at the upwind front of the group of gas storage tanks between the first and second columns in the middle between the third and fourth rows at* ***1m/s***

Figure 8.145 presents the iso-surfaces of the concentration profile of the heavy gas dispersion with the release source located at the upwind front of the group of gas storage tanks between

the first and second column in the middle between the third and fourth rows. It helps identify the spread of the cloud in each dimension. It can be seen see that the cloud forms a zig-zagged pattern and that the usual cumulated cloud concentrations near the release source are not present in this case.

According to Standard BS EN 60079-10-1:2009 [104], the following locations can be categorised:

Zone 0: The central region buildings from upwind to middle front

Zone 1: The immediate surroundings of the buildings categorised in zone 0

Zone 2: All the remaining locations not categorised in zone 0 or zone 1

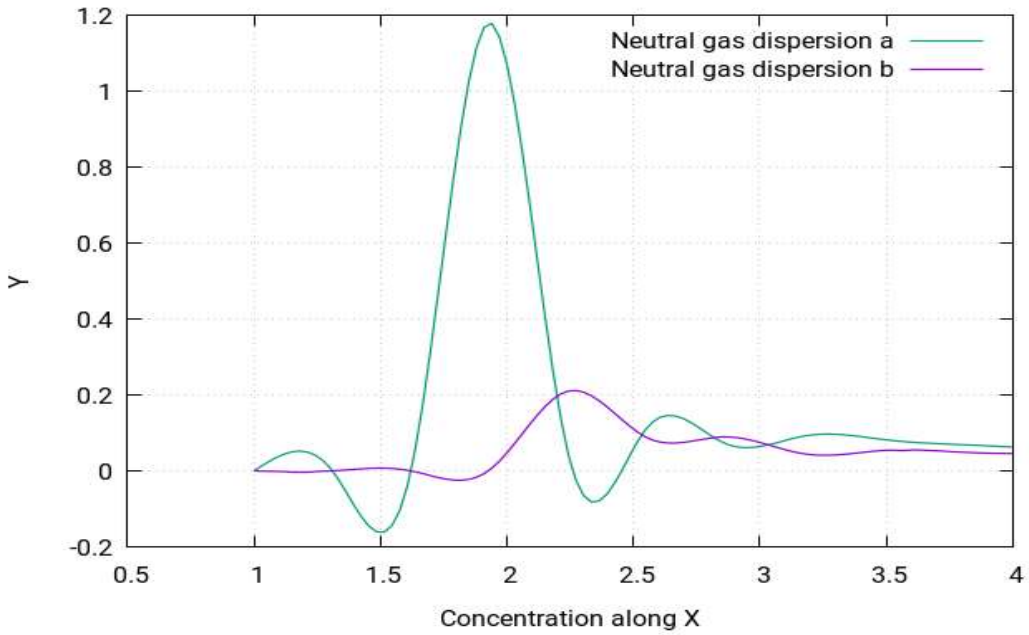

Figure 8.146: *The concentration of neutral gas dispersion profile along the* ***x****-direction at different points of (a) x=1.00m, y=2.03m, z=7.20m (b) x=1.00m, y=2.03m and z=9.84m*

In Figure 8.146 (above), two different curves for the concentration profiles are shown. They show the pattern of the concentration profile along the x-direction when the wind speed for the simulation is 1m/s. The two different curves are obtained for two different distances from the release source. Both the curves follow the same pattern but have different values due to difference in distances. From the figure, it is concluded that the concentration value of the heavy gas decreases when moved away from the source. In the figure, the curve with highest peak is obtained when nearest to the release source and vice versa.

10.6.17.5 Velocity of the neutral gas dispersion

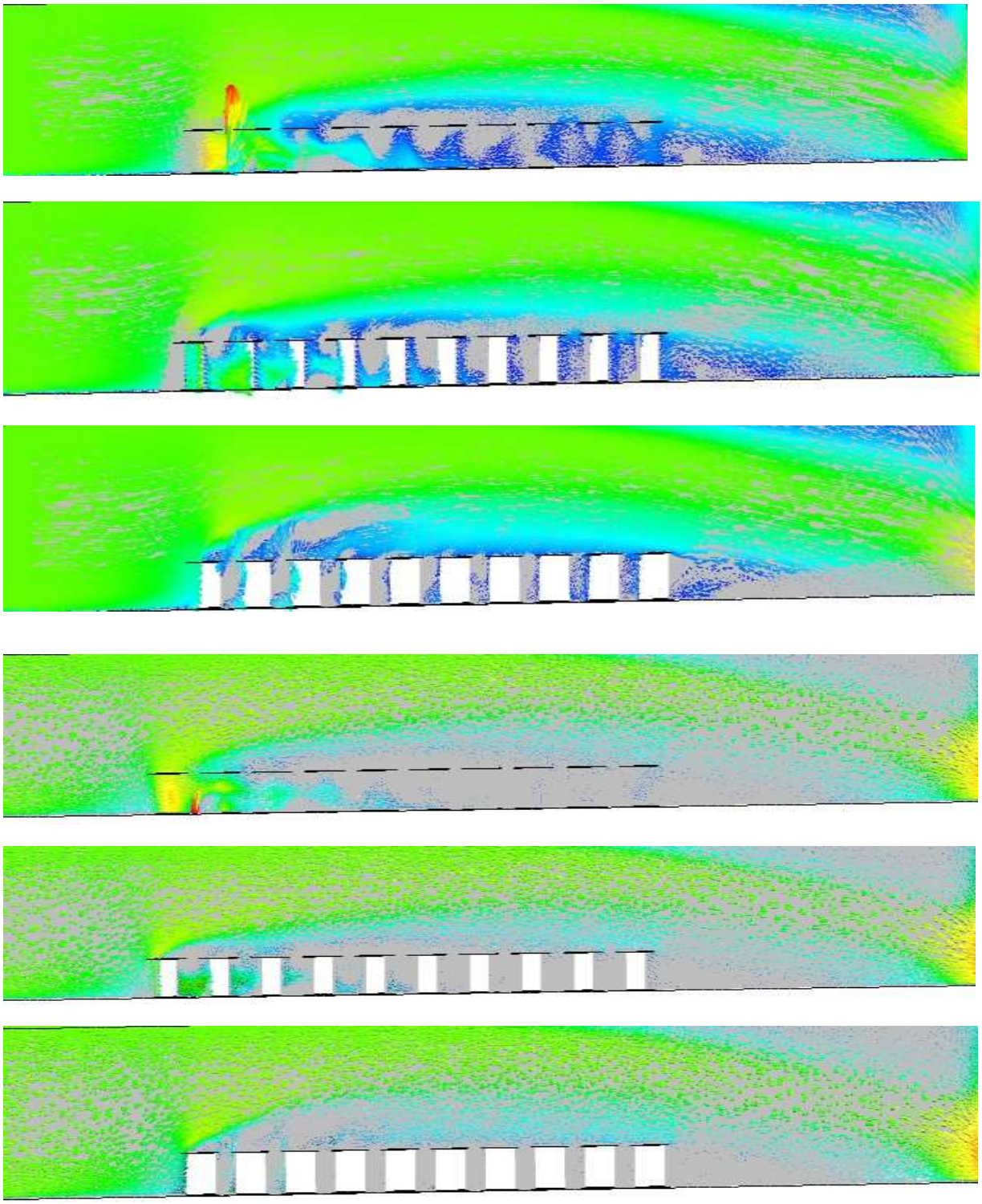

Figure 8.147: *Velocity contours of the concentration profile of the heavy gas dispersion with the release source located at the upwind front of the group of gas storage tanks between the first and second column in the middle between the third and fourth rows at* ***1m/s***

Figure 8.147 shows the velocity contours of the heavy gas dispersion for this case study with the release source located at the upwind front of the group of gas storage tanks between the first and second column in the middle between the third and fourth rows. The velocity contours

depict the intensity of the wind - or the effective wind influence - at the different locations throughout the layout. As can be seen in the figure, the wind intensity is different at different points in the layout. It is a commonly known effect that with enhanced altitudes, enhanced wind speeds are encountered. This is because the objects at the lower altitudes create resistance to the wind flow. As resistance is caused by the buildings in the flow of gas towards the direction opposite of wind, the wind flowing from left to right fails to indict the same motion of flow. Instead, various complex vertexes are formed within the buildings near the release source location, as can be seen in (Figure 8.147). The heavy gas released from the source is carried by these vertexes to the nearby mixture of the gas cloud, which then moves smoothly away from the source. Moreover, the hindrance to the wind flow caused by the buildings results in the vertexes moving in the upward direction, which enhances the shape of cloud in the upward direction.

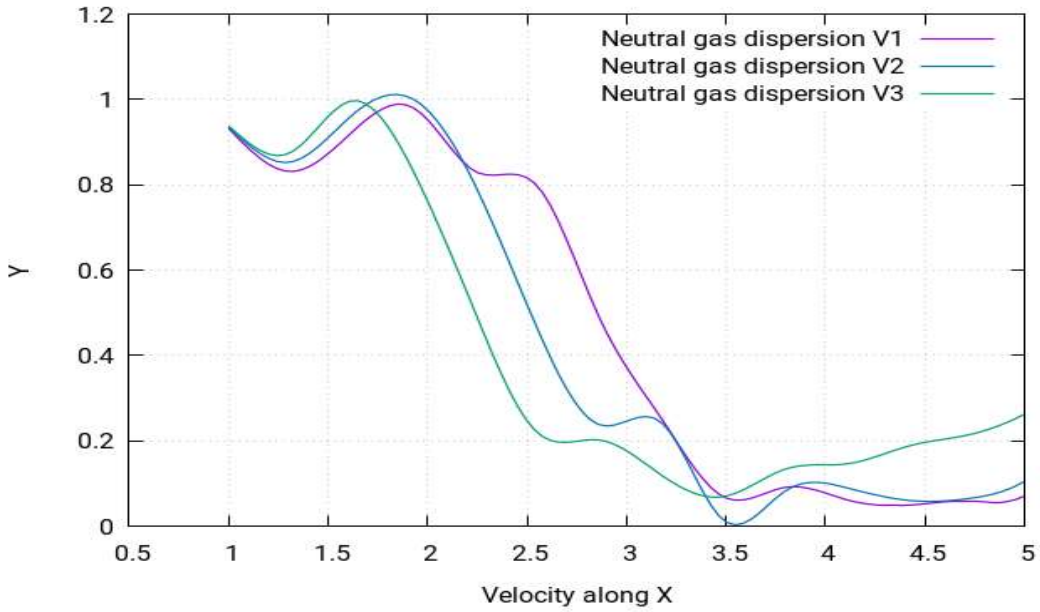

Figure 8.148: *Velocity of the neutral gas dispersion profile along the x-direction at different points of (V1) x=1.00m, y=2.03m, z=9.84m (V2) x=1.00m, y=2.03m, z=1.50m (V3) x=1.00m, y=2.03m and z=2.20m*

Figure 8.148 shows the curves for velocity profile along the x-direction. The curves follow an asymmetric pattern and have several peaks, with the highest peak being at approximately 3.5m.

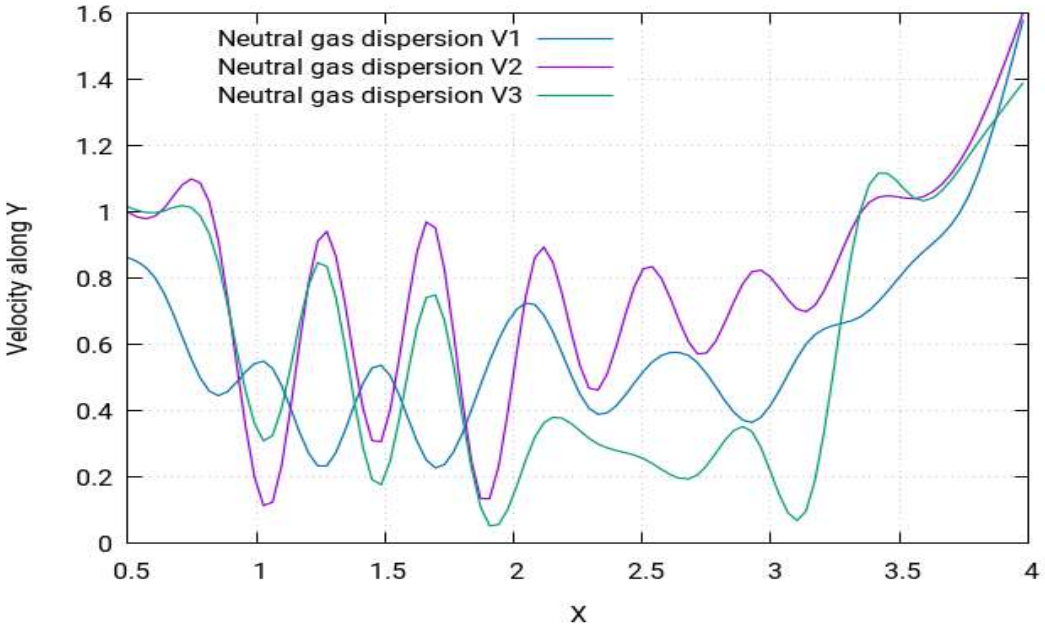

Figure 8.149: *Velocity of the neutral gas dispersion profile along the* ***y****-direction at different points of (V1) x=1.94m, y=-1m, z=7.20m (V2) x=1.94m, y=-1m, z=9.84m (V3) x=1.94m, y=-1m and z=1.50m*

Figure 8.149 shows the curves for the velocity profile along the x-direction. The curves follow an asymmetric pattern and have several peaks, with the highest peak being at approximately 3.1m.

The dispersion of the neutral gas is observed for the circular obstacles. In this case, the dispersion is seen in all the directions for the neutral gas, unlike the previous cases in which the dispersion was only in the upward direction. This is because the circular obstacles offer less resistance to the flow.

8.6.18 Location 2: Heavy gas dispersion

8.6.18.1 Structure of layout

The type of layout adopted for this case study is for the collocated layout. A layout of 60 oil storage tanks will be created with a cylinder-shaped distribution and the release source will be placed in position. The behaviour of the gas clouds will then be studied.

8.6.18.2 Release source location

The release source point (2) is located at the middle front of the building group at the middle between third and fourt row**.** The perimeters selected for this case study is stated below:

Table 8.29: *Parametric values of the high-speed heavy gas simulation (location 2)*

Density	Flow Rate	Velocity	Ambient Temperature	Release Source Temperature
2.1 kg m/s^3	1 kg/s	1 m/s	25°C	-100°C

8.6.18.3 Concentration of heavy gas dispersion

The following figure shows the concentration behaviour of the heavy gas at location 2. The whereabouts of location 2 has been stated at the beginning of the passage.

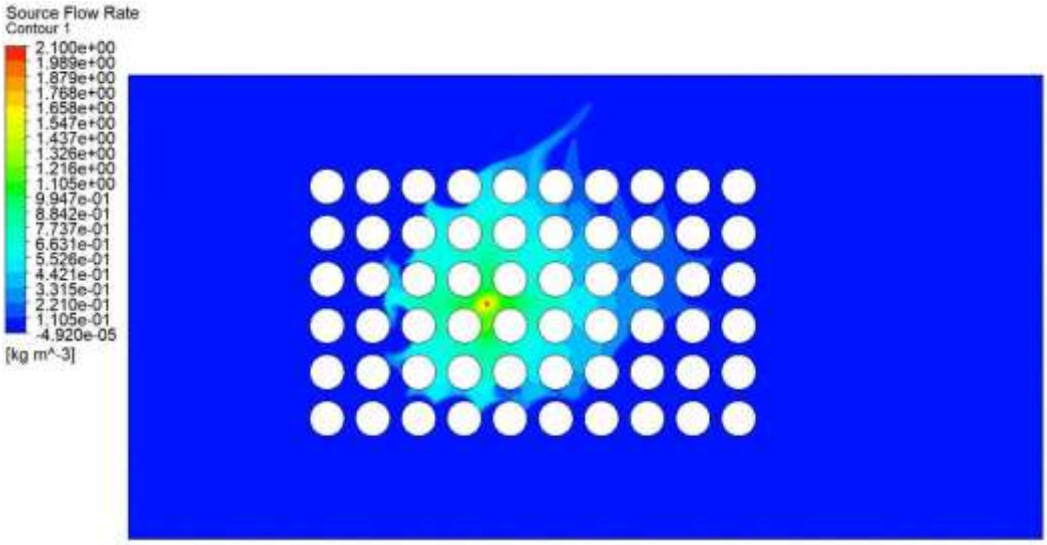

Figure 8.150: *Concentration profile of the heavy gas dispersion with the release source located at the middle front of the group of buildings in the middle between the third and fourth rows at* ***1m/s***

The concentration profile of the heavy gas at location 2 is shown above in Figure 8.150. It represents the concentration behaviour of the heavy gas when the release gas source is placed at the middle front of the group of buildings in the middle between the third and fourth rows. It can be seen in the figure that the cloud shape in this case resembles that of a circle but not exactly. Some portions of the gas cloud seem to evade the circular vicinity of the high concentration area. The gas source placed somewhat centrally may have affected the gas cloud, making it evenly spread in the horizontal directions. Nonetheless, the cloud is still inclined towards one edge of the layout, as shown in (Figure 8.150).

8.6.18.4 Iso-surfaces of the heavy gas dispersion

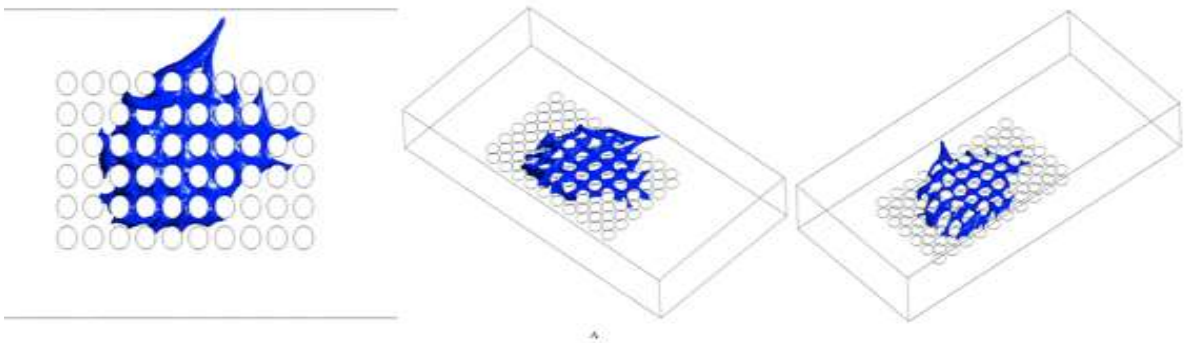

Figure 8.151: *Iso-surfaces of the concentration profile of the heavy gas dispersion with the release source located at the middle front of the group of buildings in the middle between the third and fourth rows at* ***1m/s***

Figure 8.151 shows the iso-surfaces of the concentration profile of the heavy gas dispersion with the release source located at the middle front of the group of buildings in the middle between the third and fourth rows. This helps identify the spread of the cloud in each dimension. It can be seen that the cloud shape forms a circle, but some small chunks of the gas cloud in the upper portions of the layout try to drift away from the main cloud. The cloud is spread somewhat symmetrically, but a part of cloud is inclined to move more towards one edge.

According to Standard BS EN 60079-10-1:2009 [104], the following locations can be categorised:

Zone 0: The middle front of the layout containing the release source

Zone 1: A very small portion of the gas cloud trying to drift away from the main cloud through the upper edge

Zone 2: All the remaining locations not categorised in zone 0 or zone 1

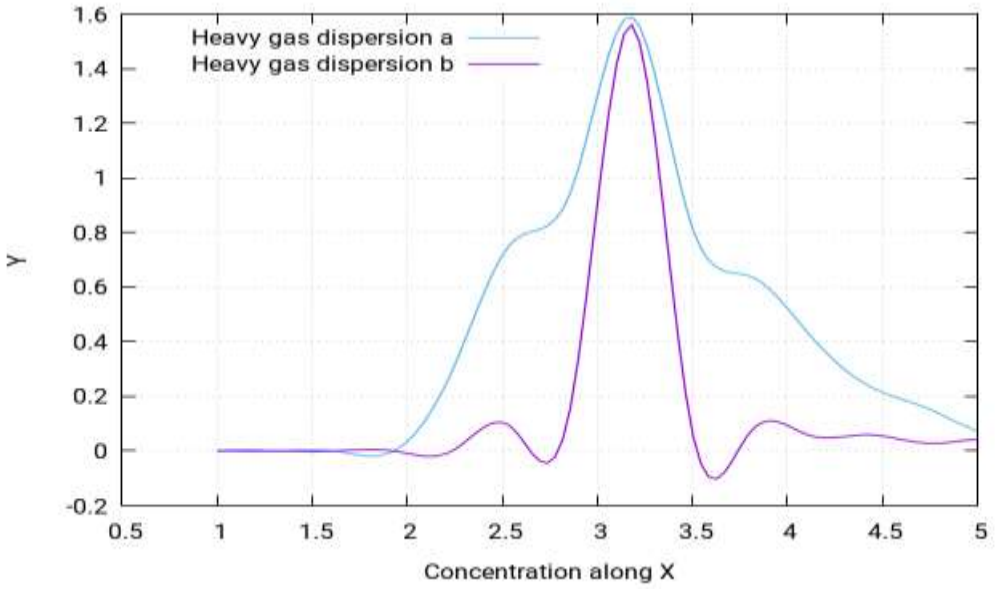

Figure 8.152: *Concentration of the heavy gas dispersion profile along the* ***x****-direction at different points of (a) x=1.00m, y=2.03m, z=7.20m (b) x=1.00m, y=2.03m and z=9.84m*

In Figure 8.152 (above), two different curves for the concentration profiles are shown. They show the pattern of the concentration profile along the x-direction when the wind speed for the simulation is 1m/s. The two different curves are obtained for two different distances from the release source. Both curves follow the same pattern but have different values due to difference in distances. From the figure, it is concluded that the concentration value of the concentration of the heavy gas decreases as it moves away from the source. In the figure, the curve with highest peak is obtained when nearest to the release source and vice versa.

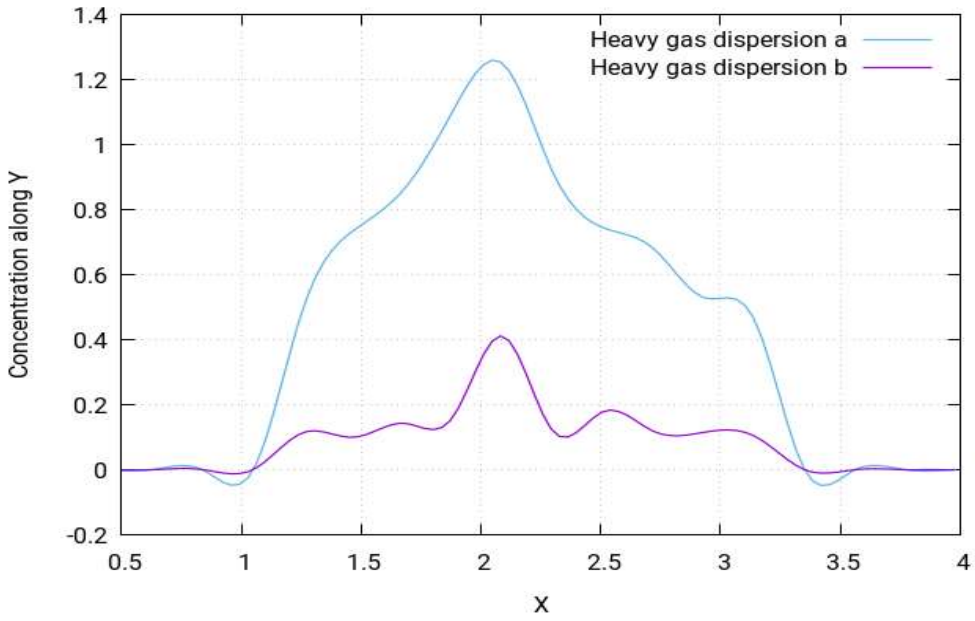

Figure 8.153: *Concentration of the heavy gas dispersion profile along the* ***y****-direction at different points of (a) x=3.14m, y=-1m, z=7.20m (b) x=3.14m, y=-1m and z=9.84m*

In Figure 8.153 (above), two different curves for the concentration profiles are presented. They show the pattern of the concentration profile along the y-direction when the wind speed for the simulation is 1m/s. The two different curves are obtained for two different distances from the release source. Both curves follow the same pattern but have different values due to difference in distances. From the figure, it is concluded that the concentration value of the heavy gas decreases when moved away from the source. In the figure, the curve with highest peak is obtained when nearest to the release source and vice versa.

8.6.18.5 Temperature of the heavy gas dispersion

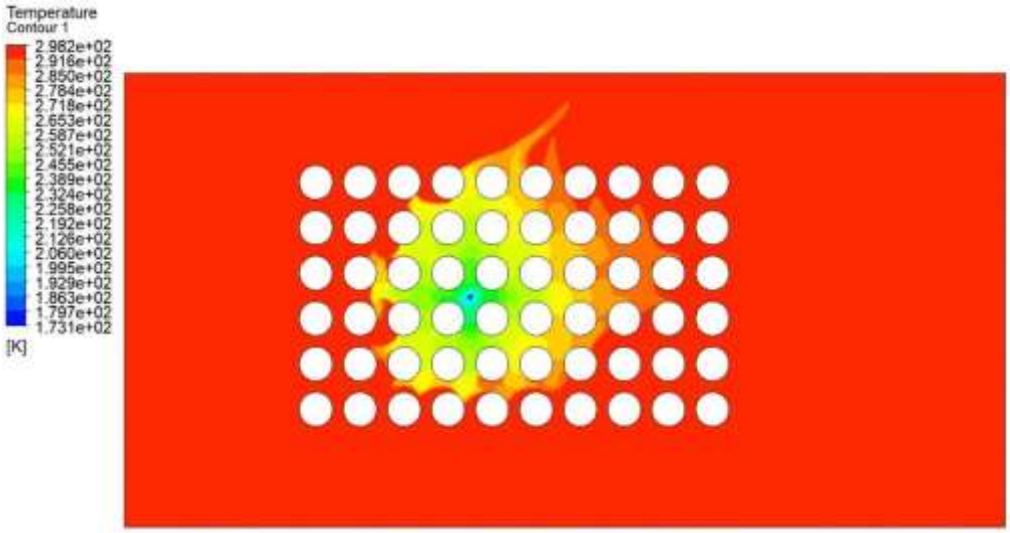

Figure 8.154: *Temperature profile of the heavy gas dispersion with the release source located at the middle front of the group of buildings in the middle between the third and fourth rows at* ***1m/s****.*

Above, Figure 8.154 shows the temperature simulation for this study. By visualising the temperature simulation, it is found out that the temperature simulation produces quite the same profile for the case study as that of the concentration profile. However, the behaviour of temperature is in fact the opposite to that of concentration. This means that the areas identified in the concentration simulation as the highly concentrated will in fact have the lowest temperatures, while the ones with moderate concentrations will have moderate temperatures and the least concentrated areas will have the highest temperatures. To further simply these findings, it should be pointed out that the simulations showed that the concentrations near the release source point tend to be the highest and start to fade away as the gas cloud moves away from the source and are the lowest as the cloud moves much further away in the layout, eventually reaching the environment where the gas cloud disappears. However, the temperature is lowest near the release source point and tends to increase as the gas cloud moves away from the source, finally achieving its highest temperature equal to the ambient temperature of the environment.

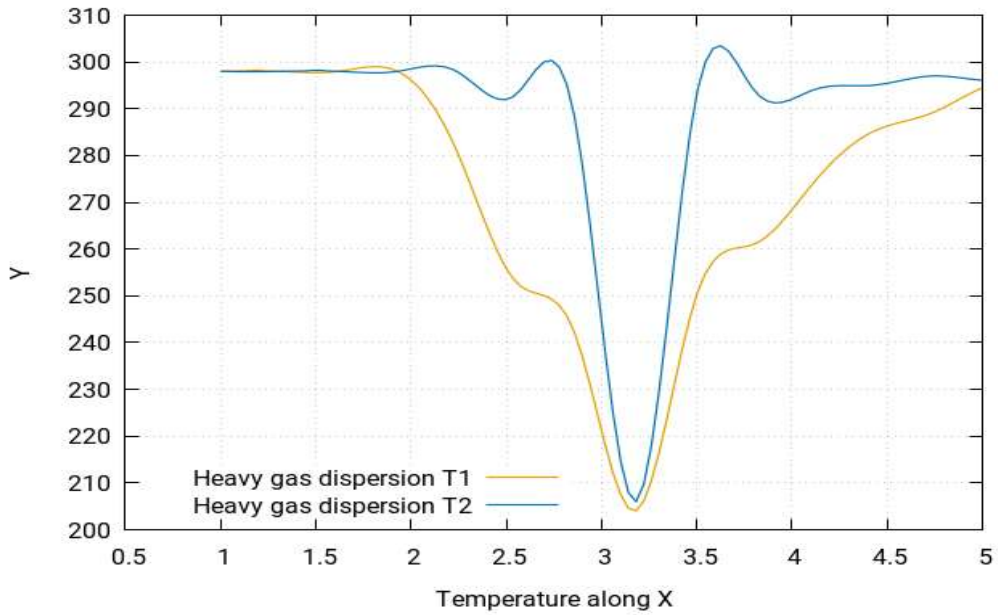

Figure 8.155: *Temperature of the heavy gas dispersion profile along the* ***x****-direction at different points of (T1) x=1.00m, y=2.03m, z=7.20m (T2) x=1.00m, y=2.03m and z=9.84m*

Figure 8.155 presents two different curves for the concentration profiles. They show the pattern of the concentration profile along the y-direction when the wind speed for the simulation is 1m/s. The two different curves are obtained for two different distances from the release source. It is seen that, along the y-direction, the profiles do not follow the same pattern unlike the y-direction, where they followed the same pattern. This is because the wind makes a significant effect in y-direction.

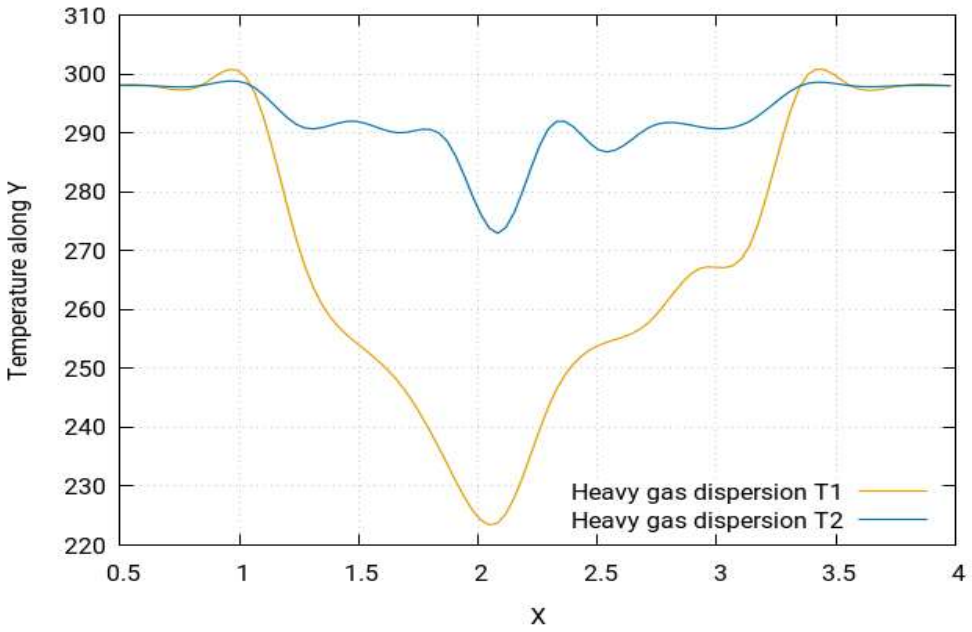

Figure 8.156: *Temperature of the heavy gas dispersion profile along the* ***y****-direction at different points of (T1) x=3.14m, y=-1m, z=7m (T2) x=3.14m, y=-1m and z=9.84m*

Above, Figure 8.156 presents two different curves for the concentration profiles. They show the pattern of the concentration profile along the y-direction when the wind speed for the simulation is 1m/s. The two different curves are obtained for two different distances from the release source. It is seen that along the y-direction the profiles do not follow the same pattern unlike the x-direction, where they followed the same pattern. This is because the wind makes a significant effect in the y-direction.

8.6.18.6 Velocity of the heavy gas dispersion

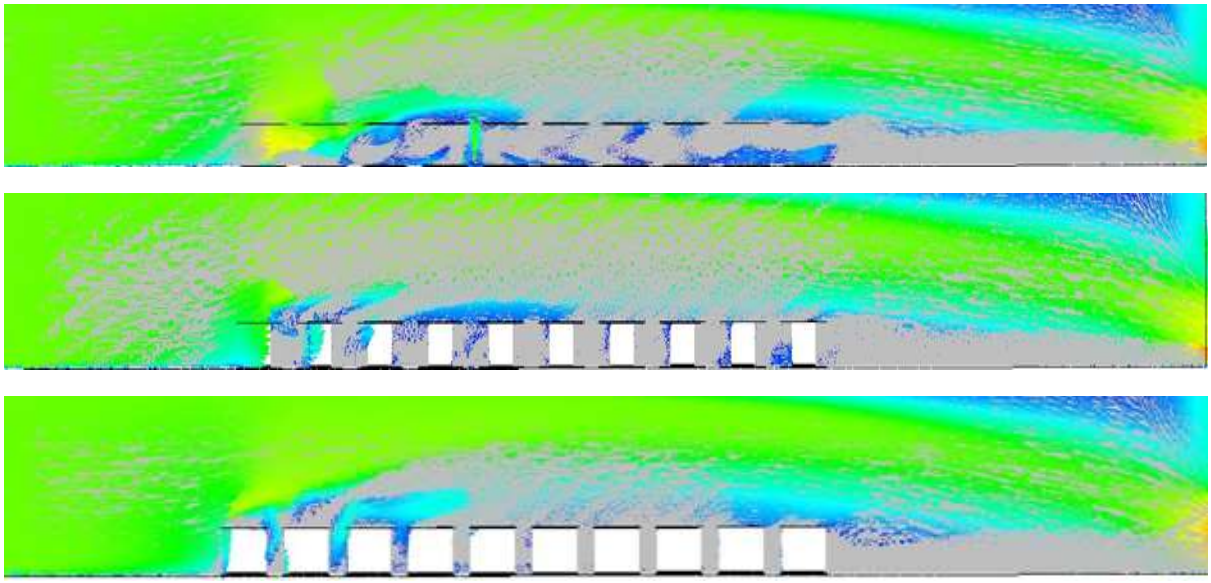

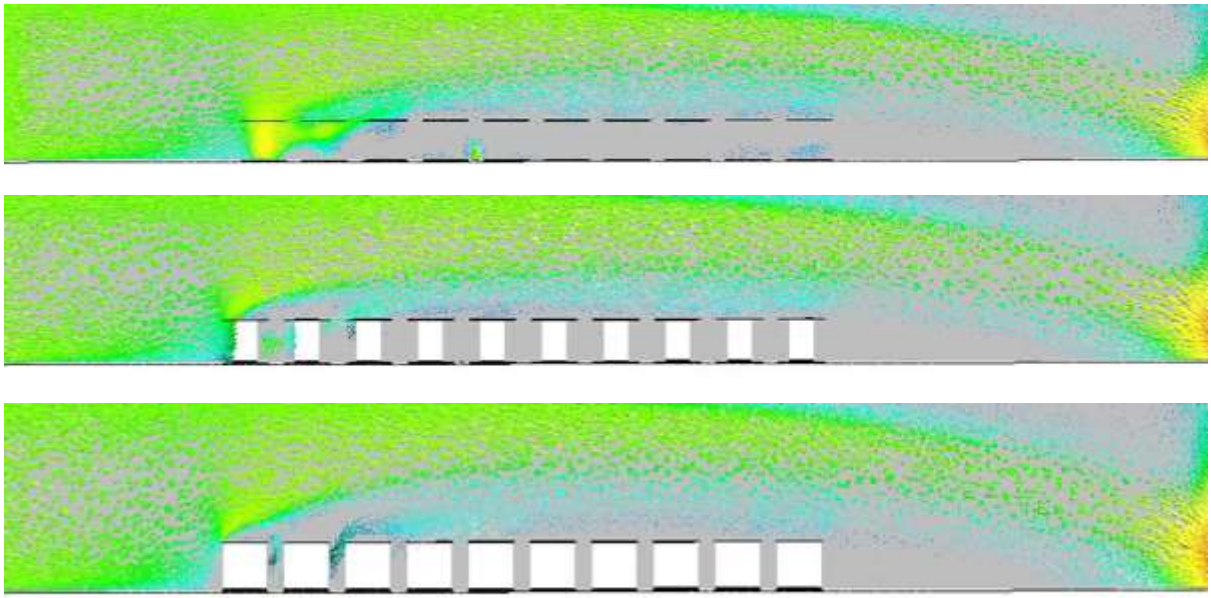

Figure 8.157: *Velocity contours of the heavy gas dispersion with the release source located at the middle front of the group of buildings in the middle between the third and fourth rows at* ***1m/s***

Figure 8.157 shows the velocity contours of the heavy gas dispersion for this case study with release source located at the middle front of the group of buildings in the middle between the third and fourth rows. The velocity contours depict the intensity of the wind - or the effective wind influence - at the different locations throughout the layout. As can be seen in the figure, the wind intensity is different at different points in the layout. It is a commonly known effect that, with enhanced altitudes, enhanced wind speeds are encountered. This is because the objects at the lower altitudes create resistance to the wind flow. As resistance is caused by the buildings to the flow of gas towards the direction opposite of wind, the wind flowing from left to right fails to indict the same motion of flow. Instead, various complex vertexes are formed within the buildings near the release source location, as can be seen in (Figure 8.157). The heavy gas released from the source is carried by these vertexes to the nearby mixture of the gas cloud, which then moves smoothly away from the source. Moreover, the hindrance to the wind flow caused by the buildings results in the vertexes moving in the upward direction, which enhances the shape of the cloud in the upward direction.

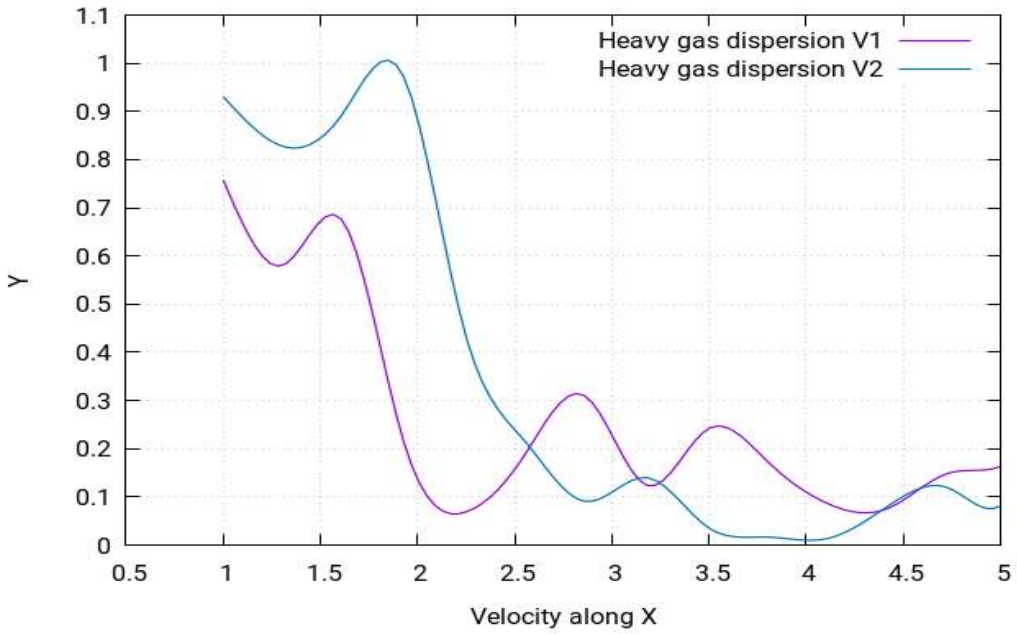

Figure 8.158: *Velocity of the heavy gas dispersion profile along the* ***x****-direction at different points of (V1) x=1.00m, y=2.03m, z=7.20m (b) x=1.00m, y=2.03m and z=9.84m*

Figure 8.158 shows the curves for the velocity profile along the x-direction. The curves follow an asymmetrical pattern and have several peaks, with the highest being at approximately 2.5m.

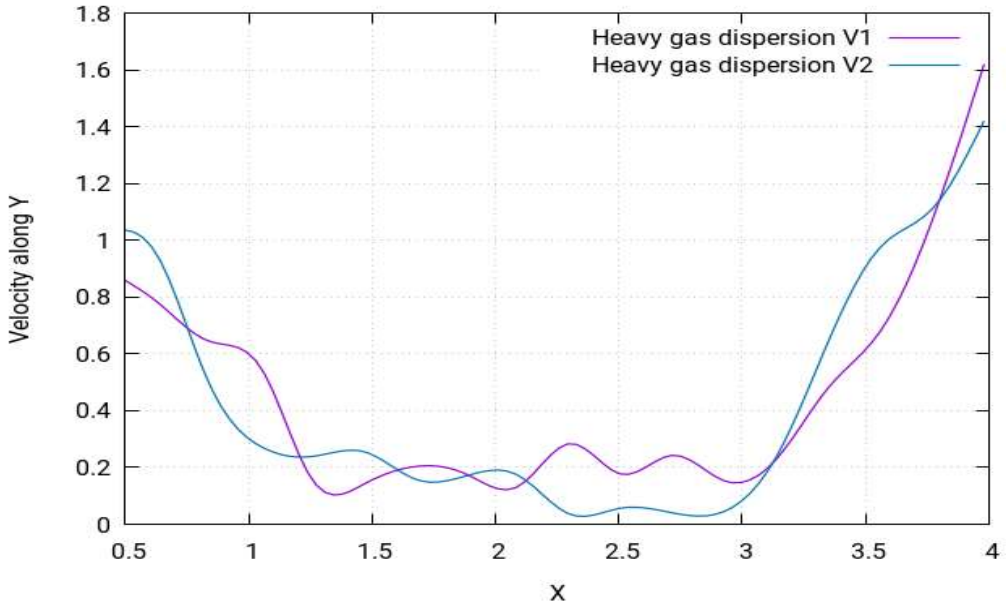

Figure 8.159: *Velocity of the heavy gas dispersion profile along the* ***y****-direction at different points of (V1) x=3.14m, y=-1m, z=7.00m (b) x=3.14m, y=-1m and z=9.84m*

Figure 8.159 shows the curves for velocity profile along the x-direction. The curves follow an asymmetrical pattern and have several peaks, with the highest being at approximately 2.5m. The dispersion of the heavy gas is now observed at location 2 of the circular obstacles. It can

be seen that the dispersion is uniform with a small accumulation around the obstacles because of less resistance.

8.6.19 Location 3: Heavy gas dispersion

8.6.19.1 Structure of layout

The type of layout adopted for this case study is for the collocated layout. A layout of 60 oil storage tanks will be created, with a cylinder-shape distribution, the release source will be placed in position. The behaviour of the gas clouds will then be studied.

8.6.19.2 Release source location

The release source point (3) is located at the middle front of the group of buildings in the 3rd row. The perimeters selected for this case study is stated below:

Table 8.30: *Parametric values of the high-speed heavy gas simulation (location 3)*

Density	Flow Rate	Velocity	Ambient Temperature	Release Source Temperature
2.1 kg m/s^3	1 kg/s	1 m/s	25°C	-100°C

8.6.19.3 Concentration of the heavy gas dispersion

The following figure shows the concentration behaviour of the heavy gas at location 3. The whereabouts of location 3 has been stated at the beginning of the passage.

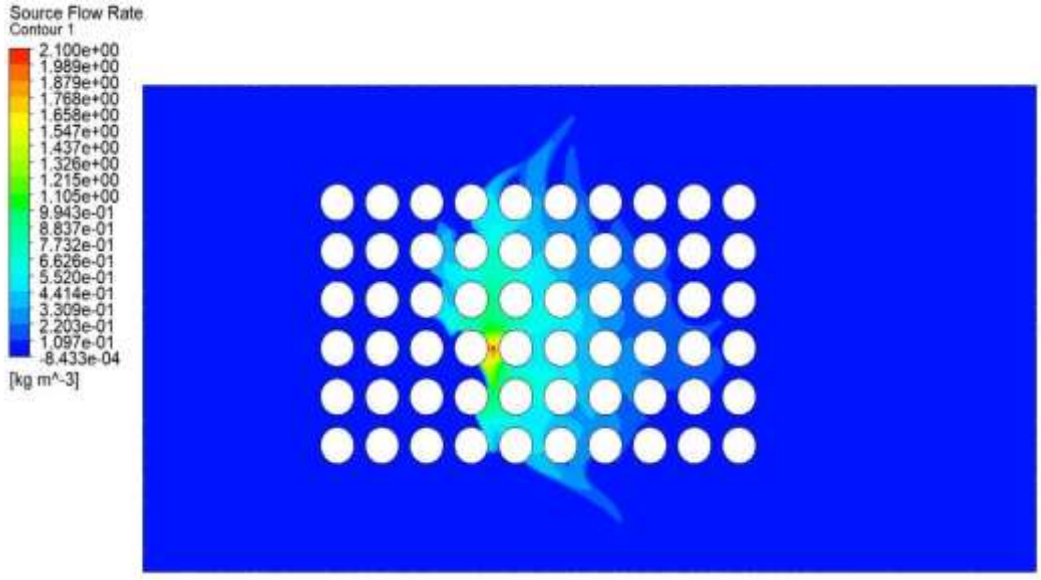

Figure 8.160: *Concentration profile of the heavy gas dispersion with the release source located at the middle front of the group of buildings in the 3rd row at* ***1m/s***

The concentration profile of the heavy gas at location 3 is shown in Figure 8.160 above. It represents the concentration behaviour of the heavy gas when the release gas source is placed at the middle front of the group of buildings in the 3rd row. It can be seen in the figure that the cloud shape in this case resembles that of a wing and appears to be symmetrical but also tilted at a slight angle. The main cloud is still near the release source location, with the gas cloud slightly more concentrated towards the upper edge than towards the lower. It should be noted that the gas cloud's vicinity is only a couple of columns in both directions, after which it starts to fade away.

8.6.19.4 Iso-surfaces of the heavy gas dispersion

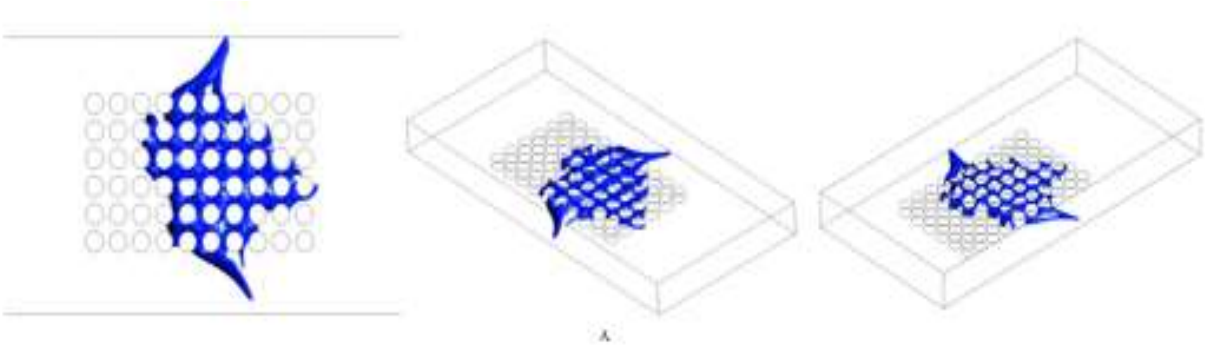

Figure 8.161: *Iso-surfaces of the concentration profile of the heavy gas dispersion with the release source located at the middle front of the group of buildings in the 3rd row at* ***1m/s***

Figure 8.161 shows the iso-surfaces of the concentration profile of the heavy gas dispersion for a/the staggered layout with the release source located at the middle front of the group of buildings in the middle between the third and fourth rows. This helps identify the spread of the cloud in each dimension. It can be seen that the cloud shape forms a tilted symmetrical wing, but some small chunks of the gas cloud at the upper portions of the layout try to drift away from the main cloud. The cloud is spread somewhat symmetrically, but a part of cloud is inclined to move more towards one edge. Another thing to note is that in this, the heavy accumulated gas cloud behaviour near the release source is not noticed.

According to Standard BS EN 60079-10-1:2009 [104], the following locations can be categorised:

Zone 0: The middle front of the layout containing the release source

Zone 1: A very small portion of the gas cloud trying to drift away from the main cloud through the upper and the lower edge

Zone 2: All the remaining locations not categorised in zone 0 or zone 1

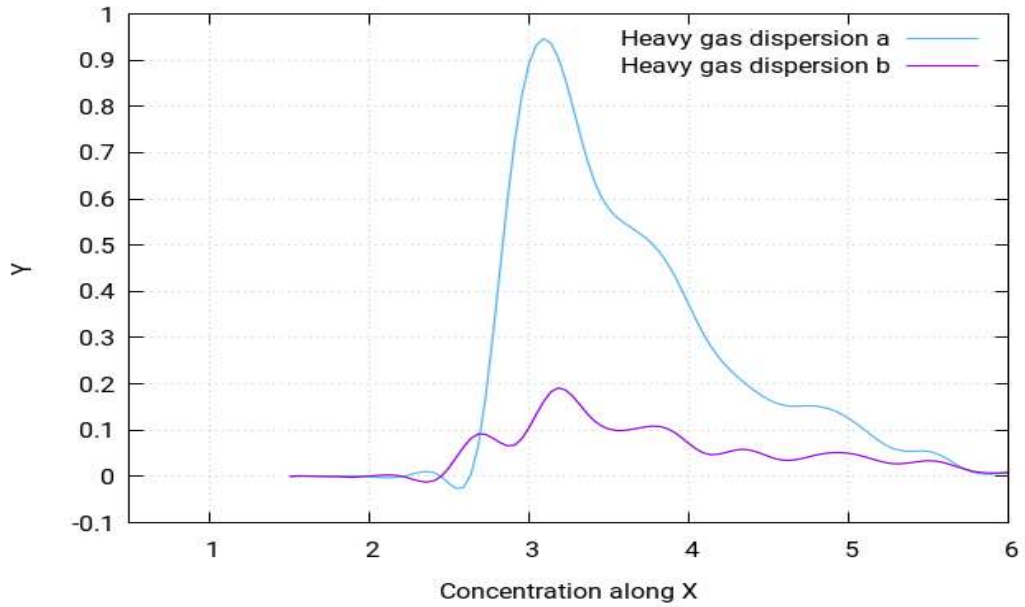

Figure 8.162: *Concentration of the heavy gas dispersion profile along the* ***x****-direction at different points of (a) x=1.50m, y=2.03m, z=7.20m (b) x=1.50m, y=2.03m and z=9.84m*

In Figure 8.162 (above), two different curves for the concentration profiles are shown. They show the pattern of the concentration profile along the x-direction when the wind speed for the simulation is 1m/s. The two different curves are obtained for two different distances from the release source. Both curves follow the same pattern but have different values due to difference in distances. From the figure, it is concluded that the concentration value of the heavy gas decreases as it moves away from the source. In the figure, the curve with highest peak is obtained when nearest to the release source and vice versa.

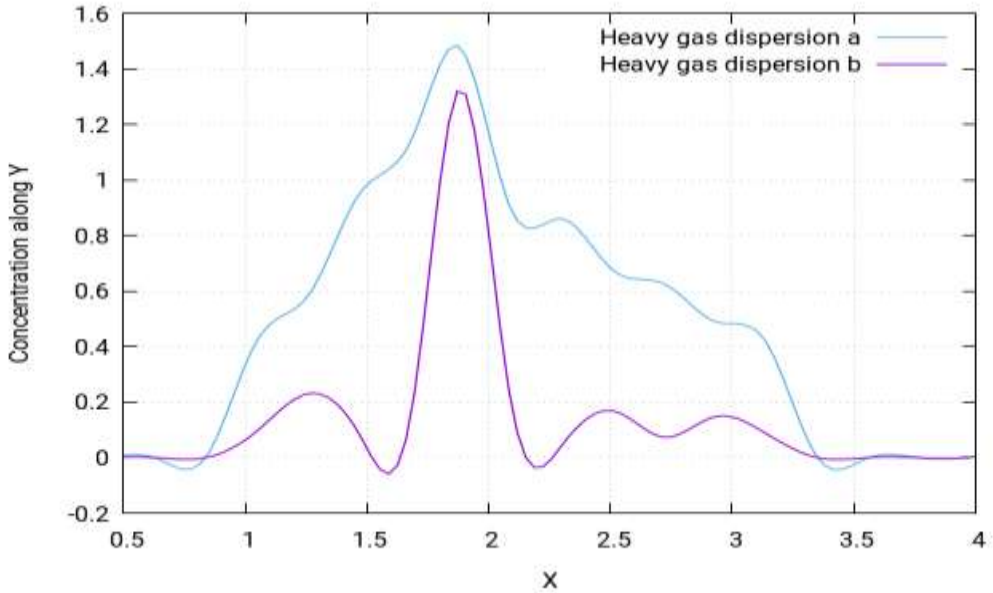

Figure 8.163: *Concentration of the heavy gas dispersion profile along the* ***y****-direction at different points of (a) x=3.14m, y=-1m, z=7.20m (b) x=3.14m, y=-1m and z=9.84m*

In Figure 8.163 (above), two different curves for the concentration profiles are shown. They show the pattern of the concentration profile along the x-direction when the wind speed for the simulation is 1m/s. The two different curves are obtained for two different distances from the release source. Both curves follow the same pattern but have different values due to difference in distances. From the figure, it is concluded that the concentration value of the heavy gas decreases as it moves away from the source. In the figure, the curve with the highest peak is obtained when nearest to the release source and vice versa.

8.6.19.5 Temperature of the heavy gas dispersion

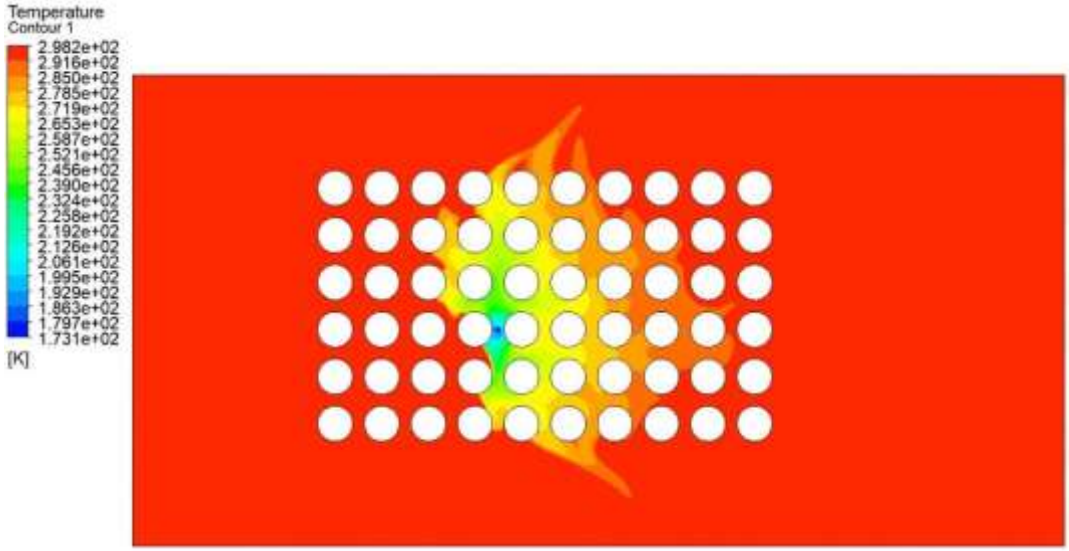

Figure 8.164: *Temperature profile of the heavy gas dispersion with the release source located at the middle front of the group of buildings in the 3rd row at* ***1m/s***

Figure 8.164 shows the temperature simulation for this study. By visualising the temperature simulation, it is found out that it produces largely the same profile for the case study as that of the concentration profile. However, the behaviour of temperature is in fact the opposite to that of concentration. This means that the areas which were identified in the concentration simulation as highly concentrated will in fact have the lowest temperatures, while the ones with moderate concentrations will have moderate temperatures and the least concentrated areas will have the highest temperatures. To further simply these findings, it should be pointed out that the simulations show that the concentrations near the release source point tend to be the highest and start to fade away as the gas cloud moves away from the source and is at its lowest when the gas cloud moves much further away in the layout, eventually reaching the environment where it disappears. However, the temperature it is lowest near the release source point and tends to increase as the cloud moves away from source and finally achieves the highest temperature equal to the ambient temperature of the environment.

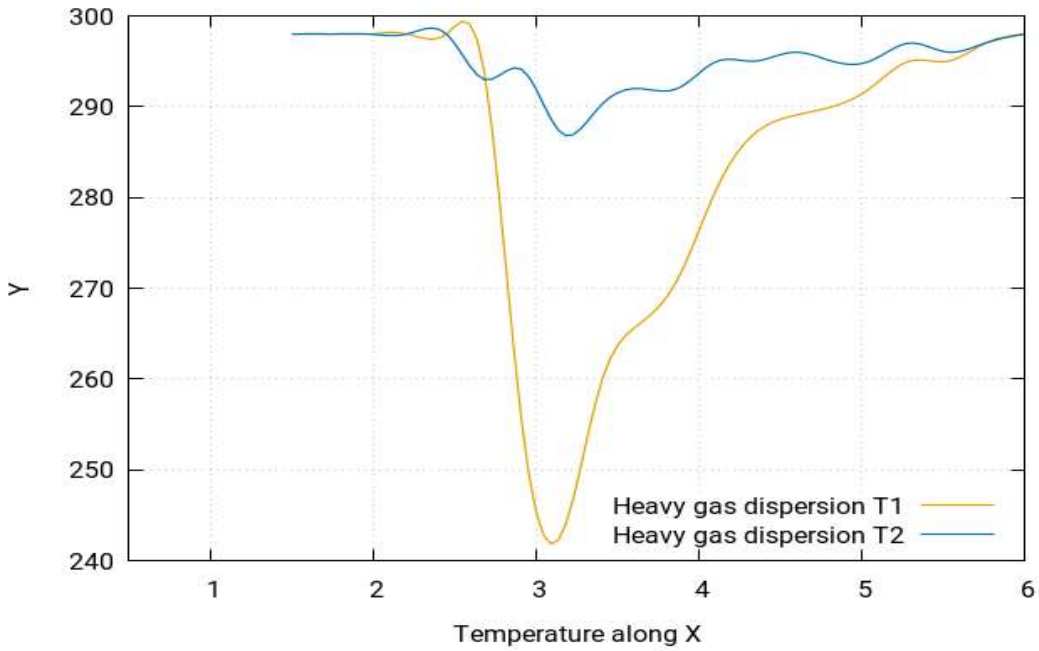

Figure 8.165: *Temperature of the heavy gas dispersion profile along the x-direction at different points of (T1) x=1.50m, y=2.03m, z=7.20m (T2) x=1.50m, y=2.03m and z=9.84m*

In Figure 8.165 (above), two different curves for the temperature profiles are shown. They show the pattern of the temperature profile along the y-direction when the wind speed for the simulation is 1m/s. The two different curves are obtained for two different distances from the release source. These results show that, at speed of 1m/s, temperature profiles are a mirror of concentration profile.

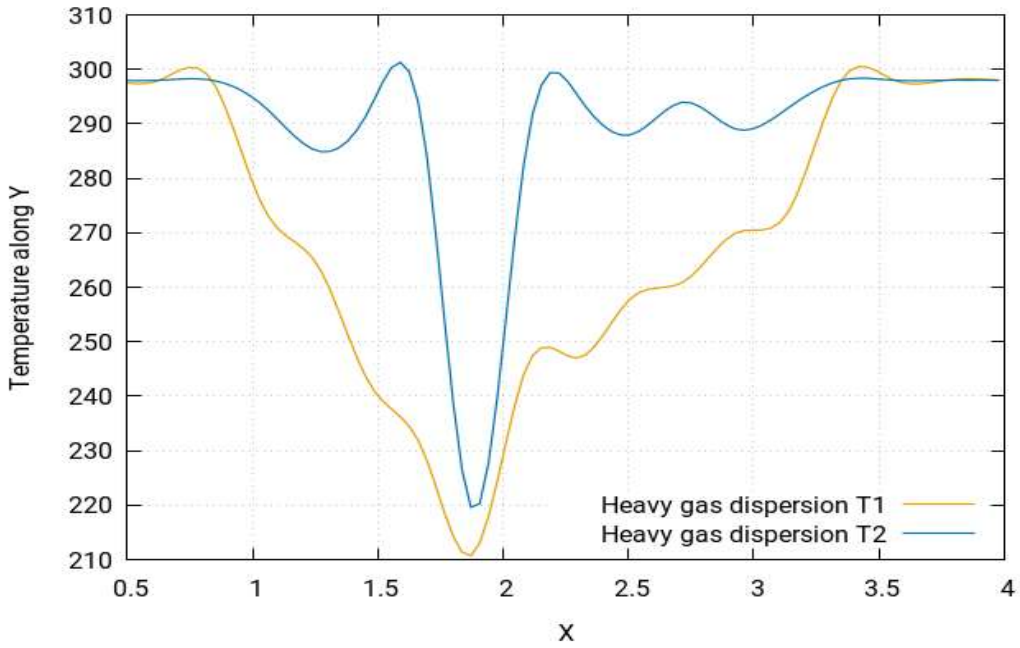

Figure 8.166: *Temperature of the heavy gas dispersion profile along the* ***y****-direction at different points of (T1) x=3.14 y=-1m, z=7.20m (T2) x=3.14m, y=-1m and z=9.84m*

In Figure 8.166, two different curves for the temperature profiles are shown. They show the pattern of the temperature profile along the y-direction when the wind speed for the simulation is 1m/s. The two different curves are obtained for two different distances from the release source. These results show that at speed of 1m/s, temperature profiles are a mirror of concentration profile.

8.6.19.6 Velocity of the heavy gas dispersion

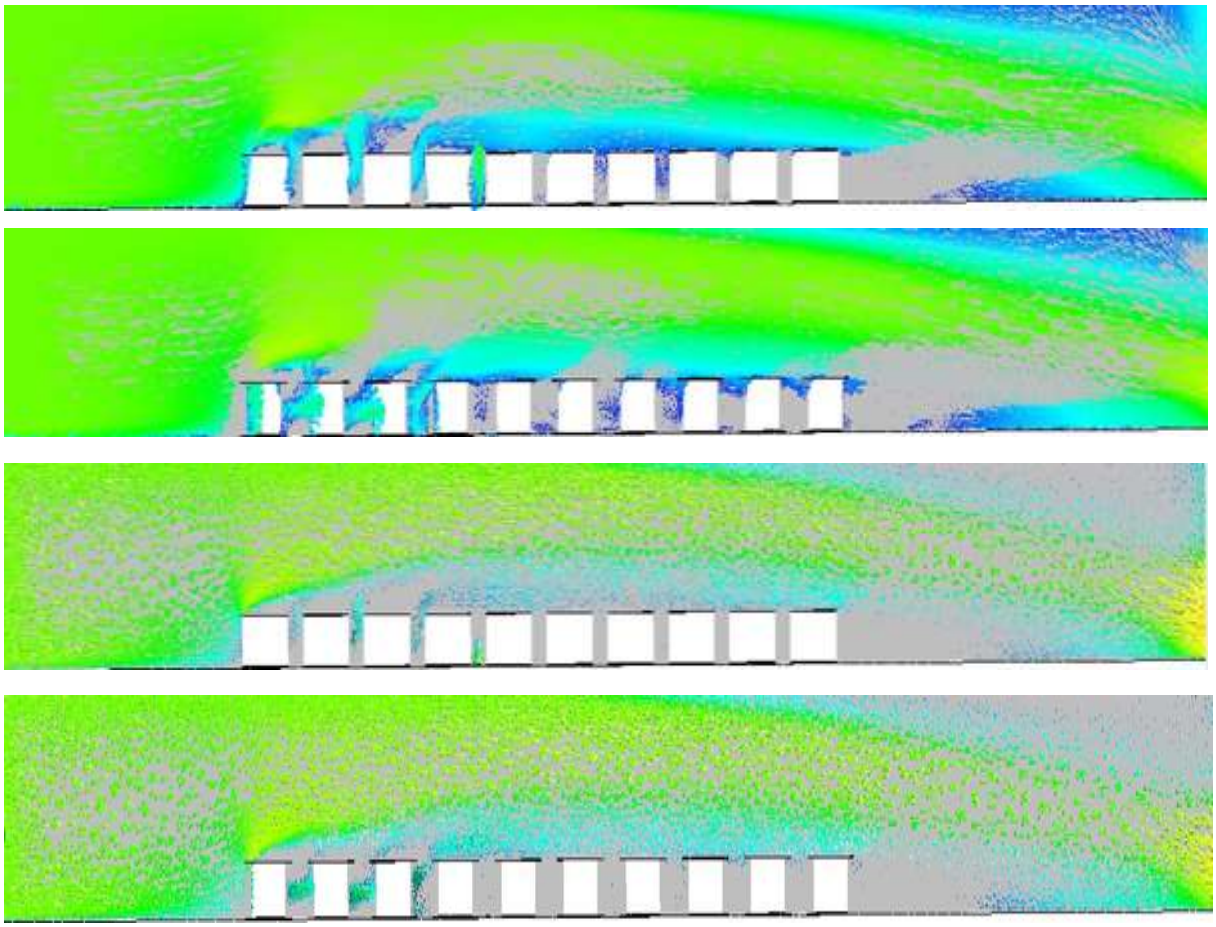

Figure 8.167: *Velocity contours of the heavy gas dispersion with the release source located at the middle front of the group of buildings in the 3rd row at* ***1m/s***

Figure 8.167 shows the velocity contours of the heavy gas dispersion for this case study with release source located at the middle front of the group of buildings in the 3rd row. Velocity contours depict the intensity of the wind - or the effective wind influence - at the different locations throughout the layout. As can be seen in the figure, the wind intensity is different at different points in the layout. It is a commonly known effect that with enhanced altitudes, enhanced wind speeds are encountered. This is because the objects at the lower altitudes create resistance to the wind flow. As resistance is caused by the buildings in the flow of gas towards the direction opposite of wind, the wind flowing from left to right fails to indict the same motion of flow. Instead, various complex vertexes are formed within the buildings near the release

source location, as can be seen in (Figure 8.167). The heavy gas release from the source is carried by these vertexes to the nearby mixture of the gas cloud, which then moves smoothly away from the source. Moreover, the hindrance to the wind flow caused by the buildings results in the vertexes moving in the upward direction, which enhances the shape of cloud in the upward direction.

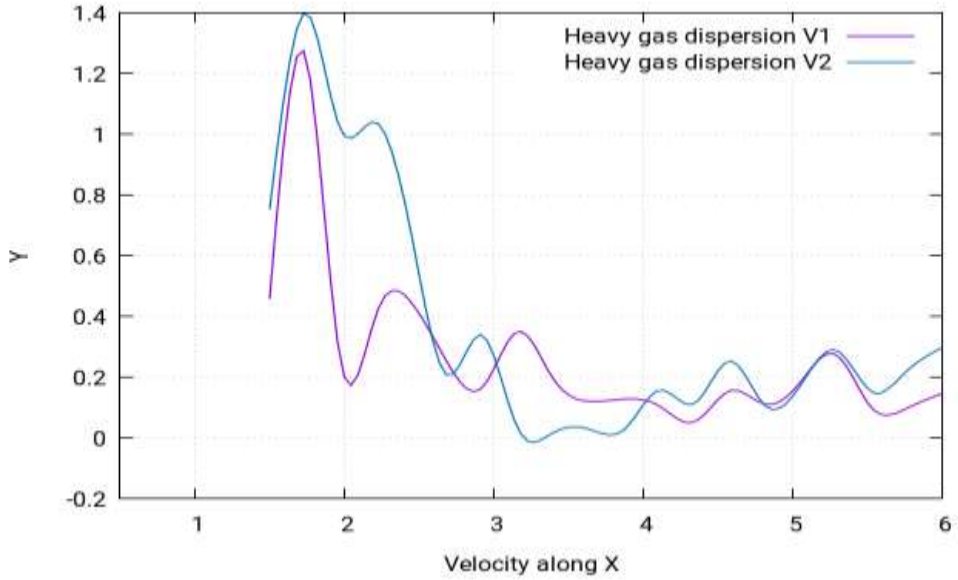

Figure 8.168: *Velocity of the heavy gas dispersion profile along the* ***x****-direction at different points of (V1) x=1.50m, y=2.03m, z=7.20m (V2) x=1.50m, y=2.03m and z=9.84m*

Figure 8.168 shows the curves for the velocity profile along the x-direction. The curves follow an asymmetrical pattern and have several peaks, with the highest peak being at approximately 3.2m.

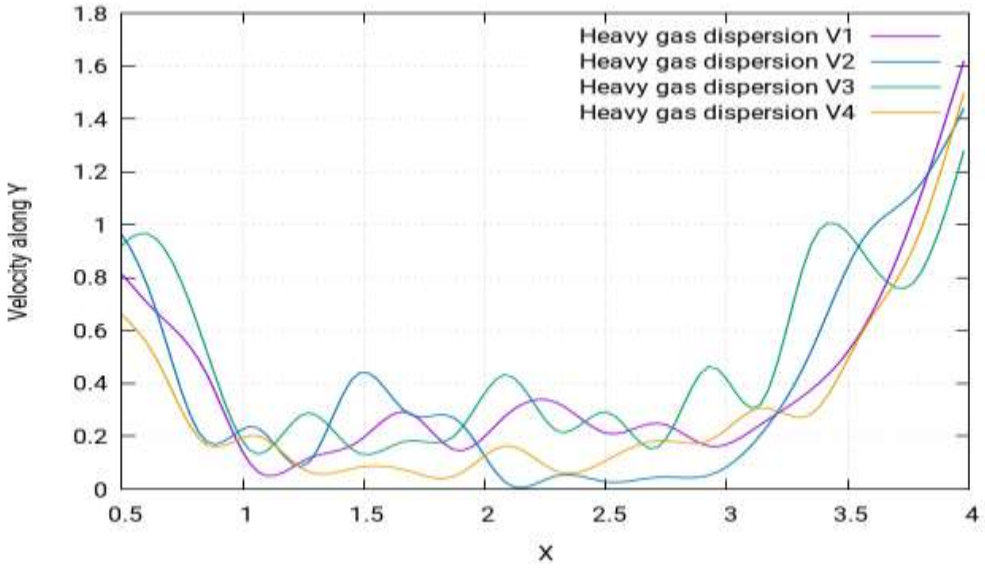

Figure 8.169: *Velocity of the heavy gas dispersion profile along the* ***y****-direction at different points of (V1) x=3.14m, y=-1m, z=7.20m (V2) x=3.14m, y=-1m, z=9.84m (V3) x=3.14m, y=-1m, z=2.00m (V4) x=3.54m, y=-1m and z=7.20m*

Figure 8.169 shows the curves for the velocity profile along the y-direction. The curves follow an asymmetric pattern and have several peaks, with the highest peak being at approximately 3.5m.

For location 3 of the circular obstacles, the heavy gas dispersion shows uniform spread in all directions. The temperature difference and the velocity aided the dispersion by creating buoyancy and turbulence. In the case of circular obstacles, the resistance is less, due to which the dispersion also occurs in the horizontal direction.

8.6.20 Location 1: Heavy gas dispersion for a safe distance

8.6.20.1 Structure of layout

The type of layout adopted for these two case studies the collocated layout. A layout of 24 Oil storage tanks will be created, in a cylinder-shape distribution for a safe distance, and the release source will be placed in the same positions. The behaviour of the gas clouds will then be studied.

8.6.20.2 Release source location

The release sources point (1) is located at the upwind front of the group of gas storage tanks between the first and second columns in the middle between the 2nd and 3rd rows. The perimeters selected for this case study are stated below:

Table 8.31: *(A) Parametric values for the high-speed heavy gas simulation (safe distance 1)*

Density	Flow Rate	Velocity	Ambient Temperature	Release Source Temperature
2.1 kg m/s^3	1 kg/s	1 m/s	25°C	-100°C

Table 8.32: *(B) Parametric values for the low-speed heavy gas simulation (safe distance 1)*

Density	Flow Rate	Velocity	Ambient Temperature	Release Source Temperature
2.1 kg m/s^3	5 kg/s	0.25 m/s	25°C	-100°C

8.6.20.3 Concentration of the heavy gas dispersion for a safe distance

The following figure shows the concentration behaviour of the heavy gas at location 1. The whereabouts of location 1 has been stated at the beginning of the passage.

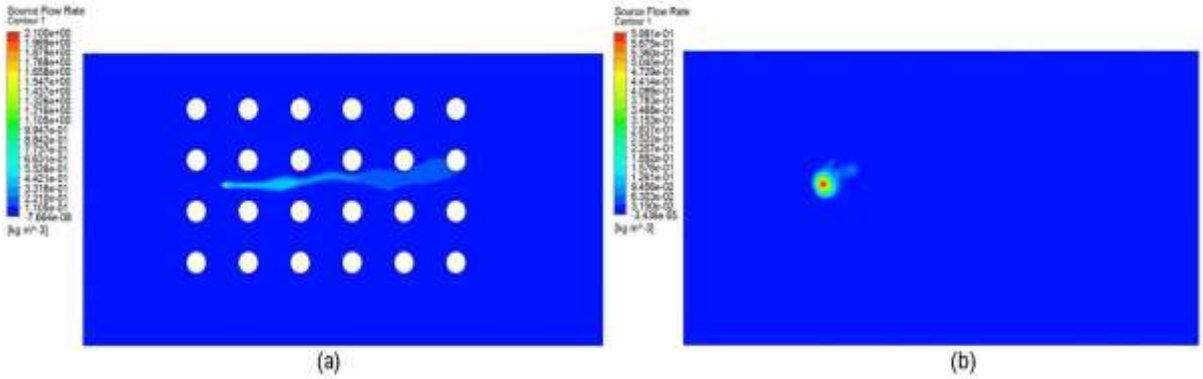

Figure 8.170: (a) *Concentration profile of the heavy gas dispersion with the release source located at the upwind front of the group of gas storage tanks between the first and second columns in the middle between the 2nd and 3rd row at 1m/s.* ***(b)*** *at 0.25m/s*

The concentration profile of the heavy gas at location 1 is shown above in Figure 8.170. It represents the concentration behaviour of the heavy gas, when the release gas source is placed at the upwind front of the group of gas storage tanks between the first and second columns in the middle between the 2nd and 3rd row. In the above figure, parts labelled (a) are at high speed and those labelled (b) are at low speed. For this particular layout, the gas cloud does not seem to be particularly concentrated and takes the shape of a small strip in the case of high speed(1m/s) and that of a semi-circle in the case of low speed (0.25m/s).

8.6.20.4 Iso-surface of the heavy gas dispersion for a safe distance

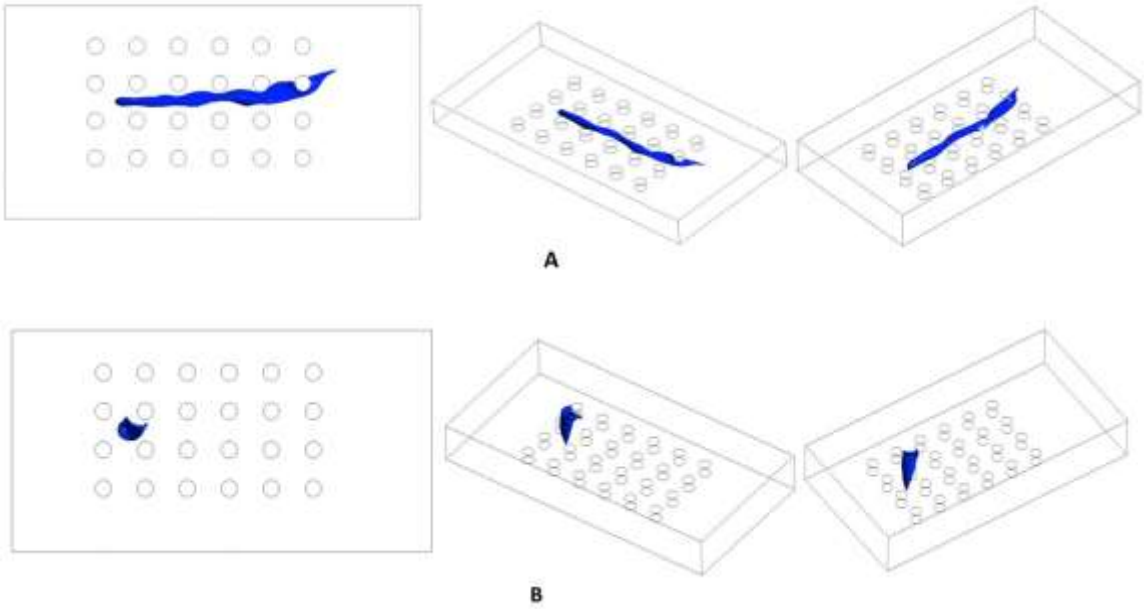

Figure 8.171: (a) *Iso-surfaces of the concentration profile of the heavy gas dispersion with the release source located at the upwind front of the gas storage tanks group between the 1st and 2nd columns at the middle between the 2nd and 3rd rows at 1m/s.* ***(b)*** *At 0.25m/s*

Figure 8.171 presents see the iso-surfaces of the concentration profile of heavy gas dispersion for a/the staggered layout with the release source located at the upwind front of the group of gas storage tanks between the first and second column at the upwind front of the group of gas storage tanks between the first and second columns in the middle between 2nd and 3rd rows. Although the small size of the cloud in both cases does not help make much of a conclusion about their spread in the layout, the iso-surfaces still somehow shed some light in the way the gas cloud travels in all the directions in the layout.

The spacing between the tanks or obstacles must be optimised. Very small spacing between the obstacles will result in the accumulation of the gases around them in the case of any leakage [24]. Too much spacing will result in the occupation of more land or will result in a smaller number of storage tanks or buildings in the specified space. For the present study's simulation, the optimisation of the spacing between the obstacles was carried out by plotting the C/Cmax ratio against the spatial distance. The C/Cmax ratio showcases the dispersion of the gases in terms of buoyancy and density. The greater the ratio, the greater the dispersion of the gas, which is advantageous in quick separation of the gases. The smaller the ratio, the slower the dispersion. This results in accumulation of the gases around the tanks or obstacles. Hence, it is necessary to optimise the distance to obtain the maximum ratio of C/Cmax [24].

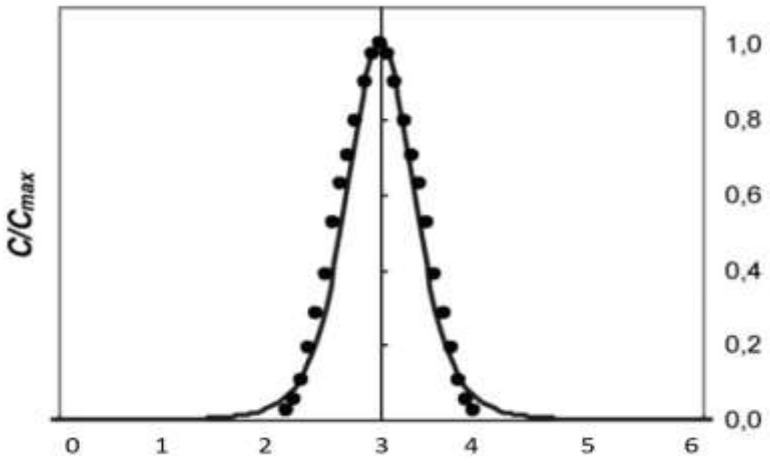

Figure 8.172: *x-axis shows the distance diagonal distance between the tanks or obstacles against the C/Cmax ratio Scargiali et.al. [24]*

From the above graph, it is clear that the ratio first increases and then starts decreasing as the distance between the storage tanks is changed. The diagonal distance between the tanks or obstacles should be maintained at 3 m for the ideal dispersion of the gases.

According to Standard BS EN 60079-10-1:2009 [104], the following locations can be categorised:

High speed:

Zone 0: The central portion of the layout

Zone 1: The immediate surrounding of the central portion of the layout

Zone 2: All the remaining locations not categorised in zone 0 or zone 1

Low speed:

Zone 0: A small semi-circular portion at the release source location

Zone 1: The immediate surrounding of the release source

Zone 2: All the remaining locations not categorised in zone 0 or zone 1

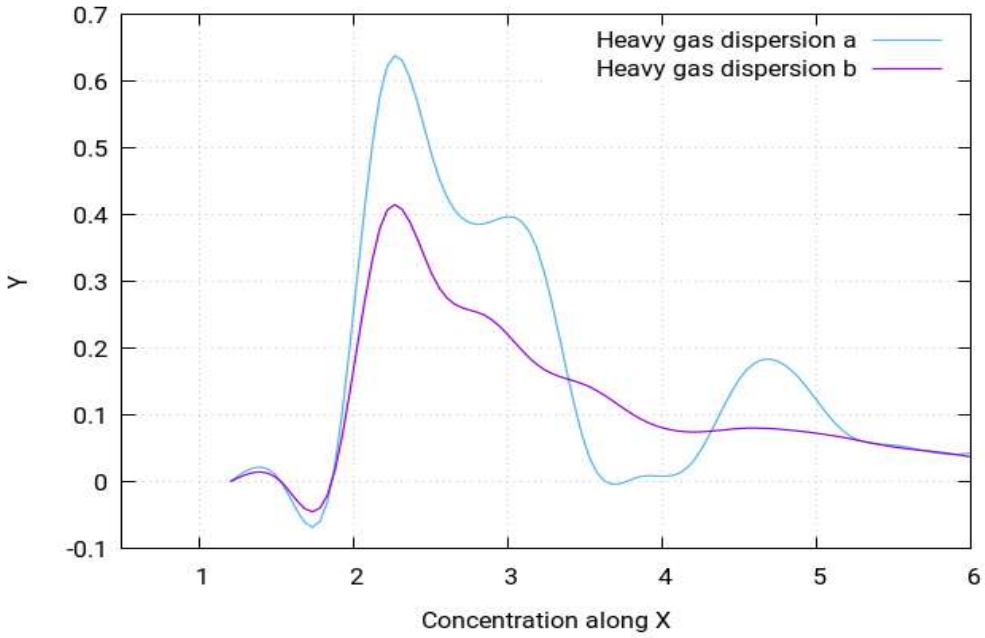

Figure 8.173: *Concentration of the heavy gas dispersion profile along the* ***x****-direction at* ***1m/s*** *at different points of (a) x=1.20m, y=2.20m, z=7.20m (b) x=1.20m, y=2.20m and z=9.84m*

The above figure shows the concentration profiles for two of the gas dispersions at two different locations depending on distance from release source. The curves show a dissimilar overall pattern but follow a similar pattern initially. The highest peak is at approximately 2.2m.

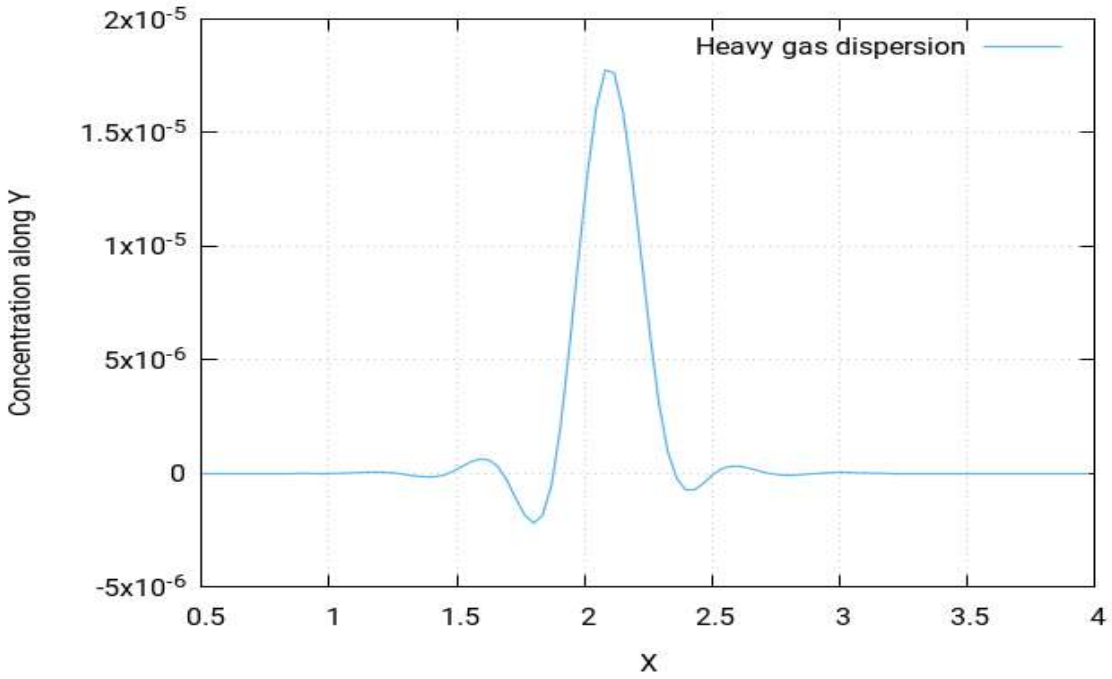

Figure 8.174: *Concentration of the heavy gas dispersion profile along the* ***y****-direction at* ***1m/s*** *at points of x=2.15m, y=-1m and z=1.00m*

Figure 8.174 shows the curve for the concentration profile along the x-direction. The curve follows a somewhat symmetrical pattern and has a single peak at almost 2.2m.

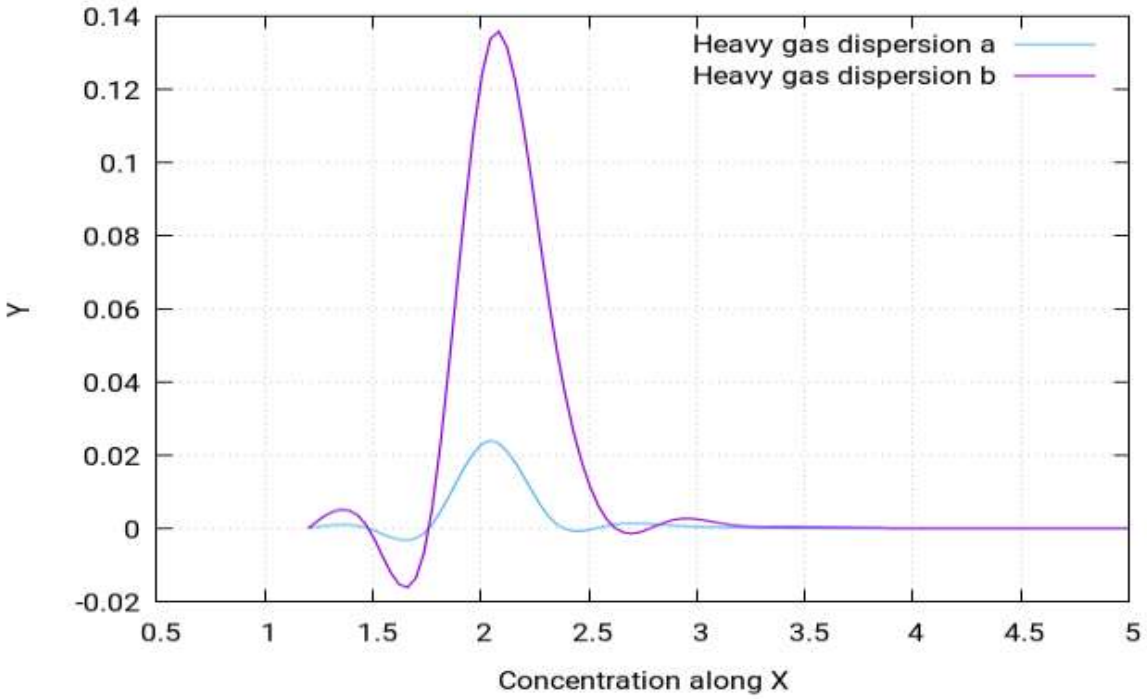

Figure 8.175: *Concentration of the heavy gas dispersion profile* with a low velocity of **0.25m/s** *along the* ***x****-direction at different points of (a) x=1.20m, y=2.20m, z=2.20m (b) x=1.20m, y=2.20m and z=3.50m*

The above figure shows the concentration profiles for two of the gas dispersions at two different locations depending on distance from release source. Both curves follow the same pattern but have different values.

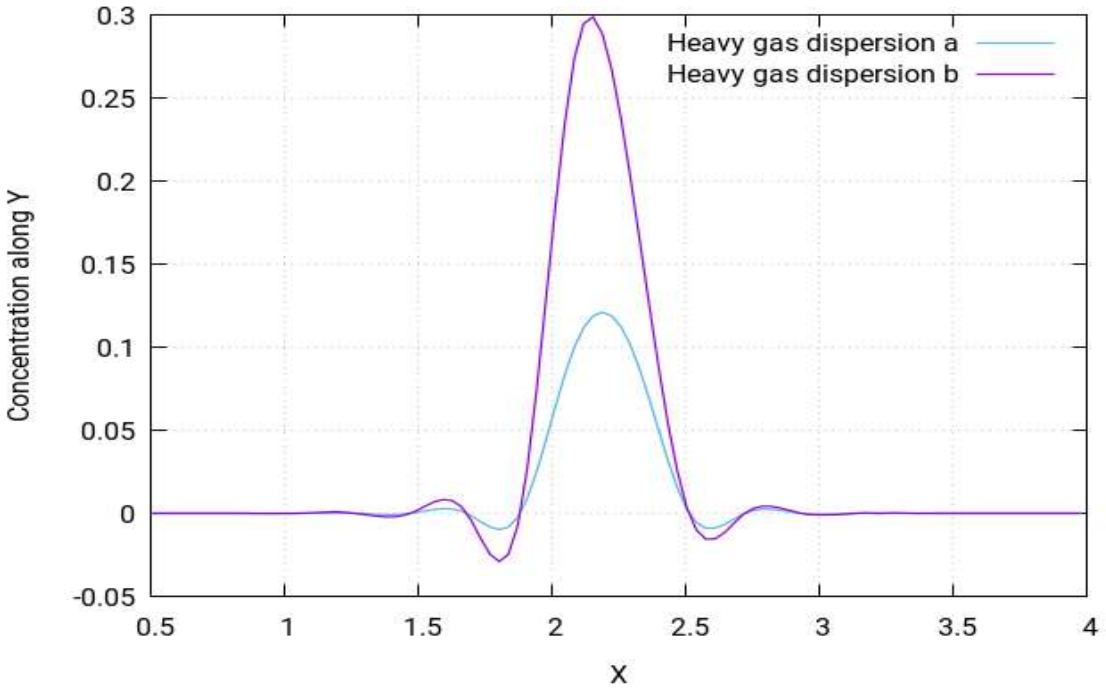

Figure 8.176: *Concentration of the heavy gas dispersion profile* with a low velocity *along the* ***y****-direction at different points of (a) x=1.15m, y=-1m, z=2.20m (b) x=2.15m, y=-1m and z=3.50m*

The above figure shows the concentration profiles for two of the gas dispersions at two different locations depending on distance from release source. Both the curves follow the same pattern but have different values.

8.6.20.5 Temperature of the heavy gas dispersion for a/the safe distance

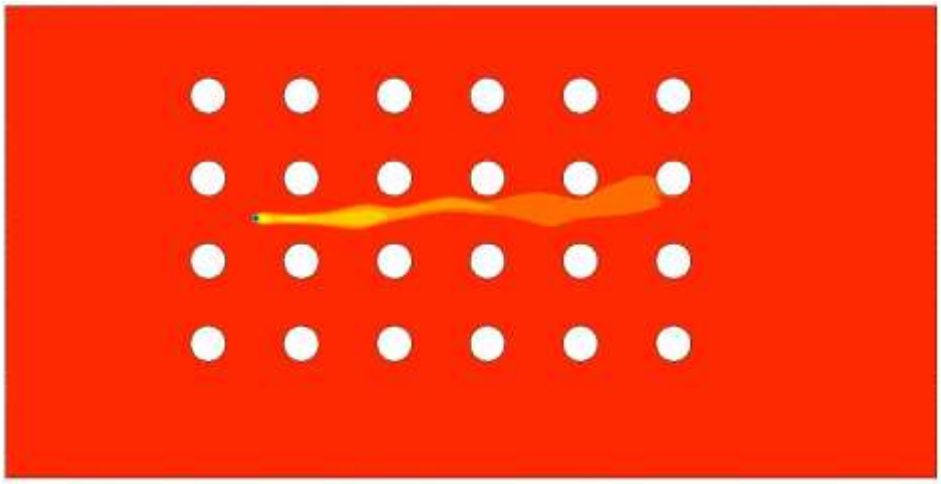

Figure 8.177: *Temperature profile of the heavy gas dispersion with the release source located at the upwind front of the group of gas storage tanks between the first and second columns in the middle between the 2nd and 3rd rows at* ***1m/s***

Figure 8.177 (above) shows the temperature simulation for this study. By visualising the temperature simulation, it is found that the temperature simulation produces largely the same profile for the case study as that of the concentration profile. However, the behaviour of temperature is in fact the opposite of that of concentration. This means that the areas which were identified in the concentration simulation as the highly concentrated will in fact have the lowest temperatures, while the ones with moderate concentrations will have moderate temperatures and the least concentrated areas will have the highest temperatures. The reason for this behaviour is that, as the temperature increases, the density of the gas decreases, which causes it to rise and expand. Hence the concentration at that specific point decreases. To further simply these findings, it should be pointed out that the simulations showed that the concentrations near the release source point tend to be the highest and start to fade away as the gas cloud moves away from the source and are the lowest as the cloud moves much further away in the layout, eventually reaching the environment where the gas cloud disappears. However, the temperature is lowest near the release source point and tends to increase as the gas cloud moves away from the source, finally achieving its highest temperature equal to the ambient temperature of the environment.

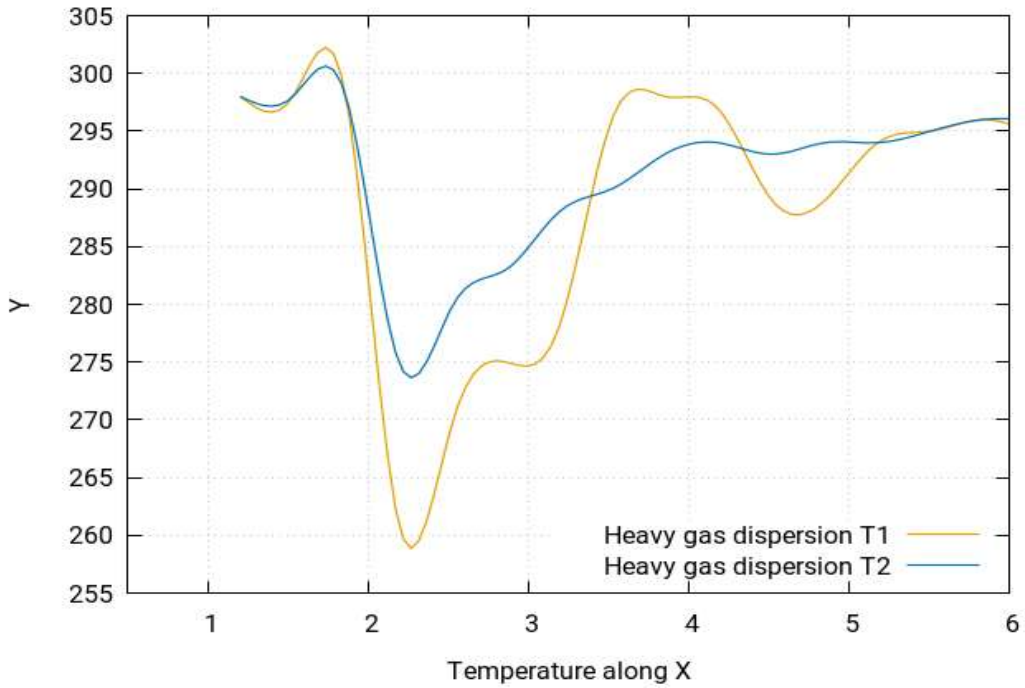

Figure 8.178: *Temperature of the heavy gas dispersion profile along the x-direction at different points of (T1) x=1.20m, y=2.20m, z=7.20m (T2) x=1.20m, y=2.20m and z=9.84m*

Figure 8.178 shows the curves for temperature profile along the x-direction. The curves follow an asymmetrical pattern and have several peaks with the highest peak being at about 2.5m.

8.6.20.6 Velocity of the heavy gas dispersion for a/the safe distance

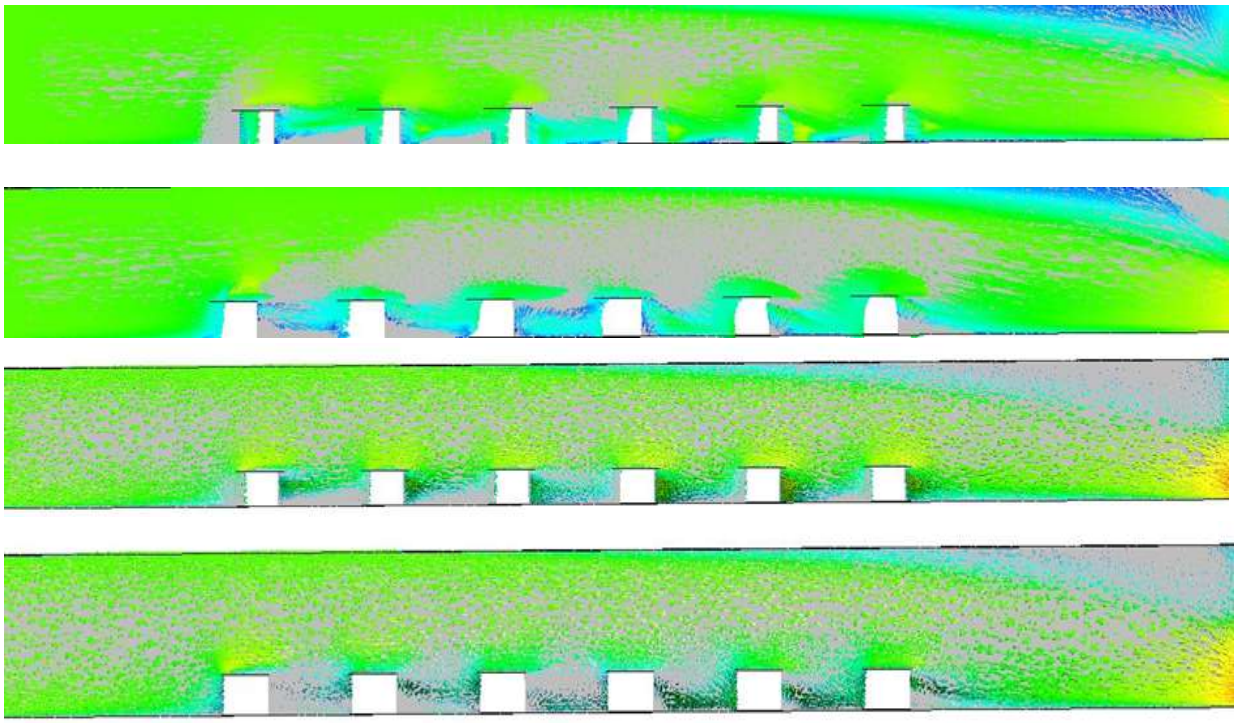

Figure 8.179: (a) *Temperature profile of the heavy gas dispersion with the release source located at the upwind front of the group of gas storage tanks between the first and second column in the middle between 2nd and 3rd rows at* ***1m/s***

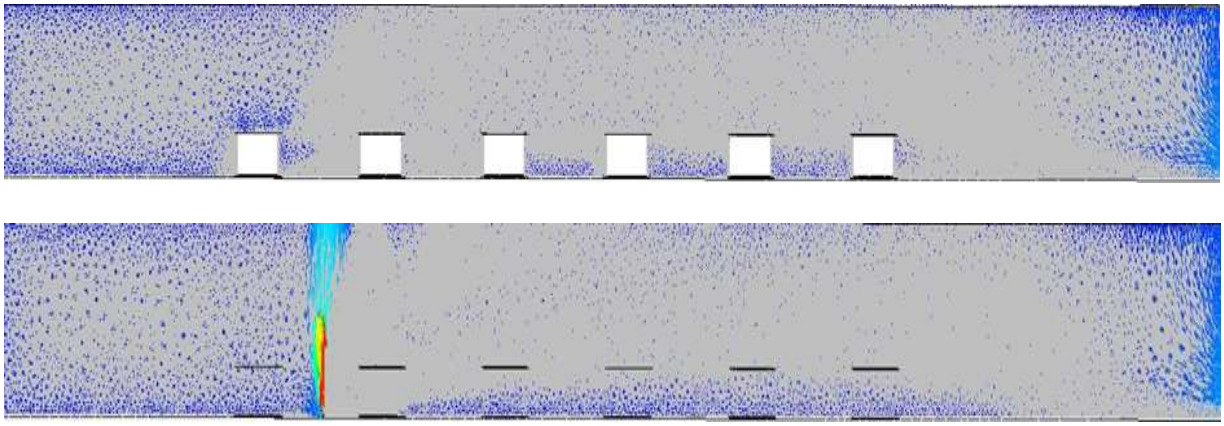

Figure 8.180: (b) *Temperature profile of the heavy gas dispersion with the release source located at the upwind front of the group of gas storage tanks between the first and second columns in the middle between the 2nd and 3rd rows at* ***0.25m/s***

The above figures show the velocity contours of the heavy gas dispersion for this case study with the release source located at the upwind front of the group of gas storage tanks between the first and second columns in the middle between the 2nd and 3rd rows. Velocity contours depict the intensity of the wind - or the effective wind influence - at the different locations throughout the layout. As can be seen in the figure, the wind intensity is different at different points in the layout. It is a commonly known effect that, with enhanced altitudes, enhanced

wind speeds are encountered. This is because the objects at the lower altitudes create resistance to the wind flow. As resistance is caused by the buildings to the flow of gas towards the direction opposite of wind, the wind flowing from left to right fails to indict the same motion of the flow. The dispersion of the heavy gas in the real environment is also influenced by the frictions caused by the buildings and other obstacles. Instead, various complex vertexes are formed within the buildings near the release source location, as can be seen in the above figures. The heavy gas release from the source is carried by these vertexes to the nearby mixture of the gas cloud, which then moves smoothly away from the source. Moreover, the hindrance to the wind flow caused by the buildings results in the vertexes moving in the upward direction, which enhances the shape of the cloud in the upward direction.

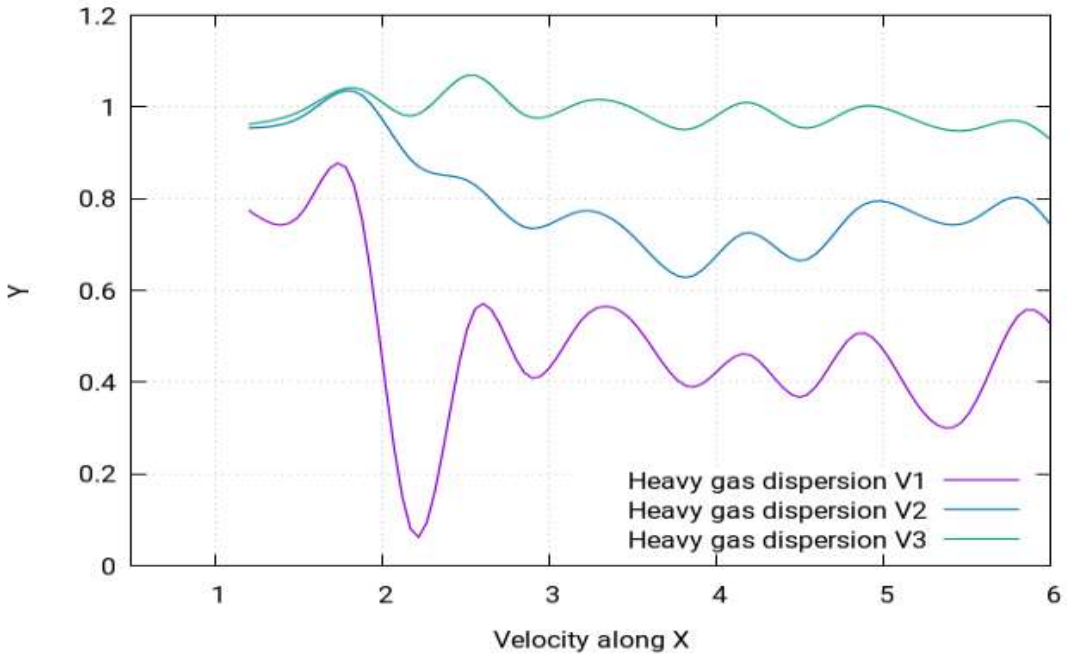

Figure 8.181: *Velocity of the heavy gas dispersion profile along the* ***x****-direction at* ***1m/s*** *at different points of (V1) x=1.20m, y=2.20m, z=7.20m (V2) x=1.20m, y=2.20m, z=9.84m (V3) x=1.20m, y=2.20m and z=2.00m*

Figure 8.181 shows the curves for velocity profile along the x-direction. The curves follow an asymmetrical pattern and has several peaks, with the highest peak being at approximately 1.8m.

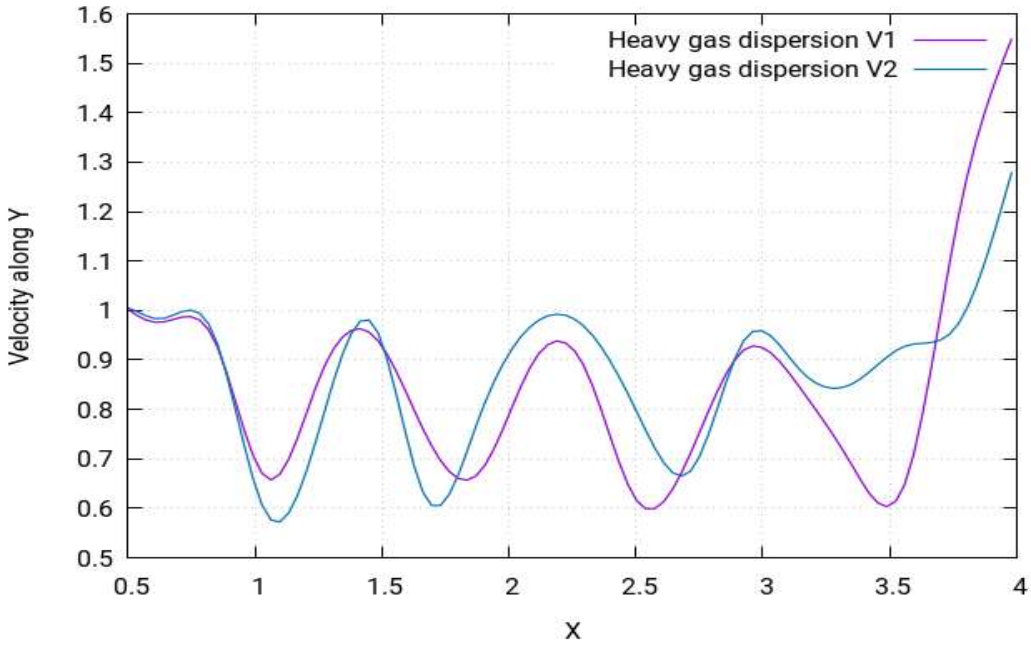

Figure 8.182: *The velocity of the heavy gas dispersion profile along the* ***y****-direction at* ***1m/s*** *different points of (V1) x=2.15m, y=-1m, z=1.00m (V2) x=2.15m, y=-1m and z=2.00m*

Figure 8.182 shows the curves for the velocity profile along the x-direction. The curves follow an asymmetrical pattern and have several peaks, with the highest peak being at approximately 2.2m

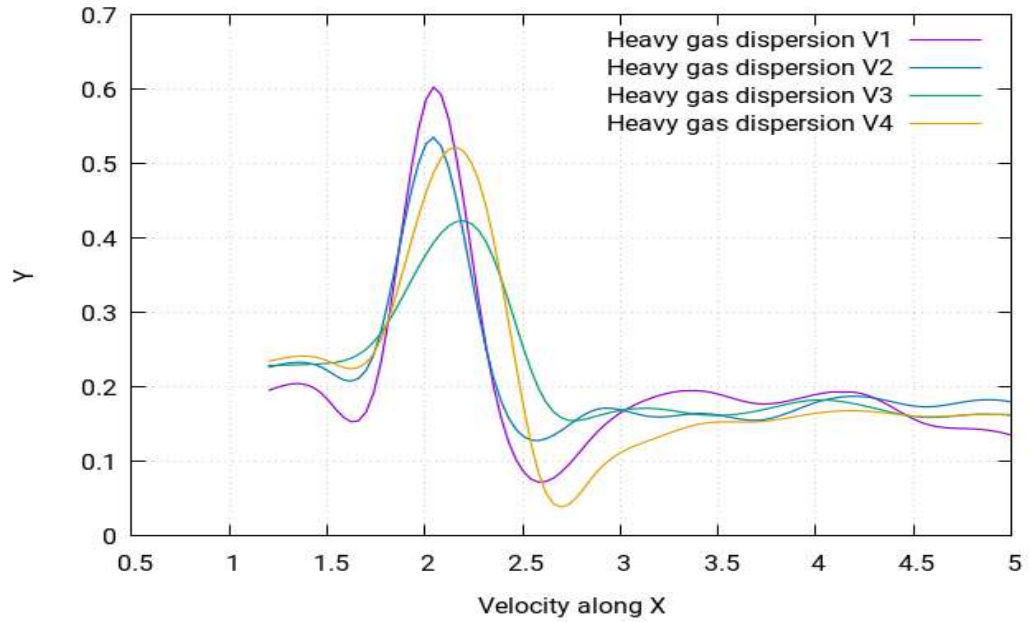

Figure 8.183: *The concentration of the heavy gas dispersion profile* with a low velocity of ***0.25m/s*** *along the* ***x****-direction at different points of (V1) x=1.20m, y=2.20m, z=7.20m (V2) x=1.20m, y=2.20m, z=1.00m (V3) x=1.20m, y=2.20m, z=2.20m (V4) x=1.20m, y=2.20m and z=3.50m*

Figure 8.183 shows the curves for velocity profile along the x-direction. The curves follow an asymmetrical pattern and have several peaks, with the highest peak being at about 2m.

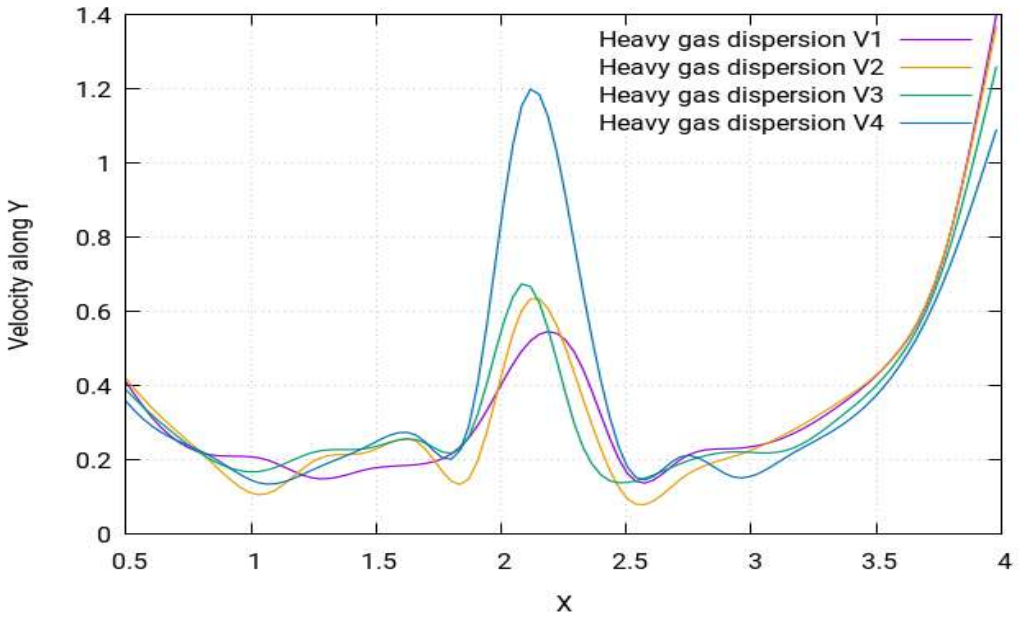

Figure 8.184: *Velocity of the heavy gas dispersion profile* with a low velocity of ***0.25m/s*** *along the* ***y****-direction at different points of (V1) x=1.15m, y=-1m, z=7.20m (V2) x=2.15m, y=-1m, z=1.00m (V3) x=2.15m, y=-1m and z=2.20m (V4) x=2.15m, y=-1m and z=3.50m*

Figure 8.184 shows the curves for velocity profile along the y-direction. The curves follow an asymmetric pattern and have several peaks, with the highest peak being at approximately 2.2m.

At location 1 of the cylindrical tanks, which are arranged at safe distance in a collocated arrangement, it is evident that the concentration of the heavy gas is minimum around the tanks. This is because the distance between the tanks allows minimum turbulence around the tanks due to the wind.

8.6.21 Location 2: Heavy gas dispersion for a safe distance

8.6.21.1 Structure of layout

The type of layout adopted for these two case studies the collocated layout. A layout of 24 Oil storage tanks will be created, with a cylinder shape distribution for safe distance, and the release source will be placed in positions. The behaviour of the gas clouds will then be studied.

8.6.21.2 Release source location

The release sources point (2) was located at the upwind front of the gas storage tanks group in the second row between the second and third columns. The perimeters selected for this case study are stated below:

Table 8.33: *(A) Parametric values for the high-speed heavy gas simulation (safe distance 2)*

Density	Flow Rate	Velocity	Ambient Temperature	Release Source Temperature

2.1 kg m/s^3	1 kg/s	1 m/s	25°C	-100°C

Table 8.34: *(B) Parametric values for the low-speed heavy gas simulation (safe distance 2)*

Density	Flow Rate	Velocity	Ambient Temperature	Release Source Temperature
2.1 kg m/s^3	5 kg/s	0.25 m/s	25°C	-100°C

8.6.21.3 Concentration of the heavy gas dispersion for a/the safe distance

The following figure shows the concentration behaviour of the heavy gas at location 2. The whereabouts of location 2 has been stated at the beginning of the passage.

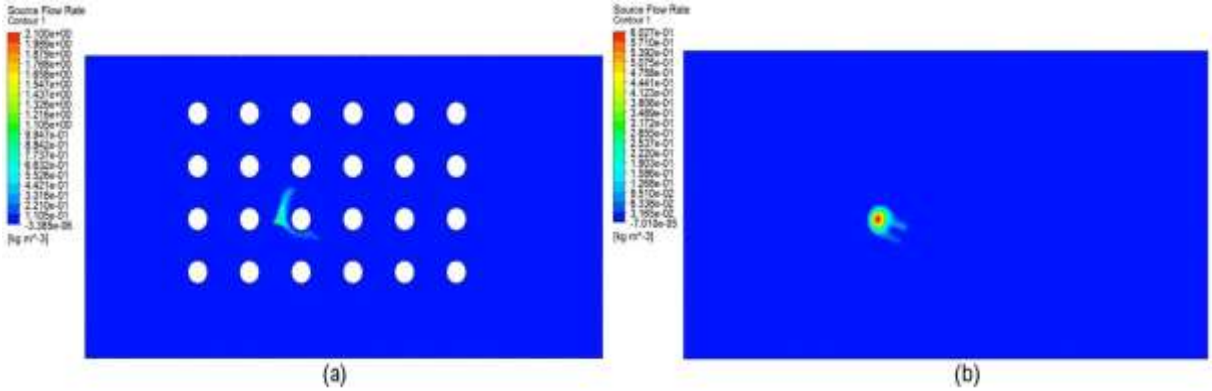

Figure 8.185: (a) *Concentration profile of the Heavy Gas Dispersion with the release source located at the upwind front of the group of gas storage tanks in the second row between the second and third columns at 1m/s.* ***(b)*** *at 0.25m/s*

The concentration profile of the heavy gas at location 2 has been shown in the above Figure 8.185. It represents the concentration behaviour of the heavy gas when the release gas source is placed at the upwind front of the group of gas storage tanks in the second row between the second and third columns. In the above figure, parts labelled (a) are at high speed and those labelled (b) are at low speed. It can be seen from the figure that, for this particular layout, the gas cloud appears to be a tiny piece of a tilted c-shaped cloud in the case of high speed (1m/s), while it is a tiny circle in the case of low speed (0.25m/s).

The separation between the tanks or obstacles is also very much dependent on the size of the tanks. For the small obstacles i.e., for the diameters less than 10 meters, the spacing between the storage obstacles ranges from 1 m to 15 m diagonally [112]. The capacity of the tanks is directly related to the diameter. By increasing the diameter of the tank, the capacity increases. The variation of the safe distance between the tanks with respect to the capacity is shown in the following graph:

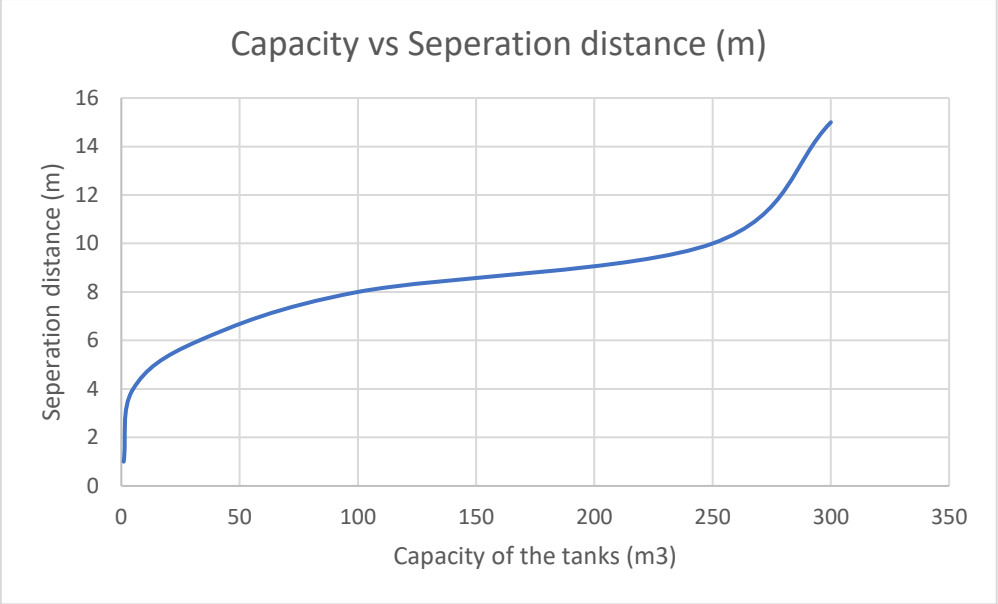

Figure 8.186: *Capacity of the tank vs the separation distance [112]*

8.6.21.4 Iso-surface of the heavy gas dispersion for a/the safe distance

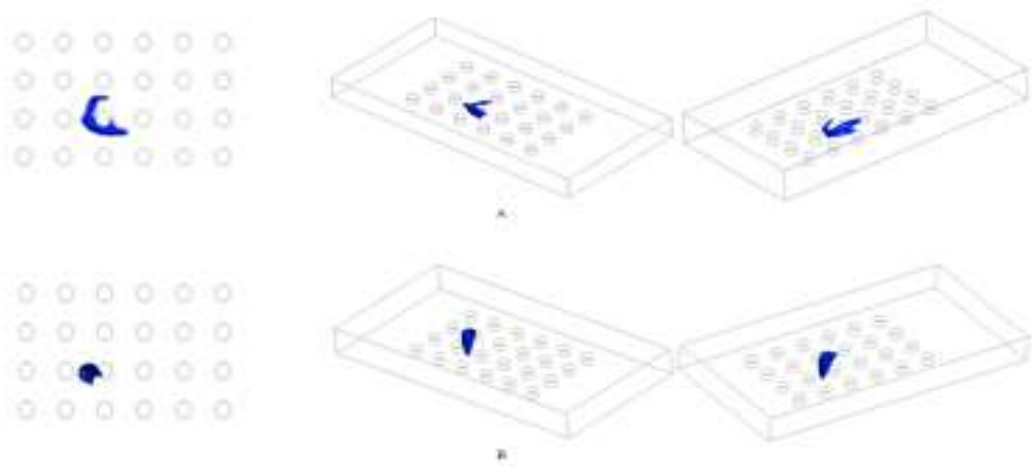

Figure 8.187: (a) *Iso-surfaces of the concentration profile of the heavy gas dispersion with the release source located at the upwind front of the gas storage tanks group in the second row between the second and third columns at 1m/s.* ***(b)*** *At 0.25m/s*

Figure 8.187 presents the iso-surfaces of the concentration profile of the heavy gas dispersion with the release source located at the upwind front of the group of gas storage tanks in the second row between the second and third columns. Although the small size of the cloud in both cases does not help make many conclusions about their spread in the layout, the iso-surfaces still somehow shed some light on the way the gas cloud travels in all the directions in the layout.

According to Standard BS EN 60079-10-1:2009 [104], the following locations can be categorised:

High speed:

Zone 0: The immediate blocks of the release source location

Zone 1: The immediate surrounding of the release source location

Zone 2: All the remaining locations not categorised in zone 0 or zone 1

Low speed:

Zone 0: A small circular portion at the release source location

Zone 1: The immediate surrounding of the release source location

Zone 2: All the remaining locations not categorised in zone 0 or zone 1

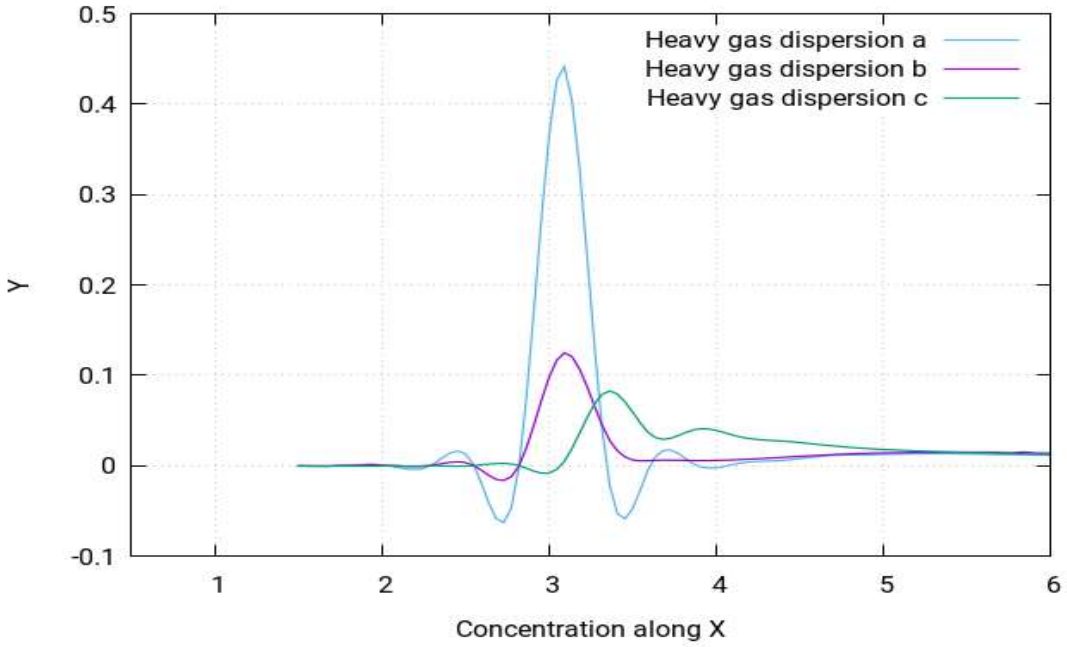

Figure 8.188: *Concentration of the heavy gas dispersion profile along the* ***x****-direction at* ***1m/s*** *different points of (a) x=1.50m, y=2.00m, z=7.20m (b) x=1.50m, y=2.20m, z=7.20m (c) x=1.50m, y=2.20m and z=8.50m*

Above, Figure 8.188 shows three different curves for the concentration profiles. They show the pattern of the concentration profile along the x-direction when the wind speed for the simulation is 1m/s. The three different curves are obtained for two different distances from the release source. The curves follow the same pattern but have different values due to the difference in distances. From the figure, it is concluded that the concentration value of the heavy gas decreases as it moves away from the source. In the figure, the curve with the highest peak is obtained when nearest to the release source and vice versa.

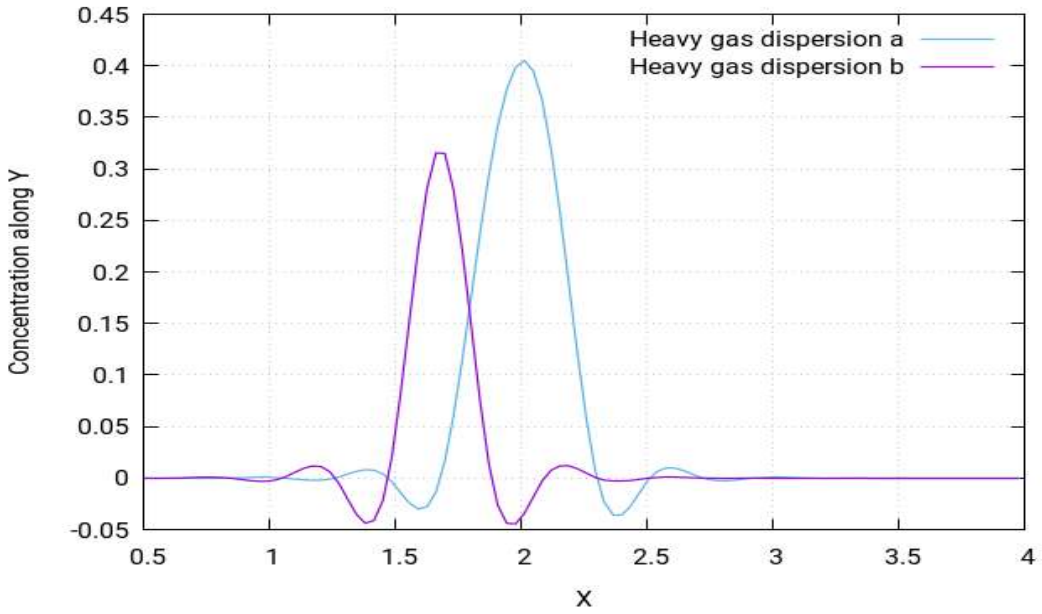

Figure 8.189: *Concentration of the heavy gas dispersion profile along the **y**-direction at **1m/s** different points of (a) x=2.10m, y=-1m, z=7.20m (b) x=2.10m, y=-1m and z=2.00m*

Above in Figure 8.189, two different curves for the concentration profiles are shown. They show the pattern of the concentration profile along the y-direction when the wind speed for the simulation is 1m/s. The two different curves are obtained for two different distances from the release source. Both curves follow the same pattern but have different values due to the difference in distances. From the figure, it is concluded that the concentration value of the concentration of heavy gas decreases as it moves away from the source. In the figure, the curve with highest peak is obtained when nearest to the release source and vice versa.

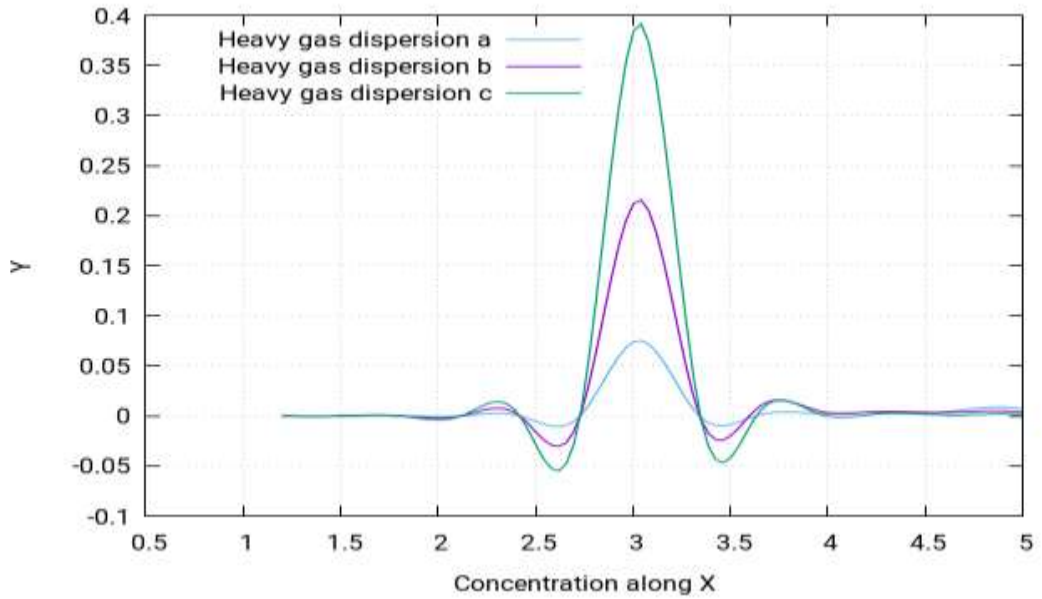

Figure 8.190: *Concentration of the heavy gas dispersion profile with a low velocity of **0.25m/s** along the **x**-direction at different points of (a) x=1.20m, y=1.80m, z=2.00m (b) x=1.20m, y=1.80m, z=3.00m (c) x=1.20m, y=1.80m and z=4.50m*

In Figure 8.190, three different curves for the concentration profiles are shown. They show the pattern of the concentration profile along the x-direction when the wind speed for the simulation is 0.25m/s. The three different curves are obtained for two different distances from the release source. The curves follow the same pattern but have different values due to difference in distances. From the figure, it is concluded that the concentration value of the concentration of heavy gas decreases as it moves away from the source. In the figure, the curve with highest peak is obtained when nearest to the release source and vice versa.

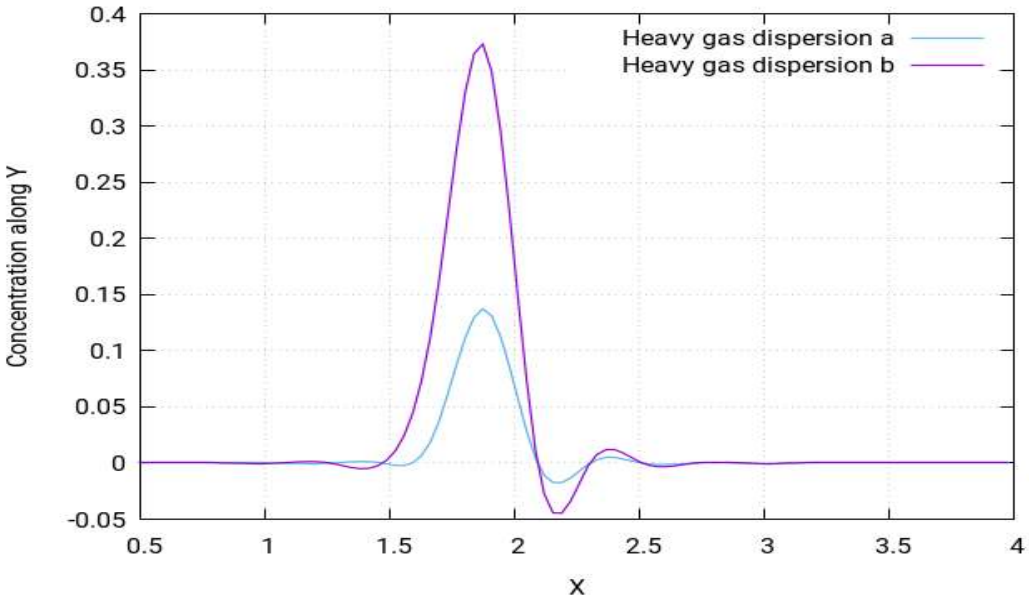

Figure 8.191: *Concentration of the heavy gas dispersion profile with a low velocity of* ***0.25m/s*** *along the* ***y****-direction at different points of (a) x=2.93m, y=-1m, z=2.00m (b) x=2.93m, y=-1m and z=3.60*

In Figure 8.191, two different curves for the concentration profiles are shown. They show the pattern of the concentration profile along the x-direction when the wind speed for the simulation is 1m/s. The two different curves are obtained for two different distances from the release source. Both curves follow the same pattern but have different values due to difference in distances. From the figure, it is concluded that the concentration value of the concentration of heavy gas decreases as it moves away from the source. In the figure, the curve with highest peak is obtained when nearest to the release source and vice versa.

8.6.21.5 Temperature of the heavy gas dispersion for a/the safe distance

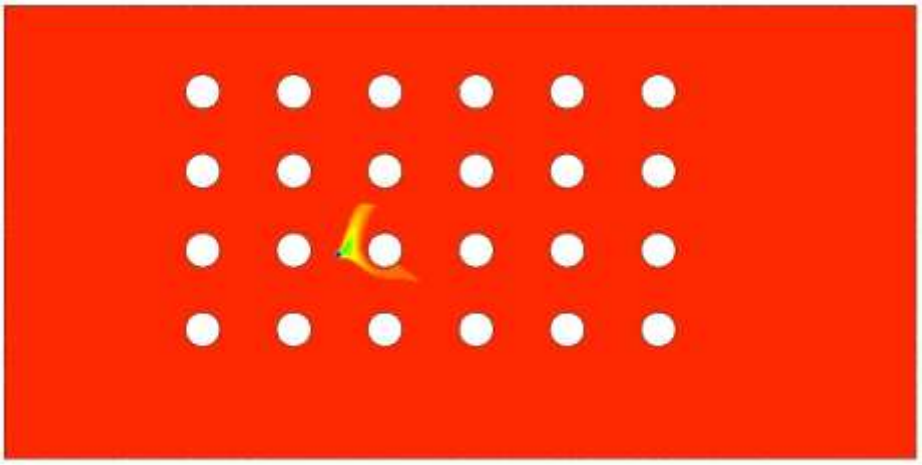

Figure 8.192: *Temperature profile of the heavy gas dispersion with the release source located at the upwind front of the gas storage tanks group in the second row between the second and third column at* ***1m/s****.*

Figure 8.192 (above) shows the temperature simulation for the present study. By visualising the temperature simulation, it is found out that the temperature simulation produces largely the same profile for the case study as that of the concentration profile. However, the behaviour of temperature is in fact the opposite to that of concentration. This means that the areas which were identified in the concentration simulation as highly concentrated will in fact have the lowest temperatures, while the ones with moderate concentrations will have moderate temperatures and the least concentrated areas will have the highest temperatures. To further simply these findings, it should be pointed out that the simulations showed that the concentrations near the release source point tend to be the highest and start to fade away as the gas cloud moves away from the source and are the lowest as the cloud moves much further away in the layout, eventually reaching the environment where the gas cloud disappears. However, the temperature is lowest near the release source point and tends to increase as the gas cloud moves away from the source, finally achieving its highest temperature equal to the ambient temperature of the environment.

According to the 'Energy Institute's Model Code of Safe Practice' [112], the separation between the tanks is also very much dependent on their operating temperatures. The operating temperature is the temperature at which the substance is stored inside the tanks. A table was drafted that shows the recommended distances between the storage tanks based on the temperature of the substances:

Table 8.35: *Recommended distance between tanks based on temperature* [112]

	LPG cylinders (>50 kg total capacity)	LPG vessels (up to 135 m³)	LPG vessel (over 135 m³)
Flammable liquid (flashpoint <32 °C)	3 m to bund wall	6 m to bund wall	15 m to bund wall
Flammable liquid (flashpoint 32–65 °C) Tank size up to 3000 litres	3 m to bund wall	3 m to bund wall	6 m to bund wall
Flammable liquid (flashpoint 32–65 °C) Tank size over 3000 litres	3 m to bund wall	3 m to bund wall	15 m to bund wall

It is clear from the above table that, as the temperature of the stored substance increases, the safe distance is increased.

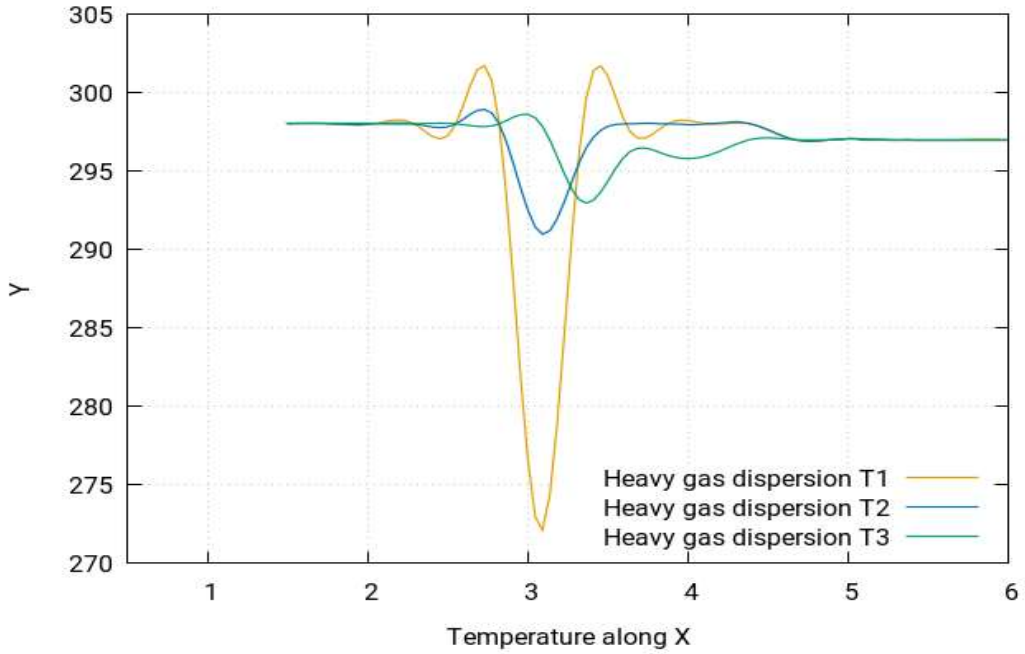

Figure 8.193: *Temperature of the heavy gas dispersion profile along the* ***x****-direction at* ***1m/s*** *different points of (T1) x=1.50m, y=2.00m, z=7.20m (T2) x=1.50m, y=2.20m, z=7.20m (T3) x=1.50m, y=2.20m and z=8.50m*

In Figure 8.193, two different curves for the temperature profiles are shown. They show the pattern of the temperature profile along the x-direction when the wind speed for the simulation is 1m/s. The two different curves are obtained for two different distances from the release source. These results show that at speed of 1m/s, temperature profiles are a mirror of concentration profile.

8.6.21.6 Velocity of the heavy gas dispersion for a/the safe distance

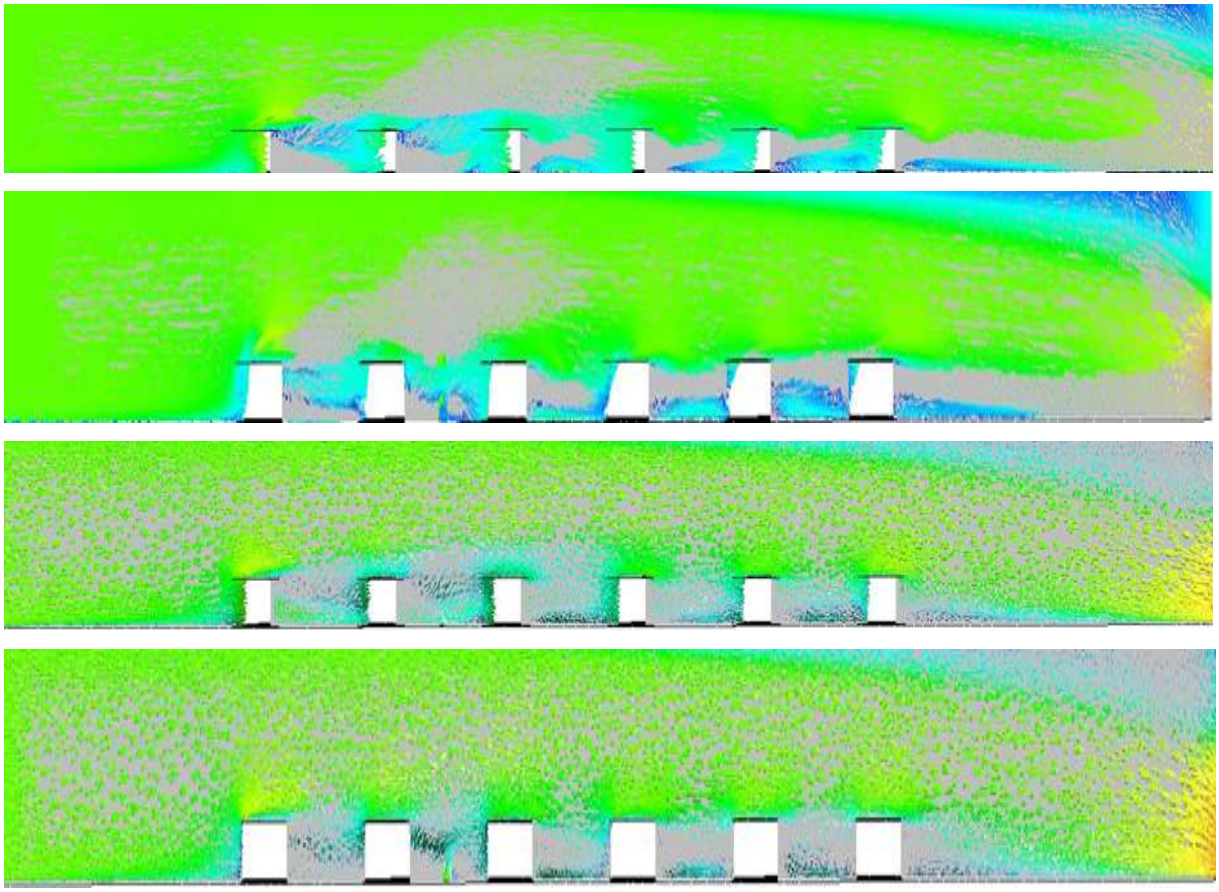

Figure 8.194: *Velocity contours of the heavy gas dispersion with the release source located at the upwind front of the group of gas storage tanks in the second row between the second and third columns at* ***1m/s****.*

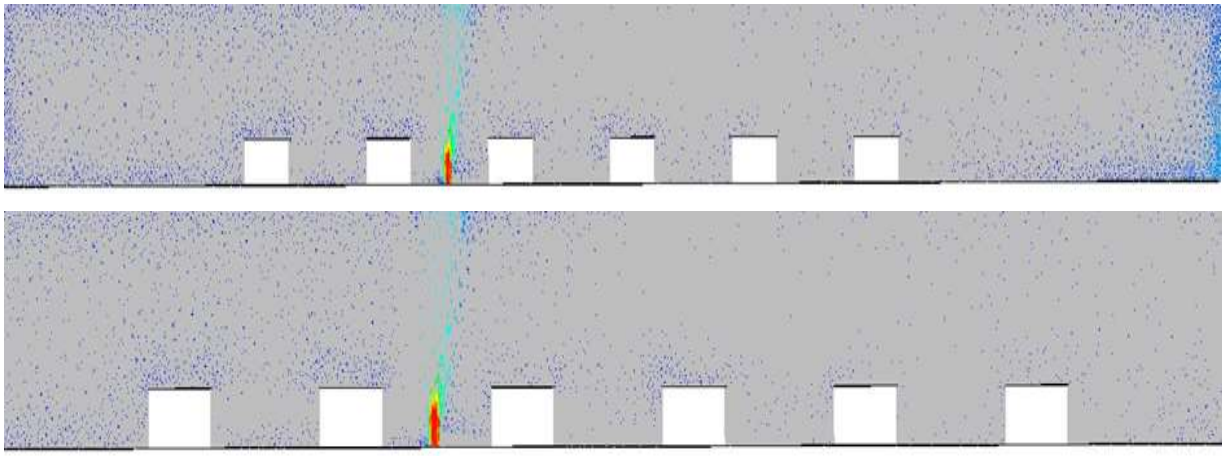

Figure 8.195: *Velocity contours of the heavy gas dispersion with the release source located at the upwind front of the group of gas storage tanks in the second row between the second and third columns at* ***0.25m/s****.*

The above figures show the velocity contours of the heavy gas dispersion for this case study with the release source located in the second row between the second and third columns. Velocity contours depict the intensity of wind - or the effective wind influence - at the different locations throughout the layout. The wind intensity is different at different points in the layout.

It is a commonly known effect that with enhanced altitudes, enhanced wind speeds are encountered. This is because the objects at the lower altitudes create resistance to the wind flow. As resistance is caused by the buildings in the flow of gas towards the direction opposite of wind, the wind flowing from left to right fails to indict the same motion of the flow. Instead, various complex vertexes are formed within the buildings near the release source location as can be seen in the above figure. The heavy gas release from the source is carried by these vertexes to the nearby mixture of the gas cloud which then moves smoothly away from the source. Moreover, the hindrance to the wind flow caused by the buildings results in the vertexes moving in the upward direction, which enhances the shape of the cloud in the upward direction.

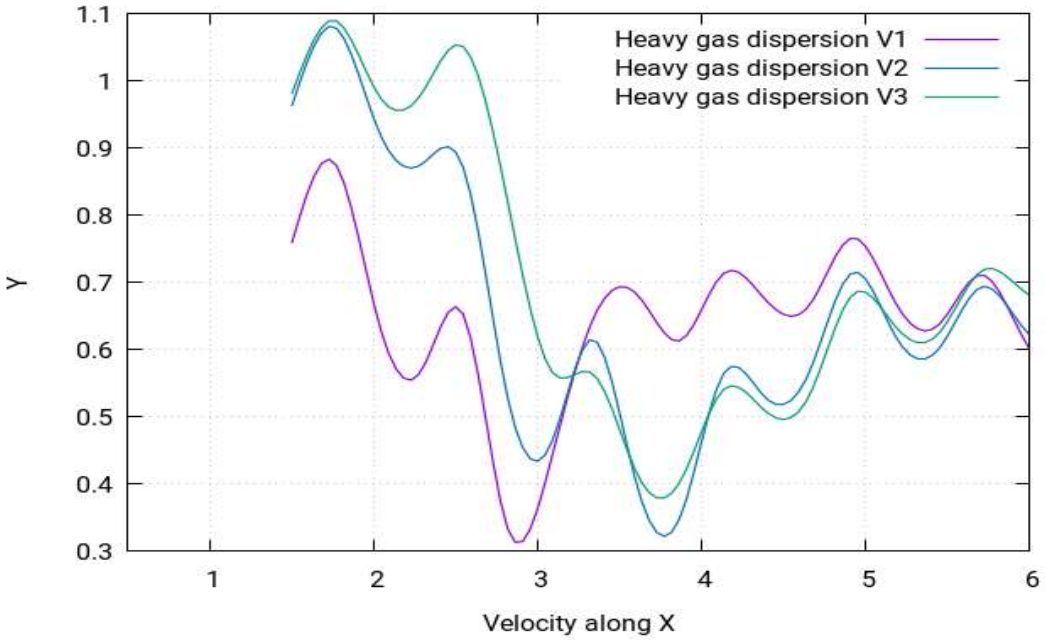

Figure 8.196: *Concentration of the heavy gas dispersion profile along the* ***x****-direction at* ***1m/s*** *different points of (V1) x=1.50m, y=2.20m and z=7.20m, (V1) x=1.50m, y=2.20m and z=8.50m, and (V3) x=1.50m, y=2.20m and z=1.60m*

Figure 8.196 shows the curves for the velocity profile along the x-direction. The curves follow an asymmetrical pattern and have several peaks, with the highest peak being at approximately 2.9m.

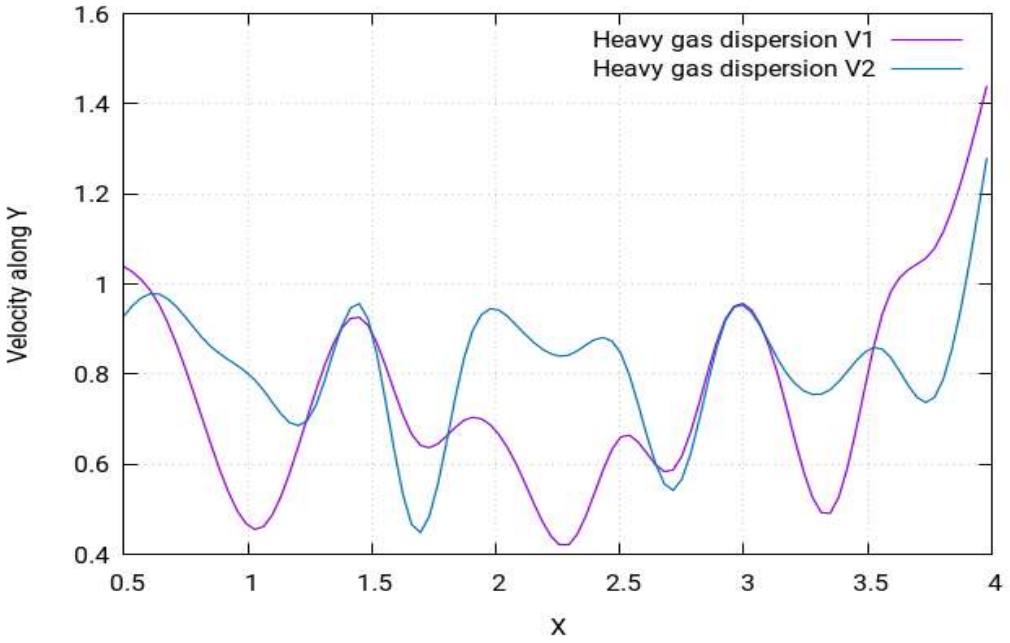

Figure 8.197: *Concentration of the heavy gas dispersion profile along the **y**-direction at **1m/s** different points of (V1) x=3.10m, y=-1m, z=8.50m (V2) x=3.10m, y=-1m, z=2.00m, y=-1m and z=7.20m*

Figure 8.197 shows the curves for the velocity profile along y-direction. The curves follow an asymmetric pattern and have several peaks, with the highest peak being at approximately 2.3m.

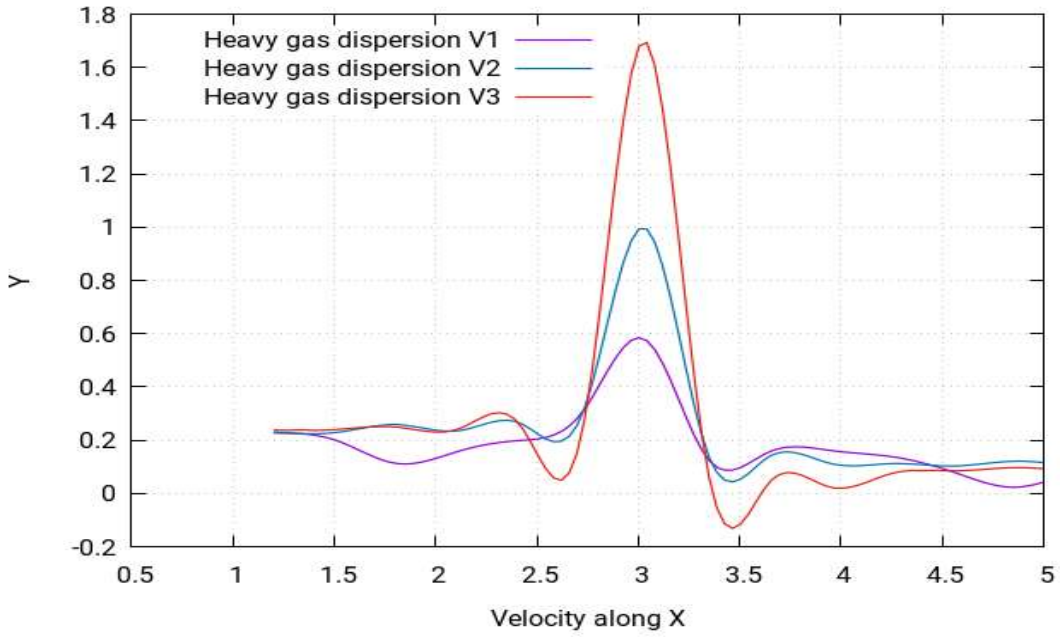

Figure 8.198: *Velocity of the heavy gas dispersion profile with a low velocity of **0.25m/s** along the **x**-direction at different points of (V1) x=1.20m, y=1.80m, z=2.00m (V2) x=1.20m, y=1.80m, z=3.00m (V3) x=1.20m, y=1.80m and z=4.50m*

The above figure shows the velocity profiles for two of the gas dispersions at two different locations depending on distance from release source. Both the curves follow the same pattern but have different values.

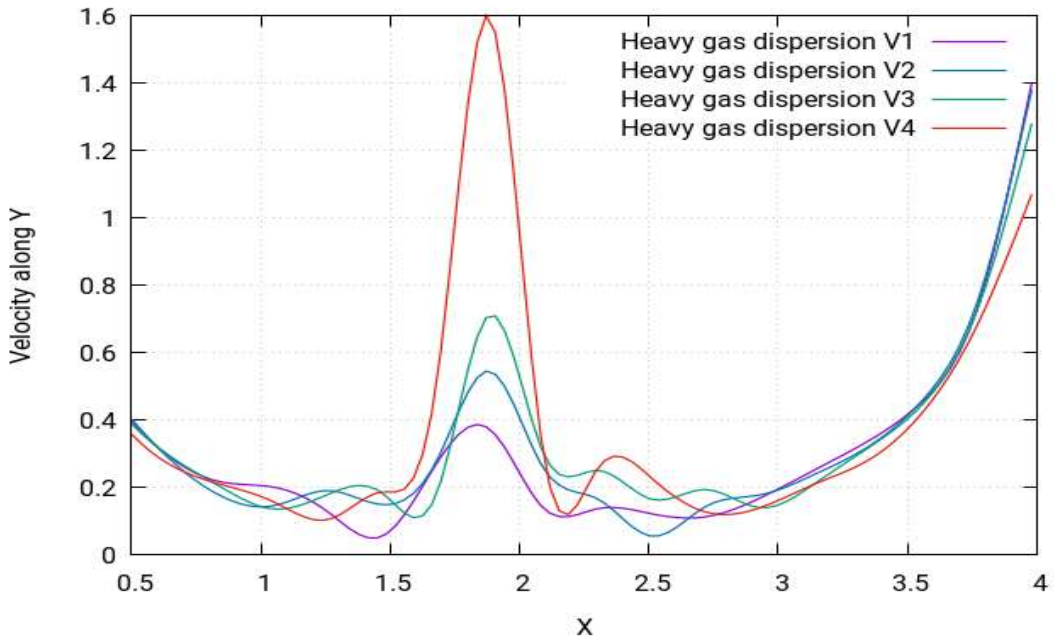

Figure 8.199: *Velocity of the heavy gas dispersion profile with a low velocity of* ***0.25m/s*** *along the* ***y****-direction at different points of (V1) x=2.93m, y=-1m, z=7.20m (V2) x=2.93m, y=-1m, z=8.50m (V3) x=2.93m, y=-1m, z=2.00m (V4) x=2.93m, y=-1m and z=3.60m*

The above figure shows the velocity profiles for four of the gas dispersions at two different locations depending on distance from release source. The curves follow the same pattern but have different values.

At location 2 of the heavy gas dispersion for the cylindrical tanks, it is clear from the simulation results that the tank which is nearest to the source has the highest concentration of the heavy gas due to the turbulence and the dispersion velocity. But since the rest of the tanks are arranged at the minimum safe distance, the turbulence of the wind around them is low, due to which the concentration is minimum.

8.6.22 Location 1: Heavy gas dispersion

8.6.22.1 Structure of layout

The type of layout adopted for this case study for the staggered layout. A layout of 90 oil storage tanks will be created, with a cylinder-shape distribution, and the release source will be placed in position. The behaviour of the gas clouds will then be studied.

8.6.22.2 Release source location

The release sources point (1) is located at the middle front of the oil storage tanks group in the 5th row. The perimeters selected for this case study is stated below:

Table 8.36: *Parametric values for the high-speed neutral gas simulation (location 1)*

Density	Flow Rate	Velocity	Ambient Temperature	Release Source Temperature
2.1 kg m/s^3	1 kg/s	1 m/s	25°C	-100°C

8.6.22.3 Concentration of the heavy gas dispersion

The following figure shows the concentration behaviour of the heavy gas at location 1. The whereabouts of location 1 has been stated at the beginning of the passage.

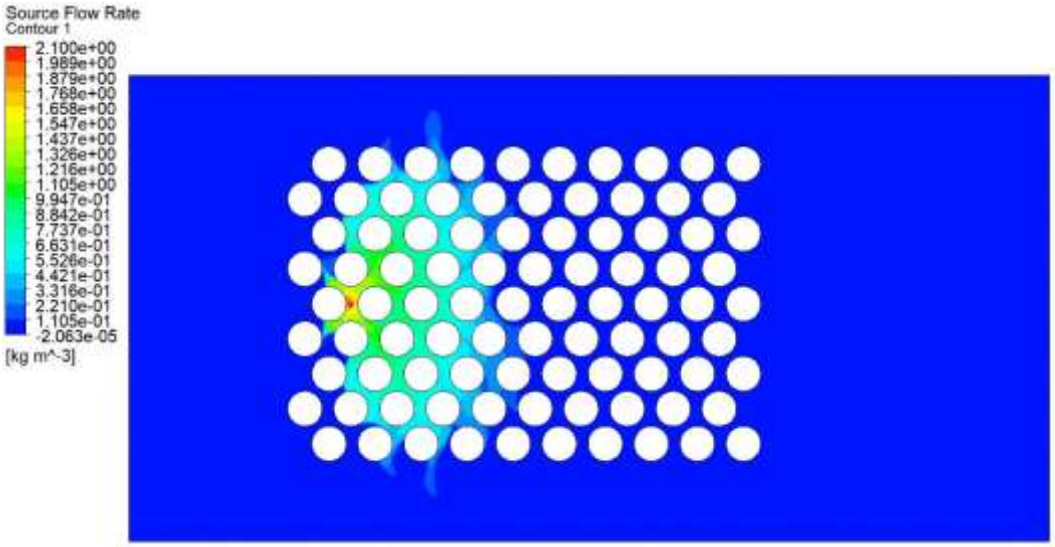

Figure 8.200: *Concentration profile of the heavy gas dispersion with the release source located at the middle front of the group of oil storage tanks in the 5th row at* ***1m/s***

The concentration profile of the heavy gas at location 1 for staggered layout is shown in the Figure 8.200. It represents the concentration behaviour of the heavy gas when the release gas source is placed at the middle front of the group of oil storage tanks in the 5th row. The same study was also performed for collocated layouts under the same parameters but in the 3rd row instead of the 5th. The simulations show that, since the release source is now not exposed to the air, the gas coming out of the release source is therefore not directly affected. As a result, the gas cloud adopts a more concentrated pattern, unlike if the gas source was exposed to the air. The change of location has affected the cloud shape in such a way that at high speed it now makes a rectangular type of cloud shape at the upwind front of the building layout extending to the middle front. The cloud shape is largely symmetrical.

8.6.22.4 Iso-surface of the heavy gas dispersion

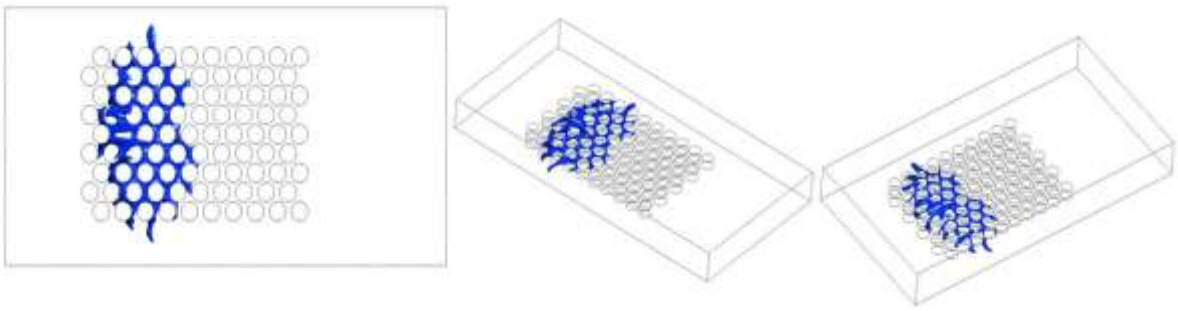

Figure 8.201: *Iso-surfaces concentration profile of the heavy gas dispersion with the release source located at the middle front of the group of oil storage tanks in the 5th row at* ***1m/s***

Figure 8.201 shows the iso-surfaces of the concentration profile of the heavy gas dispersion for a/the staggered layout with the release source located at the middle front of the group of oil storage tanks in the 5th row. It helps identify the spread of the cloud in each dimension and it can be seen that the cloud is not concentrated at the release source location like it is in other layout types. It can also be said that the cloud shape in this case is largely symmetrical and is not an exact rectangle, as it appears in the beginning.

According to Standard BS EN 60079-10-1:2009 [104], the following locations can be categorised:

Zone 0: The square shaped building containing three central rows and 1 column at each side of the release source

Zone 1: The rectangular shaped portion of the building layout starting from the upwind front extending all the way to the middle front of the building layout

Zone 2: All the remaining locations not categorised in zone 0 or zone 1

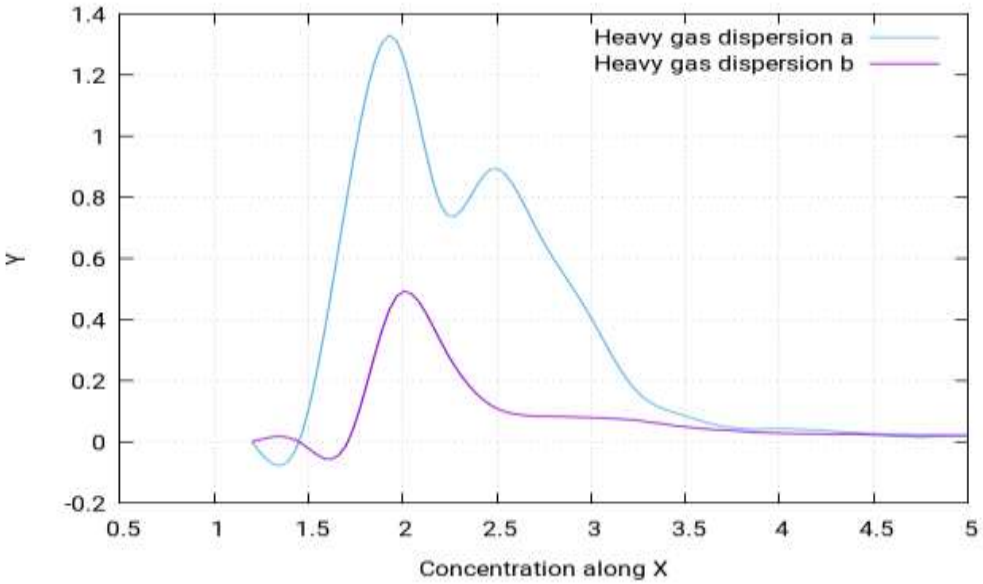

Figure 8.202: *Concentration of the heavy gas dispersion profile along the* ***x****-direction at different points of (a) x=1.20m, y=1.90m, z=7.20m (b) x=1.20m, y=1.90m and z=1.00m*

Above in Figure 8.202, two different curves for the concentration profiles are shown. They show the pattern of the concentration profile along the x-direction when the wind speed for the simulation is 1m/s. The two different curves are obtained for two different distances from the release source. Both the curves follow the same pattern but have different values due to difference in distances. From the figure, it is concluded that the concentration value of the heavy gas decreases as it moves away from the source. In the figure, the curve with highest peak is achieved when nearest to the release source and vice versa.

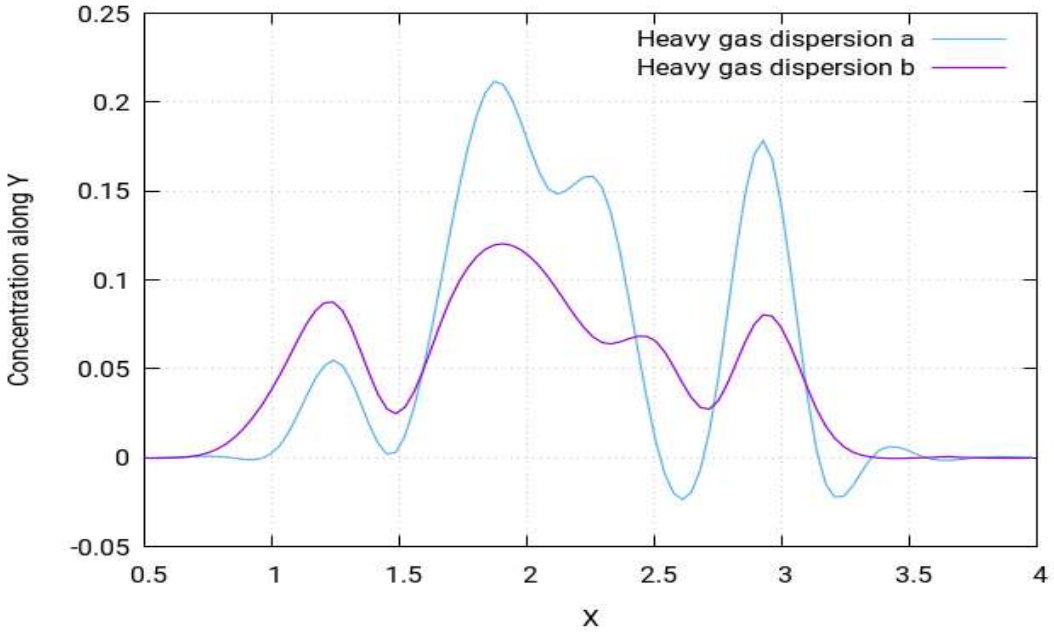

Figure 8.203: *Concentration of the heavy gas dispersion profile along the* ***y****-direction at different points of (a) x=2.12m, y=-1m, z=2.00m (b) x=2.40m, y=-1m, z=2.00m*

Figure 8.203 shows the curves for the concentration profile along the x-direction. The curves follow an asymmetric pattern and have several peaks, with the highest peak being at approximately 2.6m.

8.6.22.5 Temperature of the heavy gas dispersion

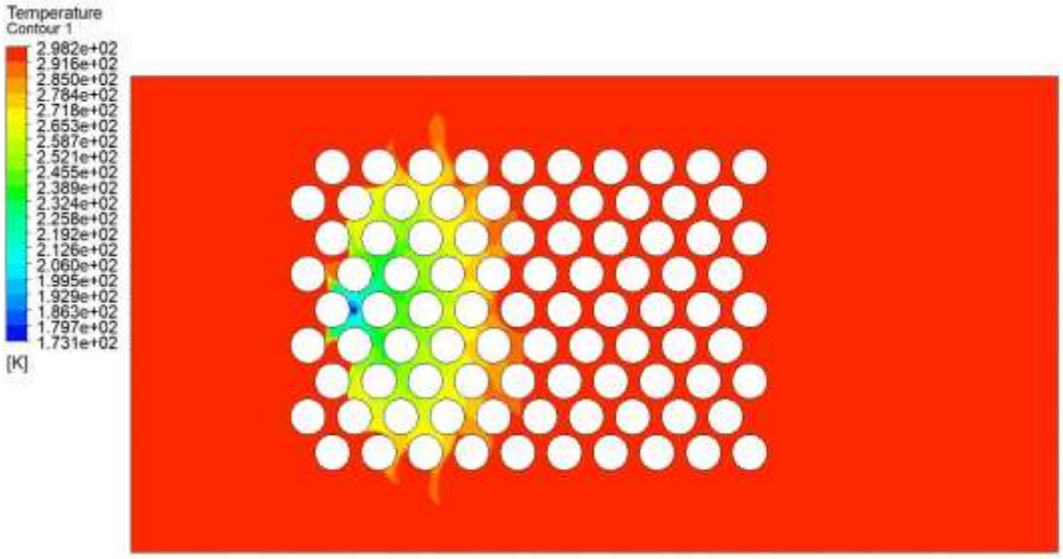

Figure 8.204: *Temperature profile of the heavy gas dispersion with the release source located at the middle front of the group of oil storage tanks in the 5th row at* ***1m/s***

Figure 8.204 (above) shows the temperature simulation for the present study. By visualising the temperature simulation, it is found out that the temperature simulation produces largely the same profile for the case study as that of the concentration profile. However, the behaviour of temperature is in fact the opposite to that of concentration. This means that the areas which were identified in the concentration simulation as highly concentrated will in fact have the lowest temperatures, while the ones with moderate concentrations will have moderate temperatures and the least concentrated areas will have the highest temperatures. To further simply these findings, it should be pointed out that the simulations showed that the concentrations near the release source point tend to be the highest and start to fade away as the gas cloud moves away from the source and is at its lowest as it moves much further away in the layout reaching the environment where the gas cloud eventually disappears. However, temperature is minimum near the release source point and tends to increase as the gas cloud moves away from source, finally achieving the maximum temperature equal to the ambient temperature of the environment.

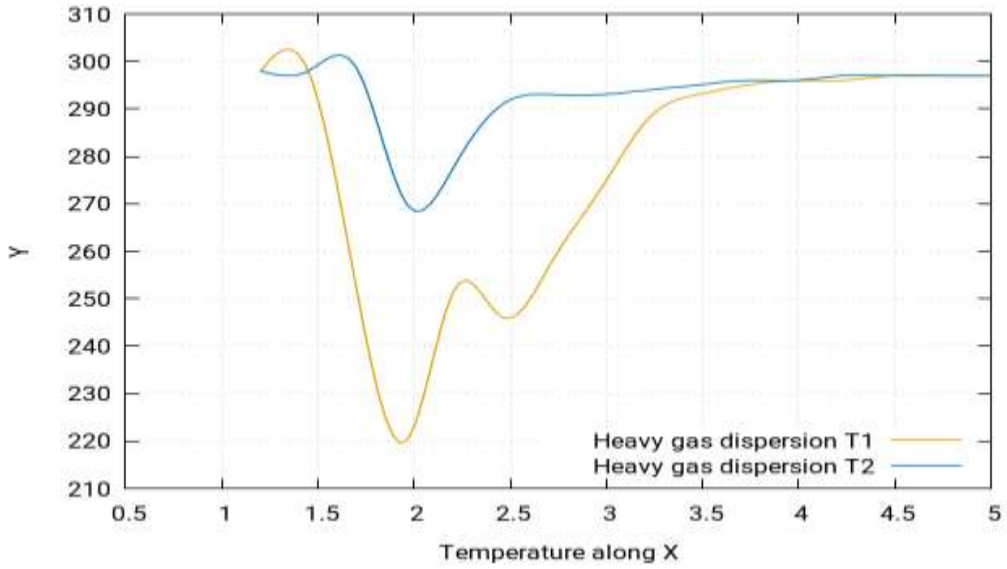

Figure 8.205: *Temperature of the heavy gas dispersion profile along the* ***x****-direction at different points of (T1) x=1.20m, y=1.90m, z=7.20m (T2) x=1.20m, y=1.90m and z=1.00m*

Above in Figure 8.205, two different curves for the temperature profiles are shown. They show the pattern of the temperature profile along the x-direction when the wind speed for the simulation is 1m/s. The two different curves are obtained for two different distances from the release source. These results show that, at a speed of 1m/s, temperature profiles are a mirror of the concentration profile.

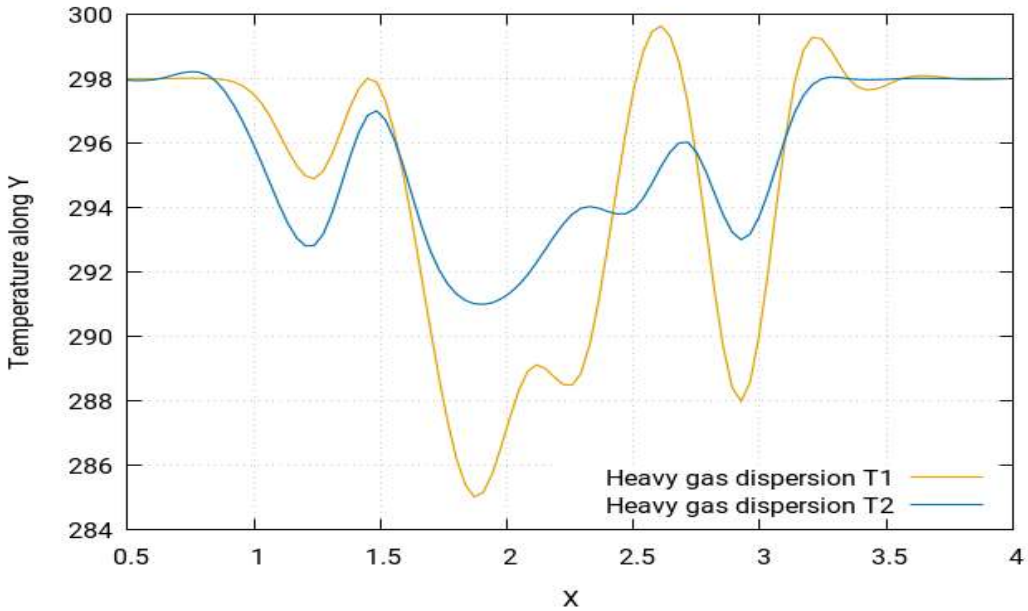

Figure 8.206: *Temperature of the heavy gas dispersion profile along the* ***y****-direction at different points of (T1) x=2.12m, y=-1m, z=2.00m (T2) x=2.40m, y=-1m and z=2.00m*

Figure 8.206 shows the curves for temperature profile along the y-direction. The curves follow an asymmetrical pattern and have several peaks, with the highest peak being at approximately 1.8m.

8.6.22.6 Velocity of the heavy gas dispersion

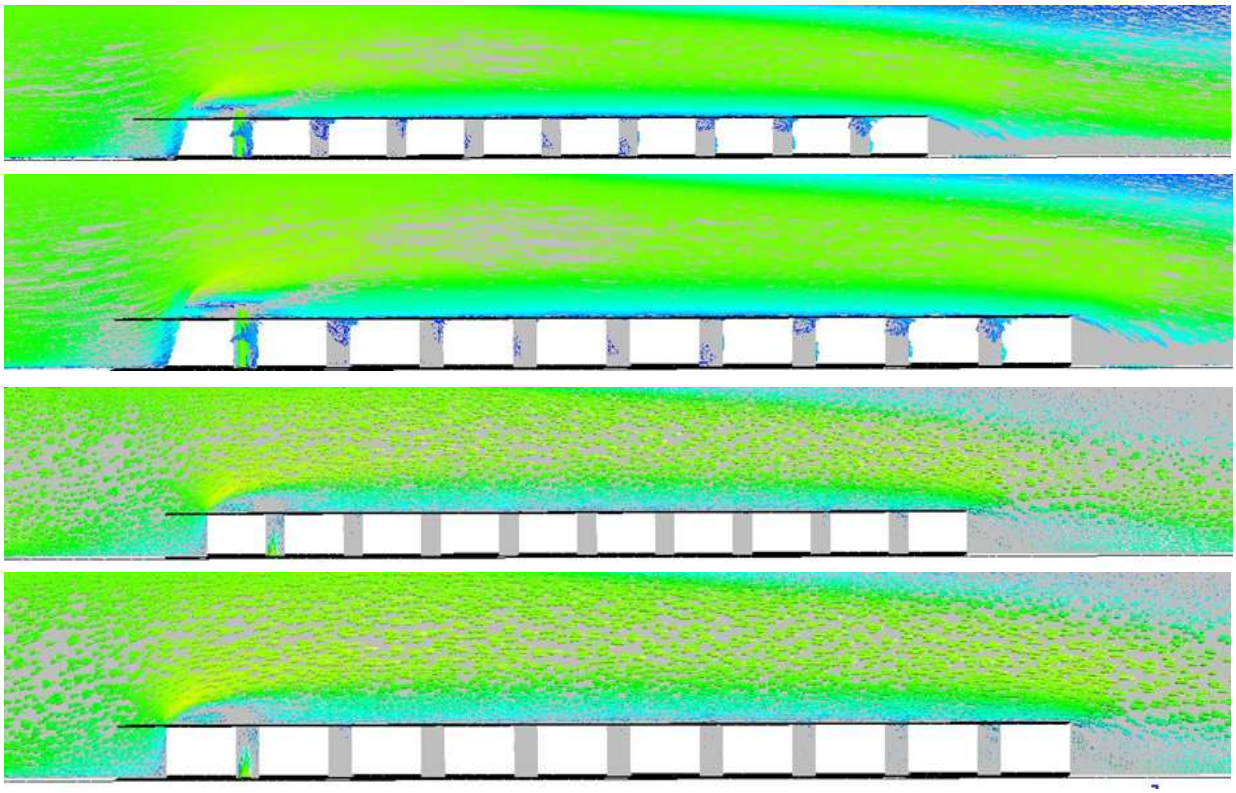

Figure 8.207: *Temperature profile of the heavy gas dispersion with the release source located at the middle front of the group of oil storage tanks in the 5th row at* ***1m/s***

Figure 8.207 shows the velocity contours of heavy gas dispersion for this case study with the release source at the middle front of the group of oil storage tanks in the 5th row. The velocity contours depict the intensity of the wind - or the effective wind influence - at the different locations throughout the layout. As can be seen in the figure, the wind intensity is different at different points in the layout. It is a commonly known effect that with enhanced altitudes, enhanced wind speeds are encountered. This is because the objects at the lower altitudes create resistance to the wind flow. As resistance is caused by the buildings in the flow of gas towards the direction opposite of wind, the wind flowing from left to right fails to indict the same motion of flow. Instead, various complex vertexes are formed within the buildings near the release source location, as can be seen in (Figure 8.207). The heavy gas release from the source is carried by these vertexes to the nearby mixture of the gas cloud, which then moves smoothly away from the source. Moreover, the hindrance to the wind flow caused by the buildings results in the vertexes moving in the upward direction, which enhances the shape of cloud in the upward direction.

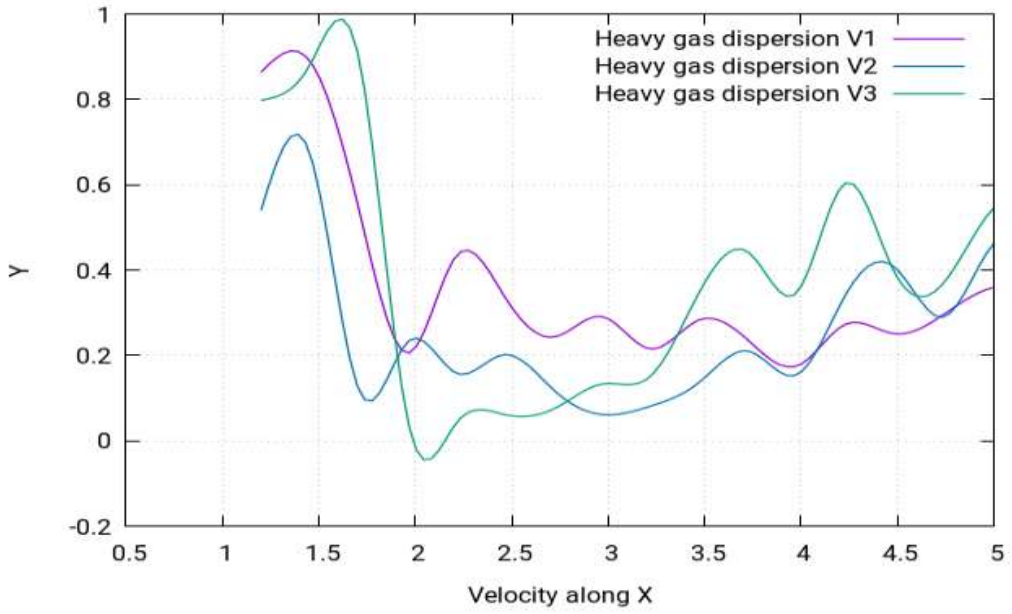

Figure 8.208: *Velocity of the heavy gas dispersion profile along the* ***x****-direction at different points of (V1) x=1.20m, y=2.03m, z=2.00m (V2) x=1.20m, y=1.90m, z=7.20m (V3) x=1.20m, y=1.90m and z=1.00m*

Figure 8.208 shows the curves for the velocity profile along the x-direction. The curves follow an asymmetrical pattern and have several peaks, with the highest peak being at approximately 2.5m.

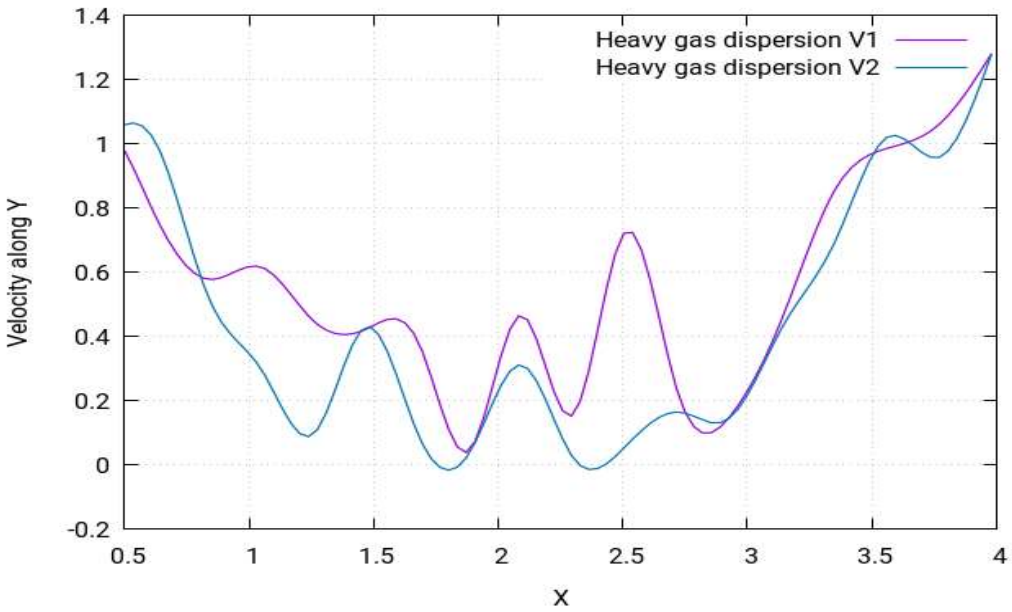

Figure 8.209: *Velocity of the heavy gas dispersion profile along the* ***y****-direction at different points of (V1) x=2.12m, y=-1m, z=2.00m (V2) x=2.40m, y=-1m and z=2.00m*

Figure 8.209 shows the curves for the velocity profile along the x-direction. The curves follow an asymmetrical pattern and have several peaks, with the highest peak being at approximately 2.3m.

In this case, the cylindrical shaped obstacles used are arranged in staggered manner. The heavy gas dispersion is observed for the heavy gas at different velocities i.e., 1 m/s and 0.25 m/s. It is seen that, despite the smooth turns, the concentration of the heavy gas is high around the obstacles. This is because the staggered arrangement offers more resistance to the flow and the turbulence of the air is high around the tanks.

8.6.23 Location 2: Heavy gas dispersion

8.6.23.1 Structure of layout

The type of layout adopted for this case study for the staggered layout. A layout of 90 oil storage tanks will be created, with a cylinder shape distribution for the release source in position. Then the behaviour of the gas clouds will be studied.

8.6.23.2 Release source location

Release sources point (2) was located at the upwind front of the group of oil storage tanks at the third row. The perimeters selected for this case study is stated below:

Table 8.37: *Parametric values for the high-speed heavy gas simulation (location 2)*

Density	Flow Rate	Velocity	Ambient Temperature	Release Source Temperature
2.1 kg m/s^3	1 kg/s	1 m/s	25°C	-100°C

8.6.23.3 Concentration of the heavy gas dispersion

The following figure shows the concentration behaviour of the heavy gas at location 2. The whereabouts of location 2 has been stated at the beginning of the passage.

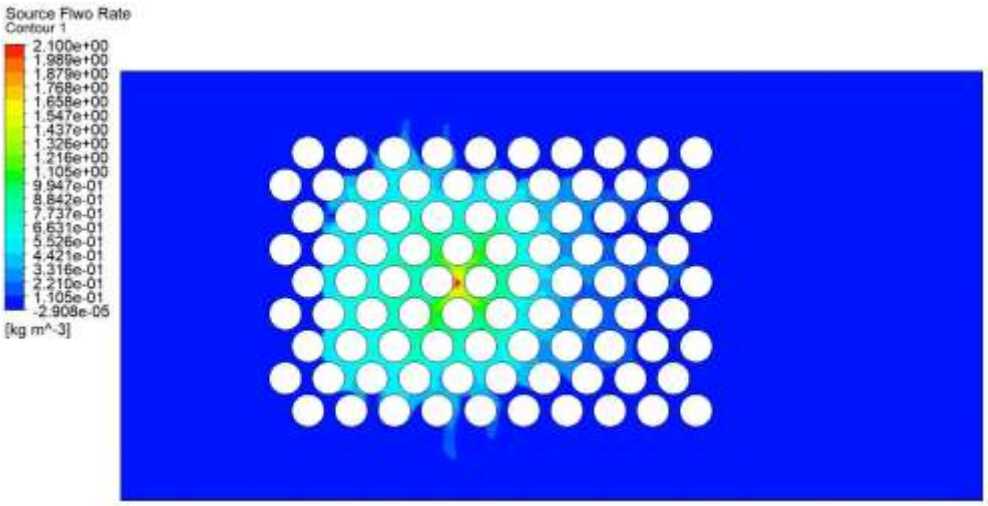

Figure 8.210: *Concentration profile of the heavy gas dispersion with the release source located at the upwind front of the group of oil storage tanks in the 3rd row at* ***1m/s***

The concentration profile of the heavy gas at location 2 for a/the staggered layout is shown in Figure 8.210 above. It represents the concentration behaviour of the heavy gas when the release gas source is placed at the middle front of the group of oil storage tanks in the 3rd row. In the previous case study, the results of the simulation were visualised with the same perimeters, but here the release source is located in the 3rd row now instead of the fifth. The simulations show that a slight change of release source location in the layout has produced a considerable change in the cloud shape. It can be seen that, although the cloud shape looks similar here, the area covered by the cloud is considerably larger than in the previous case. It can be said that almost twice the area of the layout is covered by this certain change of location of the release source.

8.6.23.4 Iso-surface of the heavy gas dispersion

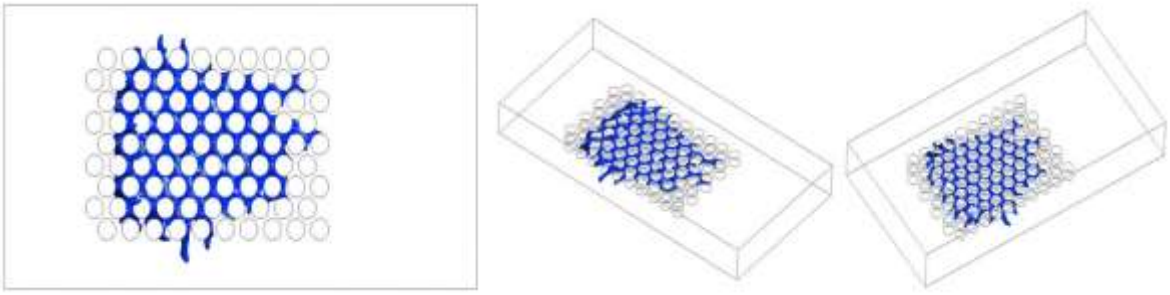

Figure 8.211: *Iso-surfaces of the concentration profile of the heavy gas dispersion with the release source located at the upwind front of the group of oil storage tanks in the 3rd row at* ***1m/s***

Figure 8.211 presents the iso-surfaces of the concentration profile of the heavy gas dispersion for a/the staggered layout with the release source located at the upwind front of the group of oil storage tanks in the 3rd row. This helps identify the spread of the cloud in each dimension. It can be seen that the cloud is not concentrated at the release source location like it is in other layout types. It can be said that the cloud shape in this case is largely symmetrical. It is not exactly rectangular and its span differs substantially from that of the previous case study. It covers twice the area of the gas cloud seen in the previous case.

According to Standard BS EN 60079-10-1:2009 [104], the following locations can be categorised:

Zone 0: The squared shape building containing three central rows and 1 column on each side of the release source at the middle front

Zone 1: The rectangular shaped portion of the building layout starting from the upwind front extending all the way to the final front of the building layout

Zone 2: All the remaining locations not categorised in zone 0 or zone 1

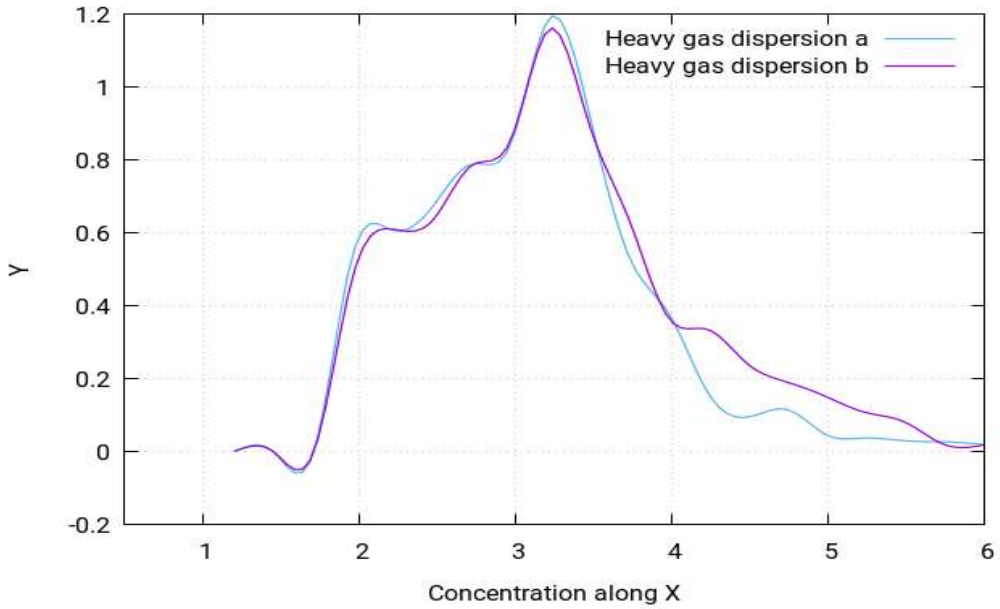

Figure 8.212: *Concentration of the heavy gas dispersion profile along the* ***x****-direction at different points of (a) x=1.20m, y=1.90m, z=7.20m (b) x=1.20m, y=2.19m and z=7.20m*

The above figure shows the concentration profiles for two of the gas dispersions at two different locations depending on distance from release source. Both curves follow the same pattern but have different values.

8.6.23.5 Temperature of the heavy gas dispersion

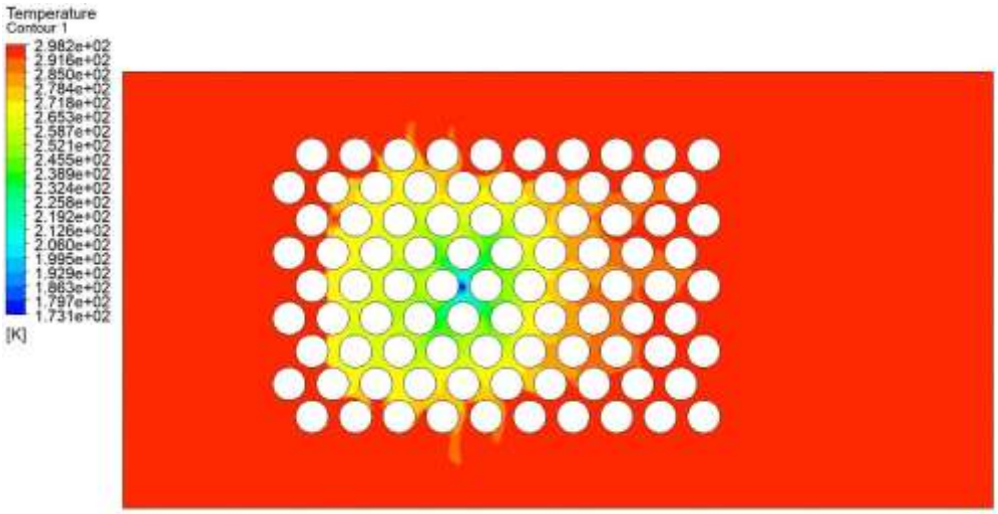

Figure 8.213: *Temperature profile of the heavy gas dispersion with the release source located at the upwind front of the group of oil storage tanks in the 3rd row at* ***1m/s***

Figure 8.213 shows the temperature simulation for the present study. By visualising the temperature simulation, it is found that the temperature simulation produces largely the same profile for the case study as that of the concentration profile. However, the behaviour of temperature is in fact the opposite to that of concentration. This means that the areas which were identified in the concentration simulation as being highly concentrated will in fact have

the lowest temperatures, while the ones with moderate concentrations will have moderate temperatures and the least concentrated areas will have the highest temperatures. To further simply these findings, it should be pointed out that the simulations showed that the concentrations near the release source point tend to be the highest and start to fade away as the gas cloud moves away from the source and is at its lowest as it moves much further away in the layout reaching the environment where the gas cloud eventually disappears. However, temperature is minimum near the release source point and tends to increase as the gas cloud moves away from source, finally achieving the maximum temperature equal to the ambient temperature of the environment. Figure 8.213 (above) has been added in order to depict this behaviour of the temperature.

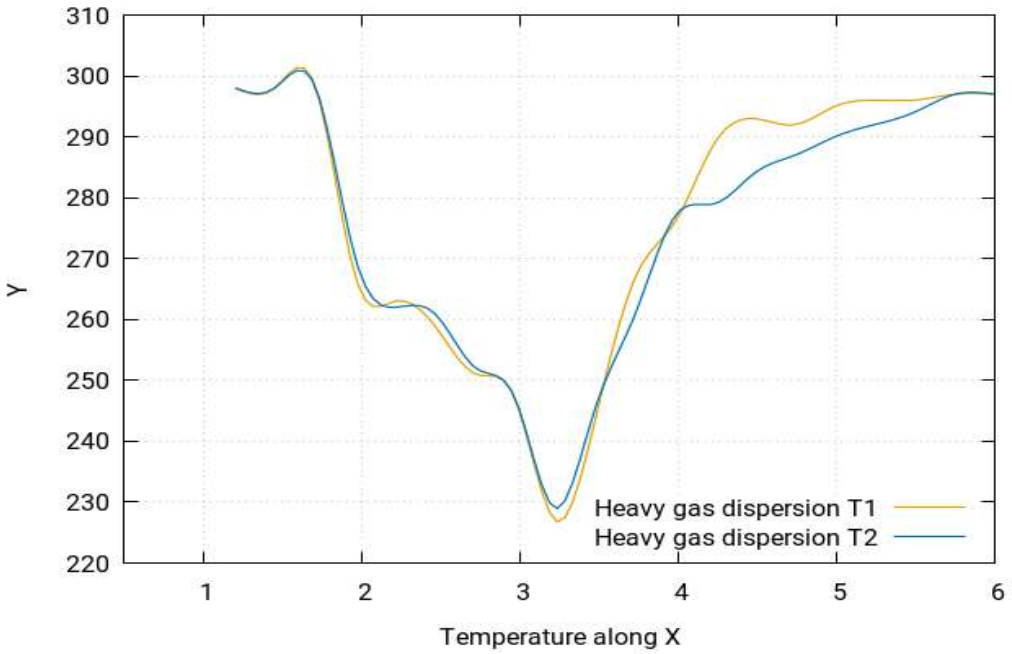

Figure 8.214: *Temperature of the heavy gas dispersion profile along the* ***x****-direction at different points of (T1) x=1.20m, y=1.90m, z=7.20m (T2) x=1.20m, y=2.19m and z=7.20m*

Figure 8.214 shows two different curves for the temperature profiles. The curves show the pattern of the temperature profile along the x-direction when the wind speed for the simulation is 1m/s. The two different curves are obtained for two different distances from the release source. These results show that, at a speed of 1m/s, temperature profiles are a mirror of the concentration profile.

8.6.23.6 Velocity of the heavy gas dispersion

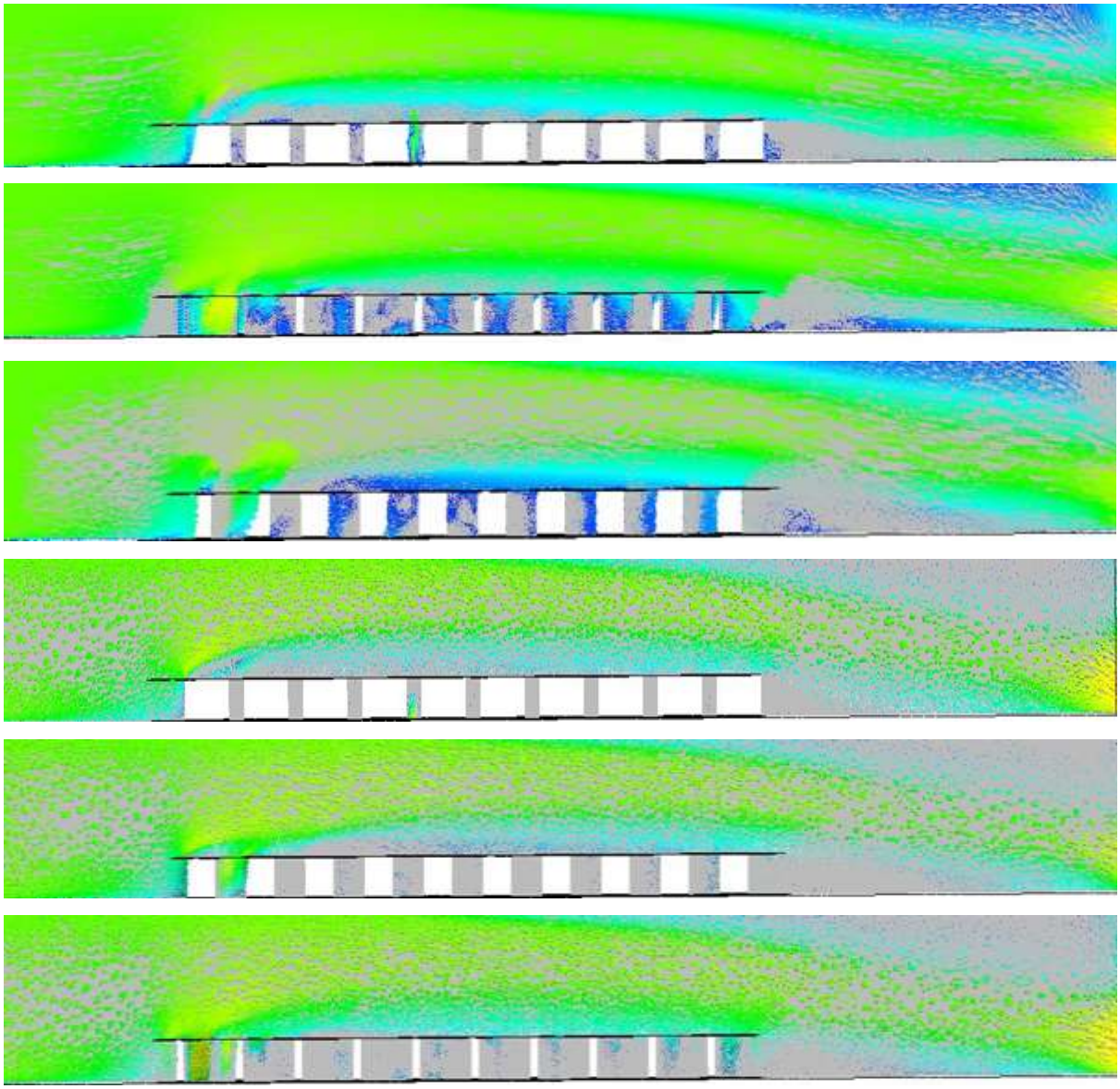

Figure 8.215: *Velocity contours of the heavy gas dispersion with the release source located at the upwind front of the group of oil storage tanks in the 3rd row at* ***1m/s***

Figure 8.215 shows the velocity contours of the heavy gas dispersion for this case study with the release source located at the upwind front of the group of oil storage tanks in the 3rd row. The velocity contours depict the intensity of the wind - or the effective wind influence - at the different locations throughout the layout. As can be seen in the figure, the wind intensity is different at different points in the layout. It is a commonly known effect that with enhanced altitudes, enhanced wind speeds are encountered. This is because the objects at the lower altitudes create resistance to the wind flow. As resistance is caused by the buildings to the flow of gas towards the direction opposite of wind, the wind flowing from left to right fails to indict the same motion of flow. Instead, various complex vertexes are formed within the buildings near the release source location, as can be seen in (Figure 8.215). The heavy gas released from

the source is carried by these vertexes to the nearby mixture of the gas cloud, which then moves smoothly away from the source. Moreover, the hindrance to the wind flow caused by the buildings results in the vertexes moving in the upward direction, which enhances the shape of the cloud in the upward direction.

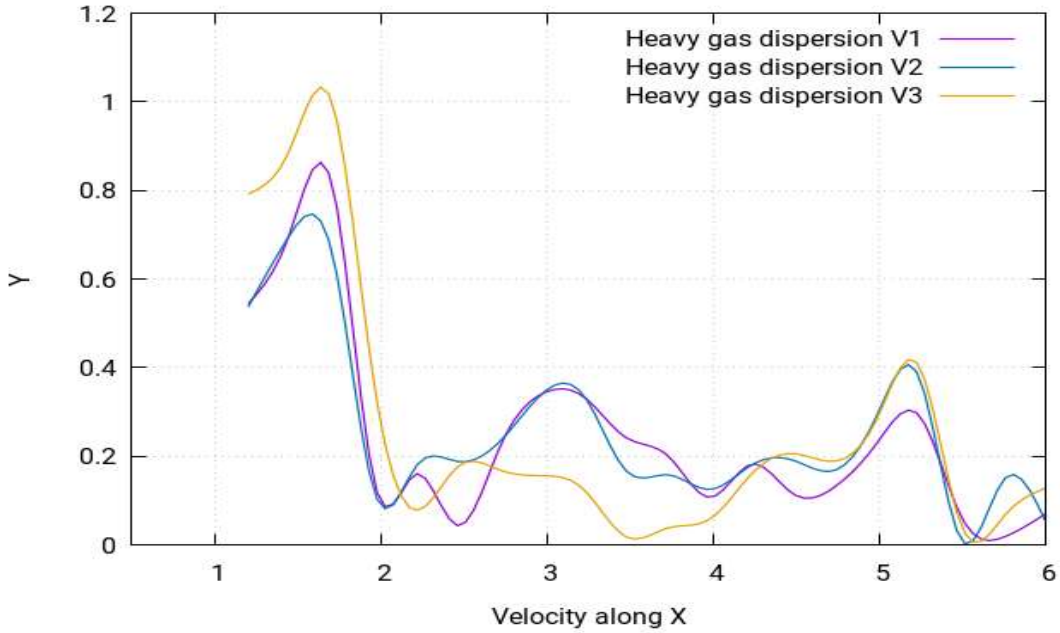

Figure 8.216: *Velocity of the heavy gas dispersion profile along the* ***x****-direction at different points of (V1) x=1.20m, y=1.90m, z=7.20m (V2) x=1.20m, y=2.19m, z=7.20m (V3) x=1.20m, y=2.19m and z=9.85m*

Figure 8.216 shows the curves for the velocity profile along the x-direction. The curves follow an asymmetric pattern and have several peaks, with the highest peak being at approximately 5.5m.

At location 2 of the staggered arrangement of the cylindrical obstacles, the dispersion of the heavy gas shows similar results. In this case, the dispersion is uniform in all directions, owing to the absence of change in the density while moving in the horizontal direction.

8.6.24 Location 1: Heavy gas dispersion for a safe distance

8.6.24.1 Structure of layout

The type of layout adopted for this case study for the staggered layout. A layout of 30 oil storage tanks will be created, with a cylinder shape distribution for safe distance, and the release source will be placed in position. Then, the behaviour of the gas clouds will be studied from a safe distance.

8.6.24.2 Release source location

Release source point (1) was located at the upwind front of the oil storage tanks group in the 3rd row. The perimeters selected for this case study is stated below:

Table 8.38: *Parametric values for the high-speed heavy gas simulation (safe distance 1)*

Density	Flow Rate	Velocity	Ambient Temperature	Release Source Temperature
2.1 kg m/s^3	1 kg/s	1 m/s	25°C	-100°C

8.6.24.3 Concentration of heavy gas dispersion for a safe distance

The following figure shows the concentration behaviour of the heavy gas at location 1. The whereabouts of location 1 has been stated at the beginning of the passage.

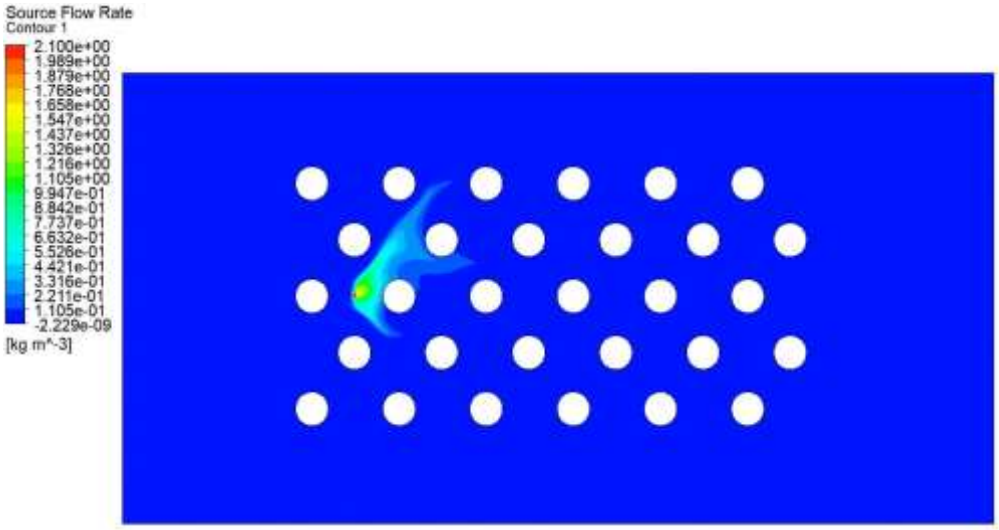

Figure 8.217: *Concentration profile of the heavy gas dispersion with the release source located at the upwind front of the group of oil storage tanks in the 3rd row at* ***1m/s***

The concentration profile of the heavy gas at location 1 is shown in Figure 8.217 above. It represents the concentration behaviour of the heavy gas when the release gas source is placed at the upwind front of the group of oil storage tanks in the 3rd row. The simulation shows that, for this layout and this particular set of perimeters, the cloud shape is hard to compare to a geometric shape. However, it should be mentioned that the cloud leans towards the upward edge more than towards the lower edge.

The safe distance between the storage tanks or obstacles is also dependent on the location at which the tanks are placed. There are different safety measures and distances for the tanks placed in the buildings compared to those that are placed underground [112].

8.6.24.4 Iso-surface of heavy gas dispersion for a safe distance

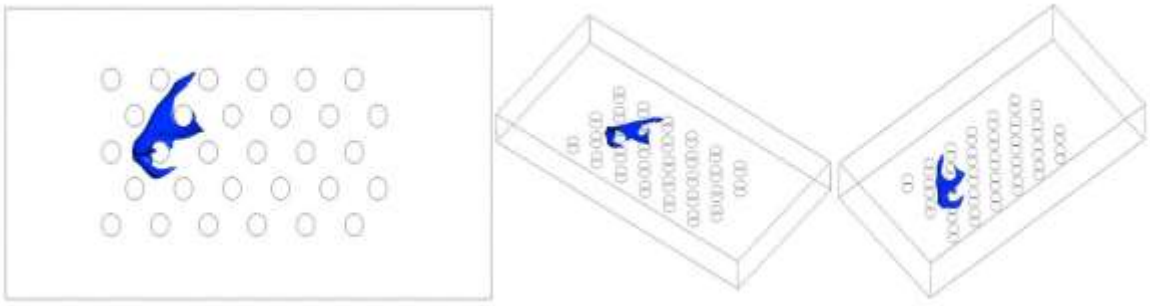

Figure 8.218: *Iso-surfaces of the concentration profile of the heavy gas dispersion with release source located at the upwind front of the group of oil storage tanks in the 3rd row at* ***1m/s***

Figure 8.218 shows see the iso-surfaces of the concentration profile of the heavy gas dispersion for a staggered layout with the release source located at the upwind front of the group of oil storage tanks in the 3rd row. This helps identify the spread of the cloud in each dimension. It can be seen that the cloud is not concentrated at the release source location, as it was in the other layout. It can also be seen that the cloud span is rather small as compared to other layouts in each dimension.

According to Standard BS EN 60079-10-1:2009 [104], the following locations can be categorised:

Zone 0: The small portion of the central row and its upper edge near the release source

Zone 1: The immediate surroundings of the areas mentioned in zone 0

Zone 2: All the remaining locations not categorised in zone 0 or zone 1

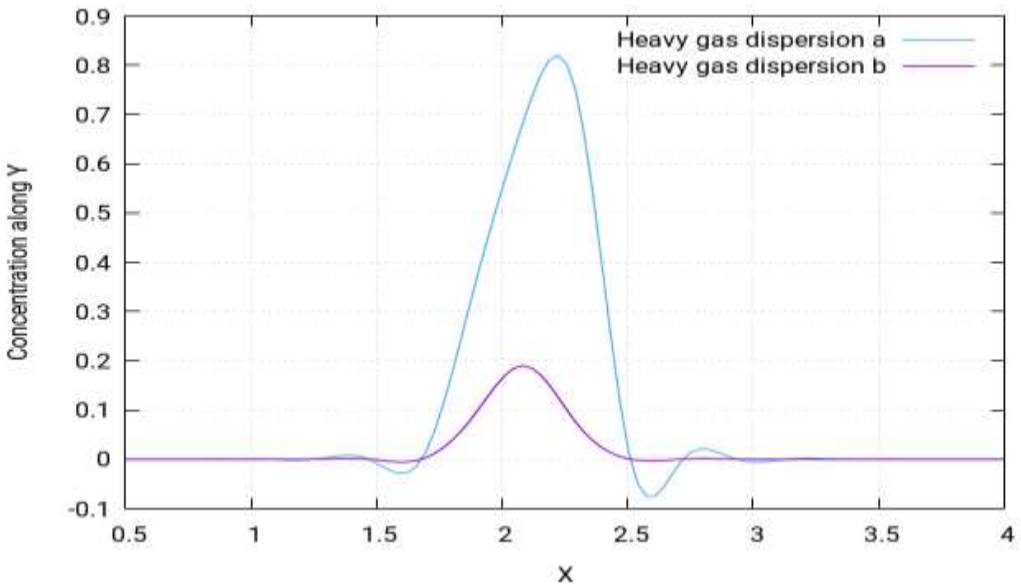

Figure 8.219: *Concentration of the heavy gas dispersion profile along the y-direction at different points of (a) x=2.33m, y=-1m, z=7.20m, (b) x=2.33m, y=-1m and z=6.00m*

In Figure 8.219 (above), two different curves for the concentration profiles are shown. They show the pattern of the concentration profile along the y-direction when the wind speed for the

simulation is 1m/s. The two different curves are obtained for two different distances from the release source. Both the curves follow the same pattern but have different values due to difference in distances. From the figure, it is concluded that the concentration value of the concentration of heavy gas decreases as it moves away from the source. In the figure, the curve with the highest peak is obtained when nearest the release source and vice versa.

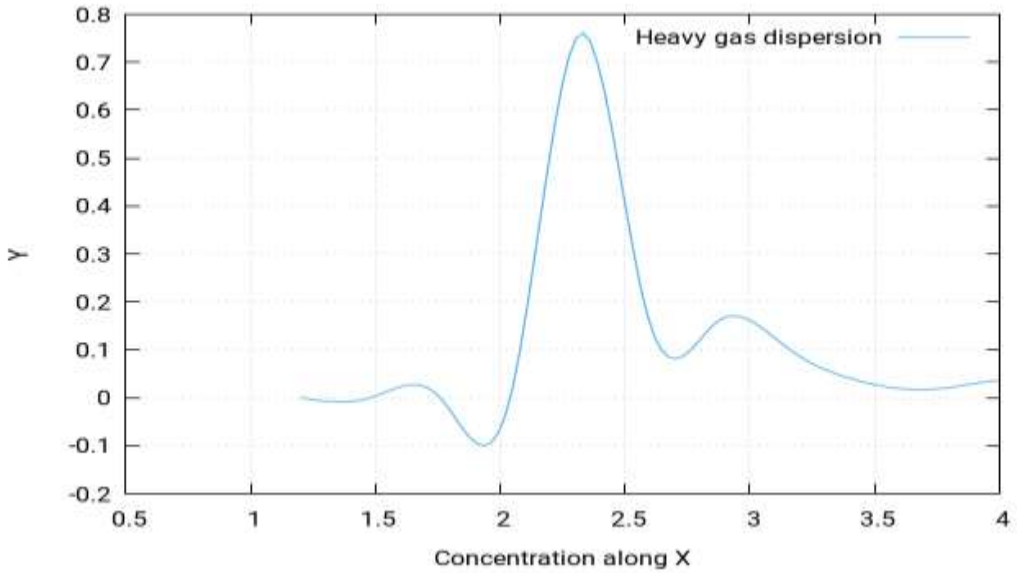

Figure 8.220: *concentration of the heavy gas dispersion profile along the* ***x****-direction at different points of x=1.20m, y=2.28m and z=7.20m*

Figure 8.220 shows the curve for the concentration profile along the x-direction. The curve follows an asymmetrical pattern and has a single peak at approximately 2.3m.

8.6.24.5 Temperature of the heavy gas dispersion for a safe distance

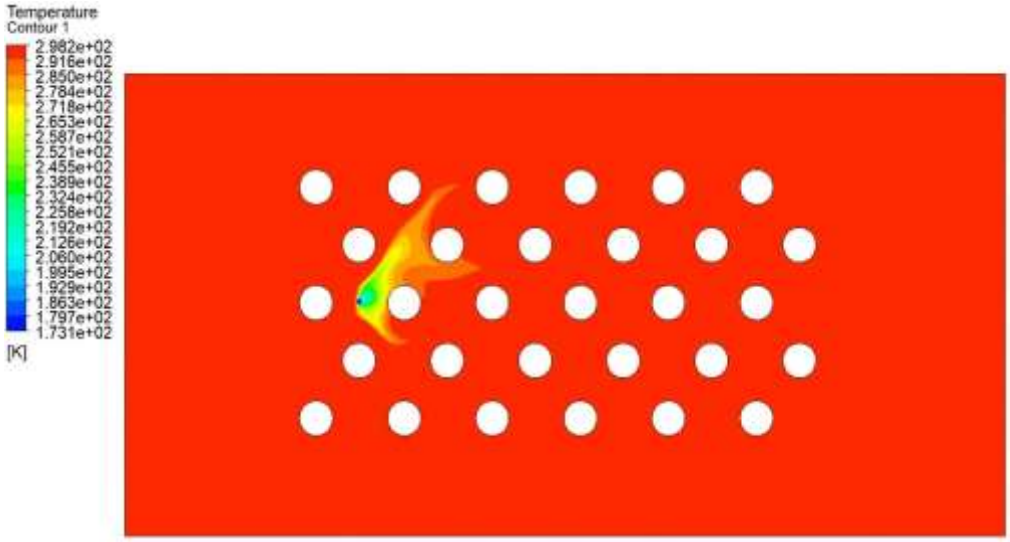

Figure 8.221: *Temperature profile of the heavy gas dispersion with the release source located at the upwind front of the group of oil storage tanks in the 3rd row at* ***1m/s***

Figure 8.221 shows the temperature simulation for this study. By visualising the temperature simulation, it is found out that the temperature simulation produces largely the same profile for the case study as that of the concentration profile. However, the behaviour of temperature is in fact the opposite to that of concentration. This means that the areas which were identified in the concentration simulation as highly concentrated will in fact have the lowest temperatures, while the ones with moderate concentrations will have moderate temperatures and the least concentrated areas will have the highest temperatures. To further simply these findings, it should be pointed out that the simulations showed that the concentrations near the release source point tend to be the highest and start to fade away as the gas cloud moves away from the source, end to being lowest as it moves much further away in the layout, eventually reaching the environment where the gas cloud disappears. However, the temperature, it is lowest near the release source point and tends to increase as one moves away from source and finally reaches the maximum temperature equal to the ambient temperature of the environment.

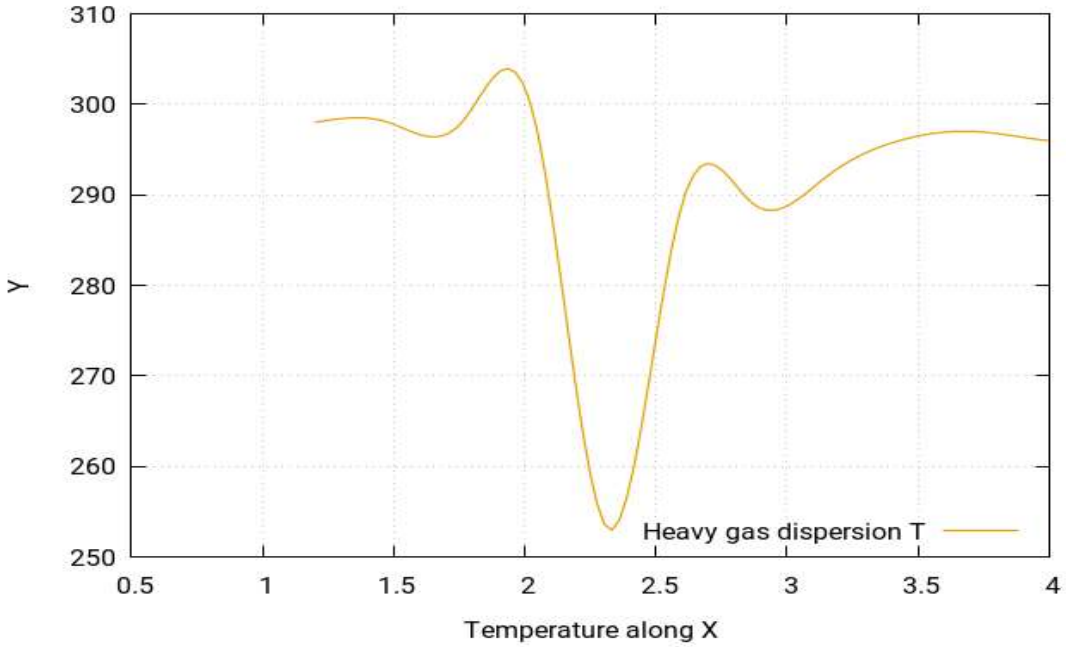

***Figure 8.222**: Temperature of the heavy gas dispersion profile along the **x**-direction at different points of (T) x=1.20m, y=2.28m and z=7.20m*

Figure 8.222 shows the curve for the temperature profile along the x-direction. The curve is a mirror pattern of the concentration profile.

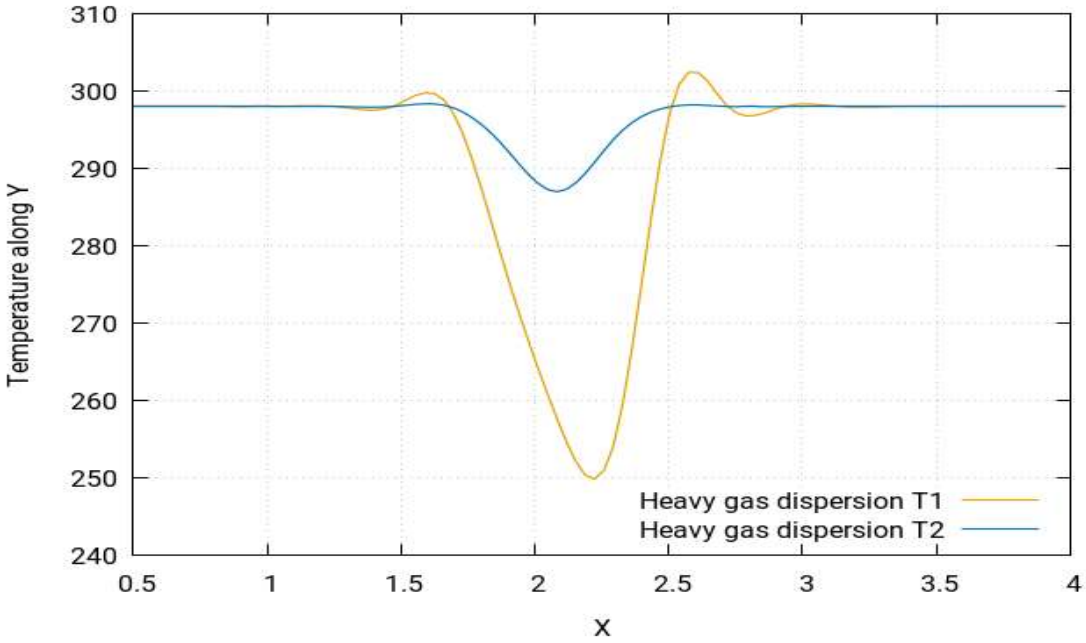

Figure 8.223: *Temperature of the heavy gas dispersion profile along the* ***y****-direction at different points of (T1) x=2.33m, y=-1m, z=7.20m (T2) x=2.33m, y=-1m and z=6.00m*

In Figure 8.223, two different curves for the temperature profiles are shown. They show the pattern of the temperature profile along the y-direction when the wind speed for the simulation is 1m/s. The two different curves are obtained for two different distances from the release source. These results show that, at speed of 1m/s, temperature profiles are a mirror of concentration profile.

8.6.24.6 Velocity of the heavy gas dispersion for a safe distance

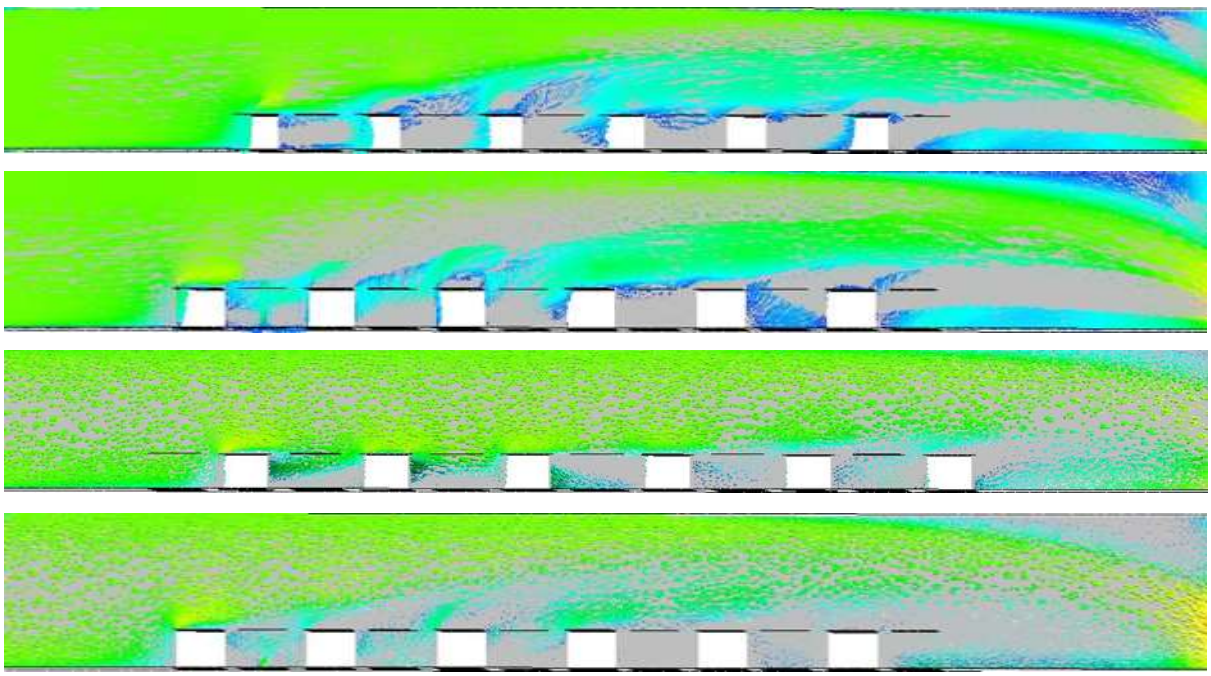

Figure 8.224: *Velocity contours of the heavy gas dispersion with the release source located at the upwind front of the group of oil storage tanks in the 3rd row at* ***1m/s****.*

Figure 8.224 shows the velocity contours of the heavy gas dispersion for this case study with the release source in the upwind front of the group of gas storage tanks in the 3rd row. Velocity contours depict the intensity of the wind - or the effective wind influence - at the different locations throughout the layout. As can be seen in the figure, the wind intensity is different at different points in the layout. It is a commonly known effect that, with enhanced altitudes, enhanced wind speeds are encountered. This is because the objects at the lower altitudes create resistance to wind flow. As their resistance is caused by the buildings to the flow of gas towards the direction opposite of wind, the wind flowing from left to right fails to indict the same motion of flow. Instead, there various complex vertexes are formed within the buildings near the release source location, as can be seen in the (Figure 8.224). The heavy gas release from the source is carried by these vertexes to the nearby mixture of the gas cloud, which then moves smoothly away from the source. Moreover, the hindrance to the wind flow caused by the buildings results in the vertexes moving in the upward direction, which enhances the shape of cloud in the upward direction.

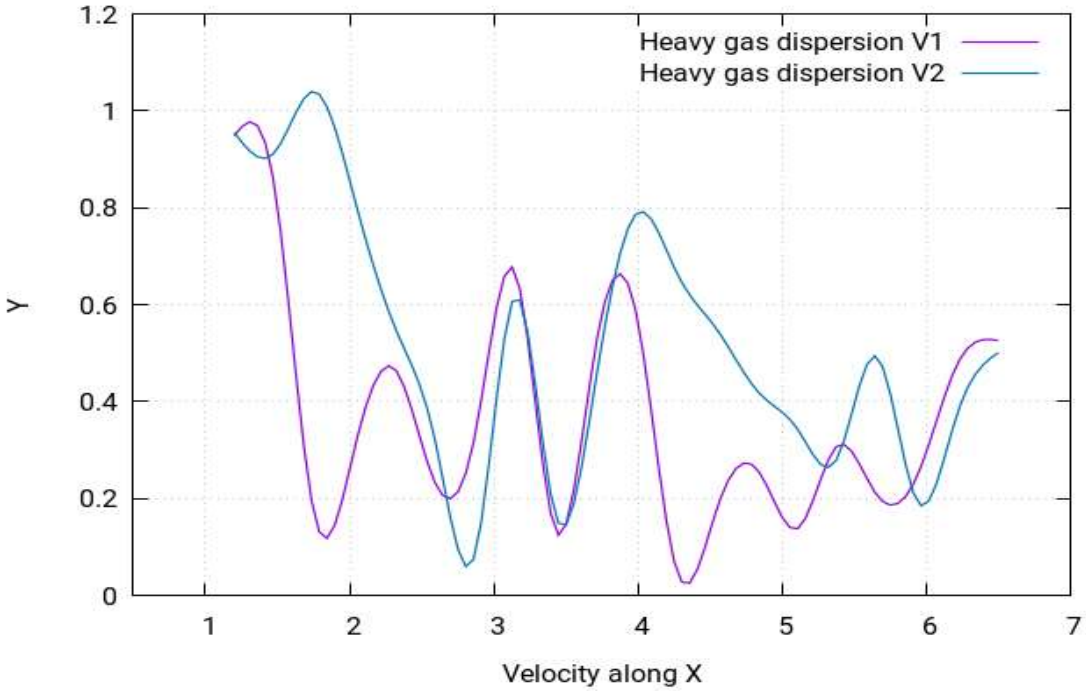

Figure 8.225: *Velocity of the heavy gas dispersion profile along the* ***x****-direction at different points of (V1) x=1.20m, y=2.03m, z=2.00m (V2) x=1.20m, y=2.03m and z=2.60m*

Figure 8.225 shows the curves for the velocity profile along the x-direction. The curves follow an asymmetrical pattern and have several peaks, with the highest peak being at approximately 1.8m.

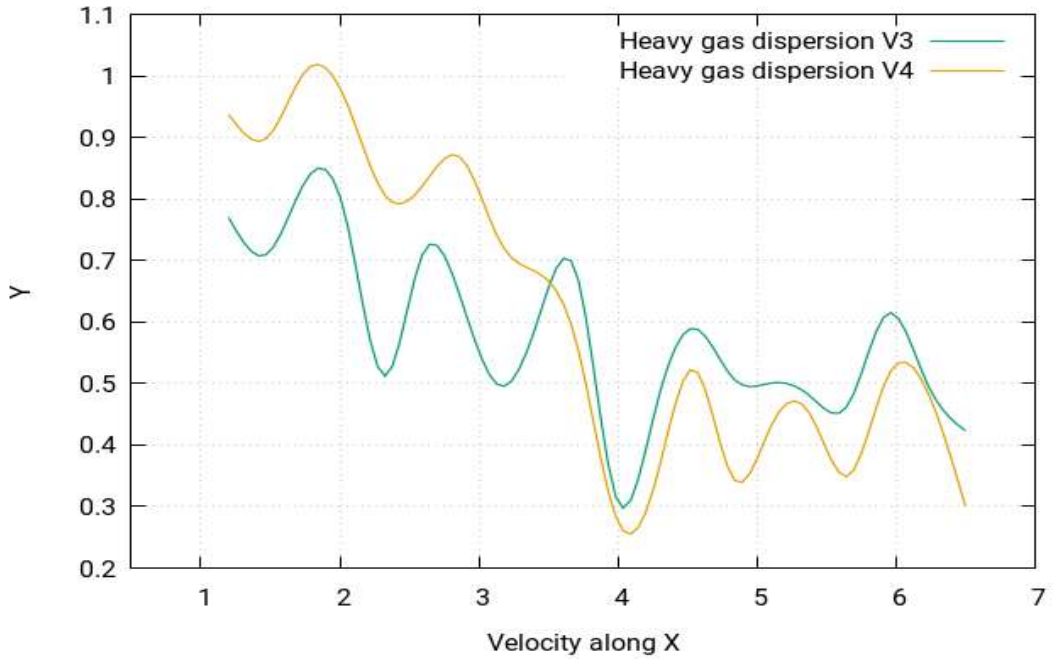

Figure 8.226: *Velocity of the heavy gas dispersion profile along the* ***x****-direction at different points of (V3) x=1.20m, y=2.28m, z=7.20m (V4) x=1.20m, y=2.28m and z=6.20m*

Above, Figure 8.226 presents two different curves for the temperature profiles. They show the pattern of the temperature profile along the x-direction when the wind speed for the simulation is 1m/s. The two different curves are obtained for two different distances from the release source. These results show that, at a speed of 1m/s, temperature profiles are a mirror of concentration profile.

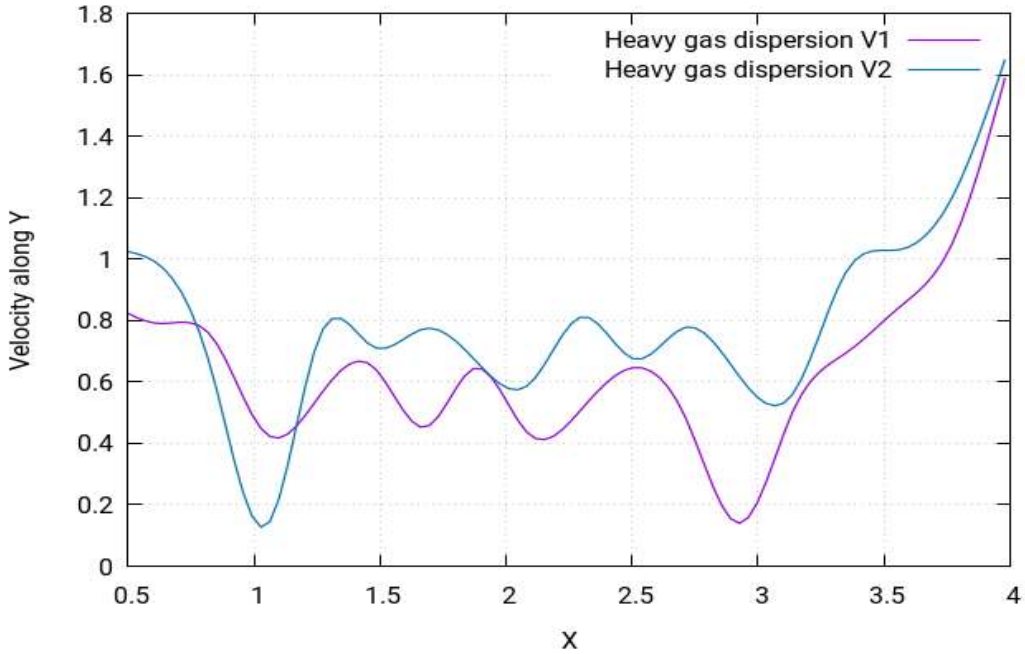

Figure 8.227: *Velocity of the heavy gas dispersion profile along the* ***y****-direction at different points of (V1) x=2.33m, y=-1m, z=7.20m (V2) x=2.33m, y=-1m and z=6.00m*

Figure 8.227 shows the curves for the velocity profile along the y-direction. The curves follow an asymmetrical pattern and have several peaks, with the highest peak being at approximately 1.1m.

At location 1 of the cylindrical storage tanks that are arranged in the staggered manner, the results show that, if the tanks are at the safe diagonal distance from each other, the concentration of the heavy gas is minimum. The safe distance between the tanks results in reduced turbulence.

8.6.25 Location 2: Heavy gas dispersion for a safe distance

8.6.25.1 Structure of layout

The type of layout adopted for this case study for the staggered layout. A layout of 30 oil storage tanks will be created, with a cylinder shape distribution for safe distance, and the release source will be placed in positions. The behaviour of the gas clouds with a safe distance will then be studied.

8.6.25.2 Release source location

Release sources point (2) was positioned at the middle front of the group of gas storage tanks in the 3rd row. The perimeters selected for this case study are stated below:

Table 8.39: *Parametric values for the high-speed heavy gas simulation (safe distance 2)*

Density	Flow Rate	Velocity	Ambient Temperature	Release Source Temperature
2.1 kg m/s^3	1 kg/s	1 m/s	25°C	-100°C

8.6.25.3 Concentration of the heavy gas dispersion for a/the safe distance

The following figure shows the concentration behaviour of the heavy gas at location 2. The whereabouts of location 2 has been stated at the beginning of the passage.

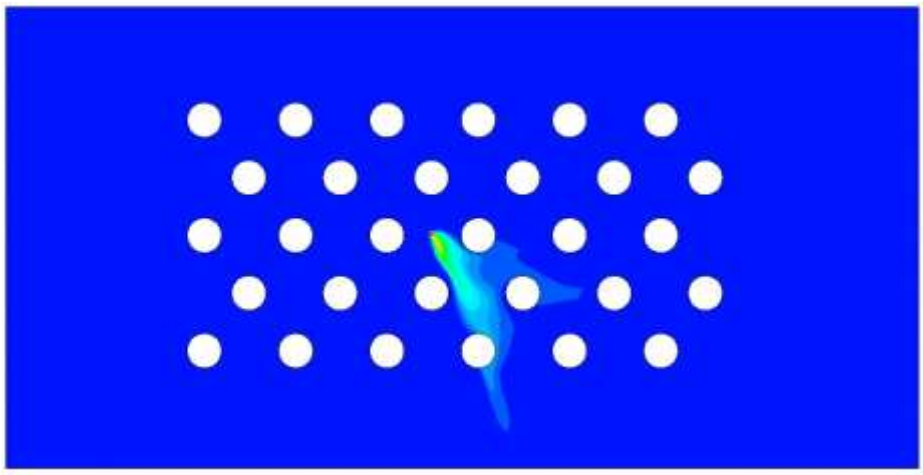

Figure 8.228: *Concentration profile of the heavy gas dispersion with the release source located at the middle front of the group of oil storage tanks in the 3rd row at* ***1m/s****.*

The concentration profile of the heavy gas at location 2 is shown in Figure 8.228 above. It represents the concentration behaviour of the heavy gas when the release gas source is placed at the middle front of the group of oil storage tanks in the 3rd row. The previous study was performed with the same perimeters. However, the release source, in that case, was at the upwind front, while in this case, it at the middle front. It can be seen that a certain change in the location of the release source has affected the cloud shape in such a way that it has inverted. The simulation shows that, for this layout and this particular set of perimeters, the cloud shape is hard to compare to a geometric shape. However, it should be mentioned that the cloud leans towards the lower edge more than it does towards the upper edge.

The safe distance in this case is dependent on the type of the heavy gas released, the average ambient conditions and the shape of the tanks. For the cylindrically shaped tanks, there is less accumulation of the heavy gas around them during the dispersion. This makes cylindrical tanks ideal for storing heavy chemicals.

8.6.25.4 Iso-surfaces of the heavy gas dispersion for a/the safe distance

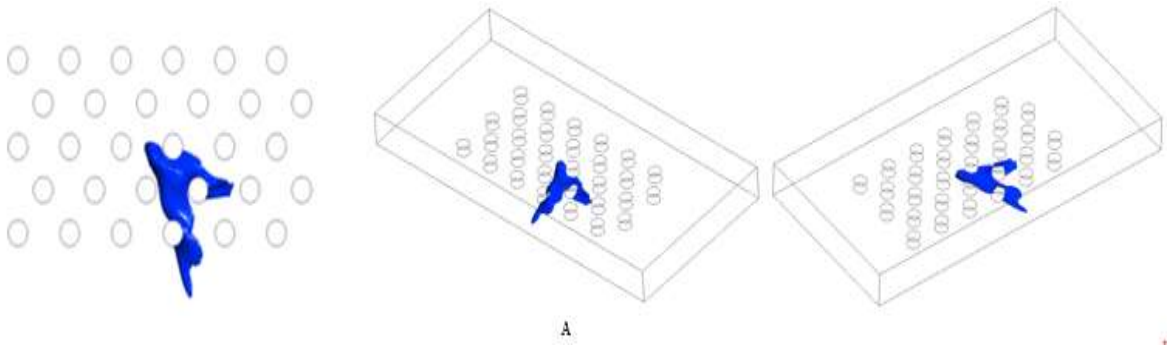

Figure 8.229: *Iso-surfaces of the concentration profile of the heavy gas dispersion with the release source located at the middle front of the group of oil storage tanks in the 3rd row at* ***1m/s***

Figure 8.229 shows the iso-surfaces of the concentration profile of the heavy gas dispersion for a staggered layout with a/the release source located at the middle front of the group of gas storage tanks in the 3rd row. This helps identify the spread of the cloud in each dimension. It can be seen that the cloud is not concentrated at the release source location as it was in the other layout. It can also be seen that the cloud span is relatively small as compared to other layouts in each dimension.

According to Standard BS EN 60079-10-1:2009 [104], the following locations can be categorised:

Zone 0: The small portion of the central row and its lower edge near the release source

Zone 1: The immediate surroundings of the areas mentioned in zone 0

Zone 2: All the remaining locations not categorised in zone 0 or zone 1

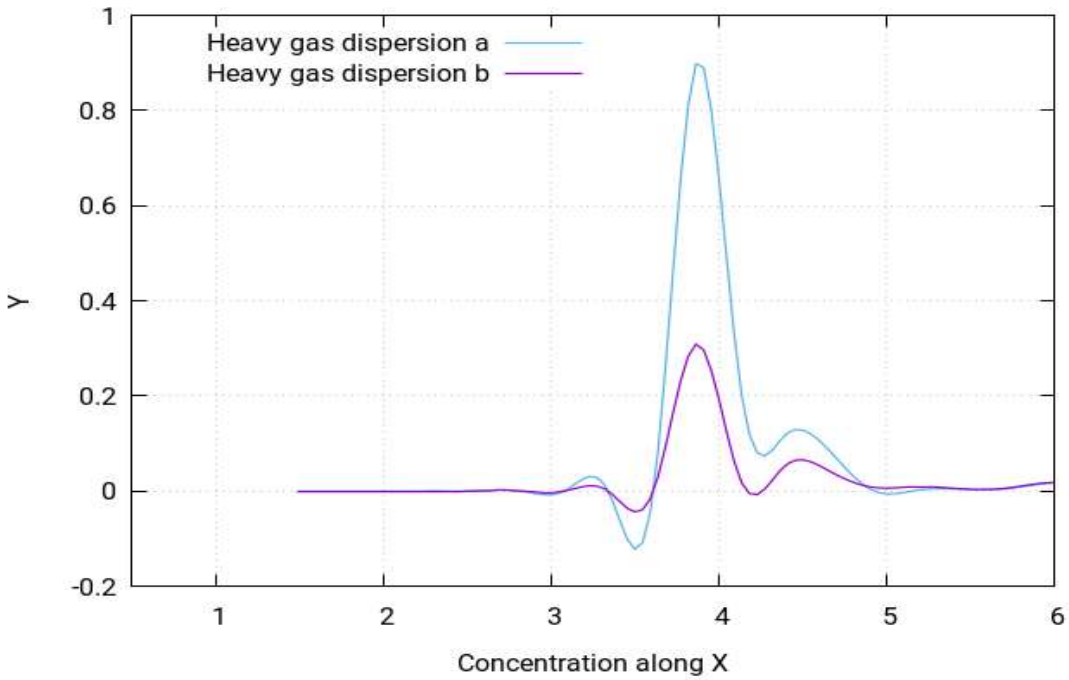

Figure 8.230: *Concentration of the heavy gas dispersion profile along the* ***x****-direction at different points of (a) x=1.50m, y=1.84m, z=7.20m (b) x=1.50m, y=1.84m and z=8.00m*

The above figure shows the concentration profiles for two of the gas dispersions at two different locations depending on distance from release source. Both curves follow the same pattern but have different values.

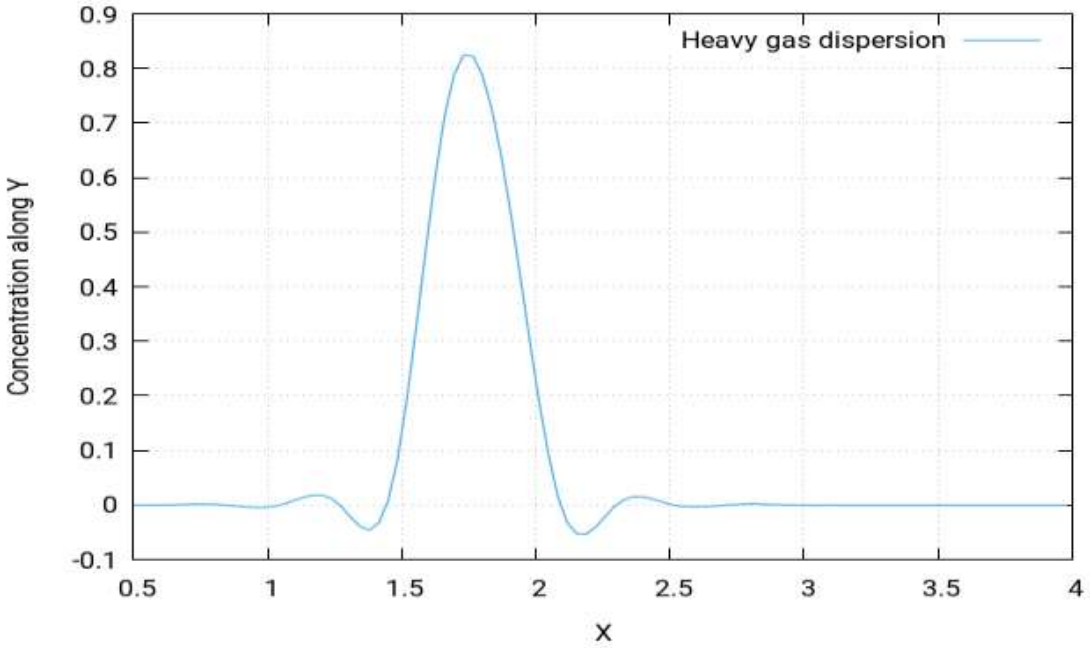

Figure 8.231: *Concentration of the heavy gas dispersion profile along the **y**-direction at different points of x=3.92m, y=-1m and z=7.20m*

Figure 8.231 shows the curve for the concentration profile along the y-direction. The curve follows a symmetrical pattern and has a single peak at almost 1.8m.

8.6.25.5 Temperature of the heavy gas dispersion for a safe distance

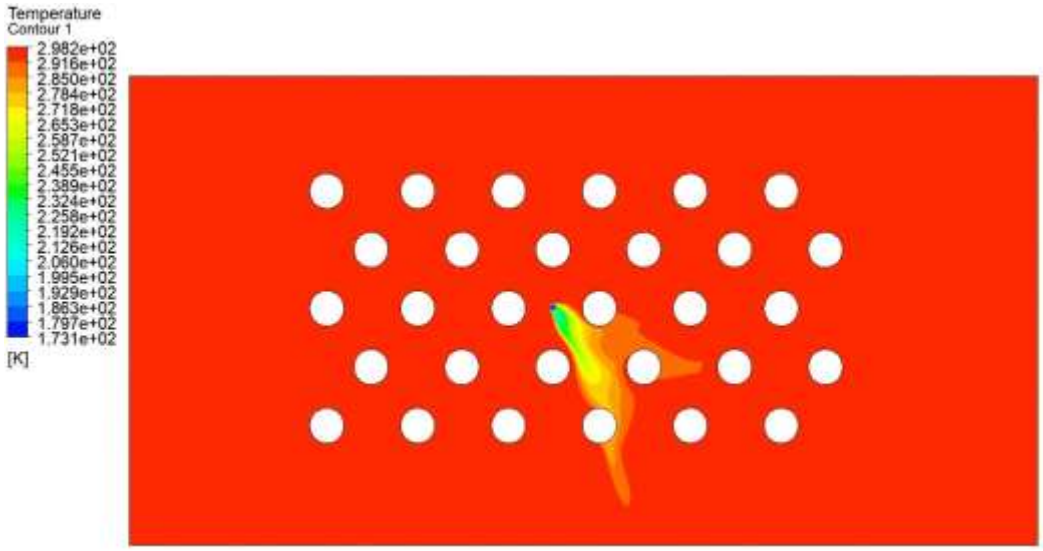

Figure 8.232: *Temperature profile of the heavy gas dispersion with the release source located at the middle front of the group of oil storage tanks in the 3rd row at **1m/s***

Figure 8.232 shows the temperature simulation for this study. By visualising the temperature simulation, it is found out that the temperature simulation produces largely the same profile for the case study as that of the concentration profile. However, the behaviour of temperature is in fact the opposite to that of concentration. This means that the areas which were identified in

the concentration simulation as the highly concentrated will in fact have the lowest temperatures, while the ones with moderate concentrations will have moderate temperatures and the least concentrated areas will have the highest temperatures. To further simply these findings, it should be pointed out that the simulations show that the concentrations near the release source point tend to be the highest and start to fade away as the gas cloud moves away from the source and are lowest when it moves much further away in the layout, eventually reaching the environment where the gas cloud disappears. The temperature is lowest near the release source point and tends to increase as the cloud moves away from source, finally reaching the maximum temperature equal to the ambient temperature of the environment.

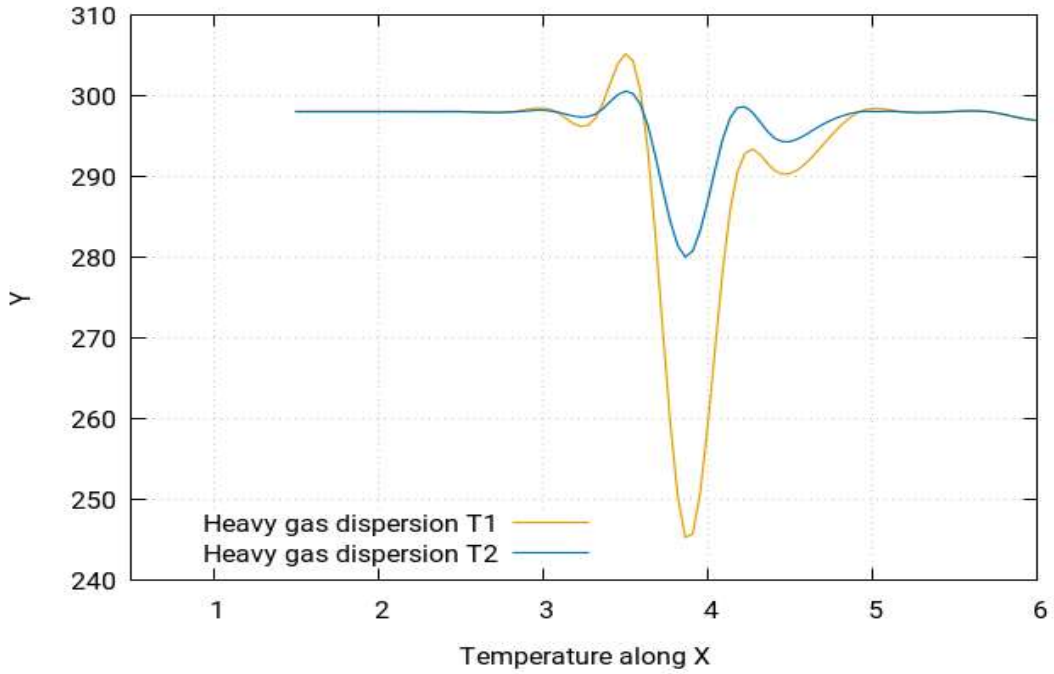

Figure 8.233: *Temperature of the heavy gas dispersion profile along the* ***x****-direction at different points of (T1) x=1.50m, y=1.84m, z=7.20m (T2) x=1.50m, y=1.84m and z=8.00m*

In Figure 8.233, two different curves for the temperature profiles are shown. They show the pattern of the temperature profile along the x-direction when the wind speed for the simulation is 1m/s. The two different curves are obtained for two different distances from the release source. These results show that, at speed of 1m/s, temperature profiles are a mirror of concentration profile.

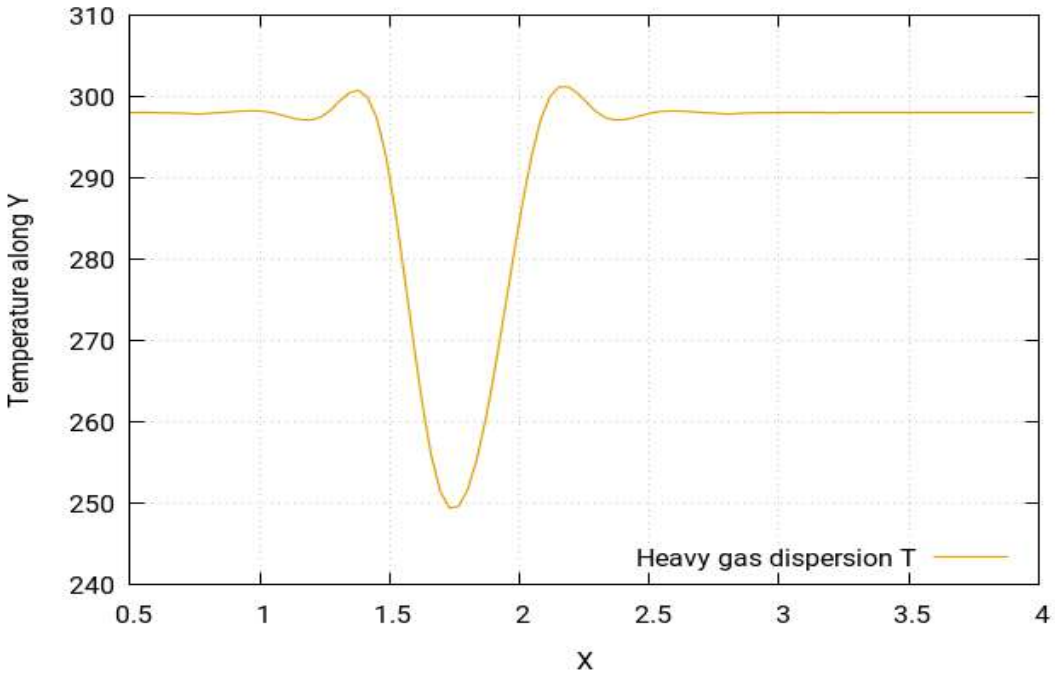

Figure 8.234: *The temperature of the heavy gas dispersion profile along the **y**-direction at different points of (T) x=3.92m, y=-1m and z=7.20m*

Figure 8.234 shows the curve for temperature profile along the y-direction. The curve follows a symmetric pattern and has a single peak at almost 1.8m.

8.6.25.6 Velocity of the heavy gas dispersion for a safe distance

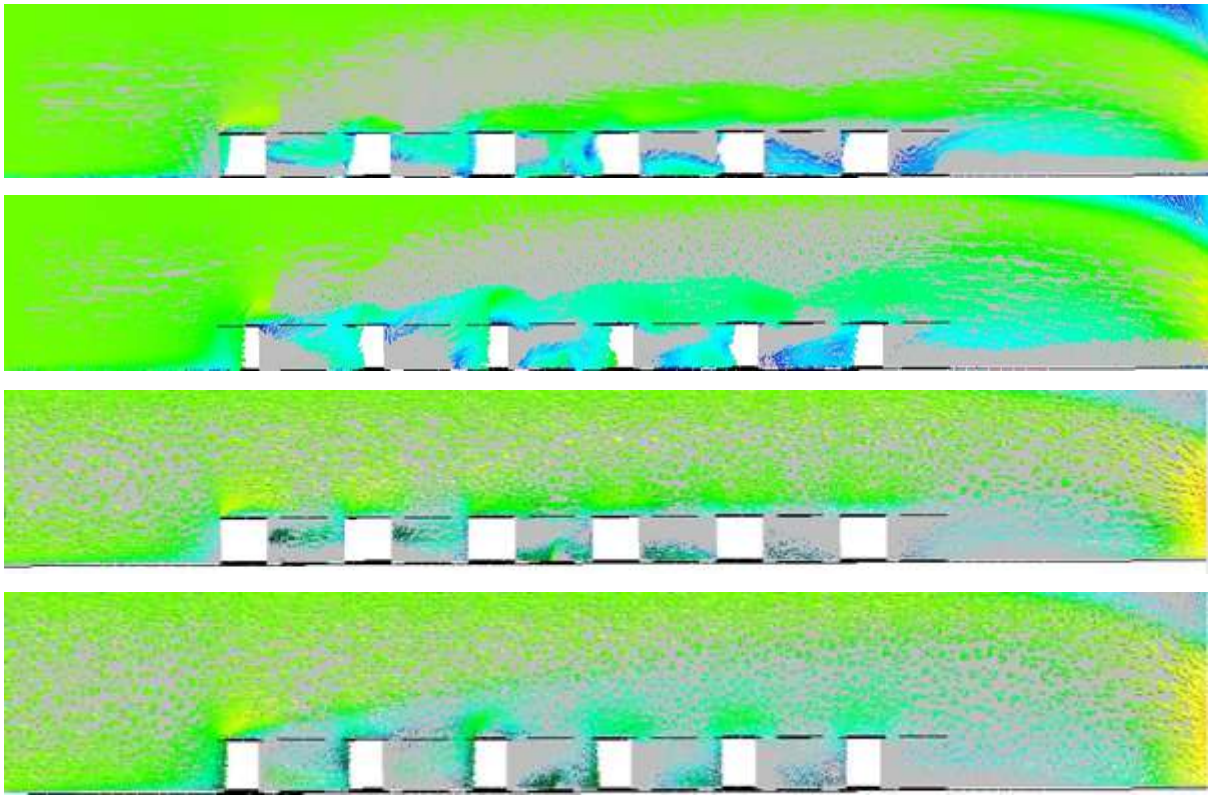

Figure 8.235: *Velocity contours of the heavy gas dispersion with release source located at the middle front of the group of oil storage tanks at the 3rd row at **1m/s***

Figure 8.235 shows the velocity contours of the heavy gas dispersion for this case study with the release source located at the middle front of the group of oil storage tanks at the 3rd row. Velocity contours depict the intensity of wind or say the effective wind influence at the different locations throughout the layout. It can be seen in the figure that the wind intensity is different at different points in the layout. It is a commonly known effect that, with enhanced altitudes, enhanced wind speeds are encountered. This is because the objects in the lower altitudes create resistance to the wind flow. Resistance is also caused by the buildings to the flow of gas towards the direction opposite of wind, so the wind flowing from left to right fails to indict the same motion of flow. Instead, various complex vertexes are formed within the buildings near the release source location as can be seen in the (Figure 8.235). The heavy gas release from the source is carried by these vertexes to the nearby mixture of the gas cloud which them moves smoothly away from the source. Moreover, the hindrance to the wind flow caused by the buildings results in the vertexes moving in the upward direction, which enhances the shape of cloud in the upward direction.

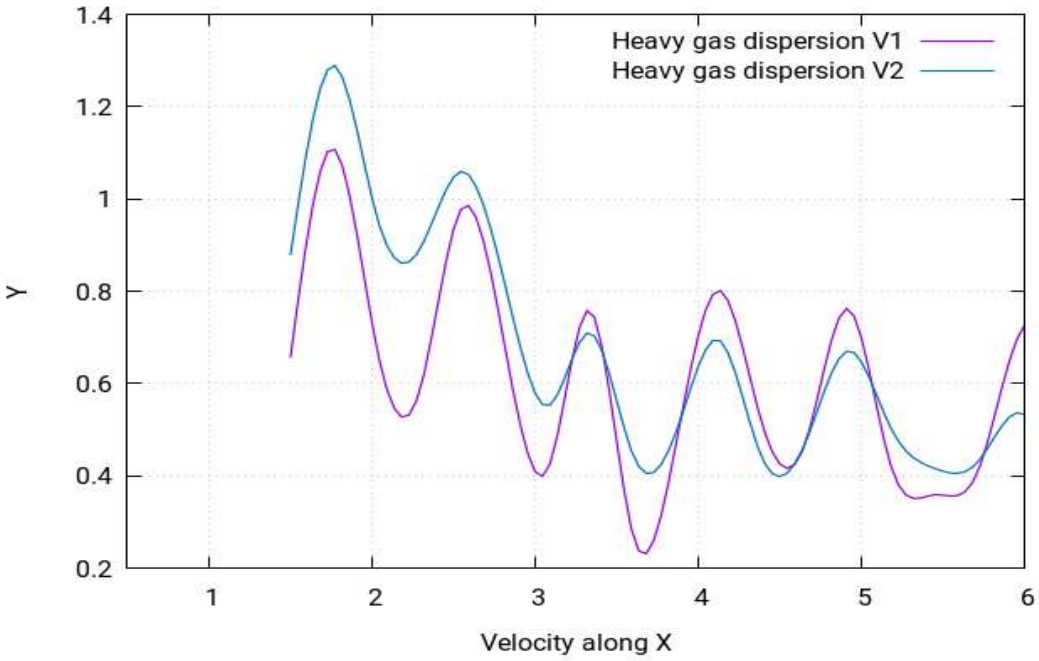

Figure 8.236: *Velocity of the heavy gas dispersion profile along the* ***x****-direction at different points of (V1) x=1.50m, y=1.84m, z=7.20m (V2) x=1.50m, y=1.84m and z=8.00m*

Figure 8.236 shows the curves for velocity profile along the x-direction. The curves follow an asymmetric pattern and have several peaks with the highest peak being at approximately 3.7m.

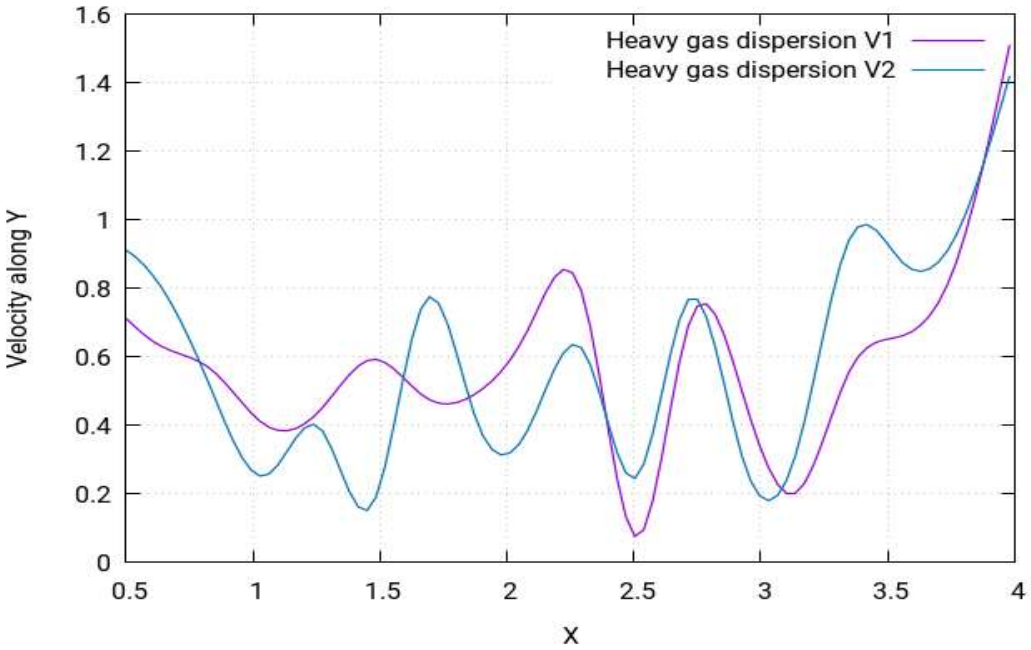

Figure 8.237: *Velocity of the heavy gas dispersion profile along the **y**-direction at different points of (V1) x=3.92m, y=-1m, z=7.20m (V2) x=3.92m, y=-1m, z=8.00m*

Figure 8.237 shows the curves for the velocity profile along the y-direction. The curves follow an asymmetrical pattern and have several peaks, with the highest peak being at approximately 2.5m.

At location 2 of the staggered arrangement of the cylindrical tanks, the concentration of the heavy gas is maximum around the tank nearest to the source. Moreover, the concentration is greater than that obtained for the collocated arrangement because the staggered arrangement causes more turbulence.

8.6.26 Location 1: Heavy gas dispersion

8.6.26.1 Structure of layout

The type of layout adopted for this case study for the collocated layout. A layout of 60 gas storage tanks will be created, with a spherical shape distribution, and the release source will be placed in different positions. The behaviour of the gas clouds will then be studied.

8.6.26.2 Release source location

The release source point (1) was located at the upwind front of the gas storage tanks group between the first and second column in the middle between the third and fourth rows. The perimeters selected for this case study are stated below:

Table 8.40: *Parametric values for the high-speed heavy gas simulation (location 1)*

Density	Flow Rate	Velocity	Ambient Temperature	Release Source Temperature
2.1 kg m/s^3	1 kg/s	1 m/s	25°C	-100°C

8.6.26.3 Concentration of the heavy gas dispersion

The following figure shows the concentration behaviour of the heavy gas at location 1. The whereabouts of location 1 has been stated at the beginning of the passage.

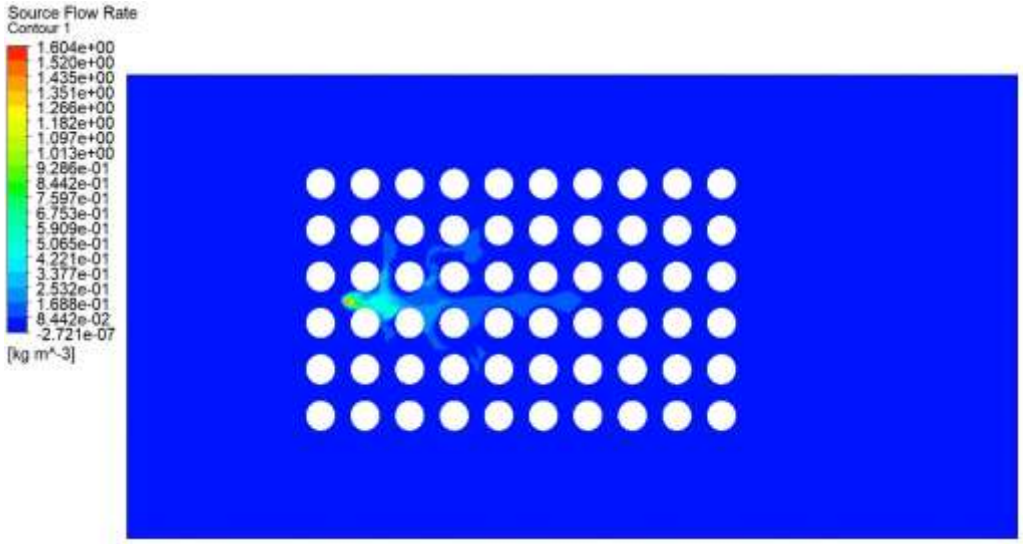

Figure 8.238: *Concentration profile of the heavy gas dispersion with the release source located at the upwind front of the group of gas storage tanks between the first and second columns in the middle between the third and fourth rows at* ***1m/s.***

The concentration profile of the heavy gas dispersion at location 1 is shown in the Figure 8.238. It represents the concentration behaviour of the heavy gas when the release gas source is placed at the upwind front of the group of gas storage tanks between the first and second columns in the middle between the third and fourth row. It can be seen that the cloud shape, in this case, looks like that of a frog, and since the gas release source is placed in between the rows, it is exposed to the air and hence the cloud is spread across the layout.

8.6.26.4 Iso-surfaces of the heavy gas dispersion

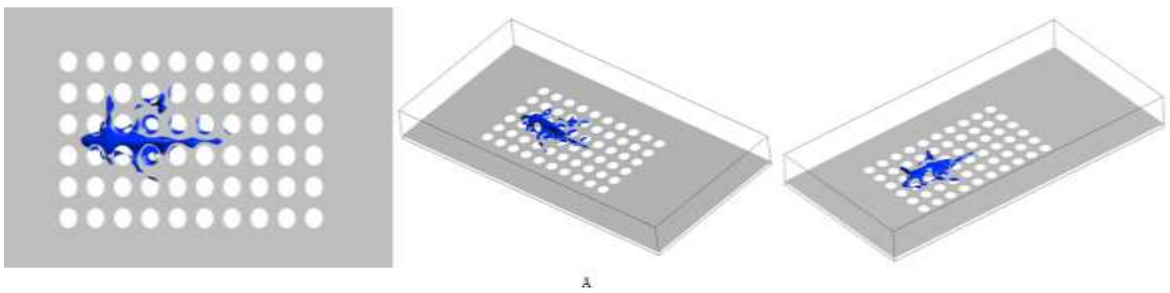

Figure 8.239: *Iso-surfaces of the concentration profile of the heavy gas dispersion with the release source located at the upwind front of the group of gas storage tanks between the first and second column at the middle between the third and fourth rows at* ***1m/s****.*

Figure 8.239 shows the iso-surfaces of the concentration profile of heavy gas dispersion with release source located at the upwind front of the group of buildings in the middle between third and fourth row. It helps identify the spread of the cloud in each dimension and it can be seen that the cloud shape seems to form a frog-shaped pattern and there are tiny bits of the cloud which have left the main cloud and settled in the nearby buildings. The cloud is spread somewhat symmetrically, but a part of cloud is inclined to move more towards one edge.

According to Standard BS EN 60079-10-1:2009 [104], the following locations can be categorised:

Zone 0: The 2nd and 3rd row buildings of the upwind and middle front containing the release source

Zone 1: Some tiny bits of the gas cloud in the immediate surroundings of the areas mentioned in zone 0

Zone 2: All the remaining locations not categorised in zone 0 or zone 1

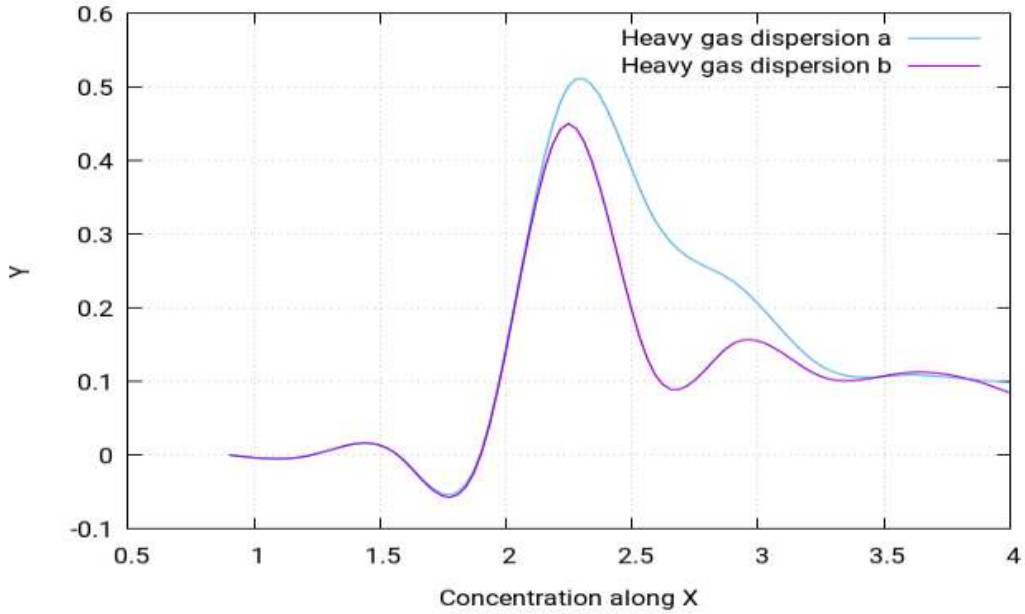

Figure 8.240*: Concentration of the heavy gas dispersion profile along the* ***x****-direction at different points of (a x=1.20m, y=2.28m, z=7.20m (b) x=1.20m, y=2.28m and z=7.20m*

The above figure shows the concentration profiles for two of the gas dispersions at two different locations depending on distance from release source. Both curves follow the same pattern but have different values.

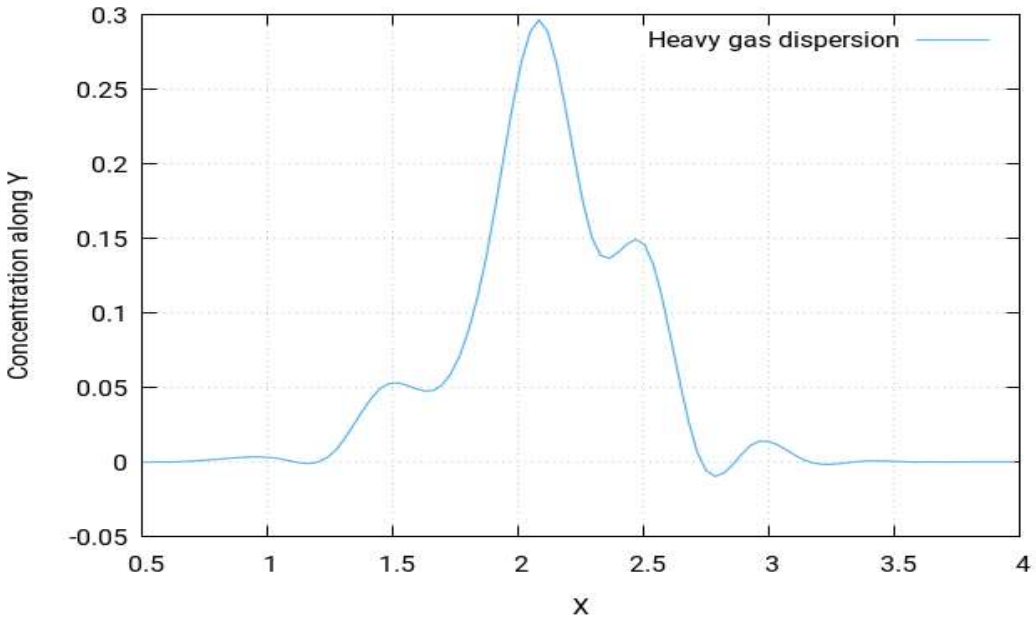

Figure 8.241: *Concentration of the heavy gas dispersion profile along the **y**-direction at different points of x=1.20m, y=2.28m and z=7.20m*

Figure 8.241 shows the curve for the concentration profile along the y-direction. The curve follows an asymmetrical pattern and has a single peak at almost 2.1m.

8.6.26.5 Temperature of the heavy gas dispersion

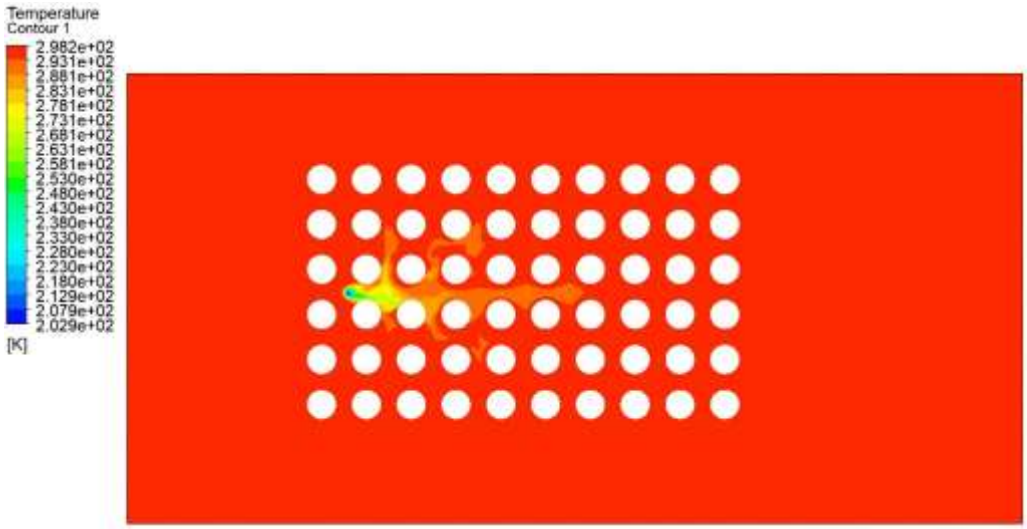

Figure 8.242: *Temperature profile of the heavy gas dispersion with the release source located at the upwind front of the group of gas storage tanks between the first and second column in the middle between the third and fourth rows at **1m/s***

Above, Figure 8.242 shows the temperature simulation for this study. By visualising the temperature simulation, it is found out that the temperature simulation produces largely the same profile for the case study as that of the concentration profile. However, the behaviour of temperature is in fact the opposite to that of concentration. This means that the areas identified

in the concentration simulation as highly concentrated will in fact have the lowest temperatures, while the ones with moderate concentrations will have moderate temperatures and the least concentrated areas will have the highest temperatures. To further simply these findings, it should be pointed out that the simulations show that the concentrations near the release source point tend to be the highest and start to fade away as the gas cloud moves away from the source and are lowest when it moves much further away in the layout, eventually reaching the environment where the gas cloud disappears. The temperature is lowest near the release source point and tends to increase as the cloud moves away from source, finally reaching the maximum temperature equal to the ambient temperature of the environment.

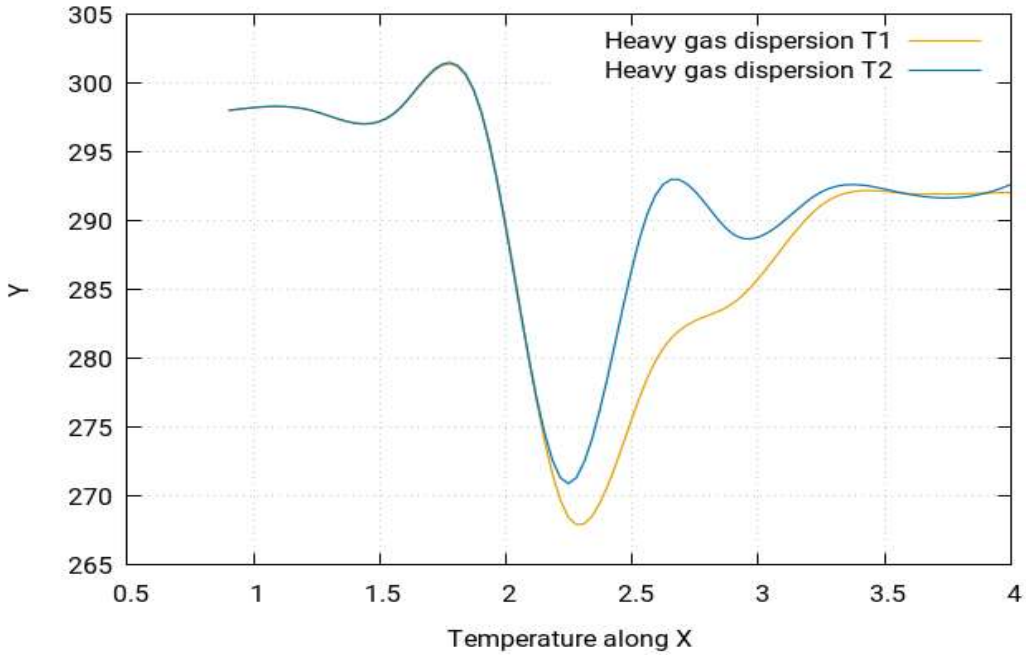

Figure 8.243: *Concentration of the heavy gas dispersion profile along the* ***x****-direction at different points of (a)x=1.20m, y=2.28m, z=7.20m (b) x=1.20m, y=2.28m and z=7.20m*

Figure 8.243 (above) shows two different curves for the temperature profiles. They show the pattern of the temperature profile along the x-direction when the wind speed for the simulation is 1m/s. The two different curves are obtained for two different distances from the release source. These results show that, at a speed of 1m/s, temperature profiles are a mirror of concentration profile.

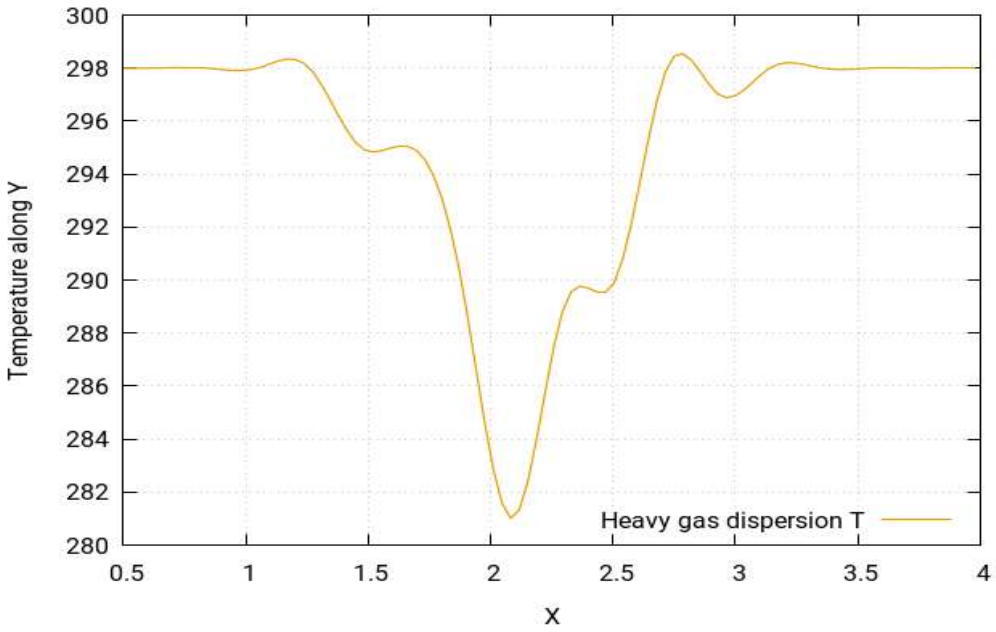

Figure 8.244: *Temperature of the heavy gas dispersion profile along the* ***y****-direction at different points of (a) x=1.20m, y=2.28m, z=7.20m (b) x=1.20m, y=2.28m and z=7.20m*

Figure 8.244 shows the curve for the concentration profile along the y-direction. The curve follows an asymmetric pattern and has a single peak at almost 2.1m.

8.6.26.6 Velocity of the heavy gas dispersion

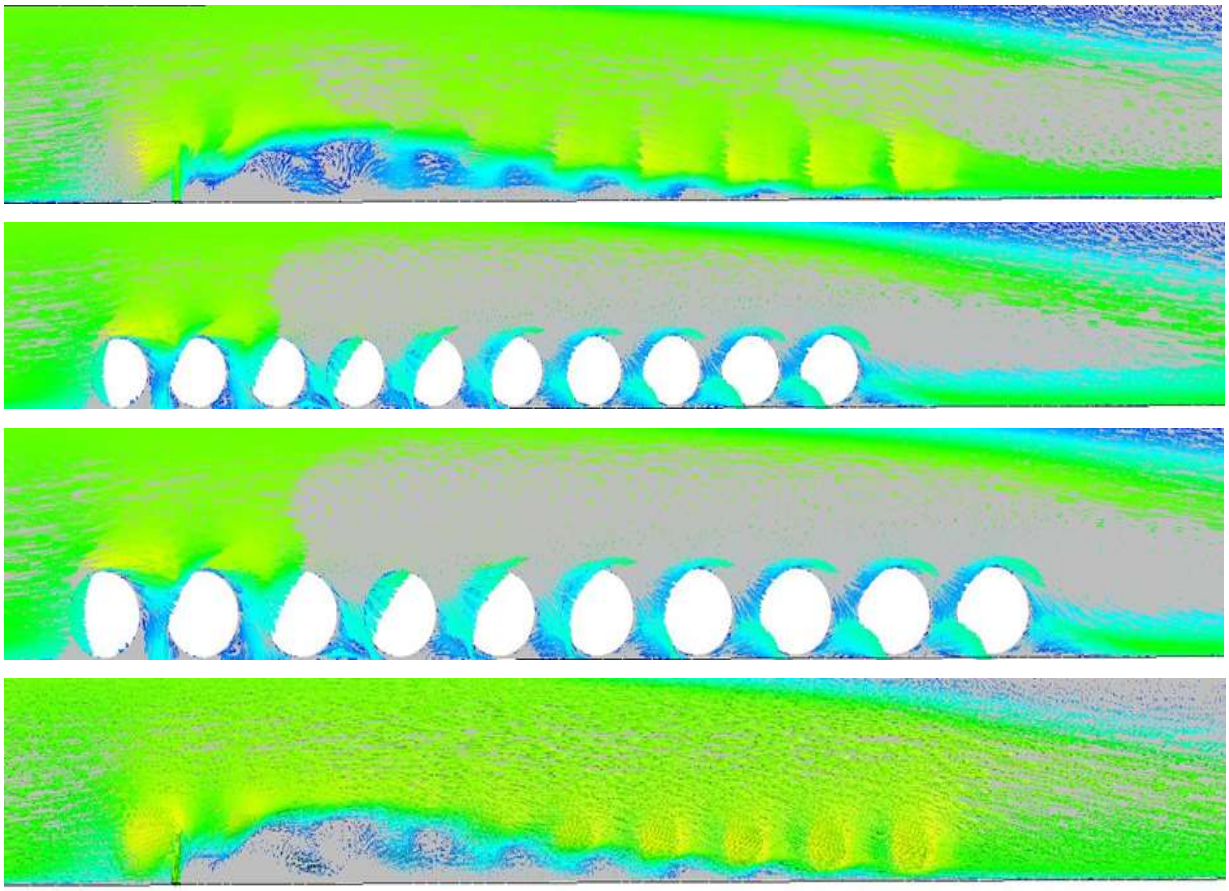

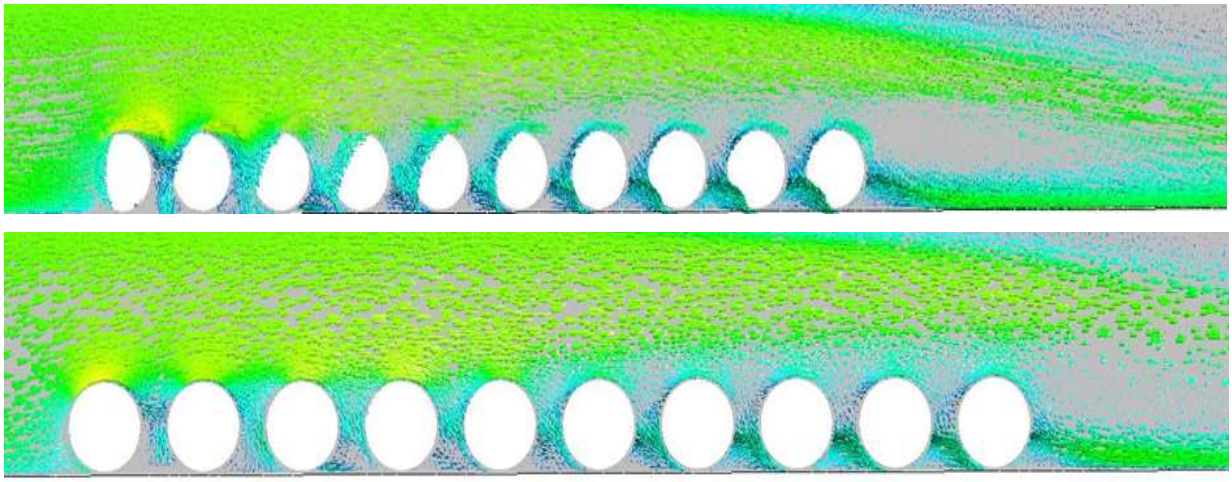

Figure 8.245: *Velocity contours of the heavy gas dispersion with the release source located at the upwind front of the group of gas storage tanks between the first and second column in the middle between the third and fourth rows at* ***1m/s***

Figure 8.245 shows the velocity contours of the heavy gas dispersion for this case study with the release source located in the middle between the third and fourth rows. The velocity contours depict the intensity of wind - or the effective wind influence - at the different locations throughout the layout. As can be seen in the figure, the wind intensity is different at different points in the layout. It is a commonly known effect that, with enhanced altitudes, enhanced wind speeds are encountered. This is because the objects in the lower altitudes create resistance to wind flow. As resistance is caused by the buildings in the flow of gas towards the direction opposite of wind, the wind flowing from left to right fails to indict the same motion of flow. Instead, various complex vertexes are formed within the buildings near the release source location, as can be seen in Figure 8.245. The heavy gas release from the source is carried by these vertexes to the nearby mixture of the gas cloud, which them moves smoothly away from the source. Moreover, the hindrance to the wind flow caused by the buildings results in the vertexes moving in the upward direction, which enhances the shape of cloud in the upward direction.

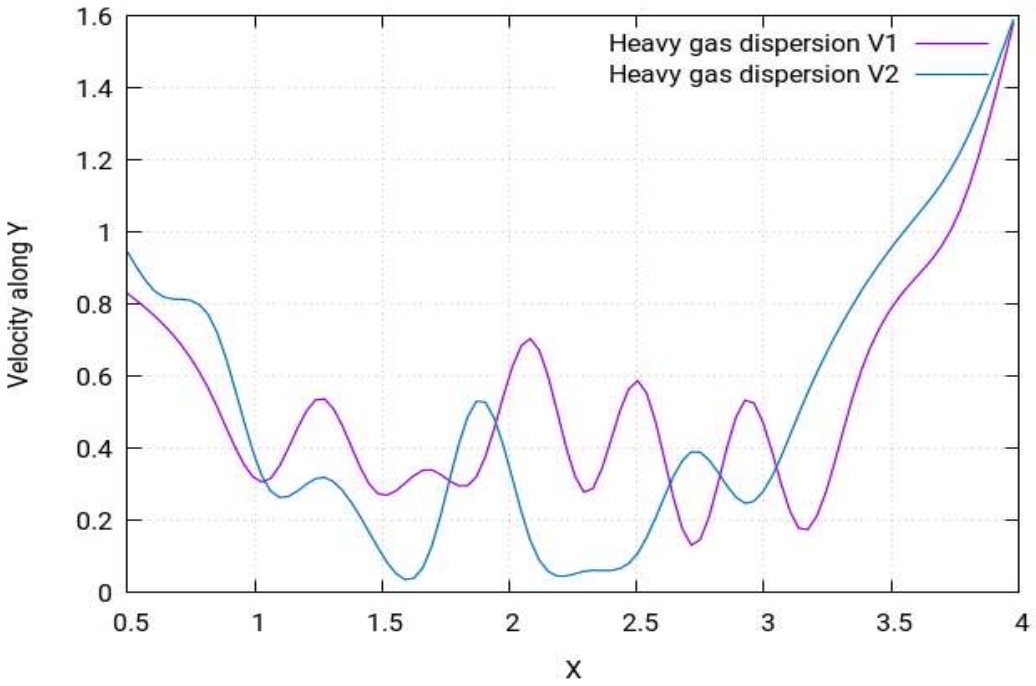

Figure 8.246: *Concentration of the heavy gas dispersion profile along the **y**-direction at different points of x=1.20m, y=2.28m, z=7.20m (b) x=1.20m, y=2.28m and z=7.20m*

Figure 8.246 shows the curves for the velocity profile along the y-direction. The curves follow an asymmetrical pattern and have several peaks, with the highest peak being at approximately 1.6m.

The dispersion of the heavy gas at high velocity in the case of a/the collocated arrangement of spherical obstacles showed uniform distribution due to the density difference between the heavy gas and the atmosphere. This difference is due to the delta temperature, which is extremely high i.e., 125 °C.

8.6.27 Location 2: Heavy gas dispersion

8.6.27.1 Structure of layout

The type of layout adopted for this case study for the collocated layout. A layout of 60 gas storage tanks will be created, with a spherical shape distribution, the release source will be placed in position. Then the behaviour of the gas clouds will be studied.

8.6.27.2 Release source location

Release source point (2) was located at the middle front of the group of gas storage tanks between the 3rd and 4th rows from the bottom. The perimeters selected for this case study are stated below:

Table 8.41: *Parametric values for the high-speed heavy gas simulation (location 2)*

Density	Flow Rate	Velocity	Ambient Temperature	Release Source Temperature
2.1 kg m/s^3	1 kg/s	1 m/s	25°C	-100°C

8.6.27.3 Concentration of the heavy gas dispersion

The following figure shows the concentration behaviour of the heavy gas at location 2. The whereabouts of location 2 has been stated at the beginning of the passage.

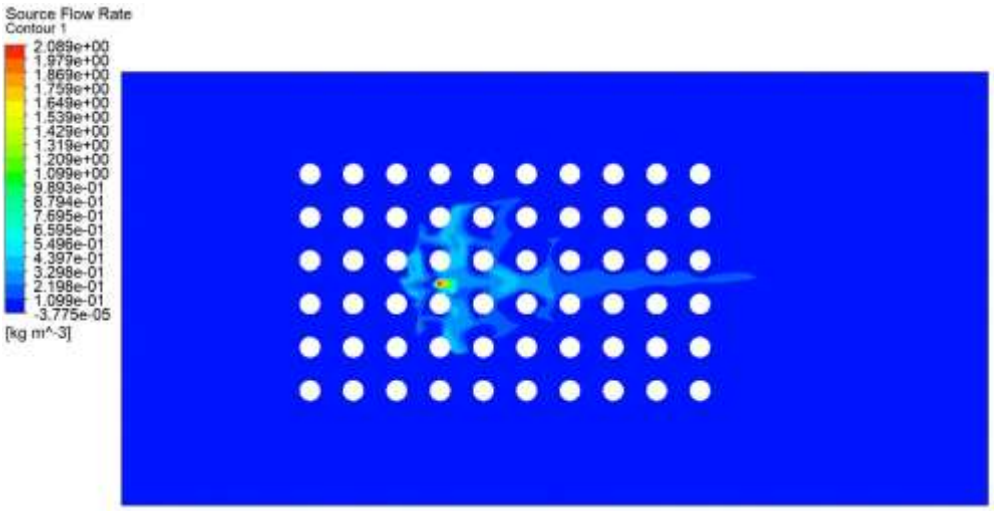

Figure 8.247: *Concentration profile of the heavy gas dispersion with the release source located at the middle front of the group of gas storage tanks between the 3rd and 4th row from the bottom at* ***1m/s***

The concentration profile of the heavy gas at location 3 is shown above in Figure 8.247. It represents the concentration behaviour of the heavy gas when the release gas source is placed at the middle front of the group of gas storage tanks between the 3rd and 4th rows from the bottom. The cloud shape in this case does not seem identical to any geometric shape and follows a somewhat screw-shaped pattern. It should also be point out that the release is placed between the buildings and not behind them. This means it is exposed to air, which is why the gas cloud is spread that way in the layout.

8.6.27.4 Iso-surfaces of the heavy gas dispersion

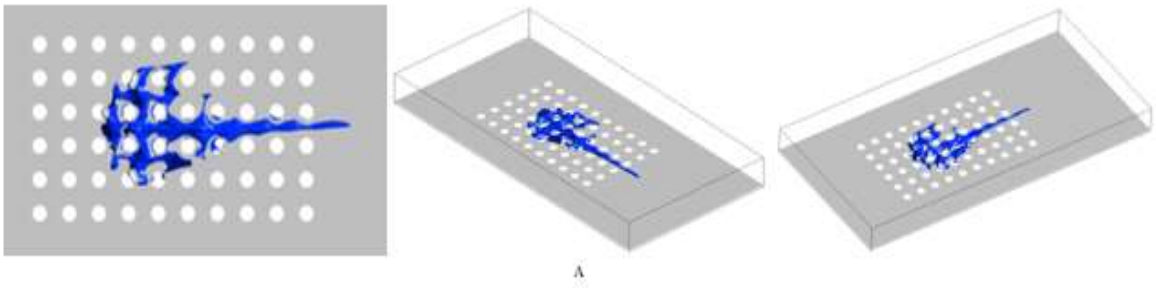

Figure 8.248: *Iso-surfaces of the concentration profile of the Heavy Gas Dispersion with the release source located at the middle front of the group of gas storage tanks between the 3rd and 4th rows from the bottom at* ***1m/s***

Figure 8.248 shows the iso-surfaces of the concentration profile of the heavy gas dispersion with the release source located at the middle front of the group of gas storage tanks between the 3rd and 4th rows from the bottom. This helps identify the spread of the cloud in each dimension. It can be seen that the cloud forms a screw-shaped pattern and does not lean towards a particular dimension that can be specifically stated. The concentrations are more towards the central rows of the layout.

According to Standard BS EN 60079-10-1:2009 [104], the following locations can be categorised:

Zone 0: The central rows of the middle front of the layout containing the release source

Zone 1: The 2nd and 3rd column buildings of the central row

Zone 2: All the remaining locations not categorised in zone 0 or zone 1

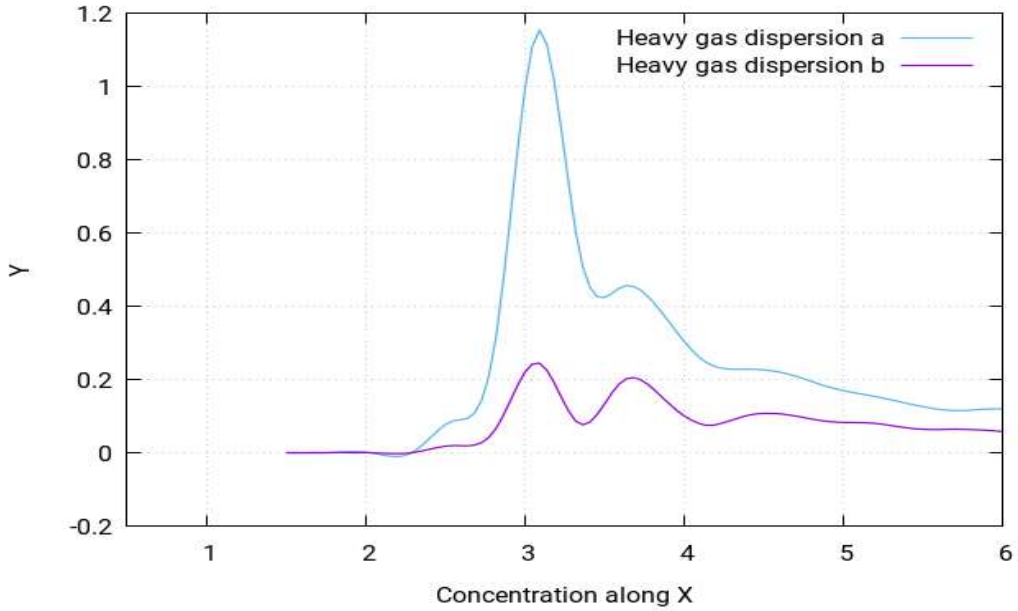

Figure 8.249: *Concentration of the heavy gas dispersion profile along the* ***x****-direction at different points of (a) x=1.50m, y=2.05m, z=7.20m (b) x=1.50m, y=2.05m and z=8.50m*

The above figure shows the concentration profiles for two of the gas dispersions at two different locations depending on distance from release source. Both curves follow the same pattern but have different values.

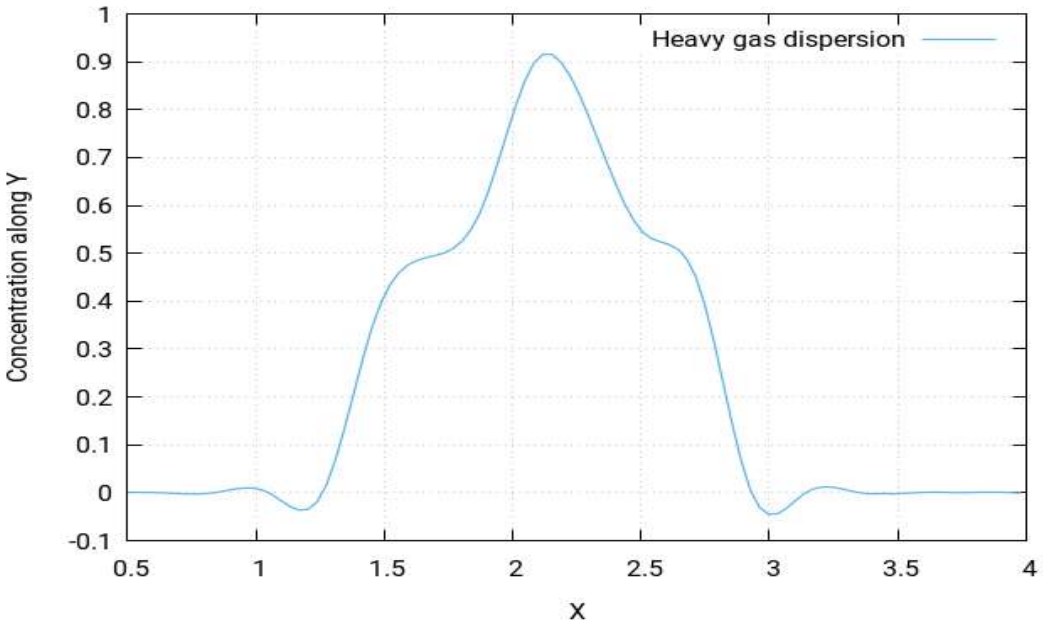

Figure 8.250: *Concentration of the heavy gas dispersion profile along the* ***y****-direction at different points of x=3.12m, y=-1m and z=7.20m*

Figure 8.250 shows the curve for the concentration profile along the y-direction. The curve follows a symmetric pattern and has a single peak at almost 2.1m.

8.6.27.5 Temperature of the heavy gas dispersion

Figure 8.251: *Temperature profile of the heavy gas dispersion with the release source located at the middle front of the group of gas storage tanks between the 3rd and 4th rows from the bottom at* ***1m/s***

Above, Figure 8.251 shows the temperature simulation for this study. By visualising the temperature simulation, it is found out that the temperature simulation produces largely the same profile for the case study as that of the concentration profile. However, the behaviour of temperature is in fact the opposite to that of concentration. This means that the areas which were identified in the concentration simulation as highly concentrated will in fact have the lowest temperatures, while the ones with moderate concentrations will have moderate temperatures and the least concentrated areas will have the highest temperatures. To further simply these findings, it should be pointed out that the simulations showed that the concentrations near the release source point tend to be the highest and start to fade. away as the gas cloud moves away from the source and is at its lowest as it moves much further away in the layout reaching the environment where the gas cloud eventually disappears. However, temperature is minimum near the release source point and tends to increase as the gas cloud moves away from source, finally achieving the maximum temperature equal to the ambient temperature of the environment.

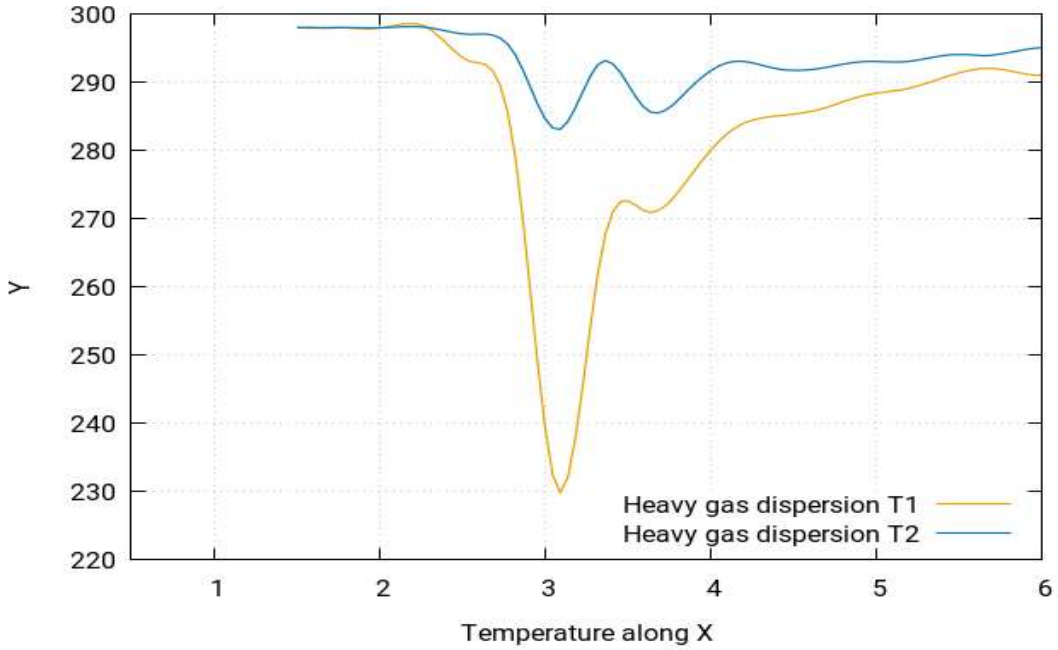

Figure 8.252: *Temperature of the heavy gas dispersion profile along the x-direction at different points of (T1) x=1.50m, y=2.05m, z=7.20m (T2) x=1.50m, y=2.05m and z=8.50m*

Figure 8.252 shows two different curves for the temperature profiles. They show the pattern of the temperature profile along the y-direction when the wind speed for the simulation is 1m/s. The two different curves are obtained for two different distances from the release source. These results show that at speed of 1m/s, temperature profiles are a mirror of concentration profile.

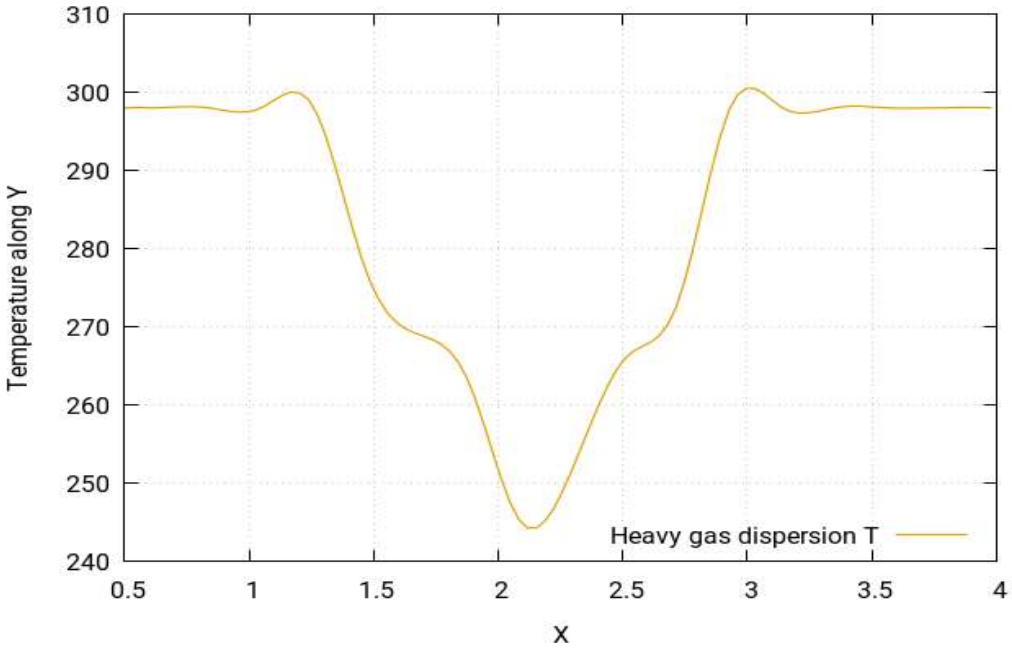

Figure 8.253: *Temperature of the heavy gas dispersion profile along the y-direction at different points of (T)x=3.12m, y=-1m and z=7.20m*

Figure 8.253 shows the curve for the temperature profile along the y-direction. The curve follows a symmetrical pattern and has a single peak at almost 2.1m.

8.6.27.6 Velocity of the heavy gas dispersion

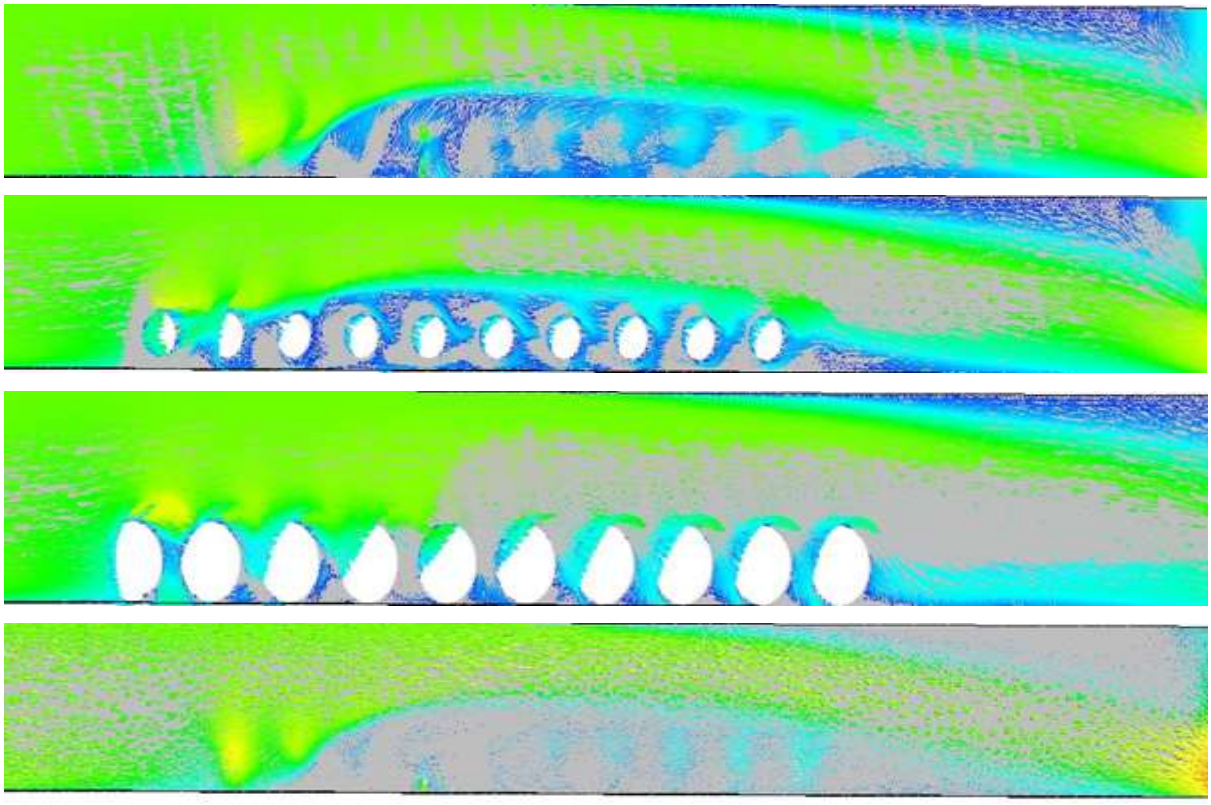

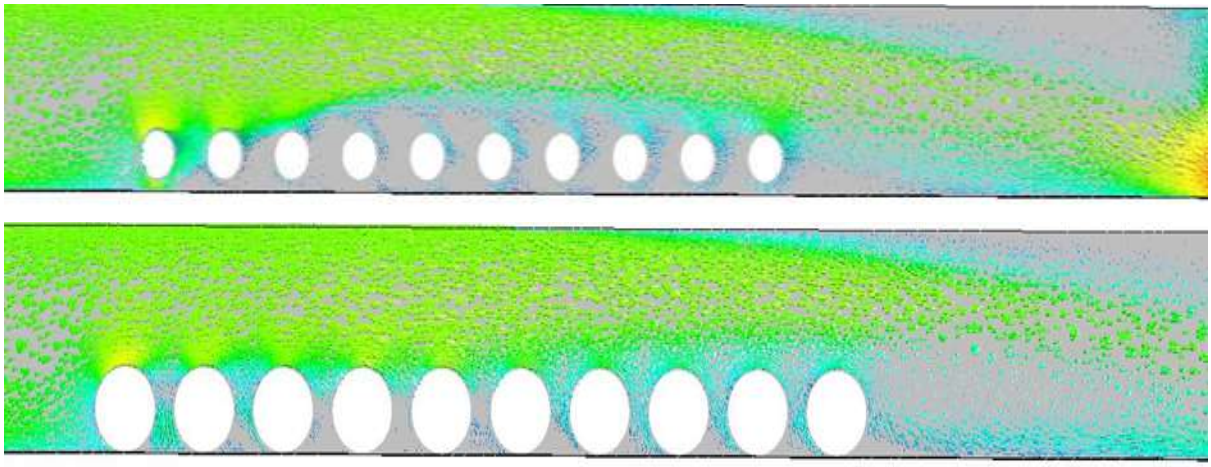

Figure 8.254: *Velocity contours of the heavy gas dispersion with the release source located at the middle front of the group of gas storage tanks between the 3rd and 4th rows from the bottom at* ***1m/s***

Figure 8.254 shows the velocity contours of the heavy gas dispersion for this case study with the release source located at the middle front of the group of gas storage tanks between the 3rd and 4th rows from the bottom. The velocity contours depict the intensity of wind - or the effective wind influence - at the different locations throughout the layout. As can be seen in the figure, the wind intensity is different at different points in the layout. It is a commonly known effect that, with enhanced altitudes, enhanced wind speeds are encountered. This is because the objects at the lower altitudes create resistance to wind flow. As resistance is caused by the buildings to the flow of gas towards the direction opposite of wind, the wind flowing from left to right fails to indict the same motion of flow. Instead, various complex vertexes are formed within the buildings near the release source location, as can be seen in (Figure 8.254). The heavy gas release from the source is carried by these vertexes to the nearby mixture of the gas cloud, which then moves smoothly away from the source. Moreover, the hindrance to the wind flow caused by the buildings results in the vertexes moving in the upward direction, which enhances the shape of the cloud in the upward direction.

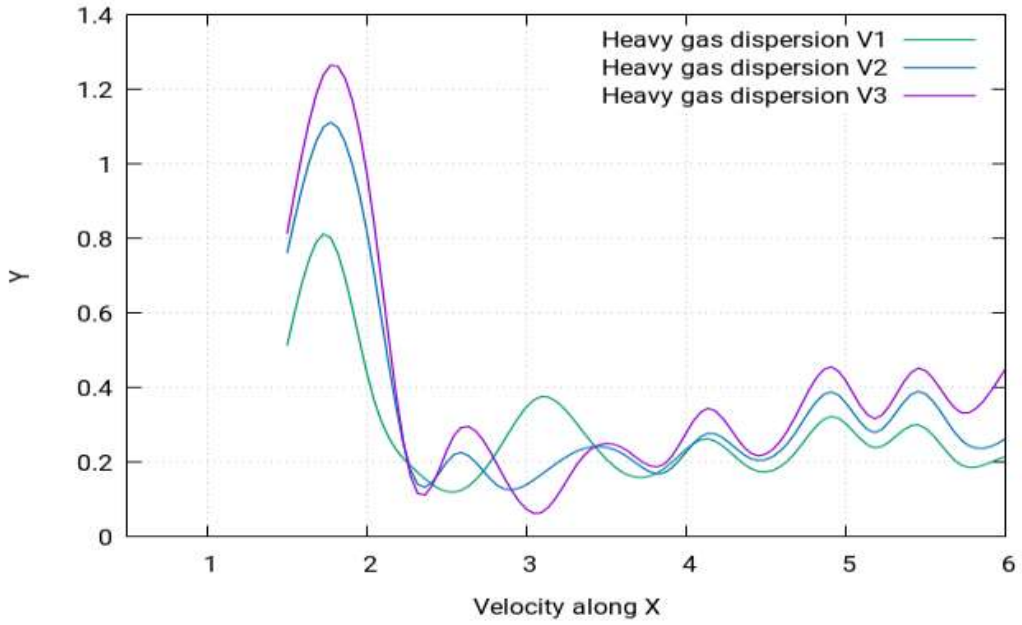

Figure 8.255: *Velocity of the heavy gas dispersion profile along the* ***x****-direction at different points of (V1) x=1.50m, y=2.05m, z=7.20m (V2) x=1.50m, y=2.05m, z=8.50m (V2) x=1.50m, y=2.05m and z=1.50m*

Figure 8.255 shows the curves for the velocity profile along the x-direction. The curves follow an asymmetrical pattern and have several peaks, with the highest peak being at approximately 1.7m.

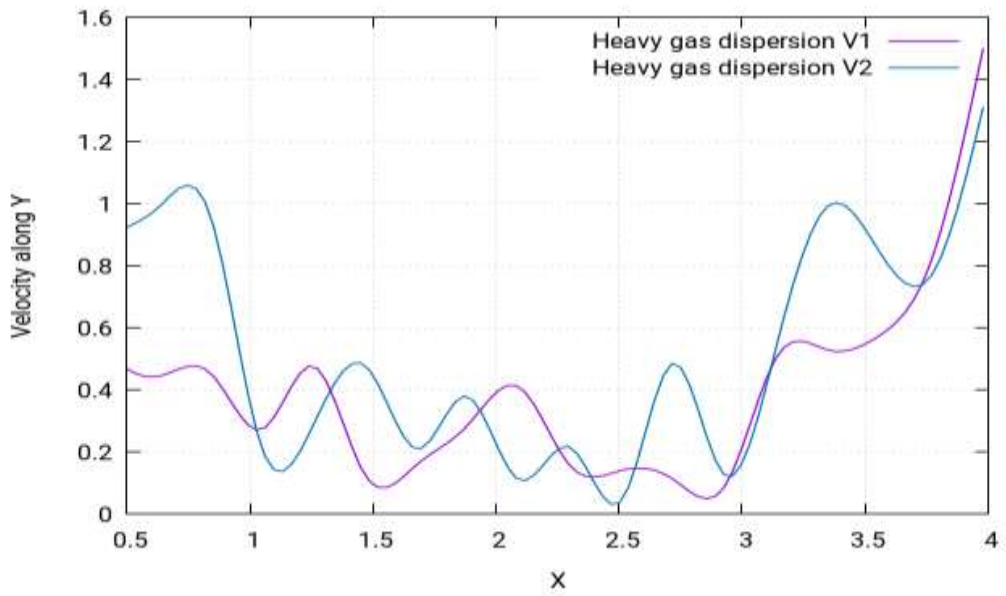

Figure 8.256: *Velocity of heavy gas dispersion profile along the* ***y****-direction at different points of (V1) x=3.12m, y=-1m, z=7.20m (V2) x=3.12m, y=-1m and z=1.60m*

Figure 8.256 shows the curves for the velocity profile along the y-direction. The curves follow an asymmetrical pattern and have several peaks, with the highest peak being at approximately 3.3m.

At location 2 of the collocated arrangement of the spherical obstacles, the dispersion showed similar results. The density difference that arose due to the temperature difference resulted in uniform dispersion of the gas.

8.6.28 Location 1: Heavy gas dispersion for a safe distance

8.6.28.1 Structure of layout

The type of layout adopted for this case study for the collocated layout. A layout of 24 gas storage tanks group will be created, with a spherical shape distribution for safe distance, and the release source will be placed in position. The behaviour of the gas clouds will then be studied.

8.6.28.2 Release source location

The release source point (1) was located at the upwind front of the group of buildings between the 1st and 2nd columns in the middle between the 2nd and 3rd rows. The perimeters selected for this case study are stated below:

Table 8.42: *Parametric values for the high-speed heavy gas simulation (safe distance 1)*

Density	Flow Rate	Velocity	Ambient Temperature	Release Source Temperature
2.1 kg m/s^3	1 kg/s	1 m/s	25°C	-100°C

8.6.28.3 Concentration of the heavy gas dispersion for a/the safe distance

The following figure shows the concentration behaviour of the heavy gas at location 1. The whereabouts of location 1 has been stated at the beginning of the passage.

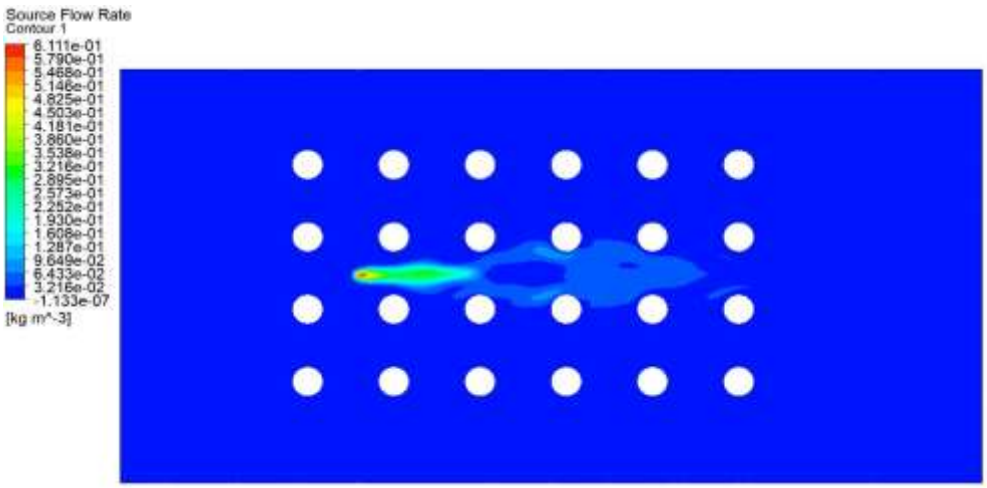

Figure 8.257: *Concentration profile of the heavy gas dispersion with the release source located at the upwind front of the group of buildings between the 1st and 2nd column in the middle between the 2nd and 3rd rows at* ***1m/s***

The concentration profile of the heavy gas at location 1 is shown above in Figure 8.257. It represents the concentration behaviour of the heavy gas when the release gas source is placed at the upwind front of the group of buildings between the 1st and 2nd columns in the middle between the 2nd and 3rd rows. It can be seen in the above figure that the cloud shape in this case again looks like an elliptical cylinder and the gas cloud does not try to swirl around the building, as at a normal distance, between the collocated and/or staggered layouts but creates a nozzling effect. The main difference caused by the safe distance between the gas storage tanks and other factors such as wind velocity and the change of obstacle layouts.

The safe distance between the obstacles is not only dependent on the size of the obstacles but is also dependent on the wind velocity. To adjust the safe distance for the storage tanks, the average velocity data is taken from the local weather station for a period of five years [112]. A safe margin is added to the average value. Based on that, the safe distance is calculated.

8.6.28.4 Iso-surface of the heavy gas dispersion for a/the safe distance

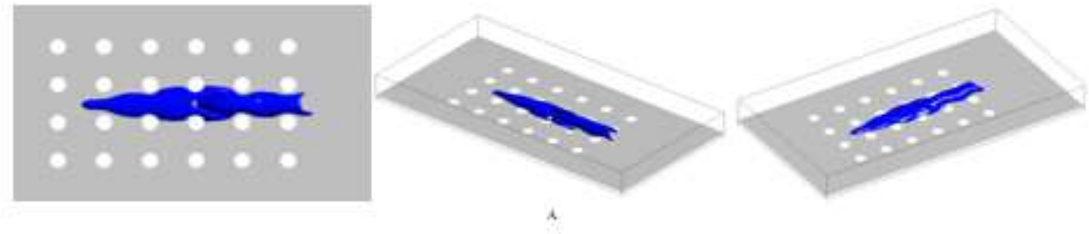

Figure 8.258: *Iso-surfaces of the concentration profile of the Heavy Gas Dispersion with the release source located at the upwind front of the group of buildings between the 1st and 2nd columns in the middle between the 2nd and 3rd rows at* ***1m/s***

Figure 8.258 presents the iso-surfaces of the concentration profile of the heavy gas dispersion with the release source located at the upwind front of the group of buildings between the 1st and 2nd columns in the middle between the 2nd and 3rd rows. This helps identify the spread of the cloud in each dimension. The cloud shape seems to form an elliptical cylindrical type shape, or it could be said that there are nodes in the cylindrical pattern of the cloud. The cloud is spread somewhat symmetrically and remains between the two central rows of the layout.

According to Standard BS EN 60079-10-1:2009 [104], the following locations can be categorised:

High speed:

Zone 0: The area between the two central rows of the layout excluding the first column

Zone 1: A partial inside area of the middle two rows of the building layout

Zone 2: All the remaining locations not categorised in zone 0 or zone 1

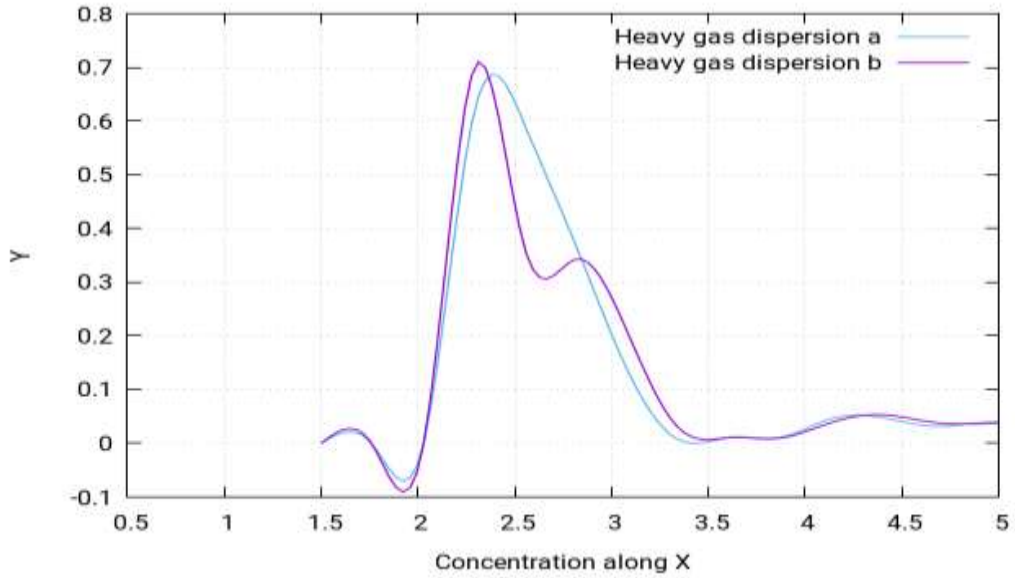

Figure 8.259: *Concentration of the heavy gas dispersion profile along the* ***x****-direction at different points of (a) x=1.50m, y=2.01m, z=7.20m (b) x=1.50m, y=2.01m and z=8.50m*

The above figure shows the concentration profiles for two of the gas dispersions at two different locations depending on distance from release source. Both curves follow the same pattern but have different values.

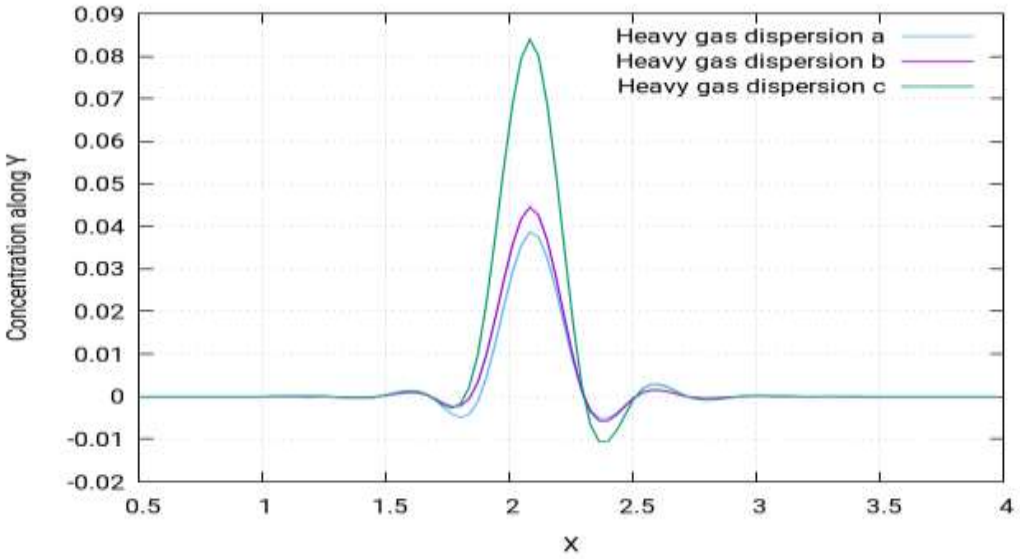

Figure 8.260: *Concentration of the heavy gas dispersion profile along the* ***y****-direction at different points of (a) x=2.38m, y=-1m, z=7.20m (b) x=2.38m, y=-1m, z=1.30m (b) x=2.38m, y=-1m and z=8.50m*

The above figure shows the velocity profiles for three of the gas dispersions at three different locations along the y-direction depending on distance from release source. The curves follow the same pattern but have different values.

8.6.28.5 Temperature of the heavy gas dispersion for a/the safe distance

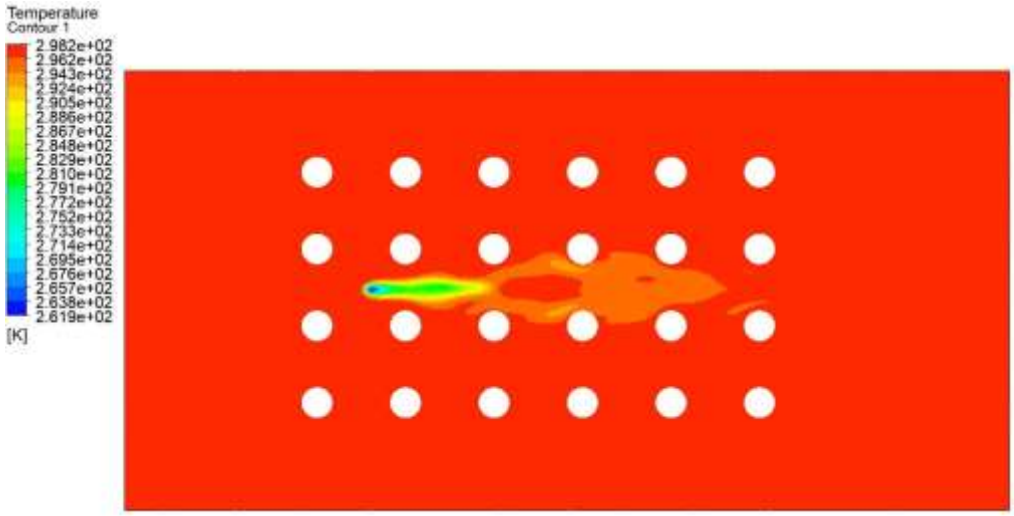

Figure 8.261: *Temperature profile of the heavy gas dispersion with the release source located at the upwind front of the group of buildings between the 1st and 2nd columns in the middle between the 2nd and 3rd rows at* ***1m/s***

Figure 8.261 shows the temperature simulation for this study. By visualising the temperature simulation, it is found out that the temperature simulation produces largely the same profile for the case study as that of the concentration profile. However, the behaviour of temperature is in fact the opposite to that of concentration. This means that the areas which were identified in the concentration simulation as highly concentrated will in fact have the lowest temperatures, while the ones with moderate concentrations will have moderate temperatures and the least concentrated areas will have the highest temperatures. To further simply these findings, it should be pointed out that the simulations showed that the concentrations near the release source point tend to be the highest and start to fade away as the gas cloud moves away from the source and are the lowest as the cloud moves much further away in the layout, eventually reaching the environment where the gas cloud disappears. However, the temperature is lowest near the release source point and tends to increase as the gas cloud moves away from the source, finally achieving its highest temperature equal to the ambient temperature of the environment.

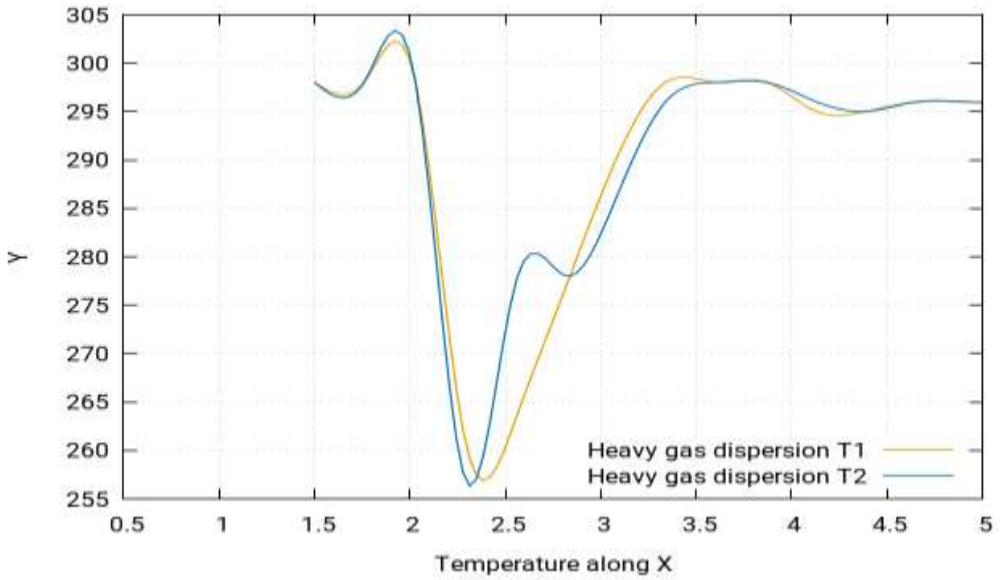

Figure 8.262: *Temperature of the heavy gas dispersion profile along the* ***x****-direction at different points of (T1) x=1.50m, y=2.01m, z=7.20m (T2) x=1.50m, y=2.01m and z=8.50m*

Figure 8.262 (above) shows two different curves for the temperature profiles. They show the pattern of the temperature profile along the y-direction when the wind speed for the simulation is 1m/s. The two different curves are obtained for two different distances from the release source. These results show that, at a speed of 1m/s, temperature profiles are a mirror of concentration profile.

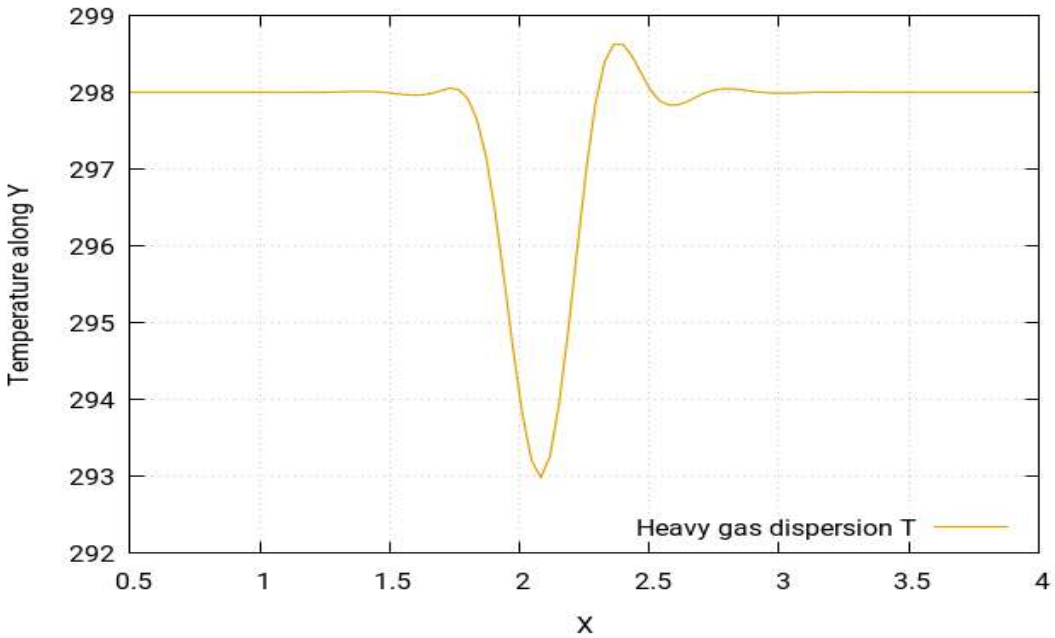

Figure 8.263: *Temperature of the heavy gas dispersion profile along the* ***y****-direction at different points of (T) x=2.38m, y=-1m and z=8.50m*

Figure 8.263 shows the curve for temperature profile along the y-direction. The curve follows an asymmetric pattern and has a single peak at almost 2.1m.

8.6.28.6 Velocity of the heavy gas dispersion for a/the safe distance

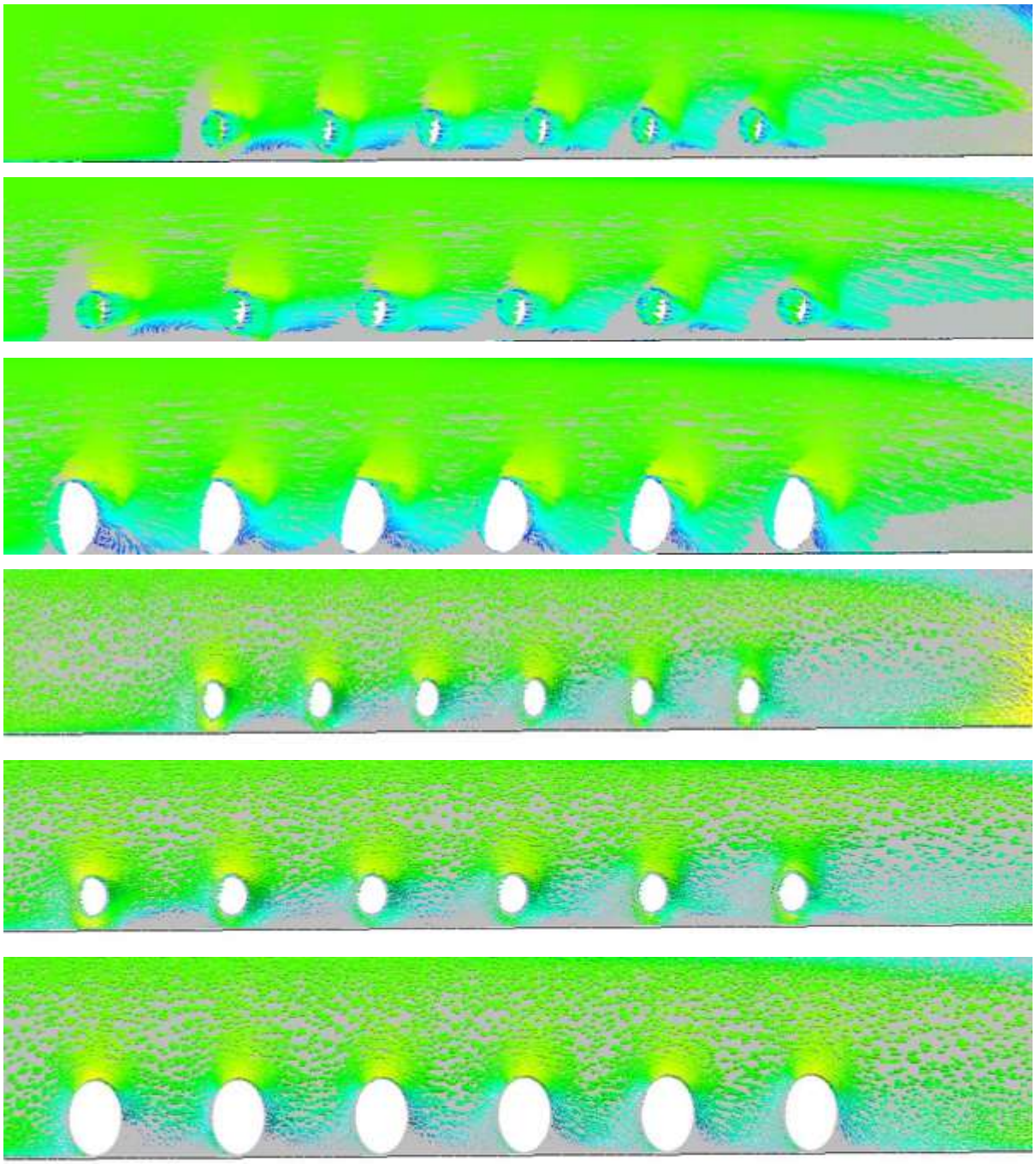

Figure 8.264: *Velocity contours of the heavy gas dispersion with the release source located at the upwind front of the group of gas storage tanks between the 1st and 2nd column in the middle between the 2nd and 3rd rows at* ***1m/s***

Figure 8.264 shows the velocity contours of heavy gas dispersion for this case study with release source located at the upwind front of the group of gas storage tanks between the 1st and 2nd columns in the middle between the 2nd and 3rd rows. The velocity contours depict the intensity of wind - or the effective wind influence - at the different locations throughout the layout. It can be seen in the figure that the wind intensity is different at different points in the

layout. It is a commonly known effect that, with enhanced altitudes, enhanced wind speeds are encountered. This is because the objects at the lower altitudes create resistance to the wind flow. As resistance is caused by the gas storage tanks to the flow of gas towards the direction opposite of wind, the wind flowing from left to right fails to indict the same motion of flow. Instead, various complex vertexes are formed within the gas storage tanks near the release source location, as can be seen in (Figure 8.264). The heavy gas release from the source is carried by these vertexes to the nearby mixture of the gas cloud, which then moves smoothly away from the source. Moreover, the hindrance to the wind flow caused by the gas storage tanks results in the vertexes moving in the upward direction, which enhances the shape of cloud in the upward direction.

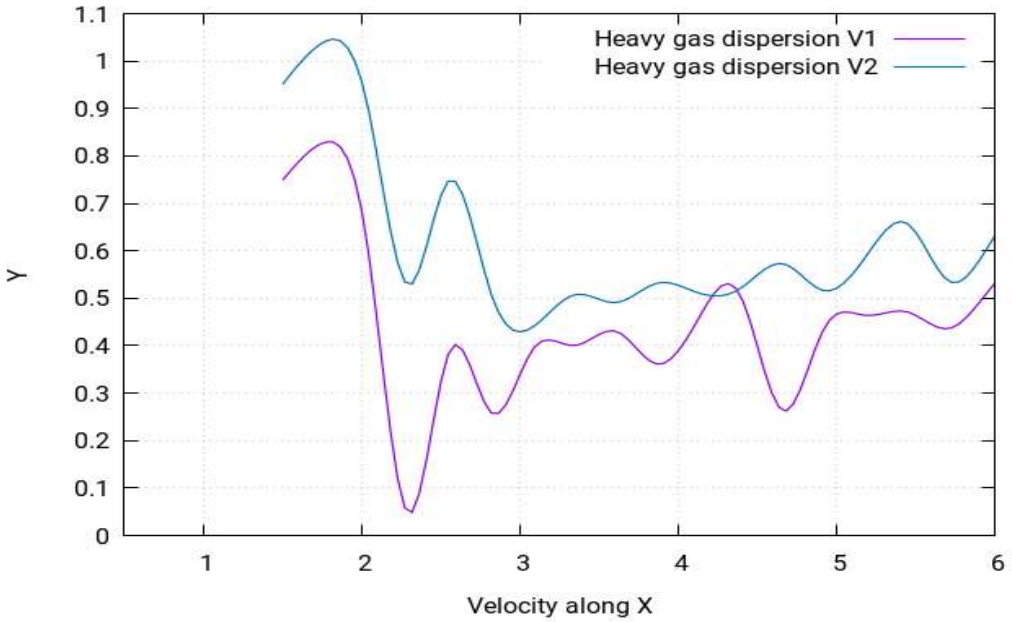

Figure 8.265: *Velocity of the heavy gas dispersion profile along the* ***x****-direction at different points of (V1) x=1.20m, y=2.28m and z=7.20m, and (V2) x=1.20m, y=2.28m and z=7.20m*

Figure 8.269 shows the curves for velocity profile along the x-direction. The curves follow an asymmetrical pattern and have several peaks, with the highest peak being at approximately 2.3m.

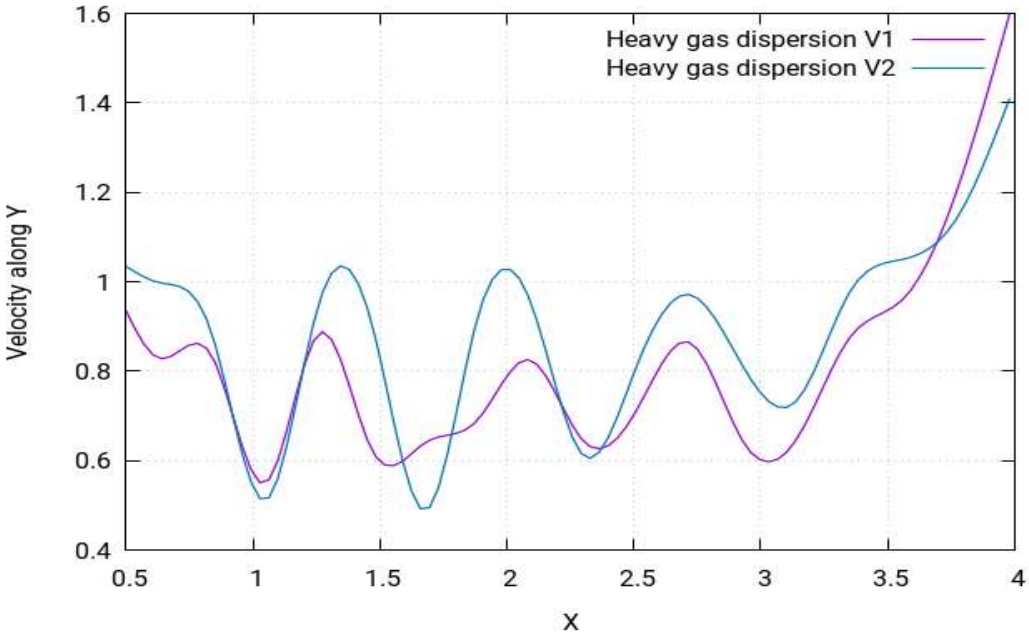

Figure 8.266: *Velocity of the heavy gas dispersion profile along the* ***y****-direction at different points of (V1) x=2.38m, y=-1m, z=8.50m (V2) x=2.38m, y=-1m and z=1.30m*

Figure 8.266 shows the curves for the velocity profile along the y-direction. The curves follow an asymmetrical pattern and have several peaks, with the highest peak being at approximately 1.3m.

At high speed, for the collocated arrangement of the spherical tank at a/the safe distance, the turbulence of the heavy gas is minimum, which is evident from the CFD results.

8.6.29 Location 2: Heavy gas dispersion for a safe distance

8.6.29.1 Structure of layout

The type of layout adopted for this case study for the collocated layout. A layout of 24 gas storage tanks will be created, with a spherical shape distribution for safe distance, and the release source will be placed in different positions. The behaviour of the gas clouds will then be studied.

8.6.29.2 Release source location

The release source point (2) was located at the middle front of the group of buildings in the 3rd column between the 2nd and 3rd rows from the bottom. The perimeters selected for this case study is stated below:

Table 8.43: *Parametric values for the high-speed heavy gas simulation (safe distance 2)*

Density	Flow Rate	Velocity	Ambient Temperature	Release Source Temperature
2.1 kg m/s^3	1 kg/s	1 m/s	25°C	-100°C

8.6.29.3 Concentration of the heavy gas dispersion for a/the safe distance

The following figure shows the concentration behaviour of the heavy gas at location 2. The whereabouts of location 2 has been stated at the beginning of the passage.

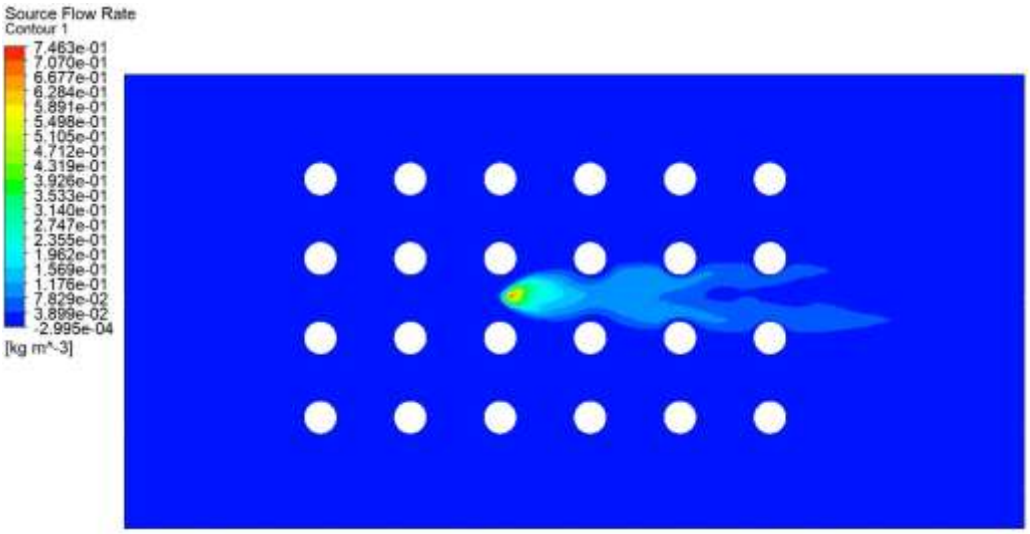

Figure 8.267: *Concentration profile of the heavy gas dispersion with the release source located at the middle front of the group of gas storage tanks in the 3rd column between the 2nd and 3rd rows from the bottom at* ***1m/s***

The concentration profile of the heavy gas at location 2 is shown in Figure 8.267 (above). It represents the concentration behaviour of the heavy gas when the release gas source is placed in the 3rd column between the 2nd and 3rd rows from the bottom. It can be seen in the above figure that the cloud shape in this case at one point looks like an elliptical sphere and the gas cloud does not try to swirl around the gas storage tanks, as that in spherical layouts, and at one point again makes a nozzle effect. The same effect was noticed in the previous case study, but the cloud size was larger than this one because, in that case, the release source was placed at the upwind front. Establishing a safe distance between the gas storage tanks and other factors, such as wind velocity and the change of obstacle, layouts play a key role in the shape of the clouds and the dispersion. For the release source located at the centre, the safe distance is solely dependent on the type of gas released and the type of storage tank layouts.

8.6.29.4 Iso-surfaces of the heavy gas dispersion for a/the safe distance

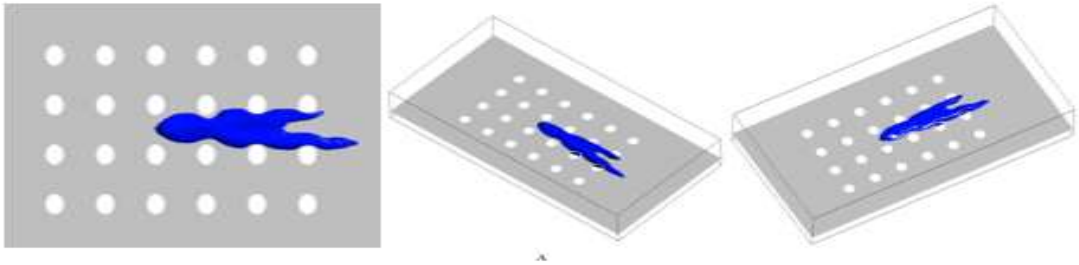

Figure 8.268: *Iso-surfaces of the concentration profile of the heavy gas dispersion with the release source located at the middle front of the group of gas storage tanks in the 3rd column between the 2nd and 3rd row from the bottom at* ***1m/s***

Figure 8.268 presents the iso-surfaces of the concentration profile of the heavy gas dispersion with the release source located at the middle front of the group of gas storage tanks in the 3rd column between the 2nd and 3rd row from the bottom. This helps identify the spread of the cloud in each dimension. It can be seen that the cloud shape is largely symmetrical and similar, and distribution is somewhat similar, as in the previous case.

According to Standard BS EN 60079-10-1:2009 [104], the following locations can be categorised:

High speed:

Zone 0: The area between the central rows starting from middle front

Zone 1: A partial inside area of the middle two rows of the building layout

Zone 2: All the remaining locations not categorised in zone 0 or zone 1

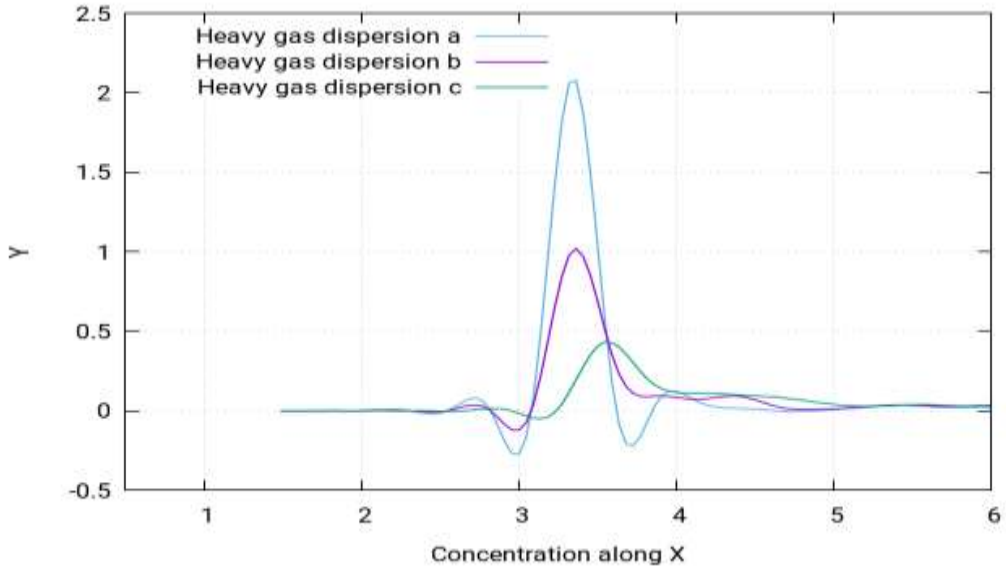

Figure 8.269: *Concentration of the heavy gas dispersion profile along the* ***x****-direction at different points of (a) x=1.50m, y=2.01m, z=7.20m (b) x=1.50m, y=2.01m, z=8.50m (b) x=1.50m, y=2.01m and z=1.60m*

Figure 8.269 shows two different curves for the concentration profiles. They show the pattern of the concentration profile along the x-direction when the wind speed for the simulation is 1m/s. The two different curves are obtained for two different distances from the release source. Both curves follow the same pattern but have different values due to difference in distances. From the figure, it is concluded that the concentration value of the heavy gas decreases as it moves away from the source. In the figure, the curve with the highest peak is obtained when nearest to the release source and vice versa.

8.6.29.5 Temperature of the heavy gas dispersion for a/the safe distance

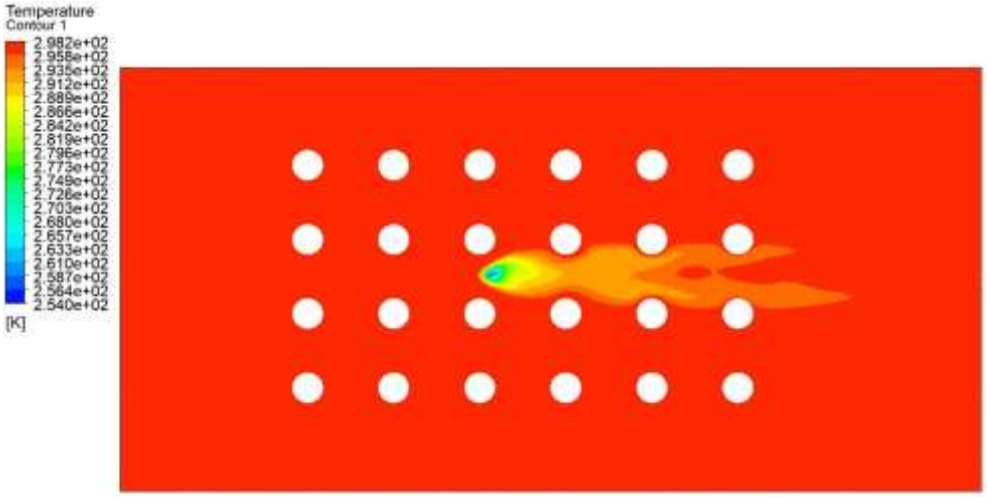

Figure 8.270: *Temperature profile of the heavy gas dispersion with the release source located at the middle front of the group of gas storage tanks in the 3rd column between the 2nd and 3rd rows from the bottom at 1m/s.*

Figure 8.274 shows the temperature simulation for this study. By visualising the temperature simulation, it is found out that the temperature simulation produces largely the same profile for the case study as that of the concentration profile. However, the behaviour of temperature is in fact the opposite to that of concentration. This means that the areas identified in the concentration simulation as highly concentrated will in fact have the lowest temperatures, while the ones with moderate concentrations will have moderate temperatures and the least concentrated areas will have the highest temperatures. To further simply these findings, it should be pointed out that the simulations showed that the concentrations near the release source point tend to be the highest and start to fade away as the gas cloud moves away from the source and are the lowest as the cloud moves much further away in the layout, eventually reaching the environment where the gas cloud disappears. However, the temperature is lowest near the release source point and tends to increase as the gas cloud moves away from the source, finally achieving its highest temperature equal to the ambient temperature of the environment.

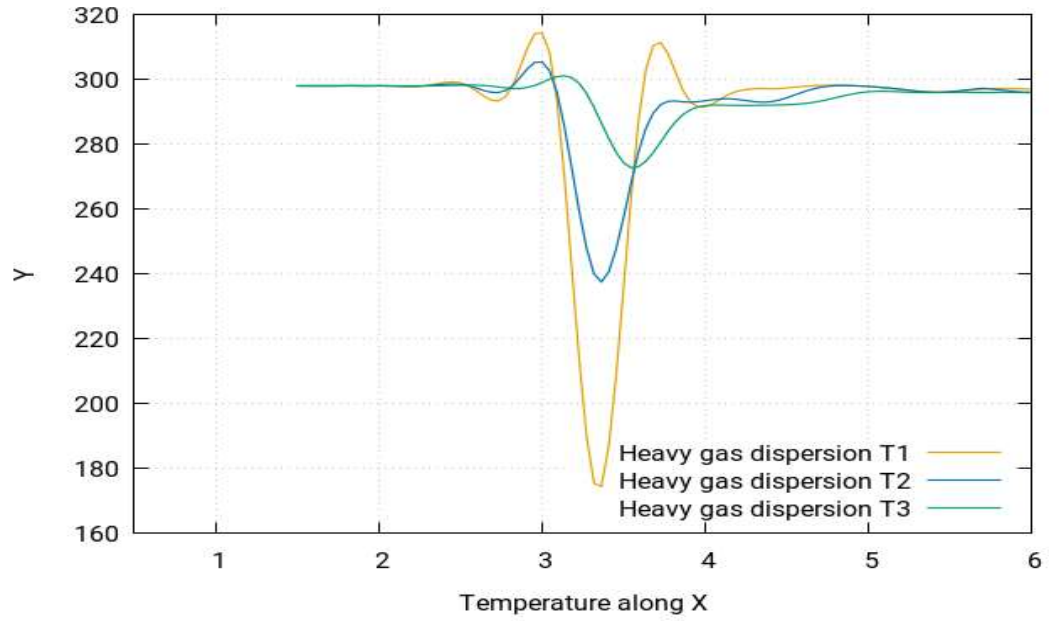

Figure 8.271: *Temperature of the heavy gas dispersion profile along the x-direction at different points of (T1) x=1.50m, y=2.01m, z=7.20m (T2) x=1.50m, y=2.01m, z=8.50m (T3) x=1.50m, y=2.01m, z=1.60m*

Figure 8.271 shows two different curves for the temperature profiles. They show the pattern of the temperature profile along the x-direction when the wind speed for the simulation is 1m/s. The two different curves are obtained for two different distances from the release source. These results show that, at a speed of 1m/s, temperature profiles are a mirror of concentration profile.

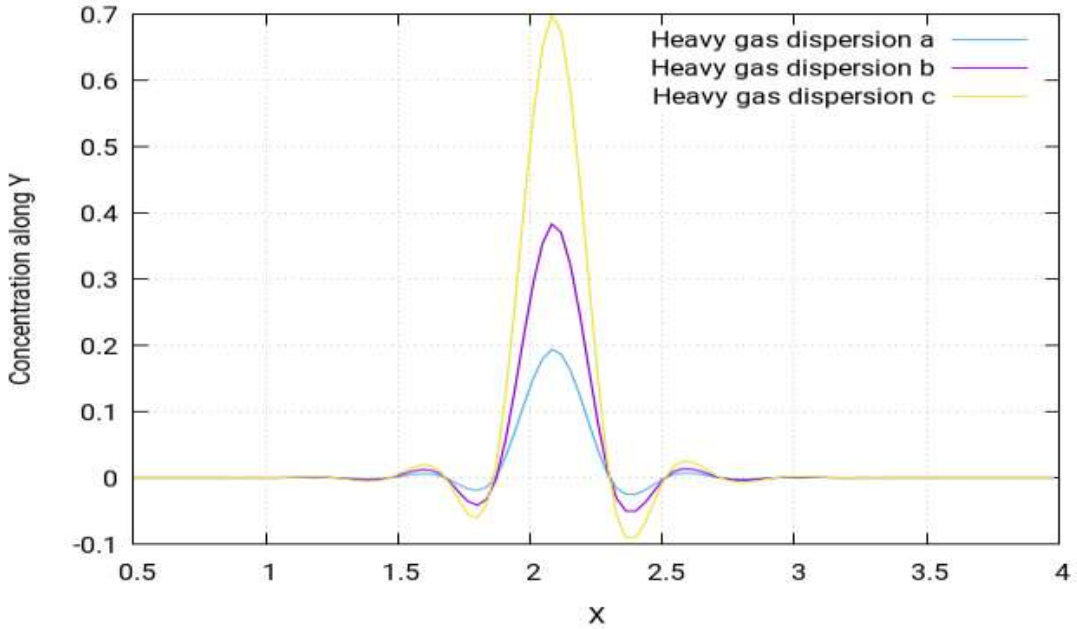

Figure 8.272: *Concentration of the heavy gas dispersion profile along the **y**-direction at different points of x=3.50m, y=-1m, z=2.50m (b) x=3.50m, y=-1m, z=8.50m (c) x=3.50m, y=-1m and z=1.60m*

The above figure shows the concentration profiles for three of the gas dispersions at three different locations along the y-direction depending on distance from release source. The curves follow the same pattern but have different values.

8.6.29.6 Velocity of the heavy gas dispersion for a/the safe distance

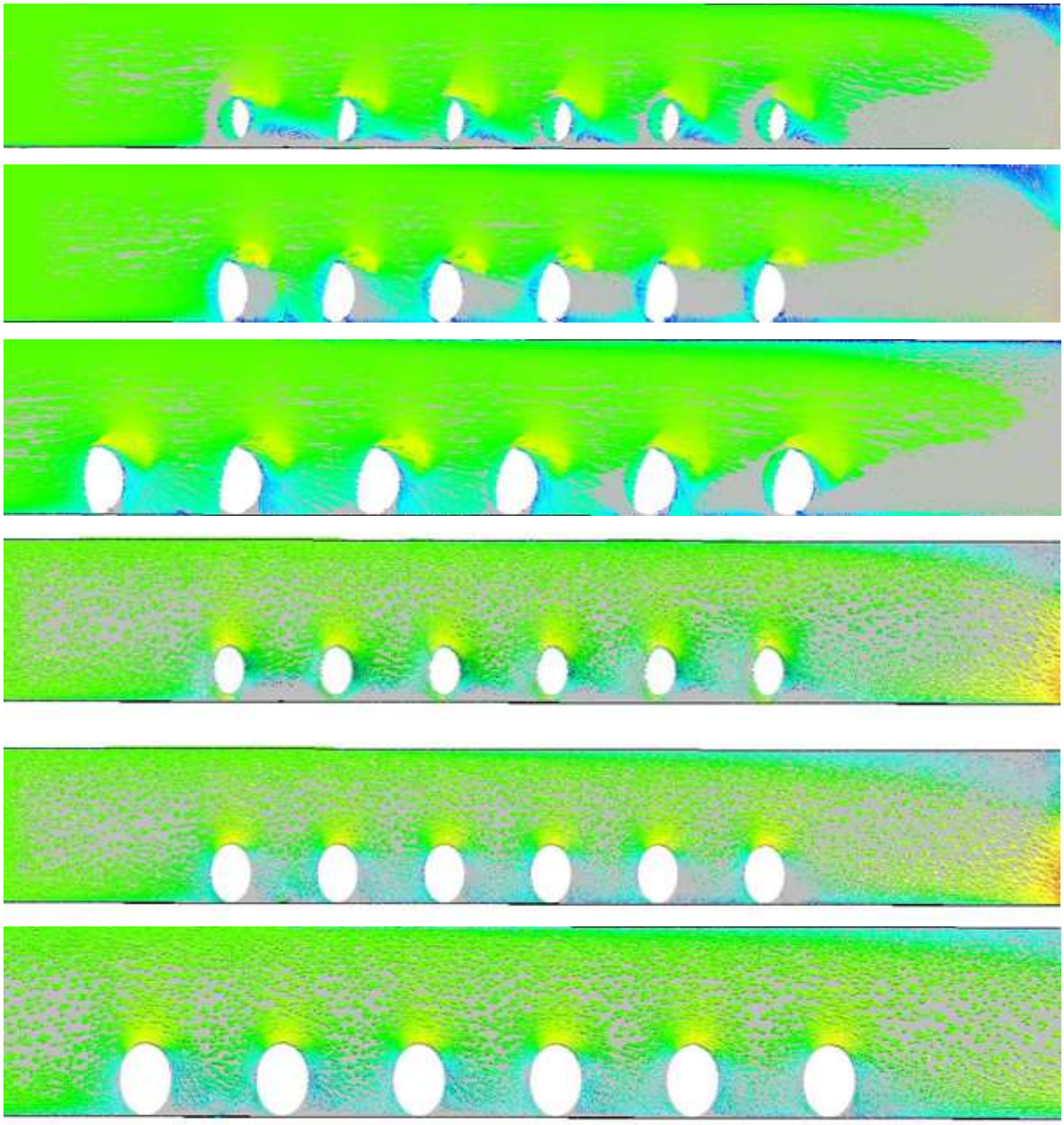

Figure 8.273: *Velocity contours of the heavy gas dispersion with the release source located at the middle front of the group of gas storage tanks in the 3rd column between the 2nd and 3rd rows from the bottom at* ***1m/s***

Figure 8.273 shows the velocity contours of the heavy gas dispersion for this case study with the release source located at the middle front of the group of gas storage tanks in the 3rd column between the 2nd and 3rd rows from the bottom. Velocity contours depict the intensity of wind -

or the effective wind influence - at the different locations throughout the layout. As can be seen in the figure, the wind intensity is different at different points in the layout. It is a commonly known effect that, with enhanced altitudes, enhanced wind speeds are encountered. This is because the objects at the lower altitudes create resistance to the wind flow. As resistance is caused by the gas storage tanks to the flow of gas towards the direction opposite of wind, the wind flowing from left to right fails to indict the same motion of flow. Instead, various complex vertexes are formed within the gas storage tanks near the release source location, as can be seen in Figure 8.273. The heavy gas release from the source is carried by these vertexes to the nearby mixture of the gas cloud, which then moves smoothly away from the source. Moreover, the hindrance to the wind flow caused by the gas storage tanks results in the vertexes moving in the upward direction, which enhances the shape of cloud in the upward direction.

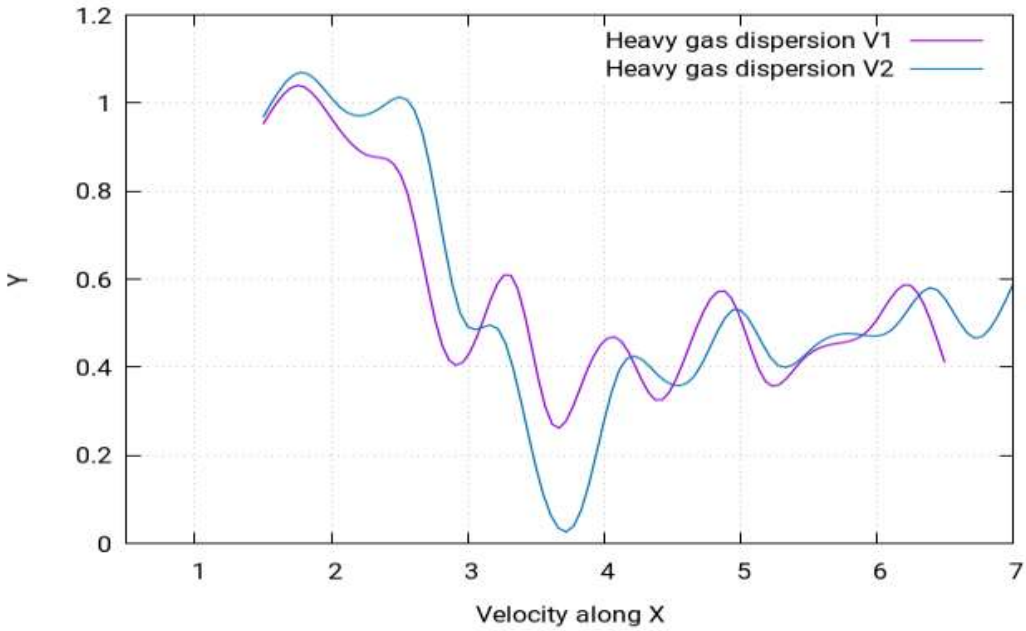

Figure 8.274: *Velocity of the heavy gas dispersion profile along the* ***x****-direction at different points of (V1) x=1.50m, y=2.01m, z=8.50m (V2) x=1.50m, y=2.01m and z=1.60m*

Figure 8.274 shows the curves for the velocity profile along the x-direction. The curves follow an asymmetrical pattern and have several peaks, with the highest peak being at approximately 3.7m.

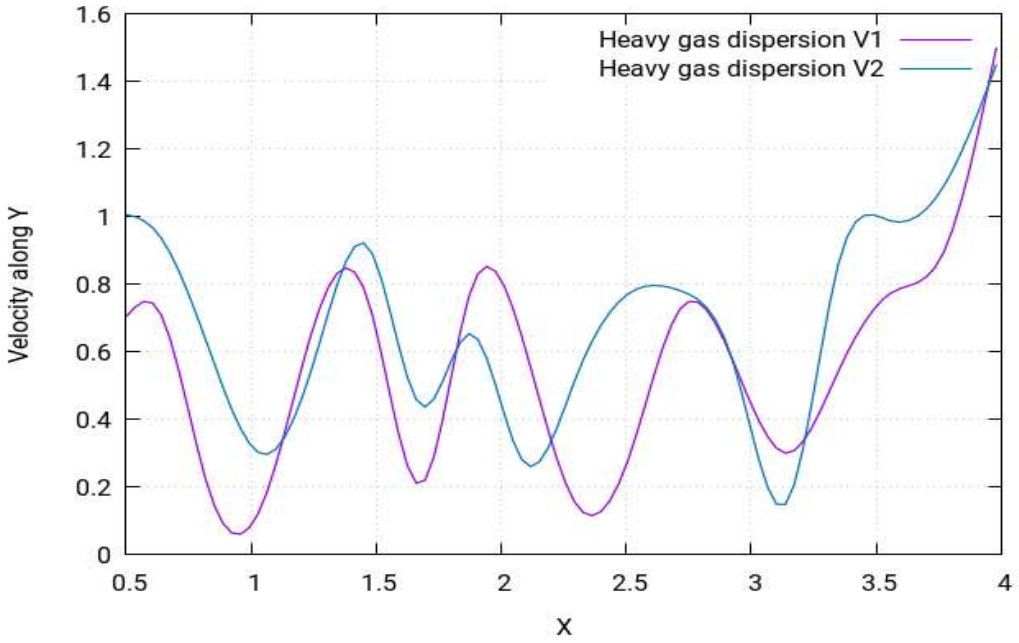

Figure 8.275: *Velocity of the heavy gas dispersion profile along the **y**-direction at different points of (V1) x=3.50m, y=-1m and z=7.20m, and (V2) x=3.50m, y=-1m and z=8.50m*

Figure 8.275 shows the curves for the velocity profile along the y-direction. The curves follow an asymmetrical pattern and have several peaks, with the highest peak being at approximately 3.5m.

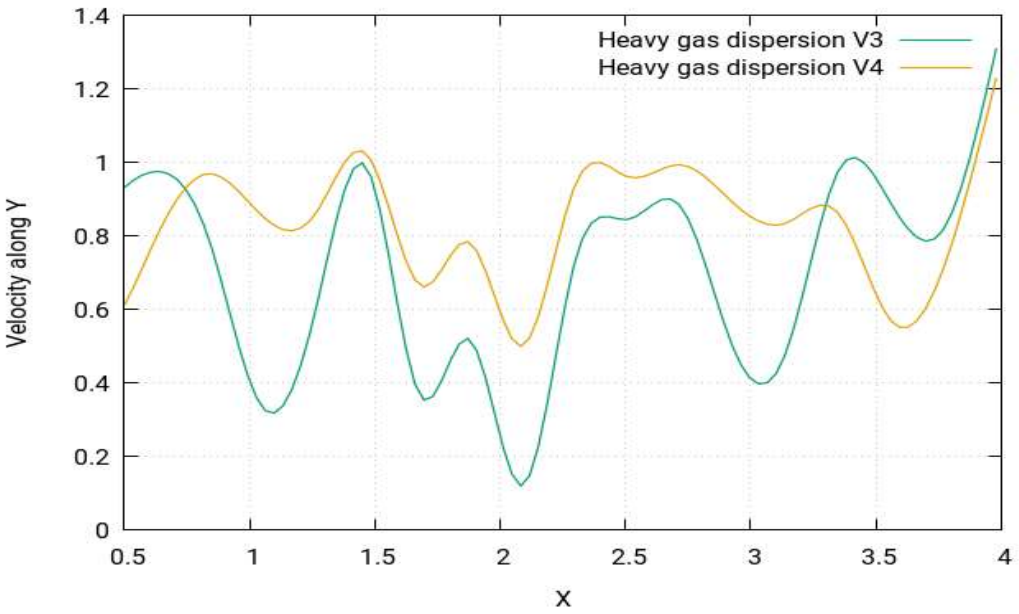

Figure 8.276: *Velocity of the heavy gas dispersion profile along the **y**-direction at different points of (V1) x=3.50m, y=-1m, z=1.60m (V2) x=3.50m, y=-1m and z=2.50m*

The above figure shows the velocity profiles for two of the gas dispersions at two different locations depending on distance from release source. Both curves follow the same pattern but have different values.

At high speeds, when the heavy gas is released at point 2 of the collocated arrangement of the spherical shaped tanks, the results show that the dispersion is maximum in the direction of the released source. This is because the velocity of the gas has caused the turbulence in that direction.

8.6.30 Location 1: Heavy gas dispersion

8.6.30.1 Structure of layout

The type of layout adopted for this case study for the staggered layout. A layout of 90 gas storage tanks will be created, with a spherical shape, and the release source will be placed in position. The behaviour of the gas clouds will then be studied.

8.6.30.2 Release source location

The release source point (1) was located at the upwind front of the gas storage tanks group in the 5th row. The perimeters selected for this case study is stated below:

Table 8.44: *Parametric values for the high-speed heavy gas simulation (location 1)*

Density	Flow Rate	Velocity	Ambient Temperature	Release Source Temperature
2.1 kg m/s^3	1 kg/s	1 m/s	25°C	-100°C

8.6.30.3 Concentration of the heavy gas dispersion

The following figure shows the concentration behaviour of the heavy gas at location 1. The whereabouts of location 1 has been stated at the beginning of the passage.

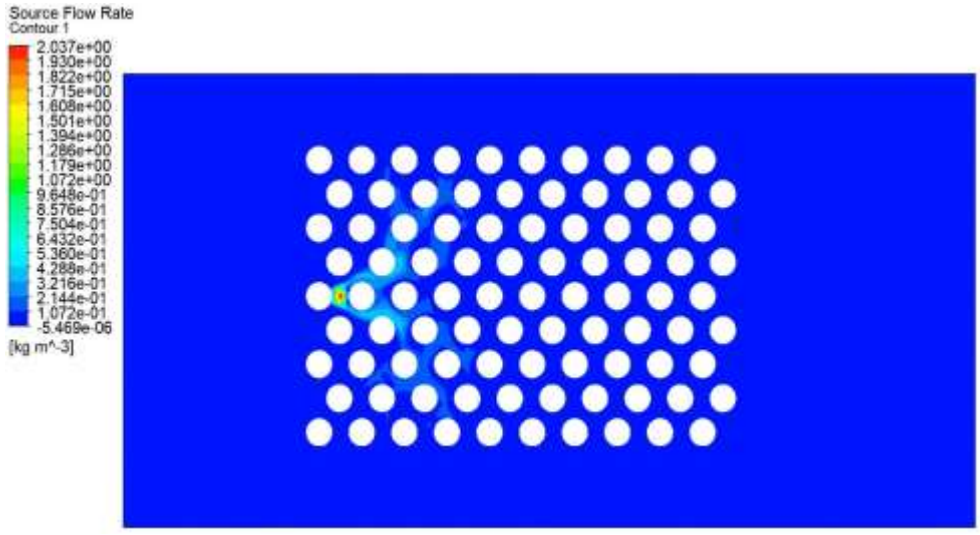

Figure 8.277**:** *Concentration profile of the Heavy Gas Dispersion with the release source at the upwind front of the group of gas storage tanks in the 5th row at* ***1m/s***

The concentration profile of the heavy gas at location 1 is shown in the above figure (Figure 8.277). It represents the concentration behaviour of the heavy gas when the release gas source is placed at the upwind front of the group of gas storage tanks in the 5th row. It can be seen that, for this particular case, the gas cloud tries to move more across the layout than along it. The release source is not exposed to air as it is placed behind the group of gas storage tanks. This explains why the cloud is not spread across a larger area of the building layout.

8.6.30.4 Iso-surface of the heavy gas dispersion

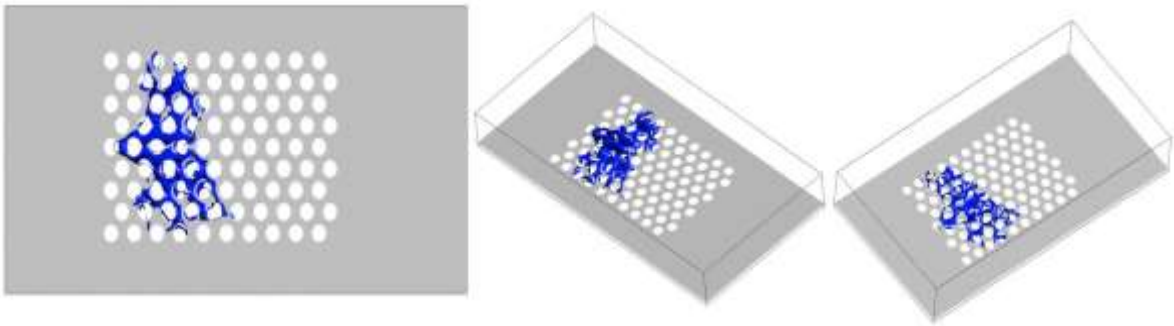

Figure 8.278: *Iso-surfaces of the concentration profile of the Heavy Gas Dispersion with release source at the upwind front of the group of gas storage tanks in the 5th row at* ***1m/s***

Figure 8.278 shows see the iso-surfaces of the concentration profile of the heavy gas dispersion with release source located at the upwind front of the group of gas storage tanks in the 5th row. This helps identify the spread of the cloud in each dimension. It can be seen that the cloud shape is largely symmetrical and that the cloud is not accumulated in on place but rather spread across most of the group of gas storage tanks at the upwind front of the layout.

According to Standard BS EN 60079-10-1:2009 [104], the following locations can be categorised:
High speed:

Zone 0: The central rows of the upwind front of the building layout

Zone 1: The extreme buildings of the upwind front of the building layout

Zone 2: All the remaining locations not categorised in zone 0 or zone 1

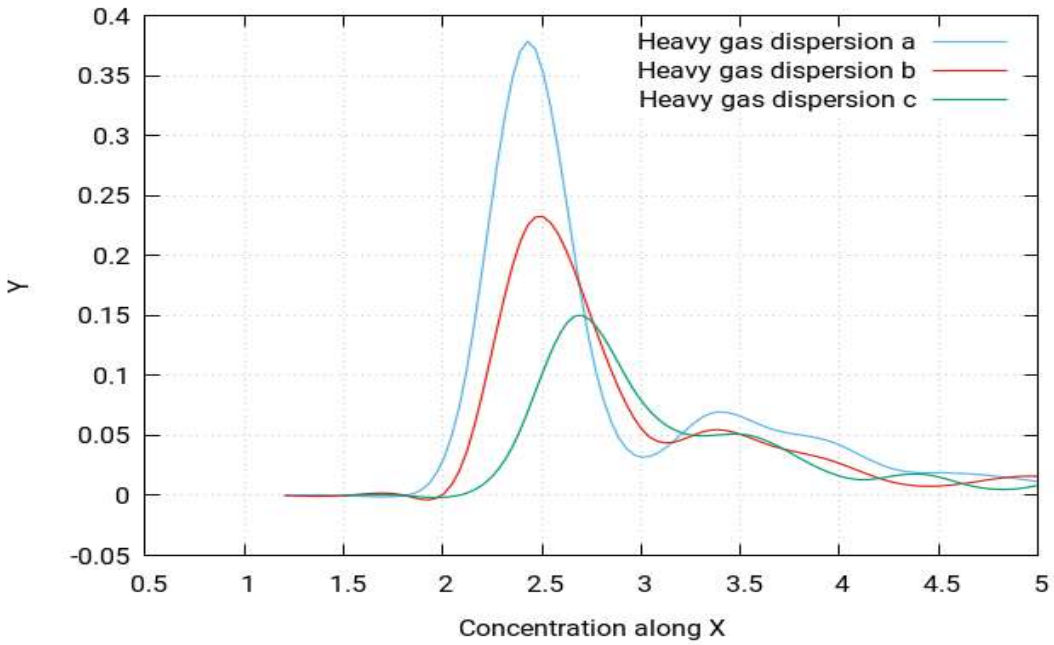

Figure 8.279: *Concentration of the heavy gas dispersion profile along the x-direction at different points of (a) x=1.20m, y=1.90m, z=8.50m (b) x=1.20m, y=1.90m, z=1.60m (c) x=1.50m, y=1.90m and z=2.20m*

Above, Figure 8.279 shows three different curves for the concentration profiles. They show the pattern of the concentration profile along the x-direction when the wind speed for the simulation is 1m/s. The three different curves are obtained for two different distances from the release source. The curves follow the same pattern but have different values due to difference in distances. From the figure, it is concluded that the concentration value of the heavy gas decreases as the cloud moves away from the source. In the figure, the curve with highest peak is obtained when nearest to the release source and vice versa.

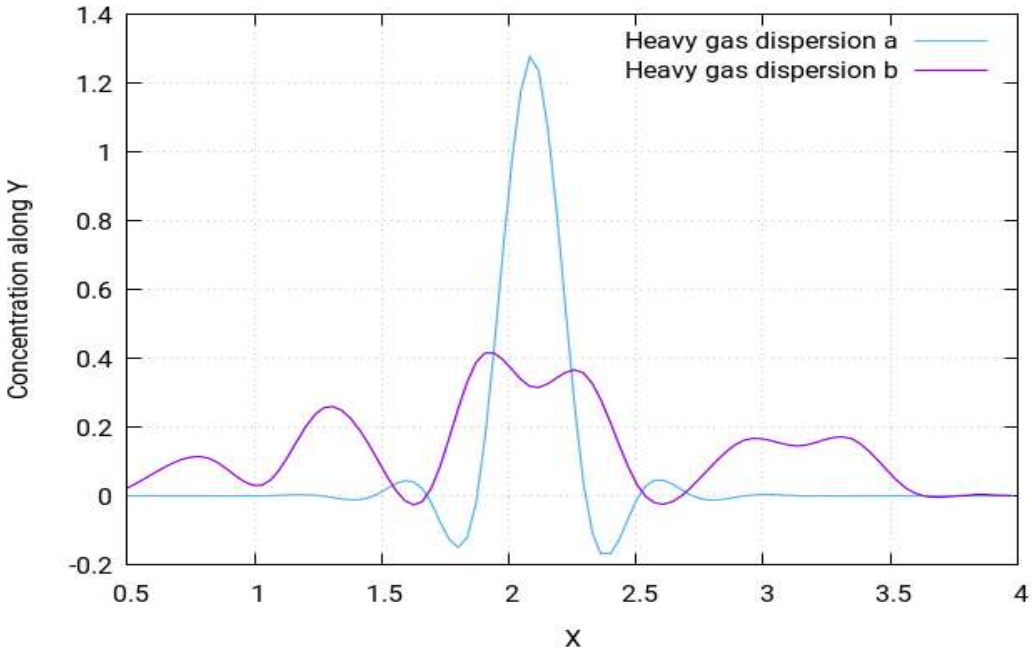

Figure 280: *Concentration of the heavy gas dispersion profile along the y-direction at different points of (a) x=2.04m, y=-1m, z=7.20m (b) x=2.44m, y=-1m and z=7.20m*

Figure 8.280 above shows two different curves for the concentration profiles. They show the pattern of the concentration profile along the y-direction when the wind speed for the simulation is 1m/s. The two different curves are obtained for two different distances from the release source. It is seen that along the y-direction, the profiles do not follow the same pattern, unlike the x-direction where they followed the same pattern. This is because the wind has a significant effect in the y-direction.

8.6.30.5 Temperature of the heavy gas dispersion

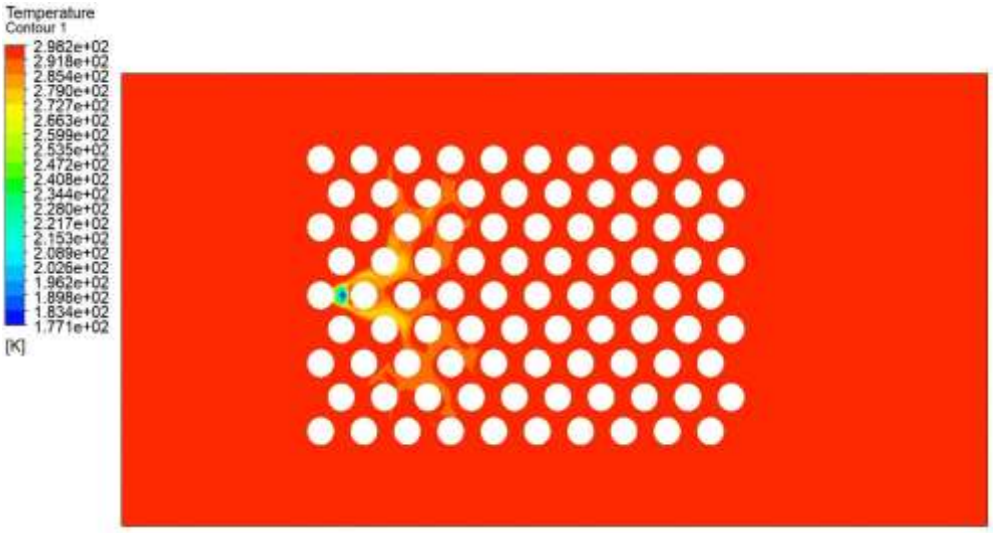

Figure 8.281: *Temperature profile of the heavy gas dispersion with the release source at the upwind front of the group of gas storage tanks in the 5th row at* ***1m/s***

Figure 8.281 shows the temperature simulation for this study. By visualising the temperature simulation, it is found out that the temperature simulation produces largely the same profile for the case study as that of the concentration profile. However, the behaviour of temperature is in fact the opposite to that of concentration. This means that the areas which were identified in the concentration simulation as the highly concentrated will in fact have the lowest temperatures, while the ones with moderate concentrations will have moderate temperatures and the least concentrated areas will have the maximum temperatures. To further simply these findings, it should be point out that the concentrations simulations showed that the concentrations near the release source point tend to be the highest and start to fade away as the gas cloud moves away from the source and are the lowest as the cloud moves much further away in the layout, eventually reaching the environment where the gas cloud disappears. However, the temperature is lowest near the release source point and tends to increase as the gas cloud moves away from the source, finally achieving its highest temperature equal to the ambient temperature of the environment.

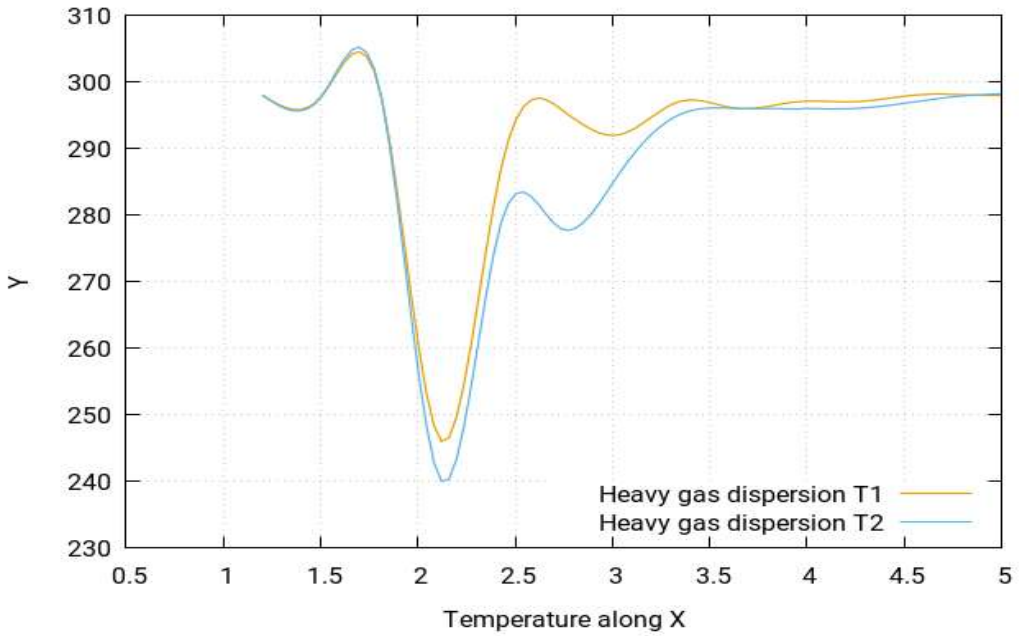

Figure 8.282: *Temperature of the heavy gas dispersion profile along the x-direction at different points of (T1) x=1.20m, y=2.04m, z=7.20m (T2) x=1.20m, y=1.90m and z=7.20m*

The above figure shows the temperature profiles for two of the gas dispersions at two different locations along the x-direction depending on distance from release source. Both curves follow the same pattern but have different values.

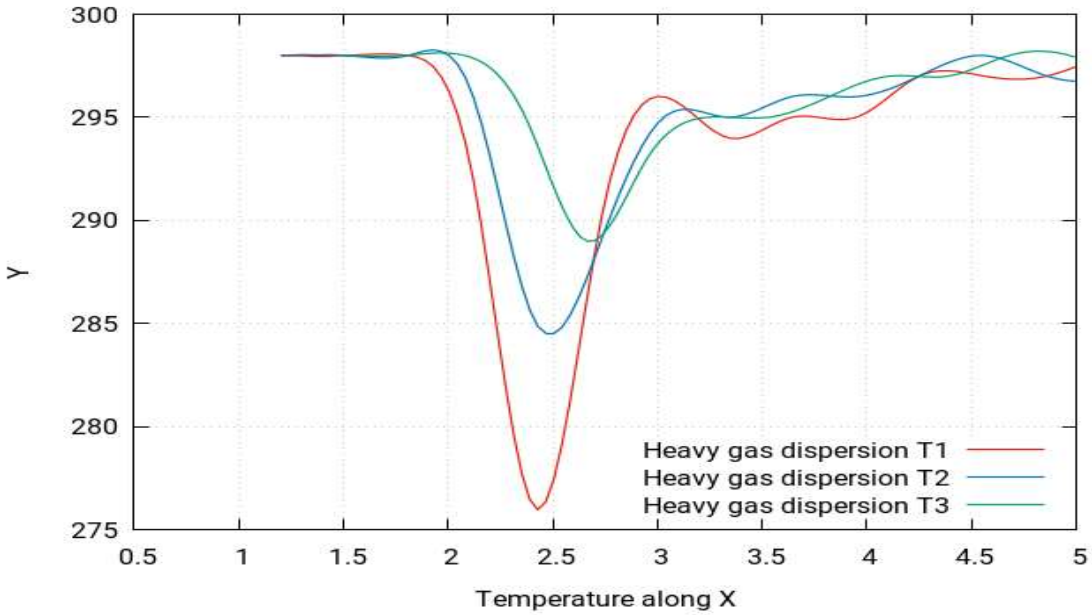

Figure 8.283: *Temperature of the heavy gas dispersion profile along the x-direction at different points of (T1) x=1.20m, y=1.90m, z=8.50m (T2) x=1.20m, y=1.90m, z=1.60m (T3) x=1.50m, y=1.90m and z=2.20m*

Figure 8.283 (above) presents three different curves for the temperature profiles. They show the pattern of the temperature profile along the x-direction when the wind speed for the simulation is 1m/s. The three different curves are obtained for three different distances from the release source. These results show that, at a speed of 1m/s, temperature profiles are a mirror of concentration profile.

8.6.30.6 Velocity of the heavy gas dispersion

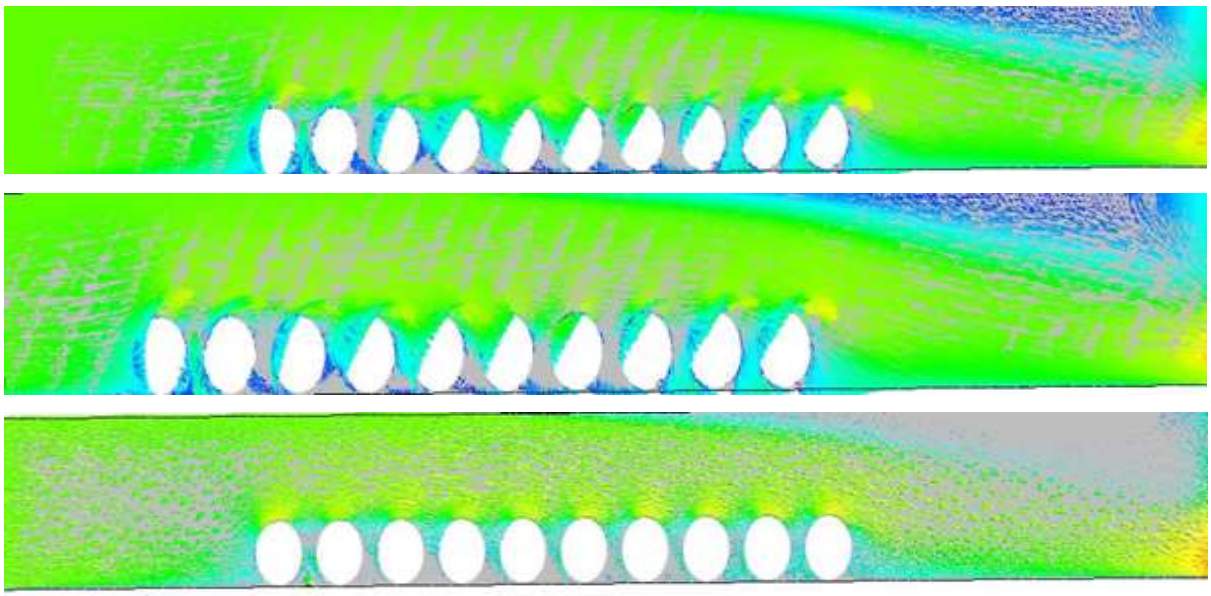

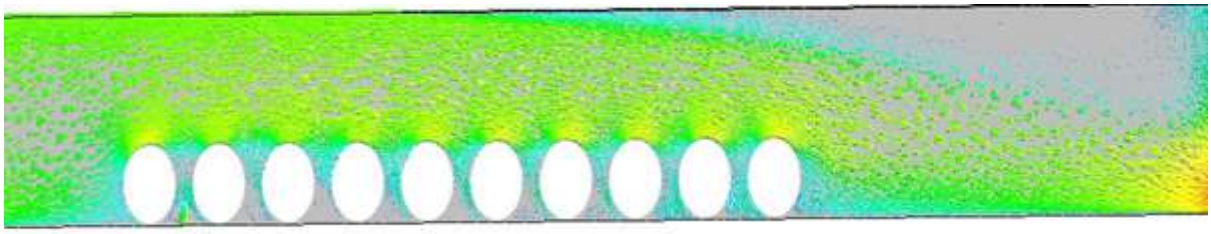

Figure 8.284: *Velocity contours of the heavy gas dispersion with the release source at the upwind front of the group of gas storage tanks in the 5th row at* ***1m/s***

Figure 8.284 shows the velocity contours of the heavy gas dispersion for this case study with release source at the upwind front of the group of gas storage tanks in the 5th row. Velocity contours depict the intensity of the wind - or the effective wind influence - at the different locations throughout the layout. As can be seen in the figure, the wind intensity is different at different points in the layout. It is a commonly known effect that, with enhanced altitudes, enhanced wind speeds are encountered. This is because the objects at the lower altitudes create resistance to the wind flow. As resistance is caused by the group of gas storage tanks to the flow of gas towards the direction opposite of wind, the wind flowing from left to right fails to indict the same motion of flow. Instead, various complex vertexes are formed within the group of gas storage tanks near the release source location, as can be seen in the (Figure 8.284). The heavy gas release from the source is carried by these vertexes to the nearby mixture of the gas cloud, which then moves smoothly away from the source. Moreover, the hindrance to the wind flow caused by the group of gas storage tanks results in the vertexes moving in the upward direction, which enhances the shape of cloud in the upward direction.

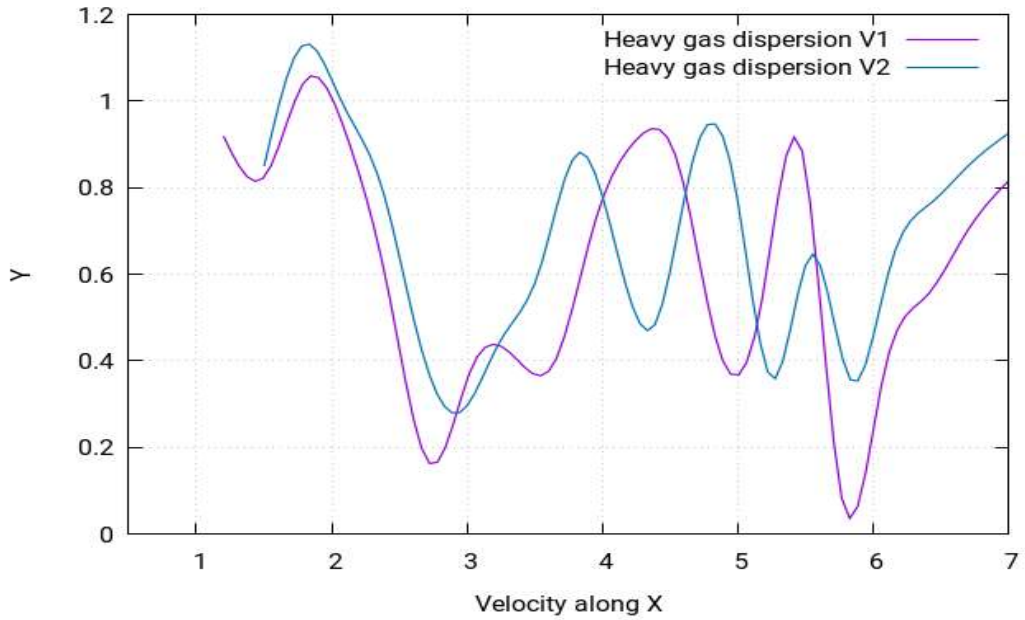

Figure 8.285: *Velocity of the heavy gas dispersion profile along the* ***x****-direction at different points of (V1) x=1.20m, y=1.90m, z=1.60m (V2) x=1.50m, y=1.90m and z=2.20m*

Figure 8.285 shows the curves for the velocity profile along the x-direction. The curves follow an asymmetrical pattern and have several peaks, with the highest peak being at approximately 1.8m.

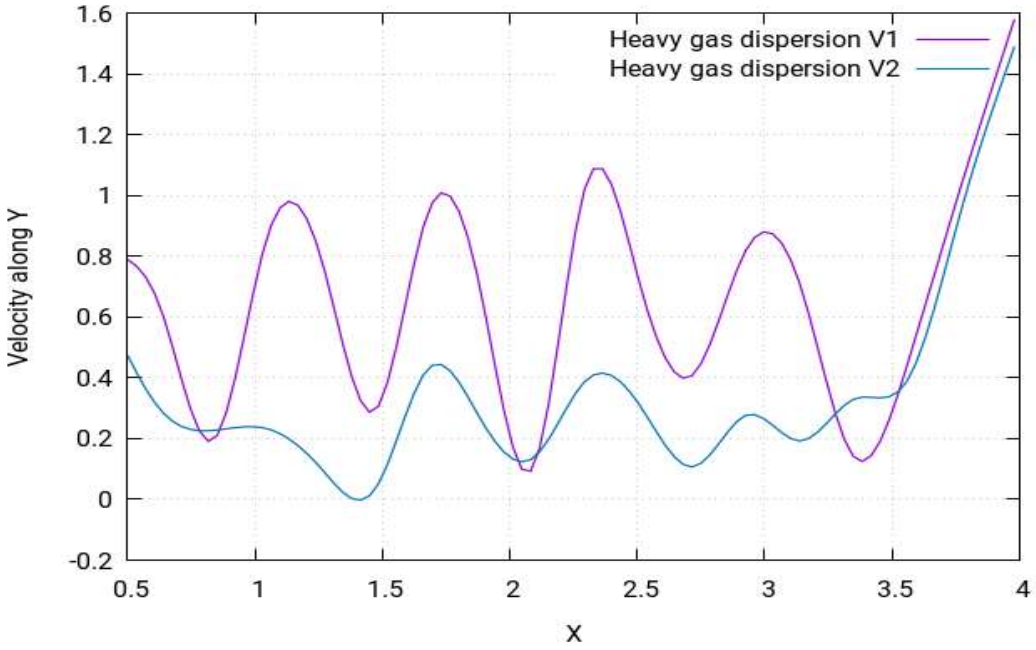

Figure 8.286: *Velocity of the heavy gas dispersion profile along the **y**-direction at different points of (V1) x=2.04m, y=-1m, z=7.20m (V2) x=2.44m, y=-1m and z=.20m*

The above figure shows the velocity profiles for two of the gas dispersions at two different locations depending on distance from release source. Both curves follow the same pattern but have different values.

At location 1 for the staggered arrangement of the spherical shaped obstacles, the dispersion shows high concentrations of the heavy gas around the obstacles near the source location. This is because of the increased resistance due to the staggered arrangement.

8.6.31 Location 1: Heavy gas dispersion for a safe distance

8.6.31.1 Structure of layout

The type of layout adopted for this case study the Staggered layout. A layout of 30 gas storage tanks will be created, with a spherical shape distribution for a/the safe distance, and the release source will be placed in a position. The behaviour of the gas clouds will then be studied.

8.6.31.2 Release source location

Release source point (1) is located at the upwind front of the group of gas storage tanks in the 3rd row. The perimeters selected for this case study are stated below:

Table 8.45: *Parametric values for the high-speed heavy gas simulation (location 1)*

Density	Flow Rate	Velocity	Ambient Temperature	Release Source Temperature
2.1 kg m/s^3	1 kg/s	1 m/s	25°C	-100°C

8.6.31.3 Concentration of the heavy gas dispersion for a/the safe distance

The following figure shows the concentration behaviour of the heavy gas at location 1. The whereabouts of location 1 has been stated at the beginning of the passage.

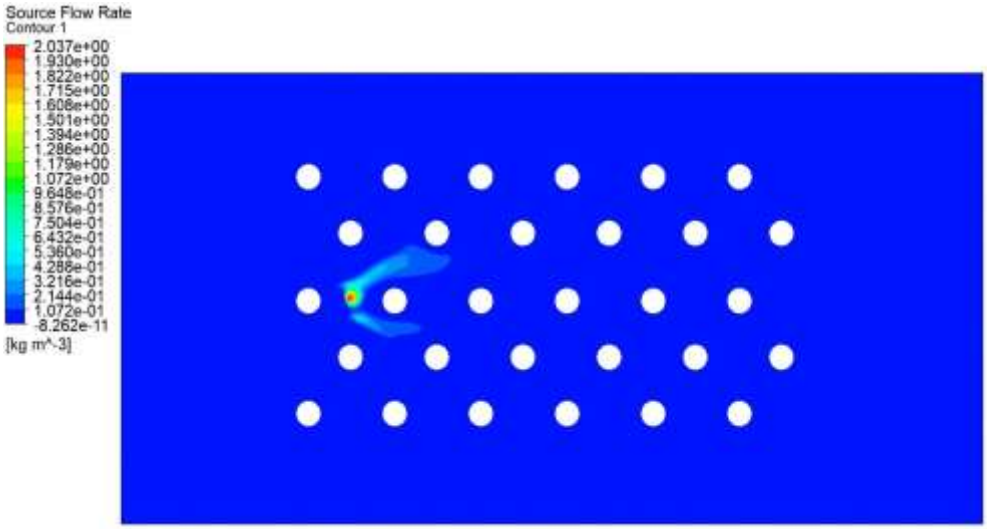

Figure 8.287: *Concentration profile of the heavy gas dispersion with the release source at the upwind front of the group of gas storage tanks in the 3rd row at* ***1m/s***

The concentration profile of the heavy gas at location 1 is shown above in Figure 8.287. It represents the concentration behaviour of the heavy gas when the release gas source is placed at the upwind front of the group of gas storage tanks in the 3rd row. It can be seen that for this particular case that the gas cloud is distributed in two small portions, with one being approximately twice the size of the other and moving at an angle towards the upper edge from the release source location, while the smaller cloud did the same towards the lower edge. The release source is not exposed to air as it is placed behind a building. This explains why the cloud is not spread across a larger area of the building layout.

8.6.31.4 Iso-surface of the heavy gas dispersion for a/the safe distance

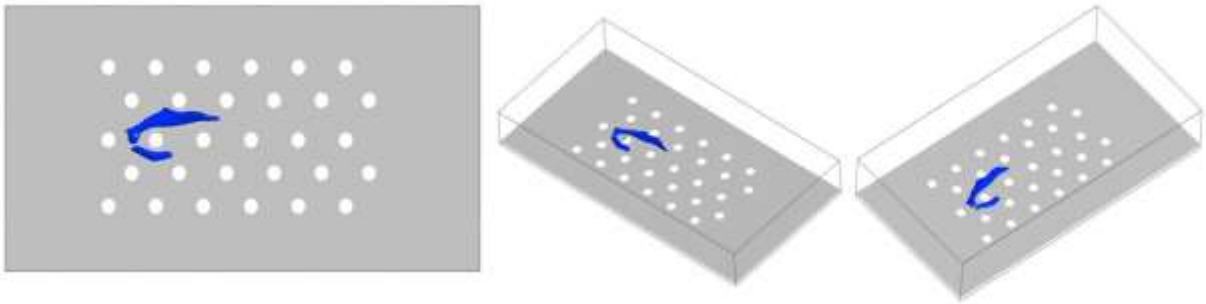

Figure 8.288: *Iso-surfaces of the concentration profile of the heavy gas dispersion with the release source at the upwind front of the group of gas storage tanks at the 5th row at* ***1m/s.***

Figure 8.288 presents the iso-surfaces of the concentration profile of the heavy gas dispersion with release source located at the upwind front of the group of gas storage tanks in the 3rd row. This helps identify the spread of the cloud in each dimension. It can be seen that the cloud shape is very small, and the cloud is not accumulated at one place.

The safe distance for a/the staggered arrangement of the spherical obstacles is dependent on the atmospheric conditions and the type of gases released.

According to Standard BS EN 60079-10-1:2009 [104], the following locations can be categorised:

High speed:

Zone 0: The central rows of the upwind front of the building layout

Zone 1: The extreme buildings at the upwind front of the building layout

Zone 2: All the remaining locations not categorised in zone 0 or zone 1

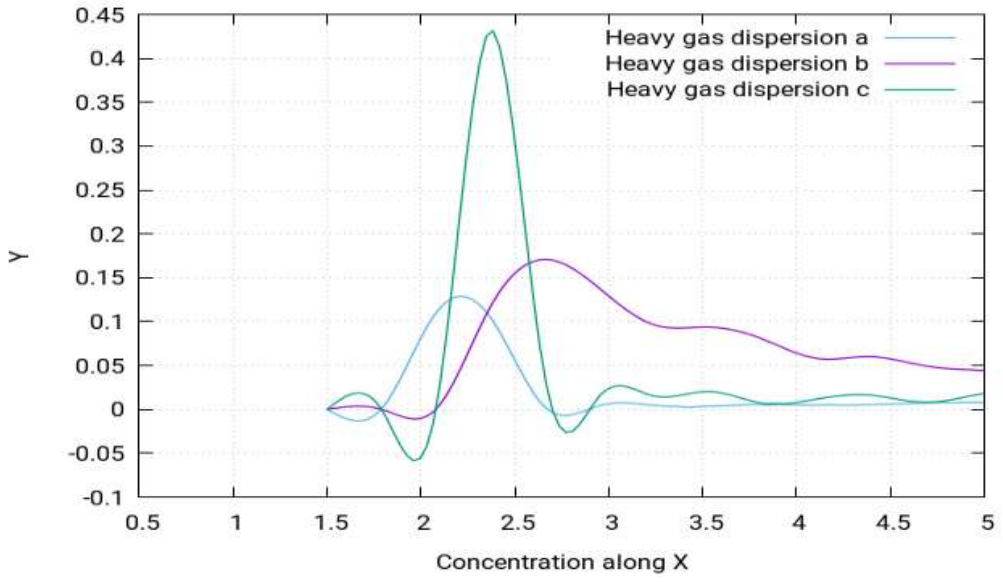

Figure 8.298: *Concentration of the heavy gas dispersion profile along the* ***x****-direction at different points of (a) x=1.50m, y=2.00m, z=7.20m (b) x=1.50m, y=2.25m, z=8.50m (c) x=1.50m, y=2.25m and z=7.20m*

Figure 8.289 shows the curves for the concentration profile along the x-direction. The curves follow an asymmetrical pattern and have several peaks, with the highest peak being at approximately 2.3m.

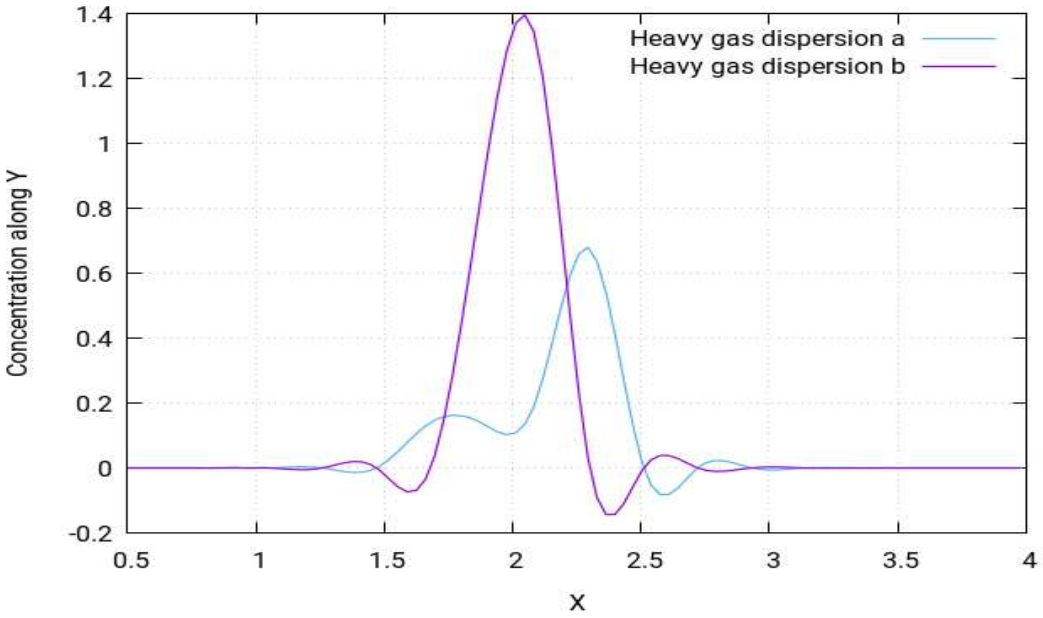

Figure 8.290: *Concentration of the heavy gas dispersion profile along the **y**-direction at different points of (a) x=2.35m, y=-1m, z=7.20m (b) x=2.13m, y=-1m and z=7.20m*

The above figure shows the concentration profiles for two of the gas dispersions at two different locations depending on distance from release source. Both curves follow the same pattern but have different values.

8.6.31.5 Temperature of the heavy gas dispersion for a/the safe distance

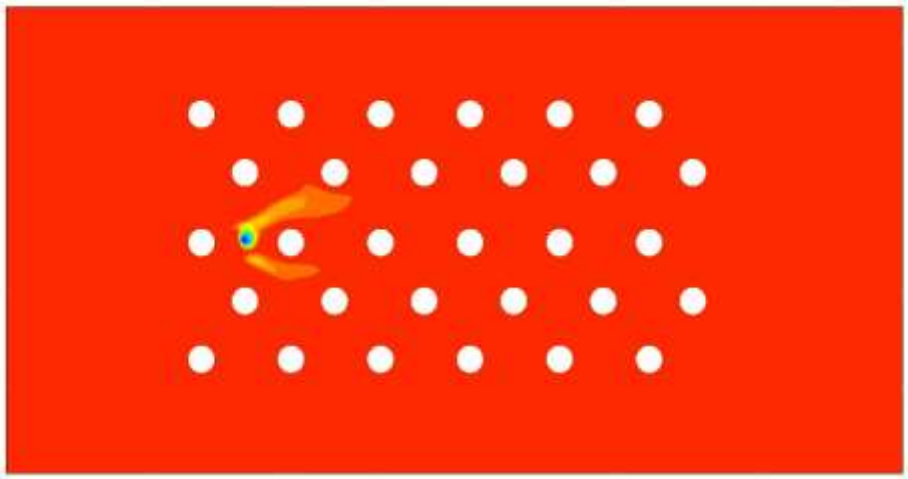

Figure 8.291: *Temperature profile of the heavy gas dispersion with the release source at the upwind front of the group of gas storage tanks in the 3rd row at **1m/s***

Figure 8.291 (above) shows the temperature simulation for this study. By visualising the temperature simulation, it is found out that the temperature simulation produces largely the same profile for the case study as that of the concentration profile. However, the behaviour of temperature is in fact the opposite to that of concentration. This means that the areas identified in the concentration simulation as highly concentrated will in fact have the lowest temperatures, while the ones with moderate concentrations will have moderate temperatures and the least concentrated areas will have the highest temperatures. To further simply these findings, it should be pointed out that the simulations show that the concentrations near the release source point tend to be the highest and start to fade away as the gas cloud moves away from the source and are the lowest as the cloud moves much further away in the layout, eventually reaching the environment where the gas cloud disappears. However, the temperature is lowest near the release source point and tends to increase as the gas cloud moves away from the source, finally achieving its highest temperature equal to the ambient temperature of the environment.

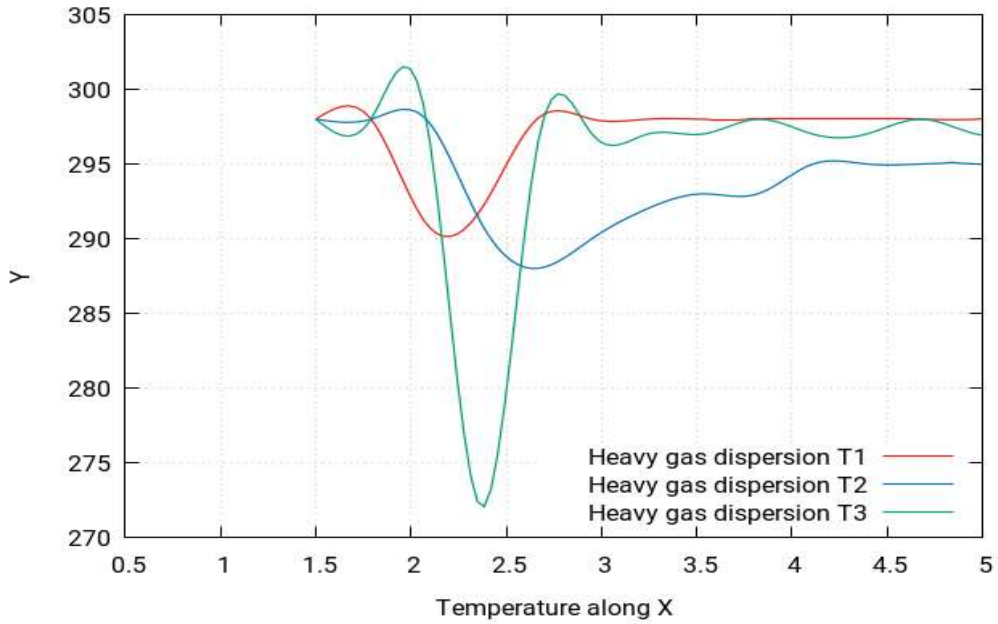

Figure 8.292: *Temperature of the heavy gas dispersion profile along the **x**-direction at different points of (T1) x=1.50m, y=2.00m, z=7.20m (T2) x=1.20m, y=2.28m, z=7.20m (T3) x=1.50m, y=2.25m and z=7.20m*

Above, Figure 8.292 presents three different curves for the temperature profiles. They show the pattern of the temperature profile along the x-direction when the wind speed for the simulation is 1m/s. The three different curves are obtained for three different distances from the release source. These results show that at a speed of 1m/s, temperature profiles are a mirror of concentration profile.

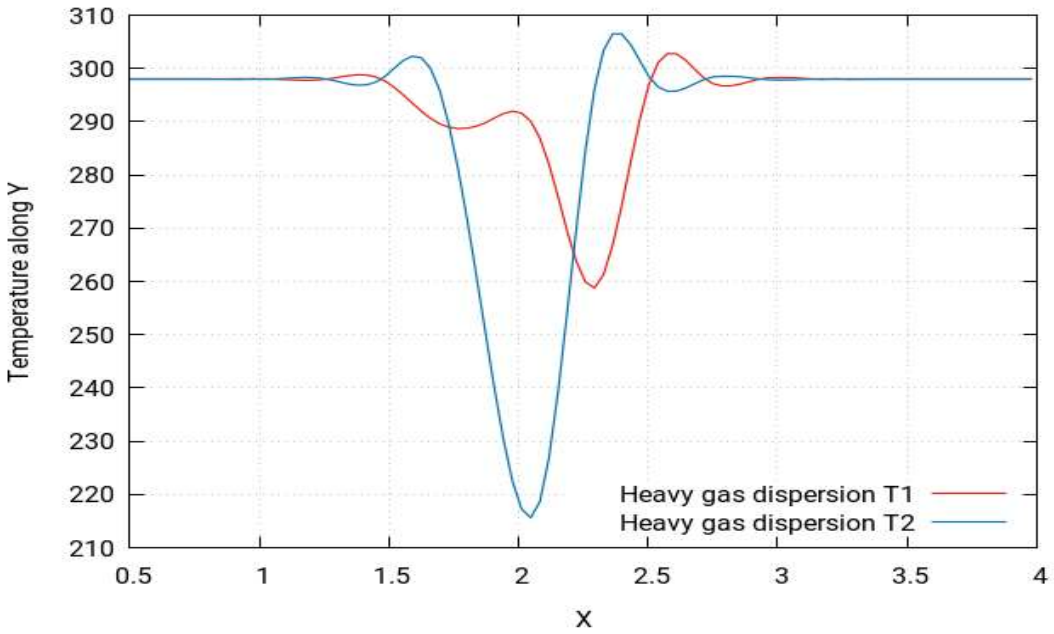

Figure 8.293: *Temperature of the heavy gas dispersion profile along the* ***y****-direction at different points of (T1) x=2.35m, y=-1m, z=7.20m (T2) x=2.13m, y=-1m and z=7.20m*

Figure 8.293 presents three different curves for the temperature profiles. They show the pattern of the temperature profile along the y-direction when the wind speed for the simulation is 1m/s. The three different curves are obtained for three different distances from the release source. These results show that, at a speed of 1m/s, temperature profiles are a mirror of concentration profile.

8.6.31.6 Velocity of the heavy gas dispersion for a/the safe distance

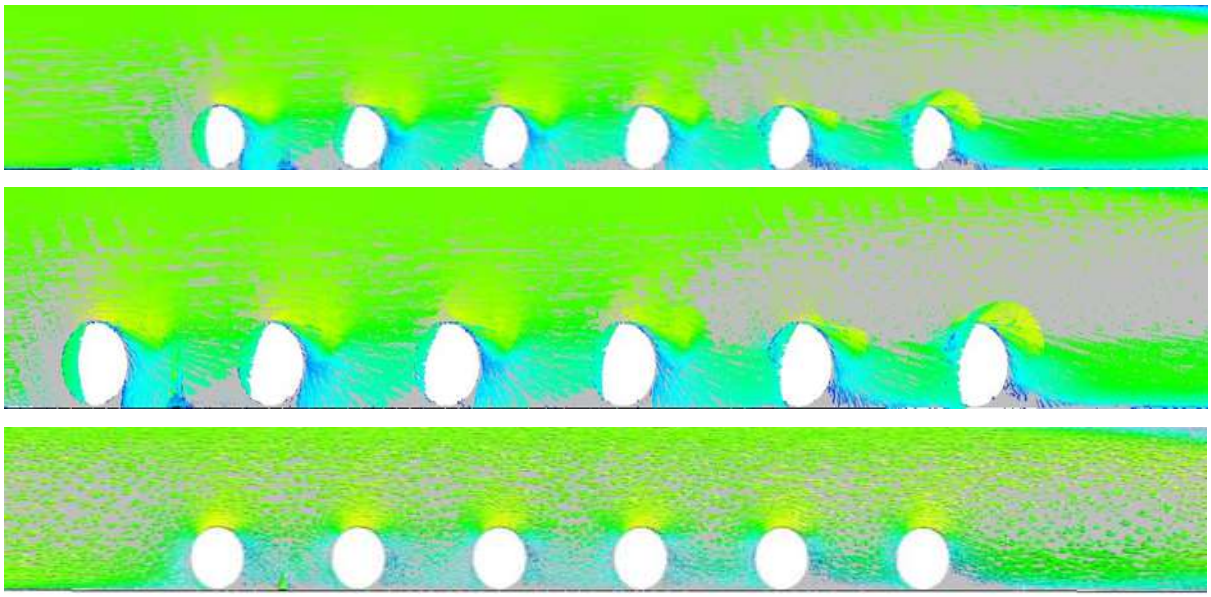

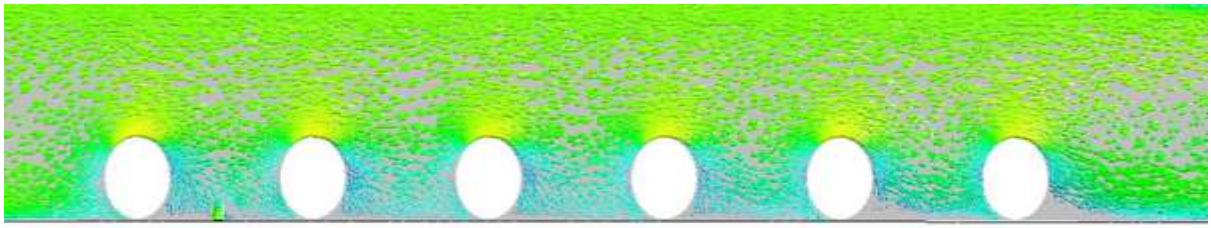

Figure 8.294: *Velocity contours of the heavy gas dispersion with the release source at the upwind front of the group of gas storage tanks in the 3rd row at* ***1m/s***

Figure 8.294 shows the velocity contours of heavy gas dispersion for this case study with the release source at the upwind front of the group of gas storage tanks in the 3rd row. Velocity contours depict the intensity of wind - or the effective wind influence - at the different locations throughout the layout. As can be seen in the figure, the wind intensity is different at different points in the layout. It is a commonly known effect that, with enhanced altitudes, enhanced wind speeds are encountered. This is because the objects at the lower altitudes create resistance to the wind flow. As resistance is caused by the buildings to the flow of gas towards the direction opposite of wind, the wind flowing from left to right fails to indict the same motion of flow. Instead, various complex vertexes are formed within the buildings near the release source location, as can be seen in Figure 8.294. The heavy gas release from the source is carried by these vertexes to the nearby mixture of the gas cloud, which then moves smoothly away from the source. Moreover, the hindrance to the wind flow caused by the buildings results in the vertexes moving in the upward direction, which enhances the shape of cloud in the upward direction.

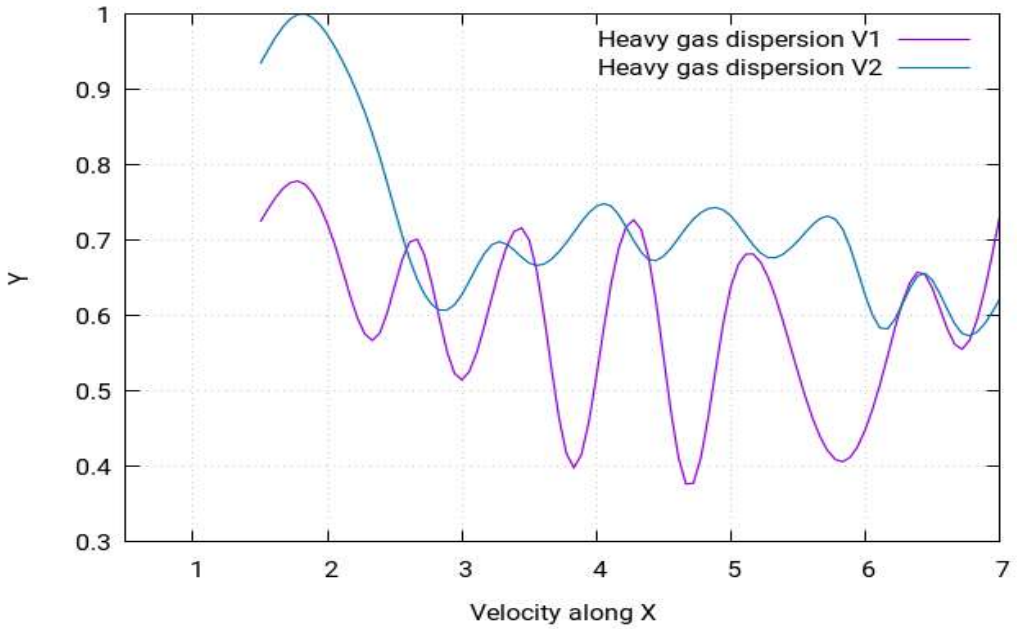

Figure 8.295: *Concentration of the heavy gas dispersion profile along the* ***x****-direction at different points of (V1) x=1.50m, y=2.25m, z=7.20m (V2) x=1.50m, y=2.25m and z=8.50m*

Figure 8.295 shows the curves for the velocity profile along the x-direction. The curves follow an asymmetrical pattern and have several peaks, with the highest peak being at approximately 1.8m.

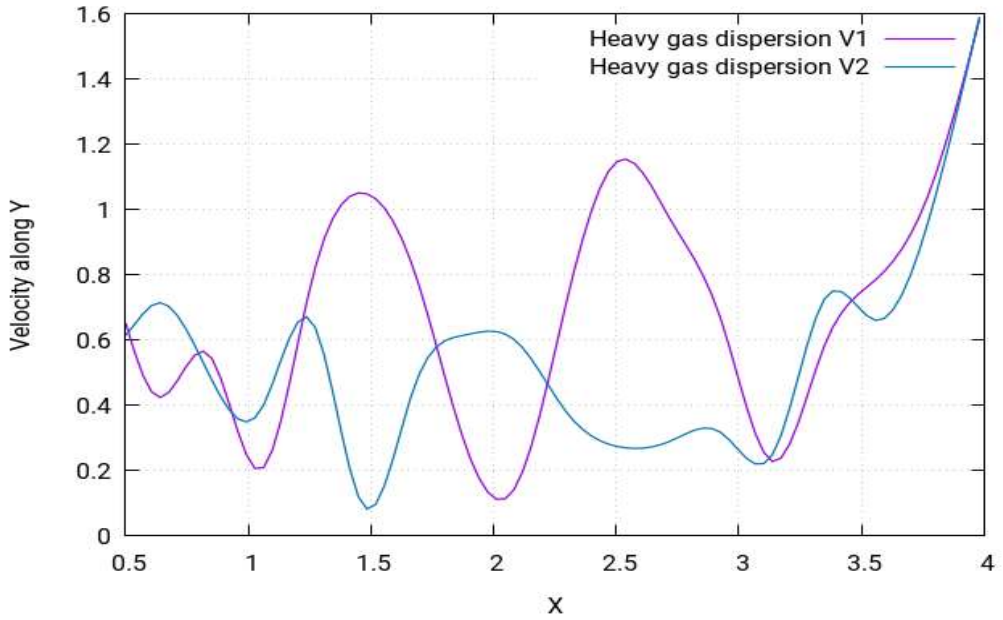

Figure 8.296: *Velocity of the heavy gas dispersion profile along the* ***y****-direction at different points of (V1) x=2.13m, y=-1m, z=7.20m (V2) x=2.35m, y=-1m and z=7.20m*

Figure 8.296 shows the curves for the velocity profile along the x-direction. The curves follow an asymmetrical pattern and have several peaks, with the highest peak being at approximately 1.8m.

Similarly, in this case, the turbulence of the heavy gas in the direction of the release has caused the high concentration around the obstacles closest to the release source.

8.7 Effect of different parameters

In this research, every effort was made to vary the values of different parameters and the behaviour of the dispersion of both heavy and neutral gas was analysed according to that. The effects produced by the difference of those perimeters are discussed below.

8.7.1 Effect of wind speed

Below, Figure 8.297 shows the results of the simulation produced at two different wind speeds.

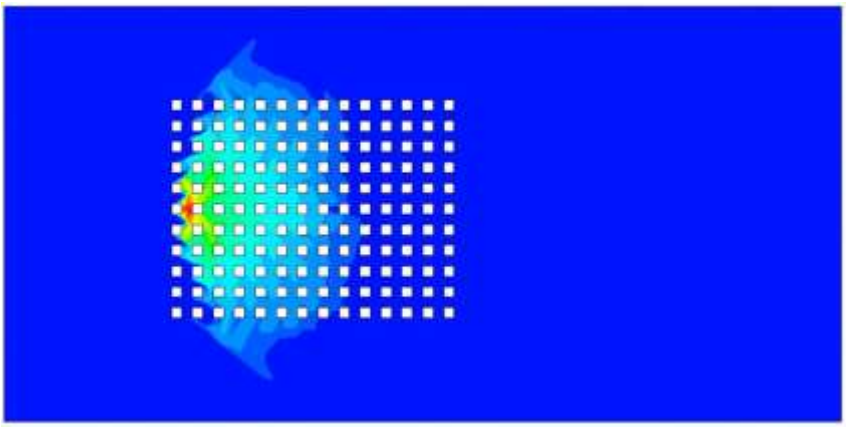

Figure 8.297: (a) *Simulation results at 1m/s*

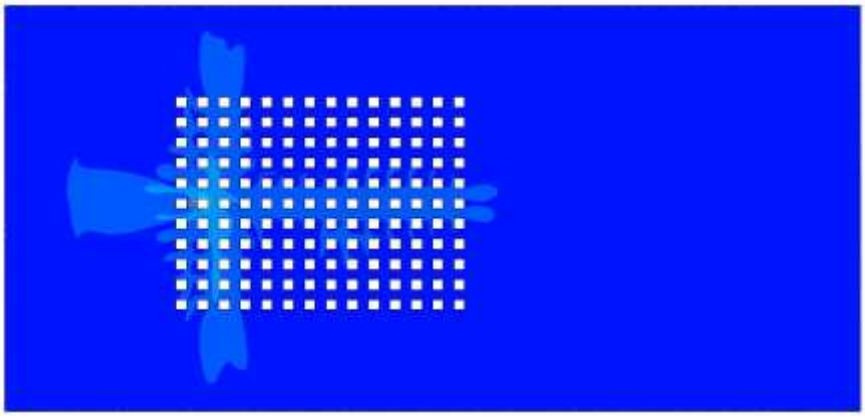

(b) *Simulation results at 0.25m/s*

Above, Figures (a) and (b) show two very different cloud shapes for wind speeds of 1m/s and 0.25m/s respectively. It is known that wind tends to increase the length of the cloud along its direction. It is also known that the effect of wind is more in the upward direction; therefore, the high winds of 1m/s enhance the cloud shape in the upward direction, as can be seen in Figure (a). On the other hand, the low speeds of 0.25m/s could not enhance the cloud shape in the upward direction. As a result, the cloud length is enhanced in the horizontal direction.

8.7.2 Effect of flow rate

The gas dispersions and cloud shape are also affected by the flow rate value. The following figures show the results of two simulations produced at two different flow rates of 1kg/s and 5kg/s.

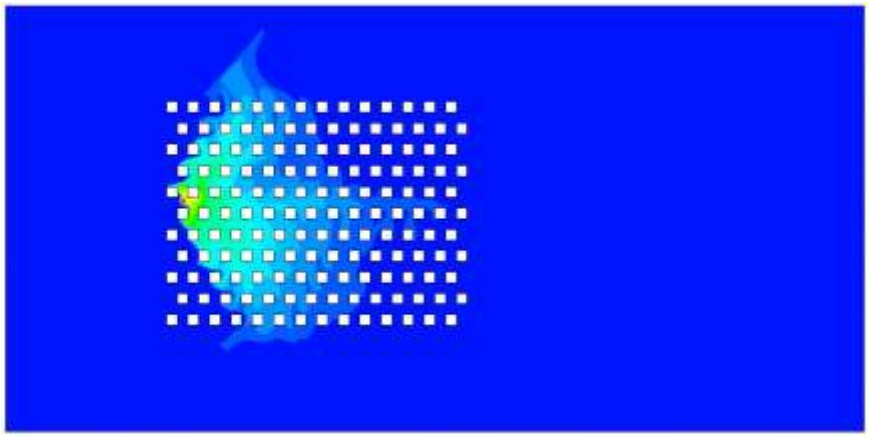

Figure 8.298: (a) *Simulation results at a flow rate of 1kg/s*

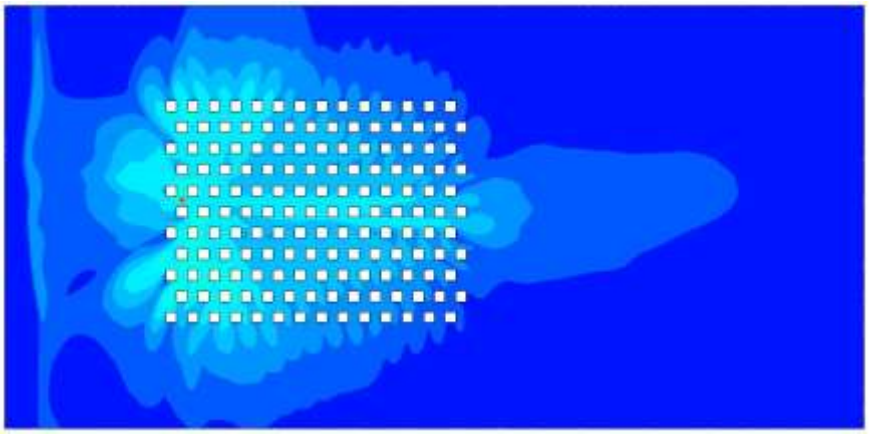

(b) *Simulation results at a flow rate of 5kg/s*

Both simulations were performed for staggered layouts of the buildings. As can be seen from the figure, the cloud dispersions at a higher flow rate of 5kg/s, as shown in Figure (b), are significantly more spread out compared to the cloud dispersions at the lower flow rate of 1kg/s shown in Figure (a). This could be because, at a lower flow rate of 1kg/s, the gas clouds move slowly and therefore settle in places near the release source location. However, the gas clouds at flow rates of 5kg/s move significantly faster and thereby tend to travel greater distances. This is why the cloud dispersions at the higher flow rate are more spread as compared to those of the lower flow rate.

8.7.3 Effect of density

In the present work, two types of gases have been used: one with a heavy gas density of 2.1 kg m/s^3 and the other being the neutral gas density of 1.1839 kg m/s^3. To determine the effect of the difference in density, the following iso-surfaces of two different density gases are shown.

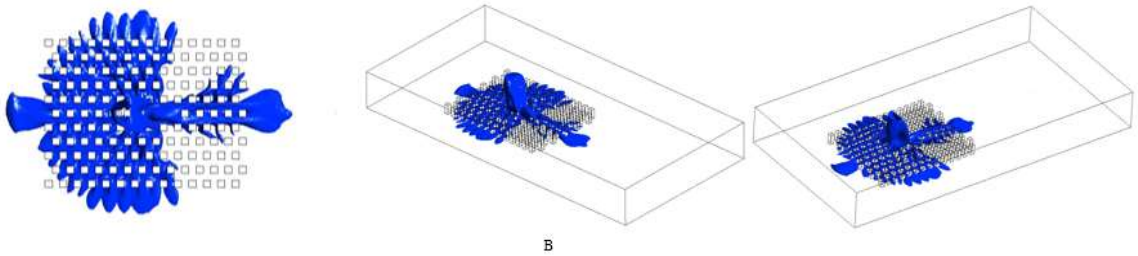

Figure 8.299: (a) *Iso-surfaces of a heavy gas density of 2.1 kg m/s^3*

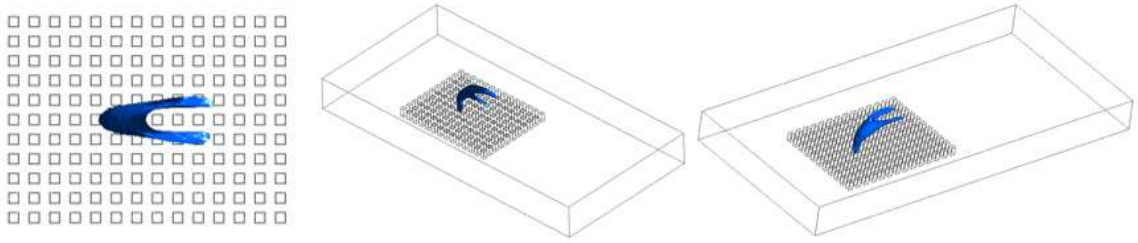

(b) Iso-surfaces of a neutral gas density of 1.1839 kg m/s^3

As can be seen from the iso-surfaces, the results of the concentrations for the heavy gas presented in (a) show that the concentration is higher near the ground, while Figure (b) shows the opposite results where the concentrations tend to move rapidly towards the upward direction. Hence, the heavy gas concentrations tend to present a greater health hazard as, if they are at ground level for a long time and make gas clouds, any high-temperature object could ignite a fire. Even if it does not catch fire, the heavy clouds present in the environment are dangerous for health.

8.7.4 Effect of temperature

The effect of temperature is actually opposite to that of concentration. Where the concentration is highest, the temperature will be lowest and vice versa. This is demonstrated in Figure 8.304 below:

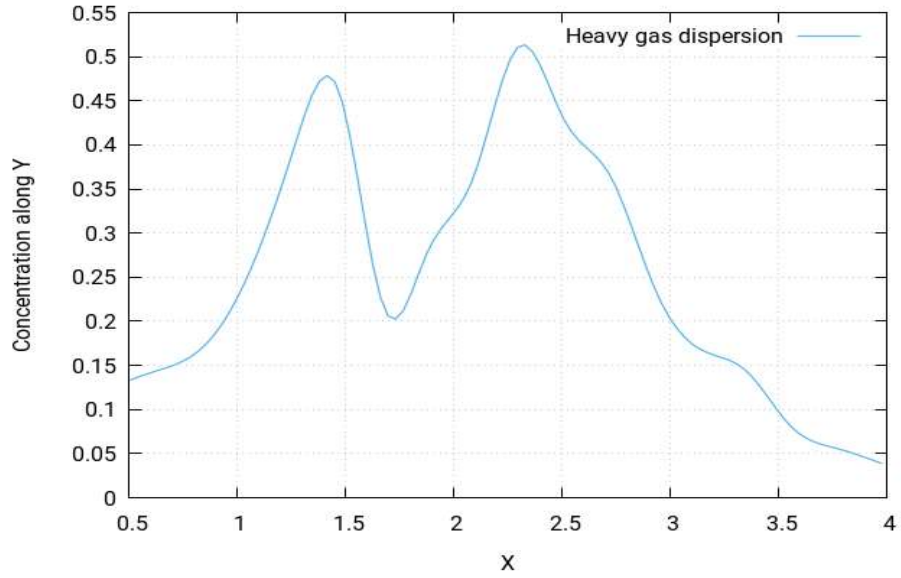

Figure 8.300: (a) *Graphical results for the concentration profile of heavy gas along the y-direction*

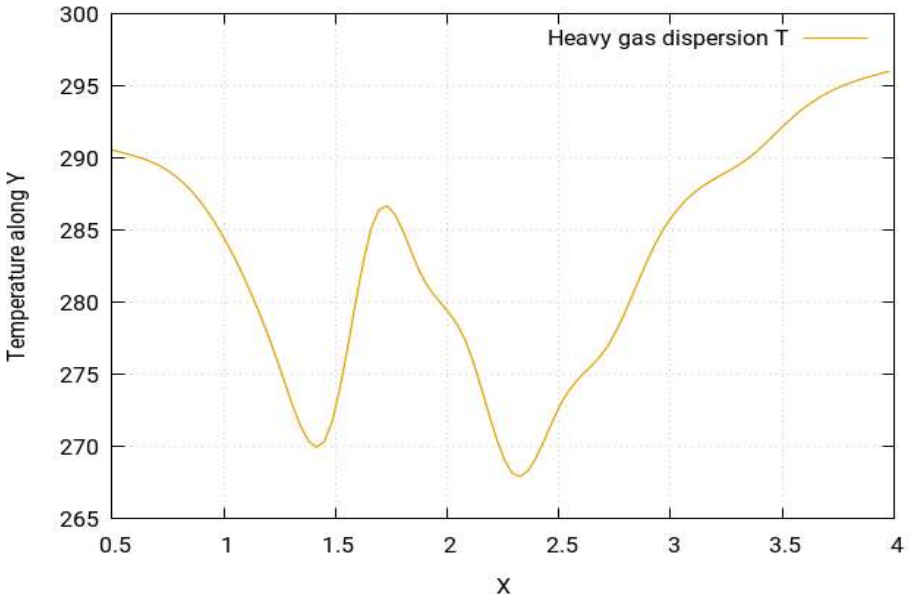

(b) *Graphical results for the temperature profile of the heavy gas along the y-direction*

The results of concentration in (a) and temperature in (b) are taken from the same case study. Figure (b) shows an exactly inverted image of Figure (a). Therefore, it is assumed that the effect of temperature is opposite to that of concentration.

8.7.5 Effect of release source location

The release source location has an influence in defining the shape of the gas cloud and gas dispersion. The following figures show the comparison of two results with two different locations for the release source:

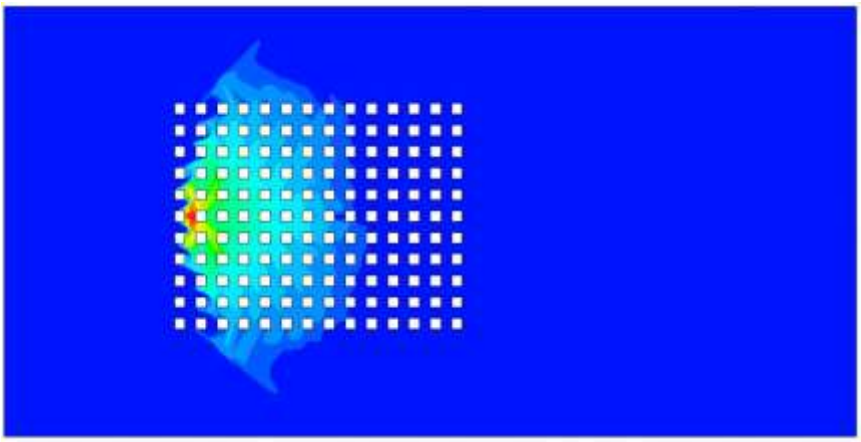

Figure 8.301: (a) *Release source located between the 1st & 2nd columns in the 6th row*

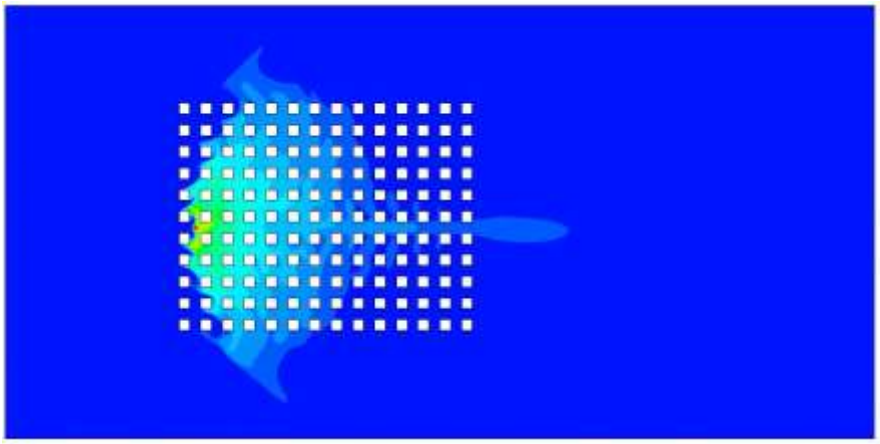

(b) *Release source located between the 1st & 2nd column in the middle between the 5th & 6th rows*

As can be seen from the above figures, there is a clear difference between the gas dispersions and cloud shapes which occurred due to the difference of release source location as all the rest of the perimeters are the same. The gas dispersions in Figure (a) are less affected by the wind in Figure (a) as the release source location is behind a building. Meanwhile, in Figure (b), the release source location is exposed to the wind, which affects the cloud shape and, as a result, the cloud shape is enhance along the horizontal and the gas dispersions are affected in such a way that the prismatic shaped high concentrated area is reduced when the release source is located between the rows.

8.8 Summary

The dispersion of heavy gas clouds using computational fluid dynamics (CFD) simulations has been studied in this work to ascertain the different patterns of the formation and dispersion of heavy gas clouds. The impact of the various factors, such as wind speed, layout and gas release source location, on the formation of heavy gas clouds and their dispersion has also been studied. The technique used in this research is Large-Eddy simulations in computational fluid dynamics (CFD) inspired by the work of Weiming et. al. [111]

Weiming Liu, Alakalabi et al. [111], in their paper "Large Eddy Simulations of Heavy Gas Dispersion within Building Group", proved that this technique yields almost the same results for the dispersion of heavy gas cloud as the experimental results. Therefore, this technique can be used as a basis to study the dispersion of heavy gas clouds in other layouts as well because the technique has already been proven to produce very effective results. Therefore, different layout types were selected and the heavy gas dispersion in those particular layouts was studied using this technique. Some particularly interesting studies, including [24],[113] and [104], have been done on this topic. Nevertheless, the experimental set-up of Heidorn et. al. [103], was selected for comparison the present study's results.

The dispersion of the gases is dependent on many factors, such as discharge velocity, temperature of the gas and the atmosphere, discharge flow rate and the release source location. The turbulence of the dispersion gas accompanied by the wind velocity results in the gases accumulating around the obstacles. Moreover, the greater the wind velocity, the greater the dispersion area will be. In the analysis, these effects of wind and gas velocity were observed in all cases. In addition, the difference in the temperatures between the dispersion gases results in the creation of buoyant forces that further increase the dispersion area in the upward direction as well as in the horizontal direction. This effect was mostly observed in the dispersion of the neutral gases at very low temperatures.

In the case of the arrangement of the storage tanks, another important parameter is to properly define the safe distance between the tanks for which the accumulation of the heavy and neutral harmful gases is minimal/um. Many industrial standards have been developed to define the safe distance between the storage tanks based on the type of the gas stored, location of the tanks, temperature of tanks, etc.

The different parameters and release source locations are mentioned against each case study. The results of these studies have helped greatly in determining the patterns of heavy gas cloud

formations and their dispersion in the closed layouts. The following points from can be deduced from the results:

1. Gas release source location is usually the most hazardous zone in terms of gas cloud formation.
2. Release source location has an impact on gas dispersion and cloud shapes.
3. Wind speed also plays a role in defining the shape of the cloud and gas dispersions.
4. Heavy gas clouds tend to move in multiple directions, unlike neutral gas clouds, which like to evade towards the vertical.
5. High wind speed tends to influence more the dispersion of heavy gas clouds more than low wind speed.
6. Gas clouds tend to be more spread out in the layout at low speed.
7. Layouts with a/the safe distance tend to be minimally hazardous due to less accumulation of the heavy gas dispersion and a decreased chance of heavy gas cloud formation.
8. Wind has very little influence on the gas cloud dispersion when the release source is not exposed to it.
9. The large eddies of the wind vertexes carry the released chunks of the gas cloud to mix them in the environment and create a poisonous zone.
10. The shapes of the gas cloud are different even if the perimeters are the same, but the release gas location is different in the same layout.
11. The wind greatly affects the dispersion of heavy gas if it has access to the location of the release source (leakage point). This leads to the conclusion that gas storage units must be placed in an environment where sufficient air is circulating so that, if the gas is leaked, it can dissipate into the environment and not accumulate in one place to form a hazardous zone.

8.9 Outcomes of this research

The present research helped study heavy gas cloud formations and the influence of different parameters and layouts on them. As a result, the following conclusions can be made:

1. The database identifies the most critical locations for cloud formation. In case of gas leakage for particular layouts, sensors should be implemented in those locations to predict the leakage of gas.

2. The database shows the patterns of cloud formations for different sources of gas leakage. In case of leakage, if the clouds could be somehow visualised, the release source could easily be identified.
3. In the event that the release location of the case has been determined, the probable locations could be filtered for the cloud formations with the help of the database.
4. Layouts of gas storage tanks could be designed on the basis of the case study.

These findings could massively help planning the transportation, storage and application of the gas as the threats and risks are now known. These results can be used as a database to help in investigating the detection, installation of the gas tanks and the risk and management purposes for the heavy gas.

Chapter 9 Conclusions

The accidental release of heavy gas occurs in petroleum and processing industries sometimes. Safety risk management employs hazard protection techniques in different layers. An area containing heavy gases often features heavy gas clouds. It is divided into three zones in management. Zone 0 has the most stringent safety protocols in which no ignition source is allowed at any time. This zone is the one that has the highest concentration of heavy gases. Meanwhile, Zone 2 has less frequent contact with heavy gas and hence has less stringent safety procedures.

In order to produce accurate knowledge of the leaked gas contents in the zones, this study numerically investigates dispersion of heavy gas clouds. Advanced mathematical models and turbulence models are developed and applied to investigate the formulation and dispersion of heavy gas clouds in this research. The mathematical models are based on the 3D Naiver-Stocks equations for low Mach number flows. The phase change of the liquefied gases, mixing processes and heat transfer of the heavy gases with the surrounding air are involved in. These mathematical models are solved numerically by the computational fluid dynamics (CFD) approach. The turbulence is modelled by the large eddy simulation and Reynolds averaged Navier-Stokes's approach.

The experimental measurements and observations are in conformity with this study's numerical simulations. There exists a small deviation between the two sets of results for the following reasons:

1) In our numerical simulations, the atmospheric conditions, like ambient temperature and wind velocity, are kept constant throughout the domain.
2) In the real time experiments, these parameters do not remain constant and hence show some deviations from the experimental approaches.

It is found that heavy gas cloud dispersion is dependent on a number of factors, including both the parameters of the heavy gases and the atmospheric conditions. The results compared through the experimental observations or even the results for the numerical simulations in this study show that the heavy gas cloud dispersion is dependent on the following parameters of the gas:

1) Velocity of the dispersion
2) Density of the cloud

3) Concentration of the heavy gas

The velocity of the heavy gas defines the area that the heavy gas cloud will cover in case of any release into the environment, both horizontally and vertically. The velocity has a direct influence on the dispersion; the higher the velocity, the greater the area of the dispersion of the heavy cloud. This is verified by the present CFD simulations results which showed similar behaviour of direct proportionality.

The density of the heavy gas cloud is dependent on the molecular mass of the gas. The molecular mass of the gas affects the dispersion of the heavy gas cloud; the lighter the gas, the more the dispersion. This is because the lighter gas is carried by the wind. The results compared with the experimental observations and the present numerical simulation are in conformity with each other on density.

The concentration of the heavy gas is very much dependent on the distance from the source. As the distance from the source increases, the concentration decreases. The results from other experiments observations and the present numerical simulations show similar behaviour.

The flashing jet has a unique property during its release, which is the formation of small droplets suspended in the heavy gas cloud. These droplets are carried away with the water during rain and remain in the atmosphere for longer durations. The diameter of these droplets was calculated both in the experimental observation and the present numerical simulation. It was found that this diameter is dependent on velocity, diameter of the nozzle and density of the heavy gas.

The flashing jet simulation and the experimental results show similar behaviour, but the following factors are particular to the flashing jet:

1) Diameter of the nozzle or the source
2) Droplet diameter
3) Pressure of the cylinder containing the liquified gas

The present CFD simulation results and experimental observations also show that, as the diameter of the nozzle releasing the flashing gas increases, the concentration of the heavy gas in the environment increases. This is because, as the diameter increases, the volumetric flow rate of the heavy gas increases.

The pressure of the cylinder has a direct influence on the dispersion. As the pressure of the cylinder increases, the heavy gas cloud dispersion area increases.

Another important parameter studied in this research is the effect of obstacles on the dispersion of the heavy gas cloud. The results show that the concentration of the heavy gas is highest around the buildings because of flow effects. This concentration also increases as the height from the ground increases; it then starts decreasing.

The ambient atmospheric properties, like temperature, wind and pressure, also have a direct influence on the dispersion of heavy gas. The wind has the greatest effect on the properties like temperature, concentration and dispersion of the heavy gas.

Recommendations and areas for further research

It is found through this work that numerical solutions of Reynolds averaged Navier - Stokes's equations are an important approach for risk assessment of heavy gas leakages. The k-epsilon turbulence model is basically able to produce correct results. To improve the accuracy of predictions, however, advanced turbulence models such as large eddy simulations and relevant numerical schemes need to be further developed. This should be one of the further research areas.

Another important aspect on hazards of the heavy combustible gas clouds is the chemical reactions with the gas dispersions. Because of the time limitation, it is missed in this study and is therefore a further research area suggested from this work.

Bibliography

[1] Ruwitch, J. Police detain nine after Qingdao oil blasts. Available at: http://www.reuters.com/article/us-china-sinopec-blasts-idUSBRE9AP02N20131126Last accessed: May 22, 2016, 2013.

[2] Cleaver, P., Johnson, M. & Hob, B. "A summary of some experimental data on LNG safety." Journal of Hazardous Materials. 140: 429–438, 2007.

[3] Ichard, M. " Numerical Computations of Pressurized Liquefied Gas Releases into the Atmosphere. " Bergen: University of Bergen, 2012.

[4] J. L. Woodward, J. Cook, and A. Papadourakis. "Modeling and validation of a dispersing aerosol jet," J. Hazard. Mater., vol. 44, no. 2–3, pp. 185–207, 1995.

[5] H. Witlox, M. Harper, P. Bowen, and V. Cleary. "Flashing liquid jets and two-phase droplet dispersion. II. Comparison and validation of droplet size and rainout formulations," J. Hazard. Mater., vol. 142, no. 3, pp. 797–809, 2007.

[6] P. J. Kay, P. J. Bowen, and H. W. M. Witlox. "Sub-cooled and flashing liquid jets and droplet dispersion II. Scaled experiments and derivation of droplet size correlations," J. Loss Prev. Process Ind., vol. 23, no. 6, pp. 849–856, 2010.

[7] Nicholas, M., & Whitfieldb, A. "The Buncefield accident and the environmental consequences for fuel storage sites and other sites in the UK, " Regulated under the Seveso directive. Chemical Engineering, 31, 2013.

[8] G. Atkinson, J. Hall, and A. Mcgillivray. "Review of Vapour Cloud Explosion Incidents Prepared by the Health and Safety Executive RR1113,",2017.

[9] G. Atkinson. "Buncefield: Lessons learned on emergency preparedness.," Loss Prev. Bull., no. 254, pp. 23–28, 2017.

[10] Zohdirad, H., Ebadi, T., & Givehchi, S. " Optimization of the calculation of hazardous zones boundaries for classification of hazardous area using risk-based approach. " Health and Safety at Work, 6(1), 13-22, 2016.

[11] H. Witlox, M. Harper, P. Bowen, and V. Cleary. "40 3 /200 2," J. Hazard. Mater., vol. 142, no. 3, pp. 797–809, 2007.

[12] Tian, S., et al., Evaluation of the use of high CO2 concentrations and cold storage to control of Monilinia fructicola on sweet cherries. Postharvest Biology and Technology, 2001. 22(1): p. 53-60.

[13] Jossi, M., et al., How Elevated CO2 Modifies Total and Metabolically Active Bacterial Communities in the Rhizosphere of Two Perennial Grasses Grown under Field Conditions. FEMS Microbiology Ecology, 2006. 55: p.339-50.

[14] 1. Kaplan, S., & Garrick, B. J. “On the quantitative definition of risk. Risk analysis,” 1(1), 11-27, 1981.

[15] 2. Gavranić, I. “Methodology of Risk Assessment in Explosive Atmosphere/Hazardous Aeeas. bilten Agencije za prostore ugrožene eksplozivnom atmosferom,” 35(1), 24-37, 2007.

[16] J. Hebrard and J. Lacome. “Evaluation of two-phase flow models for accidental release and comparison with experimental data To cite this version : HAL Id : ineris-00973315,”,2014.

[17] Ponchaut, N. F., Colella, F. and Marr, K. C. Vapor clouds, SFPE Handbook of Fire Protection Engineering, 2016.

[18] D. M. Webber and J. S. Kukkonen. “Modelling two-phase jets for hazard analysis,” J. Hazard. Mater., vol. 23, no. 2, pp. 167–182, 1990.

[19] Qi, R. Liquefied Natural Gas Vapor Dispersion Modeling with Computational Fluid Dynamics Codes. College Station: Texas A & M University, 2011.

[20] S. G. Giannissi, A. G. Venetsanos, N. Markatos, and J. G. Bartzis. “Numerical simulation of LNG dispersion under two-phase release conditions,” J. Loss Prev. Process Ind., vol. 26, no. 1, pp. 245–254, 2013.

[21] Gaber, “Gas Dispersion,” A-to-Z Guid. to Thermodyn. Heat Mass Transf. Fluids Eng., vol. g, 2006, doi: 10.1615/atoz.g.gasdis.

[22] K. J. Eidsvik, “A model for heavy gas dispersion in the atmosphere,” Atmos. Environ., vol. 14, no. 7, pp. 769–777, 1980, doi: 10.1016/0004-6981(80)90132-8.

[23] Safitri, A., Gao, X. & Mannan, S. Dispersion modeling approach for quantification of methane emission rates from natural gas fugitive leaks detected by infrared imaging technique. Journal of Loss Prevention in the Process Industries. 24: 138-145, 2011.

[24] Scargiali, F., Grisafi, F., Busciglio, A. & Brucato, A. Modeling and simulation of dense cloud dispersion in urban areas by means of computational fluid dynamics. Journal of Hazardous Materials. 197: 285– 293, 2011.

[25] Liu, X, Niu, J. & Kwok, K. Analysis of concentration fluctuations in gas dispersion around high-rise building for different incident wind directions. Journal of Hazardous Materials. 192: 1623– 1632, 2011.

[26] Havens, J., Walker, H. & Spicer, T. Bhopal Atmospheric Dispersion Revisited. Journal of Hazardous Materials. 233–234: 33–40, 2012.

[27] Kothari, K. & Meroney, R. Building Effects on National Transonic Facility Exhaust Plume. Hampton: NASA, 1979.

[28] Meroney, R. Transient Characteristics of Dense Gas Dispersion. Part II. Journal of Hazardous Materials. 9: 159–170, 1984b.

[29] Heidorn, K., Murphy, M., Irwin, P., Sahota, H., Misra, P. & Bloxam, R. Effects of obstacles on the spread of a heavy gas-Wind tunnel simulations. Journal of Hazardous Materials. 30: 151-194, 1992.

[30] Ohba, R., Hara, T., Nakamura, S., Ohya, Y. & Uchida, T. Gas diffusion over an isolated hill under neutral, stable and unstable conditions. Atmospheric Environment. 36: 5697–5707, 2002.

[31] Pontiggia, M., Derudi, M., Busini, V. & Rota, R. Hazardous gas dispersion: A CFD model accounting for atmospheric stability classes. Journal of Hazardous Materials. 171: 739–747, 2009.

[32] Hall, R. Modelling Of Dense Gas Dispersion in Tunnels. Sudbury: HSE Books, 2001.

[33] Hurley, M., Gottuk, D., Hall, J., Harada, K., Kuligowski, E., Puchovsky, M., Torero, J., Watts, J. & Wieczorek, C. SFPE Handbook of Fire Protection Engineering. Quincy: National Fire Protection Association, 2016.

[34] L. Dong, H. Zuo, L. Hu, B. Yang, L. Li, and L. Wu, "Simulation of heavy gas dispersion in a large indoor space using CFD model," J. Loss Prev. Process Ind., vol. 46, pp. 1–12, 2017, doi: 10.1016/j.jlp.2017.01.012.

[35] Baukal Jr., C. Oxygen-Enhanced Combustion. London: CRC Press, 2013.

[36] DeMarco, A. Transportation Systems and Engineering. Hershey: Engineering Science Reference, 2015.

[37] Casal, J. Evaluation of the Effects and Consequences of Major Accidents in Industrial Plants. Oxford: Elsevier, 2008.

[38] Center for Chemical Process Safety. Guidelines for Evaluating the Characteristics of Vapor Cloud Explosions. New York: American Institute of Chemical Engineers, 1994.

[39] Guo, Y., He, L., Wang, D. & Liu, S. Numerical investigation of surface conduit parallel gas pipeline explosive based on the TNT equivalent weight method. Journal of Loss Prevention in the Process Industries. 44: 360-368, 2016.

[40] Cameron, I. & Raman, R. Process Systems Risk Management. Oxford: Elsevier, 2005.

[41] Pontiggia, M., Derudi, M., Alba, M., Scaioni, M. & Rota, R. Hazardous gas releases in urban areas: Assessment of consequences through CFD modelling. Journal of Hazardous Materials. 176: 589–596, 2010.

[42] Xing, J., Liu, Z., Huang, P., Feng, C., Zhou, Y., Zhang, D. & Wang, F. Experimental and numerical study of the dispersion of carbon dioxide plume. Journal of Hazardous Materials. 256–257: 40– 48, 2013.

[43] G. Krnio-Langlo and M. Schatzmann, "Wind Tunnel Modelling of Heavy Gas Disperion," vol. 25, no. 7, 2000.

[44] C. Rauchegger, S. Bayley, and V. Schroder, "Dispersion of Heavy Gases – Experimental Results and Numerical Simulations," Process Saf. Prog., vol. 25, no. 4, pp. 326–330, 2006, doi: 10.1002/prs.

[45] Sklavounos, S., & Rigas, F. "Validation of turbulence models in heavy gas dispersion over obstacles. Journal of hazardous materials," 108(1-2), 9-20, 2004.

[46] F. Rigas, S. Sklavounos, Risk and consequence analyses of hazardous chemicals in marshalling yards and warehouses at Ikonio/Piraeus harbour, Greece, J. Loss Prevent. Process Ind. 15 (2002) 531–544

[47] F. Rigas, M. Konstandinidou, P. Centola, G.T. Reggio, Safety analysis and risk assessment in a new pesticide production line, J. Loss Prevent. Process Ind. 16 (2003) 103–109

[48] 4. F.P. Lees, Loss Prevention in the Process Industry, 2nd ed., Butterworths/Heinemann, Oxford, 1996, pp. 15 and 167.

[49] Smagorinsky, J. General Circulation Experiments with the Primitive Equations I the basic experiment, Monthly Weather Review, 91(3):99–164, 1963.

[50] Danie A. Crowl, Joseph F. Louvar. Chemical Process Safety Fundamentals with Applications, 2nd edn., The United States of America : Prentice Hall PTR, 2001.

[51] Zwillinger, D. "Handbook of differential equations (Vol. 1)." Gulf Professional Publishing, 1998.

[52] Wu, Y. S. "Multiphase fluid flow in porous and fractured reservoirs." Gulf professional publishing, 2015.

[53] Jouaneh, M. K., & Palm III, W. J. System dynamics experimentation at home. In ASME International Mechanical Engineering Congress and Exposition (Vol. 43802, pp. 413-420), (2009, January).

[54] Fiates, J., Santos, R. R. C., Neto, F. F., Francesconi, A. Z., Simoes, V., & Vianna, S. S. "An alternative CFD tool for gas dispersion modelling of heavy gas," Journal of Loss Prevention in the Process Industries, 44, 583-593, 2016.

[55] Scargiali, F., Di Rienzo, E., Ciofalo, M., Grisafi, F., & Brucato, A. Heavy gas dispersion modelling over a topographically complex mesoscale: a CFD based approach. Process safety and environmental protection, 83(3), 242-256, 2005.

[56] Jiang, Y., Xu, Z., Wei, J., & Teng, G. Fused CFD-interpolation model for real-time prediction of hazardous gas dispersion in emergency rescue. Journal of Loss Prevention in the Process Industries, 63, 103988, 2020.

[57] Zhang, Y., Wang, L., Li, A., & Tao, P. Performance evaluation by computational fluid dynamics modelling of the heavy gas dispersion with a low Froude number in a built environment. Indoor and Built Environment, 29(5), 656-670, 2020.

[58] Kruse, H., Tekiela, M. Calculatingt the consequences of a CO2 pipeline rupture. Energy Conversion and Management 37, 1013–1018, 1996.

[59] Vendrig, M., Spouge, J., Bird, A., Daycock, J. and Johnsen, O. Risk analysis of the geological sequestration of carbon dioxide. In: Crown (Ed.), Department of Trade and Industry's Cleaner Coal Technology Transfer Programme. R246 DTI/Pub URN 03/1320, 2003.

[60] Turner, R., Hardy, N., Hooper, B. Quantifying the Risks Associated with a CO2 Sequestration Pipeline: A Methodology and Case Study. Cooperative Research Centre for Greenhouse Gas Techonlogies (CO2CRC), Camberra, 2003.

[61] Reynolds, R.M. ALOHA 5.0, Theoretical description. National Oceanic and Atmospheric Administration, Seattle, Washington. NOS ORCA-65, 1992.

[62] Smith, J.C. Atmospheric Dispersion Modelling. Annual Report 1996/1997. Chilton. Didcot, Oxfordshire, National Radiological Protection Board, 1999.

[63] Mazzoldi, A., Hill, T., & Colls, J. J. CFD and Gaussian atmospheric dispersion models: A comparison for leak from carbon dioxide transportation and storage facilities. Atmospheric environment, 42(34), 8046-8054, 2008.

[64] Tang, W., Huber, A., Bell, B. and Schwarz, W. Application of CFD simulations for short-range atmospheric dispersion over open fields and within arrays of buildings. In: Proceedings of the 14th Joint Conference on the Applications of Air Pollution Meteorology with the A&WMA. Atlanta, GA, EPA, 2006.

[65] Mohan, M., Panwar, T. S., & Singh, M. P. Development of dense gas dispersion model for emergency preparedness. Atmospheric Environment, 29(16), 2075-2087, 1995.

[66] Stockie, J. M. The mathematics of atmospheric dispersion modeling. Siam Review, 53(2), 349-372, 2011.

[67] S. B. Pope. ‘Turbulent Flows’, Cambridge Univ. Press, Cambridge, UK, 2000.

[68] F. Harms, B. Leitl, M. Schatzmann, G. Patnaik. 'Validating LES-based Flow and Dispersion Models', The Fifth International Symposium on Computational Wind Engineering, 1(CWE2010), 2010.

[69] Salim Mohamed Salim. 'Numerical simulation of dispersion in urban street canyons with avenue-like tree plantings: Comparison between RANS and LES', Building and Environment, 1(1735-1746), 2011.

[70] David C. Wilcox. Turbulence Models for CFD, 1st edn., United States of America by Griffin Printing, Glendale, California: 0-9636051-0-0, 1993.

[71] Kolmogorov, A. N. Equations of motion of an incompressible turbulent fluid. Izv Akad Nauk SSSR Ser Phys, 6(6), 56-58, 1942.

[72] Wilcox, D. C. Turbulence modeling for CFD (Vol. 2, pp. 103-217). La Canada, CA: DCW industries, 1998.

[73] Durbin, P. A. Separated flow computations with the k-epsilon-v-squared model. AIAA journal, 33(4), 659-664, 1995.

[74] Patel, V. C., Rodi, W., & Scheuerer, G. Turbulence models for near-wall and low Reynolds number flows-a review. AIAA journal, 23(9), 1308-1319, 1985.

[75] Versteeg, H. K., & Malalasekera, W. An Introduction to Computational Fluid Dynamics: The Finite Volume Method, 2007.

[76] Raithby, G. D. and Chui, E. H. A Finite Volume Method for Predicting Radiative Heat Transfer in Enclosures with Participating Media, J. Heat Transfer, Vol. 112, pp. 415–423, 1990.

[77] Chui, E. H., Raithby, G. D. and Hughes, P. M. Prediction of Radiative Transfer in Cylindrical Enclosures with the Finite Volume Method, J. Thermophys. Heat Transfer, Vol. 6, No. 4, pp. 605–611, 1992.

[78] Chui, E. H., Hughes, P. M. and Raithby, G. D. Implementation of the Finite Volume Method for Calculating Radiative Transfer in a Pulverised Fuel Flame, Combust. Sci. Techn., Vol. 92, pp. 225–242, 1993.

[79] Chui, E. H. and Raithby, G. D. Computation of Radiative Heat Transfer on a Non-orthogonal Mesh Using the Finite Volume Method, Number. Heat Transfer, Pt B, Vol. 23, pp. 269–288, 1993.

[80] Chai, J. C., Lee, H. S. and Patankar, S. V. Finite-volume Method for Radiation Heat Transfer , J. Thermophys. Heat Transfer, Vol. 8, No. 3, pp. 419—425, 1994a.

[81] Chai, J. C., Parthasarathy, G., Lee, H. S. and Patankar, S. V. Finite-volume Radiation Heat Transfer Procedure for Irregular Geometries, J. Thermophys. Heat Transfer, Vol. 9, No. 3, pp. 410—415, 1994b.

[82] I. Ansys, “ANSYS CFX-Solver Theory Guide,” 2018.

[83] I. Ansys, “ANSYS Fluent-Theory Guide,” 2018.

[84] B. Kevin and P. Glenn, “Fire dynamics simulator (version 4): user’s guide.”

[85] Kelecy, F. J. Coupling momentum and continuity increases CFD robustness. Ansys Advantage, 2(2), 49-51, 2008.

[86] Caretto, L.S., Curr, R.M., and Spalding, D.B.; “Two Numerical Methods for Three

Dimensional Boundary Layers,” Methods Appl. Mech. Engrg., vol. 1, pp. 39, 1972.

[87] Vanka S.P., “Fully Coupled Calculation of Fluid Flows with Limited Use of

Computer Storage,” Argonne National Laboratory, Report ANL-83-87, 1983.

[88] Vanka, S.P. and Leaf, G.K., “Fully Coupled Solution of Pressure Linked Fluid Flow Equations,” Argonne National Laboratory, Report ANL-83-73, 1983.

[89] Braaten, M.E., “Development and Evaluation of Iterative and Direct Methods for the Solution of The equations Governing Recirculating Flows,” Ph.D. Thesis, University of Minnesota, 1985.

[90] Hanby, R. F., Silvester, D. J., & Chew, J. W. (1996). A Comparison of coupled and segregated iterative solution technique for incompressible swirling flow. International journal for numerical methods in fluids, 22(5), 353-373.

[91] McGrattan, K., Hostikka, S., McDermott, R., Floyd, J., Weinschenk, C., & Overholt, K. Fire dynamics simulator technical reference guide volume 1: mathematical model. NIST special publication, 1018(1), 175, 2013.

[92] Crowe, C. T., Troutt, T. R., & Chung, J. N. Numerical models for two-phase turbulent flows. Annual Review of Fluid Mechanics, 28(1), 11-43, 1996.

[93] Stewart, H. B., & Wendroff, B. Two-phase flow: models and methods. Journal of Computational Physics, 56(3), 363-409, 1984.

[94] Borrell, R., Jofre, L., Lehmkuhl, O., & Castro, J. Parallelization strategy for the Volume-of-Fluid method on unstructured meshes. Procedia Engineering, 61, 198-203, 2013.

[95] Kleefsman, K. M. T., Fekken, G., Veldman, A. E. P., Iwanowski, B., & Buchner, B., A volume-of-fluid based simulation method for wave impact problems. Journal of computational physics, 206(1), 363-393, 2005.

[96] R. Richtmyer and K. Morton, Difference Methods for Initial Value Problems, Interscience, New York, 1967.

[97] Glimm, J., Grove, J. W., Li, X. L., Shyue, K. M., Zeng, Y., & Zhang, Q. Three-dimensional front tracking. SIAM Journal on Scientific Computing, 19(3), 703-727, 1998.

[98] Santos, A. A., Barros, F., Jose, A., & Navarro, M. A. Verification and validation of a numeric procedure for flow simulation of a 2x2 PWR rod bundle, 2011.

[99] H. Witlox, M. Harper, P. Bowen, and V. Cleary. "Flashing liquid jets and two-phase droplet dispersion. II. Comparison and validation of droplet size and rainout formulations," J. Hazard. Mater., vol. 142, no. 3, pp. 797–809, 2007.

[100] P. J. Kay, P. J. Bowen, and H. W. M. Witlox. "Sub-cooled and flashing liquid jets and droplet dispersion II. Scaled experiments and derivation of droplet size correlations," J. Loss Prev. Process Ind., vol. 23, no. 6, pp. 849–856, 2010.

[101] Ayrault, M., Simoens, S. & Mejean, P. Dispersion Of Dense Gas Releases Downwind Of Solid Obstacles. Transactions on Ecology and the Environment. 4: 491-498, 1994.

[102] Ayrault, M., Simoens, S. & Mejean, P. Negative buoyancy effects on the dispersion of continuous gas plumes downwind solid obstacles. Journal of Hazardous Materials. 57: 79-103, 1997.

[103] K.C Heidorn, M. M. Effects of obstacles on the spread of a heavy gas-Wind. Journal of Hazardous Materials, 151-194, 1992.

[104] R. Santon, M. Ivings, D. Webber, and A. Kelsey. "New methods for hazardous area classification for explosive gas atmospheres," Inst. Chem. Eng. Symp. Ser., no. 158, pp. 339–346, 2012.

[105] H. Witlox, M. Harper, P. Bowen, and V. Cleary. "40 3 /200 2," J. Hazard. Mater., vol. 142, no. 3, pp. 797–809, 2007.

[106] K. The, "Investigation into the Flashing Jets of gas Liquefied Numerically."

[107] S. G. Giannissi, A. G. Venetsanos, N. Markatos, and J. G. Bartzis. "Numerical simulation of LNG dispersion under two-phase release conditions," J. Loss Prev. Process Ind., vol. 26, no. 1, pp. 245–254, 2013.

[108] H. W. M. Witlox et al. “Two-phase jet releases and droplet dispersion: Scaled and large-scale experiments, droplet-size correlation development and model validation,” Inst. Chem. Eng. Symp. Ser., no. 155, pp. 615–623, 2009.

[109] S. Zilitinkevich. “Transactions on Ecology and the Environment vol 2, © 1993 WIT Press, www.witpress.com, ISSN 1743-3541,” Trans. Ecol. Environ., vol. 6, pp. 54–60, 1995.

[110] Y. Tominaga and T. Stathopoulos, “CFD simulations of near-field pollutant dispersion with different plume buoyancies,” Build. Environ., vol. 131, no. January, pp. 128–139, 2018, doi: 10.1016/j.buildenv.2018.01.008.

[111] Liu, W., Alakalabi, A., Graham, T. & Gu, X. Large Eddy Simulations of Heavy Gas Dispersion within Building Group. Istanbul, Turkey: Ninth International Conference on Computational Fluid Dynamics. ICCFD9: 1-14, 2016.

[112] HSE, “HSG 176, the storage of flammable liquids in tanks,” Heal. Saf. Exec., pp. 1–69, 2015.

[113] MERONEY, R. N. TRANSIENT CHARACTERISTICS OF DENSE GAS DISPERSION. Journal of Hazardous Materials, 139-157, 1984.

Appendices

Appendix A

More results at different release source locations within a group of building and/or structures distribution layouts shapes

Location2: Heavy gas dispersion

The release source location (2) was positioned at the upwind front of the group of gas storage tanks between the first and second column in the 3rd row from bottom. The perimeters selected for this case study are stated below table:

Table 1: *Parametric values of heavy gas simulation at location 2*

Density	Flow Rate	Velocity	Ambient Temperature	Release Source Temperature
2.1 kg m/s^3	1 kg/s	1 m/s	25°C	-100°C

Concentration of heavy gas dispersion

The following figure shows the concentration behaviour of the heavy gas at location 2. The whereabouts of location 2 has been stated at the beginning of the passage.

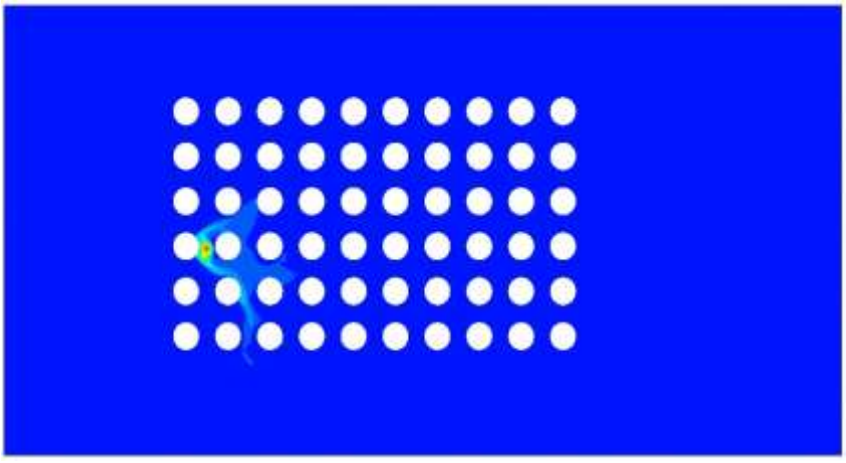

Figure 1: *Concentration profile of heavy gas dispersion with release source located at the upwind front of the gas storage tanks group between the first and second column at the 3rd row from bottom at* ***1m/s****.*

The concentration profile of the heavy gas at location 2 is shown in the above Figure 1. It represents the concentration behaviour of the heavy gas when the release gas source is placed at the upwind front of the group of gas storage tanks between the first and second column in the 3rd row. It can be seen that the cloud shape in this case is not much identical to a geometric

shape and the cloud covers the area of a few buildings only. A small portion of the gas cloud also leans downwards towards the lower edge trying to escape.

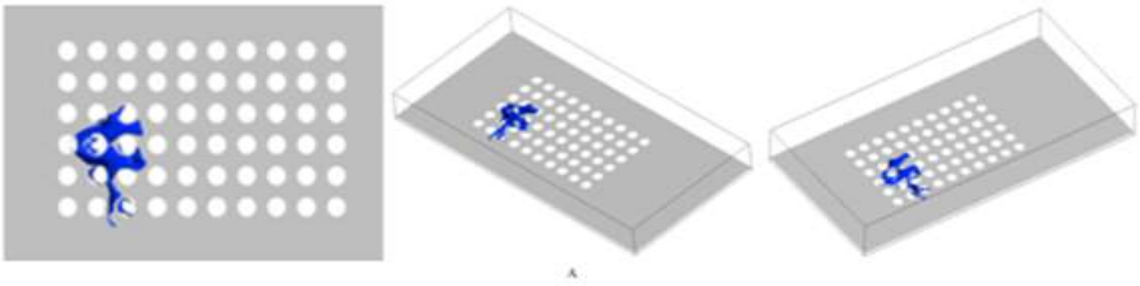

Figure 2: *Iso-surfaces of the concentration profile of heavy gas dispersion with release source located at the upwind front of the gas storage tanks group between the first and second column at the 3rd row from bottom at* ***1m/s****.*

Figure 2 shows the iso-surfaces of the concentration profile of heavy gas dispersion for collected layout with release source located at the upwind front of the group of gas storage tanks between the first and second column in the 3rd row. This helps identify the spread of the cloud in each dimension. It can be seen that the cloud shape seems to form a random pattern as discussed earlier and the iso-surfaces help us notice that the gas cloud leans more towards the vertical direction as compared to the other directions.

According to Standard BS EN 60079-10-1:2009 [104], the following locations can be categorised:

Zone 0: The 4th and 5th row buildings of the 2nd and 3rd columns

Zone 1: The immediate surroundings of the buildings mentioned in zone 0

Zone 2: All the remaining locations not categorised in zone 0 or zone 1

Temperature of heavy gas dispersion

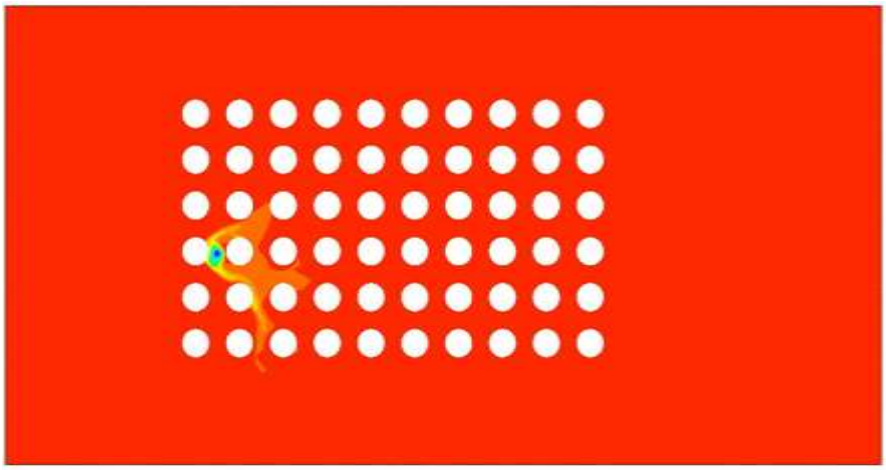

Figure 3: *Temperature profile of heavy gas dispersion with release source located at the upwind front of the group of gas storage tanks between the first and second column in the 3rd row from bottom at* ***1m/s****.*

Figure 3 shows the temperature simulation for this study. By visualising the temperature simulation, it is found out that the temperature simulation produces largely the same profile for the case study as that of the concentration profile. However, the behaviour of temperature is in fact the opposite to that of concentration. This means that the areas which were identified in the concentration simulation as the highly concentrated will in fact have the lowest temperatures, while the ones with moderate concentrations will have moderate temperatures and the least concentrated areas will have the maximum temperatures. To further simply these findings, it should be point out that the concentrations simulations showed that the concentrations near the release source point tend to be the highest and start to fade away as the gas cloud moves away from the source and are the lowest as the cloud moves much further away in the layout, eventually reaching the environment where the gas cloud disappears. However, the temperature is lowest near the release source point and tends to increase as the gas cloud moves away from the source, finally achieving its highest temperature equal to the ambient temperature of the environment.

Appendix B

Location 4: Heavy gas dispersion

Release source location was positioned in the middle front of the group of gas storage tanks at the 3rd row from bottom. The perimeters selected for this case study are stated below table:

Table 2: *Parametric values of heavy gas simulation at location 2*

Density	Flow Rate	Velocity	Ambient Temperature	Release Source Temperature
2.1 kg m/s^3	1 kg/s	1 m/s	25°C	-100°C

Concentration of heavy gas dispersion

The following figure shows the concentration behaviour of the heavy gas at location 4. The whereabouts of location 4 has been stated at the beginning of the passage.

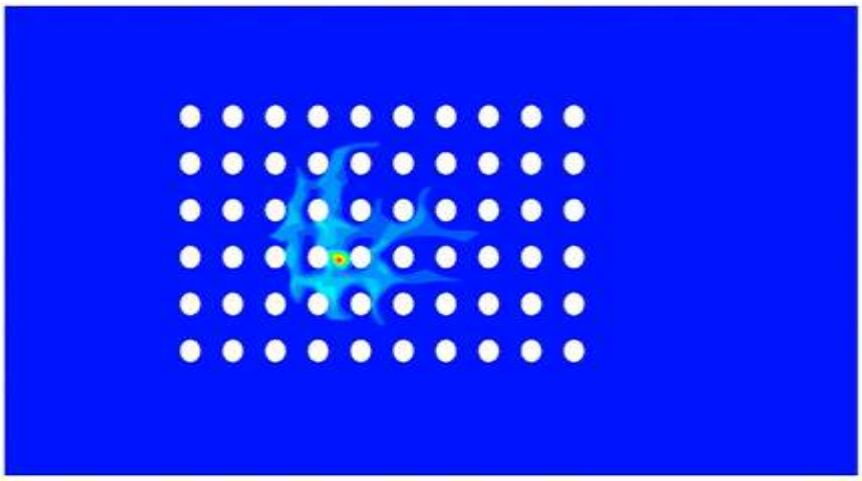

Figure 4: *Concentration profile of heavy gas dispersion with release source located in the middle front of the group of gas storage tanks at the 3rd row from bottom at* ***1m/s****.*

The concentration profile of the heavy gas at location 4 is shown in the above Figure 4. It represents the concentration behaviour of the heavy gas when the release gas source is placed at the middle front of the group of gas storage tanks in the 3rd row from bottom. It can be seen in the figure that the cloud shape is this case is a bit random and covers almost all the most central buildings of the layout. The gas cloud appears to drift away in all directions indicating the gas moves in all directions in this case. Since the release gas source is placed at the middle front therefore the effect of air on the gas cloud is not so noticeable and this is also why the gas cloud is able to move in the negative horizontal direction.

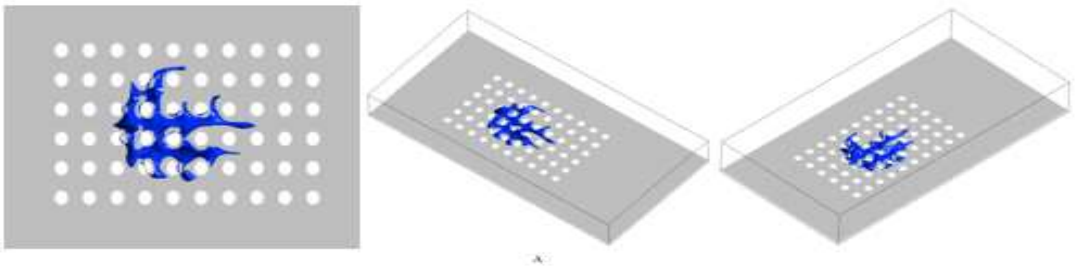

Figure 5: *Iso-surfaces of the concentration profile of heavy gas dispersion with release source located at the middle front of the group of gas storage tanks at the 3rd row from bottom at* ***1m/s****.*

Figure 5 shows the iso-surfaces of the concentration profile of the heavy gas dispersion for with release source located at the middle front of the group of gas storage tanks at the 3rd row from bottom. This helps identify the spread of the cloud in each dimension. It can be seen that the cloud forms a random pattern and tries to swirl around the circular buildings of the layout. The highest concentrations are at the middle front of the building layout which is expected as the release source is placed in the middle front. The cloud is spread somewhat symmetrically but a part of cloud is inclined to move more towards one edge.

According to Standard BS EN 60079-10-1:2009 [104], the following locations can be categorised:

High speed:

Zone 0: The middle front of the layout containing the release source excluding the first and last row.

Zone 1: A very small portion of buildings in the 2nd and the 2nd last row of the middle front.

Zone 2: All the remaining locations not categorised in zone 0 or zone 1

Temperature of heavy gas dispersion

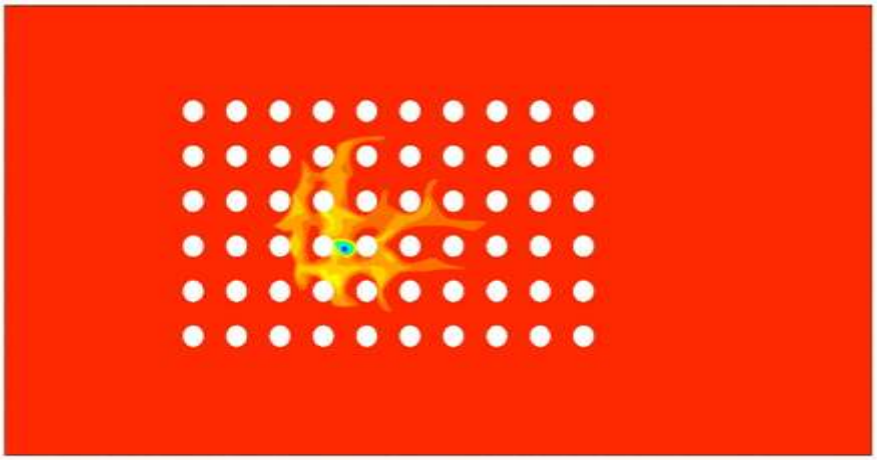

Figure 6: *Temperature profile of heavy gas dispersion with release source located in the middle front of the group of gas storage tanks at the 3rd row from bottom at* ***1m/s.***

The above Figure 6 shows the temperature simulation for this study. By visualising the temperature simulation, it is found out that the temperature simulation produces largely the same profile for the case study as that of the concentration profile. However, the behaviour of temperature is in fact the opposite to that of concentration. This means that the areas which were identified in the concentration simulation as highly concentrated will in fact have the lowest temperatures, while the ones with moderate concentrations will have moderate temperatures and the least concentrated areas will have the highest temperatures. To further simply these findings, it should be pointed out that the concentrations simulations showed that the concentrations near the release source point tend to be the highest and start to fade away as the gas cloud moves away from the source and is at its lowest as it moves much further away in the layout reaching the environment where the gas cloud eventually disappears. However, temperature is minimum near the release source point and tends to increase as the gas cloud moves away from source, finally achieving the maximum temperature equal to the ambient temperature of the environment.